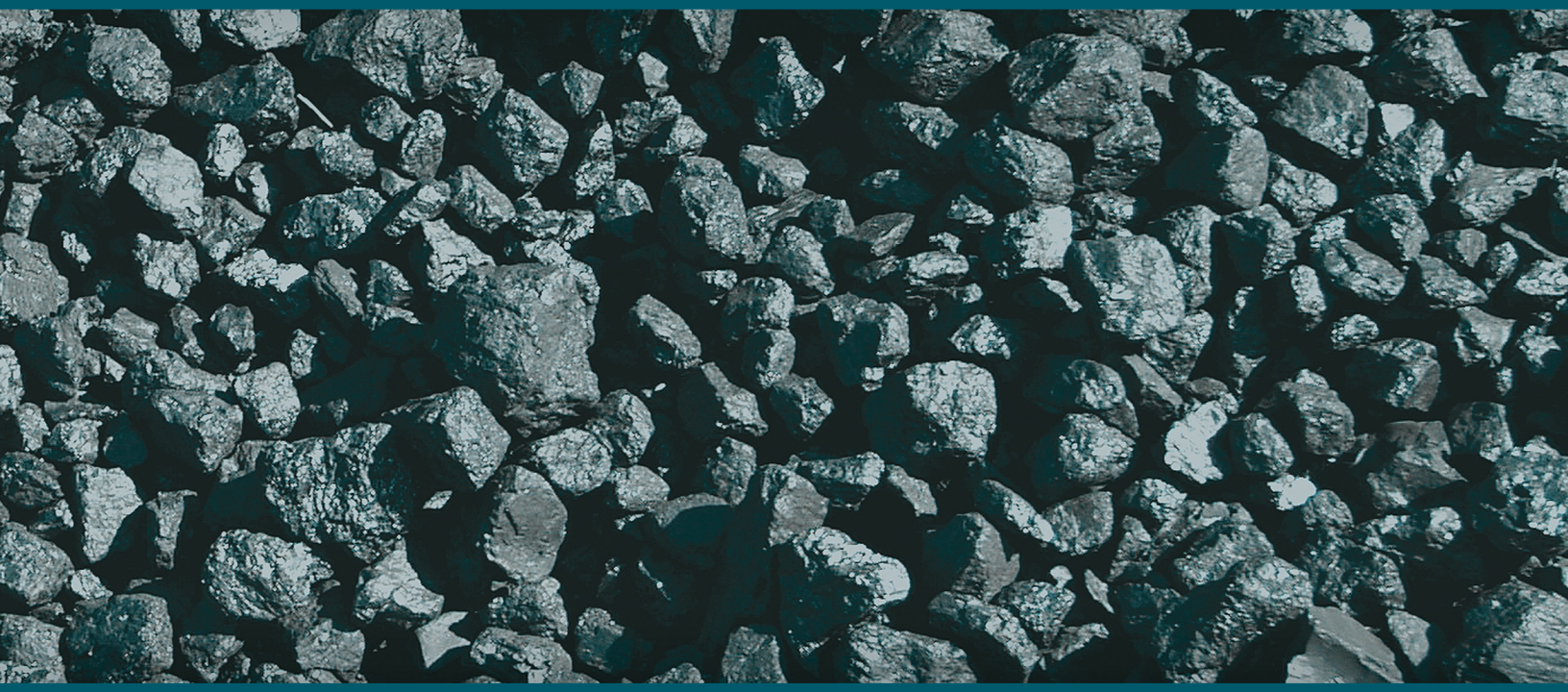
*Fundamentals of*

# COALBED METHANE

## *Reservoir Engineering*



**John Seidle**

# *Fundamentals of*
# COALBED METHANE
# *Reservoir Engineering*

PennWell®

**John Seidle**

**Disclaimer.** The recommendations, advice, descriptions, and the methods in this book are presented solely for educational purposes. The author and publisher assume no liability whatsoever for any loss or damage that results from the use of any of the material in this book. Use of the material in this book is solely at the risk of the user.

Copyright© 2011 by
PennWell Corporation
1421 South Sheridan Road
Tulsa, Oklahoma 74112-6600 USA

800.752.9764
+1.918.831.9421
sales@pennwell.com
www.pennwellbooks.com
www.pennwell.com

Marketing: Jane Green
National Account Executive: Barbara McGee

Director: Mary McGee
Managing Editor: Stephen Hill
Production Manager: Sheila Brock
Production Editor: Tony Quinn
Book Design: Susan E. Ormston
Cover Design: Therman Lee

Library of Congress Cataloging-in-Publication Data

Seidle, John.
Fundamentals of coalbed methane reservoir engineering / John Seidle.
p. cm.
Includes bibliographical references and index.
ISBN 978-1-59370-001-0
1. Gas reservoirs. 2. Coalbed methane. 3. Gas engineering. I. Title.
TN880.S45 2011
622'.3385--dc23

2011019056

All rights reserved. No part of this book may be reproduced, stored in a retrieval system, or transcribed in any form or by any means, electronic or mechanical, including photocopying and recording, without the prior written permission of the publisher.

Printed in the United States of America

1 2 3 4 5 15 14 13 12 11

To Dana and our grandchildren

# Contents

**Preface** . . . . . xi
**Acknowledgments** . . . . . xiii

**1. Introduction** . . . . . 1
What Is Coal Gas? . . . . . 1
Estimated Worldwide Coal Gas Resources . . . . . 3
Reservoir Properties of Selected Coals . . . . . 5
Construction of Coal Gas Analogs . . . . . 11
Coal Gas Pilots . . . . . 13
Statistical Nature of Coal Gas Exploitation . . . . . 15
Current Challenges to Coal Gas Exploitation . . . . . 16
References . . . . . 18

**2. Coal Fundamentals** . . . . . 19
Introduction . . . . . 19
Coal Rank . . . . . 19
Proximate and Ultimate Analyses . . . . . 22
Example 2.1. Comparison of daf and dmmf fractions . . . . . 24
Number of Samples and Confidence Limits . . . . . 25
Example 2.2. Arkoma Basin—Hartshorne coal density . . . . . 27
Sample Collection and Preservation . . . . . 28
Macerals . . . . . 29
Cleats . . . . . 30
Coal Porosity . . . . . 32
Coal Density . . . . . 36
Example 2.3. Organic fraction and ash density of San Juan Basin Fruitland coal . . . . . 38
Coal Gas Composition and Gas Properties . . . . . 40
Example 2.4. Average coal gas Z factors . . . . . 45
Gas Desorption . . . . . 47
Example 2.5. Desorption times . . . . . 50
Coal Rock Properties . . . . . 51
Nomenclature . . . . . 54
References . . . . . 56

**3. Geologic Aspects of Coal Gas Reservoir Engineering** . . . . . 59
Introduction . . . . . 59
Coal Ages, Distributions, and Depositional Environments . . . . . 60
Coal Rank . . . . . 69
Coal Cleats . . . . . 72
Coal Gas Origin and Composition—Thermogenic and Biogenic Gas . . . . . 73
Emerging Geoscience Concepts for Coal Gas Reservoir Engineering . . . . . 80
Wireline Logs . . . . . 81
Nomenclature . . . . . 87
References . . . . . 88

**4. Measurement of Coalbed Gas Content** . . . . . 93
Introduction . . . . . 93
Direct Methods . . . . . 93

Lost Gas . . . 102
Residual Gas . . . 104
USBM Direct Method . . . 105
Smith and Williams Method . . . 106
Curve Fit Methods . . . 109
Mass Normalized Gas Contents . . . 110
Sources of Error in Gas Content Measurements . . . 112
Typical Coalbed Gas Contents . . . 112
Mudlog Gas Content . . . 113
Number of Samples . . . 113
Acknowledgements . . . 121
Nomenclature . . . 122
References . . . 123

**5. Sorption of Gas on Coals** . . . 125
Introduction . . . 125
Langmuir's Equation . . . 126
Effect of Ash and Moisture, Daf and Dmmf Isotherms . . . 130
Effect of Coal Rank on Sorption . . . 133
Effect of Temperature on Sorption . . . 134
Example 5.1. Temperature effects on sorption isotherms—Dietz 3 coal, Powder River Basin . . . 136
Number of Isotherms Required . . . 139
Number of isotherms to characterize a single seam . . . 139
Number of isotherms to characterize multiple seams . . . 141
Number of isotherms to characterize a project . . . 143
Number of isotherms to characterize a basin . . . 143
Undersaturation . . . 146
Sorption Isotherms for $CO_2$, Nitrogen, and Other Gases . . . 147
Multicomponent Langmuir Isotherms . . . 148
Apparent Oversaturation . . . 149
Nomenclature . . . 151
References . . . 152

**6. Coal Permeability** . . . 155
Introduction . . . 155
Theoretical Absolute Coal Permeability . . . 156
Example 6.1. Hartshorne coal, Arkoma Basin—cleat permeability and porosity . . . 159
Stress Dependence of Coal Permeability . . . 159
Gas-Water Relative Permeabilities in Coal . . . 166
Matrix Deformation Due to Sorption . . . 174
Combined Stress and Matrix Shrinkage Influences on Coal Permeability . . . 175
Nomenclature . . . 181
References . . . 182

**7. Coal Well Pressure Transient Tests** . . . 185
Introduction . . . 185
Injection/Falloff Tests . . . 185
Example 7.1. Coal well prefrac falloff test . . . 187
Drillstem Tests . . . 192
Tank Tests . . . 193

Slug Tests . . . 194
Diagnostic Fracture Injection Tests . . . 195
Drawdown and Buildup Tests . . . 196
Example 7.2. Coal well pressure buildup test . . . 200
Sorption Compressibility . . . 205
Two-Phase Pseudopressures . . . 207
Why Dual Porosity Behavior Is Not Apparent in Coal Well Tests . . . 208
Interference Tests . . . 210
Micropilot Injectivity Tests . . . 211
Nomenclature . . . 212
References . . . 214

**8. Gas and Water Mass Balances in Coals** . . . 217
Coal Gas Mass Balance Equation . . . 217
Solution of the Coal Gas Mass Balance Equation . . . 224
Example 8.1. Coal gas reserves—King method—GRI well . . . 224
Example 8.2. Coal gas reserves—King method—Canyon coal, Powder River Basin . . . 227
Modified King Method . . . 228
Example 8.3. Coal gas reserves—modified King method—GRI coal well . . . 229
Example 8.4. Coal gas reserves—modified King method—Canyon coal well . . . 230
Jensen and Smith Modified Material Balance . . . 231
Example 8.5. Coal gas reserves—Jensen and Smith method—GRI coal well . . . 231
Example 8.6. Coal gas reserves—Jensen and Smith method—Canyon coal well . . . 232
Coal Gas Recovery Factor . . . 233
Example 8.7. Gas recovery factor—unidentified GRI well . . . 235
Example 8.8. Gas recovery factor—Canyon coal well . . . 236
Gas Mass Balance Equation for Undersaturated Coals . . . 238
Gas Mass Balance Equation for Multicomponent Gases . . . 239
Example 8.9. Multicomponent gas recovery . . . 242
Nomenclature . . . 245
References . . . 246

**9. Gas and Water Flow in Coals** . . . 247
Introduction . . . 247
Gas Flow in Coal Seams . . . 247
Example 9.1. Time to pseudosteady-state flow . . . 253
Characteristic Times for Sorption and Darcy Flow . . . 255
Bottomhole Pressure—Constant Rate Gas Production—Infinite Coal . . . 256
Example 9.2. Bottomhole flowing pressure for a Warrior Basin coal well . . . 257
Bottomhole Pressure—Constant Rate Gas Production—Bounded Drainage . . . 260
Example 9.3. Bottomhole flowing pressure for an Arkoma Basin coal well . . . 260
Gas Production Rate—Pseudosteady State . . . 262
Gas Production Rate—Constant Bottomhole Pressure—Bounded Drainage . . . 262
Water Flow in Coal Seams . . . 263
Example 9.4. Bottomhole flowing pressure of a well in an undersaturated coal . . . 264
Nomenclature . . . 267
References . . . 268

**10. Depletion of Gas and Water in Coals** . . . . . 271
Introduction . . . . . 271
Tank-Type Model of Coal Depletion . . . . . 272
Example 10.1. Depletion of Utah #25-7-6, Drunkard's Wash Field, Uinta Basin . . . . . 275
Gas Production from Dry Coals . . . . . 287
Example 10.2. Depletion of two Arkoma Basin coal wells . . . . . 287
Depletion of Undersaturated Coals . . . . . 291
Example 10.3. Depletion of a Marylee coal well, Rock Creek Project, Warrior Basin . . . . . 294
Coal Well Decline Curves . . . . . 296
Example 10.4. Decline curve analysis of Utah #25-7-6, Drunkard's Wash Field, Utah . . . . . 298
Example 10.5. Decline curve analysis of two Arkoma Basin coal wells . . . . . 299
Gas Composition during Depletion . . . . . 301
Example 10.6. Gas composition during laboratory depletion . . . . . 305
Example 10.7. Gas composition during depletion of a San Juan coal well . . . . . 310
Depletion of Variable Permeability Coal . . . . . 311
Nomenclature . . . . . 314
References . . . . . 316

**11. Simulation of Coal Well Performance** . . . . . 319
Introduction . . . . . 319
Development of Coalbed Methane Simulators . . . . . 319
Simulation Insights into Coal Reservoir Physics . . . . . 322
Probabilistic Coal Well Simulations . . . . . 323
Simulation of Enhanced Coalbed Methane Recovery and $CO_2$ Sequestration . . . . . 325
Required Inputs . . . . . 326
History Matching . . . . . 327
Example 11.1. Simulation of undersaturated coal with tank and gridded models . . . . . 331
Example 11.2. Cleat compressibility effects in undersaturated coal . . . . . 335
Example 11.3. Effect of sorption time on coal well performance . . . . . 338
Nomenclature . . . . . 343
References . . . . . 344

**12. Enhanced Coalbed Methane Recovery and $CO_2$ Sequestration** . . . . . 347
Introduction . . . . . 347
Binary Langmuir Sorption . . . . . 347
Example 12.1. Coalbed gas contents of a two-component gas mixture . . . . . 348
Early History of ECBM and $CO_2$ Sequestration in Coals . . . . . 350
Linear Flooding of a Coal Deposit . . . . . 356
Example 12.2. Nitrogen breakthrough in the Tiffany ECBM Pilot, San Juan Basin . . . . . 362
Example 12.3. Effect of Langmuir pressure on $CO_2$ breakthrough in ECBM . . . . . 366
Coal Absolute Permeability Variation during ECBM or $CO_2$ Sequestration . . . . . 372
Tank Model for $CO_2$ Sequestration . . . . . 374
Example 12.4. $CO_2$ sequestration in San Juan coal . . . . . 376
Nomenclature . . . . . 382
References . . . . . 384

Index . . . . . 387

# Preface

Coalbed methane developed from a safety hazard in coal mines to an unconventional gas reservoir in the last quarter of the 20th century. Many articles dealing with coal geoscience and reservoir engineering have been written over the last 30 or 40 years, and the field is now sufficiently mature that several good textbooks and monographs on these subjects have appeared. Why add another? Three reasons. First, coalbed methane can now be differentiated into separate specialties such as geology, geochemistry, geophysics, drilling and completions engineering, and operations and facilities engineering in addition to reservoir engineering. Secondly, the coalbed methane industry is increasingly global, allowing regional perspectives of previous work to be fused into a larger vision. Lastly, coalbed methane reservoir engineering has evolved many specialized methods in recent years. Entry into the field could perhaps be eased by a book stressing the fundamental aspects of coal gas reservoir engineering.

This book is not meant to be an exhaustive compilation of all coalbed methane reservoir engineering, a rapidly evolving field. It is meant to be a useful introduction to a unique unconventional gas resource for students and practicing engineers as well as a basic handbook for those involved in coalbed methane on a daily basis and require straightforward, practical answers in the fast-paced business world. I am grateful to all the people who have assisted me in bringing this book to completion, but all errors remain mine and mine alone. I will consider this book successful to the extent that it promotes additional developments in coalbed methane reservoir engineering that render it obsolete.

# Acknowledgments

This book took too long to write. I thank the editors and staff at PennWell who have patiently helped move this book along, in particular Marla Patterson, Steve Hill, and Tony Quinn. Coworkers John Arsenault and Leslie O'Connor were kind enough to read drafts of early chapters and offer constructive comments to a struggling author. I'm grateful to an anonymous reviewer whose comments on the first five chapters were most beneficial. My greatest thanks go to my wife, Dana, without whose steadfast love and support over the years this book simply could not have been written.

# Introduction 1

## What Is Coal Gas?

Coals were among the first gas reservoirs to be discovered and among the most recent to be exploited. Coal outcrops provided solid fuel to various early human societies, but gas held in coal deposits was unrecognized. Only when mines were driven deeper into coal deposits were gas emissions encountered, all too frequently with tragic results when the gas exploded. This gas was considered one of the many hazards of coal mining, with no thought given to capturing it for beneficial use even after exploitation of conventional oil and gas reservoirs began. Coalbed methane evolved from safety concerns in gassy coal mines, and initial coal gas geoscience and reservoir engineering concepts were rooted in this mining perspective. Only in the last generation has coal gas, along with shale gas and tight formation gas, been recognized as an unconventional gas resource. Like other unconventional gas resources, coal gas is a diffuse, heterogeneous, areally extensive resource defined by distribution and maturity of source rock, seal integrity over geological time, and occasionally by conventional traps.

Gas is generated during maturation of organic matter into coal and by microbes residing in a coal. Coal deposits of all geologic ages have generated gas, the volume increasing with coal rank. The belated development of coal gas is perhaps due to its capricious behavior, which is related to its unique storage in coal. Conventional gas is compressed into the pore space of the host reservoir rock and will easily flow to a pressure sink such as a wellbore. In contrast, the majority of the gas in a coal is typically *sorbed*, or attached to the surface of the coal itself. Coals are naturally fractured reservoirs, and the fractures, termed *cleats*, are often filled with water. Coal deposits are usually aquifers with the hydrostatic pressure of the water in the cleats holding the gas on the matrix of the coal, thereby providing the seal for this unconventional reservoir. Reduction of pressure in a coal seam by a mine shaft or wellbore will first mobilize water in the cleats, followed by gas desorbed from the matrix. Removal of this water can be costly and has bankrupted more than one attempt to produce coal gas. Only recently has coal water been recognized as a valuable natural resource rather than as oilfield brine, and future coal gas development projects should expect increased regulatory constraints on water production and disposal.

Pressure reduction in a coal seam sufficient to liberate gas from the matrix into the cleats initially results in a low gas saturation and, hence, low gas mobility and low initial gas production rates from a well. With continued dewatering of the coal deposit, gas saturation in the cleats increases, leading to increasing gas mobility and gas production rates. This rising gas production rate, a behavior opposite to that of conventional gas reservoirs, has been termed *negative decline*. Caused by the interplay between dewatering and depressuring of a coal deposit, duration of this negative decline period and the resulting peak gas production rate remain difficult to predict a priori. Gas rates can increase by a factor of 2 to 10 over a dewatering period, which can last from months to years. Examples of rapid and slow negative declines are illustrated in figures 1–1 and 1–2, respectively. After the gas production rate from a well or field has peaked and shows a clear decline, future performance and remaining reserves are often predicted with a combination of decline curve analysis, well performance analysis, and reservoir simulation.

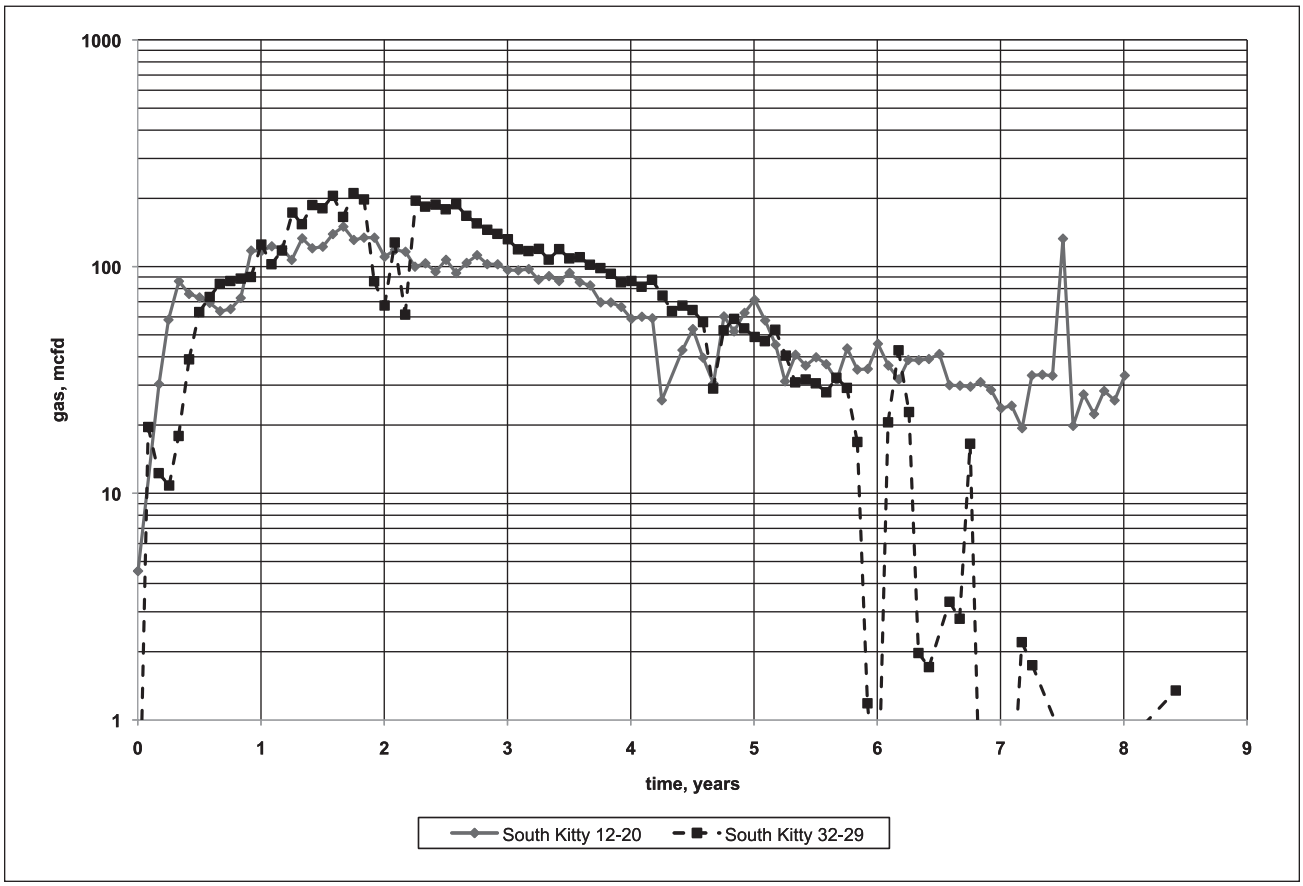



**Fig. 1–1.** Examples of rapid negative decline—Powder River Basin, Wyodak coal

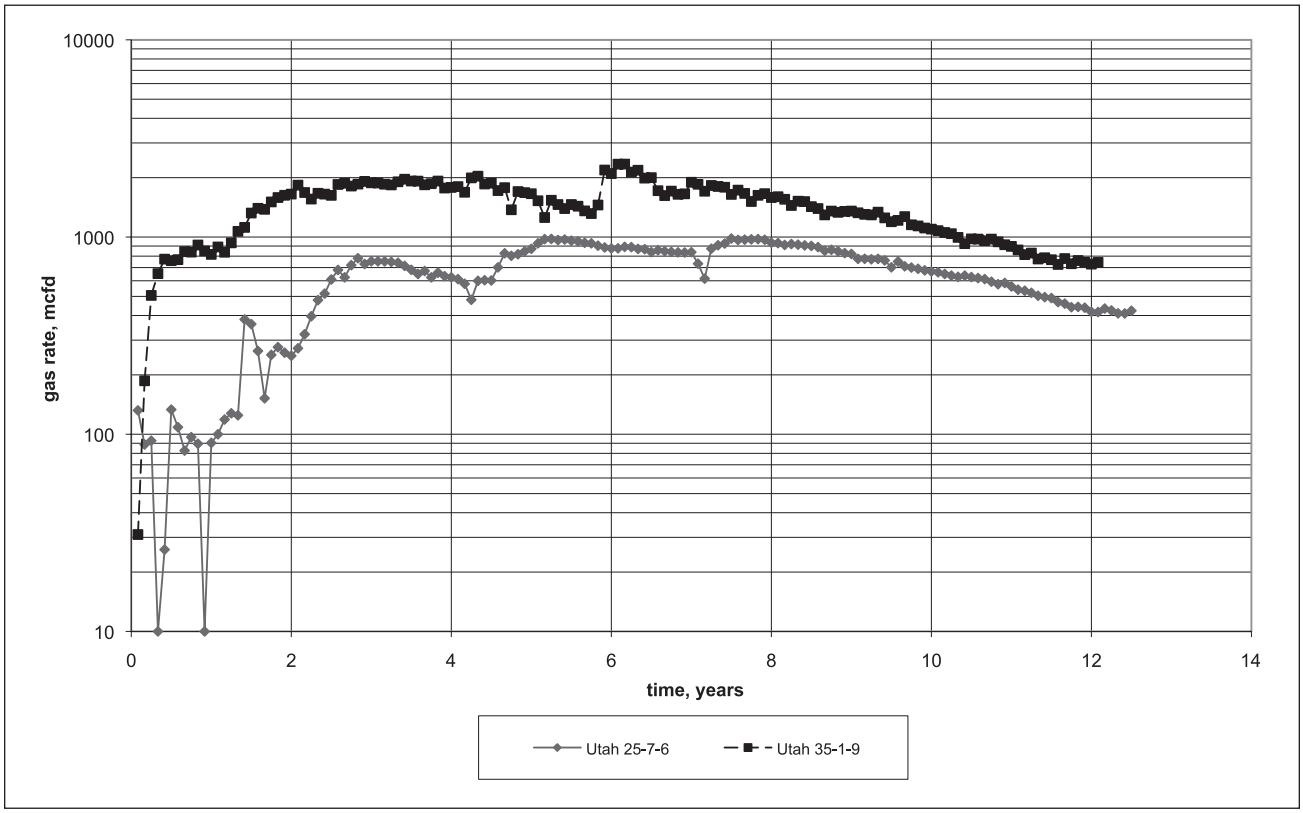



**Fig. 1–2.** Examples of slow negative decline—Uinta Basin, Ferron coal

Organic sediments subjected to pressure and temperature over geologic time slowly coalify, and as part of that process, copious amounts of gas are generated. Some of that gas escapes over geologic time, and some remains in the coal as free and sorbed gas. As sorption is a very efficient way to store gas, a unit reservoir volume of coal can hold several times more gas, sometimes an order of magnitude more gas, than a unit volume of sandstone at the same temperature and pressure. Consequently, determination of the gas resource in a coal deposit has required development of new technologies to quantify the sorbed gas volume. The most reliable technique is measurement of gas emitted by coal samples collected at the wellsite. Coals, like all unconventional hydrocarbon reservoirs, are often more heterogeneous than conventional reservoirs, compounding the difficulty of obtaining representative samples for testing.

Coals provide drilling breaks, seismic reflectors, and distinct markers on wireline logs, but definition of coal net pay is elusive. Net pay in a coal seam is generally determined from applying a bulk density cutoff to wireline logs, with occasional secondary cutoffs from gamma ray, acoustic, or resistivity logs when density logs are weak or inconclusive. Coal density cutoffs typically used in the mining industry are often too restrictive for coalbed methane reservoirs. Desorption tests routinely encounter significant gas volumes in coaly, organic rocks too dense to be considered mineable. Many early coal wells were still producing gas at economic rates after having produced all reserves assigned based upon the low density pay cutoffs employed in the mining industry. At the time of this writing, the coal gas industry standard coal pay cutoff is 2.0 g/cm$^3$.

Coal deposits hold a diffuse, continuous, and highly variable gas resource. Although hydrostatic pressure provides the seal to retain the gas in most coals, structure and stratigraphy still play significant roles in these reservoirs. Buoyancy forces can drive gas up dip, and interbedded or bounding sands can contribute gas and water flows. Productive limits of a coal deposit are often difficult to define, and gas in place calculations employ both clear geological limits, such as coal subcrops, and artificial limits, such as lease boundaries.

## Estimated Worldwide Coal Gas Resources

Coal deposits are widely and unevenly distributed over the earth. Worldwide coal reserves, listed by continent and rank in table 1–1, are primarily located in North America, Europe, and Asia. Both the volume of gas generated and sorption capacity per unit mass of coal increase with rank, making coal rank an important element of coal gas reservoir engineering. About one-half of global coal reserves are bituminous or anthracite, one-third are subbituminous, and one-sixth are lignites. Worldwide coal gas resources, listed by geographic area in table 1–2, are estimated to total more than 256 trillion cubic meters (9,051 tcf) and are located primarily in the former Soviet Union, North America, and the centrally planned economies in Asia and China. For comparison, worldwide proved natural gas reserves are 185 t m$^3$ (6,533 tcf).[1] Recovery of one-half the global coal gas resource would increase global natural gas reserves by 128 t m3 (4,520 tcf), a gain of about two-thirds. But current estimates of the global coal gas resource may be conservative for at least three reasons.

Coal deposits have historically been assessed from a mining perspective, and coal resource and reserve estimates reflect this view. Coal gas reservoir engineering developed out of safety concerns in gassy coal mines, and early estimates of coal gas resources reflected this bias. For instance, shallow coals with ash contents too high to be economically mined are rightly excluded from coal resource and reserve inventories. Consequently, they are neglected in coal gas resource estimates based upon these inventories. Similarly, coals buried too deeply to mine often hold large volumes of gas and can be commercially viable coal gas reservoirs. Focusing on an individual coal seam, the inorganic ash (or mineral matter) fraction varies vertically and horizontally throughout the seam, rendering portions unmineable. These unmineable portions of the seam, for instance, could include a basal boney coal, a shaley overburden, or an areally extensive lobe of ashy coal. Unmineable portions are correctly excluded from coal resource estimates yet can contain significant gas volumes, which should be included in coal gas resource estimates for this seam. The shallow, thick, high-purity coal deposits that are considered mineable are but a small fraction of the carbonaceous formations that may contain coal gas.

**Table 1–1.** World proved recoverable coal reserves—2005

| | Coal resources, m tonnes | | | | |
|---|---|---|---|---|---|
| **Region** | **Bituminous & anthracite** | **Subbituminous** | **Lignite** | **Total, m tonnes** | **Total, %** |
| Africa | 49,431 | 171 | 3 | 49,605 | 5.9% |
| N America | 116,592 | 101,440 | 32,661 | 250,693 | 29.6% |
| S America | 7,229 | 9,023 | 24 | 16,276 | 1.9% |
| Asia | 146,251 | 36,282 | 34,685 | 217,218 | 25.6% |
| Europe | 72,872 | 117,616 | 44,649 | 235,137 | 27.7% |
| Mid East | 1,386 | 0 | 0 | 1,386 | 0.2% |
| Oceania | 37,135 | 2,305 | 37,733 | 77,173 | 9.1% |
| World | 430,896 | 266,837 | 149,755 | 847,488 | 100.0% |

| | Coal resources by rank, % | | |
|---|---|---|---|
| **Region** | **Bituminous & anthracite** | **Subbituminous** | **Lignite** |
| Africa | 11.5% | 0.1% | 0.0% |
| N America | 27.1% | 38.0% | 21.8% |
| S America | 1.7% | 3.4% | 0.0% |
| Asia | 33.9% | 13.6% | 23.2% |
| Europe | 16.9% | 44.1% | 29.8% |
| Mid East | 0.3% | 0.0% | 0.0% |
| Oceania | 8.6% | 0.9% | 25.2% |
| World | 100.0% | 100.0% | 100.0% |

*Source*: World Energy Council. 2007. *2007 Survey of Energy Resources*. ser2007_final_online_version_1.pdf. Accessed November 30, 2008.

**Table 1–2.** World coal gas resources—2007

| **Region** | **Coal gas in place, tcf** | **Coal gas in place, t m$^3$** | **Coal gas in place,%** |
|---|---|---|---|
| North America | 3017 | 85.4 | 33.3% |
| Latin America | 39 | 1.1 | 0.4% |
| Western Europe | 157 | 4.4 | 1.7% |
| Central and Eastern Europe | 118 | 3.3 | 1.3% |
| Former Soviet Union | 3957 | 112.0 | 43.7% |
| Middle East and North Africa | 0 | 0.0 | 0.0% |
| Sub-Saharan Africa | 39 | 1.1 | 0.4% |
| Centrally planned Asia and China | 1215 | 34.4 | 13.4% |
| Pacific (OECD) | 470 | 13.3 | 5.2% |
| Other Asia Pacific | 0 | 0.0 | 0.0% |
| South Asia | 39 | 1.1 | 0.4% |
| World | 9051 | 256.1 | 100.0% |

Secondly, coals are more compressible than sandstones and limestones, and therefore, permeability of coals can decrease more rapidly with depth of burial in a given basin than that of conventional reservoirs. Early coal gas resource estimates were sometimes predicated upon a perceived depth cutoff. Subsequent developments in the Warrior and San Juan basins have demonstrated that productive coal wells, often the most productive wells in the basin, are completed in the deepest seams. Concerns about coal permeability loss with depth have given way to identification of geological controls on increased coal permeability, such as jointing, faulting, and tectonic fractures. It also has led to development of new completions, such as horizontal wellbores and improved stimulations. The gas resource potential of deep coals is not yet fully understood.

Lastly, precision of coal gas resource estimates varies inversely with occurrence of conventional oil and gas resources. In areas with significant conventional hydrocarbon resources, little incentive exists to characterize coal gas resources, which are inherently more difficult to define and more technically challenging to produce than conventional gas resources.

For these and other reasons, current estimates of the worldwide coal gas resource are conservative. Coals are an important source of clean burning gas in a world where carbon emissions are increasingly important. As coal deposits come to be assessed as natural gas reservoirs and technologies are developed to exploit that gas, estimates of the global coal gas resource will rise.

## Reservoir Properties of Selected Coals

Coals are heterogeneous reservoirs of highly variable architecture. Reservoir properties of selected coals are collected in table 1–3. Some coals are well characterized with commercial gas production (San Juan, Warrior, and Powder River), while others have not yet been fully assessed (Cook Inlet) and lack commercial production. Coals from all five geologic periods of coal deposition and all ranks have been studied as reservoirs. Reservoir settings include deep (3,000 m) and shallow (30 m) seams, and single and multiple (30+) seams. The deepest known commercial coal gas production at this time is from 2,180 m in the Cameo coals of the White River Dome Field in the Piceance Basin. The shallowest known commercial production is from 30 m deep seams in the Powder River Basin.

Inspection of table 1–3 shows gas content of these coals varies by two orders of magnitude, from 0.2 to 36 g/cm$^3$. Equally important is actual coalbed gas content relative to the theoretical maximum gas content the coal could hold at current reservoir temperature and pressure. A coal is said to be *undersaturated* when it holds less gas than its theoretical capacity at current reservoir temperature and pressure. Visualizing sorption capacity of a coal seam as similar to the gasoline tank of an automobile and the coalbed gas content as the amount of gasoline in the tank, a coal holding the theoretical maximum amount of sorbed gas is said to be *fully saturated* and is analogous to a full gasoline tank. A coal sorbing only two-thirds the maximum amount it could hold at current reservoir conditions is described as undersaturated and corresponds to a gasoline tank only two-thirds full. Some of the coals listed in table 1–3 are fully saturated (San Juan Basin, Fruitland coal), while some are modestly undersaturated (Warrior Basin, Marylee coal—93% saturation) and some are deeply undersaturated (Upper Silesian Basin, 405 coal—67% saturation, Qinshui Basin, #3 seam—56% saturation).

Coal permeability varies by four orders of magnitude, ranging from less than 0.1 md to more than 1,000 md. The well-developed, throughgoing, extensive, nearly parallel face cleats and the less-well-developed, limited, slimmer butt cleats provide an asymmetric fracture network in a coal, which intuitively suggests permeability anisotropy. However, field tests show permeability contrasts of perhaps two, and well patterns are typically controlled by aboveground issues, such as topography and culture, rather than permeability anisotropy.

Coal well gas production profiles reflect the interplay between dewatering and depressuring of the coal. Coals are often aquifers and require dewatering to attain peak gas production rate before declining. Timing and magnitude of peak gas production and the nature of the subsequent decline vary considerably among coal deposits. Coals with no moveable water, often referred to as *dry coals*, are rare, comprising perhaps 10% of all coal plays. Gas rates of wells completed in such coals steadily decline, similar to conventional gas wells. Coal well gas production profiles vary from basin to basin, from seam to seam within a basin, and from area to area within a seam. They also vary by completion. The type curves collected in figures 1–3 to 1–10 are not comprehensive of all coal wells but rather illustrative of the wide variety of such profiles.

Coal deposits are a class of heterogeneous gas reservoirs. Differences in geologic age, depositional environment, thermal maturity, geologic history, and various other controls result in a wide spectrum of coalbed gas contents and permeabilities. Coal gas reservoir engineering would be simpler if general rules existed, such as “All Jurassic coals support commercial gas production” or “Anthracitic coals never support commercial gas production.” In reality, the presence and producibility of coal gas can be neither guaranteed nor excluded with screens based upon one or more of the coal reservoir properties discussed here. These parameters are, however, rough indicators of the nature of gas production that might be expected from a coal, making analogs useful in understanding coal reservoir performance.

**Table 1–3.** Reservoir properties of selected coals

| Seq no. | Basin/area | Coal | Age | Rank | Depth, m | No. of seams | Net coal, m | In-situ gas content, $cm^3/g$ | Perm, md |
|---|---|---|---|---|---|---|---|---|---|
| 1[a] | Sydney | Bulli | Carboniferous–Permian | hi-vol.–lo-vol. | 698 | 1 | na | 20.8 | na |
| 2[b] | Surat | Walloon | Jurassic | subbit. | 150–950 | 11 | na | 3.14 | 500 |
| 3[c] | Qinshui | #3, #15 | Carboniferous–Permian | hi-vol. A–metaanth | 0–2,500 | 7–17 | 0–16 | 0–36 | 0.1–4 |
| 4[d] | Cook Inlet/ Susitna | Sterling, Beluga, Tyonek, Chickaloon | Paleocene–Miocene | lig.–anth. | 0–1,830 | 30 | 0–206 | 1.1–17 | na |
| 5[e] | San Juan | Fruitland | Cretaceous | subbit.–lo-vol. | 0–1,300 | 5? | 0–21 | na | 0.1–60 |
| 6[f] | Piceance | Cameo | Cretaceous | hi-vol. B–semianth. | 0–3,050 | 7 | 18 | 13–23 | 0.2 |
| 7[g] | WCSB | Mannville | L. Cretaceous | subbit.–lo-vol. | 1,500 | 3 | 2–12 | 7–13 | 0.1– 3 |
| 8[h] | Uinta | Ferron | U. Cretaceous | hi-vol. C–B | 370–1,040 | 6 | 1–14 | 3–17 | 5–20 |
| 9[i] | WCSB | Horseshoe Canyon | U. Cretaceous | subbit. C–A | 200–600 | 10–30 | 2–30 | 0.9–3.8 | 1–5? |
| 10[j] | Powder River | Fort Union | Paleocene | subbit. C–B | 90–610 | 2–24 | 91 | 2.2 | 10–1,000 |
| 11[k] | Arkoma | Hartshorne | Pennsylvanian | hi-vol. A–semianth | 85–1,340 | 3 | 0.2–2 | 2.2–18 | 20–45 |
| 12[l] | Scotland | na | Carboniferous | hi-vol. C–A | 500–880 | 10–30 | 10–24 | 0.2–6.3 | na |
| 13[m] | England, Northern | na | Carboniferous | hi-vol. C–lo-vol. | 710–875 | 20–30 | 12–15 | 3.2–7.5 | na |
| 14[n] | England, Central | E. Pennine | Carboniferous | hi-vol. C–A | 430–1,230 | 25–32 | 9.1–18 | 1.5–5.9 | na |
| 15[o] | England, Central | W. Pennine | Carboniferous | hi-vol. A–med. vol | 470–1,100 | 10–22 | 7.3–20 | 0.5–7.1 | na |
| 16[p] | England, Southern | multiple | Carboniferous | med.-vol.–anth. | 700–760 | 10–20 | 6.1–18 | 0.4–13 | na |
| 17[q] | Greater Green River | multiple | Cretaceous– Tertiary | subbit.– hi-vol. C | 990–1,360 | 12+ | 24 | 1.5–6.9 | 12.5 |
| 18[r] | Warrior | multiple | Pennsylvanian | hi-vol. A–lo-vol. | 60–760 | 29 | 13 | 1.6–17 | 75 |
| 19[s] | Silesian Basin | multiple | Carboniferous | hi-vol. B–lo-vol. | 250–1,750 | 5+ | 9.0 | 4–9 | 1–2 |
| 20[t] | Raton | Vermejo | Cretaceous– Paleocene | hi-vol. B–A | 75–360 | 11–20 | 23.0 | 0.8–15 | na |

*Sources:* [a]Wang, I., Choudhury, J., Barker, W., and McNally, S. 2005. Developing Coal Seam Methane in the Sydney Basin. Paper 0534 in *Proceedings of the 2005 International Coalbed Methane Symposium*. Tuscaloosa: University of Alabama. [b]Scott, S., Anderson, B., Crosdale, P., Dingwall, J., and Leblang, G. 2004. Revised geology and coal seam gas characteristics of the Walloon Subgroup—Surat Basin, Queensland. PESA Eastern Australasian Basins Symposium II. Adelaide, September 19–22. [c]Su, X., Lin, X., Zhao, M., Song, Y., and Liu, S. 2005. The upper Paleozoic coalbed methane system in the Qinshui basin, China. *AAPG Bulletin*. V. 89 (no. 1). p. 81. [d]Montgomery, S. L., Barker, C. E., Seamount, D., Dallegge, T. A., and Swenson, R. F. 2003. Coalbed methane, Cook Inlet, south-central Alaska: A potential giant gas resource. *AAPG Bulletin*. V. 87 (no. 1). p. 1. [e]Rightmire, C. T., Eddy, G. E., and Kirr, J. N. 1984. *Coalbed Methane Resources of the United States*. AAPG Studies in Geology Series #17. Tulsa: American Association of Petroleum Geologists; Scott, A. R., Kaiser, W. R., and Ayers, W. B. 1994. Thermogenic and secondary biogenic gases, San Juan Basin, Colorado and New Mexico—Implications for coalbed gas producibility. *AAPG Bulletin*. V. 78 (no. 8). p. 1,186; and Ayers, W. B., Jr. 2002. Coalbed gas systems, resources, and production and a review of contrasting cases from the San Juan and Powder River basins. *AAPG Bulletin*. V. 86 (no. 11). p. 1,853. [f]Rightmire, C. T., Eddy, G. E., and Kirr, J. N. 1984; McFall, K. S., Wicks, D. E., Kelso, B. S., and Brandenburg, C. F. 1988. An analysis of the coal-seam gas resource of the Piceance Basin, Colorado. *Journal of Petroleum Technology*. V. 40 (no. 6). p. 740; and Olson, T. M. 2003. White River Dome Field: Gas production from deep coals and sandstones of the Cretaceous Williams Fork Formation. In *Piceance Basin 2003 Guidebook*. Peterson, Olson, and Anderson, eds. Denver: Rocky Mountain Association of Geologists. [g]Beaton, A. 2003. [h]Montgomery, S. L., Tabet, D. E., and Barker, C. E. 2001. Upper Cretaceous Ferron Sandstone: Major coalbed methane play in central Utah. *AAPG Bulletin*. V. 85 (no. 2). p. 199; Lamarre, R. A., and Burns, T. D. 1997. Drunkard's Wash Unit: Coalbed methane production from Ferron coals in East-Central Utah. p. 47. *Innovative Applications of Petroleum Technology Guidebook—1997*. Denver: Rocky Mountain Association of Geologists; Lamarre, R. A., and Pratt, T. J. 2002. Reservoir characterization study: Calculation of gas-in-place in Ferron coals at Drunkard's Wash Unit, Carbon and Emery counties, Utah. *The Mountain Geologist*. V. 39 (no. 2). p. 41; and Burns, T. D., and Lamarre, R. A. 1997. Drunkard's Wash Project: Coalbed methane production from Ferron coals in East-Central Utah. Paper 9709 in *Proceedings of the 1997 International Coalbed Methane Symposium*. Tuscaloosa: University of Alabama. [i]Bastian, P. A., et al. 2005; and Beaton, A. 2003. [j]Ayers, W. B., Jr. 2002. [k]Rightmire, C. T., Eddy, G. E., and Kirr, J. N. 1984; Cardott, B. J. 2004. *Coalbed-Methane Activity in Oklahoma, 2004 Update*. Presented at the Unconventional Energy Resources in the Southern Midcontinent Conference. Oklahoma Geological Survey. Oklahoma City, Oklahoma, March 10; and Mutalik, P. N., and Magness, W. D. 2006. *Production Data Analysis of Horizontal CBM Wells in Arkoma Basin*. SPE 103206. Presented at the SPE Annual Technical Conference and Exhibition. San Antonio, Texas, September 24–27. [l]Ayers, W. B., Jr., Tisdale, R. M., Litzinger, L. A, and Steidl, P. F. 1993. Coalbed methane potential of Carboniferous strata in Great Britain. Paper 9301 in *Proceedings of the 1993 International Coalbed Methane Symposium*. Tuscaloosa: University of Alabama; and Creedy, D. P. 1991. An introduction to geological aspects of methane occurrence and control in British deep coal mines. *Quarterly Journal of Engineering Geology & Hydrogeology*. V. 24 (no. 2). p. 209. [m]Ibid. [n]Ibid. [o]Ibid. [p]Ibid. [q]Young, G. B. C., McElhiney, J. E., Dhir, R., Mavor, M. J., and Anbouba, I. K. A. 1991. *Coalbed Methane Production Potential of the Rock Springs Formation, Great Divide Basin, Sweetwater County, Wyoming*. Paper SPE 21487. Presented at the SPE Gas Technology Symposium. Houston, Texas, January 23–25; and Rightmire, C. T., Eddy, G. E., and Kirr, J. N. 1984. [r]Ancell, K. L., Lambert, S., and Johnson, F. S. 1980. *Analysis of the Coalbed Degasification Process at a Seventeen Well Pattern in the Warrior Basin of Alabama*. Paper SPE 8971. Presented at the SPE/DOE Unconventional Gas Recovery Symposium. Pittsburgh, Pennsylvania, May 18–22; and Rightmire, C. T., Eddy, G. E., and Kirr, J. N. 1984. [s]McCants, C. Y., Spafford, S., and Stevens, S. H. 2001. [t]Rightmire, C. T., Eddy, G. E., and Kirr, J. N. 1984.

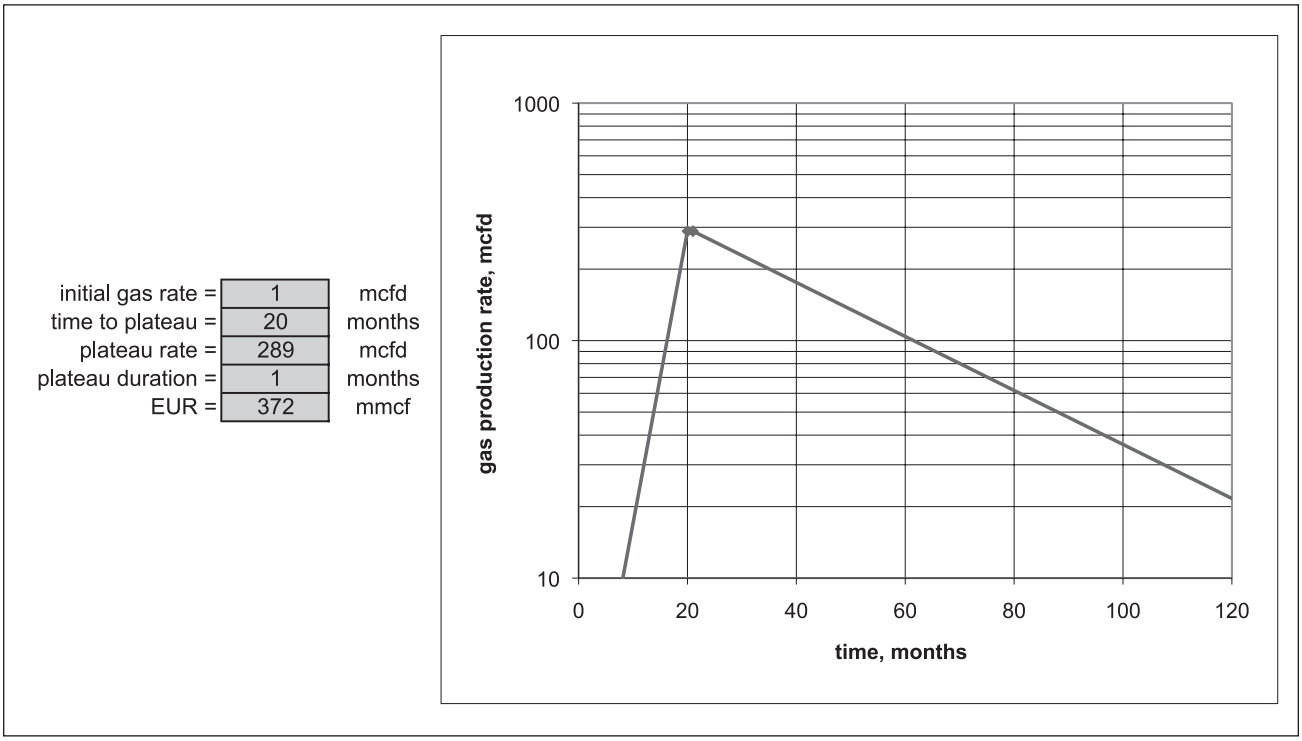



**Fig. 1–3.** Warrior Basin Cedar Cove type curve[2]

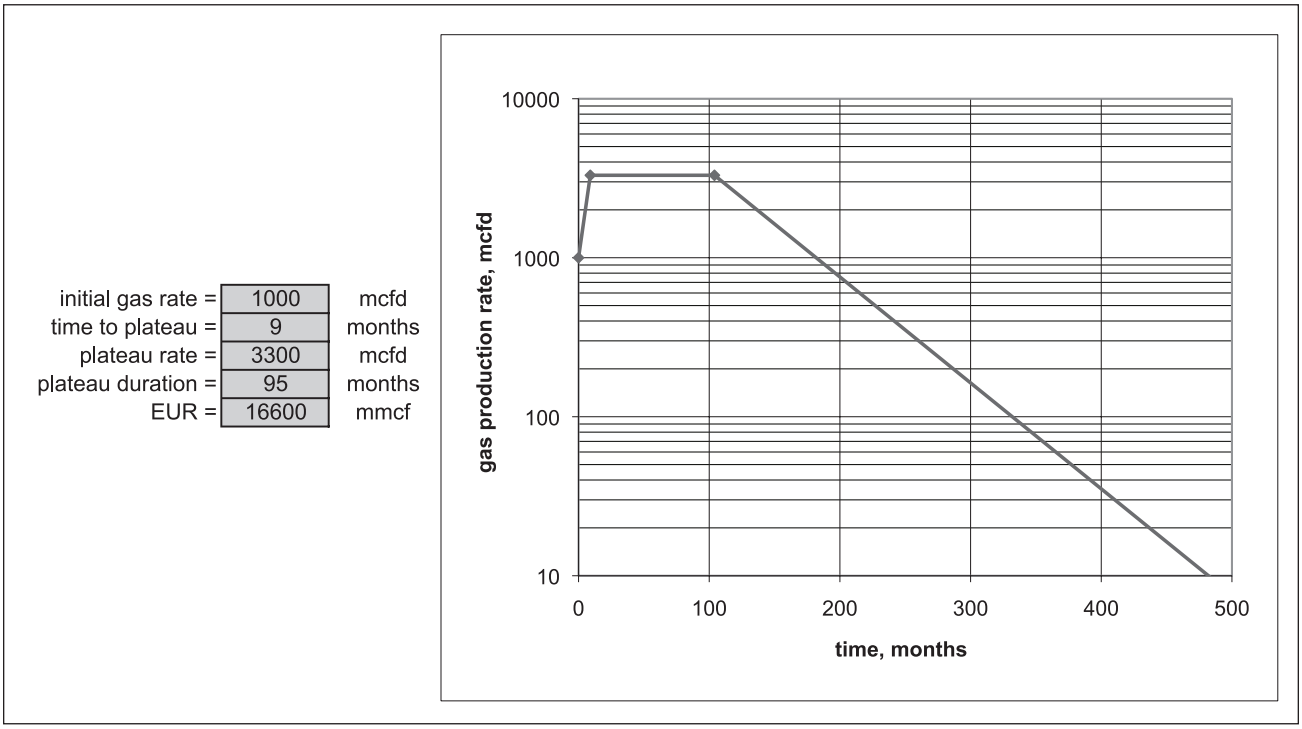



**Fig. 1–4.** San Juan Basin fairway (T30N R6W) type curve[3]

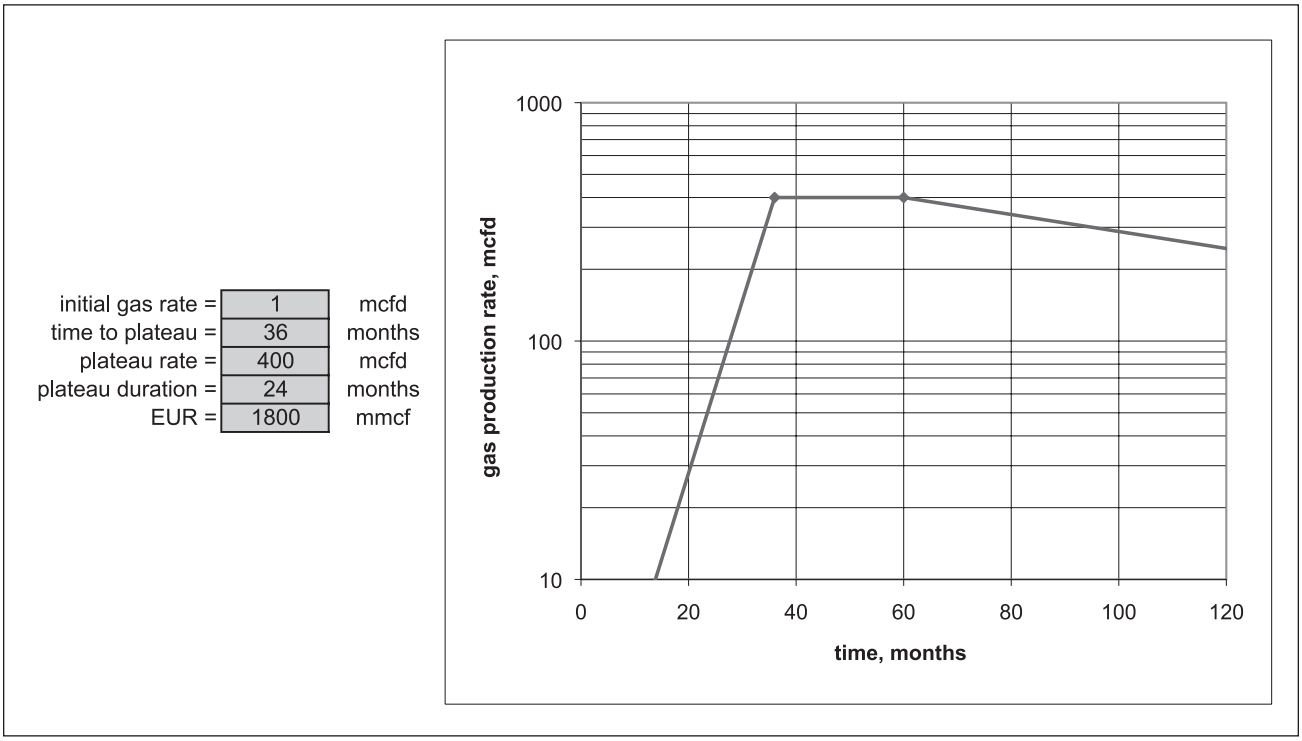



**Fig. 1–5.** Raton Basin Vermejo coal type curve[4]

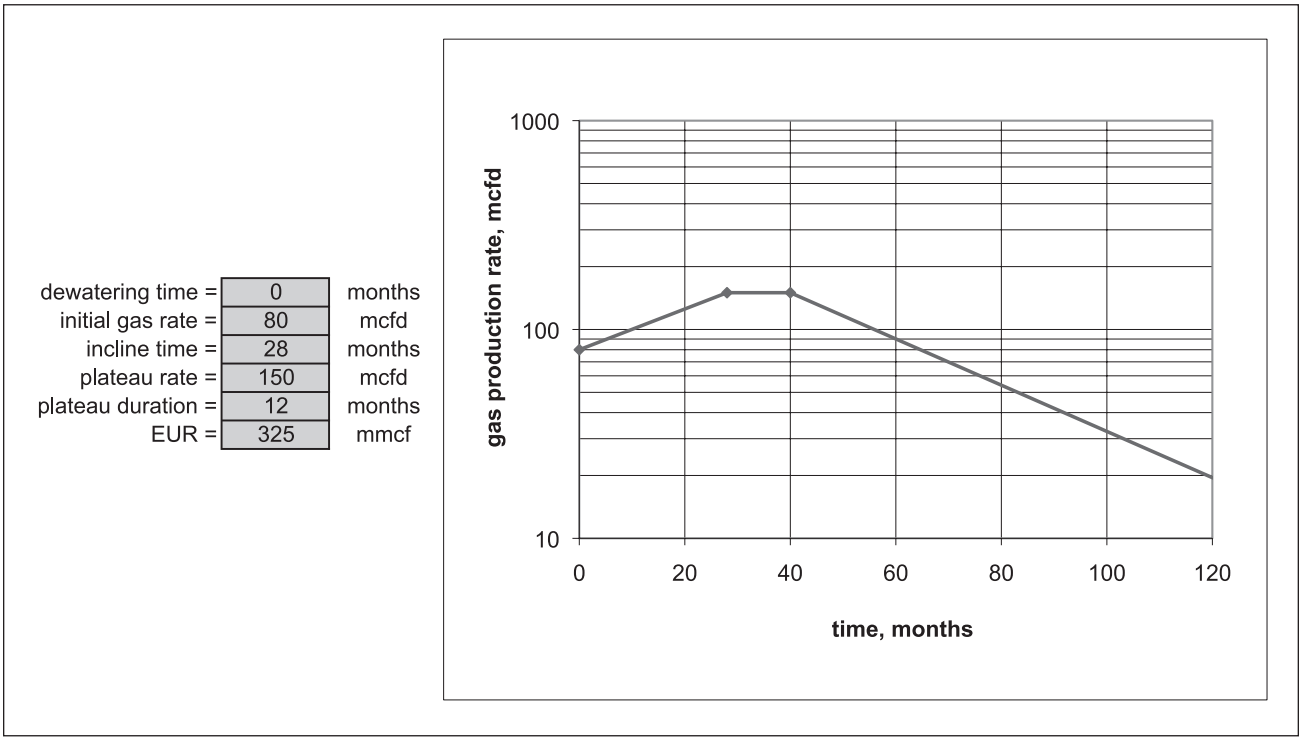



**Fig. 1–6.** Powder River Basin Wyodak coal type curve[5]

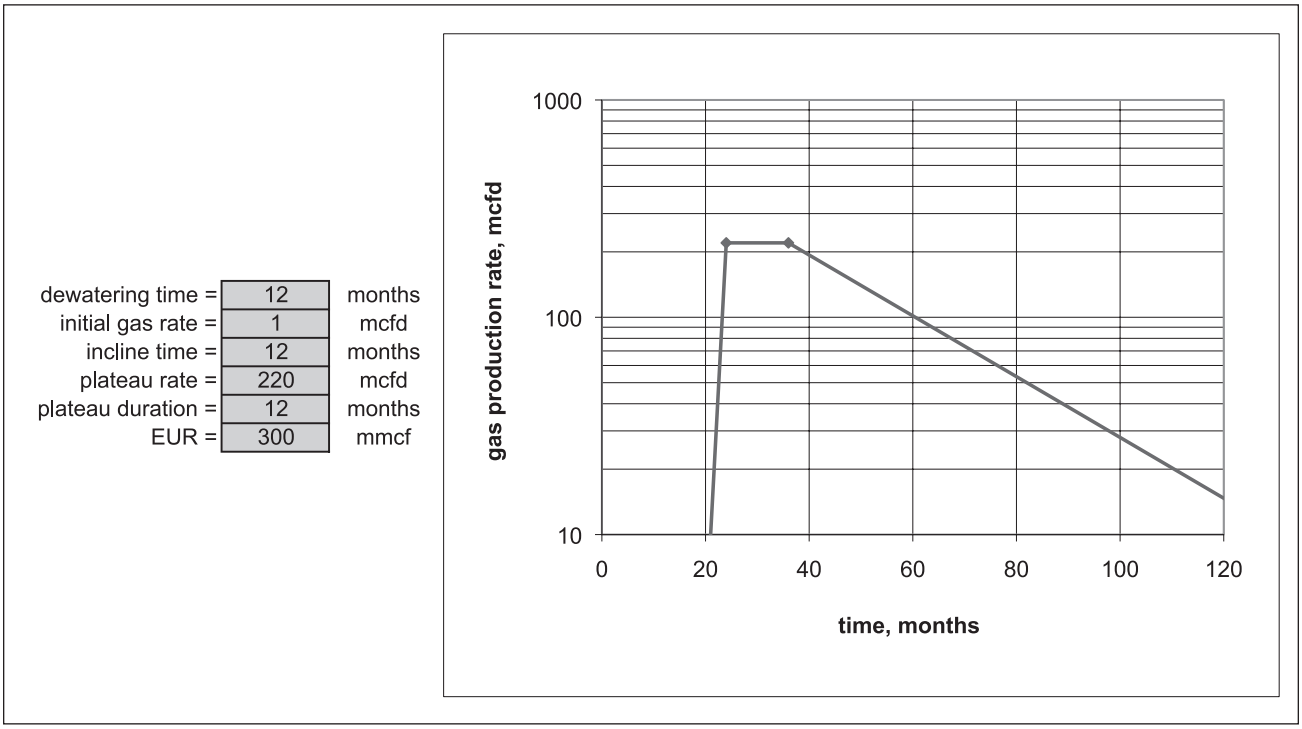



**Fig. 1–7.** Powder River Basin Big George coal type curve[6]

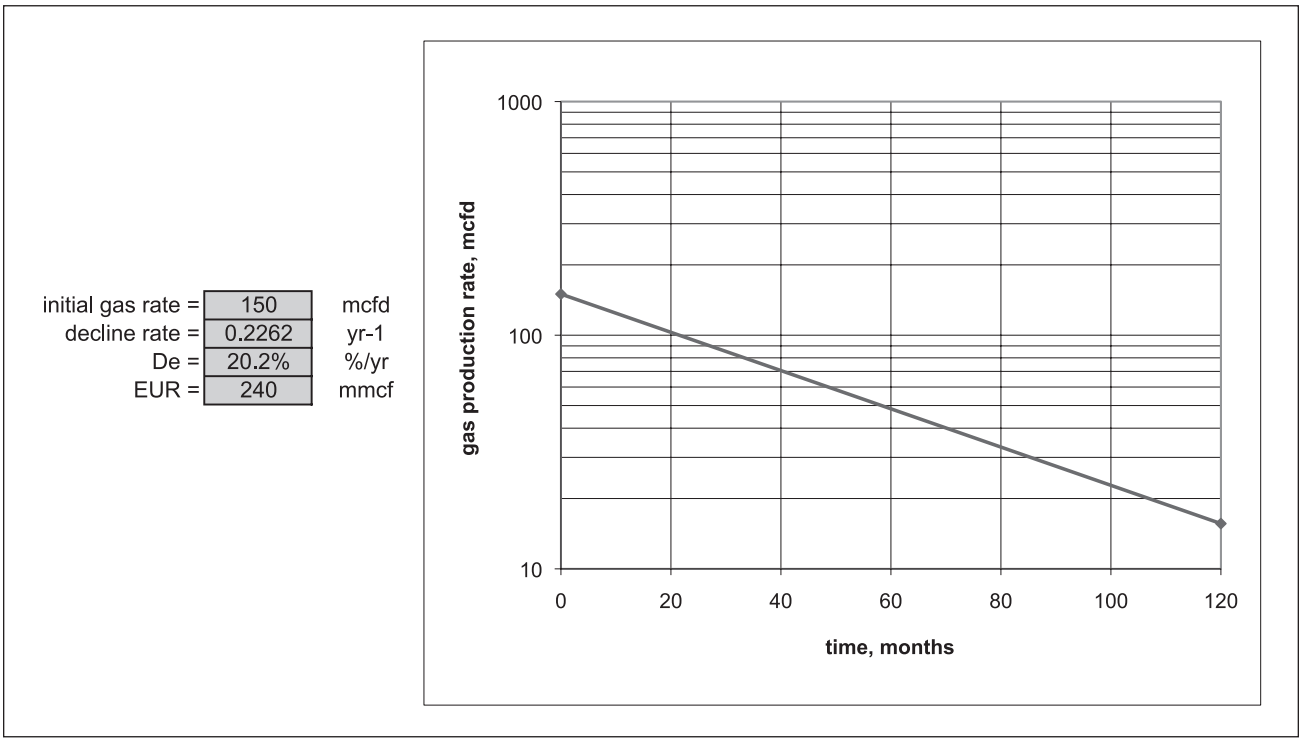



**Fig. 1–8.** Horseshoe Canyon coal type curve[7]

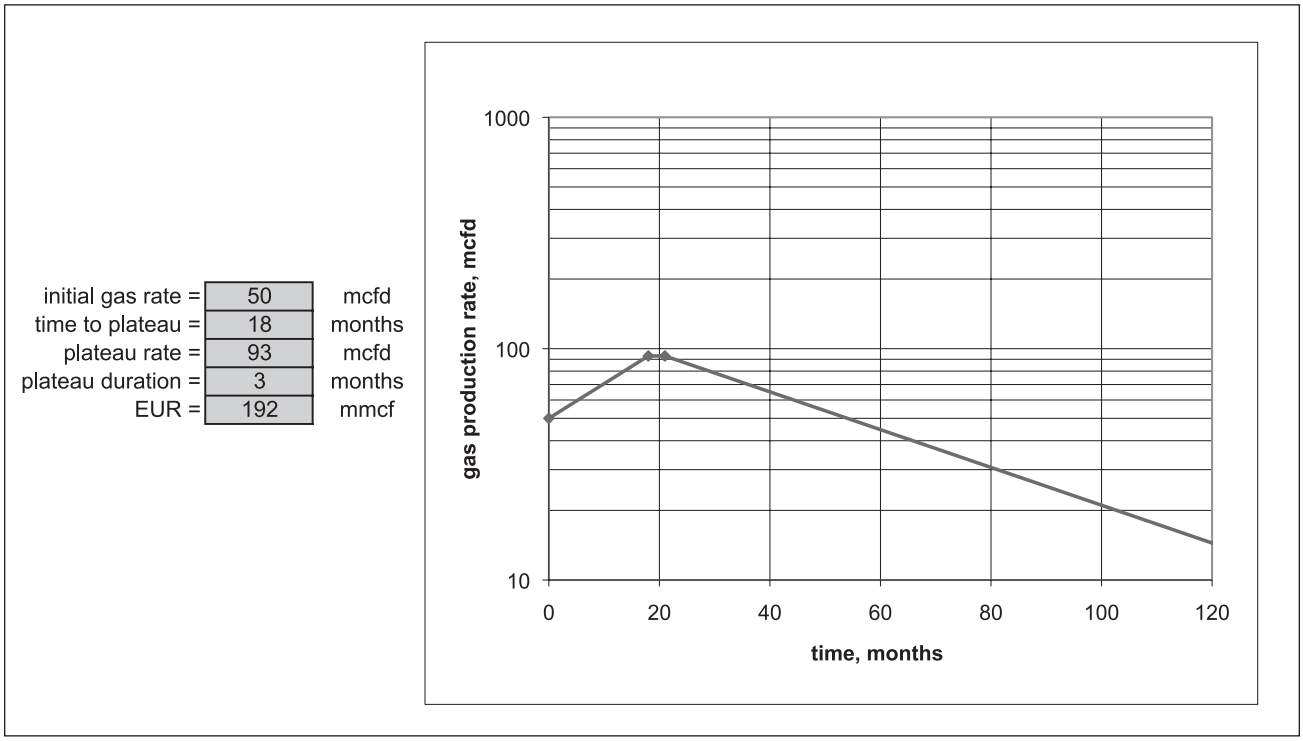



**Fig. 1–9.** Cherokee Basin type curve[8]

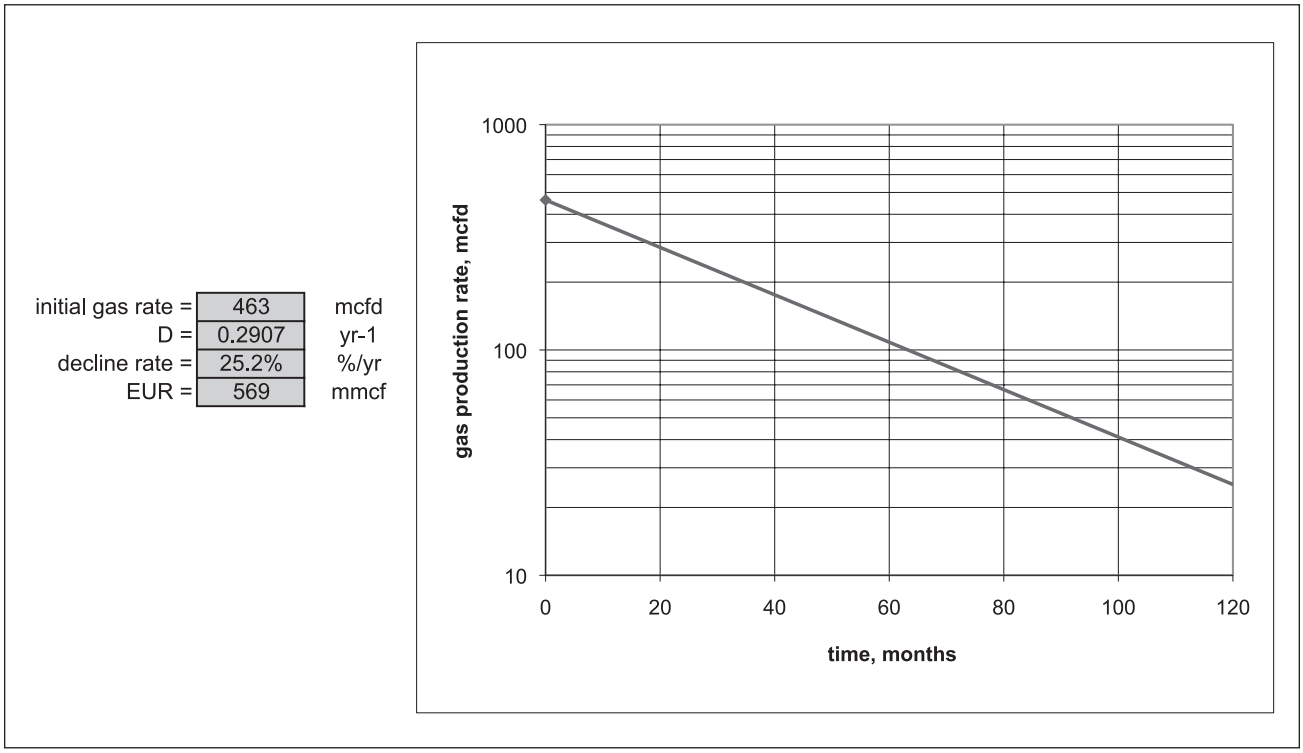



**Fig. 1–10.** Arkoma Basin horizontal well type curve (Oklahoma, T8N, R15,18, & 19E)

## Construction of Coal Gas Analogs

Analogs are often employed to better understand coal gas plays, similar to conventional hydrocarbon plays. Analogs are especially useful in the exploration and early development phases of a project when reservoir properties are incompletely known at best. Five important elements in constructing coal gas analogs are geological age, rank, permeability, gas content, and gas saturation.

Most coals were laid down in five geologic periods: the Carboniferous, Permian, Jurassic, Cretaceous, and Tertiary (sometimes divided into Neogene and Paleogene periods). Thermal maturity of coal is divided into 13 principal ranks, beginning with peat and maturing through lignite, subbituminous C, B, and A, then high-volatile C, B, and A bituminous, followed by medium-volatile and low-volatile bituminous, and lastly semianthracite, anthracite, and metaanthracite. Coalbed permeabilities range across four orders of magnitude, from 0.1 md to 1,000 md. Considering permeability on a log cycle basis, the total number of analogs based upon geologic age, rank, and permeability multiplies out to 260 possible combinations, of which only a fraction actually exist.

Gas and water production rates from a well depend on overall flow capacity of the coal volume drained by the well. Coal permeability is determined from well tests or performance analyses, which typically probe a limited fraction of that drainage volume. Overall flow capacity of a permeable coal compartmentalized by numerous leaky and sealing faults may be less than that of a low-permeability, open, unfaulted seam. Well productivity also depends on completion efficiency. Thus, permeability analogs may or may not be production rate analogs.

Gas content of a coal deposit depends on coal rank and geologic history. Gas is generated as coal matures (*thermogenic gas*) and by microbial activity (*biogenic gas*). The amount of gas generated by a coal often exceeds its sorption capacity, forcing gas to migrate out of the fully gas charged seam. Gas also migrates out of coals in response to depressurization due to uplift and erosion and, rarely, migrates into a coal that is not fully gas saturated. Ash and mineral matter reduce the sorption capacity of a coal and often vary widely across a given coal deposit. Thus, analogs based on pure coal bases (dry, ash-free or dry, mineral-matter-free) are stronger and more reliable.

A fourth important parameter for analogs is undersaturation. As discussed above, a coal is said to be undersaturated when it holds less gas than it theoretically could at current reservoir temperature and pressure. Definition of an analog by simply stating the degree of undersaturation is less than complete, as performance of a well completed in an undersaturated coal also depends on the shape of the sorption isotherm and the relative position of the initial gas content point. Figure 1–11 depicts a methane sorption isotherm from Arri et al. and a hypothetical initial gas content of 593 scf/ton at an original reservoir pressure of 1,600 psia.[9] Comparing the actual gas content with that from the isotherm, the maximum gas content at this pressure is 741 scf/ton, and the coal is 1 – 593/741 = 0.2, or 20% undersaturated. For gas to be released from the matrix, reservoir pressure must be decreased to 680 psia, a reduction of almost 1,000 psia. In contrast, figure 1–12 shows the same sorption isotherm and a hypothetical initial gas content of 329 scf/ton at an original reservoir pressure of 300 psia. As the coal could hold up to 412 scf/ton at this pressure, this coal is 1 – 329/412 = 0.2, or 20% undersaturated. Desorption pressure for this seam is 206 psia, and the pressure drop required for gas to desorb is less than 100 psia. The degree of undersaturation is the same in both examples, 20%, but the pressure drops required for gas desorption differ by an order of magnitude. Undersaturation analogs are more persuasive when both coals possess the same degree of undersaturation and their measured gas contents have the same relative positions to their respective isotherms.

Depending on the purpose for which an analog is being sought, other important parameters may be considered. These could include the microscopic character of a coal, such as ash content, cleating, and maceral composition, or the macroscopic character, including depositional environment and depth, thickness, and structure of the seams. Drilling, completions, and stimulations exert an influence on coal gas and water production behaviors equal to those of reservoir properties and architecture. Analogs that reflect such differences in wellbore conditions are stronger than those that do not.

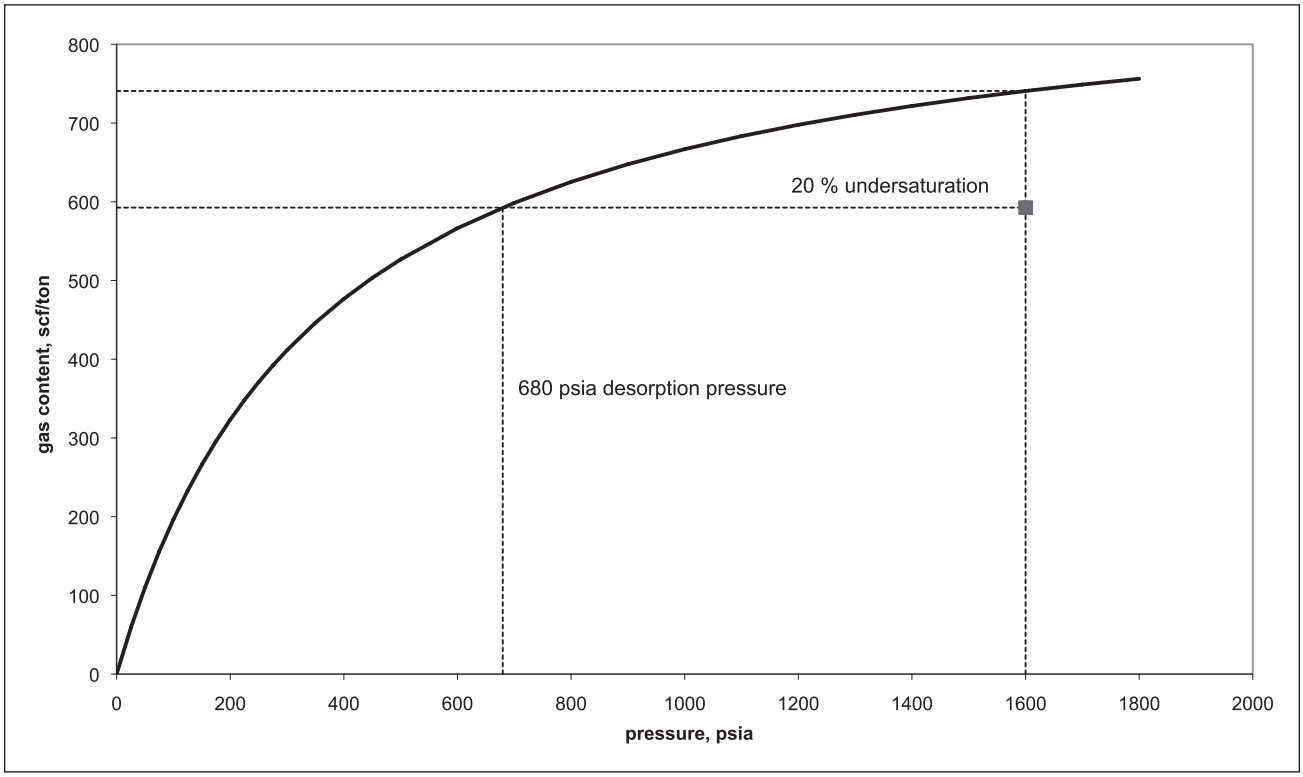



**Fig. 1–11.** Undersaturation on isotherm plateau—daf basis

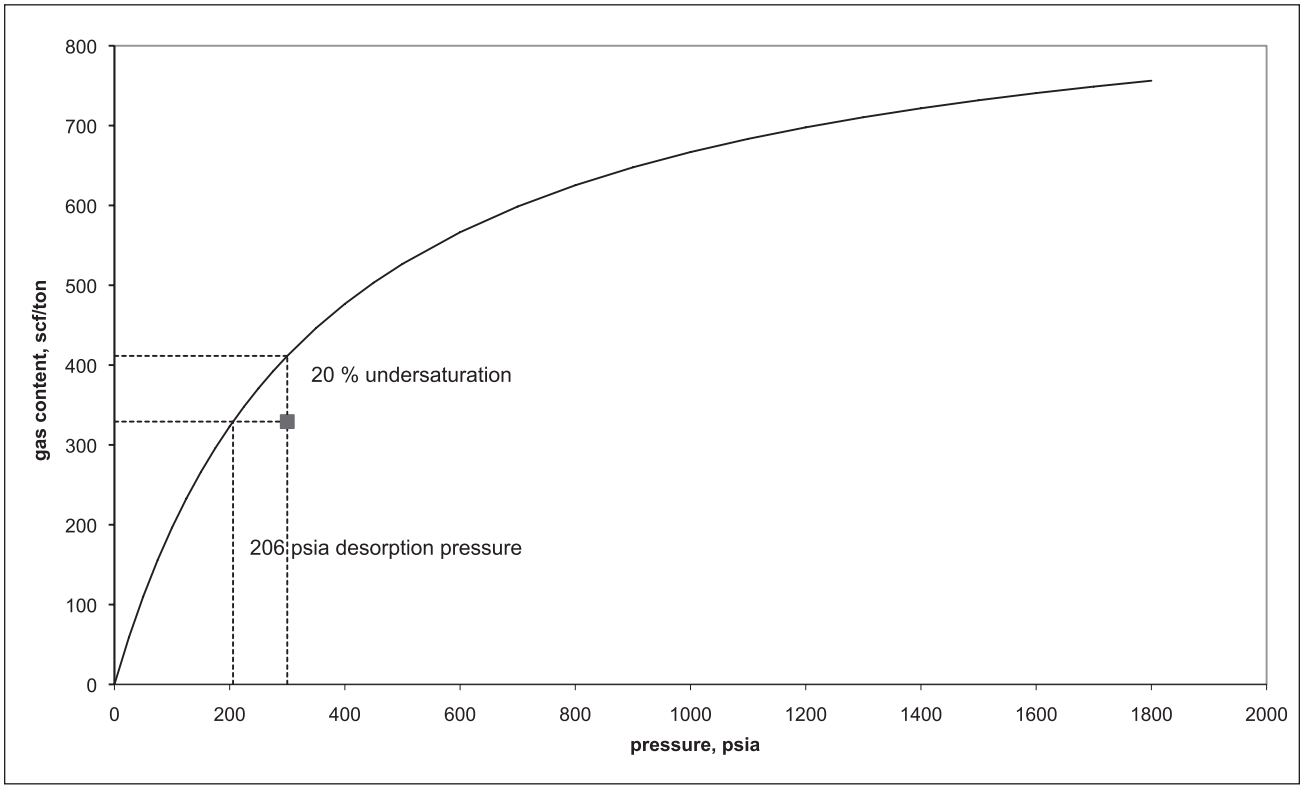



**Fig. 1–12.** Undersaturation on isotherm knee—daf basis

## Coal Gas Pilots

Production tests of single coal wells are often inconclusive. Most coals are aquifers, and an isolated well will initially produce substantial water volumes. If the coal deposit is not deeply undersaturated, water production will soon reduce reservoir pressure in the near-wellbore region to desorption pressure, liberating gas. Gas production from the well rises to a modest peak and then begins to fall as growth of the cone of depression from the lone well producing from an essentially infinite reservoir slows with time. With continued production, the cone of depression around the well grows ever more slowly, steadily decreasing gas release from the coal matrix and gas saturation in the coal cleats. Gas production from the single well continuously declines and perhaps ceases completely as the cone of depression essentially stabilizes. Eventually the well returns to nearly gas-free water production. This behavior has led to condemnation of coal plays later proven to be commercial. As an example, consider figure 1–13, which shows simulated gas and water production from a single well completed in an infinite coal seam. Inspection of figure 1–13 shows high, nearly constant water rates of 2,000 bpd, and gas rates less than 60 mcfd throughout the simulation, which utilized reservoir properties from the San Juan Basin fairway.[10] In reality, groups of fairway coal wells have seen sustained production rates of more than 1 mmcfd once the coal was dewatered.

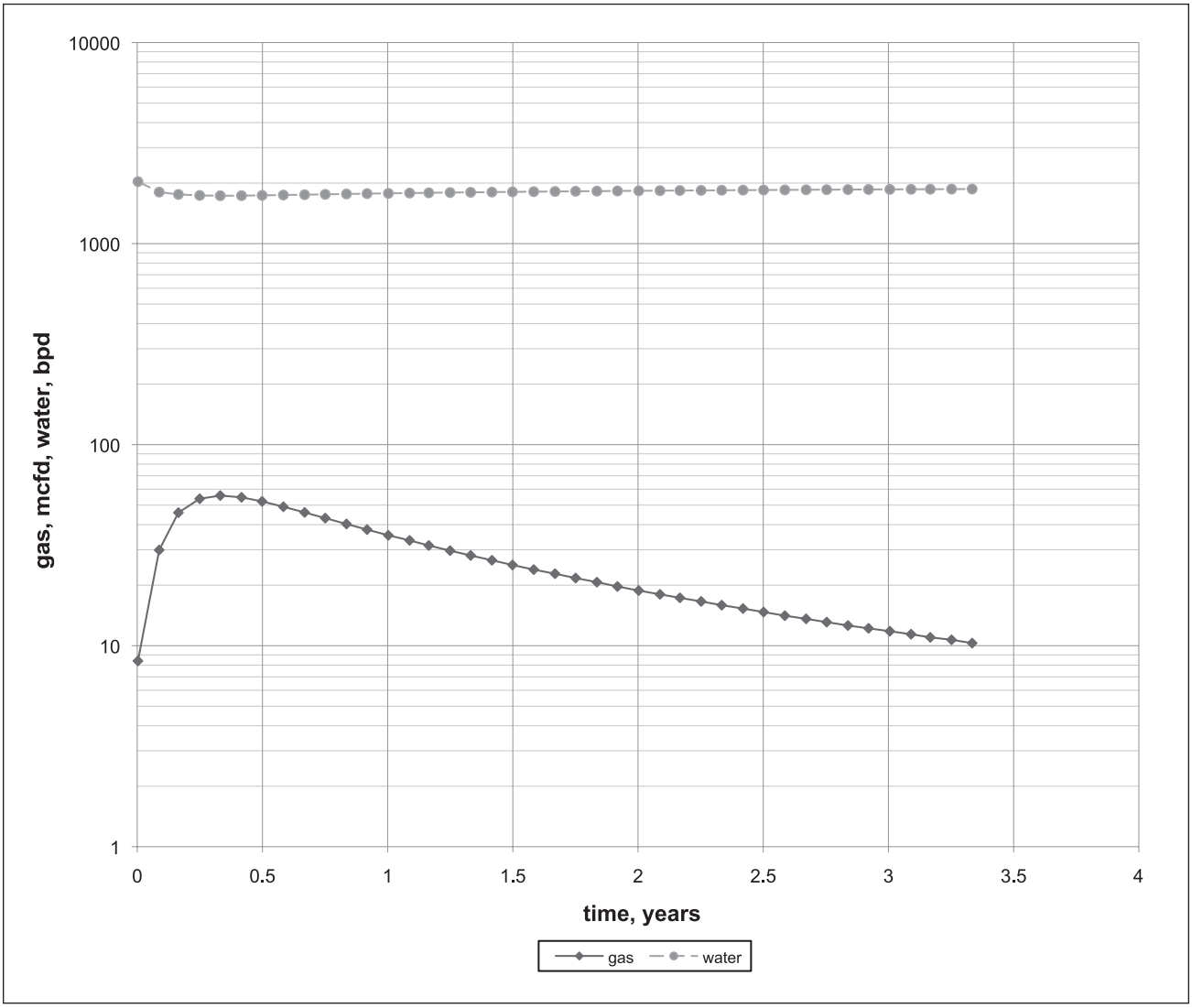



**Fig. 1–13.** Simulated single-well, infinite coal production test

Production testing of a group of closely spaced wells dewaters the interior of the pattern, providing a glimpse of the full cycle depletion behavior, which cannot be obtained from a single well test. Historically, multiwell coal pilots have employed a center well surrounded by four offset producers, dewatering the coal in unison. As with a single well production test, a multiwell coal pilot will initially produce only water until reservoir pressure in the pattern area drops to desorption pressure. In contrast to a single well test, continued pilot operation steadily liberates gas from the interior of the pattern as the offset producers shield the center well from water influx, allowing it to dewater and exhibit the negative decline that would be expected of development wells. To accelerate evaluation of a prospect, well spacing in coal pilots is often less than development spacing.

Coal pilots are expensive. Nonetheless, enforcement of rigid cost controls should be challenged by constant questions of whether the project can afford not to take a given sample or perform a proposed test. It should be remembered that coal gas pilots are designed to understand depletion performance of a given prospect, not achieve commercial gas production. Coal gas pilots are often technical successes and economic failures. Successful pilots are those that provide sufficient insight for a management decision either to proceed with full field development or to abandon the prospect.

Successful coal pilots often require several years of operation and acquisition of substantial reservoir and well data. A review of selected U. S. coal gas pilots revealed successful pilots often require three to four years of operation.[11] This same study found all successful pilots considered four elements to be essential for pilot interpretation: desorption tests, wireline logs, sorption isotherms, and pressure transient tests. Desorption of coal cores or drill cuttings provided coalbed gas contents and, hence, gas in place volumes. Wireline logs determined coal seam depth, thickness, and reservoir architecture. While a variety of wireline logs can be run in coal wells, the three common to all pilots were density, gamma ray, and caliper logs. Sorption isotherms related coalbed gas content to reservoir pressure, and when coupled with desorption and abandonment pressures, described initial matrix gas saturation and eventual coal gas recovery. Coal permeability and wellbore condition (skin) were obtained from pressure transient tests such as drawdown, buildup, or falloff tests, with the latter two also providing reservoir pressures. Early coal pilots often coincided with and promoted development of these four technologies; consequently, many of these pilots appear quite primitive by current standards. Development of coal reservoir simulators also coincided with many of the early pilots, which provided data for their validation. Current practice is to employ coal pilot performance and available geologic data to calibrate numerical simulation models, which are then used to investigate various development scenarios.

An example of the comprehensive data collection necessary for coal pilot interpretation is the five-well pilot test of coals in the Silesian Basin of Poland described by McCants et al.[12] Coalbed methane targets in this structurally complex basin are multiple thin Carboniferous seams. A total of 101 desorption samples provided an understanding of gas content variation with depth and identified the most prospective seams. Free gas composition, determined from 21 samples, was predominantly methane, with about 3% each of ethane and $CO_2$ present in the free gas. Coal seam permeabilities and pressures were determined from a series of 25 openhole injection/falloff tests. The nine methane sorption isotherms measured for these coals showed considerable variation, typical for multiple coal seams, and when combined with desorption test results, identified a zone of near saturation. This zone was then pilot tested for a period of six months. The five-well pilot utilized 20 ac spacing, and the wells, completed in 9 m (30 ft) of net coal from 1,100 to 1,400 m (3,600 to 4,600 ft), were all hydraulically fractured with cross-linked gel and sand. Total evaluation time was two years, much quicker than the historical average of three to four years reported by Seidle.[13]

Roadifer and Moore segmented assessment of a coal gas prospect into the four phases of initial screening, reconnaissance, pilot testing, and final appraisal.[14] The first two steps identify ever-smaller areas for pilot testing, with the reconnaissance phase utilizing a minimum of three low-cost coreholes to obtain samples for desorption tests, sorption isotherms, proximate analyses, and other tests. Wireline log suites and permeability tests are the final pieces of data from reconnaissance wells. Noting that all four phases are important to prospect assessment, this study concentrated on the pilot testing phase, providing nearly three dozen recommendations for pilot location, design, and implementation. This study emphasized the need for pilots to successfully dewater the coals, allowing understanding of gas depletion, rather than commercial assessment. Pilot performance is integrated with geologic data for the prospect and economic parameters for the final appraisal stage.

Two instances when pilot testing could be eliminated are dry coals and micropilot injection testing to assess coals for enhanced coalbed methane recovery or $CO_2$ sequestration. Identification of dry coals is problematic, especially early in an exploration program, as technology is not yet available to determine cleat water saturation and coals are conceptualized as water saturated. Testing and development of the dry Horseshoe Canyon coals of Alberta was discussed by Bastian et al., while micropilot testing of other Alberta coals was reported by Mavor et al.[15]

Numerical simulation of pilot response is often initiated early in the pilot life and concludes after the pilot has terminated. The reservoir description obtained from the pilot history matching exercise is used to simulate various development scenarios that are then assessed for economic viability.

Two aboveground issues affecting coal gas pilots are field operations and management focus. Coal pilots require considerable attention from field personnel, especially in the early stages of dewatering when pump repairs and replacements occur frequently. Pilot operations in new basins can be extremely frustrating, as well behavior is virtually unknown and infrastructure is nonexistent. Incremental costs to operate a pilot for another one-quarter or one-half year are usually minimal compared with the initial capital outlay for pilot installation. While multiwell pilots are begun with good intentions, time and money demands from other projects can siphon away talent and funds from a coal pilot, compromising pilot interpretability and lengthening pilot lifetime.

In summary, the purpose of a coal pilot is understanding depletion behavior of the target coal deposit. Coal pilots should focus on maintaining all wells on continuous production, measuring gas and water rates and wellhead pressures, and developing a sense of coal reservoir response as the wells progressively interfere.

## Statistical Nature of Coal Gas Exploitation

A popular slogan in the coalbed methane community states that a successful coalbed methane project requires three elements: "Gas, perm, and land." *Gas*, of course, refers to a large in-place gas resource in the coals. *Perm* refers to coal permeability and flow capacity to produce the gas resource. Implicit in this is the assumption that a viable completion technology has been identified for this play. *Land* denotes a substantial acreage position, as coal gas projects are characterized by low-rate wells draining a very heterogeneous reservoir, making coalbed methane a statistical play.

Variability in gas production rates from the Horseshoe Canyon coals of Alberta was investigated by Beaton.[16] Wells completed in these dry coals typically intercept over a dozen coal seams. Spinner logs revealed gas production from a seam did not correlate with thickness, gas content, or stratigraphic position. Comparison of spinner logs from two wells separated by a township showed very different gas production profiles. Total flow capacity of the coal seams penetrated by a well and distribution of that flow capacity among the zones were highly variable. Anecdotal evidence indicates similar productivity variations among coal wells in other basins, with productivity of wells on adjacent locations sometimes varying by an order of magnitude. This highly variable productivity is attributed to differences in the coals that are both subtle and of a length scale that is short compared to interwell distances.

Root causes of this heterogeneity are unknown, making well productivity one of the biggest risks in coal gas projects. To better understand this risk, coal gas projects are often interpreted with probabilistic methods. Initial exploration efforts typically drill a half dozen coreholes to measure coalbed gas content and permeabilities. Primitive distributions of reservoir parameters such as density, thickness, gas content, and permeability developed from corehole data can be used to drive Monte Carlo simulations of the gas resource and recovery. After development commences, individual coal well performance histories, while interesting, often provide more insight into coal depletion behavior when aggregated by seam, by geographical group, and up to the field level. Once sufficient production data are available, construction of type curves based upon performance of perhaps two dozen wells completed in a specific seam or located in a geographic area helps define expected behavior of median and end member wells, such as top and bottom deciles. With a sufficiently robust data set, probabilistic simulations with gridded, multiwell models can be utilized to understand coal gas production from a given area or field.

The process of combining Monte Carlo methods with finite-difference simulations of single-well performance was discussed by Purvis et al. and applied to stacked gas sands, coal mine methane, and coalbed methane projects.[17] Clarkson and McGovern developed a spreadsheet-based tank model that was first validated against a gridded simulator before being coupled with a Monte Carlo package to generate a suite of coal well production profiles.[18] Selected profiles (such as P90—the profile achieved by 90% of the wells, P50, and P10 cases) and economic parameters were then input to financial modules to generate various metrics such as likely capital requirements, net present values, and chances of economic success.

A large set of Monte Carlo simulations by Roadifer et al. sought to identify reservoir and wellbore parameters controlling production from coal seams and coals in conjunction with sands.[19] Thirty primary parameters (such as permeability, net coal thickness, and sand porosity) and 62 combination parameters (such as the permeability-thickness product) were identified as possible controls on well performance. A total of 100,000 Monte Carlo simulations of production from a single, bounded well showed permeability to be the most important parameter controlling wells completed in coals. Free gas saturation was shown to be the most important parameter influencing coal plus sand wells.

Expected behaviors of Horseshoe Canyon coal wells derived from Monte Carlo reservoir simulations was discussed by Bastian et al.[20] Geological heterogeneity of these coals was captured with distributions of key reservoir parameters developed from coal cores, pressure transient tests, and production logs. A bounded single-well model for a given area was calibrated by altering reservoir parameter distributions until simulated distributions of original gas in place and average production performance in the project area matched the actual distributions. A series of Monte Carlo simulations with the calibrated model was then used to derive distributions of original gas in place for the project, optimum well spacing, and to generate P90, P50, and P10 gas profiles for reserves bookings.

## Current Challenges to Coal Gas Exploitation

Coal deposits have now been exploited as unconventional gas reservoirs for over a generation. As coalbed methane evolved from a mine safety problem to a gas reservoir, the unique nature of each coal deposit and the diverse behaviors of wells draining them became apparent. On a global scale, most coals remain untested, and many challenges remain to the exploitation of the gas they hold. The following short list identifies some of those challenges.

The realization that mineable coals comprise only a small fraction of coal gas reservoirs required several years. High-density, low-gas-content carbonaceous rocks, which are neither mineable coal nor true shales, can hold substantial gas volumes. Occurring as bounding beds and stringers within traditional coal deposits or as individual, distinct strata, these zones are targets for gas recovery. As coal density increases due to higher ash (mineral) content, the gas resource in the rock steadily becomes more diffuse, and permeability decreases. A cutoff density for defining coal pay has yet to be determined.

Wireline logs are routinely employed to identify coals in the subsurface but cannot yet be used to quantify water saturation in the cleats or gas undersaturation in the matrix. Log-derived porosities remain elusive, and a relation for water saturation in coal cleats similar to Archie's equation for conventional reservoirs has yet to be developed. Wireline tools that determine partial pressure of dissolved methane and hence desorption pressure are now available.[21] However, they require a sorption isotherm and reservoir pressure to determine coalbed gas content and the degree of undersaturation.

The lowest permeability for commercial coal gas production is currently on the order of 1 to 0.l md, making exploitation of tight coals a challenge. Horizontal wells, especially surface-to-in-seam (SIS) wells, are increasingly popular completions for low-permeability, single-seam plays. An effective completion for wells draining multiple, thin, low-permeability seams remains elusive.

Coals deeper than about 2,500 m are only now being assessed as gas reservoirs. Too deep to mine, these coals can hold considerable gas due to high hydrostatic pressures, yet recovery of that gas is complicated by low coal permeabilities resulting from the lithostatic load. Commercial gas production from deep coals will require

identification of areas with increased permeability due to faulting and deformation, a geosciences problem, and improved completions, an engineering problem. Depth limits for water-bearing coals, defined by pump technology, will be less than those of dry coals and those that produce so little water it can be lifted in a gas stream produced through small diameter tubing.

Multiwell coal pilots are often a necessary step between discovery wildcat and full-field development. Reducing pilot cost and duration while maximizing interpretability is an ongoing challenge for coal gas reservoir engineers.

Well completions in coal deposits with multiple, thin seams remain challenging. Such deposits are unattractive for horizontal wells and are especially difficult when the targeted seams are encountered across stratigraphic intervals so large as to require multiple frac stages.

## References


1. *BP Statistical Review of World Energy*. 2009. London: BP p.l.c.
2. Hanby, K. P. 1991. The use of production profiles for coalbed methane valuations. Paper 9117 in *Proceedings of the 1991 International Coalbed Methane Symposium*. Tuscaloosa: University of Alabama.
3. Meek, R. H., and Levine, J. R. 2005. *Delineation of Four "Type Producing Areas" (TPAS) in the Fruitland Coal Bed Gas Field, New Mexico and Colorado, Using Production History Data*. Presented at the AAPG Annual Meeting, Calgary, Alberta, June 16–19.
4. Carlton, D. R. 2000. *RMAG Coalbed Methane 2000 Raton Basin Field Trip Guidebook*. Denver: Rocky Mountain Association of Geologists.
5. Montgomery, S. L. 1999. Powder River coalbed methane play. *Petroleum Frontiers*. V. 16 (no. 1). p. 1.
6. Bill Barrett Corporation. 2009. Analysts' presentation. November.
7. Bastian, P. A., Wirth, O. F. R, Wang, L., and Voneiff, G.W. 2005. *Assessment and Development of the Dry Horseshoe Canyon CBM Play in Canada*. Paper SPE 96899. Presented at the 2005 SPE Annual Technical Conference and Exhibition, Dallas, Texas, October 9–12.
8. McCune, D. 2003. Coalbed methane development in the Cherokee and Forest City basins. Paper 0313 in *Proceedings of the 2003 International Coalbed Methane Symposium*, Tuscaloosa: University of Alabama.
9. Arri, L. E., Yee, D., Morgan, W. D., and Jeansonne, M. W. 1992. *Modeling Coalbed Methane Production with Binary Gas Sorption*. Paper SPE 24363. Presented at the SPE Rocky Mountain Regional Meeting, Casper, Wyoming, May 18–21.
10. Young, G. C. B., McElhiney, J. E., Paul, G. W., and McBane, R. A. 1991. *An Analysis of Fruitland Coalbed Methane Production, Cedar Hill Field, Northern San Juan Basin*. Paper SPE 22913. Presented at the SPE Annual Technical Conference and Exhibition, Dallas, Texas, October 6–9.
11. Seidle, J. P. 2002. Lessons learned, lessons lost—review of selected coalbed methane pilots. In Coalbed Methane of North America II. Schwochow and Nuncio, eds. Denver: Rocky Mountain Association of Geologists. p. 7.
12. McCants, C. Y., Spafford, S., and Stevens, S. H. 2001. Five-spot production pilot on tight spacing: Rapid evaluation of a coalbed methane block in the Upper Silesian Coal Basin, Poland. Paper 0124 in *Proceedings of the 2001 International Coalbed Methane Symposium*. Tuscaloosa: University of Alabama.
13. Seidle, J. P. 2002.
14. Roadifer, R. D., and Moore, T. R. 2008. Coalbed methane pilots: Timing, design, and analysis. Paper SPE 114169. Presented at the 2008 Unconventional Reservoirs Conference, Keystone, Colorado, February 10–12.
15. Bastian, P. A., Wirth, O. F. R., Wang, L., and Voneiff, G. W. 2005. *Assessment and Development of the Dry Horseshoe Canyon CBM Play in Canada*. Paper SPE 96899. Presented at the 2005 SPE Annual Technical Conference and Exhibition, Dallas, Texas, October 9–12; and Mavor, M. J., Gunter, W. D., and Robinson, J. R. 2004. *Alberta Multiwell Micro-Pilot Testing for CBM Properties, Enhanced Methane Recovery and $CO_2$ Storage Potential*. Paper SPE 90256. Presented at the SPE Annual Technical Conference and Exhibition, Houston, Texas, September 26–29.
16. Beaton, A. 2003. *Production Potential of Coalbed Methane Resources in Alberta*. EUB/AGS Earth Sciences Report 2003-03. Edmonton, Alberta: Alberta Energy and Utilities Board.
17. Purvis, D. C., Strickland, R. F., Alexander, R. A., and Quinn, M. A. 1997. *Coupling Probabilistic Methods and Finite Difference Simulation: Three Case Histories*. Paper SPE 38777. Presented at the 1997 Annual Technical Conference and Exhibition, San Antonio, Texas, October 5–8.
18. Clarkson, C. R., and McGovern, J. M. 2003. A new tool for unconventional reservoir exploration and development applications. Paper 0336 in *Proceedings of the 2003 International Coalbed Methane Symposium*. Tuscaloosa: University of Alabama; and Clarkson, C. R., and McGovern, J. M. 2005. Optimization of coalbed-methane-reservoir exploration and development strategies through integration of simulation and economics. *Society of Petroleum Engineers Reservoir Evaluation and Engineering*. V. 8 (no. 6). p. 502.
19. Roadifer, R. D., Moore, T. R., Raterman, K. T., Farnan, R. A., and Crabtree, B. J. 2003. *Coalbed Methane Parametric Study: What's Really Important to Production and When?* Paper SPE 84425. Presented at the Annual Technical Conference and Exhibition, Denver, Colorado, October 5–8.
20. Bastian, P. A., et al. 2005.
21. Lamarre, R. A., and Pope, J. 2007. Critical-gas-content technology provides coalbed-methane-reservoir data. *Journal of Petroleum Technology*. V. 59 (no. 11). p. 108.

# Coal Fundamentals 2

## Introduction

Coal fueled the Industrial Revolution of Europe in the 18th and 19th centuries and continues to be an important source of energy throughout the world today. Scientific studies of coal have therefore focused on mineability of this resource and its combustion, chemical, and metallurgical characteristics. Much of that information is relevant for understanding coal deposits as gas reservoirs. Fundamental aspects utilized for reservoir engineering purposes include coal rank, proximate and ultimate analyses, macerals, porosity, density, rock mechanics, sorption behavior, and gas properties.

While many reservoir engineers define coal as "a black rock that burns," Schopf defined coal as a rock that is at least 50% by weight and 70% by volume carbonaceous material.[1] In addition, Schopf classified this rock by the parameters of type, grade, and rank. Coal *type* depends on the original plant precursors of the coal and is divided into two broad categories of *humic* (banded) and *sapropelic* (unbanded) coals. While coal type provides insight into coal behavior during combustion or organic chemical conversion processes, it is weakly linked to coal gas production and therefore currently sees limited use in coal gas reservoir engineering. *Grade* refers to the amount and type of inorganic impurities present in a coal. These include ash, which is of major importance in coal gas reservoir engineering, and various minerals such as pyrite and clays, some of which swell upon contact with completion fluids. Coal rank is a measure of its thermal maturity and is a major element in coal gas reservoir engineering.

## Coal Rank

Coal is a complex organic rock of variable purity and moisture content, deposited in multiple geological ages, and is often classified by rank, that is, the degree of thermal maturity or metamorphosis of the organic material in a coal. Coal rank is a primary element in the construction of coal gas analogs. Newly deposited organic material is randomly ordered and wet, with little mechanical integrity. Burial of this material deep in the earth subjects it to heat and pressure over geologic time, causing the organic material to become progressively more ordered, driving off water and gases. Thus the organic material is steadily fused into a gelled or colloidal mixture of long-chained and aromatic molecules. The resulting spectrum of rocks is chemically reactive, with moderate mechanical strength and a large surface area carpeted with gas.

Coal rank is defined by ASTM D388-05 and the 18 standards referenced therein that pertain to test procedures for specific parameters, as well as sample acquisition and preparation.[2] The nine coal ranks defined by ASTM, in order of increasing maturity, are peat, lignite, subbituminous, high-volatile bituminous, medium-volatile bituminous, low-volatile bituminous, semianthracite, anthracite, and metaanthracite. Subbituminous and bituminous rank coals are sufficiently diverse to require division into three subcategories, again in ascending maturity: C, B, and A. Alternatively, coal ranks have been defined by coking properties by the National Coal

Board of the UK.[3] They are defined primarily by vitrinite reflectance by the International Organization for Standardization (ISO 11760:2005).[4] Coal ranks are also defined by an Australian standard (1038).[5]

Coal rank depends on thermal history, not geological age, and is determined by several parameters, none unique. As seen in table 2–1, coalification is a broad process that encompasses carbonization, devolatilization, and dessication.[6] The carbon content of coals steadily increases with the degree of metamorphosis from roughly one-half, on a weight percentage basis, in peats to more than 90% in anthracites. Coal can be broadly divided into *fixed* and *volatile* portions, with the fraction of volatile matter, whose measurement is discussed below, steadily decreasing from more than 50% in peats to less than 2% in metaanthracites. Coals that are less than about one-third volatile matter, on a dry, mineral-matter-free basis, are considered high rank coals. The clear, monotonic decrease in volatile matter of medium volatile bituminous and higher maturity coals provides a convenient method of assigning rank.

**Table 2–1.** Coal rank chart

| Coal rank | Reflectance (%) | Volatile matter (%) | Carbon (% dry ash-free, vitrinite) | Bed moisture (%) | Calprific Value, Btu/lb moist, mmf |
|---|---|---|---|---|---|
| Peat | | 64 | 60 | 75 | <6,300 |
| Lignite | 0.3 | 60 | | | 6,300 - 8,300 |
| | | 56 | | 35 | |
| Sub-bituminous C | 0.4 | 52 | | | 8,300 - 9,500 |
| Sub-bituminous B | | 48 | 71 | 25 | 9,500 - 10,500 |
| Sub-bituminous A | 0.5 | | | | 10,500 - 11,500 |
| High-volatile bituminous C | 0.6 | 44 | 77 | 8-10 | 11,500 - 13,000 |
| High-volatile bituminous B | 0.7 | 40 | | | 13,000 - 14,000 |
| High-volatile bituminous A | 0.8 | 36 | | | > 14,000 |
| | 1.0 | 32 | | | |
| Medium-volatile bituminous | 1.2 | 28 | 87 | | |
| | 1.4 | 24 | | | |
| Low-volatile bituminous | 1.6 | 20 | | | |
| | 1.8 | 16 | | | |
| Semi-anthracite | 2.0 | 12 | | | |
| Anthracite | | 8 | 91 | | |
| | 3.0 | | | | |
| | 4.0 | 4 | | | |
| Meta-Authracite | > 4.5 | < 2 | > 91 | 0 | |

*Source:* Adapted from Stach, E., et al. 1982; and Mastalerz, M., and Harper, D. 1998.

Moisture content of a coal also steadily decreases from more than one-half in peats to essentially nothing in metaanthracites, but it is too variable to act as a reliable indicator of rank. Calorific content of a coal, on a moist, mineral-matter-free basis, steadily increases with maturity, showing the greatest variation in low-rank coals, thereby providing a convenient parameter for rank determination up to high-volatile bituminous A.

*Vitrinite reflectance*, a microscopic procedure using reflected light from a polished sample, steadily increases across all coal maturities, making it an increasingly common and primary determinant of rank in coal gas plays. Current industry practice is to measure reflectance from 50 to 500 points, and as it is somewhat subjective, more consistent results are obtained across a suite of samples when the measurements are made by a single individual.

The relationship between vitrinite reflectance and volatile matter on a dry, ash-free (daf) basis was described by Meissner as three linear segments whose equations are given as follows:[7]

For $VM_{daf}$ 70% to 43% and $R_o$ 0.17% to 0.52%:

$$VM_{daf} = 83.11 - 77.14R_o$$

For $VM_{daf}$ 41% to 10% and $R_o$ 0.56% to 2.30%:

$$VM_{daf} = 51.2 - 18.26R_o$$

For $VM_{daf}$ 6.7% to 2.0% and $R_o$ 2.57% to 5.00%:

$$VM_{daf} = 11.67 - 1.93R_o$$

where

$VM_{daf}$ = volatile matter, wt %, daf, and
$R_o$ = vitrinite reflectance, %.

These equations, plotted in figure 2–1, exhibit slope breaks at the "coalification jumps" across the subbituminous-bituminous and semianthracite-anthracite boundaries.

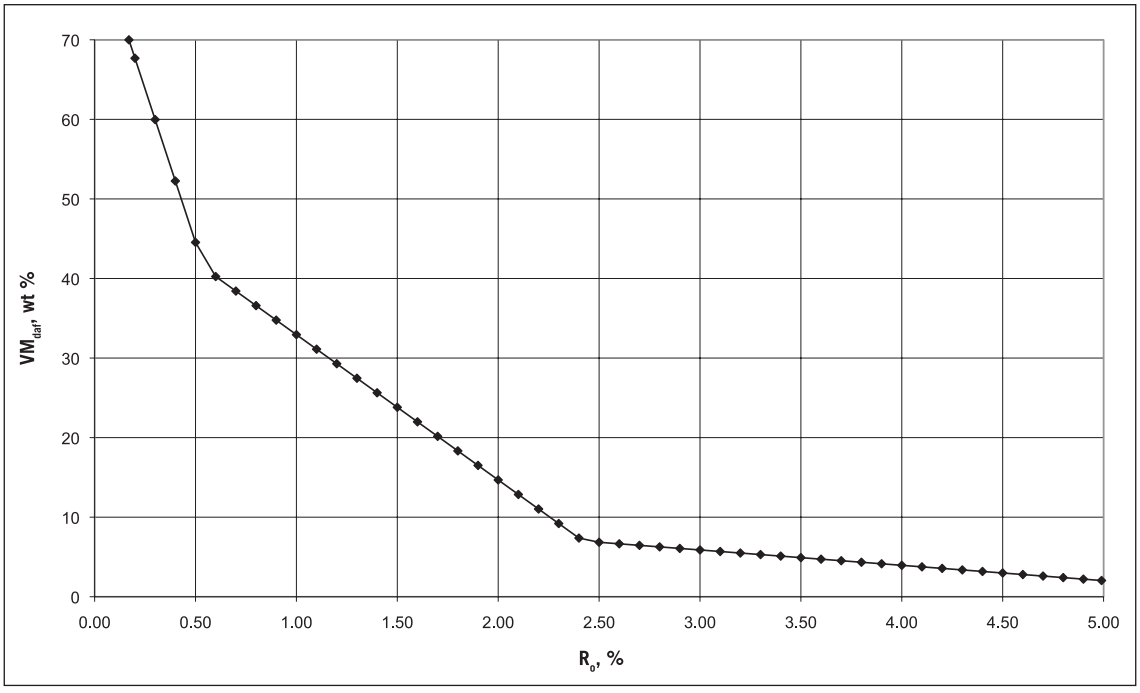



**Fig. 2–1.** Meissner relation for vitrinite reflectance vs. volatile matter, daf[8]

As rank determination is empirical, the various parameters discussed here can give slightly different ranks, especially near coalification boundaries. Consequently, rank of a given sample is often determined from multiple parameters, with the eventual rank being accompanied by its determinant, such as "high-volatile A bituminous by vitrinite reflectance."

## Proximate and Ultimate Analyses

Coal is often characterized by proximate and ultimate analyses. Proximate analysis, with origins in the coal mining industry, is the more useful of the two analyses for reservoir engineering purposes and considers coal to be comprised of four constituents, two organic and two inorganic. The organic components are fixed carbon (FC) and volatile matter (VM), while the inorganic components are moisture (w) and ash (a). Fixed carbon increases with rank, and volatile matter and moisture decrease with coal rank. Ash, a measure of coal purity, is highly variable on a local and regional scale and is related to depositional environments and cleat mineralization. A layer of sediment deposited during flooding of an otherwise quiescent swamp becomes ash in the final coal. The silica that stiffened ancient sawgrasses becomes ash in the subsequent coal. Minerals precipitated from groundwater flowing through the cleats of a coal deposit contribute to the ash content of that rock.

As discussed above, water content of a coal decreases steadily with rank. Lignites are 28% to 75% water, subbituminous coals 10% to 28%, bituminous coals less than 10%, and anthracites only a few percent. Regardless of rank, a coal deposit holds water in both cleats and pores. The relative amount of water drained from each during dewatering of a coal seam depends on several factors, including rank of the coal, specific basin hydrologies, and individual seam properties such as porosity distributions. Determination of the in-situ water in a coal deposit is important for normalizing coal properties, such as gas content, to a dry, ash-free or dry, mineral-matter-free (dmmf) basis and for estimating water disposal requirements of a given well or project. Many terms have been used historically in discussing water in coal, including *inherent moisture*, *equilibrium moisture*, *moisture-holding capacity*, *bed moisture*, and *in-situ moisture*, all expressed as a weight percent.

The first two are rigorously defined and are the most important for coal gas reservoir engineering. Inherent moisture is water that is an integral part of in-situ coal, residing in the pores but not present in macroscopically visible fractures.[9] Fractures visible in laboratory samples, although much slimmer in situ, arguably contain water that is produced during gas recovery, making inherent moisture a lower bound on water in place in a given coal seam.

Equilibrium moisture, also called *bed moisture*, is determined by first equilibrating about 5 g of coal ground to –16 mesh at 96% to 97% relative humidity and 30°C (86°F) for 48 to 72 hours.[10] After equilibration, the sample is weighed, dried at 105°C (221°F) for up to 3 hours in a low-pressure nitrogen atmosphere, then reweighed. Equilibrium moisture is defined as the difference in weights. Noting that this procedure will overestimate in-situ moisture in coals above 30°C, Testa and Pratt proposed equilibration of triplicate wet samples in an argon atmosphere at reservoir temperature, not 30°C, for periods of up to 30 days.[11]

Equilibrium moisture, essentially equal to inherent moisture for coals of bituminous and higher rank, is less than inherent moisture for coals of subbituminous and lower rank due to water loss from coal macropores during the equilibration period.[12] Testing samples of U.S. coals, Luppens and Hoeft found inherent moisture greater than equilibrium moisture by 1% to 10% in lignitic coals, 0.5% to 1.3% in subbituminous coals, and 0% to 0.5% in bituminous coals.[13] Similarly, Testa and Pratt reported their improved method resulted in moisture contents above equilibrium moistures for coal of subbituminous B and lower rank but below equilibrium moistures for ranks of subbituminous A and higher rank.[14]

Gas more than water in a coal deposit determines commerciality of its extraction. Water is often considered an unwanted by-product of gas production to be disposed of at minimal cost. However, determination of coalbed gas contents, initial gas in place, and remaining reserves requires precision in calculation of water in a coal. For coal gas calculations, consistent use of the method to characterize coal moisture is more important than a specific method. Regardless of which of the three moistures is employed, all laboratory data should be normalized to it.

A rough estimate of water in place can be obtained from any of the three moistures (inherent, equilibrium, or improved), as differences between them are typically less than uncertainties in other reservoir parameters, such as coal seam thicknesses and densities. Original water in place is the product of an area, net coal thickness, coal density, and the selected moisture fraction. Water disposal requirements for a given well or project can be estimated as the product of this water in place value multiplied by a reasonable recovery factor, typically between one-half and two-thirds.

Determination of volatile matter, as detailed in ASTM D 3175, begins with placing a 1 g sample in a covered metal crucible in the 950° ±20°C (1,742° ±36°F) zone of an oven.[15] Care must be taken to ensure the sample remains covered after disappearance of the luminous flame. After a total of seven minutes, the sample is removed from the oven, cooled in a dessicator, and then weighed. *Volatile matter* is defined as the percentage weight loss during this procedure less the inherent moisture percentage.

Proximate analysis is determined from ASTM D 3172-07a, *Standard Practice for Proximate Analysis of Coal and Coke*.[16] It incorporates procedures for equilibrium moisture and ash by reference. Equilibrium moisture, ash, and volatile matter are determined from the procedures described above, and fixed carbon by difference. For reservoir engineering purposes, comparisons of laboratory and field data are often done on a dry, ash-free basis. For example, comparison of desorbed gas contents with a laboratory sorption isotherm may seemingly indicate undersaturation of a coal deposit, when in actuality the samples in the desorption canisters contained more ash than did the subsample taken for the isotherm measurement. Reporting all gas contents and sorption isotherms on a dry, ash-free basis eliminates this problem.

*Ash* is the noncombustible portion of a coal as determined by ASTM Method D 3174.[17] As described in this procedure, a 1 g sample is heated to between 450°C and 500°C by the end of the first hour and 700°C to 750°C by the end of the second hour. The sample is held at this temperature for two additional hours before cooling in a manner to minimize moisture uptake and then weighed a second time. The *ash fraction* of the sample is final weight divided by original weight. Incapable of holding significant gas, ash is a diluent in the coal, decreasing gas-holding capacity. During the combustion process, $CO_2$ (from carbonates), $SO_2$ (from sulfates), and $H_2O$ (from clays) are driven off, making the ash fraction of a sample less than the mineral matter fraction. Ash typically varies more than equilibrium moisture for any given coal deposit, as the primary controls on ash such as shale partings, overbank deposits, or degraded organic precursors varied vertically and horizontally during deposition and coalification. Ash in a coal reservoir can vary from a few percent to more than 50% of the mass of the reservoir rock. High ash portions of a coal seam often hold sufficient gas and possess sufficient permeability to be considered part of the overall reservoir system, yet this same rock would not be commercially mineable. Consequently, viewing coals from a mining perspective will provide a conservative assessment of the reservoir potential of a coal deposit.

Data can also be normalized to a mineral-matter-free basis, either wet or dry. The dry, mineral-matter-free basis is the more common of the two in coal gas reservoir engineering. First, the sulfur content of coal is determined via ASTM D 4239-05.[18] Then the mineral-matter fraction can be calculated from the Parr formula:

$$MM = 1.08a + 0.55S$$

where

$MM$ = mineral-matter weight fraction,
$a$ = ash weight fraction, and
$S$ = sulfur weight fraction.

Gas in place depends on areal extent and thickness of a coal body as well as moisture, ash, and mineral matter. Uncertainties in area and thickness and the resulting gas in place volume are sometimes carried over to coalbed gas contents, with the daf and dmmf bases being used interchangeably. The error caused by this interchange can be illustrated with an example from the Warrior Basin of Alabama.

### Example 2.1. Comparison of daf and dmmf fractions

Proximate analyses and sulfur contents from four samples taken from the Jefferson coal seam of the Black Creek Coal Group in the Warrior Basin coal are collected in table 2–2.[19]

**Table 2–2.** Proximate analysis and sulfur content—Jefferson coal, Warrior Basin

| Seq no | County | Moisture, % | Ash, % | Volatile matter, % | Fixed carbon, % | Total, % | Sulfur, % | Mineral matter, % | Min. mat./Ash |
|---|---|---|---|---|---|---|---|---|---|
| 1 | Jefferson | 2.3 | 7.3 | 31.9 | 58.5 | 100.0 | 3.1 | 9.6 | 1.31 |
| 2 | Marion | 5.2 | 3.3 | 37.3 | 54.2 | 100.0 | 1.3 | 4.3 | 1.30 |
| 3 | Tuscaloosa | 1.4 | 4.6 | 32.6 | 61.4 | 100.0 | 1.4 | 5.7 | 1.25 |
| 4 | Walker | 4.1 | 4.2 | 36.7 | 55.0 | 100.0 | 1.5 | 5.4 | 1.28 |
| × | Average | 3.3 | 4.9 | 34.6 | 57.3 | 100.0 | 1.8 | 6.2 | 1.28 |

*Source:* Rightmire, C. T., Eddy, G. E., and Kirr, J. N. 1984.

On the basis of volatile matter, coal rank is high-volatile bituminous. Coal purity is high, with ash and mineral matter both less than 10% for all samples. Using average ash and moisture fractions, 0.049 and 0.033, respectively, for conversion of pure coal gas contents to in-situ conditions entails multiplication by

$$1 - a - w = 1 - 0.049 - 0.033 = 0.918$$

where

$a$ = ash fraction, wt %, and
$w$ = equilibrium moisture fraction, wt %.

Using the average mineral matter fraction, 0.062, and average moisture fraction for conversion of pure coal results to in-situ conditions requires multiplication by

$$1 - MM - w = 1 - 0.062 - 0.033 = 0.905$$

where

$MM$ = mineral matter fraction, wt %.

The resulting in-situ gas contents will differ by

$$\frac{0.918}{0.905} = 1.014$$

While the average mineral matter of 6.2% is about one-third larger than the average ash of 4.9%, interchange of the two for calculation of in-situ gas contents gives rise to a variation of only 1.4%. From inspection of the Parr formula above, variation between values calculated on daf and dmmf bases is greatest for high-ash, high-sulfur coals.

Ultimate analysis determines the chemical elements in a coal sample.[20] Typically reported as carbon, hydrogen, oxygen, nitrogen, and sulfur, four of the elements are determined by laboratory procedures, while oxygen is determined by difference. The active standard in the United States for ultimate analysis is ASTM D3176-89, ASTM (2002), which references an additional 14 ASTM procedures detailing sample acquisition and preparation as well as laboratory procedures.[21] Knowledge of the elemental composition of a coal is important for coal chemistry and conversion processes but gives little information about coal rank or rock properties, such as gas sorption potential or permeability. Consequently, ultimate analysis is of limited use in coal gas reservoir engineering at this time.

Procedures for determination of inherent moisture, ash, and volatile matter all contain qualitative actions. Such actions include taking care not to overly dry a sample when removing excess water by suction during equilibrium moisture determination or cooling a sample to minimize moisture uptake as part of ash fraction measurement. In addition to these subjective actions, sample history can affect proximate analyses. Coals, especially low-rank coals, oxidize rapidly upon exposure to ambient conditions. Luppens and Hoeft ascribed reproducibility differences in moisture analyses to sample oxidation.[22] Consequently, proximate analyses will vary from laboratory to laboratory and between operators within a given lab.

## Number of Samples and Confidence Limits

Characterization of a coal deposit via laboratory tests suffers from the double complications of obtaining a sufficient number of samples and preservation of those samples for selected tests. Sourced from diverse organic materials laid down in a variety of depositional settings, each coal deposit has followed a unique metamorphosis path, and the resulting heterogeneity of coal complicates acquisition of representative samples. Multiple samples are required for accurate deterministic estimates of coal properties, while even larger sample populations are necessary for construction of realistic property distributions necessary for probabilistic Monte Carlo simulations. Pratt and Baez recommend 15% to 20% of the "gross reservoir system" be sampled to obtain representative data.[23] The Gas Research Institute recommends sampling one-third of the "vertical reservoir profile" in any given well.[24]

Historically, coalbed gas content measurement has been the primary, often only, test for assessing viability gas extraction from a coal deposit. A method to estimate the required number of desorption samples based on operating characteristic curves was proposed by Mavor et al.[25] In addition to gas content samples, coal well sampling programs frequently address other coal seam parameters, such as bulk and helium density, proximate and ultimate analyses, vitrinite reflectance, sorption isotherm samples, macerals, and mechanical properties. Pratt and Baez recommend a total of 15 different parameters to characterize a coal deposit.[26] Common sense dictates uniform sampling across an acreage block as well as stratigraphically across all seams of interest. In addition to samples from visually attractive coal, samples should also be taken from dull coals, any interbedded shales, and bounding beds. While these poorer quality rocks would not be considered mineable coal, they can contain substantial amounts of gas and are necessary for rock properties tests, making them an integral part of the reservoir.

Perhaps more common is the problem of determining the confidence in a result, for example, average density, from a limited set of samples. The chi-square goodness-of-fit test can be used to address this problem and that of estimating the number of samples required to achieve a specified level of confidence as discussed above. The following intuitive derivation, while admittedly not rigorous, links the number of samples and the confidence level of a result derived from them. Introductory statistics texts define *chi-square* as the ratio of the measured spread in the data to the expected spread based upon an assumed distribution.[27] The chi-square function can be written as

$$\chi^2 = \sum_{j=1}^{N} \frac{[\,y_j - Y_j\,]^2}{\sigma^2}$$

where

$\chi^2$ = chi-square function,
$N$ = number of samples or observations,
$y_j$ = value of $j$th observation,
$Y_j$ = expected value of $j$th observation, and
$\sigma^2$ = variance of observations.

The smaller the value of $\chi^2$, the better the sample population is described by the expected distribution. For a large number of observations, this can be approximated as

$$\chi^2 = \frac{N(\mu - \mu_0)^2}{\sigma^2} \tag{2.1}$$

where

$\mu$ = mean of observations, and
$\mu_0$ = mean of assumed distribution.

Arbitrarily specifying the difference between the observed and assumed means to be within, say, 10% of the mean of the observed distribution,

$$0.1\mu = \mu - \mu_0$$

or, more generally,

$$\alpha\mu = \mu - \mu_0$$

where

α = specified difference between means.

Substituting this into equation (2.1) yields

$$\chi^2 = \frac{N\alpha^2 \mu^2}{\sigma^2} \tag{2.2}$$

With this relation, a chi-square value can be computed from a set of $N$ observations with a mean $\mu$ and standard deviation $\sigma$ coupled with an assumed difference between observed and theoretical means $\alpha$. Note that as this derivation forces a set of $N$ experimental observations to a mean, a variance, and a difference between means, the degrees of freedom are $N - 3$. From the $\chi^2$ value and the degrees of freedom, the probability of this $\chi^2$ value being exceeded can be calculated from tabulated values of $\chi^2$, collected in table 2–3, introductory statistics texts, or calculated with the Excel CHIINV spreadsheet function.[28]

Equation (2.2) can provide a crude estimate of the number of samples required to obtain a specified certainty in the resulting mean but is decidedly not rigorous and requires a primitive knowledge of the sample population mean and standard deviation. Combining the assumed mean and standard deviation with the specified certainty yields a relation between $\chi^2$ and $N$, which is solved iteratively for $N$, perhaps most easily done with the CHIDIST spreadsheet function.

Calculation of the certainty in a set of densities and estimation of the number of samples required to obtain a specified certainty are illustrated in the following example.

**Table 2–3.** Values of $\chi^2$

| Degrees of freedom | Probability | | | | | | | | | | |
|---|---|---|---|---|---|---|---|---|---|---|---|
| | 0.99 | 0.98 | 0.95 | 0.90 | 0.80 | 0.20 | 0.10 | 0.05 | 0.02 | 0.01 | 0.001 |
| 1 | 1.57E-04 | 6.28E-04 | 3.93E-03 | 0.016 | 0.064 | 1.642 | 2.706 | 3.841 | 5.412 | 6.635 | 10.828 |
| 2 | 0.020 | 0.040 | 0.103 | 0.211 | 0.446 | 3.219 | 4.605 | 5.991 | 7.824 | 9.210 | 13.816 |
| 3 | 0.115 | 0.185 | 0.352 | 0.584 | 1.005 | 4.642 | 6.251 | 7.815 | 9.837 | 11.345 | 16.266 |
| 4 | 0.297 | 0.429 | 0.711 | 1.064 | 1.649 | 5.989 | 7.779 | 9.488 | 11.668 | 13.277 | 18.467 |
| 5 | 0.554 | 0.752 | 1.145 | 1.610 | 2.343 | 7.289 | 9.236 | 11.070 | 13.388 | 15.086 | 20.515 |
| 6 | 0.872 | 1.134 | 1.635 | 2.204 | 3.070 | 8.558 | 10.645 | 12.592 | 15.033 | 16.812 | 22.458 |
| 7 | 1.239 | 1.564 | 2.167 | 2.833 | 3.822 | 9.803 | 12.017 | 14.067 | 16.622 | 18.475 | 24.322 |
| 8 | 1.646 | 2.032 | 2.733 | 3.490 | 4.594 | 11.030 | 13.362 | 15.507 | 18.168 | 20.090 | 26.124 |
| 9 | 2.088 | 2.532 | 3.325 | 4.168 | 5.380 | 12.242 | 14.684 | 16.919 | 19.679 | 21.666 | 27.877 |
| 10 | 2.558 | 3.059 | 3.940 | 4.865 | 6.179 | 13.442 | 15.987 | 18.307 | 21.161 | 23.209 | 29.588 |
| 11 | 3.053 | 3.609 | 4.575 | 5.578 | 6.989 | 14.631 | 17.275 | 19.675 | 22.618 | 24.725 | 31.264 |
| 12 | 3.571 | 4.178 | 5.226 | 6.304 | 7.807 | 15.812 | 18.549 | 21.026 | 24.054 | 26.217 | 32.909 |
| 13 | 4.107 | 4.765 | 5.892 | 7.042 | 8.634 | 16.985 | 19.812 | 22.362 | 25.472 | 27.688 | 34.528 |
| 14 | 4.660 | 5.368 | 6.571 | 7.790 | 9.467 | 18.151 | 21.064 | 23.685 | 26.873 | 29.141 | 36.123 |
| 15 | 5.229 | 5.985 | 7.261 | 8.547 | 10.307 | 19.311 | 22.307 | 24.996 | 28.259 | 30.578 | 37.697 |
| 16 | 5.812 | 6.614 | 7.962 | 9.312 | 11.152 | 20.465 | 23.542 | 26.296 | 29.633 | 32.000 | 39.252 |
| 17 | 6.408 | 7.255 | 8.672 | 10.085 | 12.002 | 21.615 | 24.769 | 27.587 | 30.995 | 33.409 | 40.790 |
| 18 | 7.015 | 7.906 | 9.390 | 10.865 | 12.857 | 22.760 | 25.989 | 28.869 | 32.346 | 34.805 | 42.312 |
| 19 | 7.633 | 8.567 | 10.117 | 11.651 | 13.716 | 23.900 | 27.204 | 30.144 | 33.687 | 36.191 | 43.820 |
| 20 | 8.260 | 9.237 | 10.851 | 12.443 | 14.578 | 25.038 | 28.412 | 31.410 | 35.020 | 37.566 | 45.315 |
| 21 | 8.897 | 9.915 | 11.591 | 13.240 | 15.445 | 26.171 | 29.615 | 32.671 | 36.343 | 38.932 | 46.797 |
| 22 | 9.542 | 10.600 | 12.338 | 14.041 | 16.314 | 27.301 | 30.813 | 33.924 | 37.659 | 40.289 | 48.268 |
| 23 | 10.196 | 11.293 | 13.091 | 14.848 | 17.187 | 28.429 | 32.007 | 35.172 | 38.968 | 41.638 | 49.728 |
| 24 | 10.856 | 11.992 | 13.848 | 15.659 | 18.062 | 29.553 | 33.196 | 36.415 | 40.270 | 42.980 | 51.179 |
| 25 | 11.524 | 12.697 | 14.611 | 16.473 | 18.940 | 30.675 | 34.382 | 37.652 | 41.566 | 44.314 | 52.620 |
| 26 | 12.198 | 13.409 | 15.379 | 17.292 | 19.820 | 31.795 | 35.563 | 38.885 | 42.856 | 45.642 | 54.052 |
| 27 | 12.879 | 14.125 | 16.151 | 18.114 | 20.703 | 32.912 | 36.741 | 40.113 | 44.140 | 46.963 | 55.476 |
| 28 | 13.565 | 14.847 | 16.928 | 18.939 | 21.588 | 34.027 | 37.916 | 41.337 | 45.419 | 48.278 | 56.892 |
| 29 | 14.256 | 15.574 | 17.708 | 19.768 | 22.475 | 35.139 | 39.087 | 42.557 | 46.693 | 49.588 | 58.301 |
| 30 | 14.953 | 16.306 | 18.493 | 20.599 | 23.364 | 36.250 | 40.256 | 43.773 | 47.962 | 50.892 | 59.703 |

*Source:* Young, H. D. 1962.

## Example 2.2. Arkoma Basin—Hartshorne coal density

Bulk coal densities of Hartshorne coal samples from the Oklahoma portion of the Arkoma Basin reported by Cardott are shown in table 2–4.[29]

**Table 2–4.** Coal densities—Hartshorne coal, Arkoma Basin

| | Depth, ft | | | |
|---|---|---|---|---|
| Sample ID | Top | Base | Midpay, feet | Bulk density, g/cm$^3$ |
| 1 | 1,182.0 | 1,182.6 | 1,182.3 | 1.34 |
| 2 | 1,182.6 | 1,182.8 | 1,182.7 | 1.35 |
| 3 | 1,182.8 | 1,183.1 | 1,183.0 | 1.53 |
| 4 | 1,183.1 | 1,183.5 | 1,183.3 | 1.30 |
| 5 | 1,183.5 | 1,184.0 | 1,183.8 | 1.30 |
| 6 | 1,184.0 | 1,184.6 | 1,184.3 | 1.77 |
| 7 | 1,184.6 | 1,184.7 | 1,184.7 | 1.66 |
| 8 | 1,184.7 | 1,185.0 | 1,184.9 | 1.65 |
| 9 | 1,185.0 | 1,186.0 | 1,185.5 | 1.36 |
| 10 | 1,186.0 | 1,186.4 | 1,186.2 | 1.34 |
| 11 | 1,186.4 | 1,186.7 | 1,186.6 | 1.37 |
| 12 | 1,186.7 | 1,187.3 | 1,187.0 | 1.30 |
| 13 | 1,187.3 | 1,188.0 | 1,187.7 | 1.34 |
| 14 | 1,188.0 | 1,187.0 | 1,187.5 | 1.45 |
| 15 | 1,187.0 | 1,188.8 | 1,187.9 | 1.69 |

*Source:* Cardott, B. J. 1998.

This set of 15 samples taken from the 6.8 ft thick coal seam has a mean density of 1.45 g/cm$^3$ and a standard deviation of 0.1645 g/cm$^3$. Assuming observed and actual means differ by at most 10%, that is, assuming an α of 0.1, the chi-square value can be calculated from equation (2.2)

$$\chi^2 = \frac{N\alpha^2\mu^2}{\sigma^2} = \frac{15(0.10)^2(1.45\text{g/cm}^3)^2}{(0.1645\text{g/cm}^3)^2}$$

$$\chi^2 = 11.656$$

With a total of 15 samples, the degrees of freedom for this example are 15 – 3 = 12. From the CHIDIST Excel function, the probability corresponding to this chi-square and degrees of freedom is 0.474. That is, the probability of the true mean exceeding the calculated mean is 47.4%. Alternatively, the probability the true and calculated means differ by less than 10% is 52.6%, leading to the conclusion of roughly 50% confidence that the true mean is within 10% of the measured mean, ranging from 1.378 to 1.595 g/cm$^3$.

How many samples would be required to achieve a 90% confidence level? As both chi-square values and the degrees of freedom depend on the number of samples, a few iterations in a $\chi^2$ table are required to obtain a $\chi^2$ value of 66.050 and 82 degrees of freedom. Consequently, a total of 82 + 3 = 85 samples would be required to be 90% confident the true mean density is within 10% of the mean of the measured densities.

In practice, both the error bounds on sample distributions and the number of samples required to achieve a high certainty in the measured value of a coal property are frequently larger than commonly believed.

## Sample Collection and Preservation

Coals, especially low-rank coals, degrade rapidly upon exposure to ambient conditions. Moisture loss and surface oxidation are among the primary mechanisms for sample degradation and complicate determination of coal properties important for coal gas reservoir engineering such as in-situ moisture, sorption behavior, and mechanical integrity. Restoration of a sample to inherent moisture content is difficult, if not impossible, while surface oxidation cannot be reversed. Although different tests require different sample preparation protocols, minimization of sample desiccation and exposure to light, air, and excessive temperatures will help ensure

sample integrity. Coal sample preservation is discussed in detail by Testa and Pratt.[30] Common tests for coal gas reservoir engineering include the following:[31]

1. Desorption tests for coalbed gas content and composition
2. Proximate/ultimate analyses to determine ash, moisture, volatile matter, fixed carbon, and sulfur
3. Vitrinite reflectance
4. Bulk and helium densities
5. Sorption isotherms
6. Macerals
7. Porosity
8. Rock properties tests, such as Young's modulus and Poisson's ratio

Desorption tests to determine coalbed gas content can be performed with whole core, sidewall cores, or drill cuttings and have the additional requirement of minimizing lost gas time. After a sample is cut from the native coal seam, gas escapes. Gas emitted by a sample during retrieval and surface handling is obviously not measured and must therefore be estimated. Various procedures for estimation of lost gas are discussed in chapter 4. Regardless of which procedure is employed for lost gas determination, the smaller the fraction of lost gas relative to the desorbed gas volume, the higher the confidence in the total gas content value. Desorption at reservoir temperature, currently industry standard practice, provides smoother and more accurate data than does desorption at ambient conditions, providing a more accurate estimate of lost gas. Procedures for sample collection and desorption tests are discussed in detail by the Gas Research Institute.[32]

Samples for various tests are often selected at the wellsite, directly after retrieval, in order to minimize sample deterioration and, in the case of desorption tests, lost gas. Desorption tests have their own protocols, as discussed in chapter 4. Current industry practice for samples selected for laboratory testing often includes a quick rinse with distilled water to remove drilling mud and other contaminants, then sealing samples in plastic bags, perhaps with moist paper towels, or submerging them in water. Whichever method of sample preservation is chosen, provisions should be made for safely venting any emitted gas. Timely transport of samples to testing facilities helps minimize sample degradation, increasing confidence in any laboratory results.

## Macerals

*Macerals* are the microscopic components of coal and originate from its organic precursors. Macerals are to coal as minerals are to sandstone. Identified optically, macerals fall into three broad groups that change independently during coalification.[33] Maceral names always have the suffix *-inite*.

*Vitrinite macerals*, with a name derived from their glassy appearance under a microscope, are derived from the woody, cellulosic tissues of plants preserved in reducing environments, often abruptly sealed from the atmosphere. Thermally immature vitrinite macerals found in lignites are termed *humitites*. Sorption capacity of a coal often correlates with increasing vitrinite content.[34]

*Liptinite macerals*, also termed *exinites*, are formed from the spores, cuticles, and resins of plants. Hydrogen-rich liptinites are often the source of the paraffinic oils sometimes found in coals.

*Inertinite macerals*, so named because of their lack of chemical reactivity, originate from burned, degraded, or oxidized plant remains. Probably sourced from the same plant components as the other maceral groups but characterized by prolonged atmospheric exposure, inertinites generate little, if any, liquid or gaseous hydrocarbons.[35]

Macerals play an important role in industrial processes requiring coal as a feedstock, such as petrochemicals and metallurgy. A concise review of maceral groups and types and their chemistry is given by Mukhopadhyay and Hatcher.[36] As noted above, sorption capacity of a coal correlates with vitrinite content. Beyond that, at this

time, the role of macerals in coal gas production in unclear, limiting their use in reservoir engineering. Maceral compositions of selected coals are given in table 2–5.

**Table 2–5.** Maceral composition of selected coals

| Seq no. | Geologic age | Rank | Country | Basin | Seam | Vitrinite | Liptinite | Inertinite | Total |
|---|---|---|---|---|---|---|---|---|---|
| 1[a] | Jurassic | subbit. | Australia | Surat | Juandah | 76.3 | 19.0 | 4.7 | 100.0 |
| 2[b] | Jurassic | subbit. | Australia | Surat | Taroom | 79.5 | 19.8 | 0.7 | 100.0 |
| 3[c] | Cretaceous | subbit. | Canada | Horseshoe Canyon | | 86.9 | 2.4 | 10.7 | 100.0 |
| 4[d] | Cretaceous | hi-vol. A | Canada | WCSB | Gates Fmn | 18.0 | 1.0 | 81.0 | 100.0 |
| 5[e] | Cretaceous | med. vol. | Canada | WCSB | Gates Fmn | 69.8 | 0.3 | 30.0 | 100.0 |
| 6[f] | Cretaceous | low vol. | Canada | WCSB | Gates Fmn | 27.7 | 1.7 | 70.7 | 100.0 |
| 7[g] | Carboniferous | hi-vol. | Poland | U. Silesian | na | 64.2 | 10.7 | 25.1 | 100.0 |
| 8[h] | Cretaceous | med. vol. | Canada | WCSB | Gates Fmn | 62.0 | 0.3 | 37.8 | 100.0 |
| 9[i] | U. Permian | hi-vol. A–low vol. | Australia | Sydney | na | 71.1 | 1.4 | 27.5 | 100.0 |
| 10[j] | Pennsylvanian | hi-vol. C | USA | Illinois | various | 78.0 | 12.3 | 9.7 | 100.0 |
| 11[k] | Paleocene | subbit C | USA | Powder | Canyon | 69.2 | 4.9 | 25.9 | 100.0 |
| 12[l] | Paleocene | subbit C | USA | Powder | Canyon | 77.7 | 3.8 | 18.5 | 100.0 |
| 13[m] | Cretaceous | med. vol. | Canada | WCSB | Sheriff | 68.8 | 0.0 | 31.2 | 100.0 |
| 14[n] | Cretaceous | med. vol. | Canada | WCSB | Bennet Dam | 46.7 | 1.4 | 51.9 | 100.0 |
| 15[o] | Cretaceous | semianth. | Canada | WCSB | Canmore | 72.8 | 0.0 | 27.2 | 100.0 |
| 16[p] | Cretaceous | hi-vol. A | USA | Uinta | Ferron | 71.4 | 5.3 | 23.3 | 100.0 |
| 17[q] | Mid- Pennsylvanian | subbit. A/hi-vol. C | USA | Forest City | Marmaton | 88.5 | 3.3 | 8.3 | 100.0 |
| 18[r] | Mid- Pennsylvanian | subbit. B/hi-vol. C | USA | Forest City | U. Cherokee | 83.2 | 2.8 | 14.1 | 100.0 |
| 19[s] | Mid- Pennsylvanian | subbit. C/hi-vol. B | USA | Forest City | L. Cherokee | 74.9 | 4.8 | 20.3 | 100.0 |
| 20[t] | Mid- Pennsylvanian | hi-vol. A | USA | Cherokee | Cherokee | 79.8 | 5.9 | 14.3 | 100.0 |
| 21[u] | Mid- Pennsylvanian | hi-vol. A/lo vol bit | USA | Arkoma | McAlester | 91.6 | 1.3 | 7.1 | 100.0 |
| 22[v] | Mid- Pennsylvanian | med. vol./semianth. | USA | Arkoma | Hartshorne | 87.0 | 0.0 | 13.0 | 100.0 |
| 23[w] | Westphalian B | hi-vol. A | Belgium | Berigen mine | | 37.9 | 18.0 | 44.1 | 100.0 |
| 24[x] | Westphalian A | med. vol. | Belgium | German mine Ruhr distrct | | 89.9 | 0.8 | 9.3 | 100.0 |
| 25[y] | Cretaceous | med. vol. | USA | San Juan | Fruitland | 95.8 | 0.6 | 3.6 | 100.0 |
| 26[z] | Cretaceous | med. vol. | USA | San Juan | Fruitland | 95.8 | 0.5 | 3.7 | 100.0 |
| 27[aa] | Cretaceous | med. vol. | USA | Piceance | Cameo | 95.3 | 1.3 | 3.4 | 100.0 |

*Sources:* [a]Scott, S., Anderson, B., Crosdale, P., Dingwall, J., and Leblang, G. 2004. *Revised Geology and Coal Seam Gas Characteristics of the Walloon Subgroup—Surat Basin, Queensland.* PESA Eastern Australasian Basins Symposium II, Adelaide, September 19–22. [b]Ibid. [c]Chikatamarla, L., and Bustin, R. M. 2003. Sequestration potential of acid gases in Western Canadian coals. Paper 0630 in *Proceedings of the 2003 International Coalbed Methane Symposium.* Tuscaloosa: University of Alabama. [d]Lamberson, M. N., and Bustin, R. M. 1993. [e]Ibid. [f]Ibid. [g]Van Bergen, F., Pagnier, H. M..M., van der Meer, L. G. H., van den Belt, F. J. G., Winthaegan, P. L. A., and Kryzstolik, P. 2003. Development of a field experiment of ECBM in the Upper Silesian Coal Basin of Poland (RECOPOL). Paper 0320 in *Proceedings of the 2003 International Coalbed Methane Symposium.* Tuscaloosa: University of Alabama. [h]Clarkson, C. R., and Bustin, R. M. 1999. The effect of pore structure and gas pressure upon the transport properties of coal: A laboratory and modeling study. 1. Isotherms and pore volume distributions. *Fuel.* V. 78 (no. 11). p. 1,333. [i]Bustin, R. M. 1997. [j]Mastalerz, M., and Kvale, E. P. 2000. *Coal Quality Variation and Coalbed Gas Content in Boreholes SDH-383 and SDH-384 in Posey County, Indiana.* IGS Open-File Study 00-5. Bloomington: Indiana Geological Survey. [k]Pratt, T. J., Mavor, M. J., and DeBruyn, R. P. 1999. [l]Ibid. [m]Chikatamarla, L., and Bustin, R. M. 2003. [n]Ibid. [o]Ibid. [p]Lamarre, R. A., and Pratt, T. J. 2002. Reservoir characterization study: Calculation of gas-in-place in Ferron Coals at Drunkard's Wash Unit, Carbon and Emery counties, Utah. *The Mountain Geologist.* V. 39 (no. 2). p. 41. [q]Pratt, T. J., and Mavor, M. J. 2005. *An Overview of Coal Gas Reservoir Properties: Core Holes from Western Interior Coal Region.* Oklahoma Geological Survey Circular 110. Norman: University of Oklahoma. [r]Ibid. [s]Ibid. [t]Ibid. [u]Ibid. [v]Ibid. [w]Wolf, K-H. A. A., Hijman, R., Barzandji, O. H., and Bruining, J. 1999. [x]Ibid. [y]Jones, A. H., Ahmed, U., Bush, D. D., Holland, M. T., Kelkar, S. M., Rakop, K. C., Bowman, K. C., and Bell, G. J. 1984. *Methane Production Characteristics for a Deeply Buried Coalbed Reservoir in the San Juan Basin.* SPE/DOE/GRI 12876. Presented at the 1984 SPE/DOE/GRI Unconventional Gas Recovery Symposium, Pittsburgh, Pennsylvania, May 13–15. [z]Bell, G. J., Seccombe, J. C., Rakop, K. C., and Jones, A. H. 1985. *Laboratory Characterization of Deeply Buried Coal Seams in the Western U.S.* Paper SPE 14445. Presented at the SPE Annual Technical Conference and Exhibition, Las Vegas, Nevada, September 12–25. [aa]Ibid.

## Cleats

Coal is a naturally fractured reservoir with two distinct sets of natural fractures called cleats. The dominant fracture system, termed *face cleat*, is comprised of well-developed, throughgoing, nearly parallel fissures. The secondary fracture system, termed *butt cleat*, is perpendicular to the face cleat and is characterized by less-well-developed fractures of limited length, also roughly parallel, and often terminating at a face cleat. Both sets of cleats, face and butt, are nominally vertical, perpendicular to the bedding planes. Cleats and other natural

fractures are the primary flow conduits in a coal seam and contain most of the moveable water but little sorbed gas. Some coals initially have free gas present in the cleats, while others are completely water saturated.

Face cleats are often planar, while butt cleats are less so. Cleats are opening-mode fractures, with little, if any, shearing or offset across the aperture. Fracture spacing for both face and butt cleats ranges from fractions of a millimeter to centimeters and is frequently less than bed, or lithotype, thickness.[37] Cleat spacing of San Juan and Warrior coals ranges from 0.3 to 5 $cm^3$.[38] Fracture spacing observed in a sample taken from the Harbour Coal seam, Nova Scotia, Canada varied from 0.5 to 7.3 $cm^3$.[39] Bustin reported fracture spacings from 0.02 to 5 mm in high-volatile A to low-volatile bituminous rank samples of Upper Permian coals from the Sydney Basin of Australia.[40] Fracture spacing of subbituminous coal from the Western Canadian Sedimentary Basin of Canada measured 0.1 cm, while that of high-volatile C bituminous coals from this basin was 0.5 $cm^3$.[41] Characterization of the size distribution of mined coal fragments implies a power law distribution for cleat spacing within a particular seam.[42]

Cleat height is variable, ranging from microscopic to seam thickness. A qualitative hierarchy of cleat height includes *master cleats*, with heights roughly equal to seam height, *primary cleats*, which cross several beds or lithotypes within a seam, *secondary cleats*, confined to a single bed, and *tertiary cleats*, poorly formed fissures confined to a single bed. Work by Laubach et al. suggests a power law relationship for cleat height within a given seam.[43]

In-situ cleat width affects coal seam permeability but is very difficult to quantify. Close estimated that aperture widths seen in coal cores from the northern San Juan Basin, ranging in size from 0.01 mm to 0.30 mm, were narrowed in situ down to 0.1 mm to 0.0001 mm.[44] Cleat widths estimated below from typical cleat spacings and porosities range from 1 to 40 microns (0.001 mm to 0.040 mm). From San Juan Basin core studies, Laubach et al. found a power law relationship between cumulative cleat frequency and aperture width.[45] With different power law constants for each core, application of this relationship to in-situ coals is limited.

Cleat length, height, and aperture are loosely correlated. Longer cleats tend to have greater vertical development, often cutting across several lithotypes or beds, and exhibit wider apertures. Shorter cleats exhibit limited vertical growth and narrow apertures.

Cleat strike is influenced by several different factors, with paleostress orientation being a principal control. Face cleats form parallel to the maximum compressive paleostress. *Cleat domains*, areas with similar cleat strike, range in size from several thousand square kilometers down to less than the area of a coal mine working the seam.[46] Close noted that face and butt cleats in many U.S. coal basins are oriented perpendicular and parallel, respectively, to major fold axes in the basin.[47] Boundaries between cleat domains can be abrupt or gradational. An example of the latter, given by Laubach et al., is in the San Juan Basin where the cleat domain on the northern San Juan Basin, with northwest trending cleats, meets that of the southern San Juan basin, with northeast trending cleats.[48] This gradational transition zone, with two sets of cleats, is coincident with the high productivity fairway of the basin.

The interplay between maturation and paleostresses in the Piceance Basin yield northeast striking cleats in the southern portion of the basin and northwest striking cleats in the northern portion of the basin.[49] Peats throughout the basin matured uniformly through lignites. Coals in the southern portion of the basin matured to subbituminous A rank 22 million years after deposition, while coals in the northern portion of the basin did not reach this maturity until 31 million years after deposition. Changes in stress orientation during coalification resulted in the different cleat orientations.

Cleat strike can vary stratigraphically. While rapid changes in paleostress orientation could conceivably result in different cleat strikes in adjacent seams, variation in cleat orientation is more common between coals in different formations. Laubach et al. note that Cretaceous and Tertiary coals in the same area of the Piceance Basin have different cleat strikes.[50]

Cleats occur in coals of all geologic ages and are related to coal rank. Cleat development begins in lignites, which often exhibit poorly developed cleats with irregular spacing and limited lengths. Bituminous coals frequently show well-developed face and butt cleats with small fracture spacings. Anthracites are often poorly cleated due to cleat healing during metamorphosis. For a given rank, brighter coal lithotypes (vitrain, clarain)

exhibit more intense cleating than do dull lithotypes (durain). Better cleat development is associated with less mineral matter and ash.

Origins of coal cleats are unknown but are probably diverse.[51] Cleats probably result from the interplay of several factors in addition to the paleostresses discussed above. Considerable water is expelled during coalification, especially at low maturities, making dessication one of the cleating mechanisms. Devolitalization occurs as various hydrocarbons are driven off a coal during maturation, and the resulting structural changes on a microscopic scale contribute to cleat formation. At very high ranks, as the polymeric coal fabric becomes increasingly aromatic, molecular rearrangement serves to anneal cleats.

## Coal Porosity

*Coal porosity* is the void space of this naturally fractured organic rock, which has a wide spectrum of pore sizes. Coal gas reservoir engineering is often concerned only with *mobile water porosity*, defined as the void space of a coal containing water that will flow through the fractures in response to an applied pressure differential. This is the porosity that is emptied, partially or totally, during "dewatering" and is suspected to be primarily cleat, macropore, and perhaps some mesopore porosities. Mobile water porosity does not include bed moisture or other immoveable water in the reservoir. Mobile water porosity is the void fraction of a coal deposit that conveys gas and water to a wellbore, and fluid flow is described by Darcy's law in conjunction with two-phase gas-water relative permeabilities. A review of various coal porosity definitions provides a better conceptual understanding of mobile water porosity but no definitive method for its measurement.

Separation of coal void space into cleat and matrix porosities for reservoir engineering purposes is artificial but useful. As estimated below, cleat or fracture porosity is on the order of 1% or less, typical of naturally fractured reservoirs.[52] Porosity of the coal matrix is comprised of irregularly shaped voids in the organic matrix. Some of the porosity is due to relict plant material, while some is the product of coalification. At the molecular level, coal is a tangle of long, complex polymers yielding highly irregular pores. Experimental evidence indicates the characteristic dimension of these voids in the matrix, often termed *pore diameter*, can vary in size by two orders of magnitude.[53] Organic components of a coal metamorphose with thermal maturation, resulting in rank-dependent pore size distributions. Regardless of geological age, rank, or purity, porosity of a coal deposit is difficult to quantify. Cleat porosities are typically estimated from conceptual models or simulation history matches, while matrix porosities are determined indirectly from laboratory experiments.

One of the conceptual models for quantifying cleat porosities combines permeabilities determined from well tests with cleat spacings observed in coal cores and hand samples. Assuming a coal deposit can be idealized as a collection of matchsticks, cleat permeability is related to cleat spacing and porosity by[54]

$$k_f = 1055.47 d^2 \phi_f^3$$

where

$k_f$ = cleat permeability, md,
$d$ = cleat spacing, cm, and
$\phi_f$ = cleat porosity, %.

Solving for cleat porosity,

$$\phi_f = 0.09822 \left[ \frac{k_f}{d^2} \right]^{1/3} \tag{2.3}$$

Cleat width is related to cleat porosity and cleat spacing by[55]

$$b = 50 d \phi_f \tag{2.4}$$

where

$b$ = cleat width, microns.

As noted above, cleat spacing can vary by two orders of magnitude. Assuming bounding permeabilities of 0.1 and 100 md and cleat spacing limits of 0.2 and 5 cm in equation (2.3) yields cleat porosities of 1% down to 0.02%. Cleat apertures, calculated from equation (2.4), range from 1 to 40 microns.

Techniques available for characterization of coal matrix porosity include low-pressure nitrogen and $CO_2$ sorption analysis, mercury and helium porosimetry, and mercury injection. However, none of these techniques provide a direct measure of the total pore volume available to methane and $CO_2$, the primary gases present in coals. Carbon dioxide can access smaller pores than other adsorbates, and low-pressure (up to 1 atm), low-temperature (0°C, 32°F) $CO_2$ sorption is commonly used to investigate microporosity of coals. Porosities derived from low-pressure sorption of nitrogen at –196°C (–321°F) are indicative of mesoporosities. Helium and mercury porosimetry are utilized to investigate total open pore volume of the samples.

Gan et al. reported porosities of American coals, dividing them into groups with diameters less than 1.2 nm, diameters between 1.2 and 30 nm, and pores with diameters greater than 30 nm.[56] Complete sample histories were not given, but measured porosities were not in-situ porosities, as the final steps in sample preparation involved heating sieved samples at 105°C (221°F) for 1 hr before degassing for 12 hr at 130°C (266°F) or 2 hr at room temperature. Thus, porosities reported by Gan et al., ranging from 4.1% to 23.2%, are almost certainly greater than in-situ porosities; however, the observed trends are probably correct. Total porosities of the laboratory samples, plotted as a function of fixed carbon (FC), % daf, in figure 2–2, decrease with increasing rank. The fraction of porosity in the smallest pores steadily increases with %C, daf, as shown in figure 2–3, while that of the largest pores shows the opposite trend. The porosity of pores of intermediate diameters is significant in subbituminous through high-volatile B bituminous rank samples. Porosity of low-rank coals, < 75% fixed carbon content, was primarily due to macropores. Porosity of medium-rank coals, with fixed carbon between 76% and 84%, was comprised mainly of micro and transitional pores. In high-rank coals, with fixed carbon > 85%, porosity was mostly due to micropores.

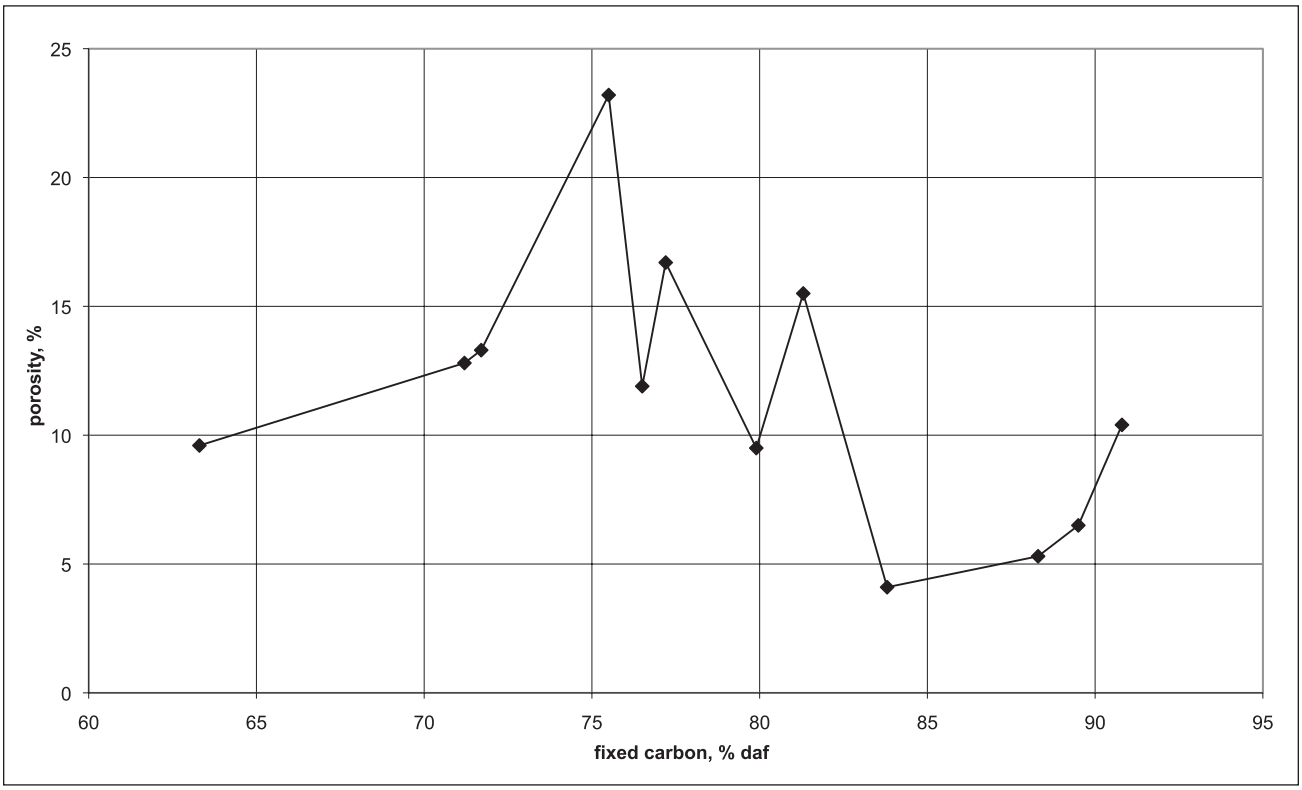



**Fig. 2–2.** Coal porosity vs. fixed carbon, % daf[57]

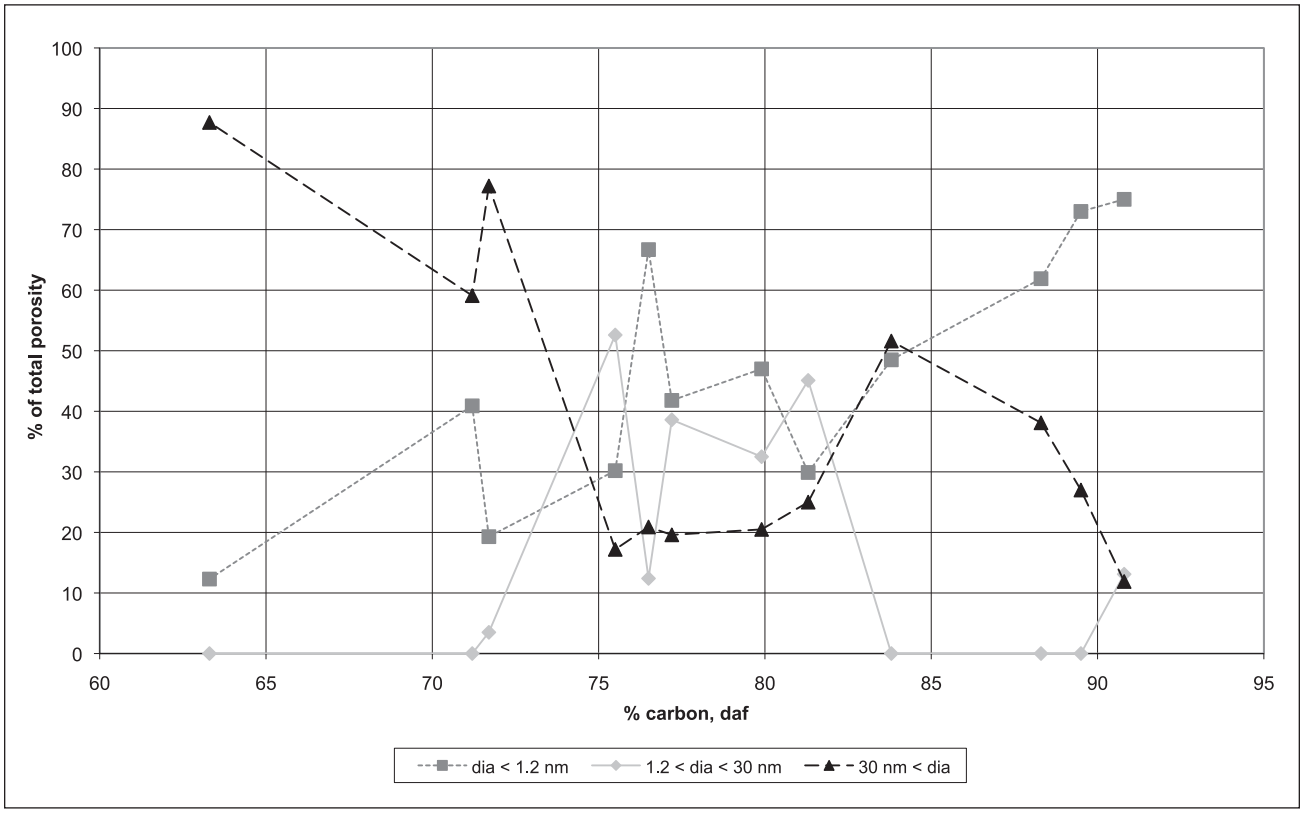



**Fig. 2–3.** Coal porosity distributions vs. rank[58]

The effect of maceral type on coal porosity was partially addressed by Gan et al. in reporting vitrinite fraction of the porosity samples on a mineral-matter-containing basis (mmcb).[59] As seen in figure 2–4, total coal porosity is roughly proportional to the volume percent vitrinite, but the significant scatter indicates a secondary control, probably mineral matter.

Levine defined water porosity as the volume percent water on an ash-free basis.[60] Water porosity of bituminous coals varied with rank, declining from a maximum of 22% in coals with 81% carbon on a dry, mineral-matter-free basis (high-volatile bituminous) to a minimum of 2% at 90% carbon (low-volatile bituminous), then rebounding to 6% at 95% carbon (anthracite). Experimental methods and sample histories were not specified, complicating extrapolation of these results to in-situ conditions.

Porosities of selected North American and Australian coals were characterized by Bustin and Clarkson using the International Union of Pure and Applied Chemistry (IUPAC) pore size classifications of micropores (diameters less than 2 nm), mesopores (diameters between 2 and 50 nm), and macropores (diameters greater than 50 nm).[61] This study found that total porosity decreases with rank, primarily due to a decline in macro and mesoporosities. In contrast, micropore volume increased with coal rank. These trends are in agreement with those of Gan et al., discussed above.[62]

Although this study had a very limited number of samples, total porosity declined from an average of 13% in the subbituminous samples to an average of 4% in the medium-volatile samples. Complete sample histories were not discussed; therefore, these reported porosity values are probably higher than in-situ coal porosities. Modal pore size for microporosity in coals of all ranks was approximately 1.2 nm, whereas mesoporosity peaked at about 4 nm in all samples with experimental indications of slit-shaped pores. For perspective, molecular diameters of gases typically found in coals are on the order of 0.5 nm.

Variation of total porosity as a function of maceral composition was not specifically addressed, but micropore porosity was seen to increase with increasing vitrinite on a mineral-matter-free basis. Bright, vitrinite-rich coals had a greater micropore volume fraction than dull, vitrinite-poor coals of equivalent rank. In contrast, the dull coals had a greater fraction of meso and macropore porosity than did the bright coals.

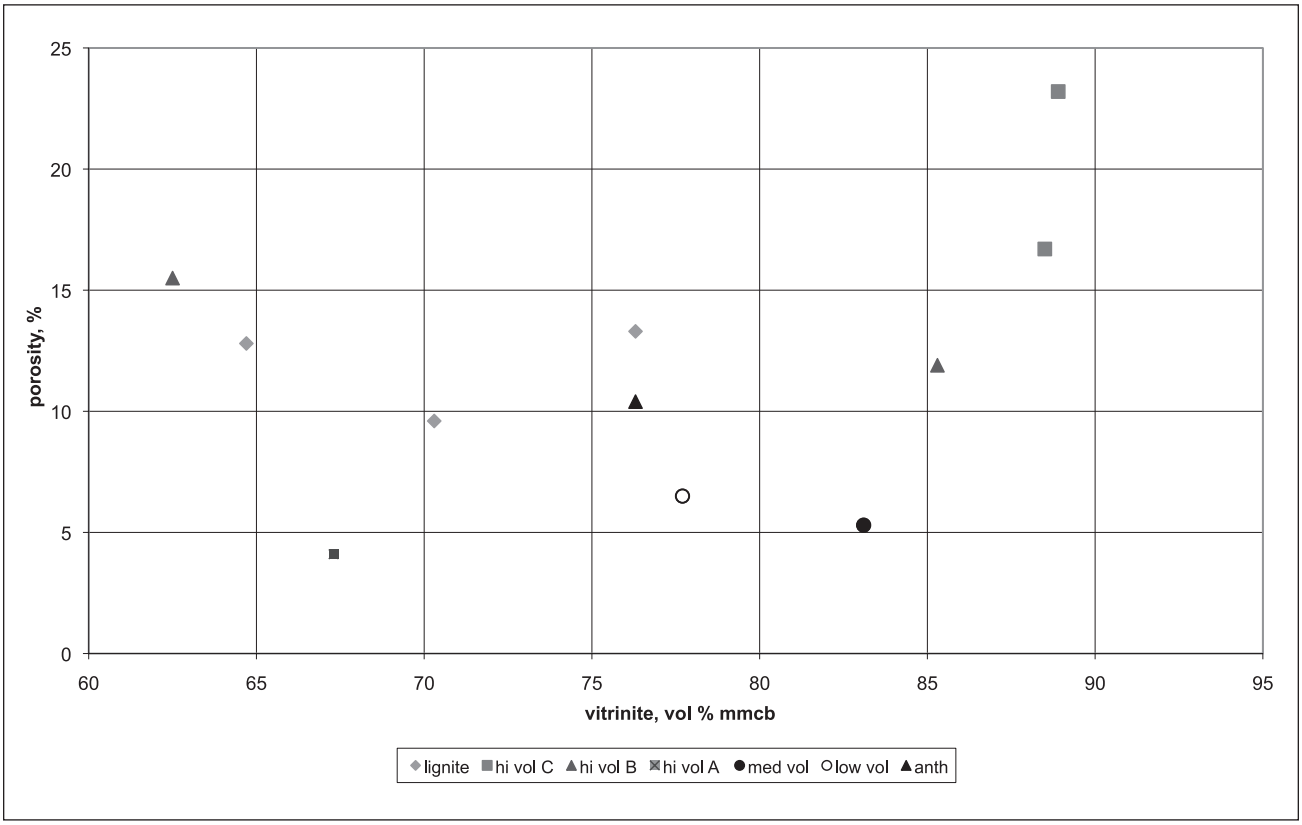



**Fig. 2–4.** Total porosity vs. vitrinite (mmcb = mineral-matter-containing basis)[63]

Sorbed gas volumes at a reservoir pressure 6 MPa (870 psia), calculated from methane sorption isotherms and assuming a sorbed gas density of 0.42252 g/cm$^3$, were compared with total porosity measurements. The comparisons led to the conclusion that sorbed gas occupied more than 90% of total porosity in the semianthracite sample, more than 60% of total porosity of the medium-volatile bituminous sample, and less than 10% of the high-volatile bituminous and subbituminous samples. Thus in high-rank coals, sorption is the dominant storage mechanism, whereas low-rank coals can hold significant free gas volumes compressed in the pores.

Nelson found that *effective porosity*, defined as the ratio of interconnected cleat volume to bulk coal volume, of Fruitland coals of the San Juan Basin was linearly related to effective stress and vitrinite reflectance.[64] Although increasing effective stress decreased effective porosity for a given sample, opposite behavior was noted for a collection of samples, indicating the role of areal and stratigraphic stress variations cannot be neglected. Effective porosities ranged from 0.6% to 1.2%.

Porosity sensitivity to stress in Carboniferous coal mine samples was reported by Wolf et al.[65] The Belgian coal was high-volatile A bituminous in rank with 44% inertinite, while the German sample was medium-volatile bituminous rank and 87% vitrinite. Initial porosities of the Belgian coal, 2% to 5.5%, decreased to 0.5% when subjected to a stress of 6 MPa (870 psi). Initial porosities of the German coal, 5.5% to 6.5%, decreased to 5.0% under the same stress loading, indicative of a stiffer coal. As the samples were vacuum dried for 24 hr and perhaps autoclaved prior to testing, reported porosities are greater than native porosities, but the overall trend of porosity reduction with stress is correct.

Simulation studies often vary coal fracture porosity, among other reservoir properties, to match performance of a well or a field. Porosities obtained from such history matching exercises are often on the order of 0.5% or less, similar to cleat porosities estimated above. Conway et al. reported a "natural fracture mobile water porosity" of 0.53% from simulation of wells completed in the Blue Creek coal in the Warrior Basin.[66] A simulation history match of Fruitland coal wells in the Tiffany area of the San Juan Basin by Ramurthy et al. yielded a porosity of 0.25%.[67] Using a blend of well test analysis and simulation, Mavor obtained a porosity of 0.45% for a well in the fairway of the San Juan Basin.[68] A modeling study of production from Rock Springs Formation coals of the Great

Divide (Greater Green River) Basin by Young et al. resulted in a porosity of 1.2%.[69] However, these simulation porosities are probably lower than actual porosities for several reasons.

Simulated water production is affected by gas-water relative permeabilities, which often have an irreducible water saturation of zero, implying the model is concerned only with mobile water porosity. This simulation porosity represents water that is important for production operations and does not reflect the true void space of a coal deposit. In addition, coal gas simulations typically use a single model layer for each coal seam, rarely breaking an actual seam into multiple model layers. This approach, while computationally efficient and often sufficient for prediction of gas and water production, neglects buoyancy-driven vertical segregation of gas and water within a seam. Gas flowing across the upper one-third or one-half of a coal with 1% or 2% total porosity is thus described in a simulator using porosities of only a fraction of a percent.

Coal porosity is smaller than that of conventional reservoirs and difficult to determine. Cleat porosities calculated from a matchstick model with reported permeabilities and observed cleat spacing yields porosities of 1% or less. Coal matrix porosities measured in laboratory studies are typically on the order of a few percent. As most studies utilize samples of uncertain history held at conditions other than in situ, these reported porosities provide an upper bound on in-situ porosities. Simulation-derived coal porosities are on the order of 1% or less but suffer from inclusion of other physics, such as buoyancy and capillary pressures, which are not treated explicitly in the reservoir model. For reservoir engineering purposes, porosity of subbituminous coals is often assumed to be 10%, while that of bituminous coals is assumed to be 1%.

## Coal Density

Coal density is less than that of conventional reservoir rocks and is highly variable, depending primarily on rank and purity. Coal seams are often identified in a wellbore by wireline log density response in conjunction with gamma ray, caliper, and other logs. Volumetric calculation of original gas in place depends on coal density and can be affected by choice of density cutoff. Bulk coal density includes the organic and inorganic fractions of this rock and the voids it contains, which are often water filled. In contrast, coal matrix density is often termed *grain density* or *helium density* after the gas used in its measurement.

In comparison to the densities of amorphous carbon, 1.80 to 2.10 g/cm$^3$, and graphite, 2.25 g/cm$^3$, densities of mineable coals are less, ranging from 1.25 to 1.70 g/cm$^3$, and generally increase with coal rank.[70] The presence of ash and moisture often dominates coal density, resulting in a high-ash, low-rank coal that is more dense than a low-ash, high-rank coal. A method for determining densities of the organic and ash fractions from laboratory densities of a set of samples is outlined below. In the absence of such laboratory data, assumed organic and ash fraction densities of 1.25 and 2.55 g/cm$^3$, respectively, are usually sufficient for reservoir engineering purposes.

Idealizing coal as a three-component mixture of organic rock, ash, and moisture with no free or sorbed gas, bulk coal density can be written as

$$\rho = \frac{1}{\frac{1-a-w}{\rho_o} + \frac{a}{\rho_a} + \frac{w}{\rho_w}} \tag{2.5}$$

where

$\rho$ = coal bulk density, g/cm$^3$,
$\rho_o$ = organic fraction density, g/cm$^3$,
$\rho_a$ = ash density, g/cm$^3$, and
$\rho_w$ = water density, g/cm$^3$.

As noted above, Schopf defined coal as a rock that is at least 50% by weight and 70% by volume carbonaceous material.[71] Assume the density of the organic fraction of coal is 1.25 g/cm$^3$, the ash density is 2.55 g/cm$^3$, and

density of the water held in the coal is 1.00 g/cm³. Further assume a bituminous coal with an equilibrium moisture of 3%. Thus, this coal is 47% ash with a density of

$$\rho = \frac{1}{\frac{0.50}{1.25\ \frac{g}{cm^3}} + \frac{0.47}{2.55\ \frac{g}{cm^3}} + \frac{0.03}{1.00\ \frac{g}{cm^3}}}$$

$$\rho = 1.63\ \frac{g}{cm^3}$$

Assuming a subbituminous coal with an equilibrium moisture of 23% and repeating the calculation yields a density of

$$\rho = 1.36\ \frac{g}{cm^3}$$

Experience shows that while the above densities provide reliable pay cutoffs for identifying mineable coal, they are often too conservative for defining a coal reservoir, as higher density rocks can hold substantial volumes of gas. Current coal gas reservoir engineering practice employs a coal pay cutoff of 2.0 g/cm³. Assuming 3% equilibrium moisture, this density cutoff corresponds to an ash fraction of 75%, whereas an equilibrium moisture of 23% yields an 84% ash fraction.

Density of the organic fraction of a coal depends on maceral composition and can be calculated from

$$\rho_o = \rho_v V_v + \rho_l V_l + \rho_i V_i \tag{2.6}$$

where

$\rho_v$ = vitrinite density, g/cm³,
$\rho_l$ = liptinite density, g/cm³,
$\rho_i$ = inertinite density, g/cm³,
$V_v$ = volume fraction vitrinite,
$V_l$ = volume fraction liptinite, and
$V_i$ = volume fraction inertinite.

Average vitrinite, liptinite, and inertinite maceral densities reported by Mavor and Nelson are 1.29, 1.18, and 1.35 g/cm³, respectively.[72] Maceral density varies with coal rank and perhaps geological age.[73] However, for reservoir engineering purposes, the organic fraction of a coal deposit can be estimated from a maceral distribution and the average maceral densities of Mavor and Nelson.

Densities of the organic fraction and the ash can be estimated from proximate analyses and bulk densities. Equation (2.5) can be rewritten as

$$\frac{\frac{1}{\rho} - \frac{w}{\rho_w}}{1 - w} = \frac{a}{1 - w}\left(\frac{1}{\rho_a} - \frac{1}{\rho_o}\right) + \frac{1}{\rho_o} \tag{2.7}$$

The left-hand side of this relation is termed the *reciprocal dry density*, and inspection of the equation shows it to be linearly related to the *dry ash weight fraction*, defined as the ash fraction divided by one minus the equilibrium moisture fraction.

A correlation relating in-situ gas content of a fully saturated coal to wireline log density can be developed from the above equations. Construction of such a relation requires substantial and expensive field and laboratory tests on samples from the initial corehole(s) or well(s). However, once developed, it minimizes coring time and costs required to estimate gas in place of a particular property or play. Solving equation (2.5) for ash fraction as a function of coal density gives

$$a = \frac{\frac{1}{\rho} - \left(\frac{w}{\rho_w} + \frac{1-w}{\rho_o}\right)}{\frac{1}{\rho_a} - \frac{1}{\rho_o}} \tag{2.8}$$

The equilibrium moisture fraction, $w$, is available from proximate analyses, while coal water density is typically assumed to be 1.0 g/cm$^3$. Densities of the organic fraction and ash are determined from the intercepts of equation (2.7). Density of the organic fraction of a coal can also be calculated from equation (2.6) if the maceral distribution is known.

As the coal is saturated, gas content can be calculated from pressure and the Langmuir isotherm

$$V = V_{Ldaf}(1 - a - w)\frac{p}{p + p_L} \tag{2.9}$$

where

$V$ = gas content, scf/t or cm$^3$/g,
$V_{Ldaf}$ = dry, ash-free Langmuir volume constant, scf/t or cm$^3$/g,
$p$ = pressure, psia or MPa, and
$p_L$ = Langmuir pressure constant, psia or MPa.

Determination of ash and organic densities and construction of a bulk density–gas content curve are illustrated in the following example.

## Example 2.3. Organic fraction and ash density of San Juan Basin Fruitland coal

Coal bulk densities and ash and moisture fractions for Fruitland coal from San Juan Basin reported by Mavor and Nelson are shown in table 2–6.[74] The samples were sourced from the Valencia Canyon 32-1 well. Reciprocal dry density, based on a brine density of 1.0 g/cm$^3$, is plotted as a function of dry ash weight fraction in figure 2–5. Fitting equation (2.7) to the data gives the line shown in the figure. The vertical axis intercept of that line gives an organic fraction density of 1.181 g/cm$^3$, while the horizontal axis intercept yields an ash density of 2.384 g/cm$^3$.

**Table 2–6.** Density, ash, and moisture—Valencia Canyon 32-1, Fruitland coal, San Juan Basin

| Seq. no. | Density, g/cm$^3$ | Ash, fraction | Moisture, fraction | Dry ash fraction | Reciprocal dry density, g/cm$^3$ |
|---|---|---|---|---|---|
| 1 | 1.40 | 0.078 | 0.012 | 0.079 | 0.711 |
| 2 | 1.26 | 0.082 | 0.018 | 0.083 | 0.790 |
| 3 | 1.25 | 0.105 | 0.014 | 0.107 | 0.797 |
| 4 | 1.24 | 0.115 | 0.023 | 0.118 | 0.802 |
| 5 | 1.10 | 0.177 | 0.007 | 0.178 | 0.908 |
| 6 | 1.28 | 0.244 | 0.008 | 0.246 | 0.780 |
| 7 | 1.72 | 0.488 | 0.007 | 0.491 | 0.578 |
| 8 | 1.80 | 0.649 | 0.013 | 0.657 | 0.550 |
| 9 | 1.82 | 0.749 | 0.026 | 0.769 | 0.537 |
| | | | Average moisture = 0.143 | | |

*Note:* Water density = 1.0 g/cm$^3$.
*Source:* Mavor, M. J., and Nelson, C. R. 1997.

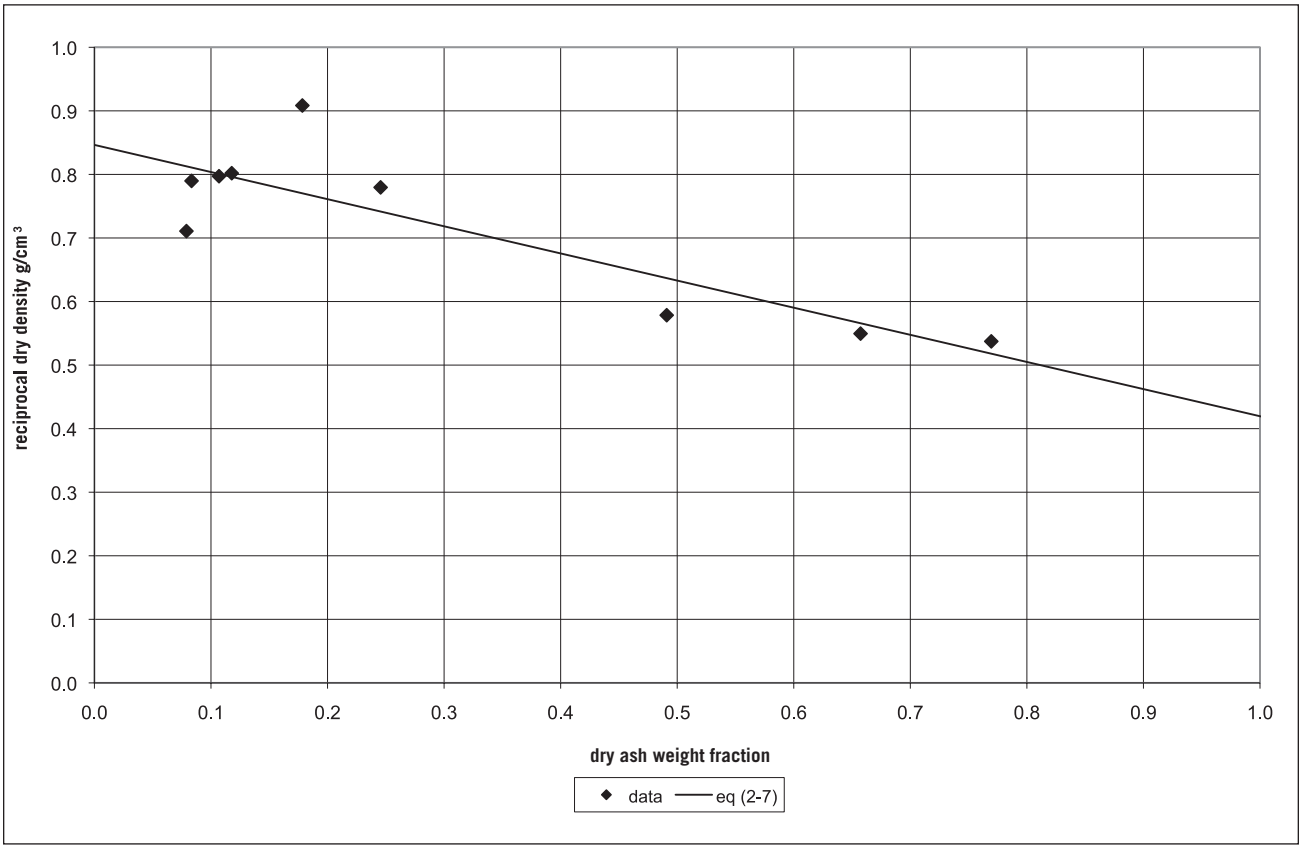



**Fig. 2–5.** Reciprocal dry density vs. dry ash weight fraction

Average maceral composition of this data set is 84.6% vitrinite, 3.1% liptinite, and 12.3% inertinite. Density of the organic component calculated from equation (2.6) with these maceral fractions and the maceral densities of Mavor and Nelson given above is 1.294 g/cm$^3$, higher than the intercept-based value derived above by about 10%. The computed ash density of 2.384 g/cm$^3$ is slightly lower than densities of materials typically comprising coal ash. For example, density of kaolinite is 2.42 g/cm$^3$, quartz is 2.65 g/cm$^3$, and feldspar ranges from 2.55 to 2.76 g/cm$^3$. Mineralogy of the coal ash was not discussed by Mavor and Nelson, and reasons for this low computed ash density are not known.

Mavor and Nelson report the Valencia Canyon 32-1 dry, ash-free Langmuir volume constant as 946.9 scf/t, and the Langmuir pressure constant as 368.5 psia. Average equilibrium moisture for this set of samples is 0.0143. The coal is slightly overpressured, with an initial reservoir pressure of 761 psia. Utilizing these constants in equations (2.8) and (2.9) yields the relation between coal density and gas content shown in figure 2–6.

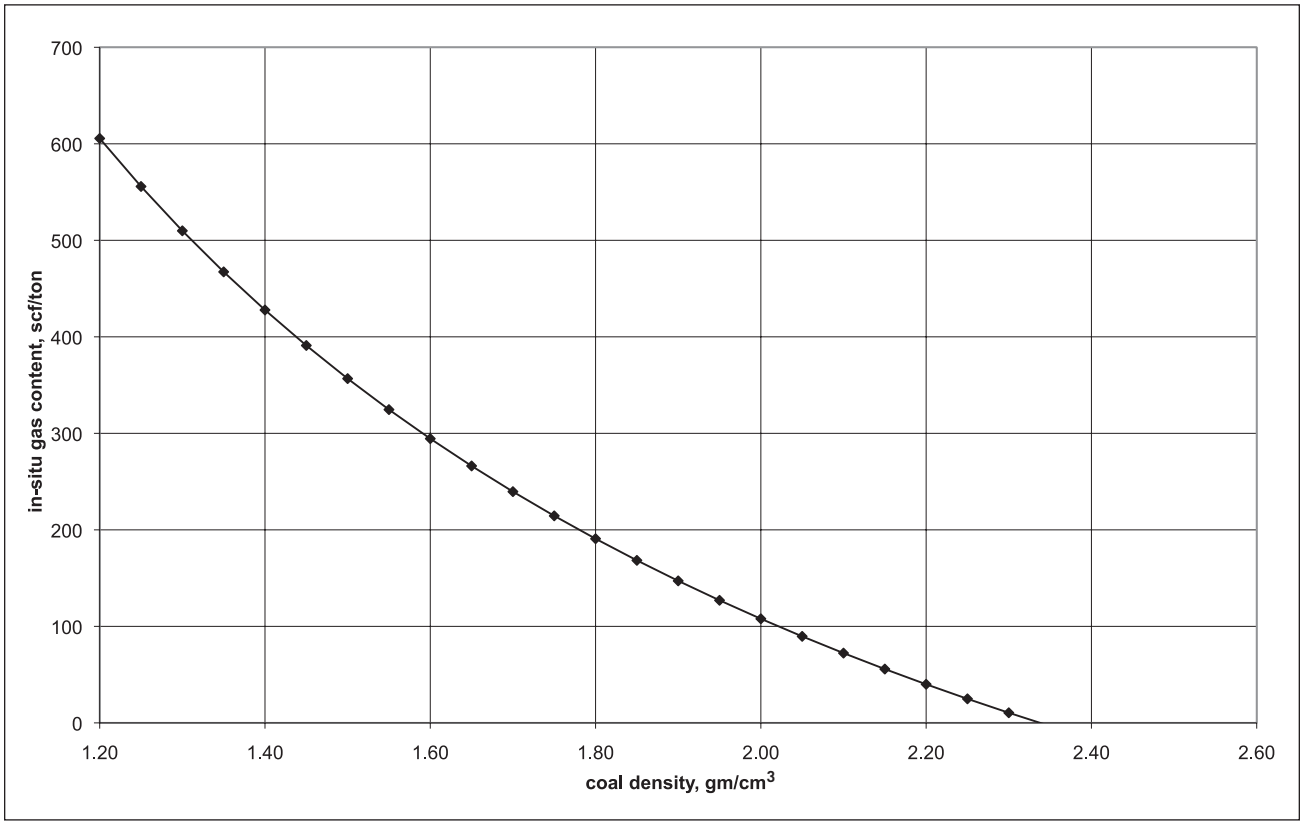



**Fig. 2–6.** Example 2.3 in-situ gas content vs. density correlation

## Coal Gas Composition and Gas Properties

Coal gas is predominantly methane, with minor amounts of nitrogen, $CO_2$, and heavier hydrocarbons. Composition of gas produced from a coal varies with depletion. Weakly sorbed species, such as methane and nitrogen, are released from the matrix before strongly sorbed species, such as $CO_2$ and ethane. Consequently, the produced gas stream from a well, project, or basin is characterized by steadily rising fractions of $CO_2$ and heavier hydrocarbon gases. Gas composition from eight U.S. coal basins averaged 93% methane, 3% each of $CO_2$ and wet gases, and 1% percent nitrogen.[75] Heating value of coal gas from these eight basins was approximately 1,000 Btu/scf, and *gas dryness indices*, defined as the methane fraction divided by the sum of methane through pentane fractions, ranged from 0.77 to 1.00.[76] Reported gas compositions from selected coals are in table 2–7.

**Table 2–7.** Selected coal gas compositions

| Seq no | Basin | Coal | Age | Rank | C1 | C2+ | $CO_2$ | $N_2$ | Total |
|---|---|---|---|---|---|---|---|---|---|
| 1 | Forest City | Upper Cherokee | Mid-Pennsylvanian | subbit. B | 81.2 | 1.2 | 0.0 | 17.6 | 100.0 |
| 2 | Forest City | Lower Cherokee | Mid-Pennsylvanian | hi-vol. B | 82.8 | 2.3 | 1.3 | 13.5 | 99.9 |
| 3 | Cherokee | Marmaton | Mid-Pennsylvanian | na | 60.8 | 19.4 | 6.0 | 13.8 | 100.0 |
| 4 | Cherokee | Cherokee | Mid-Pennsylvanian | hi-vol. A | 92.5 | 4.0 | 1.7 | 1.9 | 100.1 |
| 5 | Arkoma | MacAlester | Mid-Pennsylvanian | med. vol. | 95.1 | 2.5 | 0.5 | 1.8 | 99.9 |
| 6 | Arkoma | Hartshorne | Mid-Pennsylvanian | lo-vol. | 92.5 | 6.6 | 0.5 | 0.4 | 100.0 |
| 7 | Powder River | Canyon | Paleocene | subbit C | 90.3 | 0.0 | 7.8 | 1.9 | 99.99 |

*na = not available*

*Source:* Pratt, T. J., Mavor, M. J., and DeBruyn, R. P. 1999; and Pratt, T. J. and Mavor, M. J. 2005. *An Overview of Coal Gas Reservoir Properties: Core Holes from Western Interior Coal Region.* Oklahoma Geological Survey Circular 110. Norman: University of Oklahoma.

Coal gas composition depends primarily on coal rank and gas origin. Coal gas is predominantly methane, with the fraction of ethane and heavier hydrocarbons (C2+) steadily decreasing as rank increases. Wetter gases are more often found in subbituminous and high-volatile C bituminous coals, and leaner gases in higher rank coals. Thermogenic gases can have higher hydrocarbons (ethane, propane, butane, etc.) present, whereas biogenic gases are almost pure methane. Compared to conventional hydrocarbon plays, coals are cool, low-pressure reservoirs holding gas mixtures composed almost entirely of methane. Condensation of hydrocarbon liquids occurs rarely, if at all, in coal deposits. For reservoir engineering purposes, coals can be conceptualized as dry gas reservoirs. Consistent with this dry gas reservoir concept, coal gas mixtures remain above dewpoint pressure in the wellbore and surface equipment. More important for coal gas operations are corrosion, due to the presence of moisture and the steadily rising $CO_2$ fraction in the produced gas stream, and liquid loading in flowing coal wells due to produced and/or condensed water.

Gas properties of coal gas can be calculated similarly to conventional dry gas reservoirs as detailed in Lee and Wattenbarger or McCain.[77] Coal gas is assumed to be described by the real gas law, which can be written as

$$pV = ZnRT$$

where

$p$ = pressure, psia or MPa,
$V$ = volume, ft$^3$ or m$^3$,
$Z$ = gas deviation factor or compressibility factor,
$n$ = number of moles,
$T$ = temperature, °R or K, and
$R$ = Universal gas constant, 10.732 psia-ft$^3$/lb-mol-°R or 8.297(10)$^{-3}$ MPa-m$^3$/kg-mol-K.

Calculation of the Z factor begins with gas composition or gas gravity. Gas gravity is employed to calculate pseudocritical and reduced temperature and pressure, followed by calculation of the Z factor. If gas composition is known, gas gravity is calculated from

$$\gamma_g = \frac{\sum_j y_j M_j}{M_a}$$

where

$\gamma_g$ = gas gravity,
$y_j$ = mole fraction of component $j$,
$M_j$ = molecular weight of component $j$, and
$M_a$ = molecular weight of air, 28.96.

Molecular weights of common coal gases are collected in table 2–8.

*Critical temperature* and *critical pressure* (the *critical point*) of a pure substance are the temperature and pressure at which the properties of the liquid and vapor phases are identical. *Reduced temperature* and *reduced pressure* are defined as temperature and pressure divided by their respective critical values.

$$T_r = \frac{T}{T_c}$$

$$p_r = \frac{p}{p_c}$$

where

$T_r$ = reduced temperature,
$T_c$ = critical temperature, °R or K,
$p_r$ = reduced pressure, and
$p_c$ = critical pressure, psia or MPa.

Critical temperature and pressure for typical coal gas components are given in table 2–8.

**Table 2–8.** Physical properties of common coal gas comstituents

| Gas | Molecular weight | Critical temperature, *x*°R | Critical pressure, psia | Critical temperature, K | Critical pressure, MPa |
|---|---|---|---|---|---|
| methane | 16.04 | 343.00 | 666.4 | 190.56 | 4.595 |
| ethane | 30.07 | 549.59 | 706.5 | 305.33 | 4.871 |
| propane | 44.09 | 665.73 | 616.0 | 369.85 | 4.247 |
| i-butane | 58.12 | 734.13 | 527.9 | 407.85 | 3.640 |
| n-butane | 58.12 | 765.29 | 550.6 | 425.16 | 3.796 |
| i-pentane | 72.15 | 828.77 | 490.4 | 460.43 | 3.381 |
| n-pentane | 72.15 | 845.47 | 488.6 | 469.71 | 3.369 |
| water | 18.02 | 1164.85 | 3200.1 | 647.14 | 22.064 |
| nitrogen | 28.02 | 239.26 | 507.5 | 132.92 | 3.499 |
| $CO_2$ | 44.01 | 547.58 | 1071.0 | 304.21 | 7.384 |
| $H_2S$ | 18.02 | 672.35 | 1306.0 | 373.53 | 9.005 |

*Source:* Lee, J., and Wattenbarger, R. A. 1996.

Similarly for mixtures, pseudocritical temperature and pressure can be defined for calculating Z factors, although these computed pseudocritical values are not true critical values in that properties of the liquid and vapor phases do not become equal at this point. Pseudocritical temperature and pressure are given by

$$T_{pr} = \frac{T}{T_{pc}}$$

$$p_{pr} = \frac{p}{p_{pc}}$$

where

$T_{pr}$ = pseudoreduced temperature,
$T_{pc}$ = pseudocritical temperature, °R or K,
$p_{pr}$ = pseudoreduced pressure, and
$p_{pc}$ = pseudocritical pressure, psia or MPa.

Pseudocritical temperature and pressure for a mixture of hydrocarbon gases can be calculated from gas gravity with Sutton's correlation[78]

$$T_{pc} = 169.2 + 349.5\gamma_h - 74.0\gamma_h^2 \quad \textbf{(2.10)}$$

$$p_{pc} = 756.8 - 131.0\gamma_h - 3.6\gamma_h^2 \quad \textbf{(2.11)}$$

where

$\gamma_h$ = hydrocarbon gas gravity.

Possible contaminants in coal gas include $CO_2$, $H_2S$, water vapor, and nitrogen. Whether of thermogenic and/or biogenic origin, $CO_2$ is often present in coal gas and must be accounted for in fluid property calculations. Although sulfur is present in peats and coals of all ranks, $H_2S$ has not been reported in coal gas produced from undisturbed seams, far from coal mines. Anecdotal evidence indicates sour gas is sometimes encountered in coalmine methane when formation waters are pumped out of the mine and then recirculated for mine use, such as dust suppression. The presence of $CO_2$ and $H_2S$ in coal gas can be accounted for by correcting the pseudocritical properties using the correlation of Wichert and Aziz.[79] Mole fractions of these two gases are used to adjust the pseudocritical properties according to the following equations.

$$A = y_{H_2S} + y_{CO_2} \tag{2.12}$$

$$\xi = 120(A^{0.9} - A^{1.6}) + 15(y_{H_2S}^{0.5} - y_{H_2S}^{4}) \tag{2.13}$$

$$T_{pc}{}' = T_{pc} - \xi \tag{2.14}$$

$$p_{pc}{}' = p_{pc}\frac{T_{pc}{}'}{T_{pc} + y_{H_2S}(1 - y_{H_2S})\xi} \tag{2.15}$$

where

$A$ and $\xi$ = constants in Wichert and Aziz correlation,
$T_{pc}{}'$ = adjusted pseudocritical temperature, °R, and
$p_{pc}{}'$ = adjusted pseudocritical pressure, psia.

If the coal gas mixture contains no $CO_2$ or $H_2S$, then $T_{pc}{}' = T_{pc}$ and $p_{pc}{}' = p_{pc}$. As discussed by McCain, this correlation was developed for pressures between 154 psia and 7,026 psia, temperatures between 40°F and 300°F, $CO_2$ ranging from 0 to 54.56 mol%, and $H_2S$ from 0 to 73.85 mol%.[80] Average absolute error in the calculated Z factor was 0.97%, with a maximum error of 6.59%. Thus it is accurate for most coal seam conditions and is often applied to low-pressure coal gases.

Corrections to adjusted pseudocritical pressure and temperature to account for the presence of nitrogen and water vapor are given by Lee and Wattenbarger as[81]

$$T_{pc,cor} = -246.1y_{N_2} + 400.0y_{H_2O} \tag{2.16}$$

$$p_{pc,cor} = -162.0y_{N_2} + 1270.0y_{H_2O} \tag{2.17}$$

$$T_{pc}{}'' = \frac{T_{pc}{}' - 227.2y_{N_2} - 1165y_{H_2O}}{1 - y_{N_2} - y_{H_2O}} + T_{pc,cor} \tag{2.18}$$

$$p_{pc}{}'' = \frac{p_{pc}{}' - 493.1y_{N_2} - 3200y_{H_2O}}{1 - y_{N_2} - y_{H_2O}} + p_{pc,cor} \tag{2.19}$$

where

$T_{pc,cor}$ = pseudocritical temperature correction, °R,
$p_{pc,cor}$ = pseudocritical pressure correction, °R,
$T_{pc}{}''$ = corrected pseudocritical temperature, °R, and
$p_{pc}{}''$ = corrected pseudocritical pressure, psia.

The Z factor can be calculated from pseudocritical properties using the correlation of Dranchuk and Abou-Kassem.[82] Pseudoreduced properties of the gas mixture are defined as

$$T_{pr}'' = \frac{T}{T_{pc}''} \tag{2.20}$$

$$p_{pr} = \frac{p}{p_{pc}''} \tag{2.21}$$

The Z factor is given by

$$Z = 1 + c_1\rho_{pr} + c_2\rho_{pr}^2 - c_3\rho_{pr}^5 + c_4 \tag{2.22}$$

where

$$c_1 = A_1 + \frac{A_2}{T_{pr}} + \frac{A_3}{T_{pr}^3} + \frac{A_4}{T_{pr}^4} + \frac{A_5}{T_{pr}^5}$$

$$c_2 = A_6 + \frac{A_7}{T_{pr}} + \frac{A_8}{T_{pr}^2}$$

$$c_3 = A_9\left(\frac{A_7}{T_{pr}} + \frac{A_8}{T_{pr}^2}\right)$$

$$c_3 = A_{10}\,(1 + A_{11}\rho_{pr}^2)\left(\frac{\rho_{pr}^2}{T_{pr}^3}\right)\exp(-A_{11}\rho_{pr}^2)$$

and the pseudoreduced density is given by

$$\rho_{pr} = \left(\frac{0.27p_{pr}}{ZT_{pr}}\right)$$

The constants $A_1$ through $A_{11}$ are

$A_1 = 0.3265$ $A_7 = -0.7361$

$A_2 = -1.0700$ $A_8 = 0.1844$

$A_3 = -0.5339$ $A_9 = 0.1056$

$A_4 = 0.01569$ $A_{10} = 0.6134$

$A_5 = -0.05165$ $A_{11} = 0.7210$

$A_6 = 0.5475$

With the Z factor appearing on both sides of the equation, it is customarily solved iteratively. An expression for the derivative of $Z$ with respect to pressure at constant temperature is given by Lee and Wattenbarger.[83] They also note this correlation is within engineering accuracy for

$$0.2 <= p_{pr} < 30,\ 1.0 < T_{pr} <= 3.0$$

and

$$p_{pr} < 1.0,\ 0.7 < T_{pr} < 1.0.$$

For pure methane, the corresponding pressures and temperatures are

$$0.92 \text{ MPa} <= p < 138 \text{ MPa } (133 \text{ psia} <= p < 19{,}992 \text{ psia})$$

$$191 \text{ K} < T <= 572 \text{ K } (343°\text{R} < T <= 1{,}029°\text{R})$$

and

$$p < 4.59 \text{ MPa } (666 \text{ psia})$$

$$133 \text{ K} < T < 191 \text{ K } (240°\text{R} < T < 343°\text{R})$$

They report the correlation is poor for

$$T_{pr} = 1.0 \text{ and } p_{pr} > 1.0$$

but did not quantify the error. For pure methane, the corresponding pressures and temperatures are

$$4.59 \text{ MPa} < p \text{ (133 psia < p)}$$

$$191 \text{ K} = T \text{ (343°R} = T)$$

Thus, the correlation of Dranchuk and Abou-Kassem is adequate for calculating coal gas Z factors at reservoir conditions, and the loss of accuracy at very low wellhead pressures is usually not significant for reservoir engineering purposes.

### Example 2.4. Average coal gas Z factors

The average coal gas composition reported by Scott of 93% methane, 3% each of $CO_2$ and wet gases, and 1% nitrogen is assumed, along with properties of the wet gas fraction approximated by those of ethane.[84] Thus, the first step is calculation of normalized hydrocarbon fractions of methane, 0.9681, and C2+, 0.0319. Combining these fractions with the molecular weights shown in table 2–8 yields a hydrocarbon gas gravity of 0.569. Pseudocritical temperature and pressure calculated from Sutton's correlations, equations (2.10) and (2.11), are 344.1°R and 681.1 psia. Correcting for the presence of $CO_2$, the Wichert and Aziz correlation, equations (2.12) through (2.15), gives a ξ factor of 4.673 and adjusted pseudocritical pressure and temperature of 677.7 psia and 339.4°R. The Lee and Wattenbarger correction for nitrogen, equations (2.16) through (2.19), yields corrected pseudocritical pressure and temperature of 677.9 psia and 338.1°R.

Assuming coal seam temperatures of 65°F (18°C) and 150°F (66°C) gives pseudoreduced temperatures of 1.553 and 1.804, respectively. For pressures between 20 and 2,000 psia, the corresponding pseudoreduced pressures range from 0.0295 to 2.905. Equations (2.20)–(2.22) were used to calculate the coal gas Z factors shown in table 2–9 and plotted in figure 2–7. Inspection of these results indicates for the assumed composition and temperatures the Z factors steadily decrease with pressure. The low-temperature coal gas Z factor drops from a value near 1.0 to roughly 0.8 at 2,000 psia, a decline of about 20%, while the high-temperature coal Z factor begins at nearly the same value but drops to about 0.9 at 2,000 psia, a reduction of only 10%.

**Table 2–9.** Average coal gas Z factors

| Pressure, psia | Temp. 65°F | Temp. 150°F |
|---|---|---|
| 20 | 0.9974 | 0.9984 |
| 40 | 0.9948 | 0.9968 |
| 60 | 0.9922 | 0.9953 |
| 80 | 0.9896 | 0.9937 |
| 100 | 0.9870 | 0.9922 |
| 150 | 0.9805 | 0.9883 |
| 200 | 0.9741 | 0.9845 |
| 250 | 0.9677 | 0.9808 |
| 300 | 0.9613 | 0.9770 |
| 350 | 0.9550 | 0.9734 |
| 400 | 0.9487 | 0.9698 |
| 450 | 0.9424 | 0.9663 |
| 500 | 0.9362 | 0.9628 |
| 550 | 0.9301 | 0.9594 |
| 600 | 0.9240 | 0.9560 |
| 650 | 0.9180 | 0.9528 |
| 700 | 0.9121 | 0.9496 |
| 750 | 0.9062 | 0.9464 |
| 800 | 0.9005 | 0.9434 |
| 850 | 0.8948 | 0.9404 |
| 900 | 0.8892 | 0.9375 |
| 950 | 0.8838 | 0.9346 |
| 1,000 | 0.8784 | 0.9319 |
| 1,050 | 0.8732 | 0.9292 |
| 1,100 | 0.8681 | 0.9266 |
| 1,150 | 0.8631 | 0.9241 |
| 1,200 | 0.8583 | 0.9217 |
| 1,250 | 0.8536 | 0.9194 |
| 1,300 | 0.8490 | 0.9172 |
| 1,350 | 0.8447 | 0.9151 |
| 1,400 | 0.8405 | 0.9131 |
| 1,450 | 0.8365 | 0.9112 |
| 1,500 | 0.8327 | 0.9093 |
| 1,550 | 0.8290 | 0.9076 |
| 1,600 | 0.8256 | 0.9060 |
| 1,650 | 0.8223 | 0.9045 |
| 1,700 | 0.8193 | 0.9031 |
| 1,750 | 0.8165 | 0.9018 |
| 1,800 | 0.8139 | 0.9006 |
| 1,850 | 0.8114 | 0.8995 |
| 1,900 | 0.8093 | 0.8985 |
| 1,950 | 0.8073 | 0.8976 |
| 2,000 | 0.8055 | 0.8969 |

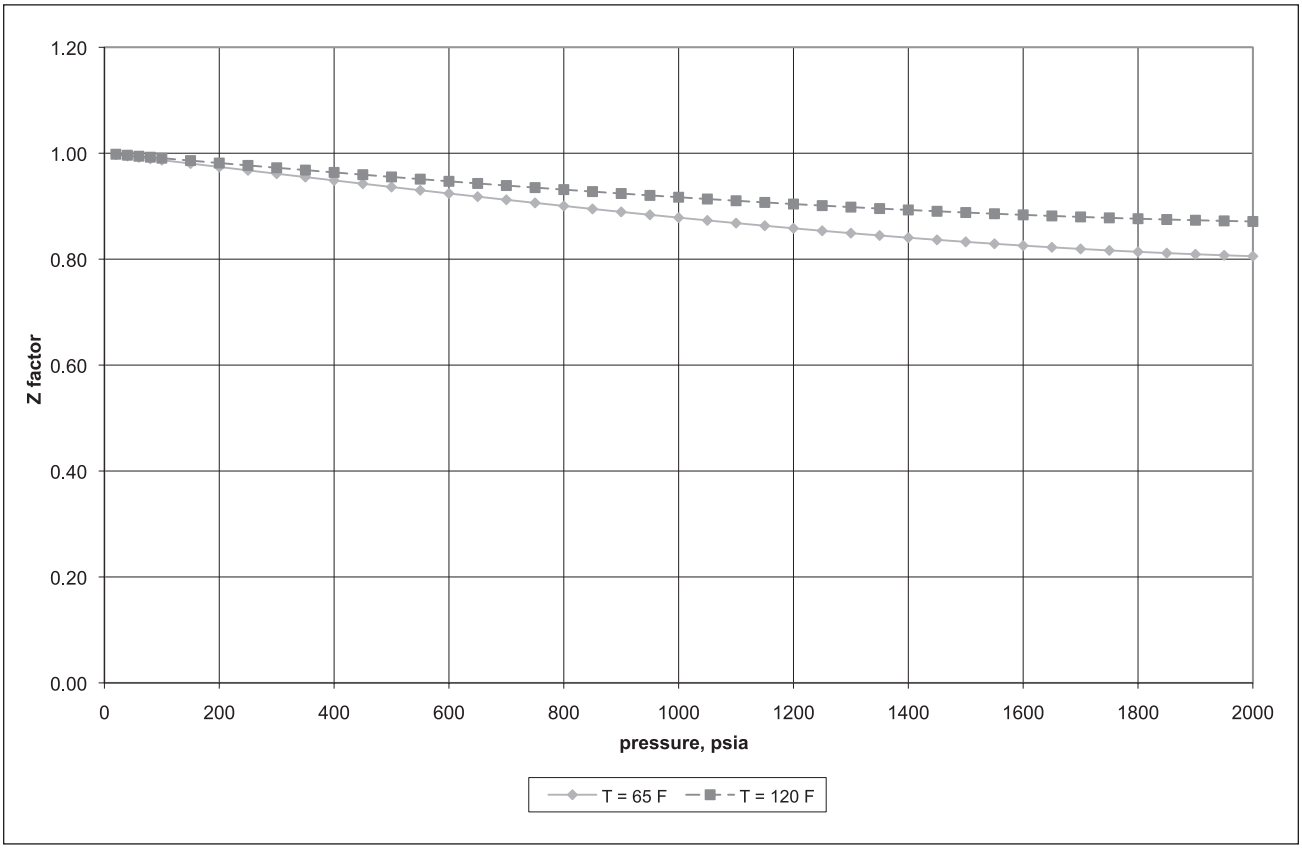



**Fig. 2–7.** Average coal gas Z factors vs. pressure

## Gas Desorption

Coals hold gas by compression of free gas in the cleats and sorption on the surface of the matrix. Sorption, also termed *adsorption*, depends on the molecular van der Waal's forces of mutual attraction between gaseous and solid molecules. Gas sorbed on a coal surface is released when pressure is reduced. The rate of gas release depends on coal temperature, coal rank and composition, porosity distribution, and gas composition.[85] The gas release rate appears to be diffusive, that is, gas release from the coal can be described by Fick's law.

For many reservoir engineering purposes, gas release from a coal can be conceptualized as gas diffusion, characterized by a single diffusion constant, out of spherical coal particles with a unipore porosity distribution. Under these assumptions, the desorbed gas fraction can be written as[86]

$$\frac{V}{V_t} = 1 - \frac{6}{\pi^2}\sum_{n=1}^{\infty}\frac{1}{n^2}\exp\left(-n^2\pi^2 t_{Ds}\right) \tag{2.23}$$

where

$V$ = desorbed gas volume, cm$^3$,
$V_t$ = total desorbed gas volume, cm$^3$, and
$t_{Ds}$ = dimensionless time, defined by

$$t_{Ds} = \frac{Dt}{r_p^2} \tag{2.24}$$

where

$D$ = diffusion coefficient, cm$^2$/sec,
$t$ = time, sec, and
$r_p$ = particle radius, cm.

The ratio $D/r_p^2$ is termed the *diffusivity* and has dimensions of sec$^{-1}$. As with many infinite series of the form of equation (2.23), convergence problems exist at small times, and a useful approximation for $V/V_t < 0.5$ is Smith and Williams[87]

$$\frac{V}{V_t} = \frac{6}{\sqrt{\pi}}\sqrt{t_{Ds}} \qquad \textbf{(2.25)}$$

The desorbed gas fraction as a function of dimensionless time is in table 2–10 and plotted in figure 2–8. The approximate solution of equation (2.25) is also plotted in figure 2–8.

**Table 2–10.** Desorbed gas fraction

| *tDs* | *V/V*$_t$ | *tDs* | *V/V*$_t$ | *tDs* | *V/V*$_t$ |
|---|---|---|---|---|---|
| 7.375E-06 | 0.01 | 0.012420 | 0.34 | 0.065540 | 0.67 |
| 3.521E-05 | 0.02 | 0.013258 | 0.35 | 0.068363 | 0.68 |
| 7.980E-05 | 0.03 | 0.014130 | 0.36 | 0.071300 | 0.69 |
| 1.426E-04 | 0.04 | 0.015038 | 0.37 | 0.074356 | 0.70 |
| 2.241E-04 | 0.05 | 0.015982 | 0.38 | 0.077538 | 0.71 |
| 3.244E-04 | 0.06 | 0.016963 | 0.39 | 0.080855 | 0.72 |
| 4.440E-04 | 0.07 | 0.017983 | 0.40 | 0.084315 | 0.73 |
| 5.832E-04 | 0.08 | 0.019042 | 0.41 | 0.087928 | 0.74 |
| 7.423E-04 | 0.09 | 0.020142 | 0.42 | 0.091704 | 0.75 |
| 9.216E-04 | 0.10 | 0.021283 | 0.43 | 0.095656 | 0.76 |
| 0.001122 | 0.11 | 0.022467 | 0.44 | 0.099797 | 0.77 |
| 0.001342 | 0.12 | 0.023696 | 0.45 | 0.104142 | 0.78 |
| 0.001585 | 0.13 | 0.024969 | 0.46 | 0.108710 | 0.79 |
| 0.001849 | 0.14 | 0.026290 | 0.47 | 0.113519 | 0.80 |
| 0.002135 | 0.15 | 0.027658 | 0.48 | 0.118594 | 0.81 |
| 0.002443 | 0.16 | 0.029077 | 0.49 | 0.123962 | 0.82 |
| 0.002775 | 0.17 | 0.030547 | 0.50 | 0.129653 | 0.83 |
| 0.003130 | 0.18 | 0.032069 | 0.51 | 0.135707 | 0.84 |
| 0.003509 | 0.19 | 0.033647 | 0.52 | 0.142167 | 0.85 |
| 0.003912 | 0.20 | 0.035282 | 0.53 | 0.149088 | 0.86 |
| 0.004341 | 0.21 | 0.036975 | 0.54 | 0.156536 | 0.87 |
| 0.004794 | 0.22 | 0.038730 | 0.55 | 0.164594 | 0.88 |
| 0.005273 | 0.23 | 0.040547 | 0.56 | 0.173366 | 0.89 |
| 0.005779 | 0.24 | 0.042430 | 0.57 | 0.182986 | 0.90 |
| 0.006312 | 0.25 | 0.044382 | 0.58 | 0.193631 | 0.91 |
| 0.006872 | 0.26 | 0.046404 | 0.59 | 0.205540 | 0.92 |
| 0.007460 | 0.27 | 0.048500 | 0.60 | 0.219051 | 0.93 |
| 0.008077 | 0.28 | 0.050674 | 0.61 | 0.234656 | 0.94 |
| 0.008723 | 0.29 | 0.052927 | 0.62 | 0.253118 | 0.95 |
| 0.009400 | 0.30 | 0.055265 | 0.63 | 0.275721 | 0.96 |
| 0.010107 | 0.31 | 0.057691 | 0.64 | 0.304867 | 0.97 |
| 0.010846 | 0.32 | 0.060209 | 0.65 | 0.345947 | 0.98 |
| 0.011617 | 0.33 | 0.062823 | 0.66 | 0.416180 | 0.99 |
| | | | | 0.649538 | 0.999 |

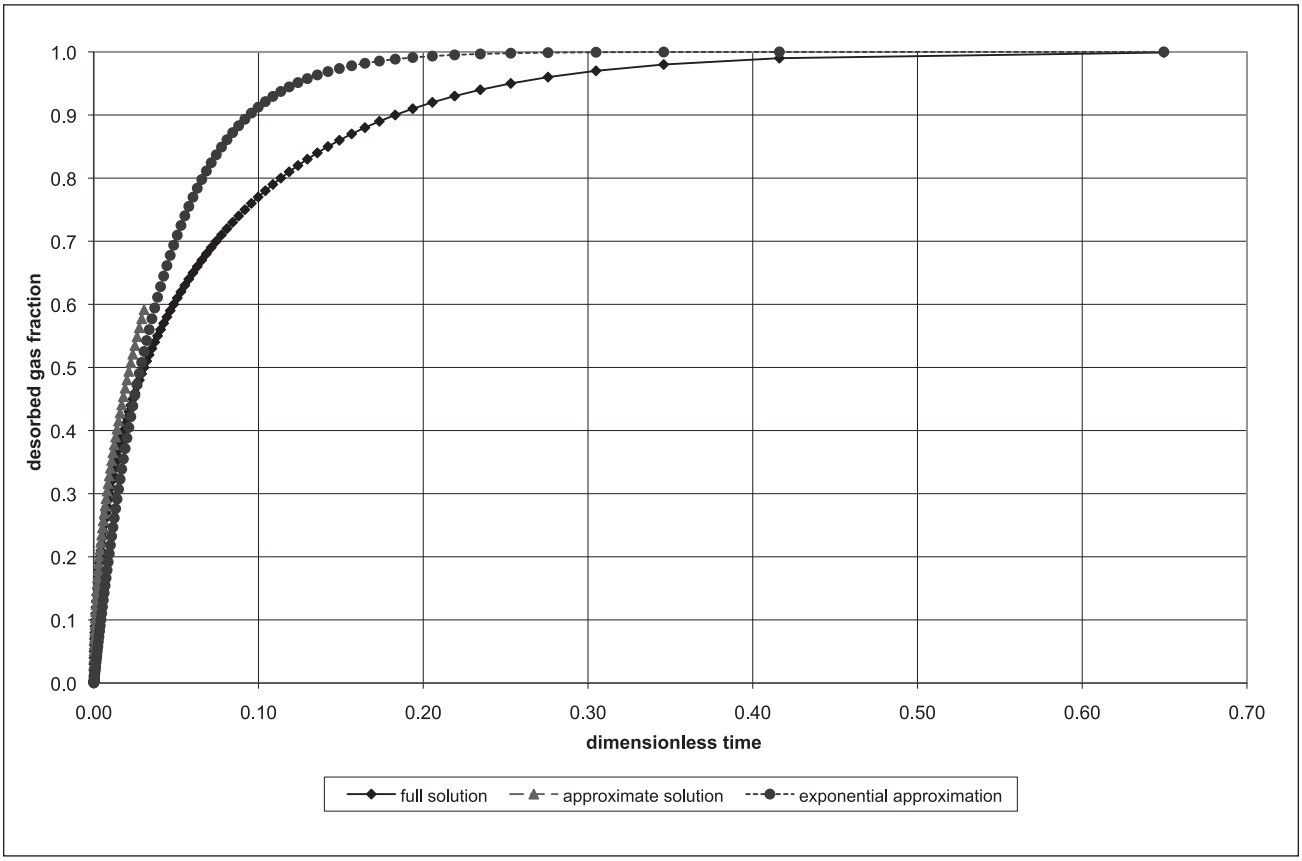



**Fig. 2–8.** Dimensionless desorbed gas function

As many reservoir engineering applications are more concerned with the time required to desorb a given volume of gas rather than the detailed physics of desorption, release of gas from the matrix is sometimes envisaged as a pseudosteady-state process described with a single exponential term. Many coal gas reservoir simulators employ this approach, describing desorption as[88]

$$\frac{V}{V_t} = 1 - \exp(-\lambda t_D) \qquad \textbf{(2.26)}$$

where

$\lambda$ = dimensionless constant.

A best fit of equation (2.26) to the full solution, shown as the third curve in figure 2–8, yields a $\lambda$ value of 20.356. This is in good agreement with the full solution for the first half of desorption but overestimates the desorbed gas volume during the second half by as much as 10% to 15%. When the exponential argument equals 1, $V/V_t = 0.632$, and 63.2% of the gas has been desorbed. Time required for desorption of 63.2% of the sorbed gas, determined from empirical desorption data, is defined as the *sorption time* and is a required input for many coal gas reservoir simulators.

The two simplified desorption models briefly discussed here, unipore spherical coal particles and exponential gas release, are employed in the following example to demonstrate the rapidity of gas release from coal. Time required to emit 90% or 95% of the sorbed gas is often very quick relative to times required for a coal well to respond to a pressure perturbation.

### Example 2.5. Desorption times

The unipore diffusion solution can be combined with empirical desorption results to calculate time required to release 90% of the sorbed gas, denoted at $t_{90}$. Desorbing samples of subbituminous Cretaceous-age coal from the San Juan Basin, Smith and Williams reported a coal diffusivity of $7.51(10)^{-4}$ min$^{-1}$.[89] Dimensionless time required to desorb 90% of the gas, from table 2–10, is 0.182986, which is combined with the diffusivity in equation (2.24) to calculate time required to release 90% of the gas.

$$t_{Ds} = \frac{Dt}{r_p^2}$$

$$0.182986 = 7.51(10)^{-4}\ \text{min}^{-1}\ t_{90}$$

$$t_{90} = 243.66\ \text{min} = 4.1\ \text{hr}$$

Similarly, dimensionless time to desorb 95% of the gas, from table 2–10, is 0.253118. Time required to desorb this fraction of the gas, defined as $t_{95}$, is

$$0.253118 = 7.51(10)^{-4}\ \text{min}^{-1}\ t_{95}$$

$$t_{95} = 337.04\ \text{min}^{-1} = 5.6\ \text{hr}$$

Initiation of gas production from a coal well, gas rate changes, or shut-ins of the well perturb gas flow in the cleats and gas desorption from the matrix. Characteristic response times of cleats and matrix to such perturbations differ. *Response time* for flow in the cleats is the time required for the well to settle into pseudosteady-state flow. As discussed in chapter 7, times required for coal wells to reach pseudosteady-state flow are often on the order of weeks or months. As these times are at least an order of magnitude larger than times required to release 90% or 95% of the sorbed gas, description of desorption physics with the simple unipore desorption model is often adequate for many reservoir engineering purposes.

*Sorption time*, the time required to desorb 63.2% of the gas, can be combined with the dimensionless time solution to calculate times required to release 90% and 95% of the gas from a coal. Pratt et al. reported sorption time, $\tau$, for a subbituminous Paleocene sample from the Canyon coal in the Powder River Basin as 54.8 hr.[90] From table 2–10, 63.2% of the gas has been desorbed at a dimensionless time of 0.055743. Time required to desorb 90% of the gas can be obtained from the ratio of the two times,

$$\frac{\dfrac{Dt_{90}}{r_p^2}}{\dfrac{D\tau}{r_p^2}} = \frac{0.182986}{0.055743}$$

Solving for $t_{90}$,

$$t_{90} = 3.28\tau$$

Thus, time to desorb 90% of the gas is

$$t_{90} = 3.28(54.8\ \text{hr}) = 179.7\ \text{hr} = 7.5\ \text{days}$$

Similarly, time required to desorb 95% of the gas is

$$t_{95} = \frac{0.253118}{0.055743}\tau = 4.54\tau$$

Time required to release 95% of the gas from this sample is therefore

$$t_{95} = 4.54(54.8 \text{ hr}) = 248.8 \text{ hr} = 10.4 \text{ days}$$

Coal permeabilities in the Powder River Basin are on the order of several hundred millidarcies, making time required for this well to reach pseudosteady-state flow on the order of one to two weeks. As response times of matrix and cleat are roughly equal, well behavior is controlled by the interplay between gas release from the matrix and gas flow in the cleats.

Recent years have seen increasing interest in enhanced coalbed methane recovery (ECBM) via injection of nitrogen, $CO_2$, and flue gas, and in $CO_2$ sequestration. On a field or well scale, uptake of injected gases onto the coal matrix can be described by the mathematics developed above. For short injection times and in the near-wellbore region, additional mathematical sophistication is required. For example, Clarkson and Bustin studied the effect of pore structure and gas pressure on the sorption behavior of methane and $CO_2$ on samples of Cretaceous coals from the Gates Formation in Western Canada.[91]

## Coal Rock Properties

As a reservoir rock, coal is more reactive than conventional reservoirs in both a mechanical and a chemical sense. Conceptualizing coal as a polymeric tangle of organic filaments, the ability of conventional rock mechanics to describe coal stress loads and the resultant deformations is surprising. Coal rock properties show little dependence on geologic age, varying primarily with rank, lithotype (maceral composition), and quality (ash and mineral matter). As coal quality is strongly influenced by local depositional events, coal rock properties can show extreme areal heterogeneity. Levine noted the dual problems of sample selection and scale dependence, which complicate measurement of coal rock properties.[92] Intact portions of coal cores sufficiently large for rock properties measurements may have survived the coring process due to anomalous mechanical behavior. Rock properties of a coal seam, with multiple heterogeneities and a thickness many times larger than the cleat spacing, may differ from those measured on laboratory samples. Typically the laboratory samples are more homogeneous and have fewer cleats. Rock properties important for coal gas reservoir engineering include Young's modulus, Poisson's ratio, unconfined compressive strength, and cleat compressibility.

*Young's modulus* is defined as the ratio of stress to strain of a sample subjected to uniaxial loading, and values for coals reported by several workers are collected in table 2–11.

While this list is not exhaustive, it does illustrate the variation seen in this important rock property. Several investigators noted that Young's modulus of a coal increases with ash fraction, and Levine suggested this parameter measured parallel to bedding planes is larger than perpendicular to bedding.[93] Reviewing Young's moduli reported for coals of bituminous rank and higher, Bromhal et al. noted the value of this parameter measured parallel to the bedding planes averaged 22% greater than that measured perpendicular to bedding planes. The average value of Young's modulus was 511,000 psia (3,500 MPa).[94] Young's moduli reported for coals are one-third to one-tenth that of sandstone and limestones and are approximately equal to that of weak shales. Until Young's modulus can be measured for a specific seam, a value of 500,000 psia (3,400 MPa) is often assumed.

*Poisson's ratio* is defined as the ratio of lateral strain to axial strain of a sample subjected to uniaxial loading. Typical values of Poisson's ratio reported for coals are collected in table 2–11, which is not comprehensive but does illustrate the variation of this rock property in coal. The range of Poisson's ratio seen in coals, from 0.2 to 0.4, is similar to that seen in sandstones and shales and somewhat greater than that of limestones. Lacking measured values of Poisson's ratio for a particular coal, a value of 0.3 is often employed.

**Table 2–11.** Rock properties of selected coals

| Basin | Coal | Rank | Young's modulus, Mpa | Young's modulus, psia | Poisson's ratio |
|---|---|---|---|---|---|
| na[a] | na | na | 2,700 | 390,000 | 0.32 |
| Warrior[b] | Blue Creek | | 2,760 | 400,000 | 0.35 |
| San Juan[c] | Fruitland | med. vol. | 3,400 | 490,000 | 0.30 |
| San Juan[d] | Fruitland | med. vol. | 5,600 | 810,000 | 0.35 |
| WCSB[e] | various | sub. B/hi-vol. C | 3,000 | 435,000 | 0.30 |
| na[f] | na | na | 1,000 | 145,000 | 0.20 |
| na[g] | na | na | 14,000 | 2,030,000 | 0.40 |
| San Juan[h] | Fruitland | hi-vol. A | 3,600 | 521,000 | 0.21 |
| San Juan[i] | Fruitland | med. vol. | 4,500 | 650,000 | 0.32 |
| Piceance[j] | Cameo | med. vol. | 2,400 | 350,000 | 0.31 |
| WCSB[k] | na | na | 1.0 to 5,000 | 1.5 to 730,000 | 0.26–0.48 |
| | | average = | 4,296 | 622,100 | 0.31 |

*na = not available*

*Sources:* [a]Gray, I. 1987. Reservoir engineering in coal seams. Part I. The physical process of gas storage and movement in coal seams. *SPE Reservoir Engineering*. V. 2 (no. 1). p. 28. [b]Layne, A. W., and Byrer, C. W. 1988. Analysis of coalbed methane simulations in the Warrior Basin, Alabama. *SPE Formation Evaluation*. V. 3 (no. 3). p. 663. [c]Jones, A. H., Ahmed, U., Bush, D. D., Holland, M. T., Kelkar, S. M., Rakop, K. C., Bowman, K. C., and Bell, G. J. 1984. *Methane Production Characteristics for a Deeply Buried Coalbed Reservoir in the San Juan Basin*. SPE/DOE/GRI 12876. Presented at the 1984 SPE/DOE/GRI Unconventional Gas Recovery Symposium, Pittsburgh, Pennsylvania, May 13–15. [d]Ibid. [e]Bustin, R. M., Cui, X., and Chikatamarla, L. 2008. [f]Levine, J. R., 1996. Model study of the influence of matrix shrinkage on absolute permeability of coal bed reservoirs. In *Coalbed Methane and Coal Geology*. Gayer and Harris, eds. Geological Society Special Publication No. 109. London: Geological Society. p. 197. [g]Ibid. [h]Mavor, M. J., Close, J. C., and Pratt, T. J. 1991. *Summary of the Completion Optimization and Assessment Laboratory (COAL) Site*. Report GRI-91/0377. Chicago: Gas Research Institute. [i]Bell, G. J., Seccombe, J. C., Rakop, K. C., and Jones, A. H. 1985. *Laboratory Characterization of Deeply Buried Coal Seams in the Western U.S.* Paper SPE 14445. Presented at the SPE Annual Technical Conference and Exhibition, Las Vegas, Nevada, September 12–25. [j]Ibid. [k]Gentzis, T., Deisman, N., and Chalaturnyk, R. J. 2007. Geomechanical properties and permeability of coals from the Foothills and Mountain regions of western Canada. *International Journal of Coal Geology*. V. 69 (no. 3). p. 153.

*Unconfined compressive strength (UCS)* is a measure of intact rock strength and is defined as the maximum load at failure divided by the sample cross-sectional area. Dependence of coal UCS on rank was discussed by Palmer, but sample origin was not given.[95] Unconfined compressive strength of subbituminous and high-volatile bituminous coals ranged from 5,000 to 8,500 psia, declined to a minimum of 1,000 psia in medium and low-volatile bituminous coals, and then rose to 5,500 psia for anthracitic coals. Gentzis et al. reported UCS values for western Canadian coals varied from 1,250 to 11,700 psia.[96] Mavor and Gunter reported a UCS for the Fruitland coal of the San Juan Basin of 11,880 psia.[97] The unconfined compressive strengths of coals are generally less than those of conventional sandstones and limestones, which range from 3,000 to 36,000 psia, and shales, 700 to 14,500 psia.

*Cleat* or *void volume compressibility* of a coal, analogous to pore volume compressibility of conventional reservoirs, is a measure of coal fracture volume loss due to applied loads. This property, also termed *formation compressibility*, primarily affects reservoir behavior in undersaturated coals above desorption pressure. As a coal seam depletes, decreases in reservoir pressure are matched by increases in rock stresses to support the lithostatic load. Voids in the coal, comprised of both coal cleats and pores of various sizes, deform over the course of depletion in response to these stress changes. Coal cleat compressibility, like pore volume compressibility of conventional reservoir rocks, is expressed mathematically as

$$c_f = \frac{1}{V_p}\frac{dV_p}{dp} \tag{2.27}$$

where

$c_f$ = formation compressibility, psia$^{-1}$ or MPa$^{-1}$, and
$V_p$ = cleat volume, ft$^3$ or cm$^3$.

To be clear of thermal expansion effects, compressibility of coal and conventional reservoir rocks should be measured at isothermal conditions, ideally at reservoir temperature but practically at ambient temperature. On a unit volume basis, equation (2.27) can be written as

$$c_f = \frac{1}{\phi}\frac{d\phi}{dp} \tag{2.28}$$

where

$\phi$ = porosity, fraction.

In practice, coal void volume compressibility is very difficult to measure, and values within a factor of two are regarded as excellent agreement. Controls on coal compressibility are poorly understood, making prediction of this parameter difficult. Coal rank and geologic age appear to minimally affect compressibility, if at all, while the role of other variables such as ash and mineral matter, maceral distribution, and coal lithotypes has not been reported. Compressibility values reported by various workers, collected in table 2–12, vary by almost an order of magnitude, ranging from a maximum of $2.50(10)^{-3}$ psia$^{-1}$ down to a minimum of $3.00(10)^{-4}$ psia$^{-1}$ (0.363 MPa$^{-1}$ to 0.044 MPa$^{-1}$). Median and average coal void volume compressibilities are $1.34\ (10)^{-3}$ psia$^{-1}$ and $1.43(10)^{-3}$ psia$^{-1}$ (0.194 MPa$^{-1}$ and 0.207 MPa$^{-1}$), respectively.

**Table 2–12.** Cleat compressibility of selected coals

| Basin | Seam | Age | Rank | Cleat compressibility, psia$^{-1}$ |
|---|---|---|---|---|
| Appalachian[a] | Pittsburgh | Pennsylvanian | na | 0.00187 |
| San Juan[b] | Menefee | na | na | 0.00134 |
| Piceance[c] | Cameo | Cretaceous | na | 0.00129 |
| Warrior[d] | na | Pennsylvanian | na | 0.00187 |
| Warrior[e] | Marylee/Blue Creek | Pennsylvanian | na | 0.000579 |
| San Juan[f] | na | Cretaceous | na | 0.000924 |
| San Juan[g] | Fruitland | Cretaceous | na | 0.000961 |
| San Juan[h] | Fruitland | Cretaceous | na | 0.001944 |
| Warrior[i] | Marylee/Blue Creek | Pennsylvanian | hi-vol. A | 0.0025 |
| San Juan[j] | Fruitland | Cretaceous | na | 0.001015 |
| Sydney[k] | Bulli | Permian | na | 0.0003 |
| Bowen[l] | Gemini | Permian | hi-vol. A–med. vol. | 0.00164 |
| Sydney[m] | na | Permian | hi-vol. A–lo-vol. | 0.002352 |

*na = not available*

*Sources:* [a]McKee, C. R., Bumb, A. C., and Koenig, R. A. 1988. Stress-dependent permeability and porosity of coal and other geologic formations. *SPE Formation Evaluation*. V. 3 (no. 1). p. 81. [b]Ibid. [c]Ibid. [d]McKee, C. R., Bumb, A. C., and Koenig, R. A. 1987. Stress-dependent permeability and porosity of coal. Paper 8742 in *Proceedings of the 1987 International Coalbed Methane Symposium*. Tuscaloosa: University of Alabama. [e]Seidle, J. P., Jeansonne, M. W., and Erickson, D. J. 1992. *Application of Matchstick Geometry to Stress Dependent Permeability in Coals*. Paper SPE 24361. Presented at the SPE Rocky Mountain Regional Meeting, Casper, Wyoming, May 18–21. [f]McKee, C. R., Bumb, A. C., and Koenig, R. A. 1987. [g]Seidle, J. P., Jeansonne, M. W., and Erickson, D. J. 1992. [h]Shi, J. Q., and Durucan, S. 2003. Changes in permeability of coalbeds during primary recovery. Part 2. Model validation and field application. Paper 0342 in *Proceedings of the 2003 International Coalbed Methane Symposium*. Tuscaloosa: University of Alabama; and Mavor, M. J., and Vaughn, J. E. 1997. Increasing absolute permeability in the San Juan Basin Fruitland Formation. Paper 9738 in *Proceedings of the 1997 International Coalbed Methane Symposium*. Tuscaloosa: University of Alabama. [i]Zuber, M. D., Sawyer, W. K., Schraufnagel, R. A., and Kuuskraa, V. A. 1987. *The Use of Simulation and History Matching to Determine Critical Coalbed Methane Reservoir Properties*. Paper SPE/DOE 16420. Presented at the SPE/DOE Low Permeability Reservoirs Symposium, Denver, Colorado, May 18–19. [j]Gash, B. W., Volz, R. F., Potter, G., and Corgan, J. M. 1993. The effects of cleat orientation and confining pressure on cleat porosity, permeability and relative permeability in coal. Paper 9321 in *Proceedings of the 1993 International Coalbed Methane Symposium*. Tuscaloosa: University of Alabama. [k]Spencer, S. J., Somers, M. L., Pinczewski, W. V., and Doig, I. D. 1987. *Numerical Simulation of Gas Drainage from Coal Seams*. Paper SPE 16857. Presented at the SPE Annual Technical Conference and Exhibition, Dallas, Texas, September 27–30. [l]Gray, I. 1987. Reservoir engineering in coal seams. Part 1. The physical process of gas storage and movement in coal seams. *SPE Reservoir Engineering*. V. 2 (no. 1). p. 28. [m]Bustin, R. M. 1997.

For comparison, pore volume compressibilities of conventional reservoir rocks range from $10^{-6}$ to $10^{-4}$ psia$^{-1}$, making coal cleat compressibility 10 to 1,000 times larger than that of conventional reservoirs.[98] At typical coal seam temperatures and pressures, water compressibility is approximately $3(10)^{-6}$ psia$^{-1}$, and gas compressibility, roughly the inverse of pressure, ranges from $4(10)^{-2}$ to $4(10)^{-4}$ psia$^{-1}$. Median coal void volume compressibility is therefore about 500 times larger than that of water and roughly equal to that of methane at 800 psia. Sorption compressibility, discussed in chapters 7 and 9, depends on gas properties and sorption characteristics and ranges from $3(10)^{-4}$ to $3(10)^{-1}$ psia$^{-1}$, at least an order of magnitude larger than the median coal cleat compressibility.

Compressibility of a coal deposit that contains both free gas and water is similar to that of a conventional reservoir plus sorption compressibility. Mathematically,

$$c_t = c_f + S_w c_w + S_g c_g + c_s \tag{2.29}$$

where

$c_t$ = total compressibility, psia$^{-1}$,
$c_f$ = cleat compressibility, psia$^{-1}$,
$S_w$ = water saturation,
$c_g$ = gas compressibility, psia$^{-1}$,
$S_g$ = gas saturation, and
$c_s$ = sorption compressibility, psia$^{-1}$.

Coal cleat compressibility is important if no free gas is present, such as an undersaturated coal above the desorption pressure. Total compressibility of the system is now

$$c_t = c_f + c_w \approx c_f$$

## Nomenclature

| | |
|---|---|
| $A$ | Constant in Wichert and Aziz correlation |
| $A_1$ through $A_{11}$ | Constants in the Dranchuk-Abou Kassem Z factor correlation |
| $a$ | Ash fraction, wt % |
| $c_1$ through $c_4$ | Functions in the Dranchuk-Abou Kassem Z factor correlation |
| $c_f$ | Cleat or void volume compressibility, psia$^{-1}$ or MPa$^{-1}$ |
| $c_g$ | Gas compressibility, psia$^{-1}$ |
| $c_s$ | Sorption compressibility, psia$^{-1}$ |
| $c_t$ | Total compressibility, psia$^{-1}$ |
| $d$ | Cleat spacing, cm |
| $D$ | Diffusion coefficient, cm$^2$/sec |
| $M_a$ | Molecular weight of air, 28.97 |
| $M_j$ | Molecular weight of component $j$ |
| $MM$ | Mineral matter weight fraction |
| $n$ | Number of moles |
| $p$ | Pressure, psia or MPa |
| $p_c$ | Critical pressure, psia or MPa |
| $p_L$ | Langmuir pressure constant, psia or MPa |
| $p_{pc}$ | Pseudocritical pressure, psia or MPa |
| $p_{pc}'$ | Pseudocritical pressure adjusted for $CO_2$ and $H_2S$, psia |
| $p_{pc}''$ | Adjusted pseudocritical pressure corrected for $N_2$ and $H_2O$, psia |
| $p_{pr}$ | Pseudoreduced pressure |
| $p_r$ | Reduced pressure |
| $R$ | Universal gas constant, 10.732 psia-ft$^3$/lb-mol-°R or 8.297(10)$^{-3}$ MPa-m$^3$/kg-mol-K |
| $r_p$ | Particle radius, cm |
| $S$ | Sulfur weight fraction |
| $S_g$ | Gas saturation, fraction |
| $S_w$ | Water saturation, fraction |
| $t$ | Time, sec |
| $T$ | Temperature, °R or K |
| $T_c$ | Critical temperature, °R or K |

| | |
|---|---|
| $T_{pc}$ | Pseudocritical temperature, °R or K |
| $T_{pc}'$ | Pseudocritical temperature adjusted for $CO_2$ and $H_2S$, °R |
| $T_{pc}''$ | Adjusted pseudocritical temperature corrected for $N_2$ and $H_2O$, °R |
| $T_{pr}$ | Pseudoreduced temperature |
| $T_r$ | Reduced temperature |
| $t_D$ | Dimensionless time, equation (2.2) |
| $V$ | Desorbed gas volume, $cm^3$, or gas content, scf/t or $cm^3/g$, or volume, $ft^3$ or $m^3$ |
| $V_i$ | Volume fraction inertinite |
| $V_l$ | Volume fraction liptinite |
| $V_{Ldaf}$ | Dry, ash-free Langmuir volume constant, scf/t or $cm^3/g$ |
| $V_p$ | Cleat volume, $ft^3$ or $cm^3$ |
| $V_t$ | Total desorbed gas volume, $cm^3$ |
| $V_v$ | Volume fraction vitrinite |
| $w$ | Equilibrium moisture fraction, wt % |
| $y_j$ | Mole fraction of component |
| $Z$ | Gas deviation factor or compressibility factor |

## Greek

| | |
|---|---|
| $\gamma_g$ | Gas gravity |
| $\gamma_h$ | Hydrocarbon gas gravity |
| $\xi$ | Constant in Wichert and Aziz correlation |
| $\rho$ | Coal bulk density, $g/cm^3$ |
| $\rho_a$ | Ash density, $g/cm^3$ |
| $\rho_i$ | Inertinite density, $g/cm^3$ |
| $\rho_l$ | Liptinite density, $g/cm^3$ |
| $\rho_o$ | Organic fraction density, $g/cm^3$ |
| $\rho_r$ | Pseudoreduced density |
| $\rho_v$ | Vitrinite density, $g/cm^3$ |
| $\rho_w$ | Water density, $g/cm^3$ |
| $\phi$ | Porosity, fraction |

## References


1. Schopf, J. M. 1956. A definition of coal. *Economic Geology*. V. 51. p. 521.
2. ASTM D388-05. 2005. *Standard Classification of Coal by Rank*. Philadelphia: American Society for Testing and Materials International.
3. Speight, J. G. 1994. *The Chemistry and Technology of Coal*. 2nd ed. New York: Marcel Dekker.
4. ISO 11760:2005. 2005. *Classification of Coals*. Geneva: International Organization for Standardization.
5. AS 1038.17: Part 17. 2000. Higher rank coal—moisture-holding capacity (equilibrium moisture). Part 17. *Coal and Coke–Analysis and Testing*. Sydney: Standards Australia Ltd.
6. Stach, E., Mackowsky, M.-Th., Teichmuller, M., Taylor, G. H., Chandra, D., and Teichmuller, R. 1982. *Stach's Textbook of Coal Petrology*. 3rd ed. Berlin: Gebruder Borntraeger; and Mastalerz, M., and Harper, D. 1998. *Coal in Indiana: A Geologic Overview*. Indiana Geological Survey. Special Report 60. Bloomington: Indiana University.
7. Meissner, F. F. 1984. Cretaceous and Lower Tertiary coals as sources for gas accumulations in the Rocky Mountain area. In *Hydrocarbon Source Rocks of the Greater Rocky Mountain Region*. Denver: Rocky Mountain Association of Geologists.
8. Ibid.
9. ASTM. 2002. Petroleum products, lubricants, and fossil fuels. V. 05.05. Gaseous fuels: Coal and coke. In *Annual Book of ASTM Standards*. Sec. 5. Philadelphia: American Society for Testing and Materials International.
10. ASTM D 3173-03. 2008. *Standard Text Method for Moisture in the Analysis Sample of Coal and Coke*. Philadelphia: American Society for Testing and Materials International; BSI. 1981. Determination of moisture-holding capacity of hard coal. Part 21 in *Methods for Analysis and Testing of Coal and Coke*. British Standard 1016: Part 21 (1981)/ISO 1018 (1975). Bristol: Standards UK; and AS 1038.3. Part 3. 1989. Proximate analysis of higher rank coal. Part 3. *Coal and Coke–Analysis and Testing*. Sydney: Standards Australia Ltd.
11. Testa, S. M., and Pratt, T. J. 2003. Sample preparation for coal and shale gas resource assessment. Paper 0356 in *Proceedings of the 2003 International Coalbed Methane Symposium*. Tuscaloosa: University of Alabama.
12. Luppens, J. A. 1988. The equilibrium moisture problem. *Journal of Coal Quality*. V. 7 (no. 2) (April–June). p. 39.
13. Luppens, J. A., and Hoeft, A. P. 1991. Relationship between inherent and equilibrium moisture contents in coals by rank. *Journal of Coal Quality*. V. 10 (no. 4) (October–December). p. 133.
14. Testa, S. M., and Pratt, T. J. 2003.
15. ASTM D 3175. 2007. *Standard Test Method for Volatile Matter in the Analysis Sample of Coal and Coke*. Philadelphia: American Society for Testing and Materials International.
16. ASTM D 3172-07a. 2007. *Standard Practice for Proximate Analysis of Coal and Coke, Revision A*. Philadelphia: American Society for Testing and Materials International.
17. ASTM D 3174. 2007. *Standard Test Method for Ash in the Analysis Sample of Coal and Coke from Coal*. Philadelphia: American Society for Testing and Materials International.
18. ASTM D 4239. 2008. *Standard Test Methods for Sulfur in the Analysis Sample of Coal and Coke Using High-Temperature Tube Furnace Combustion Methods*. Philadelphia: American Society for Testing and Materials International.
19. Rightmire, C. T., Eddy, G. E., and Kirr, J. N. 1984. Coalbed methane resources of the United States. *AAPG Studies in Geology Series #17*. Tulsa: American Association of Petroleum Geologists.
20. ASTM D 3176-89. 1989. *Standard Practice for Ultimate Analysis of Coal and Coke*. Philadelphia: American Society for Testing and Materials International.
21. ASTM D 388-05. 2005; and ASTM. 2002.
22. Luppens, J. A., and Hoeft, A. P. 1991.
23. Pratt, T. J., and Baez, L. R. G. 2003. Critical data requirements for coal and gas shale resource assessment. Paper 0367 in *Proceedings of the 2003 International Coalbed Methane Symposium*. Tuscaloosa: University of Alabama.
24. Gas Research Institute. 1995. *A Guide to Determining Coalbed Gas Content*. GRI-94/0396. Chicago: Gas Research Institute.
25. Mavor, M. J., Pratt, T. J., and Nelson, C. R. 1995. *Quantitative Evaluation of Coal Seam Gas Content Estimate Accuracy*. Paper SPE 29577. Presented at the 1995 Joint Rocky Mountain Regional/Low-Permeability Reservoirs Symposium. Denver, Colorado, March 20–22.
26. Pratt, T. J., and Baez, L. R. G. 2003.
27. Bevington, P. R. 1969. *Data Reduction and Error Analysis for the Physical Sciences*. New York: McGraw-Hill; and Young, H. D. 1962. *Statistical Treatment of Experimental Data*. New York: McGraw-Hill.
28. Young, H. D. 1962.
29. Cardott, B. J. 1998. Coal as gas-source rock and reservoir, Hartshorne Formation, Oklahoma. In *The Hartshorne Play in Southeastern Oklahoma: Regional and Detailed Sandstone Reservoir Analysis and Coalbed-Methane Resources*. Andrews, R. D., Cardott, B. J., and Storm, T. Oklahoma Geological Survey Special Publication 98-7. Norman: University of Oklahoma.
30. Testa, S. M., and Pratt, T. J. 2003.
31. Pratt, T. J., and Baez, L. R. G. 2003.
32. Gas Research Institute. 1995.
33. Galloway, W. E., and Hobday, D. K. 1996. *Terrigenous Clastic Depositional Systems*. 2nd ed. Berlin: Springer-Verlag; and Mukhopadhyay, P. G., and Hatcher, P. G. 1993. Composition of coal. In *Hydrocarbons from Coal. AAPG Studies in Geology #38*. Law, B. E., and Rice, D. D., eds. Tulsa: American Association of Petroleum Geologists. p. 79.

34. Lamberson, M. N., and Bustin, R. M. 1993. Coalbed methane characteristics of Gates Formation coals, Northeastern British Columbia: Effect of maceral composition. *AAPG Bulletin*. V. 77 (no. 12). p. 2,062.
35. Mukhopadhyay, P. G., and Hatcher, P. G. 1993.
36. Ibid.
37. Close, J. C. 1993. Natural fractures in coal. In *Hydrocarbons from Coal. AAPG Studies in Geology #38*. Law, B. E., and Rice, D. D., eds. Tulsa: American Association of Petroleum Geologists.
38. Laubach, S. E., Marrett, R. A., Olson, J. E., and Scott, A. R. 1998. Characteristics and origins of coal cleat: A review. *International Journal of Coal Geology*. V. 35 (no 1-4, special issue). p. 175.
39. Gas Research Institute. 1996. *A Guide to Coalbed Methane Reservoir Engineering*. GRI-94/0397. Chicago: Gas Research Institute.
40. Bustin, R. M. 1997. Importance of fabric and composition on the stress sensitivity of permeability in some coals, Northern Sydney Basin, Australia: Relevance to coalbed methane exploitation. *AAPG Bulletin*. V. 81 (no. 11). p. 1,894.
41. Bustin, R. M., Cui, X., and Chikatamarla, L. 2008. Impacts of volumetric strain on $CO_2$ sequestration in coals and enhanced $CH_4$ recovery. *AAPG Bulletin*. V. 92 (no. 1). p. 15.
42. Laubach, S. E., et al. 1998.
43. Ibid.
44. Close, J. C. 1993.
45. Laubach, S. E., et al. 1998.
46. Ibid.
47. Close, J. C. 1993.
48. Laubach, S. E., et al. 1998.
49. Ibid.
50. Ibid.
51. Close, J. C. 1993; and Laubach, S. E., et al. 1998.
52. Reiss, L. H. 1980. *The Reservoir Engineering Aspects of Fractured Formations*. Paris: Gulf Publishing Company.
53. Gan, H., Nandi, S. P., and Walker, P. L., Jr. 1972. Nature of the porosity in American coals. *Fuel*. V. 51 (no. 4). p. 272; and Bustin, R. M., and Clarkson, C. R. 1999. Free gas storage in matrix porosity: A potentially significant coalbed resource in low rank coals. Paper 9956 in *Proceedings of the 1999 International Coalbed Methane Symposium*. Tuscaloosa: University of Alabama.
54. Reiss, L. H. 1980.
55. Ibid.
56. Gan, H., et al. 1972.
57. Ibid.
58. Ibid.
59. Ibid.
60. Levine, J. R. 1993. Coalification: The evolution of coal as source rock and reservoir rock for oil and gas. In *Hydrocarbons from Coal. AAPG Studies in Geology #38*. Law, B. E., and Rice, D. D., eds. Tulsa: American Association of Petroleum Geologists. p. 39.
61. Bustin, R. M., and Clarkson, C. R. 1999.
62. Gan, H., et al. 1972.
63. Ibid.
64. Nelson, C. R. 2001. Geologic controls on effective cleat porosity variation in San Juan Basin Fruitland Formation coalbed reservoirs. Paper 0108 in *Proceedings of the 2001 International Coalbed Methane Symposium*. Tuscaloosa: University of Alabama.
65. Wolf, K-H. A. A., Hijman, R., Barzandji, O. H., and Bruining, J. 1999. Laboratory experiments and simulations on the environmentally friendly improvement of coalbed methane production by carbon dioxide injection. Paper 9905 in *Proceedings of the 1999 International Coalbed Methane Symposium*. Tuscaloosa: University of Alabama.
66. Conway, M. W., Mavor, M. J., Saulsberry, J., Barree, R. B., and Schraugnagel, R. A. 1995. *Multi-Phase Flow Properties for Coalbed Methane Wells: A Laboratory and Field Study*. Paper SPE 29576. Presented at the Joint Rocky Mountain Regional Meeting and Low Permeability Reservoirs Symposium, Denver, Colorado, March 20–22.
67. Ramurthy, M., Young, G. B. C., Daves, S. B., Witsell, F. 2003. *Case History: Reservoir Analysis of the Fruitland Coals Results in Optimizing Coalbed Methane Completions in the Tiffany Area of the San Juan Basin*. Paper SPE 84426. Presented at the SPE Annual Technical Conference and Exhibition, Denver, Colorado, October 5–8.
68. Mavor, M. J. 1994. *Coal Gas Openhole Well Performance*. Paper SPE 27993. Presented at the University of Tulsa Centennial Petroleum Engineering Symposium, Tulsa, Oklahoma, August 29–31.
69. Young, G. B. C., McElhiney, J. E., Dhir, R., Mavor, M. J., and Anbouba, I. K. A. 1991. *Coalbed Methane Production Potential of the Rock Springs Formation, Great Divide Basin, Sweetwater County, Wyoming*. Paper SPE 21487. Presented at the SPE Gas Technology Symposium, Houston, Texas, January 23–25.
70. Berkowitz, N. 1979. *An Introduction to Coal Technology.* New York: Academic Press.
71. Schopf, J. M. 1956.
72. Mavor, M. J., and Nelson, C. R. 1997. *Coalbed Reservoir Gas-in-Place Analysis.* GRI-97/0263. Chicago: Gas Research Institute.
73. Berkowitz, N. 1979.
74. Mavor, M. J., and Nelson, C. R. 1997.
75. Scott, A. R., Kaiser, W. R., and Ayers, W. B., Jr. 1994. Thermogenic and secondary biogenic gases, San Juan Basin, Colorado and New Mexico—implications for coalbed gas producibility. *AAPG Bulletin*. V. 78 (no. 8). p. 1,189.
76. Ibid.

77. Lee, J., and Wattenbarger, R. A. 1996. *Gas Reservoir Engineering*. Richardson, Texas: Society of Petroleum Engineers; and McCain, W. D., Jr. 1991. Reservoir fluid property correlations—state of the art. *SPE Reservoir Engineering*. V. 6 (no. 2). p. 266.
78. Sutton, R. P. 1985. *Compressibility Factors for High-Molecular-Weight Reservoir Gases*. Paper SPE 14265. Presented at the SPE Annual Technical Meeting and Exhibition, Las Vegas, Nevada, September 22–25.
79. Wichert, E., and Aziz, K. 1972. Calculation of Z's for sour gases. *Hydrocarbon Processing*. V. 51 (no. 5). p. 119.
80. McCain, W. D., Jr. 1991.
81. Lee, J., and Wattenbarger, R. A. 1996.
82. Dranchuk, P. M., and Abou-Kassem, J. H. 1975. Calculation of Z factors for natural gases using equations of state. *Journal of Canadian Petroleum Technology*. V. 14 (no. 3). p. 34.
83. Lee, J., and Wattenbarger, R. A. 1996.
84. Scott, A. R., et al. 1994.
85. Bertard, C., Bruyet, B., and Gunther, J. 1970. Determination of desorbable gas concentration of coal (direct method). *International Journal of Rock Mechanics and Mining Sciences*. V. 7. p. 43; and Clarkson, C. R., and Bustin, R. M. 1999. The effect of pore structure and gas pressure upon the transport properties of coal: a laboratory and modeling study. 2. Adsorption rate modeling. *Fuel*. V. 78 (no. 11). p. 1,345.
86. Crank, J. 1975. *Mathematics of Diffusion*. London: Oxford University Press.
87. Smith, D. M., and Williams, F. L. 1984. Diffusional effects in the recovery of methane from coalbeds. *Society of Petroleum Engineers Journal*. V. 24 (no. 5). p. 529.
88. Gas Research Institute. 1995.
89. Smith, D. M., and Williams, F. L. 1984.
90. Pratt, T. J., Mavor, M. J., and DeBruyn, R. P. 1999. *Coal Gas Resource and Production Potential of Subbituminous Coal in the Powder River Basin*. Paper SPE 55599. Presented at the SPE Rocky Mountain Regional Meeting, Gillette, Wyoming, May 15–18.
91. Clarkson, C. R., and Bustin, R. M. 1999.
92. Levine, J. R. 1993.
93. Ibid.
94. Bromhal, G. S., Sams, W. N., Jikich, S., Ertekin, T., and Smith, D. H. 2004. Simulation of the effects of shrinkage and swelling on coal seam sequestration and coalbed methane production. Paper 0418 in *Proceedings of the 2004 International Coalbed Methane Symposium*. Tuscaloosa: University of Alabama.
95. Palmer, I. D. 1992. *Review of Coalbed Methane Well Stimulation*. SPE 22395. Presented at the SPE International Meeting on Petroleum Engineering, Beijing, China, March 24–27.
96. Gentzis, T., Deisman, N., and Chalaturnyk, R. J. 2007. Geomechanical properties and permeability of coals from the Foothills and Mountain regions of western Canada. *International Journal of Coal Geology*. V. 69 (no. 3). p. 153.
97. Mavor, M. J., and Gunter, W. D. 2004. *Secondary Porosity and Permeability of Coal vs. Gas Composition and Pressure*. Paper SPE 90255. Presented at the SPE Annual Technical Meeting and Exhibition, Houston, Texas, September 26–29.
98. Earlougher, R. C. 1977. *Advances in Well Test Analysis*. SPE Monograph 5. Dallas: Society of Petroleum Engineers.

# Geologic Aspects of Coal Gas Reservoir Engineering

# 3

## Introduction

Coal gas exploitation is difficult, if not impossible, without understanding the geology of a given deposit. Geology strongly influences the nature of a coal deposit, the gas resource it may hold, and its producibility. Coals have been mined for centuries and studied extensively in recent decades. Excellent studies covering different aspects of coal geology abound, such as those of Stach et al. and Galloway and Hobday.[1] However, since coals are mined, these studies have historically focused on shallow, high-purity seams that could be accessed with mining technology available at the time. Realization of coals as an unconventional gas resource has led to consideration of a much larger population of carbonaceous rocks from a much different perspective. Coal mines develop a deep understanding of at most a few seams on length scales much smaller than typically encountered in reservoir engineering. Mineable coals represent only a small fraction of all coal deposits, and a seam that is too deep, too high in ash, or too thin to mine can be a commercial gas reservoir.

Treating coal deposits as gas reservoirs has resulted in reinterpretation of previous works and initiation of new studies investigating reservoir aspects of coals. Coal deposits are among the most heterogeneous of all hydrocarbon reservoirs. Being the metamorphosed remnants of once-living material, coals are both source rock and organic reservoir rock. Unlike conventional reservoirs with sharply defined hydrocarbon boundaries, such as gas-water contacts, coal gas is often a diffuse resource, pervasive across organic deposits with irregular, poorly defined margins. The *flow capacity* of a coal seam is its ability to transmit fluids in response to a pressure difference; the reservoir engineer quantifies this flow capacity as *permeability*. The flow capacity is controlled by geology through natural fractures formed either during coalification or as a result of postcoalification deformation. Reservoir architecture is highly variable, and that portion of a given deposit considered as a gas reservoir often changes as a play matures. The Powder River Basin play began with exploitation of the shallow, thick Wyodak seam near strip mines. In contrast, the Warrior Basin play initially targeted the mineable Marylee/Blue Creek coal but soon grew to include multiple thin coals over a stratigraphic interval spanning more than 100 m. Completion strategies for coal wells targeting a single seam include openholes and cavitation, whereas multiple zone completions often require cased holes and multiple fracture (*frac*) stages.

Far from being an exhaustive review of coal geology, this chapter selectively draws from a wide body of literature in an attempt to identify some of the geologic elements important for understanding coal deposits as gas reservoirs. With worldwide demand for natural gas steadily increasing, coal reservoir geology is rapidly evolving, and the few topics discussed here are only the initial elements of coal geology that reservoir engineers should understand. Geologic concepts discussed here include geologic age, depositional setting, and maturity of a coal, as well as the origin of the gas it holds. As with conventional reservoirs, wireline logs are important for characterization of coal reservoirs. Wireline log responses in coals are discussed, with the primary logs being density, gamma ray, and caliper logs.

## Coal Ages, Distributions, and Depositional Environments

Coals are the preserved remains of organic materials that have been metamorphosed over geologic time by temperature and pressure into complex organic rocks containing a mixture of gases. Organic materials have been deposited and removed continuously since the appearance of life on this planet but are only rarely preserved and buried sufficiently long to become coals. Coals first appear in the geological record as coaly layers derived from aquatic plants growing in shallow lagoons of the Lower Devonian.[2] The first true coal deposits, distinct from the surrounding sediments, are associated with the appearance of land-based plants in the Middle and Upper Devonian, some 400 to 350 million years ago. The five major coal-forming periods, from oldest to youngest, are the Carboniferous (355 to 290 million years ago), the Permian (290 to 245 million years ago), the Jurassic (206 to 143 million years ago), the Cretaceous (143 to 65 million years ago), and the Cenozoic or Tertiary (beginning 65 million years ago).

As seen in table 3–1, Clayton classified almost one-third of the coals that have survived to modern times as from the Permian, about one-fifth of extant coals as Cenozoic or Jurassic in age, one-sixth from the Carboniferous, and one-eighth from the Cretaceous.[3]

**Table 3–1.** Distribution of coals by geologic age

| Period | Coal, % | Cumulative coal, % |
|---|---|---|
| Cenozoic | 21.1% | 100.0% |
| Cretaceous | 12.9% | 78.9% |
| Jurassic | 18.2% | 66.1% |
| Triassic | 0.7% | 47.8% |
| Permian | 29.0% | 47.1% |
| Carboniferous | 17.1% | 18.1% |
| Devonian | 1.0% | 1.0% |

*Source:* Clayton, J. L. 1993.

A slightly different age distribution was reported by Hayes, with 40% of global coal resources from the Carboniferous and Permian, 10% from the Triassic and Jurassic, and 50% from the Cretaceous and Tertiary.[4] Knowledge of the geologic age of a coal deposit aids in understanding reservoir behavior but is a poor predictor of commerciality.

Estimates of world coal resources vary between 4 and 30 trillion tonnes, reflecting differences in technical definitions (coal density cutoffs, mineable seam thicknesses, and ash concentrations) and confusion between resources and reserves.[5] The best estimate of global coal mass is on the order of 10 trillion tonnes, of which less than 10%, only 847,533 m (million) tonnes, are classified as proved recoverable coal reserves.[6] Table 3–2 shows global coal reserves sorted by rank and continent.

**Table 3–2.** Distribution of coals by rank and location

| Continent | Bituminous including anthracite, m tonnes | Subbituminous, m tonnes | Lignite, m tonnes | Total, m tonnes | Bituminous including anthracite, % | Subbituminous, % | Lignite, % | Total, % |
|---|---|---|---|---|---|---|---|---|
| Africa | 49,431 | 171 | 3 | 49,605 | 11.5% | 0.1% | 0.0% | 5.9% |
| North America | 116,592 | 101,440 | 32,661 | 250,693 | 27.1% | 38.0% | 21.8% | 29.6% |
| South America | 7,229 | 9,023 | 24 | 16,276 | 1.7% | 3.4% | 0.0% | 1.9% |
| Asia | 146,251 | 36,282 | 34,685 | 217,218 | 33.9% | 13.6% | 23.2% | 25.6% |
| Europe | 72,872 | 117,616 | 44,694 | 235,182 | 16.9% | 44.1% | 29.8% | 27.7% |
| Middle East | 1,386 | 0 | 0 | 1,386 | 0.3% | 0.0% | 0.0% | 0.2% |
| Oceania | 37,135 | 2,305 | 37,733 | 77,173 | 8.6% | 0.9% | 25.2% | 9.1% |
| total world | 430,896 | 266,837 | 149,800 | 847,533 | 100.0% | 100.0% | 100.0% | 100.0% |
| % of total world | 50.8% | 31.5% | 17.7% | 100.0% | | | | |

*Source:* World Energy Council. 2007.

On the basis of rank, one-half of global coal reserves are bituminous or anthracite, one-third are subbituminous, and one-sixth are lignite. Most high-rank coal reserves are concentrated in Asia and North America; most subbituminous reserves are located in Europe and North America. Lignite coal reserves are evenly distributed between North America, Asia, Europe, and Oceania.

However, coal resources have historically been assessed from a mining perspective and therefore imperfectly reflect coal gas resources. The shallow, thick, high-purity coal deposits that are considered mineable are but a small fraction of the coals that may be gas bearing. Coal resources and reserves discussed above are based on various coal depth cutoffs, all less than 1,800 m (5,900 ft) and most less than 1,000 m (3,300 ft). Minimum coal seam thickness ranges from 0.1 m to more than 1 m and, within a given country, frequently varies with coal rank. Coal purity cutoffs are often related to Schopf's definition of coal as a rock that is at least 50% by weight and 70% by volume carbonaceous material.[7] Such screens are at once too conservative and too liberal for estimation of coal gas resources and reserves. They are too conservative in that deep, thin, high-ash coals may have generated significant quantities of gas and are too liberal in that a shallow, thick, low-ash coal seam may have insufficient permeability for commercial gas production.

The organic precursors to coal have been deposited at all latitudes. Galloway and Hobday noted the latitude of deposition for coals depends on geologic age.[8] Carboniferous coals were predominantly deposited in equatorial conditions, while Permian coals reflect cold, high-latitude, postglacial environments. Jurassic coals were deposited at mid- to high latitudes, Cretaceous coals originated in swamps at latitudes above 45°, and Tertiary coals were deposited at all latitudes. Latitude dictates climatic conditions of swamps, and plant communities of those swamps became more diverse over geologic time. Equatorial swamps are populated with luxuriant plant communities and commonly experience rapid, continuous accumulation of peat. A tropical swamp can renew itself in seven to nine years, with trees growing up to 30 m in height.[9] In contrast, high-latitude swamps are often characterized by reeds, mosses, and other low plants, with episodic accumulation of organic matter, such as autumnal plant litter. Plant communities in early coal swamps were characterized by mosses, shrubs, and low ferns. As plant life evolved, vegetation in the swamps became more diverse and included large trees up to 35 m in height and a variety of grasses. Evolution of flowering plants in Cretaceous times further diversified plant communities and the resulting coals.

Peats are deposited at annual rates of 0.3 mm to 3 mm and are compressed during coalification to about 10% of their original thickness.[10] Thus, a 1 m coal seam represents 3,000 to 30,000 years of stable swamp deposition. Alternatively, the slow depositional rate of 0.3 mm/year over the 5,000 years of recorded history would result in a coal seam thickness of 15 cm, roughly equal to the span of a human hand. The rapid depositional rate of 3 mm/y over the same time interval would lead to a coal seam thickness of 1.5 m, a bit less than the average height of modern humans.

Seven factors controlling coal properties identified by Stach et al. included type of deposition, plant communities, nutrient supply, swamp acidity, peat temperature, redox potential, and deposition setting.[11] Peat, the organic precursor of coal, can be laid down by in-situ vegetation (*autochthonous*) or derived from plant material washed into the swamp (*allochthonous*) or from reworked in-situ vegetation (*hypautochthonous*). Almost all mineable coal deposits are from autochthonous peats, as the other two types often have high ash. From a reservoir perspective, autochthonous coals, with generally lower ash contents, would be expected to have higher gas contents than the other two types, but coal permeability appears to be largely independent of the source of the vegetation.

Plant communities, the second element noted by Stach et al., vary continuously in time and space across a swamp.[12] For instance, a shallow lake with soft-bodied aquatic plants fills steadily from the margins as shoreline species, such as reeds and then trees, migrate inward. Or openwater swamps progress to reedy swamps and then forest swamps before fires force a return to openwater swamps. Plant communities affect a coal reservoir more on the microscopic scale, e.g., macerals, than the macroscopic scale of gas resource and producibility.

Swamps with an abundance of nutrients (*eutrophic*) are characterized by lush, robust growth of a diverse plant community. Swamps with minimal nutrients (*oligotrophic*) exhibit stunted growth from a limited number of plant species. Swamps distinct from these two end members, with mixed nutrient supply (*mesotrophic*), support sufficient growth for peat accumulation from a modest number of species. Most bituminous coals were laid

down in eutrophic swamps sustained by regular flooding of rivers, lakes, and seas.[13] The rapid, diverse growth of a eutrophic swamp can result in high-purity, relatively permeable coals, with minimal flow barriers from shaley or sandy streaks laid down in episodic floods. The slow accumulation of organic matter in oligotrophic swamps is conducive to contamination by periodic floods and airborne dust, resulting in finely dispersed ash throughout a relatively low-permeability coal body.

Acidity of swamp water, the fourth element identified by Stach et al., affects preservation of organic material.[14] Highly acidic peats promote preservation of vegetal accumulations. As pH values rise above about 5.0, a peat accumulation is subject to severe degradation.[15] In general, salt marshes are more acidic than freshwater swamps. Peat preservation is quite sensitive to acidity, and even brief episodes of elevated pH, such as seasonal flooding, can degrade peat. Highly alkaline environments support rapid degradation of plant matter and are prone to pyrite formation if sulfur is present, especially if a peat experiences a marine transgression or if iron is present in the groundwater. Pyrite, with a density of 5.0 g/cm$^3$, can affect the density log, as discussed in the section on wireline logs below.

Peat temperature also influences preservation of plant material, as optimal bacterial degradation occurs at 35°C to 40°C (95°F to 104°F). Rapid burial and subsidence of cool swamps can preserve accumulated organic materials, whereas slow burial of a tropical swamp promotes peat degradation. While peat temperature is important for primary decomposition of organic material and the genesis of coalification, it is only a minor control on coal reservoir properties.

Redox potential, the sixth factor identified by Stach et al., addresses degradation of plant materials in the presence of oxygen.[16] The low oxygen levels of anaerobic environments, often characterized by stagnant waters, promote plant preservation, whereas the high oxygen levels of aerobic swamps do not. Oxidation of peat primarily affects the resultant coal on the microscopic level through maceral formation rather than macroscopic reservoir properties.

Depositional setting, the final factor affecting coal properties identified by Stach et al., is a major control on coal reservoirs.[17] Coals have been laid down in a variety of depositional environments, including alluvial fans, fluvial, delta, shore-zone, and lacustrine systems. Detailed geologic aspects of each of these environments are discussed elsewhere.[18] Influences of depositional environment on coal gas reservoir engineering are discussed briefly here.

Alluvial fans are cone-shaped bodies built up by shifting networks of ephemeral streams (dry fans) or perennial streams (wet fans). Peats are developed on the distal edge of the cone or in intralobe depressions. Stream migrations initiate and terminate deposition of peat bodies, while episodic flooding, especially in fans with high sediment loads, increases ash content of the resulting coals. The resulting coal deposits are irregularly shaped bodies generally aligned with the alluvial cone structure or along the distal edge of the cone where groundwater nourished peat swamps or the fan merged into a lacustrine environment. Examples of coals formed in alluvial fans include those of the Karoo Basin of South Africa and the Sydney Basin of Australia.[19]

Permian coals of the Sydney Basin formed at the intersection of large, cold climate gravel fans and margins of glacial-fed lakes. The 15 or more seams commonly present in a fan cover a gross stratigraphic interval of 400 m and are typically 1–3 m thick, with a maximum thickness of 9 m. The thin coals and a net-to-gross ratio of approximately 0.1 of this coal deposit imply multizone completions. Flow capacity of a coal zone completed in a well depends not only on permeabilities of the coal bodies proper that comprise the seam, but also on permeabilities of any preserved stream channels that defined or scoured the coal bodies. Water production from channels filled with high-permeability sandstone could prolong coal dewatering, delaying gas production. In contrast, tight sandstones could retard water influx or perhaps even provide a flow barrier, accelerating dewatering and gas production. Individual seams in a Sydney Basin alluvial fan can cover up to 400 km$^2$ (150 mi$^2$). Assuming the Kokand alluvial fan of semiarid western Siberia is a modern analog of ancient alluvial fans, where a typical peat body occupies 1% of total fan area, yields a coal body area of 4 km$^2$ (400 ha or 990 ac).[20] Under the simple assumption that the peats of an alluvial fan are subjected to uniform burial and coalification with little tectonic deformation over geologic time, the resulting coal deposit is still a complex assembly of coal bodies. These coal bodies are difficult to correlate as individual seams and often provide infill opportunities during coal gas extraction.

A second coal depositional environment is *fluvial systems*, which primarily collect and transport sediment into basins by water flow.[21] Fluvial systems can persist over geologic time, but individual flow channels are dynamic, often shifting laterally, splitting and joining, abandoning and reoccupying a given course. Peats often develop in the interchannel zones and are characterized by slow depositional rates of 20 to 80 cm per millennium.[22] The resulting coals are often elongated along dip, with narrower coal bodies associated with high-energy, linear flows and wider deposits associated with meandering, lazy flows. Coals along the fluvial margin are often thin and split and show a higher ash content than those from the back swamp area, which is relatively free of sediment loading except during seasonal and major floods. Established peat swamps resist erosion, serving to stabilize flow in existing channels and preserve interchannel organic deposits.

Coals laid down in fluvial systems can be up to 20 m thick.[23] Length scales of coals deposited in fluvial systems range from tens of meters to tens of kilometers.[24] The bounding fluvial channels, which compact less than peats, can affect coal well performance, similar to those of alluvial fans described above, acting either as conduits for water or as permeability barriers. Less energetic, shorter-lived streams may simply wash out a channel from the surface of a peat swamp, leaving a sand lens or stringer in the resulting coal. Crevasse splays reduce coal quality on a small scale, both laterally and vertically, degrading coal quality, generated gas, and flow capacity. Fluvial coal reservoirs display considerable heterogeneity with a spectrum of permeabilities. Similar to alluvial fans, correlation of individual seams can be difficult over more than a few kilometers. Due to the variation in thickness and areal extent of coals deposited in fluvial systems, extraction of gas from these coals requires different development schemes. Thick, areally extensive coals can sometimes be exploited with single-zone completions in widely spaced wells, whereas thin, areally limited coal bodies can require multiple-zone completions in closely spaced wells. Examples of coals deposited in fluvial systems in the United States include the deposits of the Powder River Basin of Wyoming and Montana and those of the Gulf Coast of Texas and Louisiana.[25]

Deltas form where rivers enter a body of water. Common deltas include wave-dominated, tide-dominated, and fluvial-dominated deltas. Deltaic coals provide a variety of coal reservoir styles. Coals in wave-dominated deltas parallel the shore face, often connecting through nominally perpendicular channels and estuaries. The laterally extensive, strike-elongate seams are separated by beach ridges sandstones, and performance of wells completed in such coals is partially controlled by the permeability contrast between coals and sandstones. If permeabilities of coals and sandstones are nearly equal, coal gas could be recovered by vertical wells on regular spacing. If permeabilities of coals were larger than those of the sandstones, reservoir permeability is anisotropic, and coal gas recovery could be accomplished by horizontal wells aligned with the major coal body axes. If the coals are less permeable than the sandstones, coal gas recovery could be complicated by strong water influx from the latter. In the United States, coals of the southeastern Piceance Basin in Colorado were deposited in both the lower and upper regions of a wave-dominated delta.[26] Coals of the lower delta plain are elongate bodies, paralleling the north-south paleoshoreline, with lengths greater than the 40 km north-south dimension of the study area. Individual seams are 10 to 13 km wide in the east-west direction, with thicknesses up to 32 m. Upper delta plain coals were reported to be thinner and less extensive than those of the lower delta, but seam dimensions were not quantified.

Tide-dominated deltas are controlled by the relative strengths of freshwater and tidal influxes and are often oblate, with a major axis as much as 200 km in length.[27] Geomorphology of these deltas is discussed in detail by Galloway and Hobday.[28] Tidal flats of regressive environments support a diversity of plant communities ranging from salt-tolerant species at the progradational front to freshwater trees, shrubs, and grasses on the landward margin. In a transgressive environment, estuaries often dissect the tidal flats prior to flooding by marine waters. Tidal flats frequently support luxurious plant growth, with the resulting laterally extensive peat deposits compartmentalized by estuaries and tidal inlets. Tide-dominated deltas have sourced few commercial coals, and many technical details of this environment, including reservoir engineering aspects, of this depositional environment are not as well understood as others.[29]

Fluvially-dominated deltas source coal deposits with different geometries. During the constructive phase of the delta life cycle, peats are laid down in the interchannel region and are frequently dip-elongated bodies of limited areal extent and thickness. Distributaries tend to be stable, extending their course basinward, leaving

the adjacent peats relatively free of washouts, but detrital splits due to sediment-laden floodwaters are common. Ash contents can be high. Coals deposited during the abandonment phase of fluvially dominated deltas can be areally extensive, even blanket-type, coals covering up to 500 $km^2$.[30] Coals of the lower delta plain tend to be thinner but can cover large areas, limited by distributaries and splays. In contrast, coals deposited in the transitional area from lower to upper delta plain are generally thicker and of greater areal extent. Distributary confinement is not uncommon, leading to thick, laterally extensive, high-quality coals in the central backswamp areas. As the roof rocks deposited over these coals are among the most stable, many commercially important coals are found in this transition zone. Upper delta plain coals tend to be thick but of limited areal extent, being confined to interchannel areas. Splays from these channels can be extensive, and the resulting coal bodies are characterized by several coal "benches" interbedded with thin shales and sandstones.

Shore-zone systems support peat development in backbarrier and tidal flat settings. The shallow bays, lagoons, and marshes of the back-barrier environment reflect the interplay between freshwater fluvial and marine influences. Back-barrier coals of the Northern and Central Appalachian basins in the United States are thin, discontinuous, and high in sulfur (reflecting a strong marine influence). In contrast, those of the Gippsland Basin in Australia are individually as thick as 100 m, with up to eight mudstone partings from minor basinwide transgressions.[31] Back-barrier coals are parallel to the shoreline and may be crosscut by tidal inlets. Under favorable circumstances, these parallel peat bodies grow laterally and vertically, clogging tidal creeks and coalescing into widespread peats. Transgressive episodes favor deposition of these laterally extensive coals. Barriers of a shore-zone system help preserve delta plain peats, with the ash fraction of the resulting coals affected by splays and washovers. Higher ash content often correlates with higher energy environments. Tidal flats are frequently high-energy environments that rework or remove organic material, resulting in slow accumulation of randomly oriented peat bodies. The resulting coals are thin, defined by estuaries cutting the tidal flat, and high in sulfur. Shore-zone coal deposits are typically thin, multilayered gas reservoirs. Each layer is composed of erratically shaped coal bodies with no clear depositional orientation. Development of shore-zone coals typically requires multizone completions and tight well spacing.

Lacustrine environments can provide conditions suitable for peat development, especially in deltas, but are often on smaller scales than in other environments discussed above. Length scales of lakes tend to be smaller than those of other depositional environments, restricting peat body development accordingly. Plant communities on a lake perimeter are controlled by shoreline gradient, with more areally extensive bodies associated with shallow, gentle slopes, and river deltas, where sediment loads and thermal contrasts control deposition, and hence, peat growth. Water levels in lacustrine settings vary more frequently and over larger intervals than in other environments. Annual lake-level fluctuations on the order of 1 m, 5 m variations on the order of a century, and 350 m over 75,000 years have been recorded.[32] For perspective, coals form only where there is balance between being too low and subject to flooding with clastics and too high to prevent peat accumulation. The difference between "too low" and "too high" is on the order of a few meters.[33] Lacustrine coals reflect shoreline geometry, sometime paralleling an ancient shore, sometimes showing characteristics of interchannel peats of a fluvial delta. A warm, shallow, stable lake could be filled by organic matter as plant communities on the perimeter progressively advanced across the lake, ultimately filling it with peat.

In any given basin, depositional environments often vary areally and stratigraphically, resulting in coal bodies with different reservoir characteristics. A present-day example of concurrent depositional diversity is the Barataria Basin, which is bounded by distributary channels of the Mississippi River, one abandoned, one active, and by barrier islands between the bay and the Gulf of Mexico.[34] An elongate basin more than 150 km long and 60 km wide, the distal end is a saline marsh where the bay joins the Gulf of Mexico. Moving landward, the saline marsh gives way to a brackish marsh and then a freshwater marsh. The final upstream environment is forested wetland, including some hardwood stands, with characteristic lengths on the order of 5 km. Several lakes, present in the upper reaches of the basin, show characteristic lengths of 10 to 20 km. Crevasse splays are lobate or teardrop-shaped, with a maximum dimension of 15 km.

Reservoir complexity increases during coalification through several mechanisms, including compaction and fracturing. As noted above, peats compact in the ratio of 10:1 during burial. In contrast, Laubach noted sand body compaction is around 1.5:1.[35] Thus, concurrent deposition of peats and sands in, for example, fluvial or

deltaic environments produces roughly planar, heterogeneous accumulations that differentially compact during burial. A 10 m peat will compact to a 1 m thick coal, whereas an adjacent sand body will compact to a 6 or 7 m thick sandstone. In the extreme, a coal seam in such a sequence could be draped over sandstones six or seven times as high as the seam is thick. Many coals are brittle, especially Paleozoic coals, and these deformations fracture the coals, overprinting the cleats and providing additional anisotropic permeability on a local scale.

In addition to these fold-related fractures, regional fractures and faults are often present in coal deposits. Faults with significant throw clearly contribute to structural complexity and can also act as conduits for groundwater flows, which may precipitate minerals in coal cleats and fractures. Investigation of minerals in the joints of coals, shales, and sandstones of the Warrior Basin of Alabama by Pitman et al. revealed mainly calcite precipitates associated with fresh water plumes from meteoric recharge along the southeastern margin of the basin.[36] These plumes also facilitated late-stage biogenic methane, resulting in a compartmentalized coal reservoir with high gas contents. Inspection of fresh exposures in two coal mines indicated pervasive calcite fill in the coal cleats to a distance of 5 m from the faults. Pitman et al. noted these faults are frequently effective seals.[37] However, as a gas seep has been documented along at least one fault, the reservoir compartmentalization due to faults and any subsequent mineralization of faults and cleats are not the classical no-flow boundaries commonly assumed in reservoir engineering. Additional reservoir complexity is added by patchy, random areas of calcite-filled cleats with length scales below that of the joints and the well spacing. This same study reported carbon isotope ratios of the calcite correlated with methane producibility, perhaps providing reservoir engineers a key for coal gas exploration as well as development planning.

**Depositional environments of selected coals.** Coals of the San Juan Basin were laid down behind beach barrier deposits as an ancient seaway retreated from southwest to northeast across the basin.[38] Appearing in en echelon formation, coals rise stratigraphically to the northeast. Thickest coals are found in the northeast part of the basin where a stillstand allowed thick peat deposits to develop. Backbarrier coals are thinner but more areally extensive than delta plain coals. Individual coal body thicknesses range from 2 to 5 m (6 to 26 ft) and cover an area between 2.5 and 11 $km^2$ (1.5 to 7 $mi^2$). Maximum seam thickness is 6 to 9 m (20 to 30 ft), indicating a seam could be composed of several different coal bodies. Coal wells in this basin were initially spaced on 320 ac, which has proven adequate to drain the high-productivity fairway of the basin. However, other areas of the basin, notably the northeast portion, have seen infill drilling campaigns down to 160 acre spacing and now down to 80 acres.

Warrior Basin coals were laid down in regionally extensive depositional cycles termed *cyclothems*, which consist of a vertical repetition of shale overlain by sandstone overlain by coals. Driven by sea level fluctuations, mean frequency of a cycle was 0.2 to 0.5 million years.[39] *Coal groups*, the stratigraphic cluster of coal bodies within a cycle, are the basic geological unit in this basin, and the seven major coal groups were laid down over a period of 1.4 to 3.5 million years. Warrior Basin coals were deposited in fluvial and deltaic environments strongly influenced by structure. Thicker coals formed in flood basins on upthrown blocks, and thinner coals accumulated in fluvial systems on downthrown blocks.[40] Controls on coal seam thickness and geometry were discussed by Pashin.[41] Geometries of the resulting coal bodies include dendritic (5 mi by 10 mi), elongate (5 mi by 15 mi to 0.7 mi by 1.2 mi), lens (0.3 mi by 0.6 mi), and lenticular (0.3 mi by 2 mi). These individual coal bodies, which exhibit complex geometry on a local scale, are amalgamated into areally extensive coal seams.

In the United States, coals of the Powder River Basin of Wyoming and Montana occur in the Fort Union and Wasatch formations and are exceptionally thick (65 m, 210 ft). Coals found in the Fort Union Formation may have formed in a fluvial environment with meandering and anastomosed streams or in the deltaic margins of a lacustrine environment.[42] Wasatch coals were deposited in fluvial and alluvial fan settings, with the thickest coals bodies located between two contemporaneous systems. In the stable, favorable climates of both Fort Union and Wasatch times, channels accreted vertically, and thick peats formed in areas isolated from clastic influx. The thickest coals are thought to have been sourced by material in poorly drained back swamps subject to groundwater influx.[43] Coals formed from anastomosing stream environments tend to be discontinuous pod-shaped bodies 2 km by 8 km (1 mi by 5 mi) in area. Those associated with the meandering fluvial system are narrow, lenticular bodies 25 km by 80 km (15 mi by 50 mi).

Because of variations in depositional environments, climatic conditions, and evolution of swamp flora, coal seam thickness and lateral extent do not correlate. Coal body thicknesses and areas reported for the San Juan, Warrior, and Powder River basins by Flores are collected in table 3–3 and plotted in figure 3–1.[44] Thus, coal seam thickness encountered in an exploration well will not help determine areal extent of a possible coal gas field and the number of wells required to develop it.

**Table 3–3.** Selected coal body thicknesses and areas

| Basin | Depositional environment | Avg. thickness, m | Width, km | Length, km | Avg. area, km$^2$ | Avg. thickness, feet | Width, mi | Length, mi | Area, mi$^2$ |
|---|---|---|---|---|---|---|---|---|---|
| Powder River | fluvial | | | | | | | | |
| | meand.-anast. | 5 | 2 | 3 | 5 | 15 | 1 | 2 | 2 |
| | meandering | 10 | 24 | 80 | 2,000 | 30 | 15 | 50 | 750 |
| | anastomosed | 30+ | 2 | 5 | 8 | 100+ | 1 | 3 | 3 |
| | alluvial fan | 30+ | 5 | 30 | 160 | 100+ | 3 | 20 | 60 |
| | Lake DeSmet | 80 | 5 | 30 | 160 | 250 | 3 | 20 | 60 |
| San Juan | coastal plain | | | | | | | | |
| | deltaic | 3 | 2 | 6 | 15 | 8 | 1.5 | 4 | 6 |
| | back barrier | 2 | 8 | 30 | 250 | 6 | 5 | 20 | 100 |
| Warrior | fluvial-coastal | | | | | | | | |
| | paleovalley | 2 | 8 | 15 | 130 | 6 | 5 | 10 | 50 |
| | floodbasin | 2 | 8 | 25 | 200 | 7 | 5 | 15 | 75 |
| | downthrown block | 0.6 | 1 | 2 | 2 | 2 | 0.7 | 1.2 | 0.84 |
| | upthrown block | 0.9 | 1 | 3 | 3 | 3 | 0.6 | 2 | 1.2 |

*Source:* Flores, R. M. 1993.

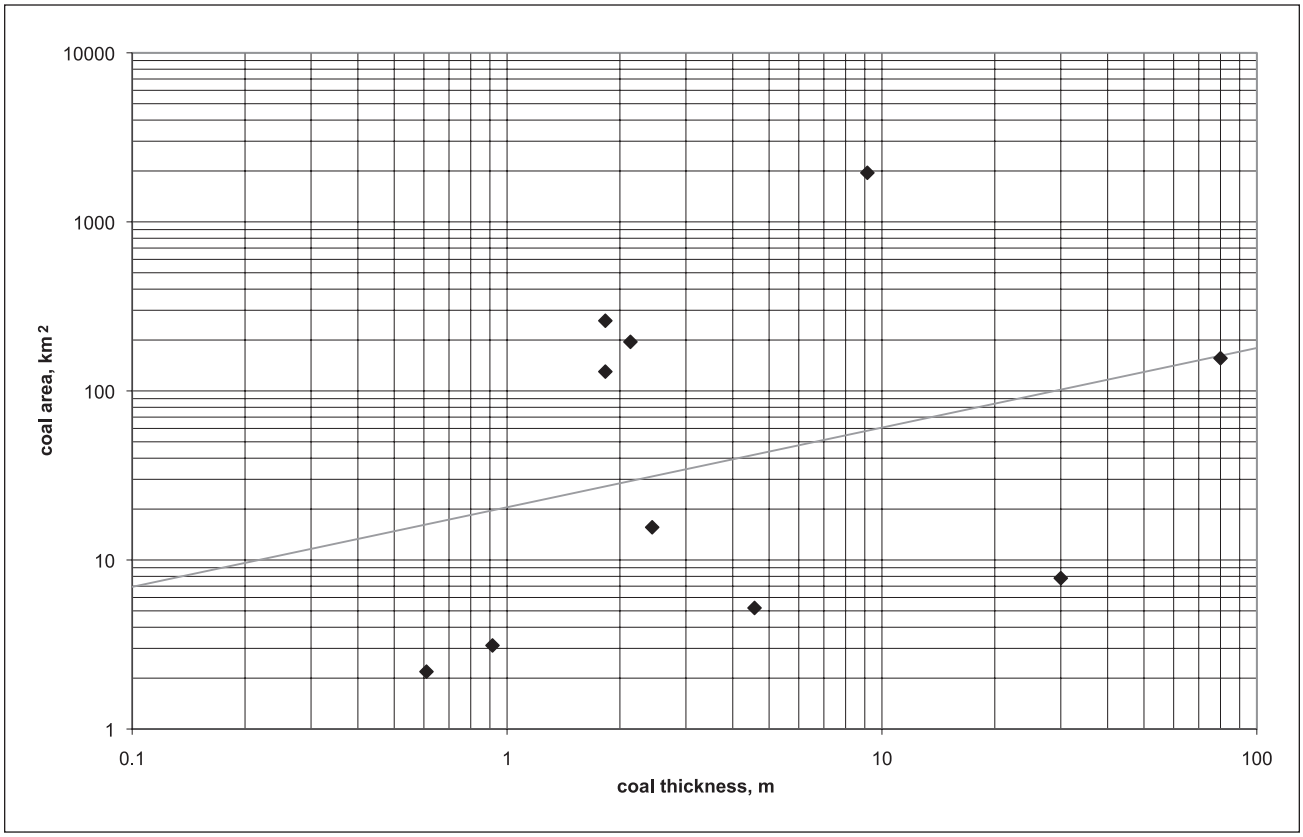



**Fig. 3–1.** Coal seam thickness vs. area

Depositional environments of many coal deposits have been described in the literature. Deposition of the organic precursors to the coals in the Cook Inlet in south central Alaska was controlled by braided, anastomosing streams meandering over a broad plain subject to overbank flooding.[45] Coalbed methane resources of the Qinshui Basin of China are held in Carboniferous and Permian coals. The Carboniferous Taiyuan coals were laid down in a system of lagoons, barrier islands, and tidal flats. The Permian Shanxi coals were deposited in a deltaic environment, with the delta plain in the north part of the basin and the delta front in the south.[46] Coals of the South Sumatra Basin, ranked as one of the most prospective Indonesian basins for coal gas exploration by Stevens et al., were deposited in a transgressive fluvial-deltaic-shoreline complex.[47] Individual seams are up to 12 m thick and lenticular in shape, with limited areal extent. Many of the most economically important coals of the Northern Appalachian Basin, the Monongahela Group, were deposited in a series of "vast lakes" and "deltaic-lake margin" settings, with no marine sedimentation.[48]

Depositional environments of selected coals in the province of Alberta, now better understood through coal gas exploitation, were discussed by Beaton.[49] The Ardley coals of the Scollard Formation were deposited in fluvial and lacustrine settings and are grouped into four separate zones, each containing multiple seams. Seams are more numerous, and individual seams are thicker and more laterally extensive in areas of increased subsidence and protection from clastic input from the major river systems. Horseshoe Canyon coals were interpreted as those of a tide-dominated delta by Galloway and Hobday.[50] However, Beaton and Bastian et al. suggested these coals were laid down on a coastal plain on the margins of the Bearpaw Sea in a variety of settings including alluvial, fluvial, lacustrine, and shoreline.[51] This reservoir is characterized by multiple thin seams that vary in lateral continuity. Bastian et al. reported some individual coal seams can be mapped over 50 km (30 mi) in a depositional strike direction and 16 km (10 mi) in a depositional dip direction, whereas other seams pinch out within 1 or 2 km (1 mi).[52] Mannville coals are associated with backbarrier, lagoonal, estuarine, and tidal flat depositional environments. Lower Mannville coals were laid down during infilling of high-relief paleoterrain, resulting in more erratic coals bodies than those of the Middle and Upper Mannville. Middle Mannville coals were deposited in shoreline and near-shoreline environments, while the Upper Mannville coals are part of a prograding clastic wedge consisting of several transgressive/regressive cycles. Gething coals (Mannville equivalent) were deposited in upper and lower delta plain settings, while coals of the Gates Formation were laid down in nonmarine coastal plain and fluvial environments. Mist Mountain coals developed in a nonmarine coastal plain setting.

**Peat mires.** Regardless of geologic age, latitude of peat formation, or depositional environment, coals seams can be regarded as groups of coal bodies, each of which originated as a peat mire. Geometry of a peat mire is heavily influenced by the water sources sustaining it. The two basic peat mire forms are planar and raised or domed. *Planar mires* are fed by surface runoff and groundwater. These water sources are high in dissolved solids, providing both mineral nutrients for plant growth and high-to-moderate ash in the resulting coal. Vegetation is robust and varied, but preservation of the resulting organic debris is limited due to high-pH waters (generally above 4). Planar swamps are susceptible to episodic and seasonal flooding that erodes organic material and introduces highly oxygenated water, retarding anaerobic decomposition. Widely dispersed fine sediments mix with the organic matter, leading to high-ash coal with reduced gas capacity and, perhaps, permeability. A major flood can leave sufficient sediments across the top of the peat to form a vertical flow barrier in the coal. Reservoir properties of coals derived from planar mires (ash content, maceral distribution, and cleating) are typically more areally homogenous than those of coals from raised mires.

*Raised* or *domed mires* form when rainfall is the major source of water to a swamp, exceeding surface runoff and groundwater. In humid environments with low evaporation, peat domes can rise as much as 15 m (50 ft) above the adjacent waterways, and with surface grades of 1 to 2 m/km, can extend 15 to 30 km laterally.[53] Rainfall supplies moisture but few nutrients to the interior of a raised mire, resulting in stunted, limited plant growth in highly acidic conditions. Consequently, peat accumulation is slower here than in planar mires but tends to be better preserved. Clastic influx is generally confined to dome margins, resulting in relatively low-ash coal in the interior of a raised mire. Coals from raised mires can show significant lateral variation in reservoir properties, with well-cleated, high-vitrinite, low-ash coals formed in the interior of the mire and variably cleated, high-inertinite, high-ash coals from the margins. The thick coal of the mire interior can feather out at the edges, sometimes splitting into two or more beds.

Knowledge of coal body geometry helps determine completion strategies and understand subsequent performance in wellbores penetrating multiple seams. Stratigraphically proximal seams may be derived from different depositional environments, with the interbedded strata laid down in geological periods devoid of swamps. This is the case of the cyclothems of Paleozoic coals in the Warrior Basin. Or adjacent coals may represent the landward edge of backbarrier swamps or the distal margins of a fluvial system, such as the Cretaceous Fruitland coals of the San Juan Basin or the Paleocene-Eocene coals of the Powder River Basin, respectively. Completing in the lowermost seam and sequentially moving to uphole coals as the producing seam depletes is a reasonable strategy in coal deposits from distinct swamps. The same completion strategy in a well penetrating a swamp margin will yield perplexing results, as a completion in the perceived basal coal is actually a completion in the lowest bench of the coal deposit. Within a short distance, a kilometer for example, this bench may merge with the main seam, formed from the interior of a peat mire. Production from this completion will be dominated by water drained from the entire seam, delaying and minimizing gas production. Subsequent completion in the perceived uphole coal is actually a completion in the upper bench of the now-dewatered coal body and will be characterized by shorter dewatering times and earlier, stronger gas production. Moving uphole, completion in a third apparent seam would show an even shorter dewatering time and stronger gas production as a fraction of the gas liberated by the lower completions has migrated up structure.

Actual coal wells often encounter a spectrum of coal body types, with planar and raised mires simply being end members. Because well behavior is a superposition of single coal body behaviors discussed above, performance of adjacent wells is often very different. Wells with essentially identical completions can exhibit rates and recoveries differing by an order of magnitude. Knowledge of the depositional environments of the seams penetrated by a well will help understand well performance and guide field development.

Various maceral indices, usually pairs, help characterize depositional environments. Galloway and Hobday discuss characterization of Gondwana coals of the Jharia Basin in India using two such indices developed by Diessel.[54] The *gelification index* (*GI*) is defined by

$$\text{gelification index} = \frac{\text{vitrinite} + \text{macrinite}}{\text{semifusinite} + \text{fusinite} + \text{inertodetrinite}}$$

The *tissue preservation index* (*TPI*) is defined by

$$\text{tissue preservation index} = \frac{\text{telinite} + \text{telocollinite} + \text{semifusinite}}{\text{desmocollinite} + \text{macrinite} + \text{inertodetrinite}}$$

Coals sourced from dry forest moors and laid down on debris-flow and stream-dominated glacial outwash fans exhibited low-GI and high-TPI values. Coals from a seasonal, warm, humid climate laid down in a fluvial system showed low-to-moderate GI ratios and variable TPIs.

Determination of mire types of 13 coal bodies of the Central Appalachian Basin in southern West Virginia by means of another pair of coal maceral indices was discussed by Staub.[55] The *groundwater index* is defined as

$$\text{groundwater index} = \frac{\text{desmocollinite} + \text{mineral matter}}{\text{telocollinite}}$$

And the *cell preservation index* is defined by

$$\text{cell preservation index} = \frac{\text{telocollinite} + \text{semifusinite} + \text{fusinite}}{\text{desmocollinite (+ exinite)}}$$

The groundwater index is a measure of groundwater influence during mire formation, with lower values indicative of minimal groundwater control. The cell preservation index indicates degree of organic preservation, with higher values reflecting better preservation.

High-sulfur coals are frequently associated with marine depositional settings or peat mires drowned by a transgressing sea. During coalification, geochemistry favors pyrite formation over sour gas generation. Consequently, occurrence of sour gas in native coals is extremely rare. Sour gas production reported from coal wells is often associated with mines that have recirculated produced water for mine usage, such as dust suppression, introducing sulfate reducing bacteria into the deposit.

Commercial coal gas production is neither guaranteed nor precluded by deposition in a specific geologic age or a given environment, making them poor screens for coal gas potential. These two elements influence but do not control gas storage and flow capacity of a coal deposit. Swamp flora, constantly evolving over geologic time, influence coal character on the maceral level, and hence, storage of both sorbed and free gas. Depositional environment affects reservoir architecture, and hence, overall flow capacity of a coal seam. Knowledge of coal age and depositional setting helps determine optimal well spacing, well completions, and the subsequent coal well behaviors.

## Coal Rank

Coal rank is a measure of thermal maturity and reflects the degree of metamorphosis of the original organic materials. It is one of the primary elements for construction of analogs and is often used as an exploration screen. As discussed in chapter 2 and shown in table 2–1, the nine coal ranks in order of maturity are peat, lignite, subbituminous, high-volatile bituminous, medium-volatile bituminous, low-volatile bituminous, semianthracite, anthracite, and meta-anthracite. Effects of time, temperature, and depth of burial on progression of organic material through these ranks are detailed in Berkowitz and Stach et al.[56] Coal rank can be determined by several methods (vitrinite reflectance, daf volatile matter, or calorific value), all of which require samples on the order of 100 g, making them essentially point source measurements in a reservoir. Rank determination of seams penetrated by a wildcat well should be part of any exploration program, as amalgamation of rank data from wells drilled throughout a coal deposit can provide insight into stratigraphic and areal variations in reservoir behavior.

Coal rank influences both thermogenic gas generation and cleating. Consequently, both the size and producibility of the gas resource in a coal deposit are related to coal rank. As discussed below, gas is generated throughout maturation of a coal, peaking in the bituminous ranks. On a dry, ash-free basis, gas generation across the bituminous portion of the rank spectrum is an order of magnitude greater than that generated by maturation up through subbituminous rank. On a cumulative basis, total gas generated by maturation of organic matter through anthracite is two orders of magnitude greater than the gas volume generated up through subbituminous rank coals.

Macroscopic fluid flow through a coal deposit depends on permeabilities of individual coal and sand bodies, interbedded shales and bony, ashy coals, and faults and large-scale, tectonic fractures. Fluid flow in the drainage area of a given well is also strongly influenced by the cleat network. Coal cleats, the two sets of natural fractures present in coals, vary with rank. Subbituminous coals have poorly developed cleats, often widely spaced and with only a weak preferential orientation. Bituminous coals often exhibit classic cleating with well-developed, extensive, closely spaced fractures organized into clearly visible networks of face and butt cleats. Anthracitic coals, with highly organized molecular structures, lose cleats with maturation, leaving a brittle rock whose anisotropic permeability comes primarily from tectonic fractures. Coal permeability, which can vary from fractions of a millidarcy to over a Darcy (four orders of magnitude), is influenced by coal maturity but at the present time cannot be predicted by rank.

Thermal maturity often varies so gradually throughout a coal deposit that coal rank in a development that exploits a small fraction of that deposit can be considered constant for engineering purposes. While this assumption is often valid for a given field, commercial coal gas exploitation on a regional or basinwide scale requires knowledge of rank variation across the target area. Examples of anisotropic rank variation include the coals of southern Alberta, where coal rank is approximately constant for more than 600 km (370 miles) in

the northwest-southeast direction, roughly paralleling the Rocky Mountains.[57] However, coal rank rises from lignite to medium- or low-volatile bituminous rank in a distance of 400 km (250 miles) perpendicular to the Rocky Mountains.

A second example of anisotropic coal rank is the Marylee coal in the southeast portion of the Warrior Basin of Alabama. Rank of this seam, controlled by variation in the paleogeothermal gradient, varies slowly across the coal gas fields here with the exception of an elliptical area along thrust faults at the basin margin.[58] In this area, vitrinite reflectance rises from 0.8 to 1.4 over a distance of 30 km (19 mi) perpendicular to the thrust fault and basin boundary. As shown in figure 3–2, coal rank changes from high- to medium-volatile bituminous across this distance.

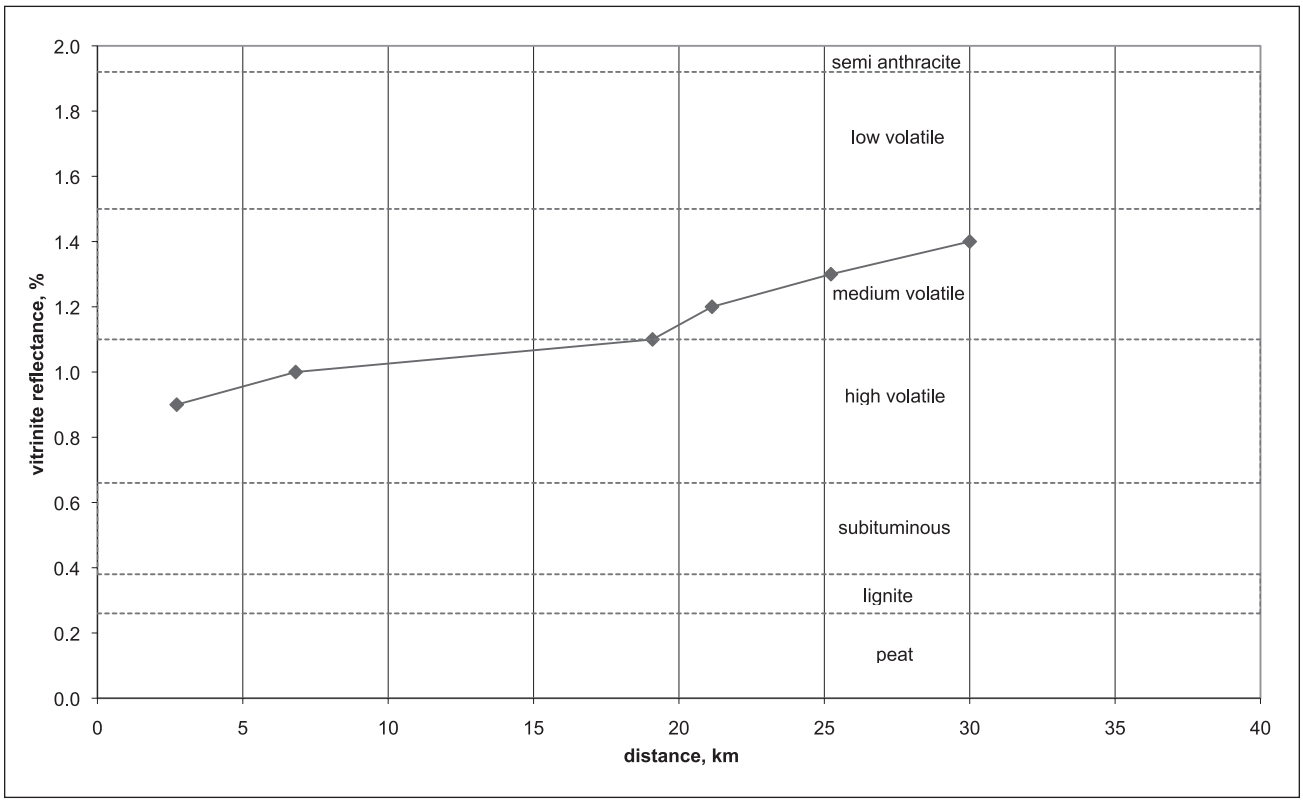



**Fig. 3–2.** Warrior Basin, Marylee coal: Vitrinite reflectance vs. distance[59]

Coal permeability is affected by both cleating and stresses. Cleat spacing in this elliptical area varies from less than 1 cm to greater than 2 cm.[60] Conceptualizing a coal seam as a collection of matchsticks and the cleats as the voids between matchsticks, permeability is inversely related to cleat spacing.[61] Thus, the rise in thermal maturity across this small area increases coal permeability by a factor of two or more, other elements being equal.

Maturity of the Ferron coals in the Uinta Basin of Utah was expressed as contours of vitrinite reflectance by Montgomery et al.[62] Isolines of vitrinite reflectance generally trend northeast-southwest, with significant rank gradients perpendicular to them. Coal rank rises from subbituminous A (0.57% $R_o$) to high-volatile B (0.71% $R_o$) over a distance of 30 km (21 mi). As discussed below, such a maturity change doubles or triples the volume of coal gas generated and shifts composition of the generated gas from predominantly $CO_2$ to a gas mixture increasingly richer in methane.

A final example is variation of coal maturity in the northern San Juan Basin due to igneous events.[63] Vitrinite reflectance along a north–south transect of the basin, shown in figure 3–3, rapidly rises from 0.78% on the northern outcrop to 1.50% before gently declining to 0.5% in the interior of the basin.

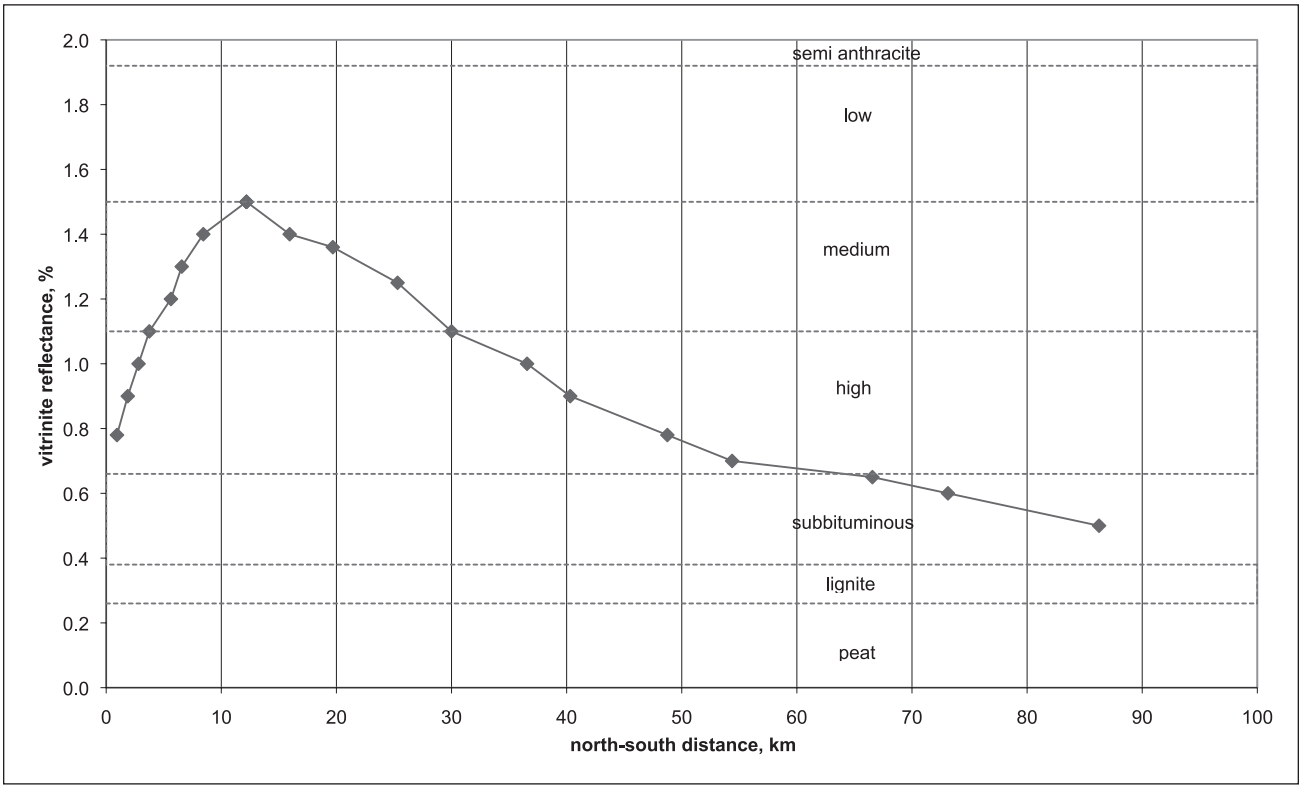



**Fig. 3–3.** San Juan Basin—vitrinite vs. distance[64]

From a rank of high-volatile bituminous B on the northern outcrop, coal rank rises to the high-volatile/medium-volatile threshold (1.1%) within about 4 km (2.5 mi). Coal rank peaks at the medium-volatile/low-volatile threshold (1.5%), approximately 12 km (8 mi) into the basin. Coal rank then slowly declines to the subbituminous/bituminous boundary (0.68%) some 62 km (38 mi) to the south of the outcrop. Coal depth varies across this transect, which includes the basin syncline, with a maximum depth of 900 m (3,000 ft). Coal permeability, affected by both rank and depth, varies from less than 5 md to more than 50 md along this north–south path.[65]

Comparison of rank contours and structural contours provides insight into the relative timing of metamorphosis and deformation of the reservoir. At the simplest, a peat accumulation that subsides uniformly, is coalified with areally uniform heating and pressures, and experiences minimal deformation after coalification will exhibit planar structures and constant rank. Rank contours across relatively undisturbed deposits often reflect geothermal heat flux variations. Deformation of a peat body prior to significant metamorphosis will result in structurally complex coals with simple, even uniform, rank contours. Deformation of a coal body with little subsequent metamorphosis will yield complex structural and rank contours. Consideration of coal rank and structure variations on a broad scale provides insight into reservoir architecture. For example, rank variation of the Marylee coal with distance across the elliptical area along thrust faults of the Warrior Basin discussed above occurs in gently dipping strata with only local deformation of the coal bodies. Considering maturity in all coal zones, Pashin et al. discovered coal rank changes appear as concentric cones in this area, with the inner cones exhibiting higher rank, indicating mild deformation of the organic deposits prior to metamorphosis into coal by paleogeothermal heating.[66]

## Coal Cleats

Coals are unique, naturally fractured reservoirs with two sets of mutually perpendicular fractures, both of which are perpendicular to the bedding planes. As discussed in chapter 2, the dominant set of roughly parallel, throughgoing, extensive fractures is termed face cleats. The second set of fractures, also roughly parallel but less well developed and often terminating at a face cleat, are called butt cleats. Cleats provide most of the permeability of a coal deposit.

Cleat development depends on coal rank but not geologic age. Lignites and subbituminous coals show sparse, disordered, poorly developed cleats, with cleat spacings on the order of centimeters. Bituminous coals exhibit closely spaced, well-ordered, highly developed face and butt cleats, with fracture spacing on the order of a centimeter or less. Anthracitic coals have fewer, more widely spaced cleats than bituminous coals due to annealing of the fractures as the matrix metamorphoses to a more ordered, planar, graphitic structure. Close noted that cleat spacing in Fruitland coals of the San Juan Basin varied from more than 6 cm in the subbituminous and high-volatile C bituminous coals of the southern portion of the basin to less than 0.6 cm in the high-volatile A bituminous coals along the northern margin of the basin.[67] Again conceptualizing a coal deposit as a collection of matchsticks, permeability is inversely dependent on cleat spacing. Thus, other influences being equal, permeability of Fruitland coals would be expected to vary by an order of magnitude due to rank variations.

Cleats are opening-mode fractures with little, if any, displacement parallel to the cleat walls. Cleats seldom exhibit shearing or deformation. Face and butt cleat spacings are usually equal but are sometimes more intense in the face cleat direction. Although cleat height and length (and usually aperture) are generally much larger than characteristic lengths of coal macerals, cleats are more abundant and better developed in bright, glassy coals rich in vitrinite. The megascopic banding apparent in hand samples of many coals is related to coal lithotype. A detailed explanation of coal lithotypes is given by Mukhopadhyay and Hatcher.[68] Thicknesses of these visual bands (*lithotypes*) are on the order of centimeters and, similar to fractures in conventional rocks, cleat spacing is typically less than lithotype thickness. Some random cleats pass through several bands or lithotypes. These master cleats are better developed than average cleats, with wider apertures and greater lengths. Laubach et al. reported a linear relationship between cleat height and aperture and found cumulative frequency of cleat apertures obeyed a power law distribution.[69] Empirical constants in the equation varied from well to well, indicative of a small length scale for characterizing cleat heterogeneity.

Extension of mathematical relations describing cleat geometries, spacings, and distribution to expressions for calculating permeability of a coal deposit is not yet possible. This could be due to sample volumes being several orders of magnitude smaller than actual drainage volumes, overly simplified equations, and coal heterogeneities.

Several processes are thought to influence cleat formation.[70] Cleats can be considered as dessication-type cracks generated by the expulsion of water in the early stages of maturation. However, dessication cracks are typically polygonal in appearance, not linear. Differential compaction of peats and clastics during burial and lithification could sufficiently stress coal bodies to fail. Although these stresses are primarily compressional, Laubach et al. discussed conditions when they are not and employed geomechanical arguments to demonstrate that all coals should be fractured to some extent.[71] Cleats are sometimes explained as brittle failures caused by deformation of mature coals. This explains the often-observed alignment of face and butt cleats parallel and perpendicular to major fold axes. The interplay of stresses is thought to dictate whether the face or butt cleats are parallel to the fold axis. Close noted that face and butt cleat strikes are nominally parallel and perpendicular to fold axis strikes in the Northern and Central Appalachian, Warrior, Illinois, Arkoma, Powder River, Hanna, Green River, Uinta, Piceance, San Juan, and Raton basins.[72]

Paleostresses during coalification are one of the controls on the constant cleat orientation seen over large portions of some coal basins. Kulander and Dean reported seven cleat domains in the Appalachian coals of West Virginia.[73] Three adjacent domains showed evidence of two cleats sets, but development to date in this basin has not identified these as exceptionally productive areas. Two and possibly three cleat orientations have been identified in the Fruitland coals of the San Juan Basin. Laubach et al. noted the high-productivity fairway of this basin occurs in the transition zone between two cleat orientations, leading to the hypothesis that overprinting

of two (or more) cleat sets increases overall seam permeability.[74] That same study noted two cleat orientations in the coals of the Piceance Basin with no apparent transition zone between them.

For reservoir engineering purposes, cleats are the primary pathways for gas and water flows in a coal deposit. Because they are slim fractures in an organic matrix, the flow capacity of cleats can be significantly reduced due to completion and fracturing fluids by mechanical plugging and chemical reactions on the cleat walls.

## Coal Gas Origin and Composition—Thermogenic and Biogenic Gas

Coals typically source the gas they hold. Occasionally coals will contain migratory gas from deeper formations but generally retain gas generated in the coal body itself. Gas derived from a coal can be either thermogenic or biogenic. Gas generated in coals during coalification is termed *thermogenic gas*, while that generated from microbes metabolizing the coal matrix is termed *biogenic gas*. Both thermogenic and biogenic coal gases are composed predominantly of methane, giving rise to the common name of *coalbed methane*, and preventing identification of origin from composition alone. A coal can simultaneously hold both thermogenic and biogenic gas mixtures in the free and sorbed states.

Regardless of origin, storage of sorbed gas on the coal surface can be described with Langmuir's equation. Storage of free gas compressed in the cleats can be described by conventional gas reservoir engineering equations. Flow of gas, whether thermogenic or biogenic, through a coal deposit is characterized by Darcy's law. However, gas origin is one of the controls on areal and stratigraphic distribution of the gas resource in a given coal deposit, making this knowledge helpful in interpretation of desorption data patterns and predicting general behavior of the gas resource in undrilled areas. Thermogenic coal gas is most often found in high-rank coals, and coalbed gas content is controlled by maturity, often increasing uniformly with depth of burial. Biogenic coal gas occurs most often in shallow, low-rank coals, and coalbed gas content is related to microbial activity sustained by water influx along major faults and other high-permeability pathways. Consequently, gas content of the coal deposit often varies erratically with depth.

Origin of the gas in a given coal, thermogenic or biogenic, cannot be reliably determined from composition, as all coal gas is predominantly methane, with minor amounts of heavier hydrocarbons, $CO_2$, and nitrogen. Composition of produced coal gases from six U.S. basins averaged 93% methane, 3% wet gases, 3% $CO_2$, and 1% nitrogen.[75] While this average is representative of coal gas mixtures worldwide, coal gas composition can show considerable variation. In the gases analyzed by Scott, $CO_2$ ranged from 0% to more than 40%, while nitrogen and ethane varied from negligible to more than 11%.[76] Smith and Pallasser noted that coal gas mixtures from the south Sydney Basin of Australia ranged from pure methane to pure $CO_2$.[77] As discussed in chapter 2, fluid properties of coal gas can be calculated from composition and standard correlations. For reservoir engineering purposes, when gas composition is unknown, gas properties are often assumed to be those of pure methane.

Although coal gas is predominantly methane, composition of the produced gas stream varies during depletion due to the different sorption strengths of methane and any minor constituents. Nitrogen sorbs less strongly than methane, while $CO_2$ and heavier hydrocarbons sorb more strongly. Knowledge of gas origin helps in design of gas treating and processing requirements and can help in blending gas from different portions of the field to meet pipeline specifications.

**Thermogenic coal gas.** Thermogenic gas is generated as a coal matures. The volume of gas generated and its composition vary as a function of rank, with no reported dependence on geologic age or maceral composition. Approximate volumes of methane, $CO_2$, and nitrogen generated at each stage of coalification are shown in table 3–4 and plotted in figure 3–4.[78]

**Table 3–4.** Coal gas generation vs. rank

| | $CH_4$ | | $CO_2$ | | $N_2$ | | Total gas | | Cumulative gas | |
|---|---|---|---|---|---|---|---|---|---|---|
| **Rank** | **scf/t** | **$cm^3/g$** | **scf/t** | **$cm^3/g$** | **scf/t** | **$cm^3/g$** | **scf/t** | **cm3/g** | **scf/t** | **$cm^3/g$** |
| lignite | 0 | 0 | 120 | 4 | 0 | 0 | 120 | 4 | 120 | 4 |
| subbit. | 0 | 0 | 200 | 6 | 0 | 0 | 200 | 6 | 320 | 10 |
| hi-vol. bituminous | 640 | 20 | 1,080 | 34 | 160 | 5 | 1,880 | 59 | 2,200 | 69 |
| med.-vol. bituminous | 2,680 | 84 | 360 | 11 | 160 | 5 | 3,200 | 100 | 5,400 | 169 |
| low-vol. bituminous | 2,160 | 67 | 240 | 7 | 80 | 2 | 2,480 | 77 | 7,880 | 246 |
| semianth. | 760 | 24 | 120 | 4 | 80 | 2 | 960 | 30 | 8,840 | 276 |
| anthracite | 880 | 27 | 216 | 7 | 320 | 10 | 1,416 | 44 | 10,256 | 320 |
| Total | 7,120 | 222 | 2,336 | 73 | 800 | 25 | 10,256 | 320 | × | × |

*Source:* Rightmire, C. T., et al. 1984.

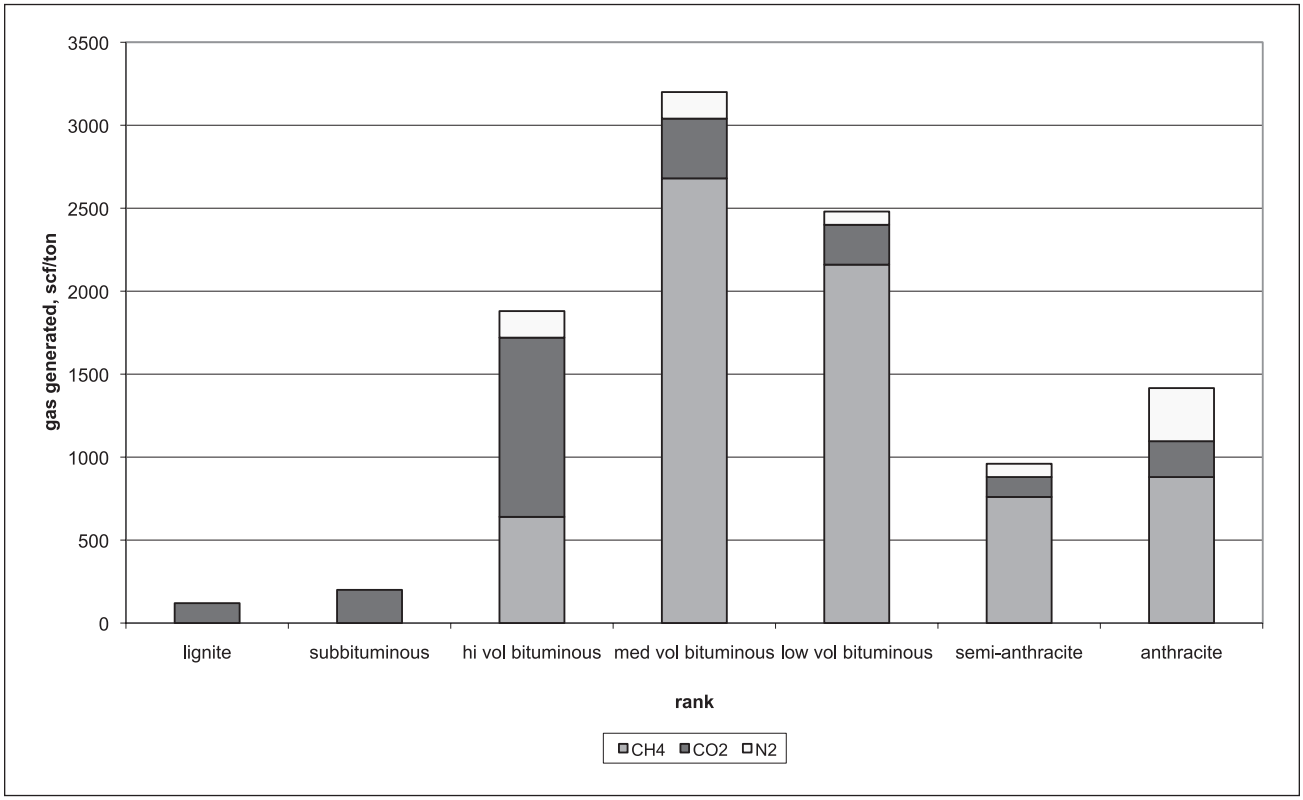



**Fig. 3–4.** Gas generation vs. coal rank[79]

Note that reference pressure and temperature were not reported. Generation of both methane and total thermogenic gas peak in medium-volatile bituminous coals. Peak $CO_2$ generation occurs at slightly lower rank, high-volatile bituminous, while nitrogen is generated in modest amounts in bituminous and higher ranks. Cumulative gas generation, plotted in figure 3–5, is negligible in lignite and subbituminous coals, jumps to more than 62 $cm^3/g$ (2,000 scf/ton) in high-volatile bituminous coals, and exceeds 321 $cm^3/g$ (10,250 scf/ton) in anthracites.

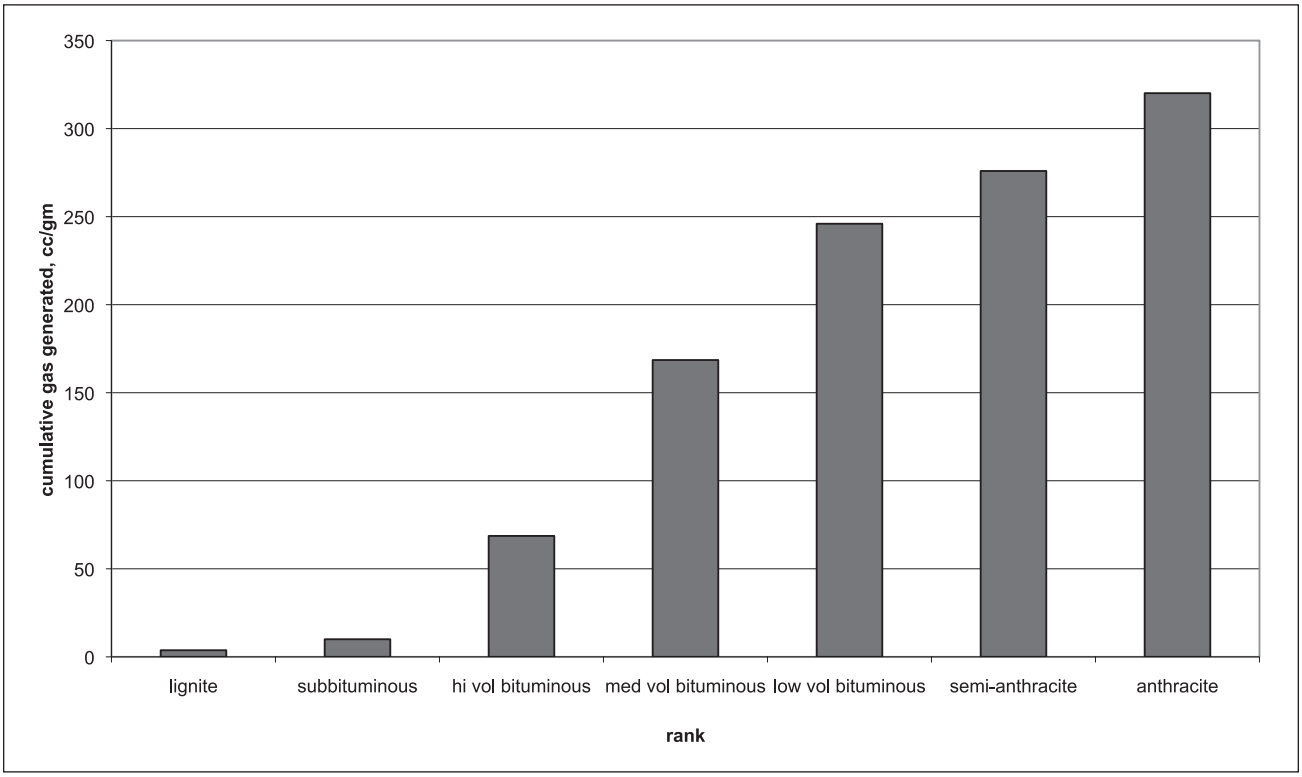



**Fig. 3–5.** Cumulative gas generation vs. coal rank[80]

On a compositional basis, the 321 $cm^3/g$ generated during coalification is 69% methane (222 $cm^3/g$ or 7,120 scf/ton), followed by 23% $CO_2$ (73 $cm^3/g$ or 2,336 scf/ton), and 8% nitrogen (25 $cm^3/g$ or 800 scf/ton). Higher hydrocarbon gases, ethane and above, occur in thermogenic coal gas in minor and highly variable amounts.[81] Ethane first appears as a coal matures across the coalification jump from subbituminous to bituminous, quickly peaks in high-volatile bituminous coals, and then steadily declines with further increases in rank.[82] Generation of propane, butanes, and higher hydrocarbon gases during coalification has not been widely studied. As coal gas typically contains only small quantities of ethane and higher hydrocarbons, they are often reported only as "C2+s" and lumped together for coal gas reservoir engineering purposes.

Meissner noted that significant gas generation commenced when volatile matter dropped below about 37.8% on a dry, ash-free (daf) basis, corresponding to a rank of high-volatile bituminous.[83] Using data from Juntgen and Karweil on a daf basis, Meissner related total methane generated to volatile matter by[84]

$$V_{C1} = -325.6 \log\left[\frac{vm_{daf}}{0.378}\right] \quad \textbf{(3.1)}$$

where

$V_{C1}$ = volume of methane generated, daf, $cm^3/g$, and
$vm_{daf}$ = volatile matter weight fraction, daf.

Meissner based the generated methane volume on a temperature of 20°C (68°F) and 1 atm pressure (14.7 psia). At oilfield standard conditions of 14.7 psia and 60°F, the constant becomes 10,273 scf/ton, and at SI standard conditions of 0°C and 1 atm pressure, the constant is 303.4 $cm^3/g$. The SI form of the Meissner equation is plotted in figure 3–6 and compared with methane gas generation reported by Rightmire et al. in figure 3–7.[85]

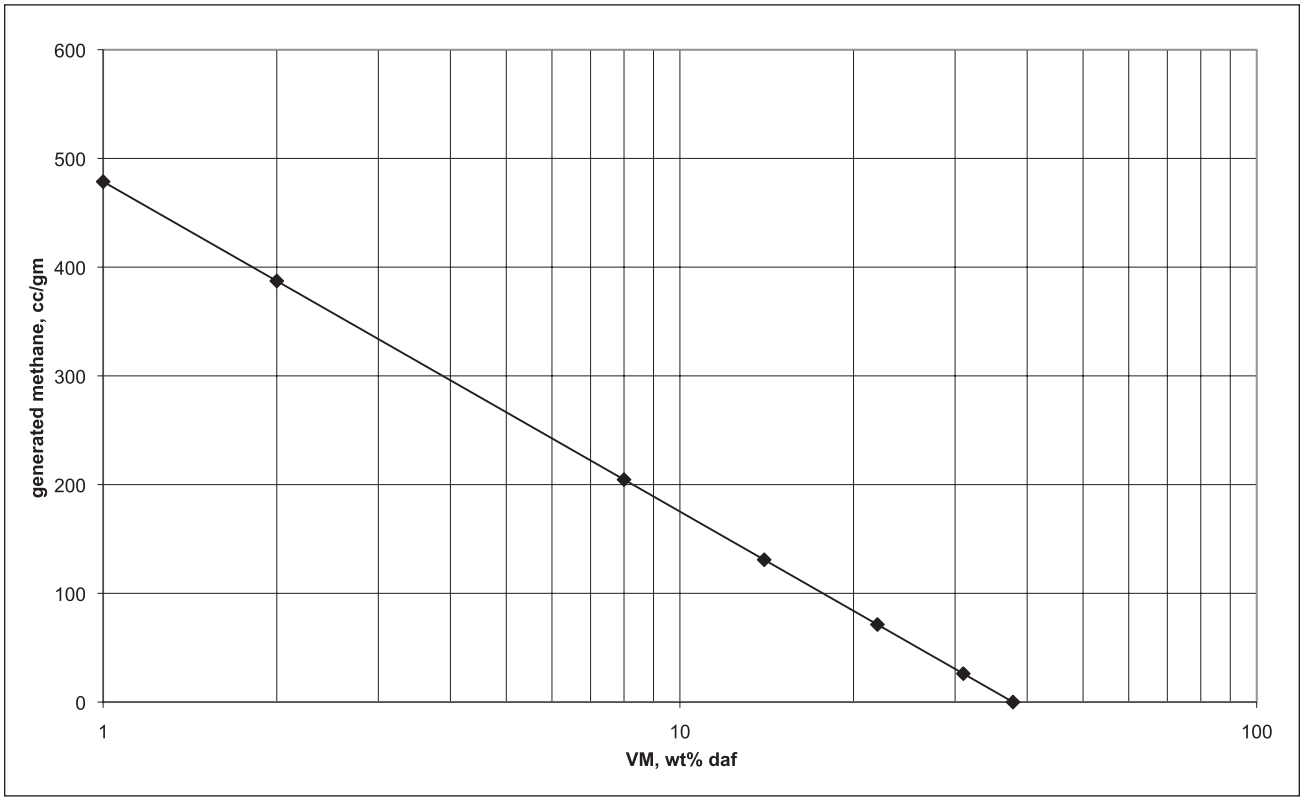



**Fig. 3–6.** Thermogenic methane vs. volatile matter[86]

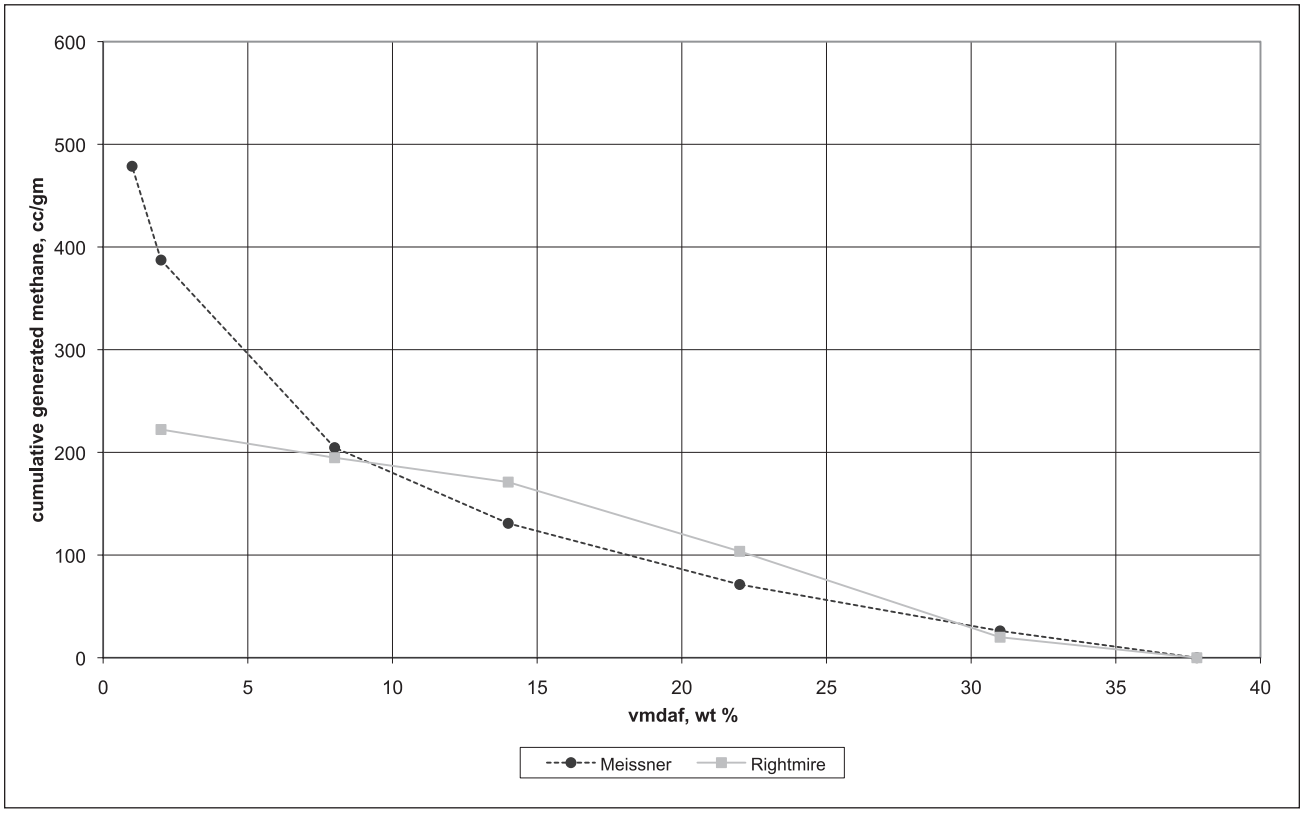



**Fig. 3–7.** Cumulative generated methane vs. coal rank—Meissner vs. Rightmire[87]

Cumulative methane volumes predicted by these two studies are in general agreement across the bituminous and semianthracite ranks. The volumes predicted by Meissner rise above those of Rightmire et al. in the anthracite range, where volatile matter (daf) drops below 8%.

The steady increase in thermogenic gas volumes with rank provides a simple exploration screen and helps to explain why the first commercial coal gas plays were in bituminous coals. However, from perspectives of mine safety and reservoir engineering, more important than generated gas volume is retained gas volume. Both surface area and cumulative generated gas volume increase with coal maturity. As a general rule, generated gas volume exceeds current sorption capacity at any given rank, implying gas expulsion over geologic time and an expectation that saturated coal deposits should be the norm. In actuality, however, coal deposits are often intermittently breached after gas generation ceases, allowing gas to drain out of the seams, leaving undersaturated coals. Correlations of coalbed gas content with depth, pressure, temperature, and rank on a regional or local basis such as that of Kim for U.S. bituminous coals and Ryan for B.C. coals are sometimes useful in the respective study areas.[88] Of course, these correlations cannot be utilized to predict coalbed gas contents in other areas. At the present time, gas content of a coal deposit cannot be predicted but must be measured.

**Biogenic coal gas.** In addition to thermogenic gases, coals can also hold biogenic gases generated by microbes present in a coal. These microbial communities flourish in anoxic, low-temperature, low-sulfate, high-pH environments, with abundant organic matter and open pore space producing gas by several metabolic pathways.[89] The two primary metabolic pathways for biogenic gas generation are acetate formation[90]

$$CH_3COOH \longrightarrow CH_4 + CO_2$$

and $CO_2$ reduction

$$CO_2 + 4H_2 \longrightarrow CH_4 + 2H_2O$$

Depending on the relative activity of the different paths, composition of biogenic coal gas varies but is predominantly methane, $CO_2$, and nitrogen.

Biogenic gas can be generated very early in the coalification process, during transformation of recently buried peats, and in recent geological history, when meteoric waters carried methanogens and/or nutrients into a coal deposit. Early- and late-stage microbial activity leads to two different conceptual distributions of a biogenic coal gas resource. Early biogenic gas generation, controlled by subsidence rate, groundwater chemistry, peat quality, and other depositional factors, would give rise to a diffuse gas resource present across the resulting coal deposit in nearly constant, slowly varying quantities. With limited sorption sites available in low-rank coals, most of this gas would be expelled. If the coal deposit was never sufficiently matured for thermogenic gas generation, distribution of this early-stage biogenic gas depends on postcoalification uplift, erosion, and breaching. Late-stage biogenic gas generation is controlled by coal temperature and outcrop connections, resulting in a gas resource concentrated along basin margins and in groundwater plumes in high-permeability corridors. In discussing thermogenic and biogenic coal gases in the San Juan Basin, Scott et al. report biogenic gas 56 km (35 mi) from the nearest outcrop.[91]

The temperature constraint on microbial activity suggests an exploration screen of maximum depth for biogenic gas generation. Known methanogens become dormant at temperatures above about 65°C (150°F), with higher temperatures essentially sterilizing the reservoir.[92] Assuming a mean surface temperature of 10°C and a geothermal gradient of 1.8°C/100 m (1°F/100 ft) implies methanogenic activity ceases below about 3,060 m (10,020 ft). Thermophilic methanogens are known to thrive at temperatures above 65°C or even 100°C (212°F), but their role in biogenic coal gas generation is uncertain at this time.

A second exploration screen for biogenic coal gas is distribution of freshwater plumes. These plumes result from connection of coal fractures, especially swarms of ordered fractures and joints, to outcrops being recharged with meteoric waters laden with microorganisms and/or nutrients.

**Determination of coal gas origin.** Coal seams may contain only thermogenic or biogenic gas, but many hold a mixture of both. Identification of gas origin in a coal deposit helps understand distribution of the gas resource, allowing development to concentrate on richer seams and richer areas. Origin of gas held in a coal is determined most reliably from carbon and hydrogen isotopes. Isotopic variation is reported as δ/1,000 (or *per mil*) defined as

$$\delta = \left( \frac{R_{\text{sample}}}{R_{\text{standard}}} - 1 \right) 1{,}000$$

where, for carbon isotopes,

$R = {}^{13}C/{}^{12}C$

and for hydorgen isotopes,

$R$ = D(euterium)/H(ydrogen)

Perhaps the $\delta^{13}C$ of methane provides the most direct method for determination of gas origin. Values more negative than –55 per mil are representative of biogenic gas, and values less negative are indicative of thermogenic origin. The boundary between biogenic and thermogenic is not sharp but exhibits only a modest overlap of about ±10 per mil. From the $\delta^{13}C$ of gases produced from the Cook Inlet of Alaska, Montgomery et al. identified gas in the subbituminous coal of the northeastern part of the basin as biogenic ($\delta^{13}$ from –63 to –56 per mil). In addition, Montgomery et al. identified the gas in the bituminous coals of the central and southern areas of the basin as thermogenic ($\delta^{13}$ from –48.9 to –44.0 per mil).[93]

A crossplot of carbon and hydrogen isotopes in the methane fraction of a coal gas mixture was employed by Rice and Clayton to discriminate between thermogenic and biogenic gas as well as determine the major metabolic pathway of biogenic gas formation.[94] As shown in figure 3–8, the methane $\delta^{13}C$ value is more negative for biogenic gas than for thermogenic gas, while the methane $\delta D$ discriminates between biogenic gas formed from the two major metabolic paths noted above.

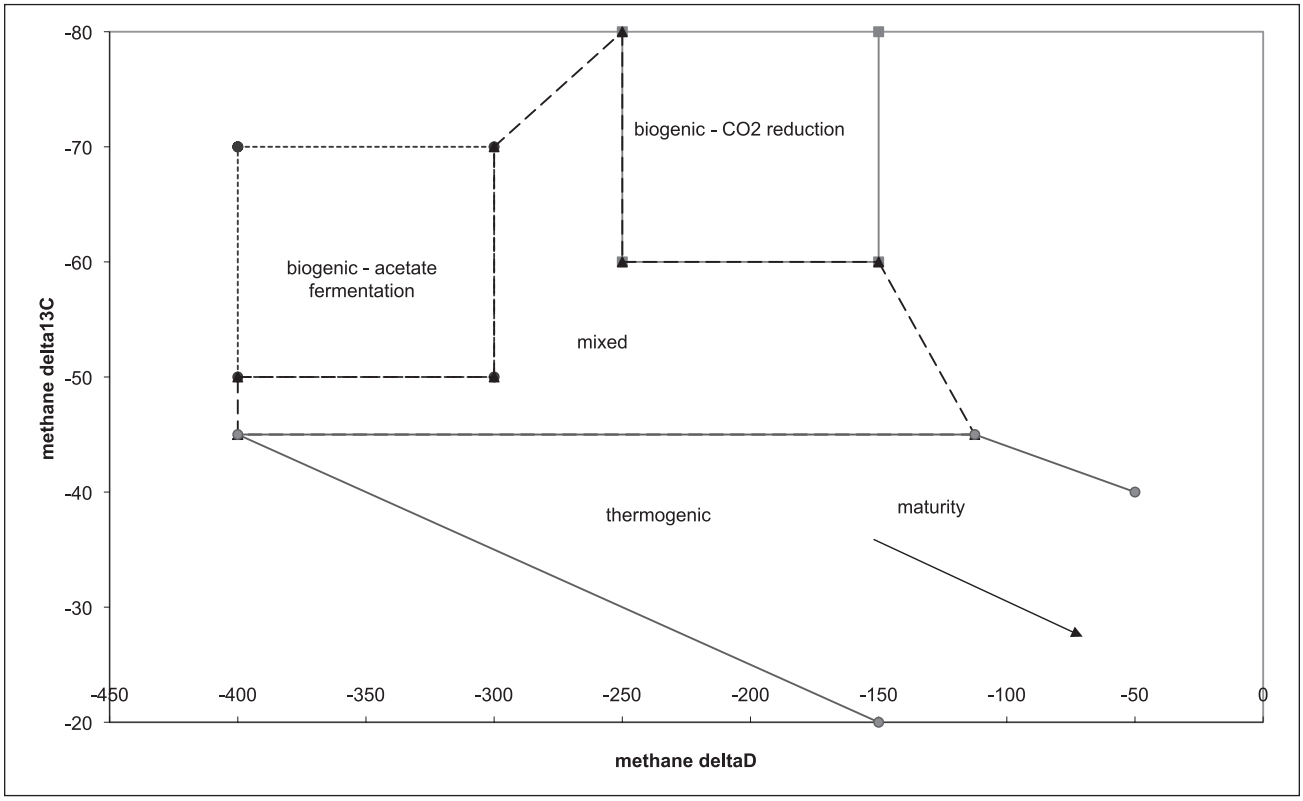



**Fig. 3–8.** Coal gas origin determined from methane carbon and hydrogen isotopes[95]

The domains of gas origin depicted in figure 3–8 are not exact, as modest variations in coal gas isotope ratios can also be due to maceral types and fractionation during desorption, as well as isotopic composition of the coal matrix.[96] Within the thermogenic envelope, both carbon and hydrogen isotope ratios vary with coal maturity but lack sufficient consistency for rank determination.

A crossplot of $\delta^{13}C$ and the *dryness ratio*, defined as the mole fraction of methane divided by the sum of the ethane and propane mole fractions, was employed by Bernard et al. to determine the origin of hydrocarbon gases in conventional reservoirs.[97] A Bernard plot, shown in figure 3–9, indicates dryness ratios of biogenic gas are one to two orders of magnitude greater than those of thermogenic gas. Similar to figure 3–8, the $\delta^{13}C$ values are less negative for thermogenic than biogenic gas.

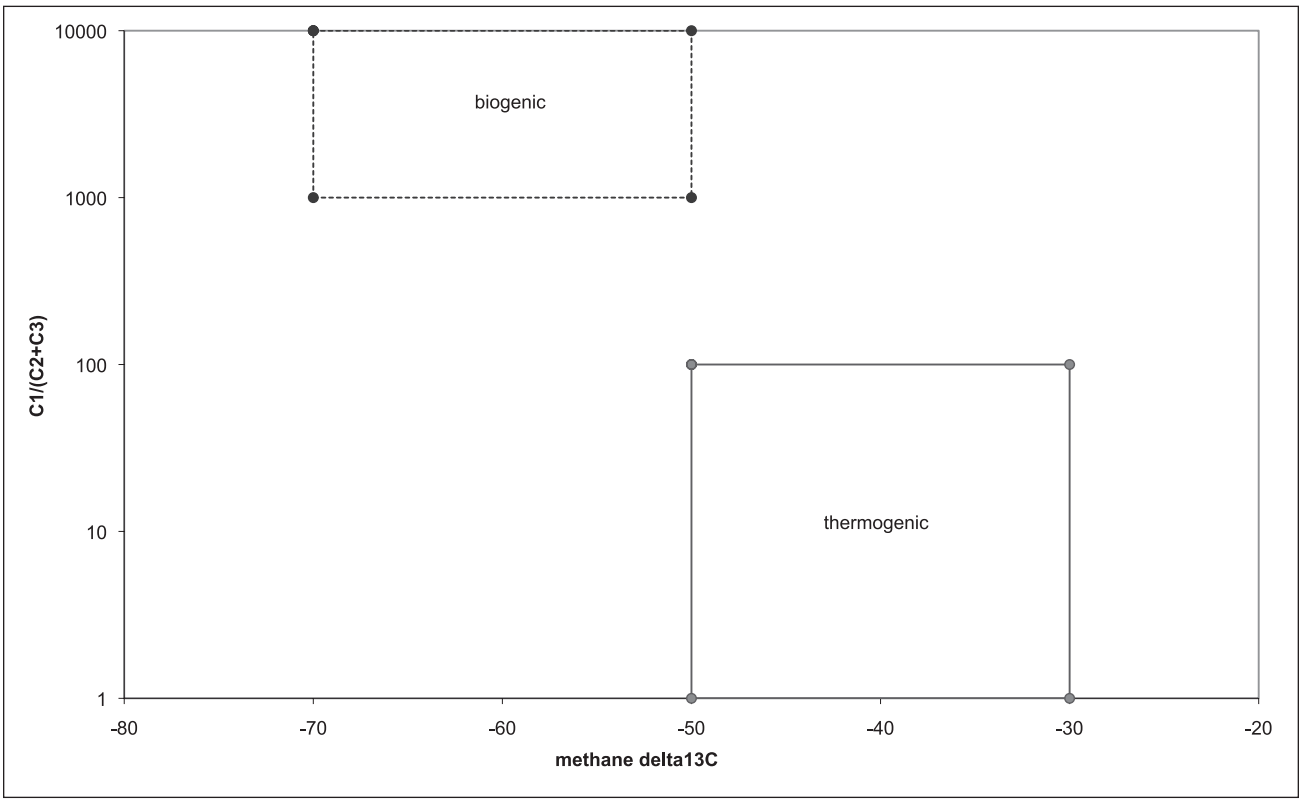



**Fig. 3–9.** Bernard plot for determination of gas origin[98]

Ruppert et al. utilized a Bernard plot, with the dryness ratio defined as the methane mole fraction divided by the sum of the mole fractions of all higher hydrocarbons in the sample, to examine coal seams in the West Virginia portion of the Appalachian Basin. They identified gases from seven of eight coal seams as thermogenic, with the remaining seam containing a mixture of both thermogenic and biogenic gas.[99]

Care must be taken when using the dryness ratio, as its definition is not unique. Dryness ratio was defined by Scott et al. as the ratio of methane mole fraction divided by the sum of methane thru pentane mole fractions.[100] Inclusion of methane in the denominator yields values between 0.7 and 1.0 for coal gases, markedly less than the variation of three orders of magnitude or more seen in the Bernard dryness ratio, and therefore of less use as a discriminator of gas origin. Proper interpretation of a reported dryness ratio requires knowledge of its definition.

Other isotopic variations that can be used to discriminate between biogenic and thermogenic gas include the $\delta^{13}D$ of coproduced water and the $\delta^{13}C$ of carbon dioxide and dissolved inorganic carbon in coproduced water.[101] Isotopic variations of coal water and $CO_2$ provide indirect evidence of methane origin and should be used with caution. For example, a coal holding thermogenic gas and hosting a microbial population that generates primarily $CO_2$ would yield a produced gas stream with an isotopic composition difficult to interpret. Thermogenic $CO_2$ exhibits $\delta$13C values from –30 to –10 per mil, which is at the lower end of the biogenic $CO_2$

spectrum, going from –30 to +25 per mil.[102] Smith and Pallasser argued for a microbial origin of coal gases in the Sydney and Bowen basins of Australia based upon the $\delta$13C and $\delta$D of methane and the $\delta^{13}$C signatures of the gas.[103]

Use of isotopic ratios of other gases and coproduced water to determine coal gas origin has been limited. Rice discussed the use of $\delta^{13}$C of ethane in coal gas for source identification.[104] Gas in the Fruitland coals of the north-central San Juan Basin was determined to be a mixture of thermogenic, biogenic, and migrated thermogenic gases by Scott et al. based on variations of the $\delta^{13}$C values of methane, $CO_2$, and the carbonate ion in the coproduced water.[105] Gas in the Ferron coals in the Drunkard's Wash Unit in the Unita Basin was determined by Burns and Lamarre to be a mixture of thermogenic and biogenic gases using the $\delta^{13}$C values of methane, $CO_2$, and ethane.[106]

## Emerging Geoscience Concepts for Coal Gas Reservoir Engineering

Although coal gas has been exploited for more than 30 years, several elements of conventional petroleum geoscience have not yet seen widespread application in these unconventional reservoirs. Geological and geophysical technologies that are routinely employed to understand conventional oil and gas reservoirs are now being adapted for coal deposits.

Geochemistry of coal waters from several U. S. basins and the plains of Alberta was addressed by Van Voast.[107] Comparison of calcium, magnesium, sodium, chlorine sulfate, and bicarbonate ions in waters from wells with and without methane production indicated an inverse correlation between sulfate and methane producibility. A dissolved sulfate content less than roughly 500 mg/l (10 meq/l) was associated with good methane production. Use of this sulfate threshold as a coal gas exploration tool has not been widely reported.

Waters found in coals are often lower in total dissolved solids (TDS) and richer in bicarbonate than waters from conventional reservoirs, allowing identification of the water source. One of the primary considerations for water disposal is total dissolved solids of injected and native waters, with disposal of waters containing higher TDS than those in the disposal formation more problematic. Van Voast noted that variability and lack of historical continuity in reported coal water TDS values often lead to erroneously high total dissolved solids, unnecessarily burdening coal water disposal.[108] Total dissolved solids were historically determined by weighing evaporative residues but with modern analytical techniques are now calculated. During sample drying, some bicarbonate is volatized and lost, and some is converted to carbonate and remains in the residue. Consequently, for continuity with historical weighed residue TDS values, calculated bicarbonate content should be multiplied by 0.4917. In the waters studied by Van Voast, this error overestimated coal water TDS concentrations by about 50%.

Coal gas is a diffuse, blanket resource whose recovery is more dependent on coal seam permeability than structure. Consequently, seismic technologies that are widely used to characterize conventional reservoirs have seen limited application in coals. As coal seams are typically shallower and thinner than those reservoirs, seismic surveys designed to investigate deeper conventional targets are problematic for characterization of coals. Historically, coalbed methane evolved from safety concerns in coal mines, where seismic was rarely employed, with the consequence that coal gas reservoir engineers now often consider seismic as a secondary tool for understanding coal deposits. Compared to seismic surveys, coal wells are relatively cheap to drill and provide quick results, prompting many operators to spend money drilling, testing, and producing wells rather than on seismic surveys with possibly long interpretation times.

As with conventional reservoirs, whenever possible, seismic results from coals should be linked with other geological and engineering data to increase confidence in the final reservoir interpretation. An example of such a fusion is provided by the work of Marroquin and Hart, where P-wave 3-D seismic data were combined with wireline logs from coal wells in the north San Juan Basin.[109] Seismic data from a 45 $km^2$ grid in the southeast portion of the fairway were combined with wireline logs from 59 wells in and around the survey area to characterize coal thickness and structure. Combining curvature analysis of the seismically defined coal deposit

with gas production data from 36 wells in the study area verified the intuitive conclusion that the highest gas rates and recoveries were associated with thick coals and seismically defined structures.

The use of digital geophones for improving imaging of coal deposits in 3-D seismic surveys was discussed by Meisheng et al.[110] Although this new technology is relatively expensive, when combined with proper seismic processing, it improves resolution of the final images. Faults, stream channels, and other structural elements of a seam are more easily discerned. Application of the method was demonstrated on a seismic survey of a coal field in China. Focusing on a single 3 m thick coal seam, faults with throws of 2 m could be identified.

*Undersaturation* describes a coal seam with actual gas contents less than the sorption capacity at reservoir temperature, pressure, and gas composition. Undersaturated coals are commercially challenging, as dewatering costs must be borne by a project for several months or years before gas production begins and revenue is generated. Coals can be undersaturated on a local, regional, or basin scale, making prediction of undersaturation difficult. As discussed below, desorption pressure measured with wireline logging tools and compared against reservoir pressure is an indicator of undersaturation but has seen limited application outside of the Powder River Basin. Desorption pressure must be combined with a sorption isotherm and reservoir pressure to quantify the degree of undersaturation. The most direct method to determine undersaturation is comparison of actual gas contents from desorption tests of coal samples with those predicted from laboratory-measured sorption isotherms utilizing the desorption samples and reservoir pressure. Quantifying undersaturation is a data-sensitive procedure, with errors in field desorption tests and reservoir and desorption pressures combining with those inherent in laboratory-measured sorption isotherms and gas analyses to compound interpretation. Consequently, actual well performance is typically seen as the definitive indicator of undersaturation.

Widespread undersaturation in a coal basin was theorized as due to uplift of coals.[111] Sorption capacity of a coal increases as temperature decreases. Tectonic uplift of a coal that is gas saturated at depth was theorized to result in cooling and depressurization such that the coal became undersaturated. This theory was tested experimentally by Bustin and Bustin with measurement of sorption isotherms for three coals at selected temperatures.[112] These results were combined with typical thermal and pressure gradients to calculate coalbed gas contents in pressure-temperature space. The results indicated undersaturation by uplift was not plausible except for pressures sufficiently high that all gas content changes were on the plateau of the isotherms or unrealistic pressure and temperature gradients. Consequently, other explanations of widespread undersaturation, such as seen in the United States in the south San Juan Basin (New Mexico) and in Poland in the Upper Silesian Basin, are necessary.

## Wireline Logs

Wireline logs are used to identify coal deposits in the subsurface, to determine seam thickness, and to measure or estimate various coal properties such as density, proximate analysis, and mechanical constants. First run to assess mineability of coal deposits, wireline logs have been adapted to coal gas exploration and development in recent years. Coal logs can be run in both open and cased holes filled with either liquid or air. More than a dozen wireline tools show response in coals, with the most useful logs for coal gas reservoir engineering being bulk density, gamma ray, and caliper logs. Identification of coal reservoirs with wireline logs is somewhat dependent on local coal properties, but for reservoir engineering purposes, coals generally exhibit densities less than 2.0 g/cm$^3$ and a gamma ray response of less than 70 API units measured in an in-gauge hole. Additional logs sometimes run in coals include compensated neutron porosity, spectral density (photoelectric), sonic, spontaneous potential (SP), desorption pressure, resistivity, microlog, laterolog, formation imaging logs, carbon/oxygen, cement, and production logs. Typical log responses in a coal, along with reservoir engineering information derived from a particular log, are listed in table 3–5. Conversely, logs to determine specific reservoir properties are shown in table 3–6. Recommended openhole logs for coal wells are gamma ray, density, and caliper. Interpretation of any wireline log is, of course, strengthened with a mud log (also referred to as a *surface log*).

**Table 3–5.** Wireline log responses in coals

| Log | Purpose | Open/cased hole | Mud/air | Response | Units |
|---|---|---|---|---|---|
| bulk density | coal identification<br>net thickness<br>coal density<br>proximate analysis<br>mechanical properties | o | m/a | 0.70–1.80 | g/cm$^3$ |
| gamma ray | coal identification<br>proximate analysis<br>mineralogy | o/c | m/a | 20–25 | API |
| caliper | hole size<br>washouts | o | m/a | varies | inches, cm |
| compensated neutron | coal identification<br>proximate analysis<br>gas content | o/c | m | >50 | × |
| spectral density (photoelectric) | lithology<br>same as bulk density | o | m/a | 0.18 | |
| sonic | coal identification<br>coal rank | o | m | 95–135 | µsec/ft |
| spontaneous potential (SP) | none | o | m | varies | mv |
| desorption pressure | desorption pressure | o | water | varies | psi, MPa |
| resistivity | coal identification | o | m | 50–2,000 | ohm-m |
| microlog | permeability<br>cleating | o | m | varies<br>varies | ohm-m<br>ohm-m |
| Laterolog | permeability<br>cleating | o | m | varies<br>varies | ohm-m<br>ohm-m |
| FMS | cleat development | o | m | varies | × |
| FMI | cleat development<br>cleat orientation | o | m | varies | × |
| carbon/oxygen | coal identification<br>coal density | o/c | m/a | varies | × |
| cement | cement integrity | c | m | varies | × |

*Source:* Hollub, V., and Schafer, P. 1992; and Hall, R. V. 2002.

As with conventional logging tools, hole conditions affect tool response, and washout, especially in friable coals, complicates log interpretation. Running logs in holes filled with heavy muds or muds containing many additives can contribute to coal seam damage, especially in dry or permeable coals, which can imbibe significant liquid into the near-wellbore region during drilling, logging, and completion. The radius of investigation of various logging tools in coals is on the order of fractions of a meter, and wireline logs provide little, if any, information about coal permeability, porosity, and fluid saturations. Production logging in coal wells, similar to that in conventional wells, serves to quantify gas and water production from completed seams. However, it is compounded by the requirement that most coal wells require artificial lift.

Perhaps the most useful wireline log for coal gas reservoir engineering is the bulk density log, especially the high-resolution bulk density log, which is often used to identify coal, determine net coal thickness, and construct ash, density, and gas content correlations. The density tool pushes pads against the side of the wellbore, causing it to read erroneously low densities in washed-out sections. Confidence in a density log is higher when the caliper log indicates an in-gauge hole. Coal density, which is less than that of conventional reservoir rocks, is a function of coal rank and purity. In order of increasing rank, bulk density of lignites ranges from 0.7 to 1.5 g/cm$^3$, subbituminous from 1.2 to 1.75 g/cm$^3$, bituminous from 1.2 to 1.5 g/cm$^3$, and anthracites from 1.4 to 1.8 g/cm$^3$.[113] The fraction of ash in a coal affects bulk density more strongly than does rank, precluding rank determination from a density log. Mullen correlated bulk density of north San Juan Basin coals with the volume fraction of ash.[114] This data was then combined with proximate analysis data to estimate fixed carbon and volatile matter on a daf basis for rank determination. Modern algorithms for coal rank determination from wireline logs are more sophisticated, utilizing multiple logs, and are more accurate when driven with local, rather than general, coal correlations.

**Table 3–6.** Wireline logs for measuring specific reservoir properties

| Property | Wireline log |
|---|---|
| coal identification | bulk density<br>spectral density<br>gamma ray<br>caliper<br>carbon/oxygen<br>sonic<br>comp. neutron<br>resisitivity |
| net thickness | bulk density<br>spectral density<br>comp. neutron |
| coal density | bulk density<br>spectral density<br>carbon/oxygen |
| proximate analysis | bulk density<br>spectral density<br>gamma ray<br>comp. neutron |
| coal rank | sonic<br>comp. neutron |
| mechanical properties | bulk density<br>spectral density |
| permeability | microlog<br>FMS<br>FMI |
| gas content | density<br>gamma ray<br>comp. neutron |

*Source:* Hollub, V., and Schafer, P. 1992: and Mavor, M. J., et al. 1994.

The density used to define coal, typically referred to as the *pay cutoff density*, influences not only seam thickness and average seam density but also volumetric gas in place calculations. Schopf's definition of coal as a rock that is at least 50% by weight and 70% by volume carbonaceous material was combined with densities of organic material, ash, and water in chapter 2 to calculate coal densities.[115] Maximum density of bituminous and subbituminous coals were calculated to be 1.63 and 1.34 g/cm$^3$, respectively. While these densities are often suitable for identification of mineable coals, poorer quality coals with higher densities are often integral components of coal gas reservoirs. As noted in chapter 2, many operators currently employ a density cutoff of 2.0 g/cm$^3$, which results in ash fractions of bituminous and subbituminous coals of 75% and 84%, respectively.

Use of a higher pay cutoff density results in thicker coal seams, higher average seam densities, and lower in-situ gas content, all of which affect volumetric gas in place calculations. The effect of density cutoff on these parameters and the resulting volumetric gas in place calculated for the Ferron coals in the Drunkard's Wash Field of the Uinta Basin was investigated by Lamarre and Pratt.[116] They concluded that increasing the pay cutoff monotonically increased gas in place. Opening up the pay cutoff from 1.75 g/cm$^3$ to 2.55 g/cm$^3$ more than doubled original gas in place. Increases in calculated gas in place volumes due to higher density cutoffs are more dramatic in dirty, shaley coals, reflective of swamps subject to frequent flooding or volcanic ashfalls. Such increases in calculated gas in place volumes are also seen in coal deposits encased in thick, shaley rinds, indicative of marginal swamp environments over relatively long geologic periods. Rapid changes in geological conditions conducive to coal swamp formation and growth results in sharp density contrasts between coal and bounding beds. Higher density cutoffs in such coals weakly affect coal seam thickness, average density, and gas in place.

Vertical resolution of the bulk density tool is on the order of 0.5 ft (0.15 m), while that of some coal mining density tools can be as small as 1 in. (0.025 m). Coal partings less than 0.5 ft in thickness, readily apparent in cores, are smoothed out in the density log curve. Comparison of density logs with coal cores from the same interval provides insight into the fine-scale vertical heterogeneity of a seam. Density tool resolution also affects definition of net coal thickness and yields erroneously high average seam densities in thin coals. In plays such as

the Cherokee and Illinois basins, where the coals are present as multiple, thin beds, many operators are currently completing coal seams as thin as 2 ft. In such plays, differences in tool calibration, logging speed, and log analysis can result in different interpretations of seam characteristics and the gas resource they hold.

Natural radioactivity in a formation is measured by the gamma ray tool. Gamma ray log response in a coal can be either low or high, depending on local conditions. Clean coals contain few radioactive minerals and consequently have gamma ray signatures less than 70 API units, sometimes as low as 25 API units, similar to that of sandstones and less than that of shales.[117] In contrast some coals, such the Ferron coals in the Drunkard's Wash Unit of the Uinta Basin, exhibit high gamma ray responses. Carbon converts soluble uranium salts to an insoluble form, and uranium precipitated from groundwater flowing through the Ferron coals clearly shows on spectral gamma ray logs. Clay and shale laminations in coals can often be identified by their high gamma ray responses compared to clean coal. Thus, gamma ray logs are useful for understanding coal seam vertical heterogeneity, for correlation of seams between wells, and for estimation of the ash fraction in proximate analysis correlations. Washouts suppress gamma ray response, and thus confidence in this log is increased if a caliper log is also available. A gamma ray log can also be run in cased holes, making it useful in perforating and production logging operations, similar to conventional reservoirs.

Neutron induced gamma ray logs can be used to identify and quantify a variety of minerals such as sulfur, calcium, and silicon. The presence of sulfur, usually pyritic, indicates a marine influence during deposition and initial burial. Calcium, especially calcium carbonate, is an indicator of cleat mineralization. Mineral concentrations, estimated from these elemental concentrations using correlations based on local conditions, are used to determine coal ash and mineral matter content.

The caliper log measures hole diameter and is more useful as a quality check on other wireline logs, such as density and gamma ray logs, than as a direct indicator of coal properties. Running this log helps prevent mistaken identification of coals from the erroneously low formation density and gamma ray responses seen across severe washouts. Washout on a caliper log is sometimes taken as an indication of permeability when in fact it is more of an indication of friable coal.

The compensated neutron log (CNL), used to measure porosity in conventional reservoirs, shows erroneously high porosity in coals, making it useful for identifying coals and determining net thickness. It is also used in some log analysis algorithms for rank determination and estimation of gas content. The CNL can be run in both open and cased holes, but like many other wireline logs run in coals, the tool is affected by washouts.

The spectral density tool, similar to the bulk density tool, provides lithology identification but employs the photoelectric effect. The photoelectric absorption index of coal is an order of magnitude less than those of sandstone and shale, providing a second means of coal identification. In addition, it is often used in conjunction with other logs in correlations to determine proximate analysis.

The sonic log can be used to identify coals and determine coal rank. Sonic travel times in coals fall between those of sandstones and shales. Due to similar travel times, discrimination between anthracite and shales is sometimes difficult. While this log is useful in assessing mineability and quality of a coal, it has seen limited application in coal gas reservoir engineering.

The spontaneous potential (SP) log response to coals is weak and inconsistent. Some coals exhibit marked SP deflection, making discrimination with a porous, wet sandstone difficult. Although SP deflection can often be qualitatively correlated with permeability development in conventional reservoirs, such interpretations are rarely possible in coal deposits.

The fraction of the coal void volume occupied by free gas is termed gas saturation, similar to conventional reservoirs. Unfortunately, the gas volume sorbed onto the surface of the coal matrix expressed as a fraction of the theoretical maximum sorbed gas at reservoir pressure and temperature is also termed gas saturation. A coal that holds this theoretical maximum sorbed gas is said to be saturated. Coals that contain less than the theoretical maximum are said to be undersaturated. Undersaturated coals are commercially challenging, as a project must bear the expenses of producing and disposing of large volumes of water prior to any gas production and revenue from gas sales. The pressure at which gas desorbs from a coal is termed *desorption pressure*, and comparison of this pressure against initial reservoir pressure provides an indication of undersaturation. Partial pressure of methane dissolved in coal formation water can be obtained via Raman spectroscopy.[118] Physical chemistry

arguments that this pressure equals methane desorption pressure allow computation of coalbed gas content if a sorption isotherm has been measured for this coal. Knowledge of coal seam pressure permits calculation of saturated coalbed gas content from that same isotherm. Division of coalbed gas content calculated from methane partial pressure by that calculated from reservoir pressure yields gas saturation of the coal matrix. Difficulties with running this log include optical clarity of the wellbore fluid and ensuring that it is representative of the native reservoir water.

Resistivity of coal is high compared to other lithologies, ranging from 50 to 2,000 ohms, and is more a function of impurities and water salinity than rank.[119] In washed-out holes, a resistivity log can be used in conjunction with density and gamma ray logs to increase confidence in identification of coal seams but is of limited use in determination of coal properties. In frontier areas, resistivity logs from logging suites run in old wells drilled to deeper, conventional targets can be used to identify coals. Vertical resolution of resistivity tools, especially older tools, is on the order of 1 ft (0.3 m), precluding accurate seam thickness measurements. Mavor et al. noted that separation of shallow, medium, and deep resistivity traces were useful indicators of coal permeability development but gave no details.[120]

Cleat detection with wireline logs is difficult. Coal mineralogy based on neutron induced gamma ray logs has been used to infer cleat development, with lower percentages of a given mineral being interpreted as indicative of a well-cleated coal and higher percentages indicative of poorly cleated coals.[121] This method is complicated by well-cleated coals with mineralized cleats or high ash contents. Johnston and Scholes combined gamma ray, density, neutron, and resistivity logs to determine coal cleating and maceral groups in Fruitland coal in the San Juan Basin.[122] Multiple assumptions and local log responses limit applicability of this method to other coals. The spectral density log is sensitive to barite, and a high photoelectric response in a coal drilled with mud containing barite is sometimes interpreted as an indicator of coal cleat development and, hence, coal permeability. The photoelectric absorption index of barite is nearly three orders of magnitude greater than coal (266 versus 0.3). As a result, the photoelectric trace of the spectral density log run in wells drilled with muds containing barite additives is useful for identifying thick mudcake, and by inference, well-cleated, highly permeable coals. Mullen noted that reliable identification of cleating in north San Juan Basin coals with this method requires mud weights of 11.5 lb/gal or higher, increasing the risk of drilling damage to the coal seams.[123]

The microlog, which measures mudcake and formation resistivities, can show significant separation in some well-cleated coals but should be used with caution, as the response can vary from basin to basin and seam to seam.[124] The degree of separation of the resistivity traces is influenced by mud additives and viscosity and hole washouts, as well as coal cleat aperture and intensity. Thus, this tool is limited to qualitative indications of coal permeability at best. Correlation of microlog response with well productivity on a local basis can predict productivity of new wells, but quantification of permeability with this log remains elusive.

A method for qualitative assessment of coal cleating in San Juan Basin coals was developed by Mullen based on a microlog index defined as[125]

$$I = \frac{(R - R_m)}{(R_c - R_m)}$$

where

$I$ = microlog index,
$R_m$ = mud resistivity corrected to bottomhole temperature,
$R_c$ = cutoff resistivity, typically 30 × mud resistivity, $R_m$, and
$R$ = average microlog resistivity.

Average microlog resistivity is defined by

$$R = \frac{(R_{ml} - R_{mn})}{2}$$

where

$R_{ml}$ = microlateral resistivity, and
$R_{mn}$ = micronormal resistivity.

This microlog index, conveniently independent of mud resistivity and ranging from 0 to 1, was used to characterize the degree of cleating in selected wells. *Well-developed cleats* were defined to be those intervals with a microlog index less than 0.3. *Moderately developed cleats* had a microlog index between 0.3 and 0.6, and *poorly cleated sections* had microlog index values greater than 0.6. Comparison of cleat development in a half dozen wells with subsequent performance allowed producibility prediction of newly drilled wells.

Cleat development in Fruitland coals in the north San Juan Basin was evaluated by Hoyer using the Dual-Laterolog.[126] Although this tool cannot resolve cleat aperture width or spacing, the conductivity differential between shallow and deep laterologs permitted estimation of seam productivity. Cleat development in a single seam, similar to the work done by Mullen, should be possible with this tool but was not reported by Hoyer. Response from the Dual-Laterolog was employed by Aguilera to determine cleat spacing and aperture and, by extension, cleat porosity and permeability.[127] Application to a San Juan Basin coal well indicated the method needed additional refinement but could be a reasonable predictor of well productivity after initial logging results were correlated with subsequent well performance.

Schlumberger's Formation Microscanner (FMS) and Formation Micro Imager (FMI) have been employed to characterize coal cleating with various degrees of success. Hollub and Schafer reported orientation of Warrior Basin coal cleats determined by the FMS tool and oriented cores were in good agreement.[128] The FMI tool can be used to determine cleat orientation and, because cleat geometries are often at the resolution limits of the tool, qualitative cleat development. Characterization of coals in the Alberta plains with the FMI is discussed by Schlumberger, where this tool was also used to identify a fault in a coal seam.[129] The tool can be run in both the static and dynamic mode, with the preferred mode being determined by experience in a given area.

Popular cased-hole logs for coal gas reservoir engineering are the carbon/oxygen, gamma ray, compensated neutron, and cement bond logs. Carbon content of a formation and the fluids it holds is measured by the carbon/oxygen log. Virtually all of the carbon in conventional reservoirs occurs as hydrocarbon fluids in the pores, allowing determination of fluid saturations from this log. Coals, composed primarily of a carbonaceous matrix with small, water-filled porosities, gives a distinctive signature on a carbon/oxygen log that can be correlated with coal density. This log can be run in both open and cased holes, permitting identification of behind-pipe coals in wells drilled to deeper conventional targets. Sensitive to washouts, interpretations from a carbon/oxygen log are strengthened when a caliper log is available.

Gamma ray and compensated neutron logs are employed in cased holes to identify coals and determine net coal thickness. The pulsed neutron log can also be used to identify coals but requires determination of the pulsed neutron ratio cutoff to determine coals, sometimes on a well-by-well basis but certainly on a regional basis. All three of these logs are sensitive to washouts behind pipe.

Cement bond logs are employed in coal wells, as in conventional wells, to assess integrity of cement. Often required by regulations, these logs provide little information about the coal reservoir, including the degree of cement damage or infiltration.

Production logs are difficult to run in coal wells because these wells often require artificial lift. Once a coal well is dewatered and the pump removed, little incentive exists for running production logs, as most of the flow is simply single-phase gas. Hollub and Schafer discuss use of various production logging tools, including downhole video.[130]

While wireline logs are fundamental for characterization of coal reservoirs, currently they cannot determine coal permeability, porosity, or water saturation. Several tools, including the microlog, Dual-Laterolog, and Formation Microscanner, can often be utilized to estimate well productivity, especially on a local basis when log response can be calibrated against subsequent gas and water production. Effective permeabilities to gas and water in a coal seam are best determined from well tests or performance analysis.

Coal is primarily a solid, organic matrix with little void space. This small void space, divided between matrix porosity and fractures, is often only a few percent of the coal seam volume. The matrix porosity typically contains

a mixture of sorbed gases with densities approaching their respective liquid densities. In contrast, the fracture porosity is composed of slim, orderly, orthogonal cleat networks filled with water, gas, or a mixture of both. Consequently, logging tools for characterizing porosity in conventional reservoirs have limited utility in the small, heterogeneous void space of coals. Effective porosity, that void volume of the coal that is important for reservoir engineering purposes, is very difficult, often impossible, to quantify with wireline logs. For reservoir engineering purposes, effective porosity is usually assumed to be on the order of 1% for bituminous and anthracitic coal and 10% for subbituminous coals. Sometimes effective porosity can be determined by analysis of well performance or reservoir simulation.

Water saturation in coal cleats, and hence, gas saturation, cannot be calculated from wireline logs and Archie-type equations. Coals are typically aquifers with little, if any, free gas initially present in the cleats; thus, reservoir engineering calculations often assume an initial water saturation of 100%. Once wells are on production, average gas and water saturations can be estimated from the producing gas-water ratio, relative permeability curves, and Darcy's law.

## Nomenclature

| | |
|---|---|
| $a$ | Ash weight fraction |
| $b$ | Kim temperature constant, $cm^3/g\text{-}°C$ |
| $fc$ | Fixed carbon weight fraction |
| $k$ | Kim pressure constant, $cm^3/g\text{-}atm$ |
| $n$ | Kim pressure exponent, dimensionless |
| $p$ | Pressure, atm |
| $T$ | Temperature, °C |
| $V$ | In-situ coalbed gas content, $cm^3/g$ |
| $V_{C1}$ | Volume of methane generated, daf, $cm^3/g$ |
| $Vm$ | Volatile matter weight fraction |
| $w$ | Equilibrium moisture weight fraction |

### Greek

| | |
|---|---|
| $\rho$ | Coal bulk density, $g/cm^3$ |
| $\rho_a$ | Ash density, $g/cm^3$ |
| $\rho_o$ | Organic fraction density, $g/cm^3$ |
| $\rho_w$ | Water density, $g/cm^3$ |

## References


1. Stach, E., Mackowsky, M.-Th., Teichmuller, M., Taylor, G. H., Chandra, D., and Teichmuller, R. 1982. *Stach's Textbook of Coal Petrology*. 3rd ed. Berlin: Gebruder Borntraeger; and Galloway, W. E., and Hobday, D. K. 1996. *Terrigenous Clastic Depositional Systems*. 2nd ed. New York: Springer-Verlag.
2. Stach, E., et al. 1982.
3. Clayton, J. L. 1993. Composition of crude oils generated from coals and coaly organic matter in shales. In *Hydrocarbons from Coal, AAPG Studies in Geology #38*. Law, B. E., and Rice, D. D., eds. Tulsa: American Association of Geologists. p. 185.
4. Hayes, E. T. 1979. Energy resources available to the United States in 1985–2000. *Science*. V. 203 (no. 4,377). p. 233.
5. Landis, E. R., and Weaver, J. N. 1993. Global coal occurrence. In *Hydrocarbons from Coal, AAPG Studies in Geology #38*. Law, B. E., and Rice, D. D., eds. Tulsa: American Association of Petroleum Geologists. p. 1.
6. Ibid.; and World Energy Council. 2007. *2007 Survey of Energy Resources*. London: World Energy Council.
7. Schopf, J. M. 1956. A definition of coal. *Economic Geology*. V. 51. p. 521.
8. Galloway, W. E., and Hobday, D. K. 1996.
9. Stach, E., et al. 1982.
10. Ibid.; and Pashin, J. C. 1994. Coal-body geometry and synsedimentary detachment folding in Oak Grove Coalbed Methane Field, Black Warrior Basin, Alabama. *AAPG Bulletin*. V. 78 (no. 6). p. 960.
11. Stach, E., et al. 1982.
12. Ibid.
13. Ibid.
14. Ibid.
15. Galloway, W. E., and Hobday, D. K. 1996.
16. Stach, E., et al. 1982.
17. Ibid.
18. Stach, E., et al. 1982; Galloway, W. E., and Hobday, D. K. 1996; and Flores, R. M. 1993. Coal-bed and related depositional environments in methane gas-producing sequences. In *Hydrocarbons from Coal, AAPG Studies in Geology #38*. Law, B. E., and Rice, D. D., eds. Tulsa: American Association of Petroleum Geologists. p. 13.
19. Galloway, W. E., and Hobday, D. K. 1996.
20. Flores, R. M. 1993.
21. Galloway, W. E., and Hobday, D. K. 1996.
22. Flores, R. M. 1993.
23. Galloway, W. E., and Hobday, D. K. 1996.
24. Ibid.
25. Ibid.
26. Nowak, H. C. 1991. Depositional environments and stratigraphy of Mesaverde Formation, Southeastern Piceance Basin, Colorado—implications for coalbed methane exploration. In *Coalbed Methane of Western North America*. Schwochow, S. D., Murray, D. K., and Fahy, M. F., eds. Denver: Rocky Mountain Association of Geologists. p. 1.
27. Flores, R. M. 1993.
28. Galloway, W. E., and Hobday, D. K. 1996.
29. Ibid.
30. Ibid.
31. Ibid.
32. Ibid.
33. Ferm, J. C., and Staub, J. R. 1984. Depositional controls of minable coal bodies. In *Sedimentology of Coal and Coal-bearing Sequences: International Association of Sedimentologists Special Publication 7*. England: Wiley-Blackwell. p. 275.
34. Galloway, W. E., and Hobday, D. K. 1996; Barataria Bay. http://www.gulfbase.org/bay/view.php?bid=barataria. Accessed December 26, 2008; and http://www.lacoast.gov/landchange/basin/ba. Accessed December 26, 2008.
35. Laubach, S. E., Marrett, R. A., Olson, J. E., and Scott, A. R. 1998. Characteristics and origins of coal cleat: A review. *International Journal of Coal Geology*. V. 35 (February). p. 175.
36. Pitman, J. K., Pashin, J. C., Hatch, J. R., and Goldhaber, M. R. 2003. Origin of minerals in joint and cleat systems of the Pottsville Formation, Black Warrior Basin, Alabama: Implications for coalbed methane generation and production. *AAPG Bulletin*. V. 87 (no. 5). p. 713.
37. Ibid.
38. Flores, R. M., 1993; Fassett, J. E. 1988. Geometry and depositional environment of Fruitland Formation coal beds, San Juan Basin, New Mexico and Colorado: Anatomy of a giant coal-bed methane deposit. In *Geology and Coalbed Methane Resources of the Northern San Juan Basin, Colorado and New Mexico*. Denver: Rocky Mountain Association of Geologists. p. 23.; and Ayers, W. B. 2002. Coalbed gas systems, resources, and production and a review of contrasting cases from the San Juan and Powder River basins. *AAPG Bulletin*. V. 86 (no. 11). p. 1,853.
39. Pashin, J. C. 1994; and Pashin, J. C. 1998. "Stratigraphy and structure of coalbed methane reservoirs in the United States: An overview. *International Journal of Coal Geology*. V. 35. p. 209.
40. Flores, R. M. 1993.
41. Pashin, J. C. 1994.

42. Flores, R. M. 1993; and Ayers, W. B. 2002.
43. Flores, R. M. 1993.
44. Ibid.
45. Montgomery, S. L., Barker, C. E., Seamount, D., Dallegge, T. A., and Swenson, R. F. 2003. Coalbed methane, Cook Inlet, south-central Alaska: A potential giant gas resource. *AAPG Bulletin*. V. 87 (no. 1). p. 1.
46. Su, Xianbo, Lin, Xiaoying, Zhao, Mengjun, Song, Yan, and Liu, Shaobo. 2005. The upper Paleozoic coalbed methane system in the Qinshui Basin, China. *AAPG Bulletin*. V. 89 (no. 1). p. 81.
47. Stevens, S. H., and Hadiyanto. 2004. *Indonesia: Coalbed Methane Indicators and Basin Evaluation*. Paper SPE 88630. Presented at the SPE Asia Pacific Oil and Gas Conference and Exhibition, Perth, Australia, October 18–20; and Horkel, A. 1990. On the plate-tectonic setting of the coal deposits of Indonesia and the Philippines. *Mitteilungen der Österreichischen Geologischen Gesellschaft*. V. 82 (December). p. 119. Vienna.
48. Rightmire, C. T., Eddy, G. E., and Kirr, J. N. 1984. *Coalbed Methane Resources of the United States, AAPG Studies in Geology Series #17*. Tulsa: American Association of Petroleum Geologists.
49. Beaton, A. 2003. *Production Potential of Coalbed Methane Resources in Alberta*. EUB/AGS Earth Sciences Report 2003–03. Edmonton: Alberta Energy and Utilities Board/Alberta Geological Survey.
50. Galloway, W. E., and Hobday, D. K. 1996.
51. Beaton, A. 2003; and Bastian, P. A., Wirth, O. F. R., Wang, L., and Voneiff, G. W. 2005. *Assessment and Development of the Dry Horseshoe Canyon CBM Play in Canada*. Paper SPE 96899. Presented at the SPE Annual Technical Conference and Exhibition, Dallas, Texas, October 9–12.
52. Bastian, P. A., et al. 2005.
53. Flores, R. M. 1993; and Staub, J. R. 1999. Reservoir sequences in the coal beds of southern West Virginia. Paper 9915 in *Proceedings of the 1999 International Coalbed Methane Symposium*. Tuscaloosa: University of Alabama.
54. Galloway, W. E., and Hobday, D. K. 1996; and Diessel, C. F. K. 1986. On the correlation between coal facies and depositional environments. *Proceedings of the 20th Sydney Basin Symposium*. Newcastle, New South Wales: Department of Geology, University of Newcastle.
55. Staub, J. R. 1999.
56. Berkowitz, N. 1979. *An Introduction to Coal Technology*. New York: Academic Press; and Stach, E., et al. 1982.
57. Horkel, A. 1990.
58. Pashin, J. C., Carroll, R. E., Hatch, J. R., and Goldhaber, M. B. 1999. Interplay among cleating, maturation, and mineralization in coalbed methane reservoirs of the Black Warrior Basin. Paper 9942 in *Proceedings of the 1999 International Coalbed Methane Symposium*. Tuscaloosa: University of Alabama.
59. Ibid.
60. Ibid.
61. Reiss, L. H. 1980. *The Reservoir Engineering Aspects of Fractured Reservoirs*. Houston: Gulf Publishing Company.
62. Montgomery, S. L., Tabet, D. E., and Barker, C. E. 2001. Upper Cretaceous Ferron Sandstone: Major coalbed methane play in central Utah. *AAPG Bulletin*. V. 85 (no. 2). p. 199.
63. Ayers, W. B. 2002.
64. Ibid.
65. Ibid.
66. Pashin, J. C., et al. 1999.
67. Close, J. C. 1993. Natural fractures in coal. In *Hydrocarbons from Coal, AAPG Studies in Geology #38*. Law, B. E., and Rice, D. D., eds. Tulsa: American Association of Petroleum Geologists. p. 185.
68. Mukhopadhyay, P. K., and Hatcher, P. G. 1993. Composition of coal. In *Hydrocarbons from Coal, AAPG Studies in Geology #38*. Law, B. E., and Rice, D. D., eds. Tulsa: American Association of Petroleum Geologists. p. 185.
69. Laubach, S. E., et al. 1998.
70. Close, J. C. 1993.
71. Laubach, S. E., et al. 1998.
72. Close, J. C. 1993.
73. Kulander, B. R., and Dean, S. L. 1993. Coal-cleat domains and domain boundaries in the Allegheny Plateau of West Virginia. *AAPG Bulletin*. V. 77 (no. 8). p. 1,374.
74. Laubach, S. E., et al. 1998.
75. Scott, A. R. 1994. Composition of coalbed gases. *In Situ*. V. 18 (no. 2). p. 185.
76. Ibid.
77. Smith, J. W., and Pallasser, R. J. 1996. Microbial origin of Australian coalbed methane. *AAPG Bulletin*. V. 80 (no. 6). p. 891.
78. Rightmire, C. T., et al. 1984.
79. Ibid.
80. Ibid.
81. Ibid.
82. Rice, D. D. 1993. Composition and origins of coalbed gas. In *Hydrocarbons from Coal, AAPG Studies in Geology #38*. Law, B. E., and Rice, D. D., eds. Tulsa: American Association of Petroleum Geologists. p. 185.
83. Meissner, F. F. 1984. Cretaceous and Lower Tertiary coals as sources for gas accumulations in the Rocky Mountain area. In *Hydrocarbon Source Rocks of the Greater Rocky Mountain Region*. Denver: Rocky Mountain Association of Geologists. p. 401.

84. Juntgen, H. and Karweil, J. 1966. Gasbildung und gasspeicherung in steinkohlenflozen. Part I and II. *Erdöl und Kohle, Erdgas, Petrochemie*. V. 19. pp. 251 and 339.
85. Rightmire, C. T., et al. 1984.
86. Meissner, F. F. 1984.
87. Meissner, F. F. 1984; and Rightmire, C. T., et al. 1984.
88. Kim, A. G. 1977. *Estimating Methane Content of Bituminous Coalbeds from Adsorption Data*. U.S. Bureau of Mines Report of Investigations RI 8245, 1977; and Ryan, B. D. 1992. An equation for estimation of maximum coalbed-methane resource potential. Paper 1992-1 in *Geological Fieldwork 1991*. Victoria, B.C.: British Columbia Geological Survey.
89. Rice, D. D. 1993.
90. Martini, A. M., Walter, L. M., Ku, T. C. W., Budai, J. M., McIntosh, J. C., and Schoell, M. 2003. Microbial production and modification of gases in sedimentary basins: A geochemical study from a Devonian shale gas play, Michigan Basin. *AAPG Bulletin*. V. 87 (no. 8). p. 1,355.
91. Scott, A. R., Kaiser, W. R., and Ayers, W. B., Jr. 1994. Thermogenic and secondary biogenic gases, San Juan Basin, Colorado and New Mexico: Implications for coalbed gas producibility. *AAPG Bulletin*. V. 78 (no. 8). p. 1,189.
92. Ibid.
93. Montgomery, S. L., et al. 2003.
94. Rice, D. D. 1993; and Clayton, J. L. 1998. Geochemistry of coalbed gas—A review. *International Journal of Coal Geology*. V. 35 (February). p. 159.
95. Ibid.
96. Ibid.
97. Bernard, B. B., Brooks, J. M., and Sackett, W. M. 1978. Light hydrocarbons in recent Texas continental shelf and slope sediments. *Journal of Geophysical Research*. V. 83. p. 289.
98. Ibid.
99. Ruppert, L. F., Fedorko, N., Warwick, P. D., Grady, W. C., Crangle, R. D, Jr., and Britton, J. Q. 2004. *Results of Coal Bed Methane Drilling, Mylan Park, Monongalia County, West Virginia*. USGS Open-File Report 2004-1402.
100. Scott, A. R., et al. 1994.
101. Martini, A. M., Walter, L. M., and McIntosh, J. C. 2008. Identification of microbial and thermogenic gas components from Upper Devonian black shale cores, Illinois and Michigan basins. *AAPG Bulletin*. V. 92 (no. 3). p. 327.
102. Scott, A. R., et al. 1994.
103. Smith, J. W., and Pallasser, R. J. 1996.
104. Rice, D. D. 1993.
105. Scott, A. R., et al. 1994.
106. Burns, T. D., and Lamarre, R. A. 1997. Drunkard's Wash project: Coalbed methane production from Ferron coals in east-central Utah. Paper 9709 in *Proceedings of the 1997 International Coalbed Methane Symposium*. Tuscaloosa: University of Alabama.
107. Van Voast, W. A. 2003. Geochemical signature of formation waters associated with coalbed methane. *AAPG Bulletin*. V. 87 (no. 4). p. 667.
108. Ibid.
109. Marroquin, I. D., and Hart, B. S. 2004. Seismic attribute-based characterization of coalbed methane reservoirs: An example from the Fruitland Formation, San Juan Basin, New Mexico. *AAPG Bulletin*. V. 88 (no. 11). p. 1,603.
110. Meisheng, W., Hong, L., Zhensheng, Z., and Peiming, L. 2008. The application of DSU1 high density 3-D in coal field exploration. In *Proceedings of the SEG Las Vegas 2008 Annual Meeting*. Tulsa: Society of Exploration Geophysicists. p. 1,157.
111. Ayers, W. B. 2002; and Lamarre, R. A. 2005. Undersaturation in coals: How does it happen and why is it important. Rocky Mountain Section, AAPG Annual Meeting, Jackson, Wyoming, September 24–26, 2005. Search and Discovery Article 40195. www.searchanddiscovery.net/documents/ 2006/06034lamarre/index.htm. Accessed April 10, 2009.
112. Bustin, A. M. M., and Bustin, R. M. 2008. Coal reservoir saturation: Impact of temperature and pressure. *AAPG Bulletin*. V. 92 (no. 1). p. 77.
113. Hollub, V., and Schafer, P. 1992. *A Guide to Coalbed Methane Operations*. Chicago: Gas Research Institute; and Campen, E. B., and Campen, E. B. 2002. Basic log analysis in coalbed methane exploration. In *Coalbed Methane of North America II*. Denver: Rocky Mountain Association of Geologists. p. 17.
114. Mullen, M. J. 1989. *Coalbed Methane Resource Evaluation from Wireline Logs in the Northeastern San Juan Basin: A Case Study*. Paper SPE 18946. Presented at the SPE Joint Rocky Mountain Regional/Low Permeability Reservoirs Symposium, Denver, Colorado, March 6–8.
115. Schopf, J. M. 1956.
116. Lamarre, R. A., and Pratt, T. J. 2002. Reservoir characterization study: Calculation of gas-in-place in Ferron coals at Drunkard's Wash Unit, Carbon and Emery counties, Utah. *The Mountain Geologist*. V. 39 (no. 2). p. 41.
117. Hollub, V., and Schafer, P. 1992; and Hall, R. V. 2002. *Geophysical Well-log Interpretation for Coalbed Methane*. OGS Open-File Report 9-2002. Norman: Oklahoma Geological Survey.
118. Lamarre, R. A., and Pope, J. 2007. Critical-gas-content technology provides coalbed-methane-reservoir data. *Journal of Petroleum Technology*. V. 59 (no. 11). p. 108.
119. Hall, R. V. 2002.
120. Mavor, M. J., Close, J. C., and McBane, R. A. 1994. Formation evaluation of exploration coalbed-methane wells. *SPE Formation Evaluation*. V. 9 (no. 4). p. 285.

121. Anderson, J., et al. 2003. Producing natural gas from coal. *Schlumberger Oilfield Review*. Autumn 2003. p. 8.
122. Johnston, D. J., and Scholes, P. L. 1991. Predicting cleats in coal seams from mineral and maceral composition with wireline logs. In *Coalbed Methane of Western North America*. Schwochow, S. D., Murray, D. K., and Fahy, M. F., eds. Denver: Rocky Mountain Association of Geologists. p. 123.
123. Mullen, M. J. 1988. Log evaluation in wells drilled for coalbed methane. In *Geology and Coalbed Methane Resources of the Northern San Juan Basin, Colorado and New Mexico Guidebook*. Fassett, J. E., ed. Denver: Rocky Mountain Association of Geologists. p. 113.
124. Mavor, M. J., et al. 1994.
125. Mullen, M. J. 1991. Cleat detection in coalbeds using the microlog. In *Coalbed Methane of Western North America*. Schwochow, S. D., Murray, D. K., and Fahy, M. F., eds. Denver: Rocky Mountain Association of Geologists. p. 137.
126. Hoyer, D. L. 1993. Evaluation and confirmation of coal seam fractures from Dual-Laterolog. Paper 9396 in *Proceedings of the 1993 International Coalbed Methane Symposium*. Tuscaloosa: University of Alabama.
127. Aguilera, R. 1994. Formation evaluation of coalbed methane formations. *Journal of Canadian Petroleum Technology*. V. 33 (no. 9). p. 22.
128. Hollub, V., and Schafter, P. 1992.
129. Anderson, J., et al. 2003.
130. Hollub, V., and Schafer, P. 1992.

# Measurement of Coalbed Gas Content

# 4

## Introduction

Determination of the gas volume held in a coal deposit is critical to economic exploitation of that gas. Gas contained in coal deposits was initially considered a mining hazard, and gassy coal mines sought to quantify the amount of gas released per ton of coal mined. Early researchers expressed gassiness of a coal deposit with dimensions of standard cubic centimeters of gas per gram ($cm^3/g$) or standard cubic feet of gas per ton (scf/ton). Both of these dimensions are still employed in coal gas reservoir engineering today.[1] The two broad categories for gas content determination are direct and indirect methods. *Direct methods* involve collection of fresh coal samples at the wellsite and measurement of gas emitted over weeks or months. *Indirect methods* rely on correlations, equations, or laboratory isotherms (see chapter 5), coupled with the assumption that the coal deposit is fully saturated with gas at the current pressure, to estimate gas content of a coal deposit. Both categories determine sorbed gas; neither determines free gas. This is not a serious limitation for low-porosity, water-saturated coals, but both methods can seriously underestimate the gas resource in high-porosity coals with substantial free gas.

## Direct Methods

Initially, coalbed gas contents were determined by measuring the gas released from whole core samples with the objective of improving mine safety. As coals came to be recognized as gas reservoirs, protocols were developed to collect and desorb drill cuttings and sidewall cores in addition to whole cores. In parallel, mathematical models to analyze desorption data were developed. All models assume gas release from the coal sample is controlled by desorption, not flow in the cleats. Currently, the following are the three most popular methods for analysis of desorption data:[2]

1. The U.S. Bureau of Mines direct method
2. The Smith and Williams method
3. Curve fit methods

It should be noted that any of the three methods can be applied to desorption data from cores, cuttings, or sidewall cores. With three types of desorption samples and three methods of analyzing desorption data, there are nine avenues to measure coalbed gas content. In theory, none are fundamentally flawed, and all nine should give the same answer. In practice, however, accuracy of the methods varies, and each has its unique limitations. The current industry standard for gas content determination is desorption of whole core samples maintained at reservoir temperature and analysis of the data according to the U. S. Bureau of Mines (USBM) direct method.

Direct methods first measure gas emitted by a sample. Next, that data is used to estimate gas lost by the sample during cutting, retrieval, and surface handling prior to being hermetically sealed. Then remaining gas is measured or estimated once desorption measurements are terminated. Early workers defined three categories of gas emitted by a coal sample.[3] Gas emitted by the sample during coring or drilling, the subsequent trip up hole, and on the surface prior to being sealed in a desorption canister clearly cannot be measured. This gas volume, defined as *lost gas*, is estimated from the initial desorbed gas volumes. Once the sample has been sealed in an airtight container, desorbed gas volumes are measured over several days, weeks, or months until the rate drops below a somewhat arbitrary threshold value. Incremental desorbed gas volumes at each step must be corrected to standard temperature and pressure (STP). Cumulative measured gas volume, corrected to STP, is termed *desorbed gas*. When the gas emission rate for a given sample drops below a threshold value, desorption measurements are terminated, and the canister is opened. Any remaining gas, labeled *residual gas*, is determined either from laboratory procedures or analytic methods.

**Sample collection.** Desorption samples include whole core, either conventional or wireline retrieved, sidewall cores, and cuttings. Historically, the coalbed methane industry first used conventional, whole core samples. This was soon followed by use of drill cuttings and continuous wireline retrieval cores. Rotary sidewall core technology was adapted to cut coals, but reliable gas contents from sidewalls requires painstaking field and laboratory techniques due to the small gas volumes released. More than one type of sample is often collected on a given well. For example, cuttings collected during coring provide alternative gas contents that can be especially useful if core recovery is poor or retrieval is problematic. Regardless of sample type, acquisition of high-quality coalbed gas content measurements is enhanced by involving the desorption company as early as possible in design of a drilling, coring, and testing program.

Conventional whole cores provide the largest samples and can be cost-effective when only one or two seams are to be cored. Picking the core point is often difficult, and frequently the top few feet of the target coal are drilled up before the drilling assembly is tripped out of the hole and the core barrel is run. Pulling times of conventional cores from 2,000 ft (600 m) can easily be three hours or more, leading to large lost gas volumes. Current practice restricts whole cores to coal seam depths of less than about 3,000 ft (900 m).

Wireline retrieved cores, also called *continuous cores*, provide samples of bounding strata as well as the target coal seams. As a general rule, wireline cores cut faster and have higher recoveries than conventional cores, especially in friable coals. With retrieval rates on the order of 100 to 200 ft/min (30 to 60 m/min), pulling times of wireline retrieved cores are typically much less than those of conventional cores. Current technology limits wireline retrieved cores to depths less than about 4,000 ft (1,200 m).

Sidewall cores are frequently the most cost-effective sample type for coals more than 4,000 ft (1,200 m) in depth or when multiple seams are to be tested. Rotary cores are preferable to percussion cores, which can shatter a brittle coal. Factors affecting sidewall core recovery include hole washout and filtercake buildup. Service companies routinely achieve 80% sidewall core recoveries. Sidewall cores are, of course, cut after drilling and logging. If the well is being drilled underbalanced or with air or mist, gas begins to escape as soon as the coal is penetrated. Minimizing drilling below the coal as well as logging runs to identify sidewall core points help reduce lost gas time. Careful desorption of sidewall cores utilizing special equipment can yield coalbed gas contents as reliable as those obtained from conventional or wireline retrieved cores.

Determination of coalbed gas content from drill cuttings is quicker and cheaper than whole core or sidewall core desorption. Cuttings can be collected when drilling through coal seams to deeper targets, allowing assessment of the coal gas resource for small incremental cost. Gas contents obtained from desorption of drill cuttings are routinely less than those obtained by other methods. For reasons not entirely understood, particle size affects rate of gas release, and cuttings from wells drilled with air or foam are too small to desorb. In wells drilled with mud or water, the cuttings lag rate of 30 to 100 ft/min (10 to 30 m/min) limits use of cuttings desorption to coal depths less than about 4,000 ft (1,200 m).

Any cuttings sample contains a variety of contaminants, with drilling solids and additives (such as lost circulation material) as well as uphole cavings being among the most common. Once desorption is complete, rinsing the cuttings sample with distilled water containing 2% KCl removes some contaminants. Separation of

coal cuttings from other cuttings in the sample was initially done with heavy brines. If this method of separation is employed, density of the heavy brine should be reported and compared against the bulk density used to define pay cutoff. A typical brine density for float/sink separation is 1.75 g/cm$^3$, while many operators use a pay cutoff of 2.0 g/cm$^3$. Such a practice will minimize coal mass and maximize coalbed gas content, and it can lead to erroneously high reserves when combined with a 2.0 g/cm$^3$ pay cutoff on wireline logs. Heavy brines often compromise the coal cuttings for further laboratory testing. Current practice is to determine ash content, as is done in proximate analyses, and report the cuttings gas content on a dry, ash-free (daf) basis. Note that contamination of a cuttings sample with cavings from uphole coals is virtually undetectable and could result in computed gas contents lower than actual.

Pressure cores have sometimes been employed to determine coalbed gas content as they virtually eliminate any lost gas. However, they are expensive and result in a single sample over the cored interval, eliminating the redundancy of multiple samples, which is the most effective strategy against the inevitable gas leaks. While the single gas content from a pressure core characterizes the cored interval, that single in-situ gas content cannot be correlated with bulk density, precluding determination of gas content in offset wells with density logs.

Core and cuttings desorption sample canisters range from 6 in. to 3 ft in length, with the 1 ft size being by far the most popular, probably due to weight and tipping considerations in the field and laboratory. The Gas Research Institute (GRI) gives a more detailed discussion of coal sampling techniques (chapter 7) and representative collection protocols (chapter 8).[4] The GRI summary of desorption sampling techniques is reproduced here as table 4–1.

**Table 4–1.** Summary of desorption sampling techniques

| Recovery technique | Advantages | Disadvantages |
|---|---|---|
| **Pressure Coring** | • Minimized lost gas volume.<br>• Direct measurement of producible gas from the cored interval.<br>• Minimized contamination by atmospheric gases.<br>• Evolution of gas species can be measured for the overall cored section.<br>• Intact, large-diameter "preserved" core samples are available for other flow or mechanical properties tests.<br>• Geological evaluation (cleat mapping, petrology, etc.) is possible. | • Most expensive option. Potential tool operation problems (sealing).<br>• Net gas content for the entire core barrel is measured, rather than for discrete zones. Do not know precisely where gas is coming from (can be approximated indirectly from proximate analysis).<br>• Cannot infer relationships between gas content and ash content for logging calibration (can be estimated indirectly from proximate analysis).<br>• Requires extensive field labor.<br>• Drilling fluid may impact desorption.<br>• Picking core point may be difficult. |
| **Full Diameter Conventional Core (Usually 3.5 in. diameter)** | • Less expensive than pressure coring.<br>• Nominally intact, large-diameter core samples are available for other tests (i.e., permeability, mechanical properties, formation damage, etc.)<br>• Potential for lost gas is less than for drill cuttings.<br>• Possible to evaluate geology (cleat mapping, petrology, etc.).<br>• Least amount of contamination from drilling fluids.<br>• Possible to evaluate desorption characteristics of discrete lithologies. | • Potential for lost gas is greater than for pressure core.<br>• Potential for lost gas may be greater than for drilled or shot sidewalls or wireline core because of greater trip time.<br>• Probably more expensive than slimhole coring.<br>• Usually more expensive than sidewalls or drill cuttings.<br>• Picking core point may be difficult (may unintentionally drill through the zone of interest). |
| **Slimhole or Wireline Recovery (Continuous Coring) (e.g., NX core size)** | • If recovered by wireline, lost gas time can be reduced significantly.<br>• May be less expensive than conventional coring.<br>• Identifying lithologic boundaries is easier (i.e., selection of core point is improved).<br>• Cleat mapping and petrology may be possible.<br>• Some additional testing (e.g., well testing) may be possible.<br>• Coring rigs may be possible.<br>• Possible to evaluate the desorption characteristics of discrete lithologies. | • Smaller diameter may lead to accelerated lost gas evolution.<br>• Slimhole logging tools may be required and may not be readily available. However, this is not true when using new generation oilfield continuous coring methods.<br>• Though it does not affect desorption, casing, completions, and production options may be seriously restricted, particularly if artificial lift is anticipated. However, this is not true when using new generation oilfield continuous coring methods.<br>• Complementary laboratory testing (i.e., permeability, mechanical properties) may be possible. However, tests such as these on coal should be performed on the largest samples possible. |

**Table 4–1.** Cont.

| Recovery Technique | Advantages | Disadvantages |
|---|---|---|
| **Drilled Sidewall Core (less than 1 in. diameter)** | • If run after logging, sampling zones can be high graded.<br>• Technology has rapidly improved to allow better sample recovery. However, operational difficulties can still be encountered because of friability and cleating.<br>• Minimized lost gas due to reduced trip time.<br>• Reduced labor. | • Intact sampling may be difficult.<br>• Potential for "accelerated" lost gas evolution due to sample size.<br>• Small volume samples. |
| **Shot Sidewall Core (not recommended)** | • Relatively inexpensive.<br>• If run after logging, sampling zones can be high graded.<br>• Reduced labor in the field. | • May give significant underestimation of gas content values.<br>• Perforation gas and debris can contaminate the samples.<br>• Samples are completely disaggregated, with frequently poor recovery.<br>• Most other measurements (other than proximate and ultimate) are not possible.<br>• Large surface area accelerates the evolution of lost gas, despite reduced recovery time.<br>• Because of its many disadvantages, this method is not recommended. |
| **Drill Cuttings** | • Least expensive.<br>• Can be considered as a viable methodology when calibrated with other desorption measurements (i.e., whole core, etc.).<br>• Gas content data typically are available in a shorter time period. | • May give significant underestimation of gas content values.<br>• Potential for substantial lost gas volume due to sample size and large exposed surface area.<br>• Great potential for contamination with adjacent formation material, drilling material, and moisture.<br>• Precise depth assessment is difficult.<br>• Selective concentration of some seam components.<br>• Potential plugging of canister valves. |

*Source:* Gas Research Institute. 1995.

**Measurement of desorbed gas volumes.** Fresh coal samples emit gas rapidly. Whether the sample is whole core, sidewall core, or drill cuttings, determination of coalbed gas content entails capturing and measuring as much emitted gas as possible.

Regardless of sample type, it is important to promptly retrieve the samples to the surface, to minimize surface handling time, and to seal the samples in airtight canisters as quickly as possible. Typical desorption canisters for whole and sidewall core samples are shown in figure 4–1.[5]

Note the large canister for whole core samples can also be employed for cuttings desorption. Ideally, a sample should nearly fill the desorption container, leaving little headspace. Ulery and Hyman reported gas content errors on the order of 30% when headspace and desorbed gas volumes were roughly equal but minimal error when headspace volume was small compared to total desorbed gas volume.[7] Service companies commonly minimize headspace error by filling void space in a desorption canister with produced formation water, plastic packing peanuts, or sand. Cuttings, especially those from gassy coals, can be lifted into the canister exhaust valve when it is opened for a desorption measurement. Sufficient cuttings can accumulate in the valve to form a pressure seal, necessitating opening of the canister to clear the valve. The attendant loss of early-time data often taints lost gas estimates. To prevent cuttings movement into the valve, service companies use steel wool or fine screens on top of the cuttings.

Rate of gas release depends on coal sample temperature. Mavor et al. reported gas contents from ambient temperature desorption tests were one-third lower than those obtained from reservoir temperature desorption tests.[8] The importance of desorbing whole core samples at reservoir temperature was discussed by the GRI.[9] During retrieval and surface handling, the core cools. Long pulling times and/or slow surface operations exacerbate temperature loss. Once a core sample is sealed in a desorption canister and placed in a temperature bath, it begins to return to reservoir temperature. Time required to restore thermal equilibrium is approximately equal to cooling time.[10] Consequently, service companies now routinely desorb whole core samples at reservoir temperature using preheated canisters to minimize temperature recovery time. In contrast, current practice is to desorb drill cuttings at mud temperature, while no consensus has yet evolved for sidewall cores.

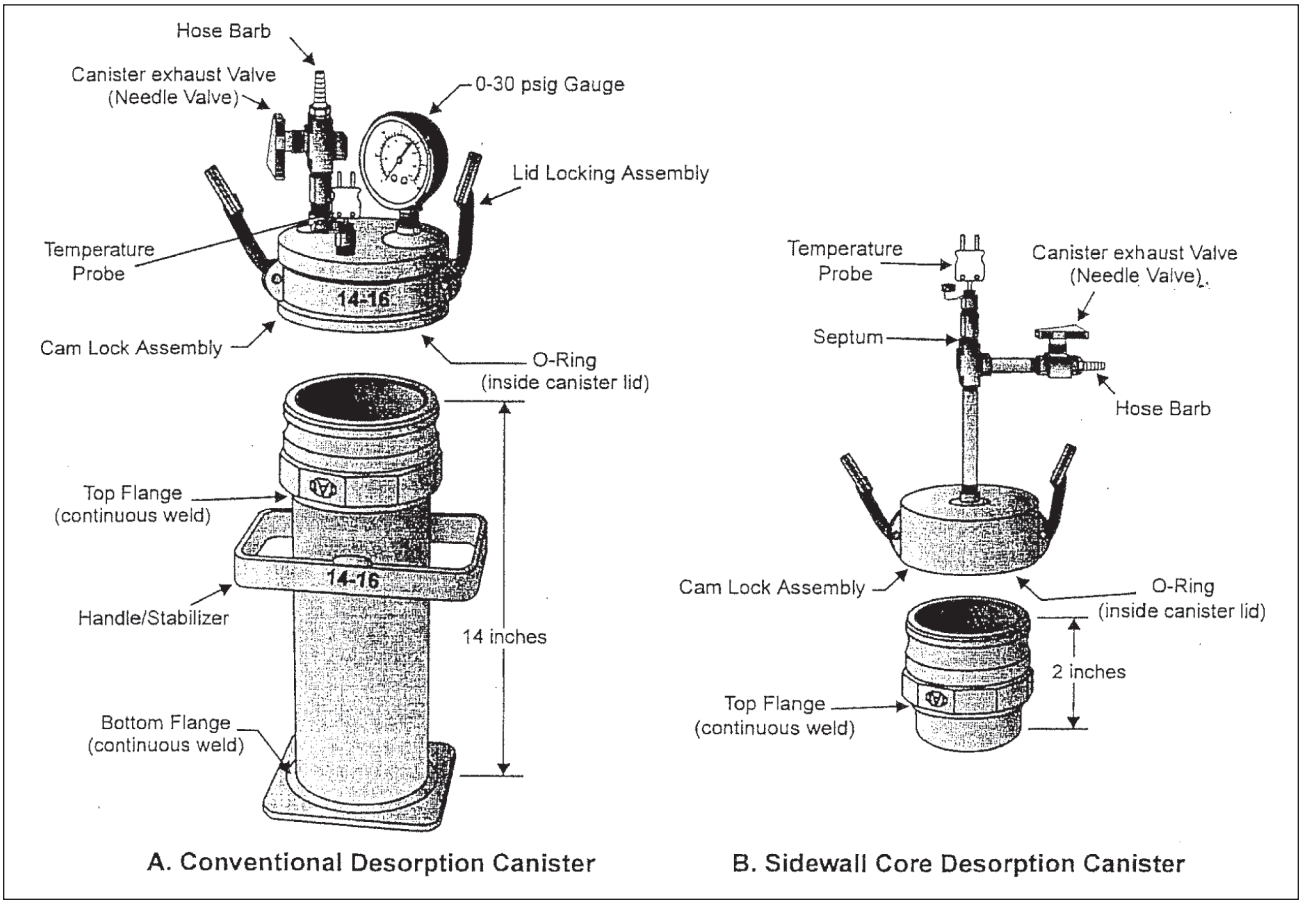



**Fig. 4–1.** Whole core and sidewall core desorption canisters[6]

As shown in figure 4–2a, desorbed gas volumes were first measured by periodically venting desorbed gas through a plastic tube into an inverted, water-filled graduated cylinder or burette. Subsequent workers refined the USBM method by adjusting the water-filled cylinder to align the fluid level with midpoint of the canister (fig. 4–2b), thus minimizing the pressure head from the water column on the sample. Additional improvements rapidly followed, and a current desorption apparatus is shown in figure 4–2c. Many service companies have now dispensed with the water-filled burettes in favor of continuous mass or flow rate meters maintained at atmospheric pressure.

Some coals contain significant amounts of $CO_2$, which is readily soluble in water. The Standards Association of Australia recommended use of an acidified brine in the desorption apparatus to mitigate $CO_2$ dissolution.[12] However, acidified brine may simply prevent formation of carbonate ions, with little impact on $CO_2$ dissolution.[13]

Once sufficient data have been acquired to estimate lost gas, many service companies will heat samples to 50°C (122°F) in order to accelerate gas release and shorten test time. This practice results in a second hump in the gas desorption plot, and the data cannot be used in determination of lost gas.

Desorbed gas volumes are measured as a function of time, with frequent sampling early in the desorption test and decreased sampling at late times. To provide clear and sufficient data, desorbed gas volumes should be measured at least every 3 to 5 min for the first hour of desorption. Regardless of the method employed to analyze the desorption data, early-time data is critical for estimation of lost gas. As the rate of gas release slows, the frequency of desorbed gas measurements also relaxes. After the first few hours of desorption, sample frequency drops off to every 15 min. After a few more hours, gas readings are taken once per hour. In the latter part of the test, desorbed gas volumes are typically measured once per day. Experience plays a large part in knowing when to take another gas reading. When in doubt, a gas measurement should be taken. Sparse data collection has ruined many desorption tests. A typical desorption data set (courtesy of HWA) from a wireline retrieved whole core is shown in table 4–2.

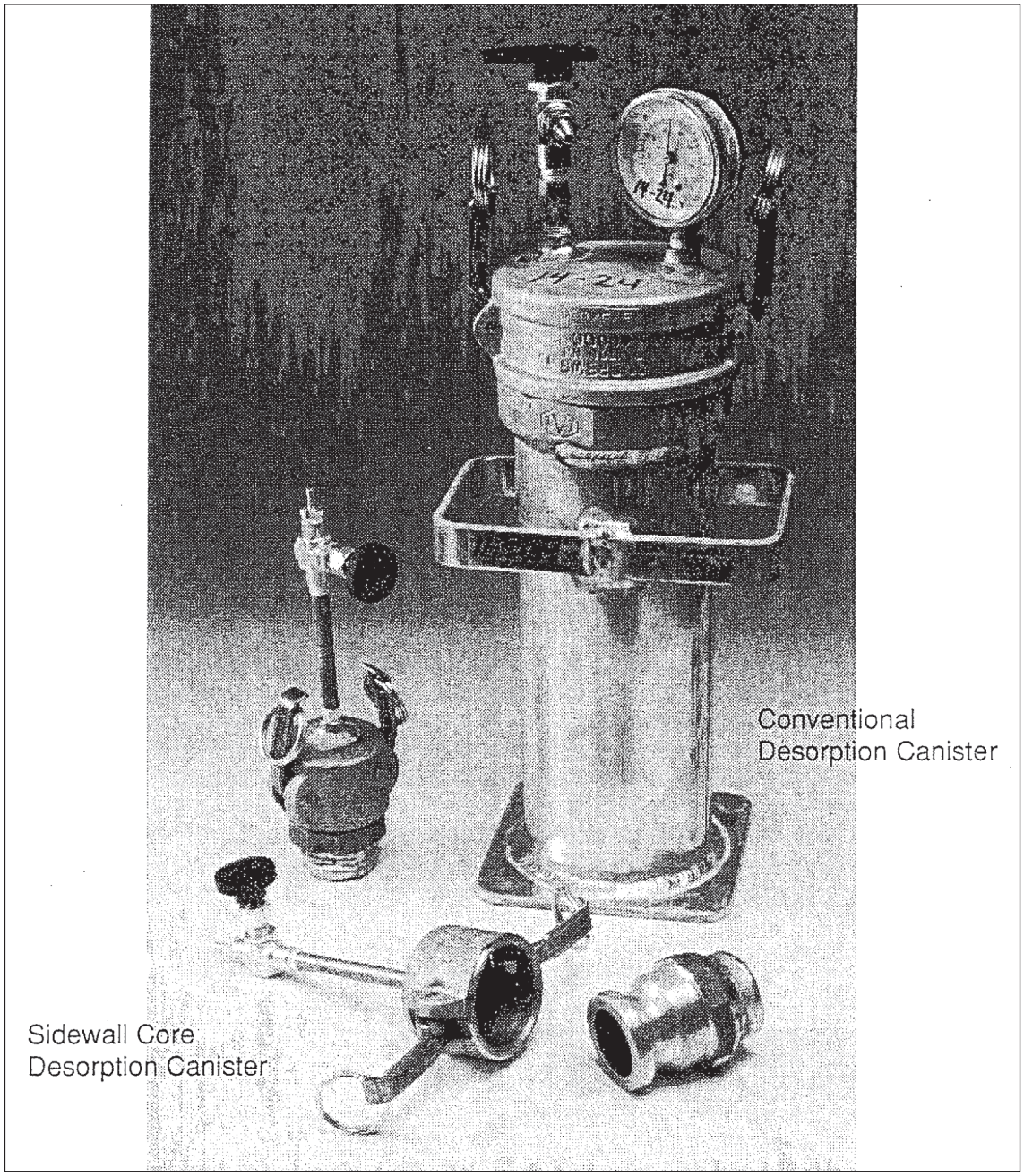



**Fig. 4–2.** Desorption test apparatus development[11]

**Table 4–2.** Desorption data set (courtesy of HWA)

**ABC Desorption & Isotherm Company**
**123 Main Street**
**Denver, Colorado 80122**
**Phone: 303-123-4567**
**Website:**

***Coalbed Methane Desorption Specialists***

**Coalbed Methane Desorption Report**

| | | | | |
|---|---|---|---|---|
| Company: | Coal Gas Forever, Inc | Sample Type: | Wireline Core | |
| Well Name: | Bad Idea # 13 | Geologist: | Col. E. Drake | |
| Location: | SWNW, SEC 37, T1N-R185W, Sorption County, NJ | Surface Elevation: | 1234 | |
| **Canister Number:** | **CGF-BI#13-122** | Coalbed Encountered: | 8/24/2001 | 20:34:00 |
| Seam Identification: | Old Swamp | Time Coal Started Out of Hole: | 8/24/2001 | 21:28:00 |
| Top of Test Interval: | 1257.6 feet | Time Coal Reached Reservoir Pressure: | 8/24/2001 | 21:28:31 |
| Bottom of Test Interval: | 1259.3 feet | Coal Half Way to Surface: | 8/24/2001 | 21:33:16 |
| Interval Thickness: | 1.7 feet | Coal Reached Surface: | 8/24/2001 | 21:38:00 |
| Bulk Sample Weight: | 2177.0 grams | Coal Sealed in Canister: | 8/24/2001 | 21:54:00 |
| Air-Dried Weight of Coal: | 1959.3 grams | | | |
| DAF Weight of Coal: | 1830.8 grams | | | |
| DMMF Weight of Coal: | 1791.8 grams | | | |
| Moisture (Residual) | 1.97% | | | |
| Moisture (Total) | 11.77% | | | |
| Ash Content (As Received) | 4.13% | | | |
| Sulfur Content (As Received) | 2.66% | | | |
| Bit Size: | 5.50 inches | | | |
| Core Diameter: | 3.00 inches | | | |
| Drilling Medium: | Mud | | | |
| Mud Weight: | 8.800 lb/gal | | | |
| Canister Size: | 2.0 feet | | | |
| Canister Headspace Volume: | 3488.4 cc | | | |
| Depth Core at Reservoir Press: | 1193 feet | | | |
| Flowline Temperature: | 25.6 deg C | | | |
| Outdoor Temperature: | 16.7 deg C | | | |
| Reservoir Temperature: | 35.0 deg C | | | |
| Lithology: | Coal, blk, vit, brit, hd, vert fracs, g face cleats, occ butt cleats | | | |
| Comments: | | | | |

**Gas Content Results:**

| | **Polynomial Fit for Lost Gas** | **Linear Fit for Lost Gas** |
|---|---|---|
| Time Lost: | 20.7 minutes | 20.7 minutes |
| Desorbed Gas: | 15931 cc, STP | 15931 cc, STP |
| Lost Gas: | 1904 cc, STP | 1647 cc, STP |
| Projected Residual Gas: | 362.0 cc, STP | 362.0 cc, STP |
| Measured Residual Gas: | na | na |
| Total Gas: | 18197 cc, STP | 17940 cc, STP |
| Total Gas Volume/Bulk Coal Weight: | 8.3587 cc/gram | 8.2408 cc/gram |
| **GAS CONTENT-Bulk Sample - des + lost** | **262.5 scf/ton** | **258.7 scf/ton** |
| **GAS CONTENT-Bulk - des + lost + proj resid** | **267.8 scf/ton** | **264.0 scf/ton** |
| **GAS CONTENT-Bulk - des + lost + meas resid** | **na** | **na** |
| **GAS CONTENT-Dry Ash-free** | **318.4 scf/ton** | **313.9 scf/ton** |
| **GAS CONTENT-Dry Mineral Matter-free** | **325.4 scf/ton** | **320.8 scf/ton** |

**Table 4–2.** cont.

| Reading Number | Date | Time (hr:min) | Minutes Elapsed | Gas Desorbed Ambient Cond. (cc) | DESORPTION READINGS: Headspace Correction, STP (cc) | Canister Temp (deg C) | Ambient Pressure (in. Hg) | Desorbed Gas, STP (HS Corrected, cc) | SQRT Time | Total Gas Desorbed, (STP, cc) | Ambient Temp (deg C) | Comments |
|---|---|---|---|---|---|---|---|---|---|---|---|---|
| 1 | 8/24/2001 | 22 : 5 | 32 | 478 | 0.0 | 35.4 | 23.64 | 364 | 5.6340 | 364 | 26.8 | |
| 2 | 8/24/2001 | 22 : 14 | 41 | 342 | –1.7 | 35.2 | 23.64 | 262 | 6.3829 | 625 | 27.1 | blue flame |
| 3 | 8/24/2001 | 22 : 24 | 51 | 346 | –0.3 | 34.9 | 23.62 | 263 | 7.1233 | 889 | 26.7 | |
| 4 | 8/24/2001 | 22 : 34 | 61 | 286 | –1.7 | 34.7 | 23.62 | 219 | 7.7937 | 1108 | 26.6 | |
| 5 | 8/24/2001 | 22 : 44 | 71 | 309 | –0.9 | 34.6 | 23.62 | 236 | 8.4108 | 1344 | 26.4 | |
| 6 | 8/24/2001 | 22 : 54 | 81 | 270 | 5.5 | 35.5 | 23.64 | 200 | 8.9856 | 1544 | 26.2 | |
| 7 | 8/24/2001 | 23 : 4 | 91 | 244 | –0.9 | 35.4 | 23.64 | 187 | 9.5258 | 1731 | 26.0 | |
| 8 | 8/24/2001 | 23 : 14 | 101 | 245 | –0.9 | 35.3 | 23.64 | 188 | 10.0370 | 1919 | 26.0 | |
| 9 | 8/24/2001 | 23 : 24 | 111 | 242 | –1.7 | 35.1 | 23.64 | 186 | 10.5234 | 2105 | 25.9 | |
| 10 | 8/24/2001 | 23 : 34 | 121 | 206 | –1.7 | 34.9 | 23.64 | 159 | 10.9883 | 2264 | 25.8 | |
| 11 | 8/24/2001 | 23 : 44 | 131 | 211 | –1.7 | 34.7 | 23.64 | 163 | 11.4342 | 2427 | 25.8 | |
| 12 | 8/24/2001 | 23 : 54 | 141 | 220 | –0.9 | 34.6 | 23.64 | 169 | 11.8635 | 2596 | 25.7 | |
| 13 | 8/25/2001 | 0 : 4 | 151 | 188 | 6.1 | 35.3 | 23.64 | 137 | 12.2777 | 2733 | 25.7 | |
| 14 | 8/25/2001 | 0 : 14 | 161 | 190 | 0.9 | 35.4 | 23.64 | 144 | 12.6784 | 2877 | 25.6 | |
| 15 | 8/25/2001 | 0 : 24 | 171 | 161 | 0.0 | 35.4 | 23.64 | 123 | 13.0668 | 3000 | 25.6 | |
| 16 | 8/25/2001 | 0 : 34 | 181 | 180 | –1.7 | 35.2 | 23.64 | 139 | 13.4440 | 3139 | 25.6 | |
| 17 | 8/25/2001 | 0 : 44 | 191 | 148 | –1.7 | 35.0 | 23.64 | 115 | 13.8109 | 3254 | 25.7 | |
| 18 | 8/25/2001 | 0 : 54 | 201 | 155 | –1.7 | 34.8 | 23.64 | 120 | 14.1683 | 3374 | 25.7 | |
| 24 | 8/25/2001 | 2 : 4 | 271 | 121 | –1.7 | 34.7 | 23.64 | 94 | 16.4542 | 4118 | 25.2 | |
| 25 | 8/25/2001 | 2 : 44 | 311 | 484 | 6.1 | 35.4 | 23.64 | 364 | 17.6279 | 4483 | 24.9 | Gas sample A, reading estimated |
| 26 | 8/25/2001 | 3 : 4 | 331 | 199 | –4.6 | 35.0 | 23.65 | 157 | 18.1863 | 4639 | 25.0 | |
| 73 | 8/26/2001 | 21 : 1 | 2,848 | 157 | 1.2 | 35.4 | 23.66 | 119 | 53.3642 | 10769 | 24.2 | |
| 74 | 8/27/2001 | 0 : 46 | 3,073 | 285 | –5.4 | 34.9 | 23.67 | 223 | 55.4323 | 10992 | 25.6 | Gas sample B, reading estimated |
| 75 | 8/27/2001 | 3 : 36 | 3,243 | 206 | 6.1 | 35.6 | 23.67 | 152 | 56.9451 | 11144 | 25.3 | |
| 78 | 8/27/2001 | 12 : 45 | 3,792 | 146 | 2.5 | 35.4 | 23.66 | 109 | 61.5771 | 11557 | 24.9 | |
| 79 | 8/27/2001 | 21 : 46 | 4,333 | 247 | –138.5 | 34.9 | 24.86 | 335 | 65.8236 | 11892 | 27.8 | Move to Denver |
| 80 | 8/28/2001 | 10 : 34 | 5,101 | 390 | –8.2 | 34.0 | 24.86 | 323 | 71.4195 | 12215 | 24.4 | |
| 86 | 8/31/2001 | 9 : 38 | 9,365 | 241 | 0.7 | 34.7 | 24.88 | 194 | 96.7716 | 13575 | 24.4 | |
| 87 | 9/1/2001 | 14 : 30 | 11,097 | 310 | 12.9 | 35.0 | 24.79 | 236 | 105.3411 | 13811 | 24.5 | Gas sample C, reading estimated |
| 88 | 9/2/2001 | 16 : 18 | 12,645 | 305 | –2.5 | 35.1 | 24.82 | 245 | 112.4488 | 14056 | 28.4 | |
| 89 | 9/3/2001 | 9 : 49 | 13,696 | 152 | –20.8 | 34.3 | 24.94 | 143 | 117.0288 | 14199 | 25.5 | |
| 90 | 9/4/2001 | 11 : 26 | 15,233 | 210 | 0.5 | 34.6 | 24.96 | 169 | 123.4210 | 14368 | 25.6 | |
| 91 | 9/5/2001 | 11 : 4 | 16,651 | 195 | –10.5 | 32.1 | 24.85 | 167 | 129.0378 | 14536 | 24.8 | |
| 92 | 9/6/2001 | 13 : 30 | 18,237 | 180 | 49.0 | 34.1 | 24.58 | 95 | 135.0435 | 14630 | 24.3 | |
| 93 | 9/7/2001 | 10 : 21 | 19,488 | 115 | –9.0 | 34.6 | 24.70 | 101 | 139.5985 | 14731 | 24.5 | |
| 94 | 9/8/2001 | 15 : 5 | 21,212 | 130 | –25.4 | 34.8 | 24.94 | 131 | 145.6425 | 14862 | 24.2 | |
| 95 | 9/9/2001 | 16 : 16 | 22,723 | 125 | 4.5 | 34.8 | 24.90 | 96 | 150.7406 | 14958 | 25.1 | |
| 96 | 9/10/2001 | 11 : 15 | 23,862 | 120 | –16.0 | 33.8 | 24.96 | 114 | 154.4725 | 15072 | 23.2 | |
| 97 | 9/11/2001 | 16 : 59 | 25,646 | 118 | 0.6 | 33.5 | 24.93 | 95 | 160.1429 | 15166 | 24.0 | |
| 98 | 9/12/2001 | 17 : 18 | 27,105 | 117 | 9.1 | 34.0 | 24.89 | 85 | 164.6352 | 15252 | 24.0 | |
| 99 | 9/13/2001 | 11 : 17 | 28,184 | 80 | 3.7 | 34.4 | 24.89 | 61 | 167.8801 | 15313 | 23.6 | |
| 100 | 9/15/2001 | 16 : 46 | 31,393 | 108 | 4.8 | 34.8 | 24.88 | 82 | 177.1800 | 15395 | 25.4 | |
| 101 | 9/17/2001 | 10 : 31 | 33,898 | 92 | –4.1 | 34.6 | 24.90 | 78 | 184.1134 | 15473 | 24.4 | |
| 102 | 9/19/2001 | 10 : 43 | 36,790 | 50 | –1.4 | 34.2 | 24.88 | 42 | 191.8065 | 15515 | 23.8 | |
| 103 | 9/27/2001 | 11 : 52 | 48,379 | 200 | –1.1 | 34.2 | 24.89 | 163 | 219.9517 | 15678 | 24.5 | Gas sample D, reading estimated |
| 104 | 9/29/2001 | 14 : 25 | 51,412 | 90 | 13.6 | 35.8 | 24.90 | 59 | 226.7416 | 15737 | 23.4 | |
| 105 | 10/3/2001 | 12 : 23 | 57,050 | 120 | 7.0 | 35.7 | 24.83 | 90 | 238.8509 | 15827 | 23.3 | |
| 106 | 10/8/2001 | 15 : 24 | 64,431 | 70 | 11.6 | 35.1 | 24.68 | 45 | 253.8321 | 15872 | 23.1 | |
| 107 | 10/12/2001 | 11 : 42 | 69,969 | 50 | –19.0 | 35.0 | 24.84 | 59 | 264.5161 | 15931 | 23.8 | |

**Analysis of desorption data.** Raw desorbed gas volumes from each step must be corrected to standard temperature and pressure (STP) conditions. Note that English STP conditions are defined as 60°F and 14.7 or 14.65 psia, whereas metric STP conditions are 0°C and 101 kPaa. For each and every data point, it is important to record ambient temperature and atmospheric pressure to allow correction to STP. As desorbed gas typically contains some water vapor, especially early in the test, most service companies also correct measured gas volumes for the presence of water vapor. Note that at 100°F, vapor pressure of water is on the order of 1 psia, making a saturated gas mixture at 14.7 psia approximately 7% water vapor. If the samples are being desorbed at reservoir temperature, canister temperature should also be reported. Corrected incremental volumes from each step are summed to provide desorbed gas as a function of time with the final, cumulative value being termed *desorbed gas*.

Inspection of raw desorption data in table 4–2 indicates the coal seam was penetrated about 8:30 p.m., and the core was off bottom approximately an hour later. Trip time was 10 min. Surface operations (removing the core from the barrel, inspecting it to select samples, breaking the core into samples of the appropriate lengths, and canistering them) required an additional 16 min. Table 4–2 contains desorbed gas volumes corrected to STP, as well as coalbed gas contents calculated from the raw desorption data. Cumulative desorbed gas volume, corrected to STP, is plotted in figure 4–3.

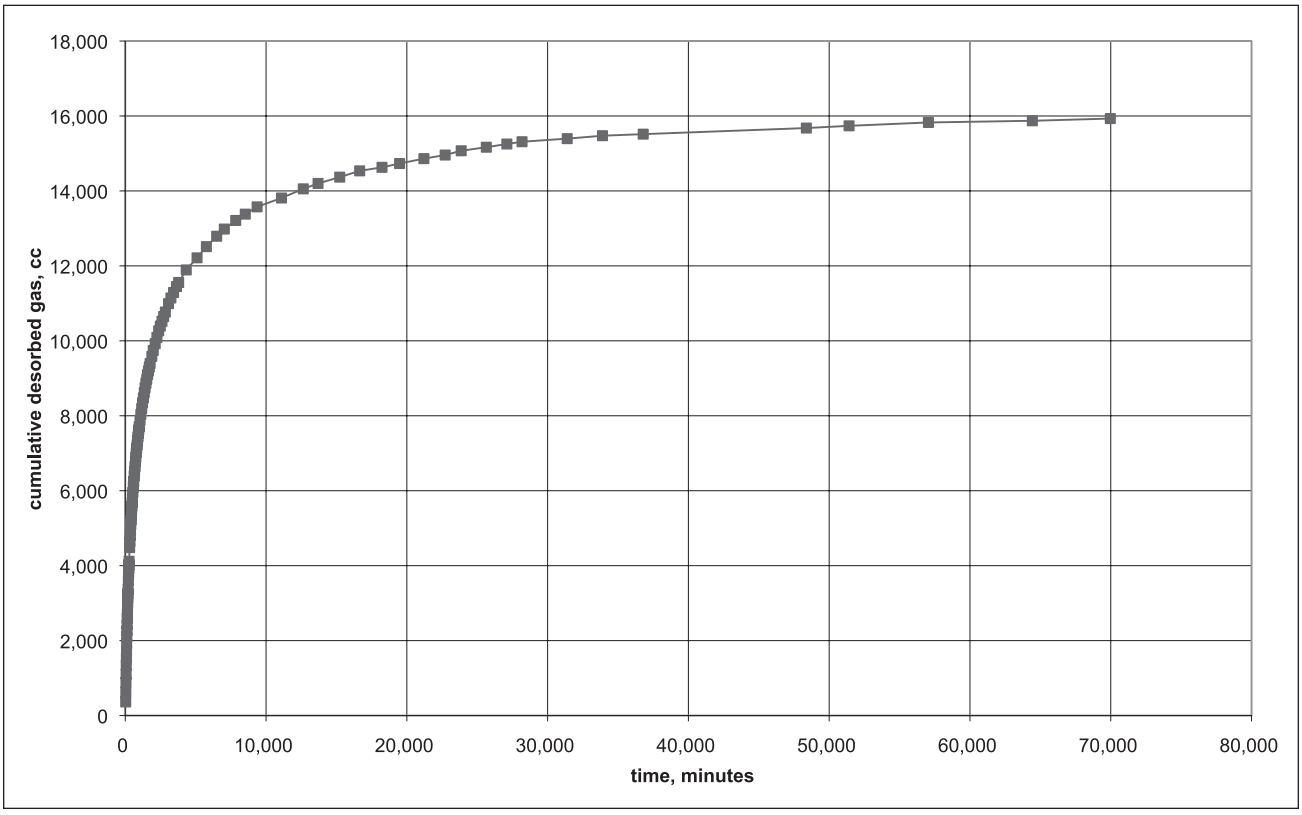



**Fig. 4–3.** Cumulative desorbed gas—sample CGF-BI#13-122

Coal gas is typically methane, with minor amounts of nitrogen, $CO_2$, and heavier hydrocarbons. The average coal gas composition is 93% methane, 3% each of nitrogen and $CO_2$, and 1% heavier hydrocarbons.[14] Gas composition varies during both sample desorption and reservoir depletion. Efforts to relate desorbed gas composition to in-situ sorbed gas composition have been problematic. Variation in gas composition during depletion was first studied by Ulery and Hyman.[15] Analysis of gas sampled at each desorption step showed nitrogen came off early in the test, while $CO_2$ and heavy hydrocarbons were released late in the test. Early workers, unaware of such compositional variations, often assumed an unchanging gas composition and calculated in-situ gas volume based on one or two desorbed gas analyses. Ulery and Hyman utilized gas

analyses each time desorbed gas was measured with the goal of determining sorbed gas composition. Intuitively, integration of gas composition over time or gas volume, similar to gas chromatography, should yield in-situ gas compositions. In practice, difficulties encountered in sampling at the wellsite and small desorbed gas volumes have complicated understanding desorbed gas compositional behavior. Pratt and Baez reported gas composition behavior during coal sample desorption is distinctly different from that observed during coal seam depletion but did not explain why.[16]

## Lost Gas

Gas desorption from a coal sample appears to be diffusive, and early workers described gas emission from coal samples using Fick's law of diffusion and solutions taken from heat flow analogs. For example, the solution for a spherical coal sample geometry assuming a uniform initial concentration and a zero boundary condition at zero time was given by Mavor et al. as[17]

$$C_{Da} = 1 - \frac{6}{\pi^2} \sum_{n=1}^{\infty} \frac{\exp\left(-n^2 \pi^2 t_D\right)}{n^2} \tag{4.1}$$

with dimensionless concentration and time defined as

$$C_{Da} = \frac{C_a - C_0}{C_b - C_0}$$

and

$$t_D = t\frac{D}{r^2} \tag{4.2}$$

where

$C_{Da}$ = dimensionless sorbed gas concentration,
$C_0$ = initial sorbed gas concentration, cm³/g or scf/ton,
$C_a$ = average sorbed gas concentration, cm³/g or scf/ton,
$C_b$ = sorbed gas concentration at the boundary, cm³/g or scf/ton,
$t_D$ = dimensionless time,
$t$ = time, min,
$D$ = diffusion coefficient, cm²/min, and
$r$ = particle radius, cm.

The diffusion coefficient, $D$, and spherical radius, $r$, are combined into a simple fraction, $D/r^2$, defined as the *diffusivity*. A measure of how fast gas is released from the coal, diffusivity provides dimensionless time in equation (4.2) and is also used in simulation of coal gas recovery.

For short times, these solutions indicate cumulative gas released is proportional to the square root of time. Bertard et al. noted this proportionality held for the first 20% of emitted gas, while Smith and Williams argued it held for the first one-half of gas desorption.[18] Kissell et al. reported experimental results from several U.S. coals showing gas emitted was linearly related to the square root of time for the first several hours of desorption.[19] Mavor et al. defined dimensionless time as the product of actual time and the diffusion coefficient divided by the square of the effective desorption radius and noted that gas release is proportional to the square root of time for dimensionless times less than 0.01.[20] Thus a plot of cumulative desorbed gas (corrected to STP) versus square root of time is expected to be linear, and an extrapolation back to zero time yields an estimate of lost gas.

Determination of zero time is, however, problematic. The original work by Kissell et al. calculated zero time based upon drilling fluid.[21] For coals drilled with air, zero time was assumed to be off-bottom time. For coals drilled with liquid muds, zero time was chosen to be when the core was "halfway out of the hole." Kissell et al. did not specify whether this was one-half the pulling time or the time when the core was raised to one-half the depth at which it was cut. Most workers consider zero time for cores cut with liquid muds to occur at one-half the pulling time. When coal samples are cut underbalanced, many workers define zero time as time of penetration.

For sidewall cores, choice of zero time is more difficult than with whole cores or cuttings. In an air-drilled hole, gas is emitted as soon as the borehole penetrates the coal. Before sidewall cores can be cut, it is necessary to run a log and pick core points. Theoretically, gas can be desorbing from a coal for several hours or days prior to cutting sidewall cores from it.

If a coal deposit is undersaturated, gas will not be released until sample pressure is reduced to desorption pressure. Careful and thorough notes by wellsite personnel enable reconstruction of the pressure history of a given sample and, thus, identification of the time when sample pressure declined to desorption pressure and gas emission commenced. In practice, lost gas ranges from a few percent to more than one-half of total gas content. Lost gas values above 25% of the total gas volume should be treated with caution, as this implies a significant fraction of the total gas was emitted under unknown conditions that are only approximately accounted for.

Lost gas for the sample desorption set contained in table 4–2 will be calculated as an example. Coring began about 20:34:00 and started out of the hole 54 min later at 21:28:00. The core reached reservoir pressure roughly one-half minute later, at 21:28:31, and was halfway out of the hole after 5 min and 16 sec, at 21:33:16. The core was on the surface at 21:38:00. Thus, retrieval required 10 min exactly, and time when the core was halfway up the borehole is nearly coincident with one-half the trip time. Once on the surface, 16 min were required to open the core barrel, inspect the core, select desorption samples, and canister this particular sample, making sealing time 21:54:00.

The service company assumed gas emission from the core began when it was halfway to the surface, at 21:33:16, making lost gas time 20 min 44 sec, or 20.7 min. Cumulative desorbed gas, corrected to STP, is plotted as a function of the square root of time in figure 4–4.

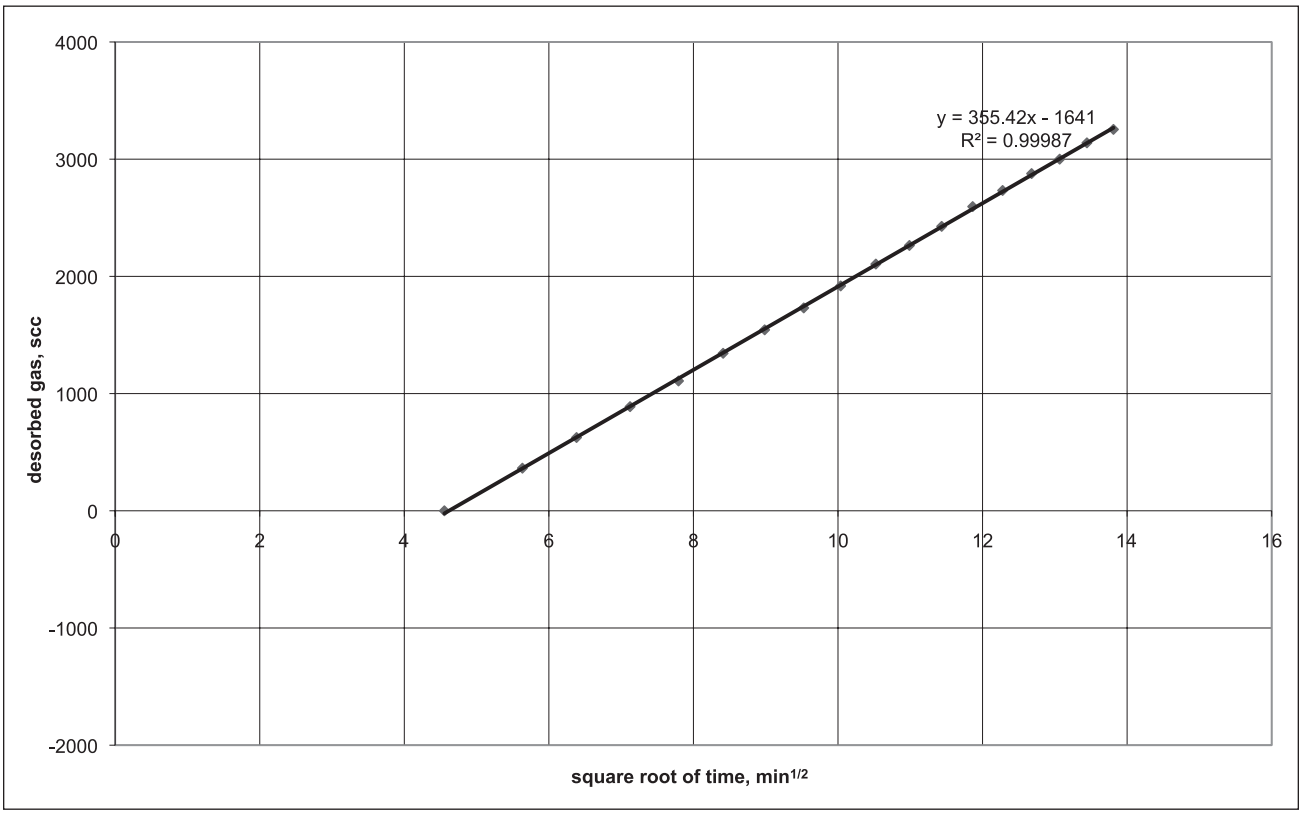



**Fig. 4–4.** Lost gas plot—sample CGF-BI#13-122

Extrapolating back to zero time, lost gas is 1,641 $cm^3$, in good agreement with the reported lost gas value of 1,647 $cm^3$ reported in table 4–2 using the linear fit. This exercise can be repeated assuming that gas release begins during core retrieval when mud pressure drops below reservoir pressure, at 21:28:31, some 4.75 minutes earlier than the lost gas time of 20.7 min above. The results indicate a lost gas volume of 1,844 $cm^3$, which differs by just over 3% from the polynomial lost gas value.

Many service companies currently fit a polynomial equation to early-time desorption data. However, the resulting lost gas volumes are almost always higher than those obtained from the linear extrapolation prescribed by the USBM direct method. Thus, even though this method is promising, it must be regarded as unproven until publication of comparison with established methods. Based on the above example, it is speculated the linear extrapolation on a square root of time plot will yield the correct lost gas volume when zero time is defined as the time at which pressure on the core drops below desorption pressure.

Regardless of the method employed to analyze desorption data, early-time data are used to estimate lost gas. As discussed above, Mavor et al. reported gas contents from ambient temperature desorption were one-third lower than those obtained from reservoir temperature desorption.[22] The difference was even more pronounced for lost gas estimates, with ambient temperature results averaging 61% less than reservoir temperature gas contents, making lost gas errors one of the largest sources of error in coalbed gas content determination. In practice, one of the greatest sources of error in lost gas estimation is insufficient early-time data. The early-time desorption measurement schedule described above should provide ample early-time data for accurate lost gas estimation.

## Residual Gas

Gas emission rates fall to very low levels late in a desorption test, typically a few cubic centimeters per day, and can linger at intermittent rates for several days or weeks. While the desorption rate will never again climb to initial values, the continuous, low-level emissions lead to the suspicion that substantial gas volumes yet remain in the sample. Two methods have been developed to estimate this remaining gas, termed *residual gas*; one empirical, the other analytical.

In the empirical method, once gas emission from a sample has fallen below a threshold value, typically 0.05 $cm^3$/g/day for a week, desorption measurements are terminated. The sample is removed from the canister and ground in a ball mill to release any remaining gas. Use of a threshold value is difficult, as the mass of coal in a canister is not known until the canister is opened and the mass of coal in the sample determined. Coal mass in a cuttings sample can vary widely, as they are often contaminated with drilling fluids and/or uphole cavings. Crushing of large samples is often impractical, especially pressure cores; consequently, only a portion of a given sample is crushed to determine residual gas. To ensure accurate residual gas values, service companies routinely crush two or three pieces from any given sample followed by determination of coal mass in the original desorption sample and all residual gas samples. Residual gas volume of the entire sample is then calculated from knowledge of the respective mass fractions. Due to economic and time pressures, this empirical process has been steadily shortened over time, with many service companies currently crushing a sample once sufficient data have been acquired to estimate lost gas.

The analytical method determines residual gas from a plot of reciprocal time versus cumulative desorbed gas. Gas emission from a coal sample can be described with exponential functions, such as equation (4.1) in the lost gas section above. At late time, these solutions are linear in reciprocal time. Thus, a plot of cumulative desorbed gas, corrected to STP, versus reciprocal time should eventually yield a straight line that can be extrapolated to zero reciprocal time to estimate total desorbed gas at infinite time.

A reciprocal time plot for the last 20 data points from table 4–2 is shown in figure 4–5.

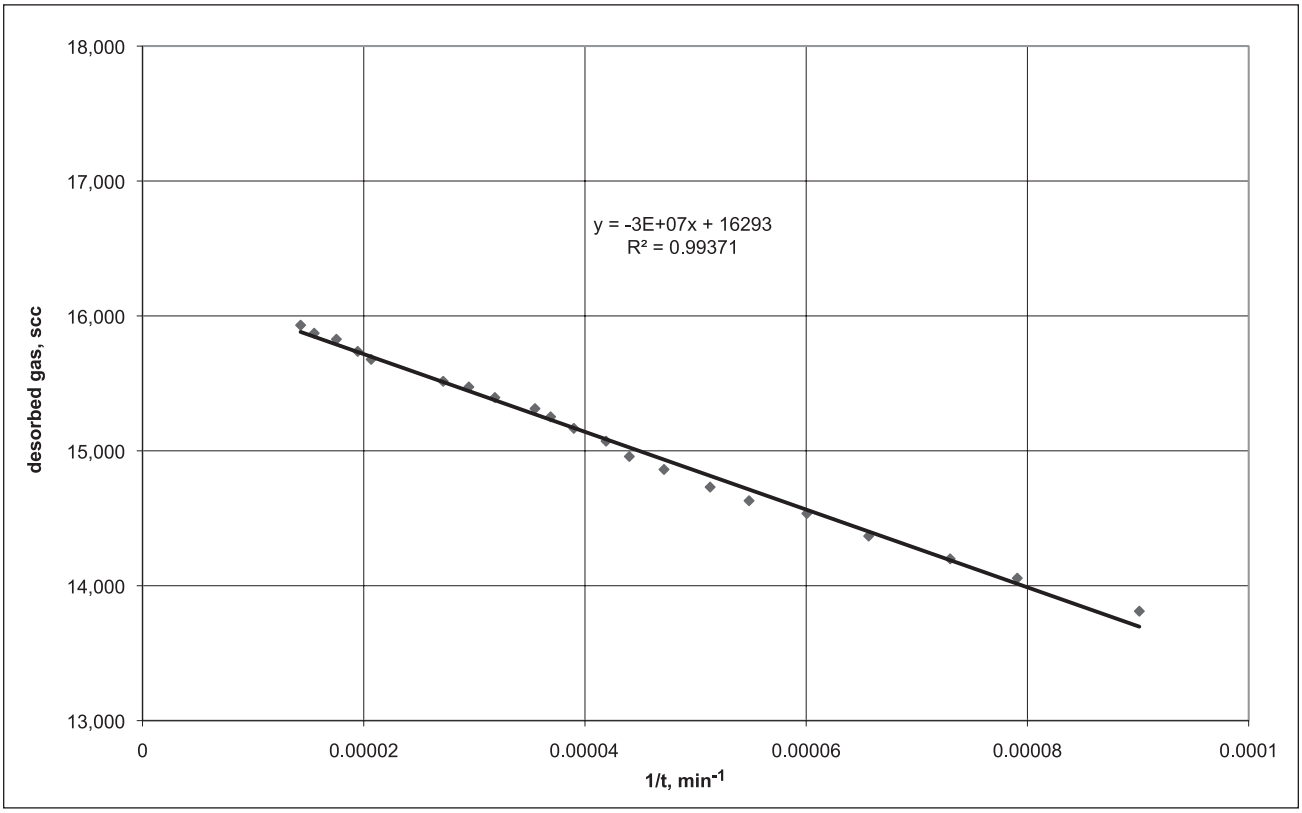



**Fig. 4–5.** Reciprocal time plot—sample CGF-BI#13-122

A trendline fit to the data yields an intercept of 16,293 $cm^3$. Subtracting the last reported desorption value of 15,931 $cm^3$ yields a residual gas volume of 362 $cm^3$. While these late-time data do indeed exhibit the expected linear behavior, acquisition of the data required considerable patience. The first point corresponds to a time of 11,097 min (7.7 days) and the last to a time of 69,969 min (48.6 days), a span of 58,872 min (40.9 days). Using only the data for the first 12 days, the final data point would be 14,536 $cm^3$ at 16,651 min, and these would be the rightmost 5 points shown in figure 4–5. Fitting a straight line through these data yields an intercept gas volume of 15,946 $cm^3$, approximately 2% lower than the 16,293 $cm^3$ obtained using the final 20 data points. As discussed above, gas emission could be accelerated by heating the samples to 50°C, thereby shortening desorption time necessary to construct a valid reciprocal time plot.

Both the empirical and analytical methods are suitable for determination of residual gas. Which one is chosen for a particular project will depend on laboratory backlogs, availability of canisters for long-term desorption tests, and cost.

## USBM Direct Method

The oldest method to determine coalbed gas content was developed by Kissell et al. at the U.S. Bureau of Mines in 1973, and it is still one of the most frequently used.[23] Termed the *direct method*, it was based on work by Bertard et al.[24] Although this method was developed for whole cores used to assess gas emissions for mine safety, it is robust and has become the industry standard for coal gas evaluation. The USBM direct method defines *coalbed gas content* as the sum of desorbed, lost, and residual gas. Lost gas is determined from a square root of time plot, and residual gas by crushing.

Analyzing the desorption data of table 4–2 with the USBM direct method yields 1,641 $cm^3$ of lost gas, 15,931 $cm^3$ of desorbed gas, and 362 $cm^3$ of residual gas, where the analytical residual gas was employed since no residual gas by crushing was reported. Total gas content is therefore 1,641 $cm^3$ + 15,931 $cm^3$ + 362 $cm^3$ = 17,934 $cm^3$. Note that for this sample, 9.2% of the total gas was lost gas, and 2% was residual gas.

Diffusivity, the diffusion coefficient divided by particle radius squared, was used to define dimensionless time in equation (4.2). It can be estimated from the slope of the line in the square root of time plot using the equation[25]

$$\frac{D}{r^2} = \left( \frac{m}{3.3851 V_{LD}} \right)^2$$

where

$m$ = slope of square root of time plot, cm$^3$/min$^{1/2}$, and
$V_{LD}$ = sum of lost plus desorbed gas, cm$^3$.

From figure 4–4, the slope of the lost gas line is 355.42 cm$^3$/min$^{1/2}$, and lost gas is 1,641 cm$^3$. From table 4–2, total desorbed gas is 15,931 cm$^3$. Thus,

$$\frac{D}{r^2} = \left( \frac{355.42 \text{ cm}^3/\text{min}^{1/2}}{3.3851 \times (15{,}931 + 1{,}641)\text{scm}^3} \right)^2 = 3.57E - 5 \text{ min}^{-1}$$

## Smith and Williams Method

A method for determination of coalbed gas content from drill cuttings was developed by Smith and Williams.[26] Coal drill cuttings are collected onsite, usually at the shale shaker, and desorbed gas is measured over time, as is done with the USBM direct method. Smith and Williams mathematically described gas release from drill cuttings using a spherical diffusion equation with a surface boundary condition that reflected the cuttings pressure history. Drill cuttings were assumed to travel up the borehole at a constant velocity, thus gas concentration at the surface of the sphere decreased linearly with time from initial reservoir conditions down to zero when the cuttings reached the surface. Once on the surface, drill cuttings are, of course, subject to atmospheric pressure. After sealing in a desorption canister, pressure will increase modestly between gas measurements. Consequently, once the drill cuttings reached the surface, gas concentration at the surface of the sphere was assumed to be zero. The mathematical solution to this differential equation was cast as an infinite series of exponentially decreasing terms. While the solution is mathematically elegant, it is difficult to apply in practice.

To facilitate practical application, Smith and Williams employed three times to define two ratios to obtain a single correction factor from a family of curves. The three times, all measured from the time the chips are cut, are the following:

- Time for the chips to travel from the drill bit to the surface, denoted as $t_d$
- Time until sample sealing, labeled $t_s$
- Time to collect 25% of the total desorbed gas volume, $t_{25\%}$

The *lost time ratio*, *LTR*, is defined as

$$LTR = \frac{t_s}{t_{25\%}} \tag{4.3}$$

where

$t_s$ = time until sample sealing, min, and
$t_{25\%}$ = time to collect 25% of the total desorbed gas volume, min.

The *surface time ratio*, *STR*, is defined as

$$STR = \frac{t_s - t_d}{t_s} \tag{4.4}$$

where

$t_d$ = time for the chips to travel from the drillbit to the surface, min.

These two ratios define a correction factor, denoted *CF*, which is multiplied by the desorbed gas volume, $V_{des}$, to obtain total emitted gas, $V_{tot}$,

$$V_{tot} = CF \times V_{des} \tag{4.5}$$

Values of the correction factor are tabulated for selected values of the LTR and STR in table 4–3 and are plotted in figure 4–6.

This correction factor accounts for gas lost by the sample prior to being sealed in a canister. The Smith and Williams method assumes all gas is rapidly released from the drill cuttings, leaving little, if any, residual gas. Although the Smith and Williams method was developed for analysis of cuttings desorption data, it was soon applied to data from whole and sidewall cores as well.

Use of this method will be illustrated using the desorption data reported in table 4–2. The core was cut slightly overbalanced with 8.8 lb/gal mud, and gas loss during coring is assumed negligible. Off-bottom time was 21:28:00, which will be used as zero time here. The core reached the surface 10 min later, at 21:38:00; thus, $t_d$ = 10 min. The time required to remove the core from the barrel and seal this particular sample in the canister was 16 min, at 21:54:00; consequently, $t_s$ = 26 min. Total collected gas was 15,931 cm$^3$. One-quarter of this volume, 3,983 cm$^3$, was collected after 257 min, making $t_{25\%}$ = 257 min + 26 min, as collection time is defined as zero when the canister is sealed. Calculating the two ratios,

$$LTR = \frac{26 \text{ min}}{283 \text{ min}} = 0.0919$$

$$STR = \frac{26 - 10 \text{ min}}{26 \text{ min}} = 0.6154$$

From table 4–3 and figure 4–6, the correction factor, CF, is 1.0962. Total emitted gas is then

$$V_{tot} = 1.0962 \times 15{,}931 \text{ cm}^3 = 17{,}464 \text{ cm}^3$$

When the USBM direct method was applied to this same data above, total gas was 17,934 cm$^3$, which is 2.7% higher than the value obtained from analyzing the data with the Smith and Williams method.

The lost gas is simply total gas less collected gas, or

$$\text{Lost gas} = 17{,}464 \text{ cm}^3 - 15{,}931 \text{ cm}^3 = 1{,}533 \text{ cm}^3$$

This is 108 cm$^3$ (6.6%) less than the 1,641 cm$^3$ lost gas estimate from the USBM direct method square root of time plot and 371 cm$^3$ (19%) less than the 1,904 cm$^3$ lost gas estimate resulting from the polynomial curve fit.

**Table 4–3.** Smith and Williams correction factors

| Lost time ratio | Surface time ratio | | | | | | | | |
|---|---|---|---|---|---|---|---|---|---|
| | 0.00 | 0.05 | 0.10 | 0.20 | 0.30 | 0.40 | 0.50 | 0.60 | 0.70 |
| 0.00 | 1.0000 | 1.0000 | 1.0000 | 1.0000 | 1.0000 | 1.0000 | 1.0000 | 1.0000 | 1.0000 |
| 0.05 | 1.0361 | 1.0382 | 1.0401 | 1.0437 | 1.0470 | 1.0501 | 1.0531 | 1.0605 | 1.0633 |
| 0.10 | 1.0630 | 1.0667 | 1.0701 | 1.0763 | 1.0820 | 1.0873 | 1.0923 | 1.1020 | 1.1068 |
| 0.15 | 1.0881 | 1.0936 | 1.0985 | 1.1073 | 1.1154 | 1.1231 | 1.1305 | 1.1426 | 1.1495 |
| 0.20 | 1.1137 | 1.1210 | 1.1275 | 1.1393 | 1.1502 | 1.1606 | 1.1706 | 1.1853 | 1.1947 |
| 0.25 | 1.1405 | 1.1500 | 1.1585 | 1.1738 | 1.1880 | 1.2014 | 1.2142 | 1.2320 | 1.2441 |
| 0.30 | 1.1698 | 1.1819 | 1.1924 | 1.2116 | 1.2295 | 1.2465 | 1.2629 | 1.2843 | 1.2999 |
| 0.35 | 1.2022 | 1.2172 | 1.2304 | 1.2543 | 1.2769 | 1.2984 | 1.3191 | 1.3448 | 1.3646 |
| 0.40 | 1.2391 | 1.2575 | 1.2739 | 1.3060 | 1.3333 | 1.3605 | 1.3868 | 1.4180 | 1.4394 |
| 0.45 | 1.2870 | 1.3114 | 1.3326 | 1.3711 | 1.3970 | 1.4291 | 1.4621 | 1.5000 | 1.5318 |
| 0.50 | 1.3379 | 1.3666 | 1.3913 | 1.4362 | 1.4756 | 1.5163 | 1.5564 | 1.6027 | 1.6427 |
| 0.55 | 1.3910 | 1.4281 | 1.4600 | 1.5179 | 1.5715 | 1.6246 | 1.6768 | 1.7339 | 1.7840 |
| 0.60 | 1.4655 | 1.5120 | 1.5518 | 1.6277 | 1.6971 | 1.7646 | 1.8299 | 1.9012 | 1.9670 |
| 0.65 | 1.5629 | 1.6230 | 1.6742 | 1.7715 | 1.8628 | 1.9513 | 2.0395 | 2.1326 | 2.2193 |
| 0.70 | 1.6876 | 1.7670 | 1.8403 | 1.9737 | 2.0959 | 2.2174 | 2.3390 | 2.4641 | 2.5840 |

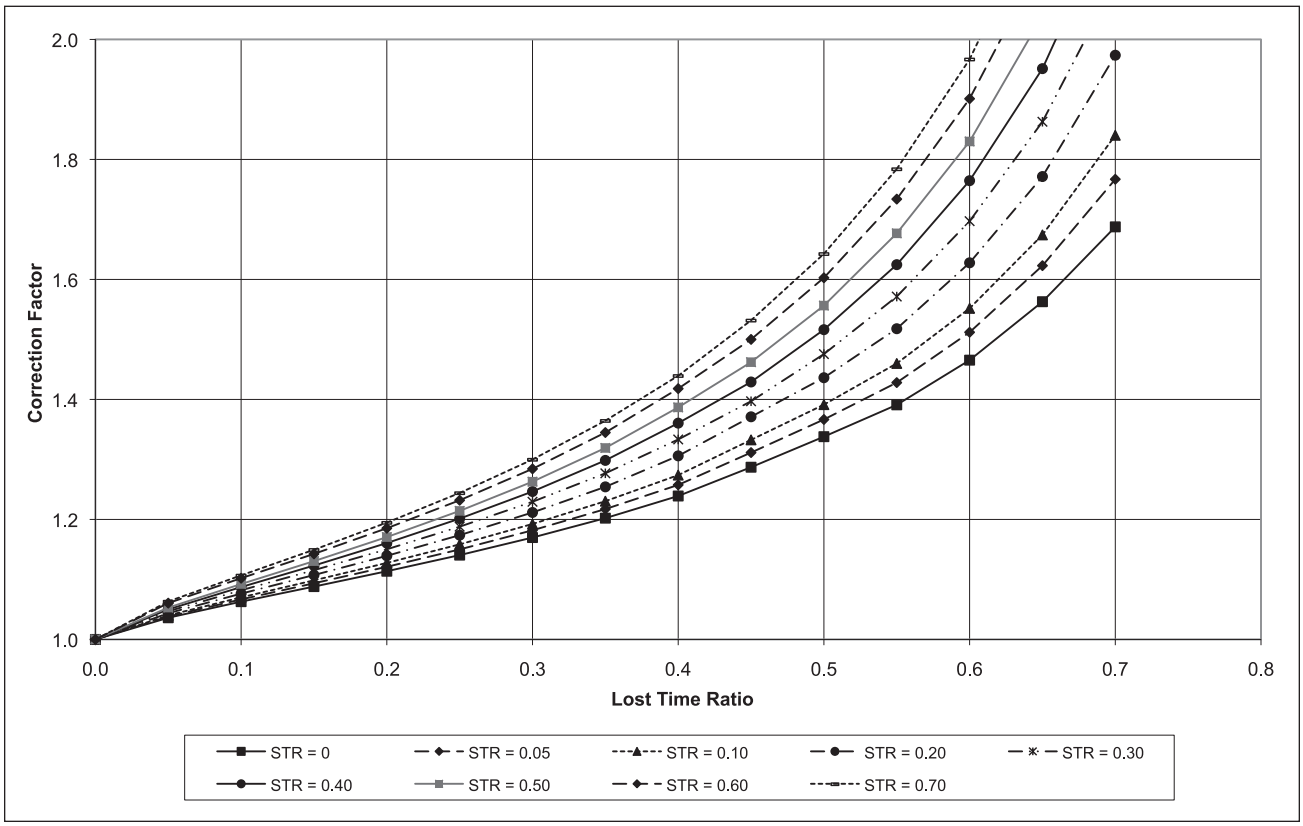



**Fig. 4–6.** Smith and Williams correction factors plot

## Curve Fit Methods

Coalbed gas content is sometimes determined by fitting desorption data to a given equation. The earliest such method was that of Chase, which was based on the observation that gas emission from a coal sample was analogous to gas production from a volumetric gas reservoir.[27] Coalbed gas content is determined from a semilog plot of desorption rate and cumulative desorbed gas. A straight line is fit to the data, with coalbed gas content being the intercept on the axis of cumulative desorbed gas. Note that a semilog rate-cumulative plot of exponential decline is not linear, leaving little theoretical basis for gas content determination from such a plot.[28] To illustrate this method, a decline curve plot of desorption data from table 4–2 is presented in figure 4–7.

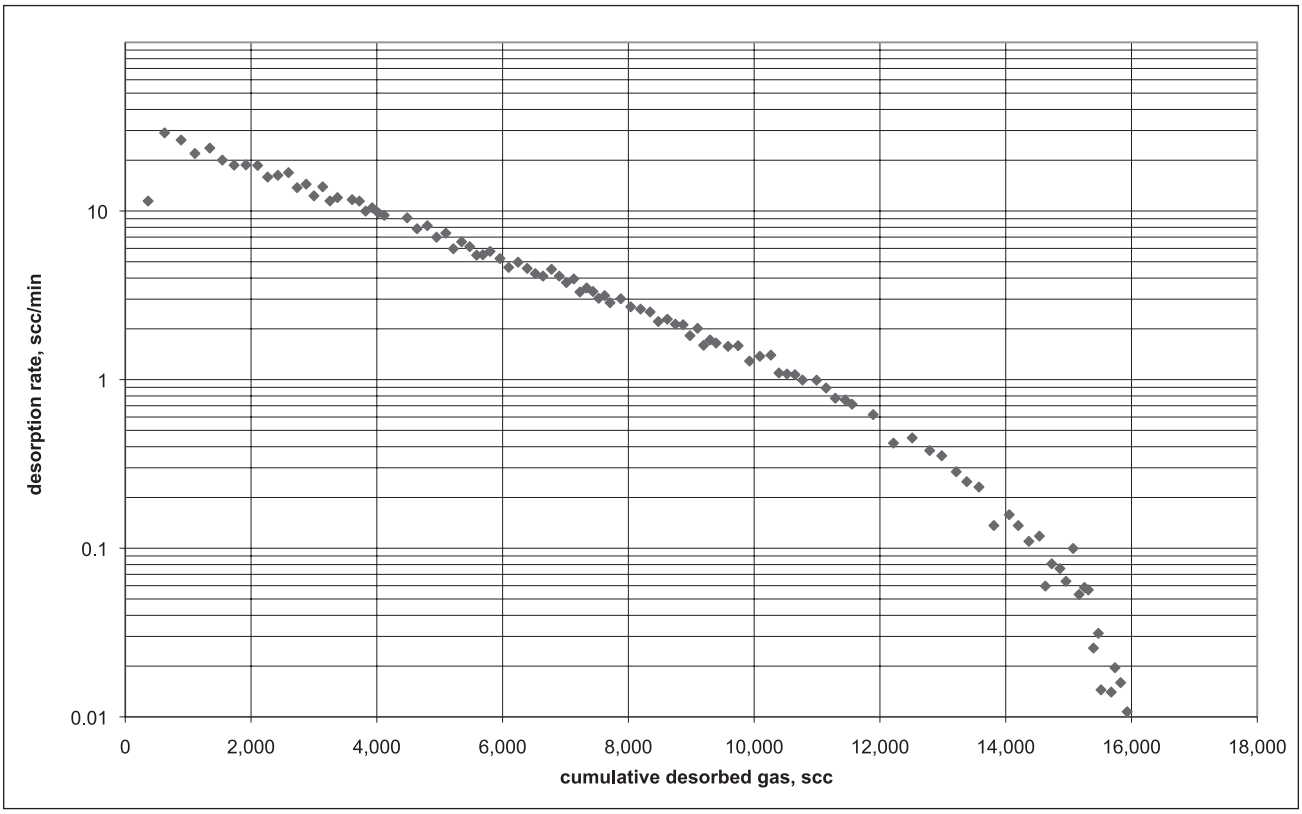



**Fig. 4–7.** Desorption decline curve—sample CGF-BI#13-122

The data for the first 11,000 min (7.6 days) are quite linear and extrapolate to a cumulative desorbed gas content of 33,112 $cm^3$ at a desorption rate of 1 $cm^3$/day. Subsequent desorption data show an actual desorbed gas volume of slightly less than 16,000 $cm^3$. Total gas content determined by the USBM direct method, 17,934 $cm^3$, is 54% of the decline curve cumulative and corresponds to a desorption rate of 40 $cm^3$/day. Use of desorption decline curves to determine coalbed gas contents is not recommended.

A second curve fit method, termed the *Amoco method*, fits cumulative desorbed gas data as a function of time to[29]

$$V_{des}(t) = V_{LD}\left[1 - \frac{6}{\pi^2}\exp\left(-\pi^2\frac{D}{r^2}t\right)\right] - V_L \qquad \textbf{(4.6)}$$

where

$V_L$ = lost gas, $cm^3$.

Fitting equation (4.6) to the desorption data in table 4–2 yields a lost plus desorbed gas volume, $V_{LD}$, of 16,156 $cm^3$, a lost gas volume, $V_L$, of 6,370 $cm^3$, and a diffusivity of 1.93E–4 $min^{-1}$. The sum of lost and desorbed gas, $V_{LD}$, from the Amoco method is 8% less than that from the USBM direct method. In contrast, the lost gas, $V_L$, from the Amoco method is higher than that from the USBM direct method by a factor of 3.9. As will be seen below, overestimation of lost gas is a common problem with this method. Diffusivity from the Amoco curve fit is 5.4 times smaller than that obtained from the USBM direct method.

Curve fit methods account for all gas emitted by a sample and thus do not require residual gas measurements.

## Mass Normalized Gas Contents

Regardless of the method employed to determine total gas sorbed by a sample, after that volume has been calculated, it is normalized to a unit mass basis. The seven most common gas content normalizations are as follows:

1. In-situ basis
2. Dry, ash-free basis (daf)
3. Air-dry basis
4. Dry, mineral-matter free (dmmf) basis
5. Moist, ash-free basis
6. Dry, with-ash basis
7. "Pure coal" basis

For reservoir engineering purposes, the most useful gas contents are those normalized on an in-situ basis and a dry, ash-free basis. Proximate and ultimate analyses are required to normalize gas contents and thus should be run on every sample. Gas contents are reported in cubic centimeters per gram and standard cubic feet per ton. Multiplication of gas content in cubic centimeters per gram by 32.037 converts the dimensions to standard cubic feet per ton. If gas content in $cm^3$/gm were measured at one base temperature and pressure, and the final units of scf/ton utilize another base temperature and pressure, an additional correction factor is necessary. For instance, if gas contents in $cm^3$/gm were measured at a standard temperature of 0°C and the final gas contents in scf/ton utilize a base temperature of 60°F, multiplication by a factor of 1.131 will transform the gas contents in scf/ton to a base pressure of 60°F.

Calculation of original gas in place and estimation of gas reserves requires in-situ gas contents, which are determined by dividing total sorbed gas volume by sample mass.

Two methods are currently employed to determine in-situ sample mass. Some service companies simply rinse the sample with distilled water, wipe it dry, and weigh it. Others allow the sample to dry at laboratory conditions until it reaches an equilibrium weight, typically 24 to 48 hr, before weighing it and reporting gas content on an air-dry basis. Coalbed gas resource calculations combine in-situ gas content with coal density, which is typically obtained from wireline logs. Native coal deposits contain water, ash, sulfur, and other impurities that are reflected in the bulk densities measured with wireline logs. For consistency, gas content on an in-situ basis must reflect these impurities. Despite the difficulties with simply rinsing the sample immediately after removing it from the desorption canister, wiping it dry, and weighing it, this technique often provides the best measure of in-situ sample mass of high-rank coals.

Air drying does not remove all moisture in a sample but always decreases sample weight, increasing gas content. This results in a modest gas content error in higher rank coals that typically have porosities of only a few percent. However, in low-rank coals, the error can be substantial. As seen in chapter 2, moisture content of subbituminous coals can be on the order of 25%, and air drying such samples can yield erroneously low sample masses, and consequently, overestimate gas in place.

Coring of coal seams with little, if any, moveable water in the cleats can result in flooding the cleats with drilling fluids. Subsequent rinsing of the samples will add additional moisture to the sample, while air drying in the laboratory will leave drilling mud residue in the cleats. Both techniques will yield erroneous sample masses. Compounding this difficulty, coals are often aquifers, and the dry nature of the target coal seam is often only evident long after core desorption has been completed.

Coals are heterogeneous reservoirs, and seam-to-seam gas content comparisons as well as variation within a given seam are often best understood on a dry, ash-free basis. Comparison of gas content from a desorption test with that calculated from a sorption isotherm should be performed on a daf basis due to different impurities in the desorption and isotherm samples. This is true even when the isotherm is measured on a subsample from the original desorption sample.

Returning to the desorption test reported in table 4–2, bulk sample mass was 2,177.0 g, and total moisture was 11.77%. Residual moisture was 1.97%, and ash and sulfur were 4.13% and 2.66%, respectively. In-situ gas content calculated with the USBM direct method is 17,934 $cm^3$/2,177.0 g or 8.24 $cm^3$/g. Multiplying by 32.037 yields an in-situ gas content of 263.9 scf/ton. Total emitted gas calculated with the Smith and Williams method was 17,464 $cm^3$, which yields a gas content of 8.02 $cm^3$/g or 257.0 scf/ton (2.6% lower). The curve fit method, using the Amoco equation, estimated total gas as 16,156 $cm^3$, giving in-situ coalbed gas contents of 7.42 $cm^3$/g and 237.8 scf/ton (9.9% lower than the USBM direct method value).

Correcting the bulk mass for ash and moisture gives a daf mass of 2,177.0 g × (1 – 0.0413 – 0.1177) = 1,830.9 g, very close to the reported daf weight of 1,830.8 g. Thus, the USBM direct method daf gas content is 17,934 $cm^3$/1,830.9 g = 9.80 $cm^3$/g or 314.0 scf/ton. The daf gas contents from the Smith and Williams and curve fit methods are 9.54 $cm^3$/g (305.6 scf/ton) and 8.82 $cm^3$/g (282.6 scf/ton), respectively.

The mineral matter fraction is calculated from the Parr formula (chapter 2),

$$mm = 1.08a + 0.55S$$

where

$mm$ = mass fraction mineral matter,
$a$ = mass fraction ash, and
$S$ = mass fraction of sulfur.

The mineral-matter fraction for this sample is 1.08 x 0.0413 + 0.55 × 0.0266 = 0.0592, making the dry, mineral-matter free weight 1,791.9 g, as compared to a reported dmmf weight of 1,791.8 g. Thus, dmmf gas contents are 10.0 $cm^3$/g (320.4 scf/ton), 9.75 $cm^3$/g (312.4 scf/ton) and 9.02 $cm^3$/g (289.0 scf/ton) for the USBM direct method, the Smith and Williams method, and the Amoco method, respectively.

With the exception of the "pure coal" basis, calculation of gas content using the remaining bases is straightforward and left to the reader as an exercise. The "pure coal" gas content was arbitrarily defined as the intercept of a regression line fit through a plot of air-dry gas contents versus weight percent of dry ash and residual moisture.[30] Thus, calculation of gas content on a "pure coal" basis is not possible for the single sample reported in table 4–2. Note, however, the moisture fraction lost during air drying was 0.1177 – 0.0197 = 0.0980, making the air-dry weight 2,177g × (1 – 0.0980) = 1,963.7 g, about 0.2% above the reported air-dry weight of 1,959.3 g. The air-dry gas content based on the USBM direct method volume is 17,934 $cm^3$/1,963.7 g = 9.13 $cm^3$/g or 292.6 scf/ton. The dry ash fraction is 0.0413 × 2,177g/[2,177g × (1 – 0.1177)] = 0.0468. Adding this to the residual moisture value of 0.0197 allows approximate correction to "pure coal" gas content, 292.6 scf/ton/(1 – 0.0468 – 0.0197) = 313.4 scf/ton, which is 0.2% below the USBM direct method daf gas content calculated above.

Field experience has shown that regardless of the method employed to analyze a given set of cuttings desorption data, gas contents from cuttings are routinely lower than those obtained from whole cores. Although they felt their data sets too few for general conclusions, Mavor et al. noted that as a general rule, gas contents from whole cores were about one-third higher than those determined from drill cuttings.[31] Nelson et al. had a much larger data set from desorption tests of Powder River Basin coals and reported gas contents from whole core desorption were 36% larger than those obtained from desorption of drill cuttings.[32] Thus, as a general rule,

gas content determined from drill cuttings is multiplied by 4/3 to obtain whole core equivalent gas content. Mavor et al. found that gas contents from sidewall core samples compared to whole core gas contents varied widely but did not speculate as to why.[33] In the decade since that work was done, sidewall core desorption techniques have improved considerably. As a result, gas contents from these techniques are now generally equal to those obtained from whole core desorption tests.

In summary, coalbed gas contents can be calculated on seven different bases. Any of them can be used if care is taken in all calculations, and all gas contents are reported on a consistent basis. In practice, the two most commonly used are the in-situ and dry, ash-free bases.

## Sources of Error in Gas Content Measurements

Mavor et al. critically assessed sources of error in coalbed gas content measurements and identified the six primary sources of such errors.[34] The most significant error resulted from desorption at off-reservoir temperatures. Gas release from a coal depends on temperature, and maintaining samples at a constant reservoir temperature is one of the most critical aspects of desorption tests. Desorption at ambient temperatures resulted in gas contents too low by one-third.

Other sources of error include desorption volume measurement error, which can be especially significant when samples, such as sidewall cores or undersaturated coals, emit small volumes of gas. The third source of error in gas content measurements stems from failure to convert desorbed gas volumes to standard conditions. Not only does this result in erroneous desorbed gas volumes, but lost gas calculations are also affected. Neglect of canister headspace volumes can lead to significant errors, especially in samples with low desorbed gas volumes. As discussed above, Ulery and Hyman reported gas content errors on the order of 30% when headspace and desorbed gas volumes were roughly equal but minimal error when headspace volume was small compared to total desorbed gas volume.[35]

Sample weight measurement errors also affect coalbed gas contents. Sample mass should be determined by weighing the actual sample. Subtracting the filled canister weight from the tare weight can introduce significant errors, especially when the sample is heavily contaminated with drilling fluids or, in the case of drill cuttings, noncoal particles.

The final source of error identified by Mavor et al. was failure to determine residual gas content. While neither the Smith and Williams nor curve fit methods require determination of residual gas, neglecting to measure it can result in erroneously low gas contents, especially in samples that are desorbed only long enough to determine lost gas.

Ulery and Hyman studied composition of desorbed gases and reported significant underestimation of coalbed gas contents due to oxygen uptake into low-gas-content coals, which slowly released the little gas they held.[36] Nelson et al. reported similar results from desorption of subbituminous samples from the Canyon coal of the Powder River Basin.[37]

Mavor et al. compared gas contents determined by the USBM direct method, the Smith and Williams method, and the Amoco method to benchmark gas contents from nine San Juan Basin coal wells.[38] The most accurate technique was found to be the USBM direct method applied to data from heated desorption samples. Average gas content error in this case was 7% high, well within engineering accuracy. Gas contents determined with the Smith and Williams method averaged 24% low, while those from the Amoco method were 30% too high. The large errors for both these two methods are probably due to the estimation of lost gas. The linear boundary condition assumed by Smith and Williams for the trip up hole could be overly simplistic, while the lost gas estimation by Amoco curve fit is too aggressive for short trip times.

## Typical Coalbed Gas Contents

Interpretation of desorbed gas contents is facilitated by comparison with other results. In-situ gas contents from various U.S. coal basins compiled by Rightmire et al. are collected in table 4–4.[39]

**Table 4–4.** Typical in-situ coalbed gas contents

| Basin | Gas content scf/ton | Gas content $m^3/t$ |
|---|---|---|
| San Juan | 23–587 | 0.7–18.3 |
| Warrior | 64–595 | 2.0–18.6 |
| Piceance | 15–569 | 0.5–17.8 |
| Central Appalachian | 10–563 | 0.3–17.6 |
| Raton | 26–510 | 0.8–15.9 |
| Powder River | 20–45 | 0.62–1.4 |

*Source:* Rightmire, C. T., et al. 1984.

Gas contents within any given basin can vary by an order of magnitude, with lower values from dirty, shallow, lower rank coals and higher values from deeper, cleaner, higher rank coals. Curiously, regardless of coal age, rank, or geographic location, maximum in-situ gas content is about 600 scf/ton. In practice, gas contents above 600 scf/ton should be viewed with caution, as they are often due to small sample mass and/or significant $CO_2$ in the adsorbed gas.

## Mudlog Gas Content

A mudlog method for determination of coalbed gas content was developed by Donovan.[40] This method assumes all gas is emitted from the drill cuttings before their arrival on the surface. A somewhat extreme assumption, this method implies all gas from the cuttings is lost gas. This method requires the following:

1. A calibrated gas chromatograph for detection and quantification of gas volumes liberated from the coal drill cuttings
2. Openhole wireline logs to determine hole diameter, coal seam thickness, and average coal density
3. Drilling penetration rate

The gas chromatograph is calibrated from the acetylene response during carbide lag measurements and detector relative sensitivity to acetylene and methane. This allows quantification of methane gas volumes. Coal seam thickness, density, and hole size from wireline logs permit calculation of the tons of coal drilled up to liberate the measured methane volumes. Dividing that volume by pulverized coal mass yields gas content in standard cubic feet per ton. In practice, this method tends to be very data sensitive, with small changes in the measured quantities translating to large changes in calculated gas contents.

While this method is promising, it must be regarded as unproven until comparisons of this method with more traditional methods of gas content determination have been published. The basic assumption behind the mudlog gas content method is that virtually all gas is liberated from drill cuttings into the mud stream before the drill cuttings reach the surface. However, this assumption conflicts squarely with the assumption underlying more traditional methods—that when drill cuttings arrive at the surface, they retain sufficient gas for desorption tests.

## Number of Samples

The number of desorption samples that should be taken from a given well depends on several factors. Characterizing a single seam in an infill well requires fewer samples than does characterizing multiple coals intercepted by a wildcat exploration corehole. Many operators restrict the number of samples in an effort to minimize costs without realizing that the cost of desorbing of a few additional samples is relatively small compared to overall well costs. In addition, the cost of bad decisions based on inadequate data can be enormous compared to the cost of additional desorption samples. In practice, the minimum number of samples is often two per seam for dominant coals and one per seam for minor coals. At the other extreme, some operators elect to canister all recovered coal.

Not only is the number of samples recovered important, but the type of samples is also important. Desorbing only low-density, high-quality coal intervals will provide no information on the gas resource held in denser rocks and will preclude correlation of gas content with bulk density. In spite of the importance of this topic, only a few workers have considered it theoretically.

Diamond and Schatzel recommend canistering the entire recovered coal section, splitting the core at natural breaks, such as shale partings, into several discrete samples.[41] Note that exclusion of shales and bone coals precludes determination of gas held in them, and reserve estimates must be reduced accordingly. The Gas Research Institute recommends sampling one-third of the "vertical reservoir profile" but does not address the number of samples required to do so.[42] Mavor et al. employed statistical arguments to determine the number of samples required to estimate gas content to within 10% at a 95% confidence level.[43] An example calculation using a San Juan well determined that 9 ft of the 57 ft of net coal, approximately 16%, were required. Note that this example required a bulk density distribution obtained from offset wells. Thus, from a theoretical basis, the recommended sample interval ranges from one-sixth of the coal seam to the entire coal seam.

Review of four sets of published gas contents will demonstrate that at least 80% of the samples from a single seam should be desorbed to determine gas content with over 90% confidence. However, sampling only one-third of the coals in a borehole will give an approximate idea of gas content distribution across the seams.

Seven whole core desorption samples from the Southern Ute 5–7 well discussed by Mavor et al. are reproduced here as table 4–5.[44]

**Table 4–5.** Southern Ute 5–7 measured gas contents

| Zone | Top depth, ft | Bottom depth, ft | Gross thickness, ft | Average density, g/cm$^3$ | Average ash, % | Average in-situ gas content, scf/ton |
|---|---|---|---|---|---|---|
| 1 | 1,312.50 | 1,314.50 | 2.3 | 1.740 | 0.5772 | 209.3 |
| 2 | 1,321.25 | 1,339.00 | 18.0 | 1.489 | 0.2991 | 353.5 |
| 3 | 1,340.75 | 1,347.75 | 7.3 | 1.619 | 0.4428 | 279.0 |
| 4 | 1,349.00 | 1,362.25 | 13.5 | 1.466 | 0.2729 | 367.1 |
| 5 | 1,449.25 | 1,449.50 | 0.5 | 2.081 | 0.9555 | 13.1 |
| 6 | 1,451.00 | 1,472.75 | 22.0 | 1.440 | 0.2442 | 382.0 |
| 7 | 1,484.50 | 1,486.75 | 2.5 | 1.502 | 0.3136 | 346.0 |
| | | | 66.1 | | 0.4436 | 278.6 |
| | | | | | stdev = | 131.64 |
| | | | | | stdev/avg = | 0.473 |

*Source:* Mavor, M. J., et al. 1996.
*Note:* Thickness-weighted average gas content = 349.8 scf/ton.

These gas contents are sound, with minimal experimental error. For the sake of argument, they are assumed to be completely accurate, giving an average gas content of 278.6 scf/ton. Gas content determined from a single sample, then two samples, then three samples, etc. will be discussed. If a single sample were selected for desorption, only one would be within 20% of the correct number. That is, only one sample, sample 3, with a gas content of 279.0 scf/ton, would be within 20% of the correct value of 278.6 scf/ton. Desorption of a single sample in seven, or 14.3% of all samples, gives a gas content within 20% of the true gas content. Desorption of any of the other six samples will yield a gas content varying from the correct gas content by more than 20%. Repeating the exercise with a tolerance of 10% gives the same result of one sample in seven, sample 3, being sufficiently close to the true value. Because the gas content of sample 3 is so close to the correct gas content, the same conclusion of gas content from only one sample in seven results from tolerances of 1% and 5% around the correct gas content.

Turning the other way, if true gas content is desired to be known only to within 25%, then three samples, samples 1, 3, and 7, or 43% of the samples are sufficiently close to the true gas content. These three samples represent 43% of the total population of seven samples, so randomly selecting a single sample for desorption will give a gas content within 25% of the correct gas content in only 43% of the cases.

Repeating this exercise with two samples of the seven, there are 21 different pairs of samples. The number of sample sets is the combination of *n* total samples taken *r* at a time. For seven total samples taken two at a time, the number of possible combinations is

$$\frac{7!}{2!(7-2)!} = \frac{7(6)5!}{2(5!)} = 21$$

Averaging the gas contents of the pairs, 43% of them will provide a gas content within 25% of the true value, while only 5% of them will yield a gas content within 1% of true gas content. These results, along with those from gas content uncertainty tolerances of 5%, 10%, and 20% uncertainty, are collected in table 4–6.

**Table 4–6.** Gas content uncertainty vs. number of samples—example #1

| Uncertainty in gas content | One sample | Two samples | Three samples | Four samples | Five samples | Six samples |
|---|---|---|---|---|---|---|
| 1% | 14.3% | 4.8% | 5.7% | 5.7% | 9.5% | 14.3% |
| 5% | 14.3% | 14.3% | 11.4% | 11.4% | 28.6% | 57.1% |
| 10% | 14.3% | 19.0% | 17.1% | 40.0% | 42.9% | 85.7% |
| 20% | 14.3% | 42.9% | 57.1% | 74.3% | 95.2% | 100.0% |
| 25% | 42.9% | 42.9% | 74.3% | 97.1% | 100.0% | 100.0% |

*Note:* Five samples are required to be 95% certain that gas content is known to within 20%.

If three samples of the seven are desorbed, a total of 35 triplets are possible. Only 6% of these triplets will yield an average gas content within 1% of the true number, yet almost three-quarters of them, 74.3%, will give an average gas content within 25% of the correct value. Repeating this exercise for four samples (also 35 possible combinations), five samples (21 possible combinations), and six samples (7 possible combinations) fills out table 4–6.

Table 4–6 quantifies the intuitive conclusions that increasing the number of desorption samples taken from a given seam provides a more accurate estimate of coalbed gas content. Many reservoir parameters such as thickness and drainage area are not known to within better than 20%, thus the 20% row of table 4–6 can be considered. Desorbing a single sample will provide the true gas content within 20% in only one out of seven samples. Gas contents from six of the seven samples will differ from true gas content by more than 20%. Desorbing a pair of samples gives true gas content within 20% in just under one-half, 42.9%, of all possible pairs. Just over one-half of all possible triplets, 57.1%, give an average gas content within 20% of the true value. Almost three-quarters of all possible sets of four samples, 74.3%, give average gas contents within 20%. Over 95% of the various combinations of five and six samples provide an average gas content within 20% of the true value. Consequently, to be 95% certain that true gas content is known to within 20%, at least five samples must be desorbed. In other words, five out of seven samples, or 71%, of the samples must be desorbed.

Further complicating determination of "true" gas content, Mavor et al. reported a thickness-weighted gas content of 349.8 scf/ton.[45] Note that determination of this gas content required use of wireline logs, which would not be available when the core barrel was opened up and the decision of how many samples to desorb must be made.

As a second example, consider the sidewall core (SWC) gas contents provided by Waechter and reported in table 4–7.[46]

Assuming the average gas content from the five samples, 213.4 scf/ton, is the true gas content and repeating the above exercise of gas content determination with one, two, three, or four samples yields table 4–8. From the table, it is seen that to be 95% certain the gas content is known to within 20% requires three or four samples.

**Table 4–7.** HWA sidewall core measured gas contents

| Zone | Depth, ft | In-situ gas content, scf/ton |
|---|---|---|
| 1 | 1,252.60 | 239.8 |
| 2 | 1,253.00 | 208.7 |
| 3 | 1,254.00 | 237.7 |
| 4 | 1,258.00 | 78.7 |
| 5 | 1,258.40 | 301.9 |
| | average = | 213.4 |
| | stdev = | 82.6 |
| | stdev/avg = | 0.387 |

*Source:* Waechter, N. B. 2003.

**Table 4–8.** Gas content uncertainty vs. number of samples—example #2

| Uncertainty in gas content | One sample | Two samples | Three samples | Four samples |
|---|---|---|---|---|
| 1% | 0.0% | 0.0% | 0.0% | 20.0% |
| 5% | 20.0% | 10.0% | 20.0% | 60.0% |
| 10% | 20.0% | 20.0% | 40.0% | 60.0% |
| 20% | 60.0% | 50.0% | 90.0% | 100.0% |
| 25% | 60.0% | 50.0% | 100.0% | 100.0% |

*Note:* Three samples are required to be 90% certain that gas content is known to within 20%.

The third set of gas contents was reported by Kelso et al. from coals of the Great Divide Basin, part of the Greater Green River Basin.[47] Cores and cuttings were desorbed from three wells that penetrated several coals over a 3,000 ft interval. Gas contents from two cores from the UPRC-9 well were selected for investigating the number of samples required to characterize these coals. Gas contents of five samples from 2,183.5 ft to 2,187.5 ft, labeled core 1 here and collected in table 4–9, were deeply undersaturated, with an average gas content of 6.68 scf/ton.

**Table 4–9.** UPRC-9—core 1 measured gas contents

| Zone | Top depth, ft | In-situ gas content, scf/ton |
|---|---|---|
| 1 | 2,183.5 | 1.79 |
| 2 | 2,184.5 | 4.32 |
| 3 | 2,186.5 | 17.57 |
| 4 | 2,186.5 | 6.50 |
| 5 | 2,187.5 | 3.22 |
| | average = | 6.68 |
| | stdev = | 6.33 |
| | stdev/avg = | 0.947 |

*Source:* Kelso, B. S., et al. 1991.

Repeating the exercise of calculating average gas contents from various numbers of samples gives table 4–10. Reported gas contents varied widely, leading to the confusing result that one-fifth of the single samples would be within 20% of true gas content but only one-tenth of the pairs would. Moreover, to determine gas content within 20% at greater than an 80% confidence level would require desorbing all five samples.

**Table 4–10.** Gas content uncertainty vs. number of samples—example #3

| Uncertainty in gas content | One sample | Two samples | Three samples | Four samples |
|---|---|---|---|---|
| 1% | 0.0% | 0.0% | 0.0% | 20.0% |
| 5% | 20.0% | 0.0% | 0.0% | 20.0% |
| 10% | 20.0% | 0.0% | 0.0% | 40.0% |
| 20% | 20.0% | 10.0% | 20.0% | 80.0% |
| 25% | 20.0% | 10.0% | 20.0% | 80.0% |

*Note:* Four samples are required to be 80% certain that gas content is known to within 20%.

The fourth example comes from gas contents from a second core in this same well. Gas contents of four samples taken from a deeper seam, between 2,515.8 ft and 2,518.5 ft, are in table 4–11.

**Table 4–11.** UPRC-9—core 2 measured gas contents

| Zone | Top depth, ft | In-situ gas content, scf/ton |
|---|---|---|
| 1 | 2,515.8 | 12.57 |
| 2 | 2,516.5 | 9.48 |
| 3 | 2,517.5 | 5.82 |
| 4 | 2,518.5 | 11.97 |
| | average = | 9.96 |
| | stdev = | 3.07 |
| | stdev/avg = | 0.308 |

*Source:* Kelso, B. S., et al. 1991.

This coal is also deeply undersaturated, with an average gas content of 9.96 scf/ton. The number of samples required to determine gas contents with selected degrees of confidence and selected tolerances are displayed in table 4–12.

**Table 4–12.** Gas content uncertainty vs. number of samples—example #4

| Uncertainty in gas content | One sample | Two samples | Three samples |
|---|---|---|---|
| 1% | 0.0% | 0.0% | 0.0% |
| 5% | 25.0% | 0.0% | 25.0% |
| 10% | 25.0% | 33.3% | 75.0% |
| 20% | 25.0% | 66.7% | 100.0% |
| 25% | 50.0% | 100.0% | 100.0% |

*Note:* Three samples are required to be virtually certain that gas content is known to within 20%.

Note that to determine gas content to within 20% with 95% confidence would require desorbing at least three of the four possible samples. Undersaturation is only known after samples have been desorbed, isotherms measured, and reservoir pressure determined. Selection of desorption samples, cores or cuttings, is almost always completed before any indication of undersaturation. In practice, if undersaturation is suspected, the operator frequently elects to desorb additional, perhaps all, samples from the seam.

These four examples of single-seam desorption tests considered whole core samples and sidewall cores from saturated and undersaturated coals. From the four examples, it can be concluded that it is generally necessary to desorb at least 80% of the samples from the seam to determine gas content to within 20% with 90% or greater confidence.

The question of how many seams should be tested in a given prospect can be addressed with data from three wells drilled in the Rock Springs Formation of the Great Divide Basin.[48] Data from two cores taken from one of the wells, the UPRC-9, were discussed above. Data for all 74 samples are presented in table 4–13, where cuttings data have been corrected to whole core equivalent by multiplying by 4/3. Average in-situ gas content was 178.2 scf/ton.

**Table 4–13.** Great Divide Basin measured gas contents

| Well 1 UPRC-9 | | Well 2 UPRC-1 | | | Well 3 UPRC-33 | | |
|---|---|---|---|---|---|---|---|
| Core depth, ft | Gas content, scf/ton | Cuttings depth, ft | Gas content, scf/ton | WCE gas content, scf/ton | Cuttings depth, ft | Gas content, scf/ton | WCE gas content, scf/ton |
| 1,769.5 | 26.25 | 3,036.5 | 34.16 | 45.55 | 519.5 | 809.10 | 1,078.80 |
| 1,782.5 | 5.66 | 3,126.0 | 34.23 | 45.64 | 1,459.5 | 1.00 | 1.33 |
| 1,797.5 | 22.86 | 3,162.5 | 35.07 | 46.76 | 1,769.5 | 1.00 | 1.33 |
| 1,804.5 | 52.04 | 3,162.5 | 29.90 | 39.87 | 2,819.0 | 87.50 | 116.67 |
| 1,819.4 | 15.87 | 3,345.0 | 117.75 | 157.00 | 2,838.0 | 79.50 | 106.00 |
| 1,825.5 | 43.42 | 3,345.0 | 127.90 | 170.53 | 3,061.5 | 233.80 | 311.73 |
| 1,827.5 | 22.32 | 3,399.0 | 155.94 | 207.92 | 3,119.5 | 183.70 | 244.93 |
| 2,183.5 | 1.79 | 3,479.0 | 80.68 | 107.57 | 3,210.0 | 58.20 | 77.60 |
| 2,184.5 | 4.32 | 3,539.0 | 161.10 | 214.80 | 3,393.0 | 205.20 | 273.60 |
| 2,186.5 | 17.57 | 3,629.0 | 225.18 | 300.24 | 3,475.0 | 591.20 | 788.27 |
| 2,186.5 | 6.50 | 3,667.0 | 371.68 | 495.57 | 3,566.0 | 475.90 | 634.53 |
| 2,187.5 | 3.22 | 3,707.0 | 396.42 | 528.56 | 3,674.0 | 373.40 | 497.87 |
| 2,292.0 | 1.79 | 3,786.0 | 434.98 | 579.97 | 3,790.0 | 386.30 | 515.07 |
| 2,295.5 | 1.86 | 3,835.0 | 336.60 | 448.80 | 3,891.0 | 290.30 | 387.07 |
| 2,313.9 | 4.05 | 3,917.0 | 269.90 | 359.87 | 4,206.0 | 369.20 | 492.27 |
| 2,316.8 | 5.84 | 3,961.0 | 203.01 | 270.68 | | | |
| 2,321.2 | 5.92 | 4,037.0 | 363.64 | 484.85 | | | |
| 2,324.8 | 4.51 | 4,065.0 | 262.23 | 349.64 | | | |
| 2,325.5 | 2.89 | 4,119.0 | 226.21 | 301.61 | | | |
| 2,329.7 | 6.79 | 4,146.0 | 281.76 | 375.68 | | | |
| 2,330.5 | 1.11 | 4,173.0 | 270.76 | 361.01 | | | |
| 2,332.5 | 4.78 | 4,219.0 | 226.63 | 302.17 | | | |
| 2,336.9 | 5.92 | 4,256.0 | 268.56 | 358.08 | | | |
| 2,365.4 | 6.63 | 4,296.5 | 337.32 | 449.76 | | | |
| 2,367.6 | 7.96 | 4,372.0 | 74.59 | 99.45 | | | |
| 2,479.0 | 2.12 | 4,397.5 | 150.70 | 200.93 | | | |
| 2,515.8 | 12.57 | | | | | | |
| 2,516.5 | 9.48 | | | | | | |
| 2,517.5 | 5.82 | | | | | | |
| 2,518.5 | 11.97 | | | | | | |
| 2,535.5 | 9.17 | | | | | | |
| 2,587.7 | 4.94 | | | | | | |
| 2,589.8 | 21.18 | | | | | | |

*Note:* WCE = whole core equivalent = cuttings × 4/3.
Avg. WCE gas content = 178.2 scf/ton.

If only every fourth sample was desorbed, average gas content is 200.3 scf/ton, 12% higher than the full average, and a plot of gas content versus depth, figure 4–8, shows erratic gas content behavior.

The gas content of the shallowest sample, at a depth of 520 ft, appears spuriously high, while the remaining data fall into two intervals. In the first interval, from 1,700 to 2,600 ft, the coals appear to be deeply undersaturated. Below 2,600 ft, gas content increases with depth, as expected, but questions of undersaturation cannot be resolved without isotherms. The deepest sample, from 4,400 ft, appears erroneously low. Based on gas content alone, production tests should be confined to coals below depths of 3,400 ft.

Assuming every third sample was desorbed, average content rises to 202.1 scf/ton (13% high), and a plot of in-situ gas content versus depth, figure 4–9, shows the same behavior as before, although the data exhibit more scatter.

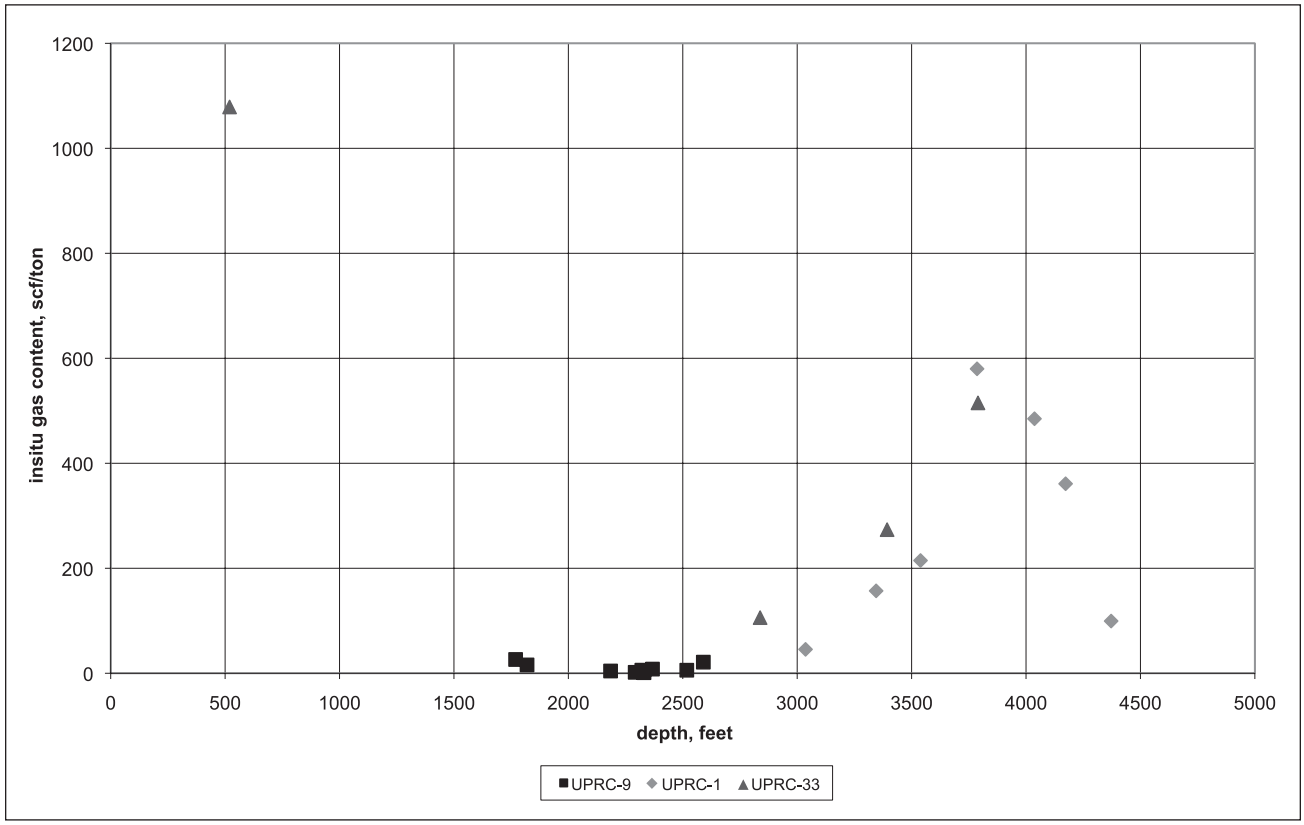



**Fig. 4–8.** Great Divide Basin—gas content vs. depth (1/4 of samples desorbed)

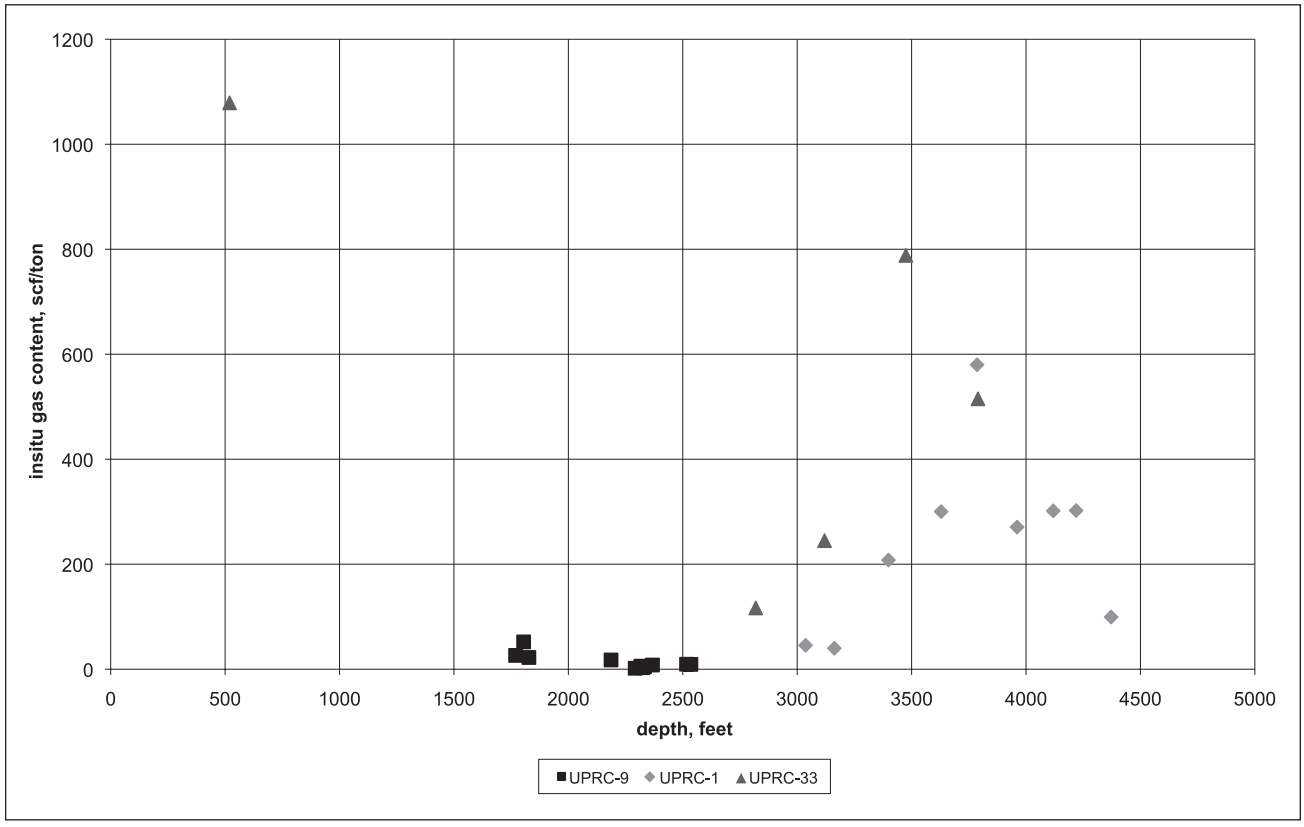



**Fig. 4–9.** Great Divide Basin—gas content vs. depth (1/3 of samples desorbed)

With gas content as the sole criterion, production tests should be confined to those coals deeper than 3,200 ft. Using every other sample results in an average gas content of 190.4 scf/ton (7% high), and the character of the gas content versus depth plot, figure 4–10, suggests three intervals, not two.

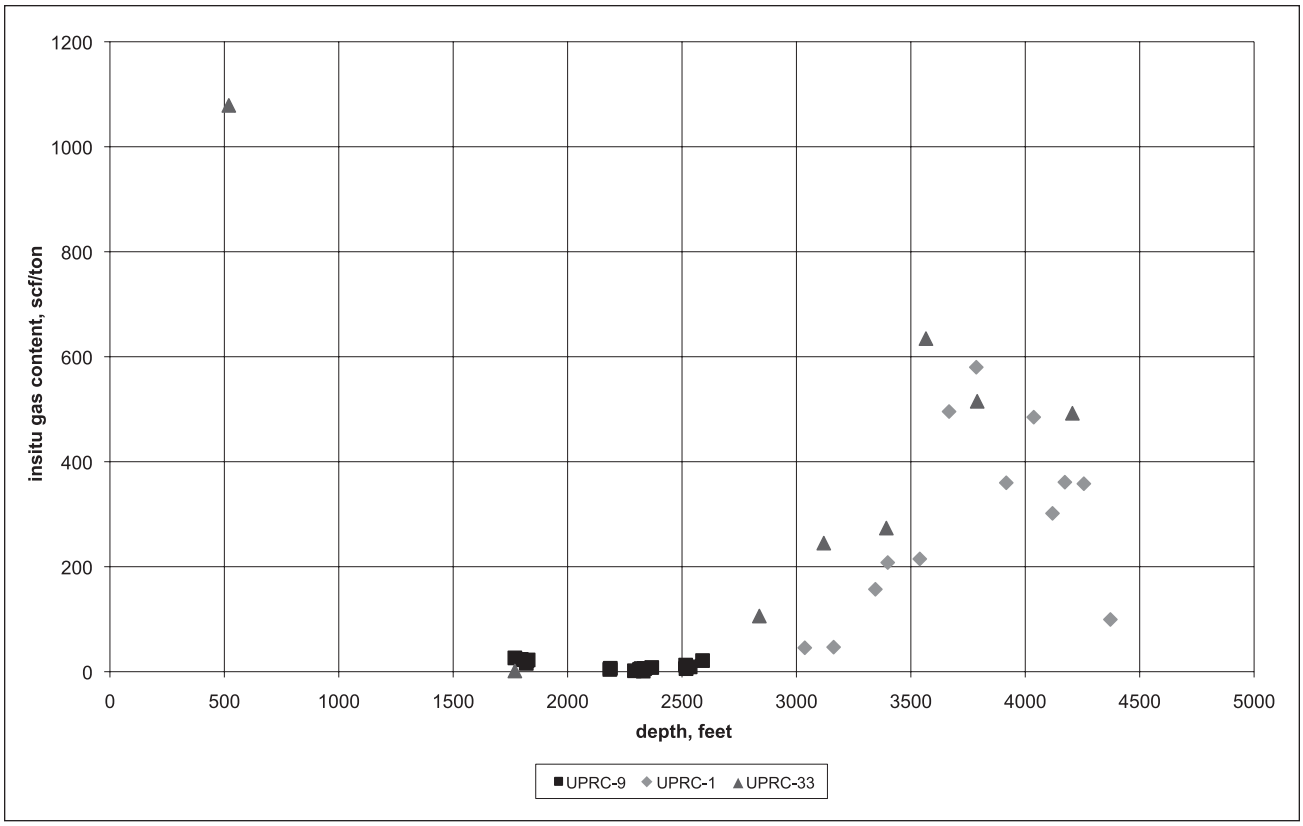



**Fig. 4–10.** Great Divide Basin—gas content vs. depth (1/2 of samples desorbed)

The first interval, from depths of 1,700 to 2,600 ft, remains unchanged. Between 2,600 feet and 3,600 ft, gas contents increase with depth, as before. Below 3,600 ft, gas contents could be interpreted either as roughly constant at 450 scf/ton or declining with depth. Production tests should be confined to zones below 3,100 ft.

A plot of all data, figure 4–11, is best interpreted as three separate intervals with gas content steadily falling with depth below 3,600 ft. Production tests should be confined to coals in the interval between 3,100 ft and 4,300 ft deep.

Although this example is somewhat transparent, it demonstrates that reasonable average gas contents could be obtained by desorbing as few as 25% of the samples, in good agreement with the GRI recommendation of sampling one-third of the "vertical reservoir profile."[49] However, behavior of gas content with depth—deep undersaturation in shallow seams, then gas content increasing with depth, followed by gas content decreasing with depth—was suggested when every other sample was desorbed but only fully evident when all samples were desorbed. As expected, identification of zones for possible production tests was clearer when all data were employed.

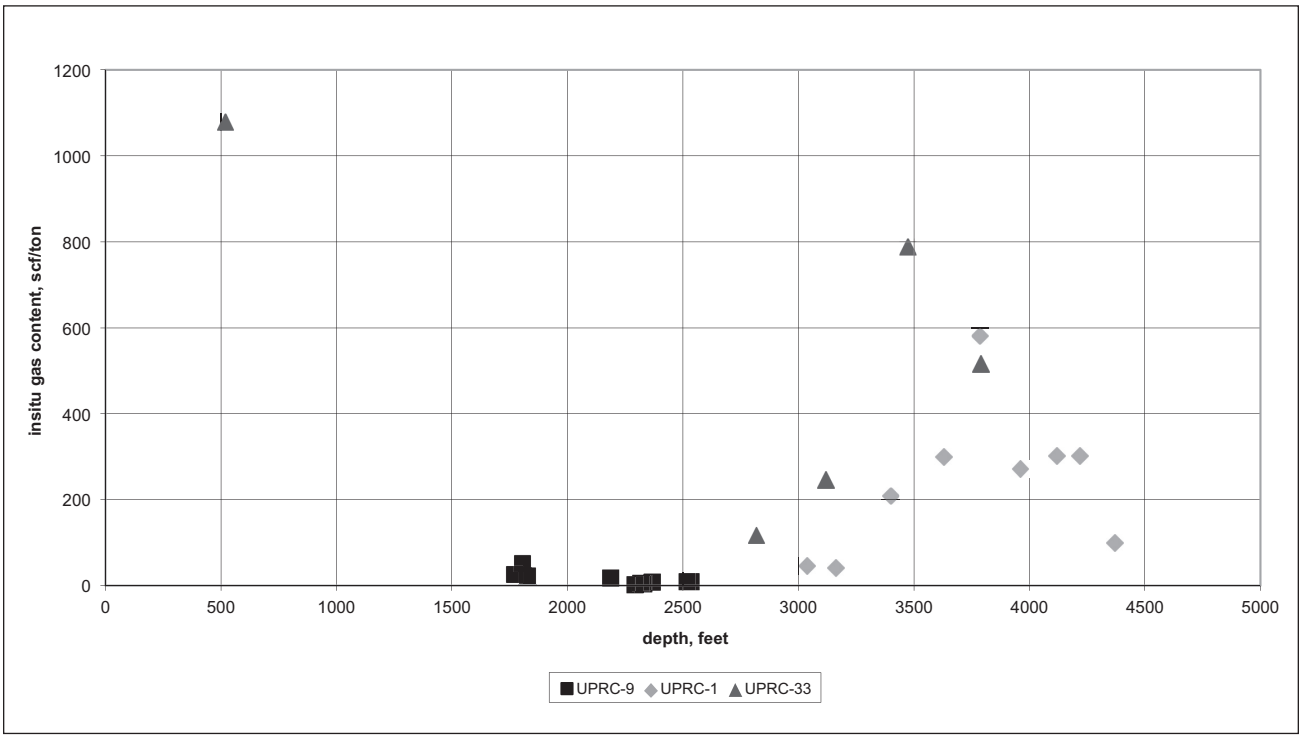



**Fig. 4–11.** Great Divide Basin—gas content vs. depth (all samples desorbed)

## Acknowledgements

The raw desorption data, the desorption test report, and sidewall core gas contents provided by Hampton, Waechter, and Associates is gratefully acknowledged.

## Nomenclature

| | |
|---|---|
| $a$ | Mass fraction ash |
| $C_0$ | Initial sorbed gas concentration, $cm^3/g$ or scf/ton |
| $C_a$ | Average sorbed gas concentration, $cm^3/g$ or scf/ton |
| $C_b$ | Sorbed gas concentration at the boundary, $cm^3/g$ or scf/ton |
| $C_{Da}$ | Dimensionless sorbed gas concentration |
| $CF$ | Smith and Williams correction factor [eq. (4.5)] |
| $D$ | Diffusion coefficient, $cm^2/min$ |
| $D/r^2$ | Diffusivity, $min^{-1}$ |
| $LTR$ | Smith and Williams lost time ratio [eq. (4.3)] |
| $m$ | Slope of square root of time plot, $cm^3/min^{1/2}$ |
| $mm$ | Mass fraction mineral matter |
| $r$ | Particle radius, cm |
| $S$ | Mass fraction of sulfur |
| $STR$ | Smith and Williams surface time ratio [eq. (4.4)] |
| $t$ | Time, min |
| $t_{25\%}$ | Time to collect 25% of the total desorbed gas volume, min |
| $t_d$ | Time for the chips to travel from the drillbit to the surface, min |
| $t_D$ | Dimensionless time |
| $t_s$ | Time until sample sealing, min |
| $V_{des}$ | Desorbed gas, $cm^3$ |
| $V_L$ | Lost gas, $cm^3$ |
| $V_{LD}$ | Sum of lost plus desorbed gas, $cm^3$ |
| $V_{tot}$ | Smith and Williams total gas emitted, $cm^3$ or scf |

# References


1. Bertard, C. B., Bruyet, B., and Gunther, J. 1970. Determination of desorbable gas concentration of coal (direct method). *International Journal of Rock Mechanics and Mining Sciences*. V. 7. p. 43; and Kissell, F. N., McCulloch, C. M., and Elder, C. H. 1973. *The Direct Method of Determining Methane Content of Coalbeds for Ventilation Design*. U.S. Bureau of Mines. RI 7767.
2. Kissell, F. N., et al. 1973; Smith, D. M., and Williams, F. L. 1981. A new technique for determining the methane content of coal. In *Proceedings of the 16th Intersociety Energy Conversion Engineering Conference*. New York: American Society of Mechanical Engineers. p. 1,272; Chase, R. W. 1979. *A Comparison of Methods Used for Determining the Natural Gas Content of Coalbeds from Exploratory Cores*. U. S. Dept of Energy. METC/CR-79/18; and Metcalfe, R. S., Yee, D., Seidle, J. P., and Puri, R. 1991. *Review of Research Efforts in Coalbed Methane Recovery*. Paper SPE 23025. Presented at the SPE Asia-Pacific Conference, Perth, Australia, November 4–7.
3. Bertard, C. B., et al. 1970; and Kissell, F. N., et al. 1973.
4. Gas Research Institute. 1995. *A Guide to Determining Coalbed Gas Content*. GRI-94/0396. Chicago: Gas Research Institute.
5. Ibid.
6. Ulery, J. P., and Hyman, D. M. 1991. The modified direct method of gas content determination: Application and results. Paper 9163 in *Proceedings of the 1991 International Coalbed Methane Symposium*. Tuscaloosa: University of Alabama.
7. Mavor, M. J., Pratt, T. J., and Nelson, C. R. 1995. *Quantitative Evaluation of Coal Seam Gas Content Estimate Accuracy*. Paper SPE 29577. Presented at the 1995 Joint Rocky Mountain Regional/Low Permeability Reservoirs Symposium, Denver, Colorado, March 20–22.
8. Gas Research Institute. 1995.
9. Ibid.
10. Ibid.
11. Standards Association of Australia. 1991. *Australian Standard AS 3980: Guide to the Determination of Desorbable Gas Content of Coal Seams—Direct Method*. North Sydney, NSW: Standards Association of Australia.
12. Saghafi, A., Williams, D. J., and Roberts, D. B. 1995. *Determination of Coal Gas Content by Quick Crushing Method*. CSIRO Investigation Rep. CET/IR391R.
13. Gas Research Institute. 1995.
14. Scott, A. R. 1994. Composition of coalbed gases. *In Situ*. V. 18 (no. 2). p. 185.
15. Ulery, J. P., and Hyman, D. M. 1991.
16. Pratt, T. J., and Baez, L. R. G. 2003. Critical data requirements for coal and gas shale resource assessment. Paper 0367 in *Proceedings of the 2003 International Coalbed Methane Symposium*. Tuscaloosa: University of Alabama.
17. Mavor, M. J., Owen, L. B, and Pratt, T. J. 1990. *Measurement and Evaluation of Coal Sorption Isotherm Data*. Paper SPE 20728. Presented at the 65th Annual Technical Conference and Exhibition, New Orleans, Louisiana, September 23–26.
18. Bertard, C. B., et al. 1970; and Smith, D. M., and Williams, F. L. 1984. Diffusional effects in the recovery of methane from coalbeds. *Society of Petroleum Engineers Journal*. V. 24 (no. 5). p. 529.
19. Kissell, F.N., et al. 1973.
20. Mavor, M. J., et al. 1990.
21. Kissell, F. N., et al. 1973.
22. Mavor, M. J., et al. 1995.
23. Kissell, F. N., et al. 1973.
24. Bertard, C. B., et al. 1970.
25. Gas Research Institute. 1995.
26. Smith, D. M., and Williams, F. L. 1981.
27. Chase, R. W. 1979.
28. Lee, J., and Wattenbarger, R. A. 1996. *Gas Reservoir Engineering*. Richardson, Texas: Society of Petroleum Engineers.
29. Metcalfe, R. S. et al. 1991.
30. Gas Research Institute. 1995.
31. Mavor, M. J., et al. 1995.
32. Nelson, C. R., Hill, D. G., and Pratt, T. J. 2000. *Properties of Paleocene Fort Union Formation Canyon Seam Coal at the Triton Federal Coalbed Methane Well, Campbell County, Wyoming*. Paper SPE 59786. Presented at the 2000 SPE/CERI Gas Technology Symposium, Calgary, Alberta, April 3–5.
33. Mavor, M. J., et al. 1995.
34. Ibid.
35. Ulery, J. P., and Hyman, D. M. 1991.
36. Ibid.
37. Nelson, C. R., et al. 2000.
38. Mavor, M. J., et al. 1995.
39. Rightmire, C. T., Eddy, G. E., and Kirr, J. N. 1984. *Coalbed Methane Resources of the United States, AAPG Studies in Geology Series #17*. Tulsa: American Association of Petroleum Geologists.
40. Donovan, W. S. 2000. Mudlogging method calculates coalbed gas content. *Oil & Gas Journal*. February 14, 2000. p. 64.
41. Diamond, W. P., and Schatzel, S. J. 1998. Measuring the gas content of coal: A review. *International Journal of Coal Geology*. V. 35 (nos. 1–4). p. 311.

42. Gas Research Institute. 1995.
43. Mavor, M. J., et al. 1995.
44. Mavor, M. J., Pratt, T. J., Nelson, C. R., and Casey, T. A. 1996. *Improved Gas-In-Place Determination for Coal Gas Reservoirs*. Paper SPE 35623. Presented at the Gas Technology Symposium, Calgary, Alberta, April 28–May 1.
45. Ibid.
46. Waechter, N. B. 2003. Personal communication.
47. Kelso, B. S., Leel, W. G., Jr., and Carr, D. L. 1991. Coalbed methane resource and producibility potential of the Rock Springs Formation, Great Divide Basin, Wyoming. In *Coalbed Methane of Western North America*. Schwochow, S. D., Murray, D. K., and Fahy, M. F., eds. Denver: Rocky Mountain Association of Geologists. p. 201.
48. Ibid.
49. Gas Research Institute. 1995.

# Sorption of Gas on Coals 5

## Introduction

Perhaps one of the most distinguishing elements of coals is their storage of gas by sorption. *Sorption*, the attachment of gas molecules to the solid surface of the coal matrix by van der Waals forces, controls coal reservoir behavior much as free gas physics dictates conventional reservoir depletion. Uptake of gas molecules to the coal matrix is sometimes labeled *adsorption*, while release of gas from the surface is sometimes described as *desorption*. In a coal deposit, sorbed gas molecules carpet the coal matrix, forming a monolayer on the surface with a density approaching that of liquid methane. As a result, the coal can store more gas by sorption on the matrix than by compression in the cleats. Coals typically contain more gas per unit volume than sandstone reservoirs at the same temperature and pressure. Sorption is a very effective method of storing gas, resulting in equivalent sandstone porosities on the order of 20% or more.

The amount of gas sorbed by a coal depends on pressure. The gas content–pressure relation for a given coal cannot be predicted from coal properties nor determined by wireline logs and must, therefore, be measured in the laboratory. Various equations have been fit to gas content–pressure data over time, but the most successful is that of Langmuir. While fitting gas content and pressure data to the Langmuir equation is straightforward, measurement of that data in the lab is time consuming and relatively expensive. The question of how many such experiments must be done to characterize a given seam, a given play, or a given basin must be addressed.

The amount of gas sorbed by a coal also depends on temperature. Transformation of the sorption capacity of a given coal measured at one temperature to another is frequently useful in exploration plays, as well as advantageous in reconciling lab data measured at off-reservoir temperatures.

Gas generated by a coal can escape over geologic time, leaving the coal holding less gas than it theoretically could. This condition, termed *undersaturation*, has strong economic ramifications and can be quantified by combining sorption characteristics of the given coal with desorption test results and reservoir pressure.

The opposite case, called *oversaturation*, where a coal appears to hold more gas than is predicted from laboratory measurements, is a physical impossibility. Reasons for such a situation are discussed.

Coals often hold a mixture of gases that is predominantly methane. Assuming this mixture to be only methane allows simplification of the sorption physics, but knowledge of the sorption behavior of the other constituent gas is required for some aspects of coal gas reservoir engineering. Single-component gas content–pressure data are used to predict sorption behavior of the gas mixture rather than measuring sorption behavior of the specific combination of gases.

## Langmuir's Equation

The volume of gas that can be sorbed on a coal depends on pressure and temperature. As a laboratory coal sample is repressured with methane, initial pressure increases result in increased sorbed gas. Further pressure increases yield, decreasing incremental sorbed gas volumes until at sufficiently high pressures, no more gas can be sorbed, as all available coal surface area is carpeted with sorbed gas molecules. At any given pressure, the amount of sorbed gas varies inversely with temperature. Consequently, cooler coals hold more gas, and warmer coals hold less. For purposes of coal gas, the appropriate temperature is reservoir temperature, and the pressure–gas content relationship is called a *sorption isotherm*.

A sorption isotherm, or simply an *isotherm*, for a given coal is measured in a laboratory by readsorbing a gas onto the coal sample or charging a coal sample with gas and measuring the gas content as pressure is reduced. Coal sample preservation and preparation techniques are critically important in order to obtain accurate laboratory test results for all coal reservoir properties, including sorption isotherms.[1] Detailed laboratory procedures for measurement of a sorption isotherm were presented by Mavor et al., Arri et al., and Greaves et al.[2] Sorption isotherms are typically measured with pure component gases rather than gas mixtures. Gas content of coal holding a mixture of gases can be calculated from pure component isotherms and the extended Langmuir equation. As discussed in chapter 10, both free and sorbed gas compositions vary during depletion, something not captured with a mixed gas isotherm.

For reservoir engineering purposes, density of the sorbed gas is usually assumed to be density of the liquid at the atmospheric pressure boiling point. Density of sorbed methane is assumed to be 0.421 g/cm$^3$, while nitrogen is assumed to be 0.808 g/cm$^3$.[3] As carbon dioxide is a solid at its atmospheric pressure boiling point, the density of the saturated liquid at the triple point, 1.18 g/cm$^3$, is commonly used.[4]

Experimental gas content and pressure data for methane gas sorbed on a moist sample of medium-volatile bituminous coal from the San Juan Basin are presented in table 5–1 and plotted in figure 5–1.[5] Initial increases in pressure are accompanied by additional sorbed gas. However, with increasing pressure, fewer and fewer gas molecules can find sorption sites, and the gas content asymptotically approaches a limit of about 700 scf/ton. At infinite pressure, the coal would be completely saturated with a monolayer of sorbed gas. Coal ash, moisture, and rank all affect the amount of gas a coal can hold, and coal deposits are so heterogeneous that even adjacent samples often exhibit different in-situ isotherms. Understanding of sorption behavior of a specific coal is greatly aided by proximate analyses of the isotherm samples.

Equations from various sorption models have been employed to describe experimental coal gas sorption data. Among the most popular are the Langmuir and Freudlich isotherm equations.[6] Interestingly, to date, virtually all experimental sorption data obtained from coals of all ranks and all geologic ages charged with pure gases of interest to coal gas engineering can be described with Langmuir's equation:

$$V = V_L \frac{p}{p + p_L} \tag{5.1}$$

where

$V$ = gas content, scf/ton or cm$^3$/g,
$V_L$ = Langmuir volume constant, scf/ton or cm$^3$/g,
$p$ = pressure, psia or MPaa, and
$p_L$ = Langmuir pressure constant, psia or MPaa.

Consequently, over the years, virtually all coal gas plays have described sorption behavior with the Langmuir equation. This fortuitous circumstance is perhaps due to the fact that Langmuir's equation accurately describes microporous sorption behavior, when sorbent pore dimensions and gas molecule sizes are comparable.

As pressure increases without bound, equation (5.1) indicates gas content approaches $V_L$, the Langmuir volume constant. In a physical sense, the Langmuir volume constant represents the maximum amount of gas that can be sorbed onto the given sample at infinite pressure. When pressure equals the Langmuir pressure constant, $p_L$, gas content calculated from equation (5.1) is ½ $V_L$. Thus, the Langmuir pressure constant represents the *half-saturation pressure*, that is, the pressure at which the coal holds one-half the maximum gas volume.

**Table 5–1.** Fruitland gas content and pressure data

| | Gas Content | |
|---|---|---|
| **Pressure, psia** | **scf/ton** | **cc/gm** |
| 95.4 | 146.5 | 4.57 |
| 203.0 | 242.1 | 7.56 |
| 401.1 | 364.3 | 11.37 |
| 604.4 | 447.1 | 13.95 |
| 802.6 | 505.5 | 15.78 |
| 1002.0 | 548.8 | 17.13 |
| 1201.4 | 589.7 | 18.41 |
| 1401.8 | 621.6 | 19.40 |
| 1598.3 | 654.3 | 20.42 |
| 1798.9 | 682.3 | 21.30 |

*Source:* Hall, F. E., et al. 1994.

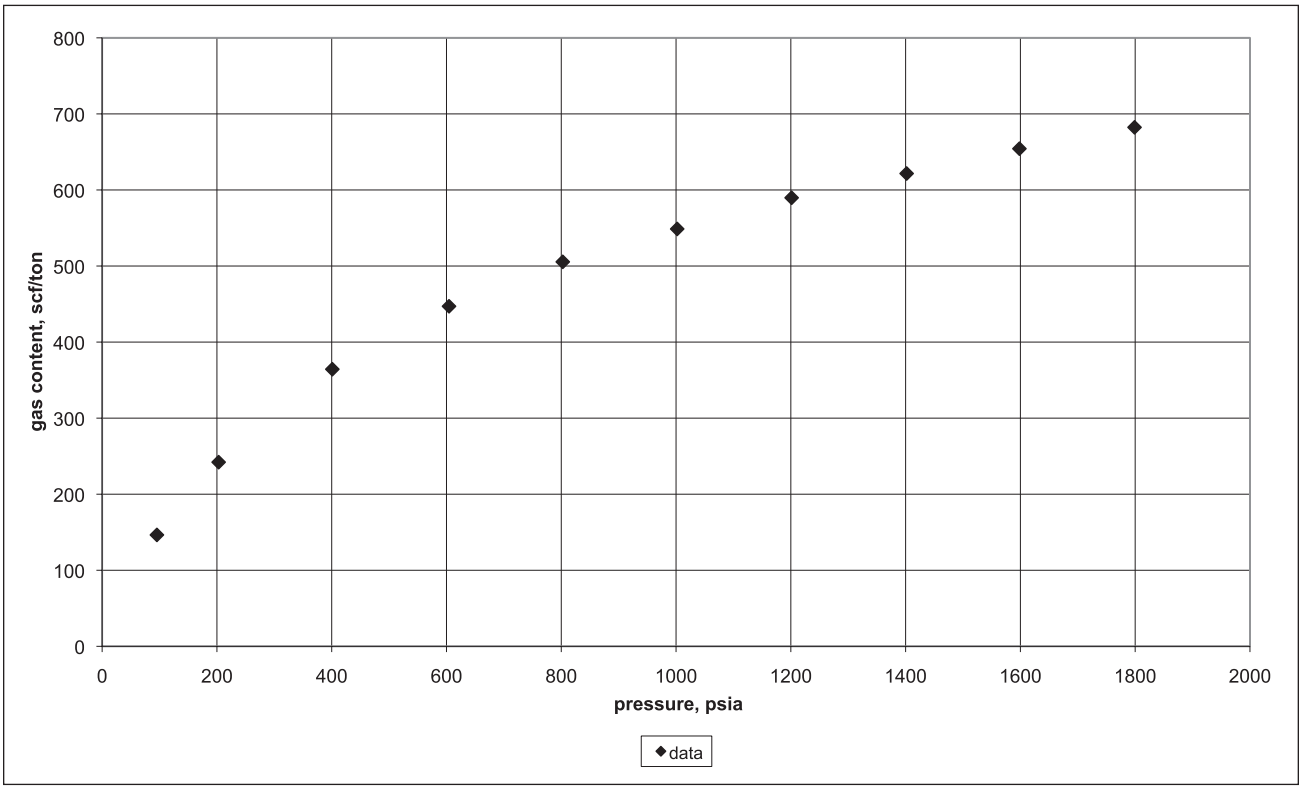



**Fig. 5–1.** Methane sorption data—San Juan Basin, Fruitland coal[7]

Early studies in coalbed methane employed a slightly different form of Langmuir's equation:

$$V = V_L \frac{bp}{1 + bp} \tag{5.2}$$

where

$b$ = the archaic Langmuir pressure constant; the reciprocal of the current Langmuir pressure constant, $p_L$.

While either form of Langmuir's equation describes gas sorption on coal, the form employing $p_L$ usually provides more physical insight.

Determination of Langmuir constants from a given set of sorption data has traditionally been done by fitting the data to a rewritten version of equation (5.1):

$$\frac{p}{V} = \frac{p}{V_L} + \frac{p_L}{V_L} \tag{5.3}$$

The Langmuir volume constant, $V_L$, is the reciprocal of the slope. The pressure constant, $p_L$, is determined by dividing the intercept by the slope. Widespread availability of curve fit routines in various software packages and spreadsheets now permits fitting laboratory data directly to Langmuir's equation. While this is a convenient approach, it loses the visual quality check easily done with the linearized form of equation (5.3). Data of Hall et al., plotted in the linearized form of equation (5.3) in figure 5–2, yields a Langmuir volume constant, $V_L$, of 865.2 scf/ton and a Langmuir pressure, $p_L$, of 536.4 psia.[8] Figure 5–3 repeats the sorption data of figure 5–1 and the fitted Langmuir isotherm.

The relative efficiency of gas storage in coals and sandstones can be illustrated by calculating the equivalent sandstone porosity required to hold the same volume of gas as is sorbed in a coal. Mathematically,

Free gas in pore space = sorbed gas in coal

On a unit volume basis,

$$\phi_{eq} S_{gi} \frac{1}{B_{gi}} = V_L \rho_B \frac{p_i}{p_i + p_L}$$

where

$\phi_{eq}$ = equivalent sandstone porosity, decimal,
$S_{gi}$ = initial gas saturation, decimal,
$B_{gi}$ = the initial gas formation volume factor, ft³/scf,
$\rho_B$ = bulk coalbed density, g/cm³, and
$p_i$ = initial reservoir pressure, psia.

Solving for equivalent porosity,

$$\phi_{eq} = V_L \rho_B \frac{p_i}{p_i + p_L} \frac{B_g}{S_{gi}}$$

Typical temperature and pressure for a north San Juan Basin coal are 110°F and 1,500 psia, respectively, making the gas formation volume factor $9.40(10)^{-3}$ ft³/scf. Assume a bulk density of 1.8 g/cm³ for the coal and an initial gas saturation of 100% in the sandstone.

$$\phi_{eq} = 865.2 \frac{\text{scf}}{\text{ton}} 1.8 \frac{\text{g}}{\text{cm}^3} \frac{1500 \text{ psia}}{1500 + 536.4 \text{ psia}} \frac{9.40(10)^{-3} \frac{\text{ft}^3}{\text{scf}}}{1.00} \frac{\text{ton} - \text{cm}^3}{32.037\text{g} - \text{ft}^3}$$

$$\phi_{eq} = 0.337$$

Thus, a sandstone at this temperature and pressure would require a porosity of almost 34% to contain as much gas as this sample of San Juan Basin coal.

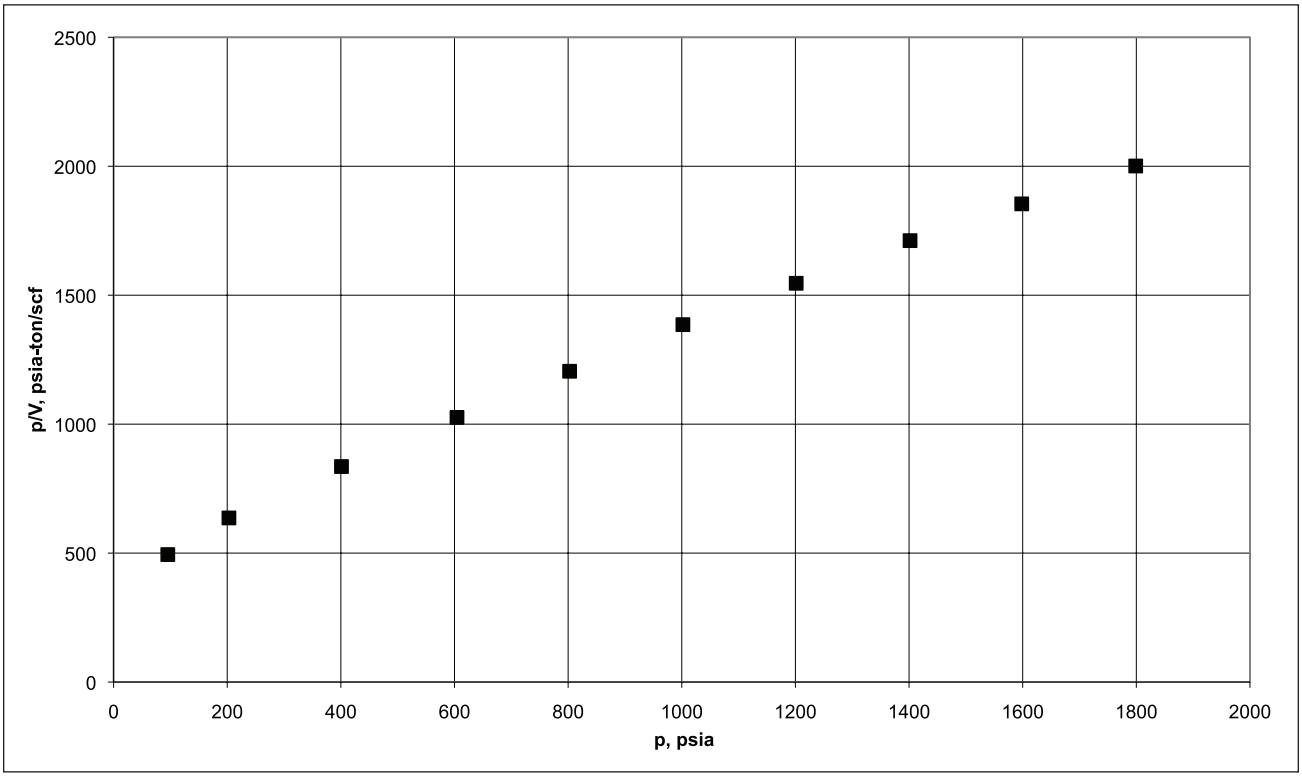



**Fig. 5–2.** Linearized gas content plot[9]

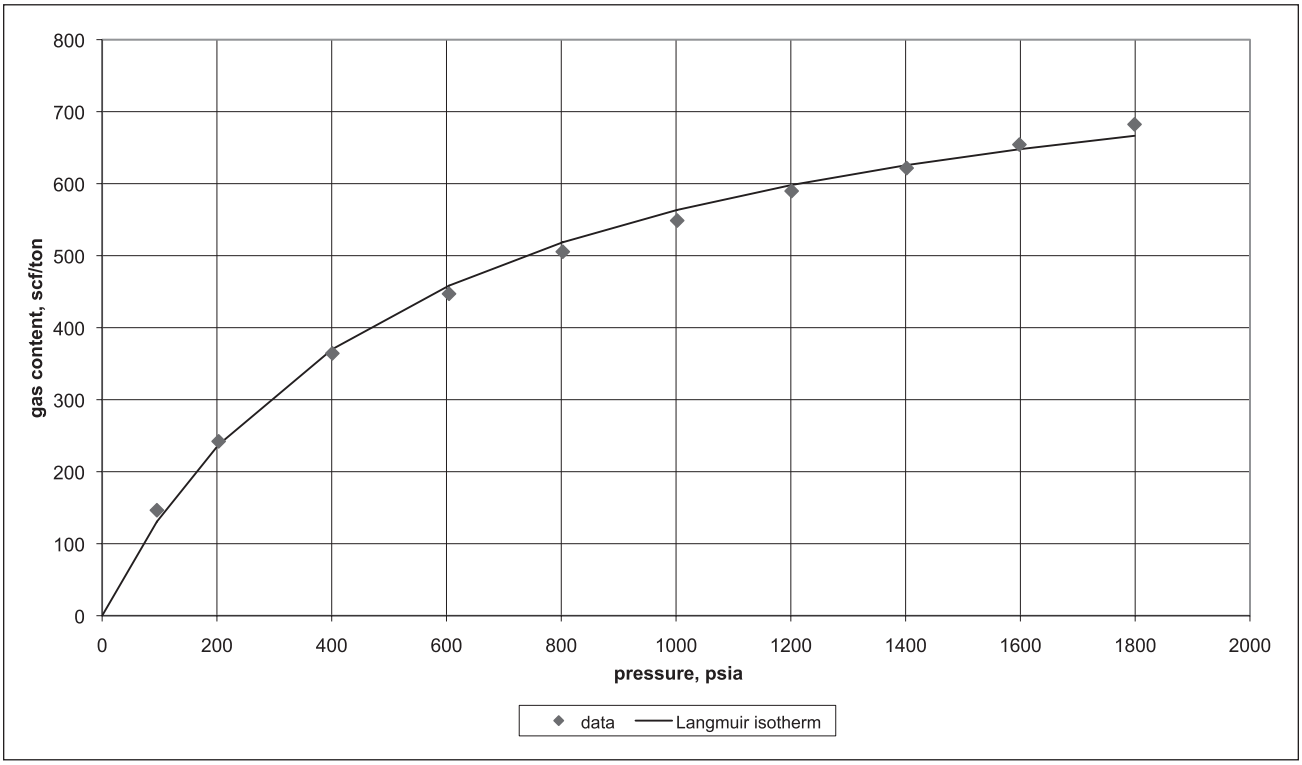



**Fig. 5–3.** Methane sorption data and Langmuir isotherm—San Juan Basin, Fruitland coal[10]

## Effect of Ash and Moisture, Daf and Dmmf Isotherms

Water blocks gas sorption sites, decreasing the volume of gas that can be sorbed at a given pressure. This especially affects low-rank coals, which preferentially sorb water over methane at many sorption sites.[11] Testa and Pratt reported the amount of methane or $CO_2$ held by a subbituminous Powder River Basin coal sample at an unspecified reservoir pressure fell by approximately an order of magnitude or a factor of three, respectively, as moisture content was increased from 3% to 37%.[12] Joubert et al. reported gas content fell as moisture was increased up to equilibrium moisture.[13] Above this critical moisture value, gas sorption capacity was not reduced further. Figure 5–4 depicts methane isotherms measured by Joubert et al. on an Illinois Basin coal at four different moisture contents.[14] Equilibrium moisture for this sample was 9.9%, and sorption above this value, at 10.7% and 14.3% moisture, gave the same isotherm. Figure 5–5 demonstrates the effect of moisture on methane sorption isotherms for a Vermejo coal of unreported rank from the Raton Basin measured by Yee et al. below and above the equilibrium moisture of 3.54%.[15] Again sorption data measured at moisture contents above equilibrium moisture fall on the same isotherm. Consequently, laboratory isotherms should be measured at moisture contents at or above equilibrium moisture to be representative of gas contents at in-situ conditions.

Ash, like moisture, decreases sorption capacity of a coal. Mathematically, the Langmuir volume must be corrected for ash and moisture, but not the Langmuir pressure. Thus, the dry, ash-free (daf) Langmuir volume constant, $V_{Lda}$f, is given by

$$V_{Ldaf} = \frac{V_{Lis}}{(1 - a - w)}$$

where

$V_{Ldaf}$ = dry, ash-free Langmuir volume constant, scf/ton or cm³/g,
$V_{Lis}$ = in-situ Langmuir volume constant, scf/ton or cm³/g,
$a$ = ash mass fraction, and
$w$ = equilibrium moisture mass fraction.

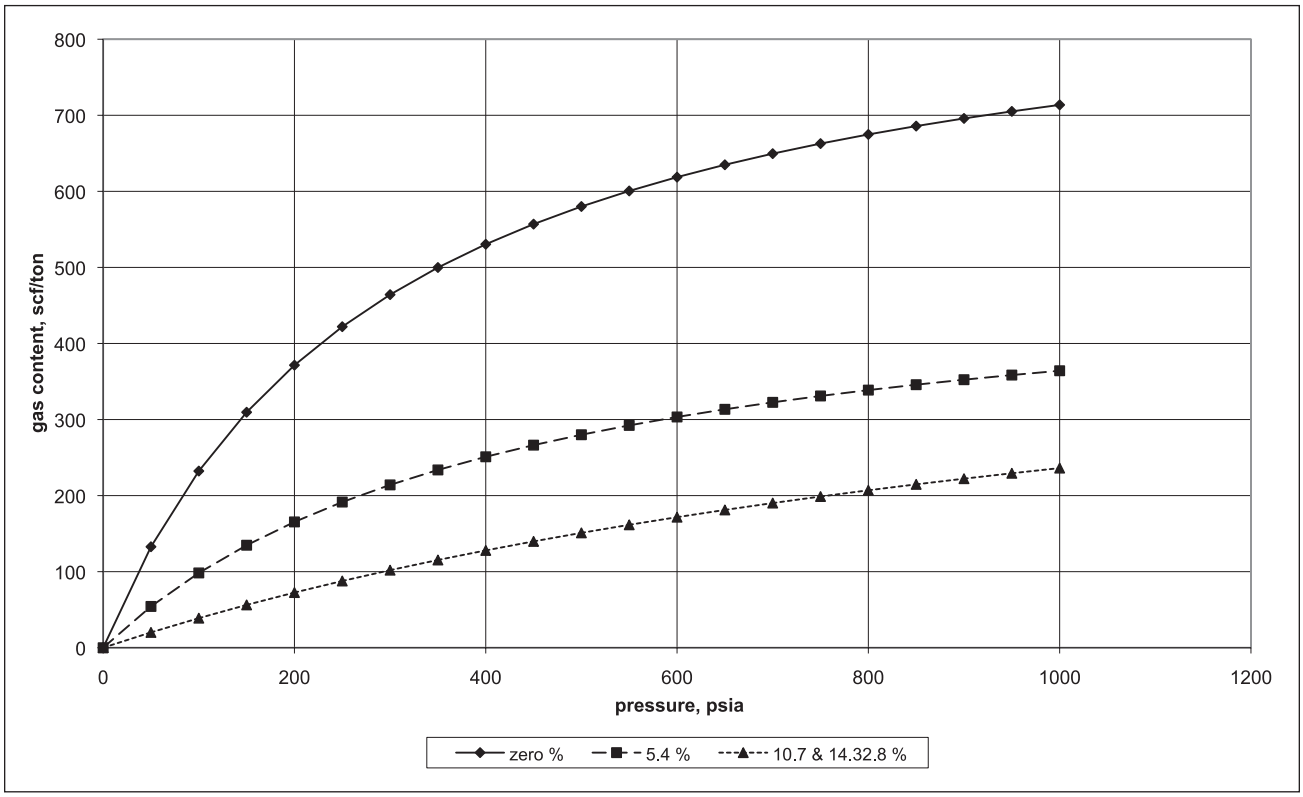



**Fig. 5–4.** Effect of moisture on Illinois no. 6 coal sorption capacity[16]

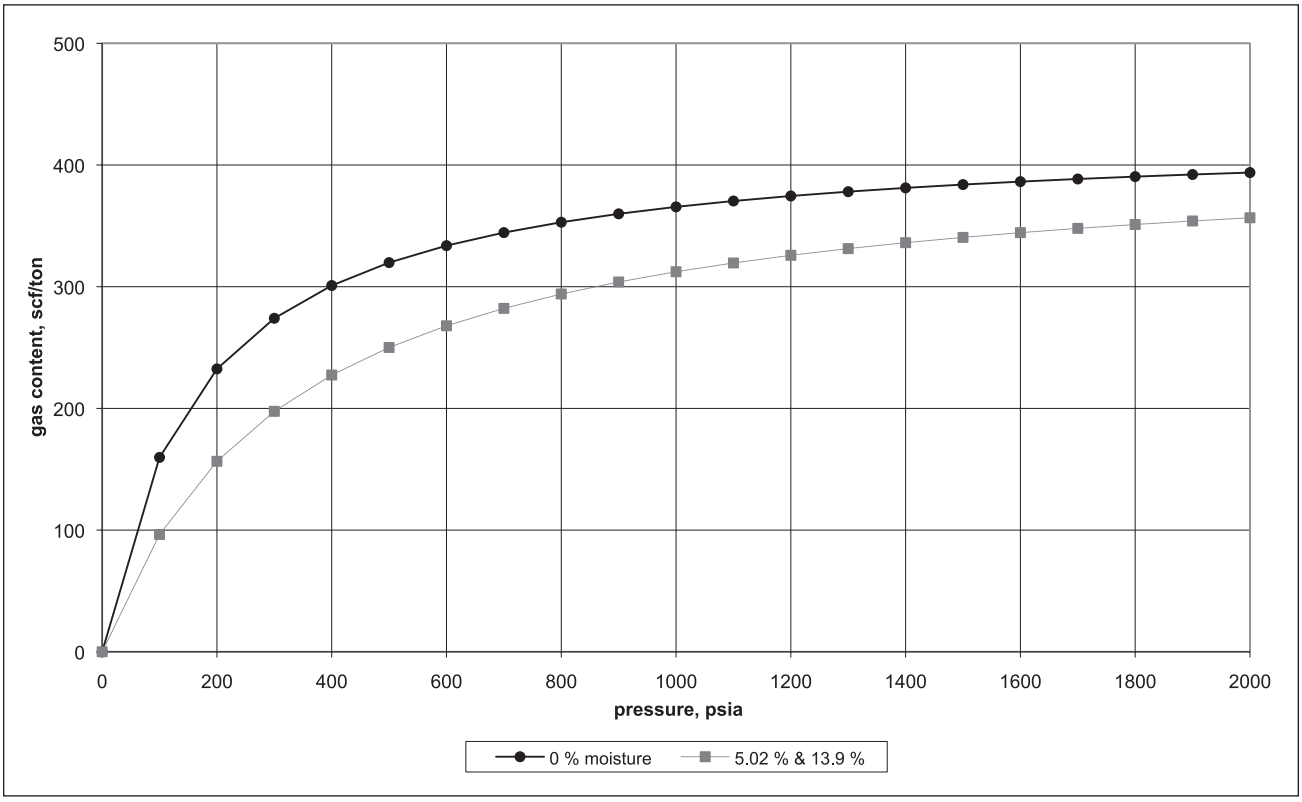



**Fig. 5–5.** Effect of moisture on Raton Basin, Vermejo coal isotherm[17]

Sorption data taken by Hall et al., which was discussed above, was measured on a sample with an ash content of 20.00% and an equilibrium moisture of 2.203%.[18] The dry, ash-free Langmuir volume constant is

$$V_{Ldaf} = \frac{865.2\ \frac{\text{scf}}{\text{ton}}}{(1 - 0.2000 - 0.02203)} = 1{,}112.1\ \frac{\text{scf}}{\text{ton}}$$

The resulting daf isotherm is compared with the data and in-situ isotherm in figure 5–6.

Coals properties can vary from bedding plane to bedding plane. Consequently, even in a single seam, sorption isotherms should be compared on a dry, ash-free or a dry, mineral-matter free (dmmf) basis. If the organic components of a given seam were uniform, all daf or dmmf isotherms from that seam should plot on top of one another. In practice, however, same-seam isotherms vary due both to errors inherent in any laboratory procedure and to the heterogeneous nature of coal. Slight differences in maceral distributions of coal samples, for example, will affect gas storage properties. Nonetheless, comparison of multiple daf or dmmf isotherms from a given project provides a quick quality check on laboratory results. Metcalfe et al. corrected sorption data measured on three samples of unreported rank taken from different wells in the Cedar Hill Field of the San Juan Basin to a dmmf basis.[19] As seen in figure 5–7, all three data sets yielded essentially the same dmmf isotherm.

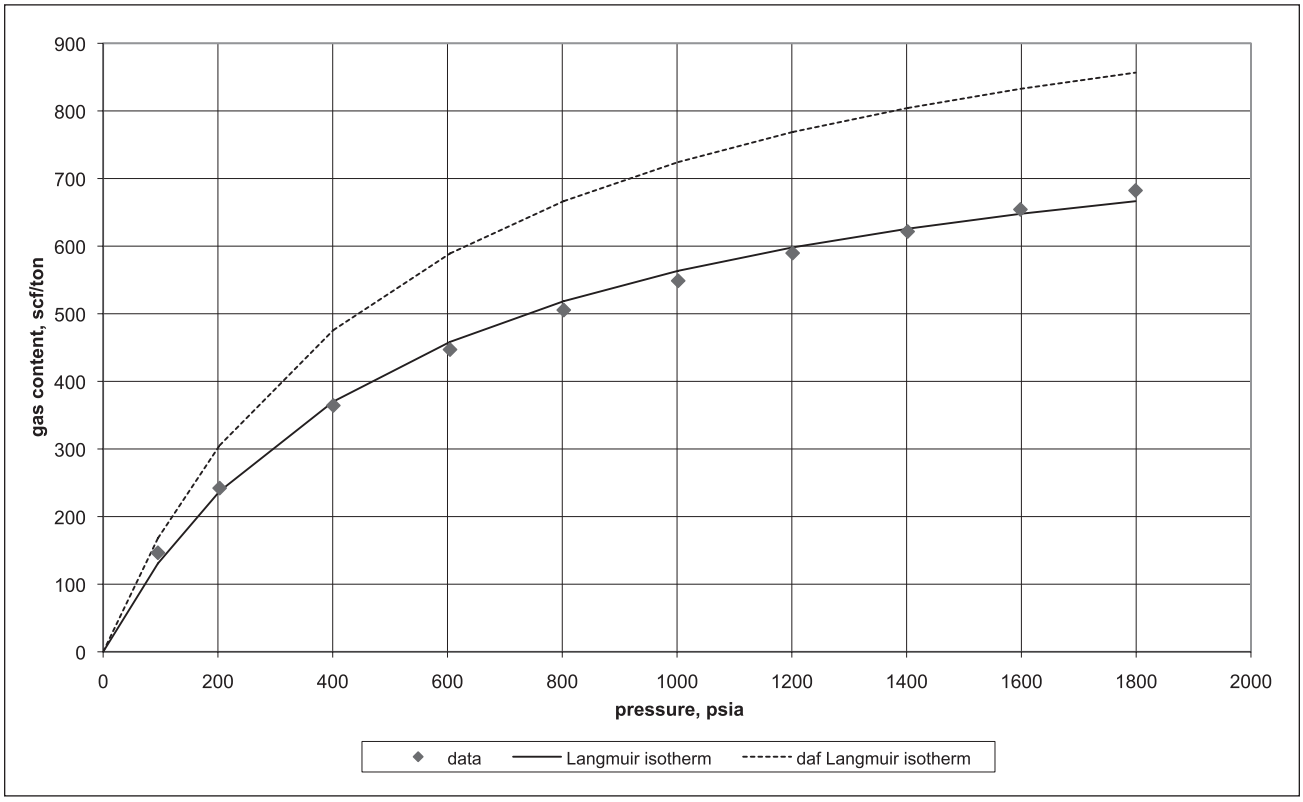



**Fig. 5–6.** Daf and in-situ methane isotherms—San Juan Basin, Fruitland coal[20]

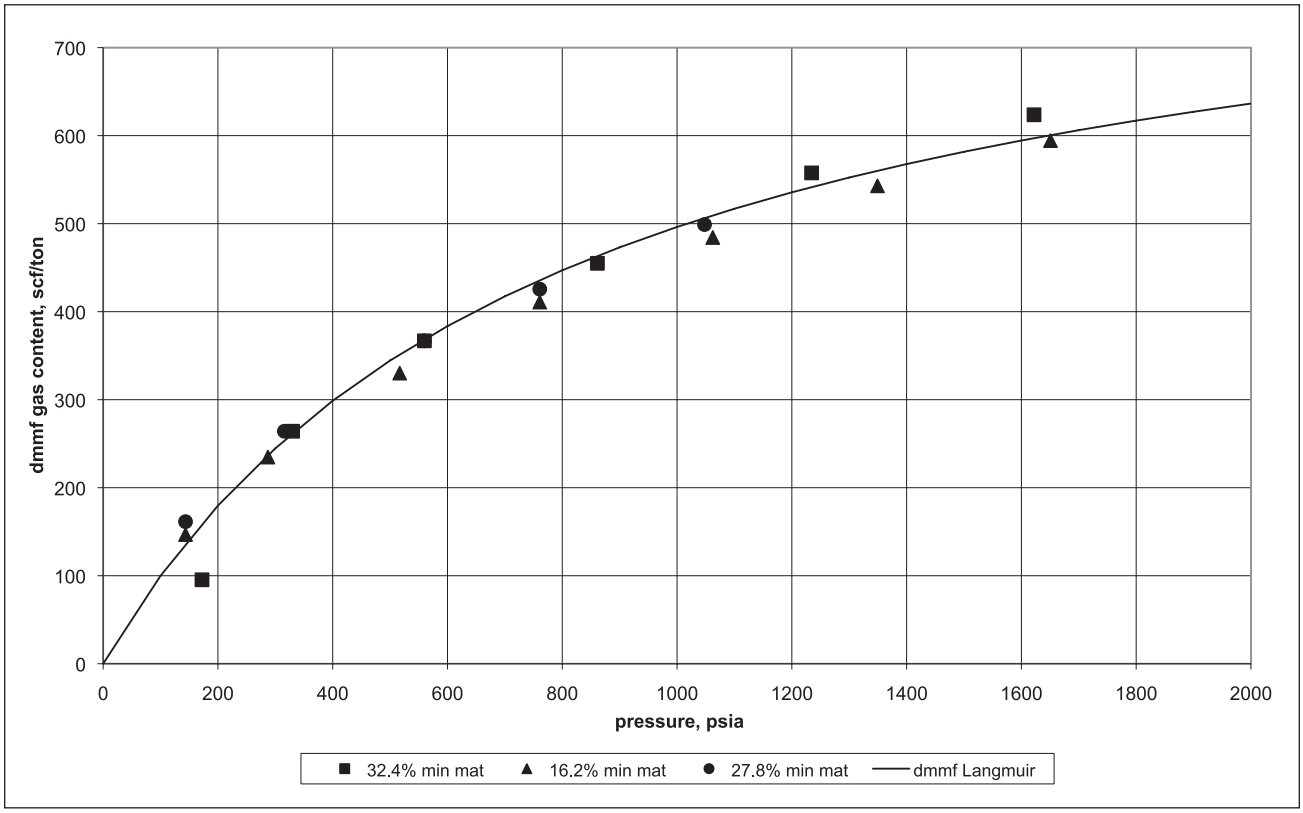



**Fig. 5-7.** Dry, mineral-matter-free Langmuir isotherms—San Juan Basin, Cedar Hill Field[21]

## Effect of Coal Rank on Sorption

Sorption capacity of coals generally increases with rank. Pore structure and size distribution varies with coal rank, and higher rank coals have larger surface areas than low-rank coals, generally allowing them to hold more gas.[22] Dry, ash-free methane sorption isotherms for four coals of various ranks are shown in figure 5–8. At high pressures, the high- and medium-volatile samples from the San Juan Basin hold about four times as much gas as the subbituminous sample from the Powder River Basin. The low-volatile bituminous sample from the Appalachian Basin holds about a one-third more gas than the San Juan samples.

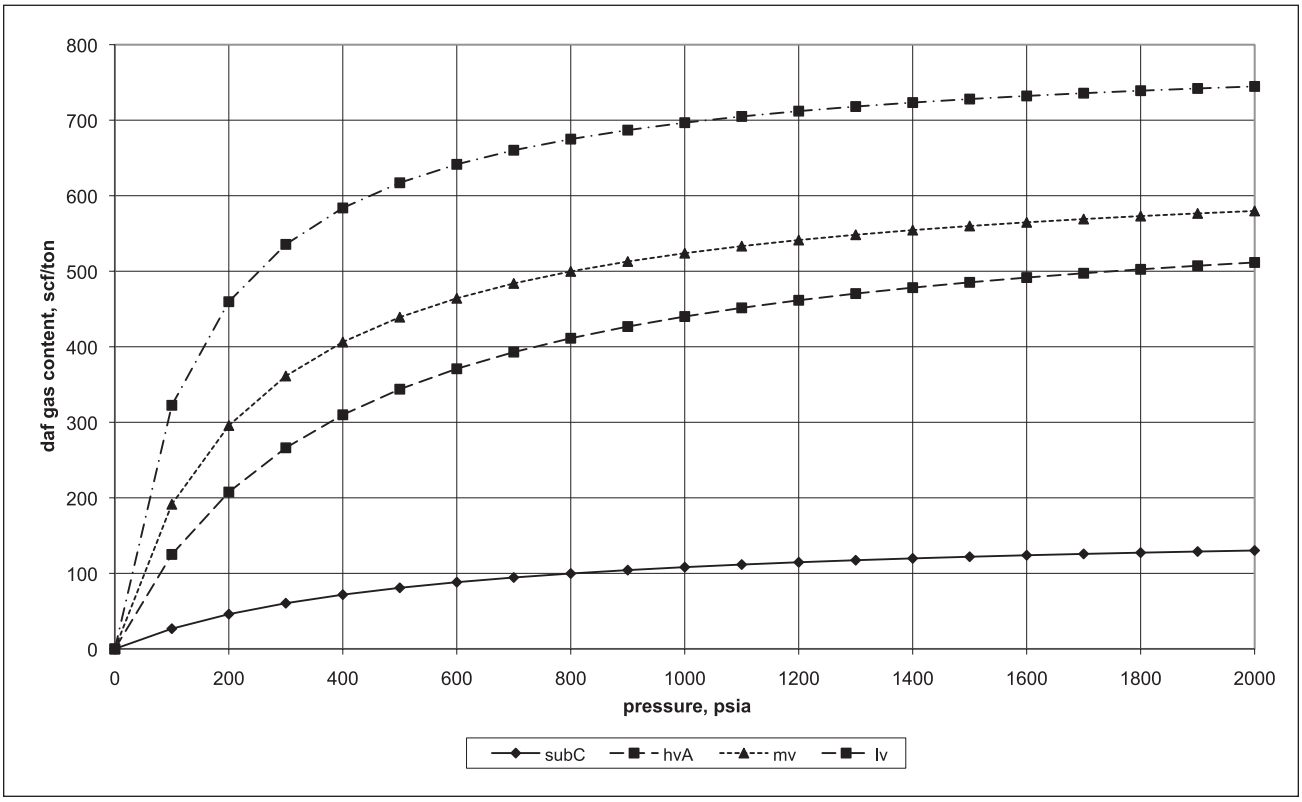



**Fig. 5–8.** Sorption isotherm variation with coal rank[23]

A counter example of this general rule of increasing sorption capacity with rank is seen in figure 5–9, which presents three daf San Juan isotherms.[24] At low pressures, the amount of gas sorbed increases with rank, but at high pressures, sorption capacity of the medium-volatile coal exceeds that of the low-volatile sample. Reasons for this reversal of expected behavior are unknown but are suspected to include maceral composition and pore size distribution.

Levine discussed sorption behavior of dry coals at a pressure of 1,000 atm.[25] The data, measured on coals with ranks ranging from high-volatile bituminous to anthracite, show considerable scatter and were interpreted as showing a minimum in the low-volatile range. It is unclear whether this same trend would be exhibited by in-situ coals.

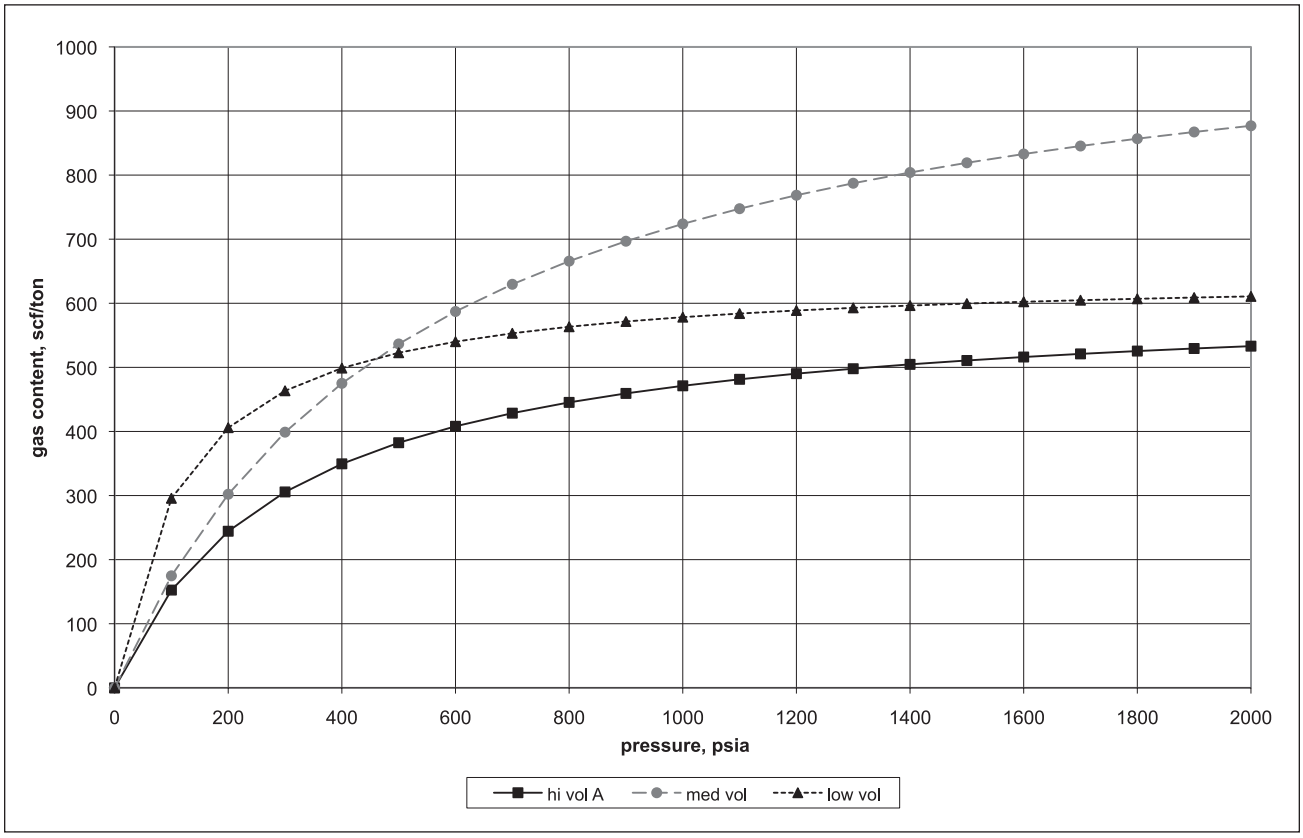



**Fig. 5–9.** Effect of rank on methane daf sorption isotherms—San Juan Basin[26]

## Effect of Temperature on Sorption

Increasing the temperature of a coal decreases the amount of gas it can sorb at a given pressure. Furthermore, the curvature of a sorption isotherm changes with temperature, becoming more concave downward as the coal warms. In practice, coal gas reservoir engineering sometimes requires coalbed gas contents or sorption isotherms at temperatures different than those at which available data were acquired. One such example is the inadvertent measurement of sorption isotherms at off-reservoir temperatures. Another possibility is that the only available gas contents for an exploration prospect are from samples at a cool, shallow depth and must be extrapolated to a hotter, deeper portion of the basin.

The effect of temperature on sorption capacity of a Dietz 3 coal sample from the Powder River Basin was studied by Bustin and Downey.[27] In-situ, not daf, gas contents for a sample at equilibrium moisture were measured at six temperatures, and the results are reproduced here as figure 5–10. Theoretically, at infinite pressure, a coal surface will be saturated with gas, regardless of coal temperature. As seen in figure 5–10, however, at pressures normally encountered in coal gas exploration, reservoir temperature strongly affects gas sorption potential of the coal deposit.

An approximate relation for the effect of temperature on gas content can be developed from experimental work. Boxho et al. reported that for bituminous coal starting at a temperature of 23°C, sorption capacity drops 0.8%/°C.[28] Methane sorption data from Hofer et al., measured on dry samples of high-volatile A bituminous Pittsburgh and low-volatile bituminous Pocahontas coals, indicated gas content decreased an average of 2.2%/°C.[29] Gas contents reported by Bustin and Downey fall at 1%–3%/°C. Thus, as a first approximation, gas content drops about 1%/°C (0.6%/°F). Thus, for a temperature increase of 10°F, gas content drops 6%.

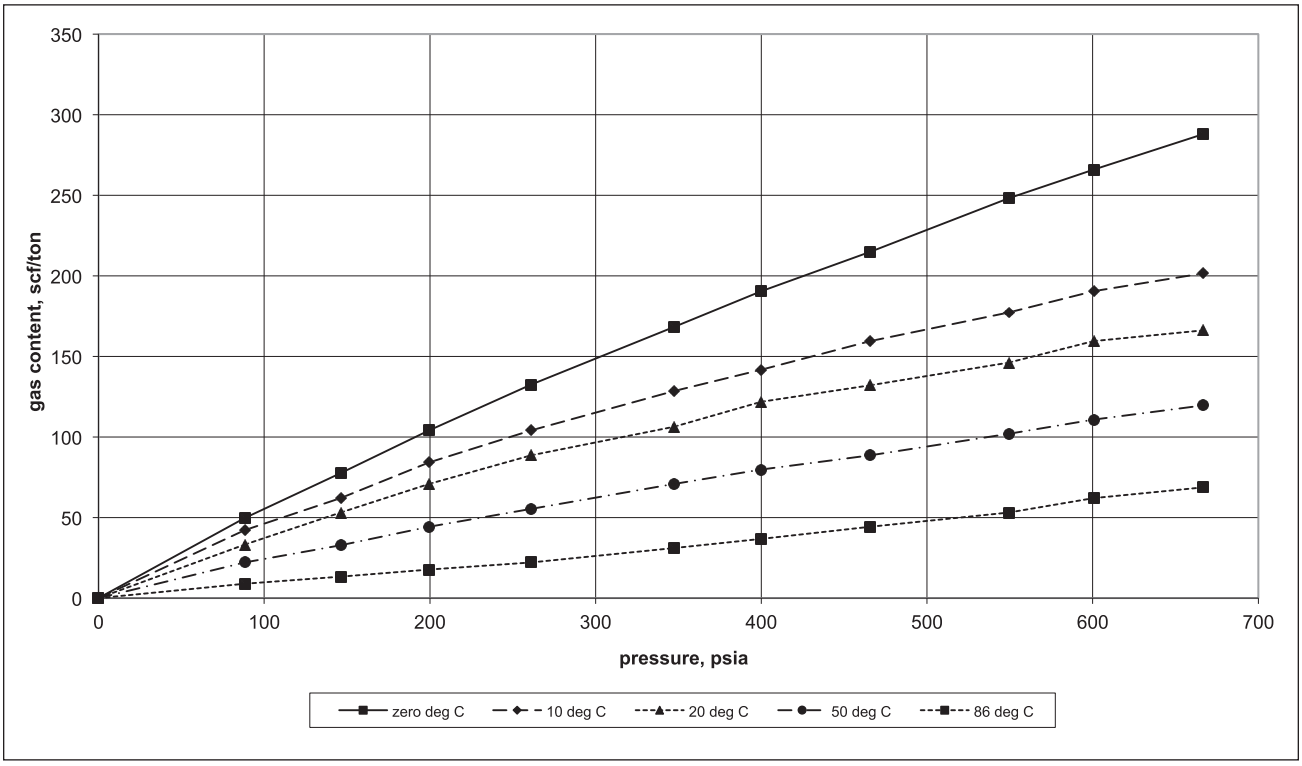



**Fig. 5–10.** Effect of temperature on sorption isotherms—Dietz 3 coal, Powder River Basin[30]

Semiempirical treatments of thermal influences on sorption typically address the Langmuir volume or pressure constants. Ettinger et al. found an exponential relation between coal temperature and the Langmuir volume constant.[31] They developed an equation whereby the Langmuir volume constant of dry coal at a given temperature could be estimated from that at 30°C using empirical temperature coefficients in the exponential arguments. Yee et al. discussed the effect of temperature on the Langmuir pressure constant but neglected the Langmuir volume constant.[32] Heats of sorption required by the Yee formulation were measured by Hofer et al. for two dry Appalachian coals.[33]

Theoretical treatment of the effect of temperature on coalbed gas content requires a different conceptual model of sorption. In contrast to the Langmuir theory of sorption, in which the sorbed gas is assumed to be a monolayer coating the surface of the coal, Dubinin theory assumes the sorbed gas fills the micropores of the coal.[34] Based upon this theory, two equations have been developed that account for the effect of temperature on sorbed gas volumes. Both the Dubinin-Radushkevich equation,

$$W = W_0 \exp\left[ -\left( \frac{RT}{\beta E} \ln \frac{p}{p} \right)^2 \right] \quad \textbf{(5.4)}$$

and the Dubinin-Astakhov equation,

$$W = W_0 \exp\left[ -\left( \frac{RT}{\beta E} \ln \frac{p_s}{p} \right)^n \right]$$

where

$W$ = sorbed gas volume, cm$^3$/g,
$W_0$ = volume of micropores, cm$^3$/g,
$R$ = universal gas constant, psi-ft$^3$/lb-mole-°R,
$T$ = absolute temperature, °R,
$\beta$ = sorbate affinity coefficient, dimensionless,
$E$ = characteristic energy, psi-ft$^3$/lb-mole,

$p_s$ = saturation vapor pressure, atm,
$p$ = pressure, atm, and
$n$ = a small integer, typically between 1 and 4,

exhibit a declining exponential relationship between sorbed gas volume and temperature. As the temperature of many coal seams is above the critical temperatures of gases sorbed on them, the concept of vapor pressure is ill-defined. There are two relations for the saturation vapor pressure at temperatures exceeding the critical temperature. The first is the Dubinin equation[35]

$$P_s = p_c \left( \frac{T}{T_c} \right)^2 \tag{5.5}$$

where

$p_c$ = critical pressure, atm, and
$T_c$ = critical temperature, °R.

The second equation is the reduced Kirchoff equation[36]

$$p_s = p_c \exp\left[ \ln p_c \left( \frac{T_{nbp}}{T_c - T_{nbp}} \right) \frac{T - T_c}{T} \right] \tag{5.6}$$

where

$T_{nbp}$ = normal boiling point temperature, °R.

Note that equation (5.6) requires critical pressure be in units of atmospheres. At the time of this writing, validity of the above expressions for saturation vapor pressure for coal gas sorption physics has not been addressed.

The above relations enable correction of isotherms and coalbed gas contents to another appropriate temperature. Experimental sorption data are used to evaluate the two constants of the Dubinin-Radushkevich equation ($W_0$ and the product $\beta E$) or the three constants of the Dubinin-Astakhov equation ($W_0$, the product $\beta E$, and the exponent $n$), followed by calculation of gas contents at the desired temperature and pressures. The following example applies the Dubinin-Radushkevich equation to the Powder River Basin coals studied by Bustin and Downey.[37]

### Example 5.1. Temperature effects on sorption isotherms—Dietz 3 coal, Powder River Basin

As noted above, Bustin and Downey reported sorption capacity of the Dietz 3 coal of the Powder River Basin at selected temperatures.[38] Using data taken at 20°C, sorption capacity at 10°C and 50°C can be estimated and compared with the reported isotherms. Saturation vapor pressures are calculated with both the Dubinin and reduced Kirchoff equations using methane properties[39]

$$T_{nbp} = 201°\text{R}$$

$$T_c = 344°\text{R}$$

$$p_c = 673 \text{ psia} = 45.78 \text{ atm}$$

At 20°C (528°R), saturation vapor pressure from the Dubinin relation, equation (5.5), is

$$p_s = 45.78 \text{ atm} \left( \frac{528°\text{R}}{344°\text{R}} \right)^2 = 107.86 \text{ atm}$$

Saturation vapor pressure from the reduced Kirchoff equation is

$$p_s = 45.78 \text{ atm} \exp\left[ \ln 45.78 \text{ atm} \left( \frac{201°\text{R}}{344 - 201°\text{R}} \right) \frac{528 - 344°\text{R}}{528°\text{R}} \right]$$

$$p_s = 45.78 \text{ atm}$$

Gas contents calculated from Bustin and Downey's isotherm at 20°C were fit to the Dubinin-Radushkevich equation using both saturation pressures to determine the two constants in equation (5.4). Results are summarized in table 5–2, and gas contents plotted in figure 5–11. In spite of the Dubinin and reduced Kirchoff saturation vapor pressures differing by a factor of almost three, both appear to work well for this coal at this temperature.

**Table 5–2.** Calculated and measured gas contents—20°C

| 20 deg C = 68 deg F = 528 deg R | | Dubinin | Reduced Kirchoff |
|---|---|---|---|
| ps = saturation vapor pressure, atm | ps = | 107.86 | 297.96 |
| Wo = volume of micropores, cc/gm | Wo = | 6.0 | 8.5 |
| βE = energy constant, psi-ft$^3$/lb-mole | βE = | 11,705.5 | 15,018.3 |

| Pressure, psia | Gas content, scf/ton | P, pressure, atm | Gas content, cc/gm | Calculated gas content, cc/gm | Calculated gas content, cc/gm |
|---|---|---|---|---|---|
| 0.0 | 0.0 | 0.0 | 0.00 | 0.0 | 0.0 |
| 88.3 | 33.2 | 6.0 | 1.04 | 0.9 | 1.0 |
| 146.0 | 53.2 | 9.9 | 1.66 | 1.6 | 1.6 |
| 199.5 | 70.9 | 13.6 | 2.21 | 2.2 | 2.2 |
| 261.0 | 88.6 | 17.8 | 2.77 | 2.8 | 2.8 |
| 347.4 | 106.3 | 23.6 | 3.32 | 3.5 | 3.4 |
| 400.0 | 121.8 | 27.2 | 3.80 | 3.9 | 3.8 |
| 465.7 | 132.0 | 31.7 | 4.12 | 4.2 | 4.2 |
| 549.3 | 146.2 | 37.4 | 4.56 | 4.6 | 4.6 |
| 600.5 | 159.5 | 40.8 | 4.98 | 4.8 | 4.9 |
| 666.7 | 166.1 | 45.4 | 5.19 | 5.0 | 5.2 |

*Source:* Bustin & Downey data

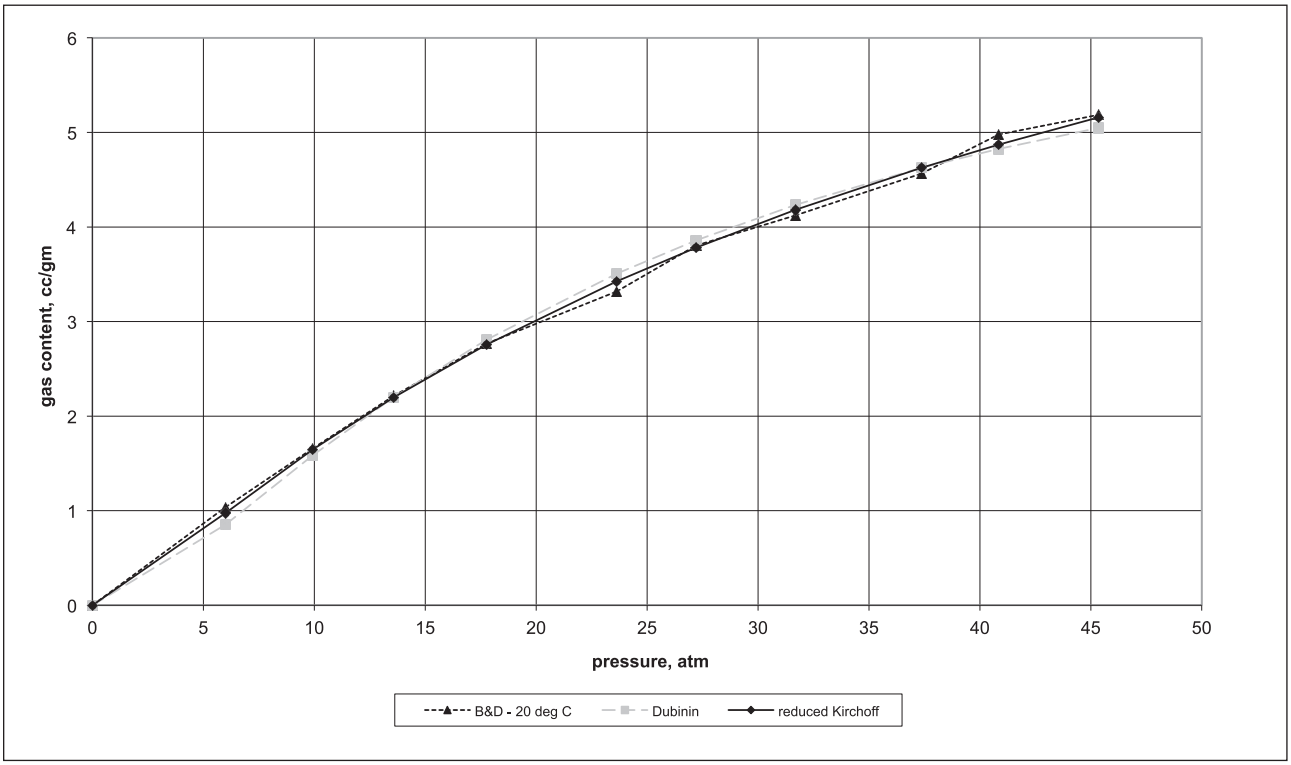



**Fig. 5–11.** Comparison of reported and calculated isotherms—20°C[40]

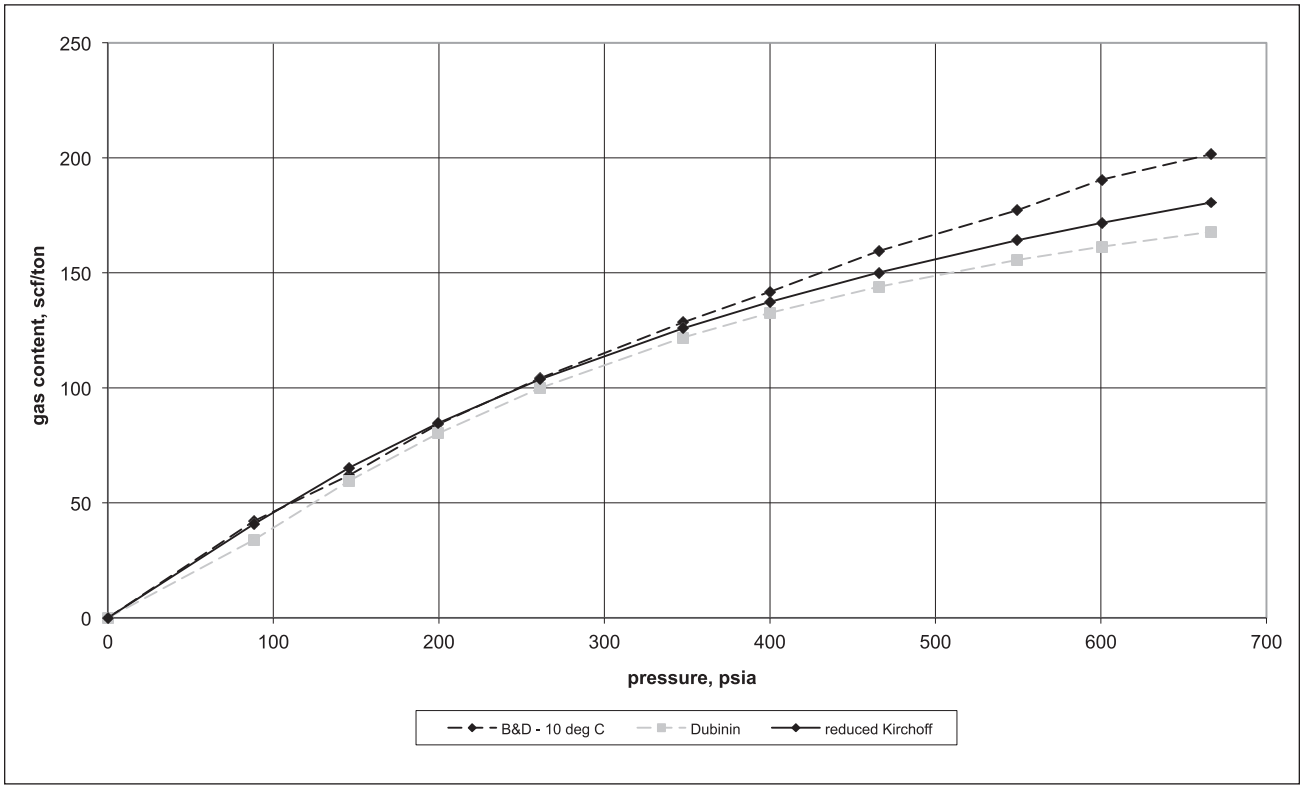



**Fig. 5–12.** Comparison of reported and calculated isotherms—10°C[41]

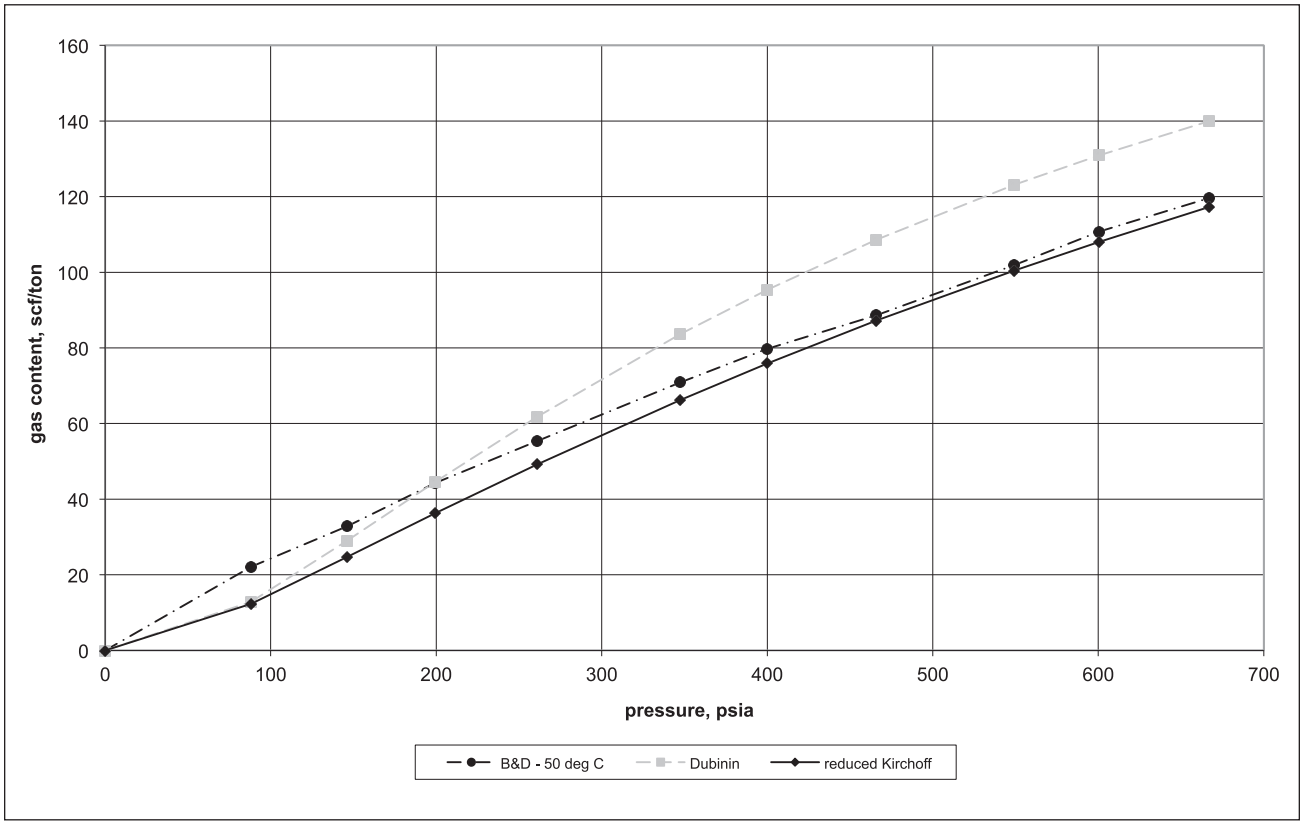



**Fig. 5–13.** Comparison of reported and calculated isotherms—50°C[42]

Gas contents at 10°C were estimated from equation (5.4) using micropore gas volumes and energy constants obtained from fitting the 20°C data. Reported and calculated gas contents are shown in figure 5–12. Gas contents based on either saturation vapor pressure, Dubinin or reduced Kirchoff, are in good agreement with reported values at low pressures. Above 400 psia, calculated gas contents fall below measured values, with the reduced Kirchoff saturation vapor pressure yielding more accurate gas contents than that of Dubinin.

Repeating the exercise for 50°C, calculated and reported gas contents are in figure 5–13. Regardless of the saturation pressure employed, plots of gas contents from the Dubinin-Radushkevich equation show unrealistic flexure at low pressures. Again, the reduced Kirchoff saturation vapor pressure relation gave more accurate results than did that from the Dubinin equation.

## Number of Isotherms Required

One of the most difficult questions in developing a coal gas project is the number of isotherms required for accurate characterization. Sorption isotherms are often internally consistent, and only when compared with other relevant isotherms is any discrepancy apparent. Avoiding the simplistic answer of measuring isotherms until one is no longer surprised, this discussion begins with the observation that the number of isotherms required depends on the number of targeted coal seams and their areal extent compared to that of the project. The question of how many isotherms are necessary can be broken into three parts. First, the number of isotherms to characterize a single seam will be considered. This will be followed by consideration of multiple seams in a single well and will conclude with the number of isotherms to characterize a project and a basin.

### Number of isotherms to characterize a single seam

The most direct case is when only a single seam is being exploited. As discussed above, Metcalfe et al. found a single dmmf isotherm described sorption behavior of basal Fruitland coal samples taken from three unnamed wells in the Cedar Hill Field.[43] Two daf methane sorption isotherms for this seam in this field reported by Mavor et al. are compared with the dmmf isotherm of Metcalfe et al. in figure 5–14.[44] The isotherms from Mavor et al. were measured on two samples of high-volatile A bituminous coal from a depth of 2,880 ft in the Hamilton #3 well. Both studies measured isotherms at the reservoir temperature, 115°F, but reported results on slightly different bases. Metcalfe et al. reduced data to a dmmf basis, while Mavor et al. reported data on a daf basis. Neither study supplied sufficient information to convert from one basis to the other, but as San Juan coal is a low-sulfur coal, the two bases are roughly equivalent. In this instance, five samples provided a band of isotherms sufficiently accurate to characterize a single seam for reservoir engineering purposes.

Methane sorption isotherms measured on two samples taken from the Canyon coal seam of the Powder River Basin are plotted on a daf basis in figure 5–15.[45] The close agreement between the two daf isotherms samples is ascribed to the very uniform character of Powder River Basin coals (the samples were separated by roughly one mile) and meticulous field and laboratory procedures.

In conclusion, a practical rule of thumb is that a minimum of three dry, ash-free isotherms in good agreement will be necessary to characterize a given coal seam. Variation in depositional setting and postcoalification history will affect the areal extent to which these isotherms are applicable.

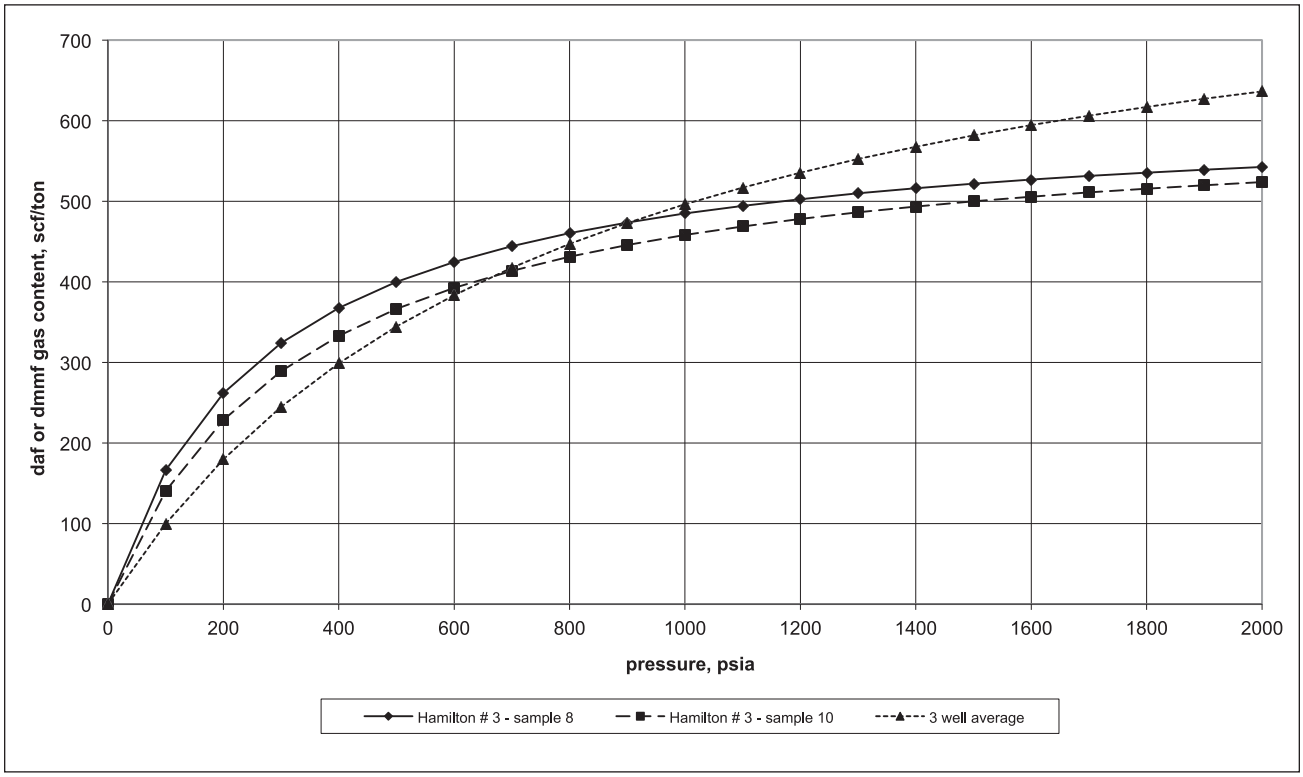



**Fig. 5–14.** Isotherm variation in a single seam—Basal Fruitland coal, Cedar Hill Field, San Juan Basin[46]

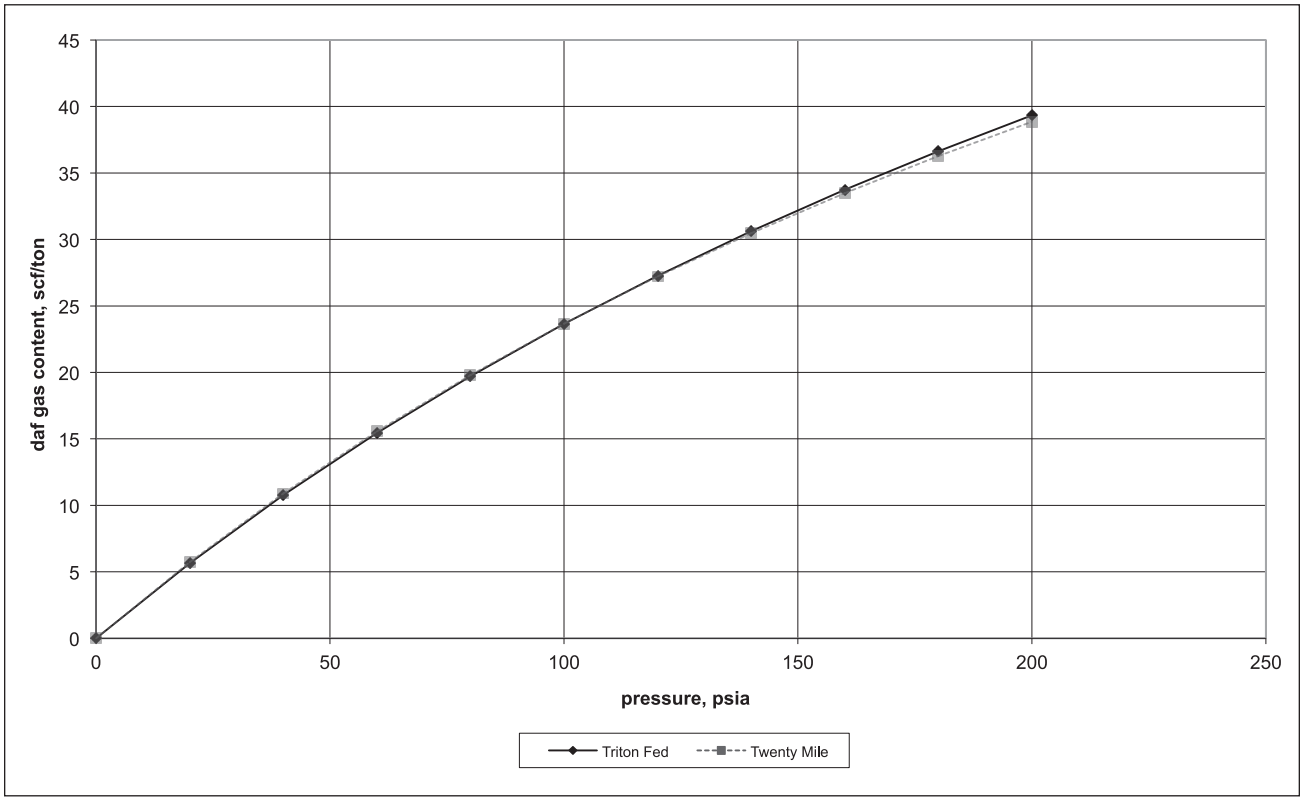



**Fig. 5–15.** Daf methane sorption isotherms—Canyon coal, Powder River Basin [47]

## Number of isotherms to characterize multiple seams

Coal wells are frequently completed in more than one seam, yet calculation of original gas in place, recovery factors, and reserves are overly simplified by characterizing all seams with a single isotherm. Such a simplification is valid when differences in in-situ sorption capacity are minimal due to coal seams with roughly the same maturity and little variation in coal ash content, quality, and depth.

Mavor et al. reported isotherms from samples taken from depths of 876 and 943 ft in the USM #1 well, an Appalachian Basin coal well.[48] As the samples were of the same rank, low-volatile bituminous, and were from seams only 67 ft apart, it is not surprising the isotherms, displayed in figure 5–16, are similar. Use of a single isotherm to describe sorption behavior in both seams is clearly justified.

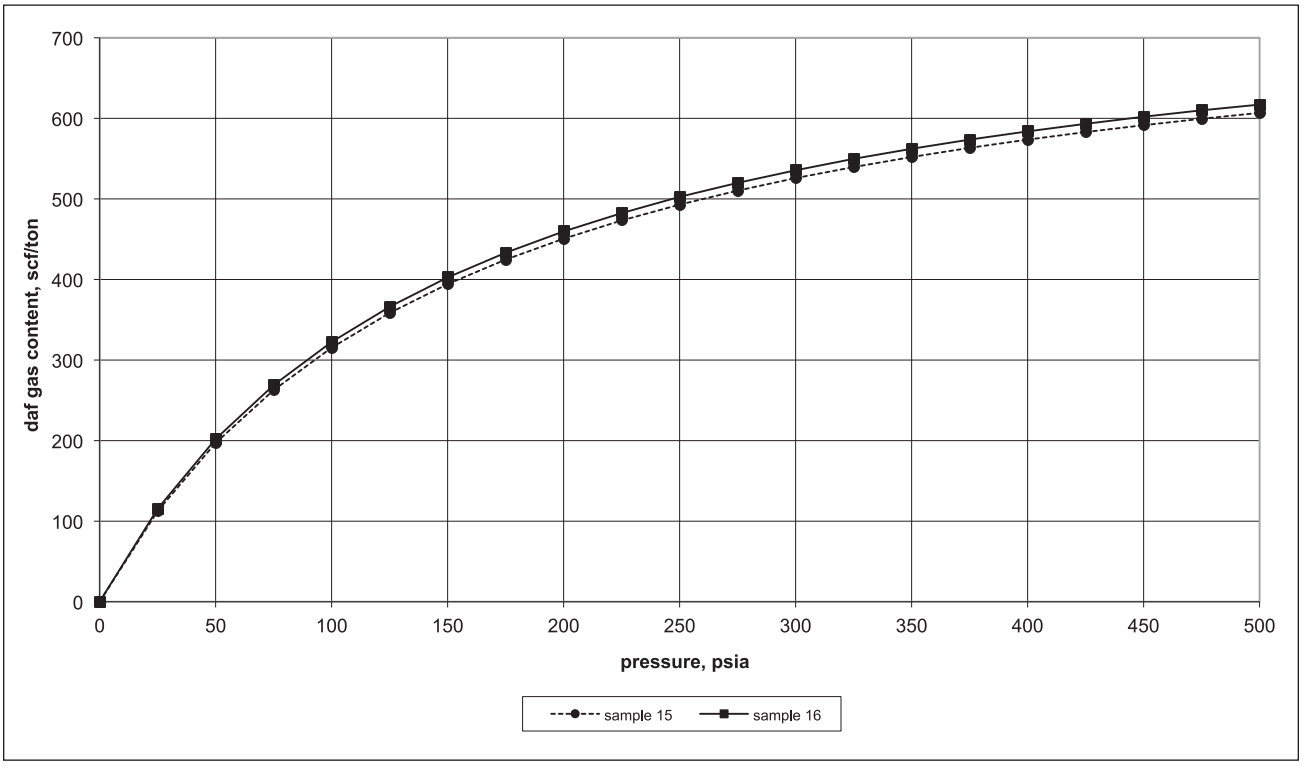



**Fig. 5–16.** Isotherm variation between seams—USM#1 well, Appalachian Basin, West Virginia[49]

Contrast this with the daf isotherms from the CO 3277-9 well in the San Juan Basin, shown in figure 5–17.[50] Both samples were low-volatile bituminous in rank and differed in depth by only 39 ft, yet the daf gas contents at a reservoir pressure of 1,200 psia differ by nearly 30%.

A third example of multiseam isotherms comes from the Hamilton #3 well studied by Mavor et al.[51] In addition to the isotherms discussed above, an isotherm was also measured on an uphole coal at a depth of 2,677 ft. This isotherm is plotted in figure 5–18 along with those from figure 5–14. As seen in the figure, the daf isotherms of the two seams differ little, even though the seams are separated by 203 ft.

To properly characterize the gas resource in a multiseam coal well completion, isotherms should be measured for every coal seam of interest. Timing of sorption isotherm measurements can vary from the initial exploration phase of prospect development to full-field development and depends on the degree of uncertainty with which the operator is comfortable. A good rule of thumb for condensing isotherms from multiple seams into a single average isotherm is when isotherm variation between seams is less than isotherm variation within the seams themselves.

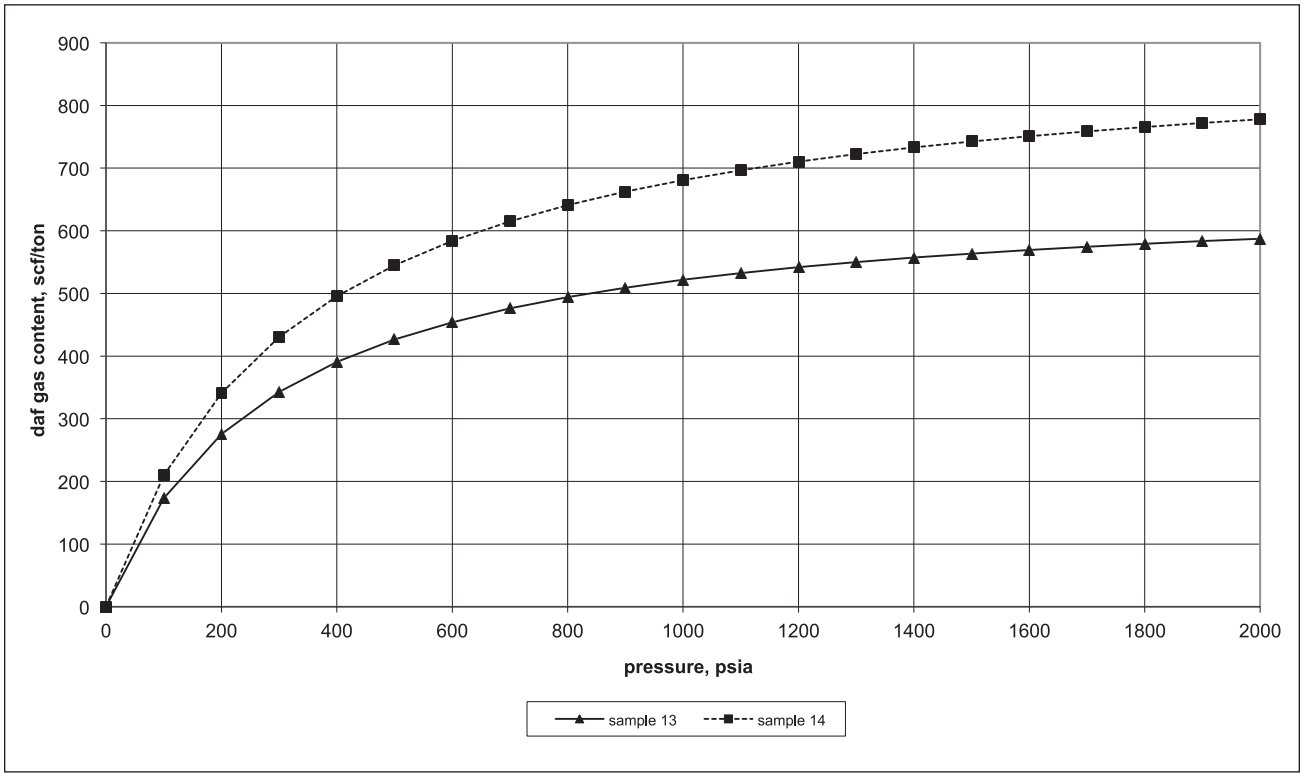



**Fig. 5–17.** Isotherm variation between seams—CO 3277-9 well, San Juan Basin[52]

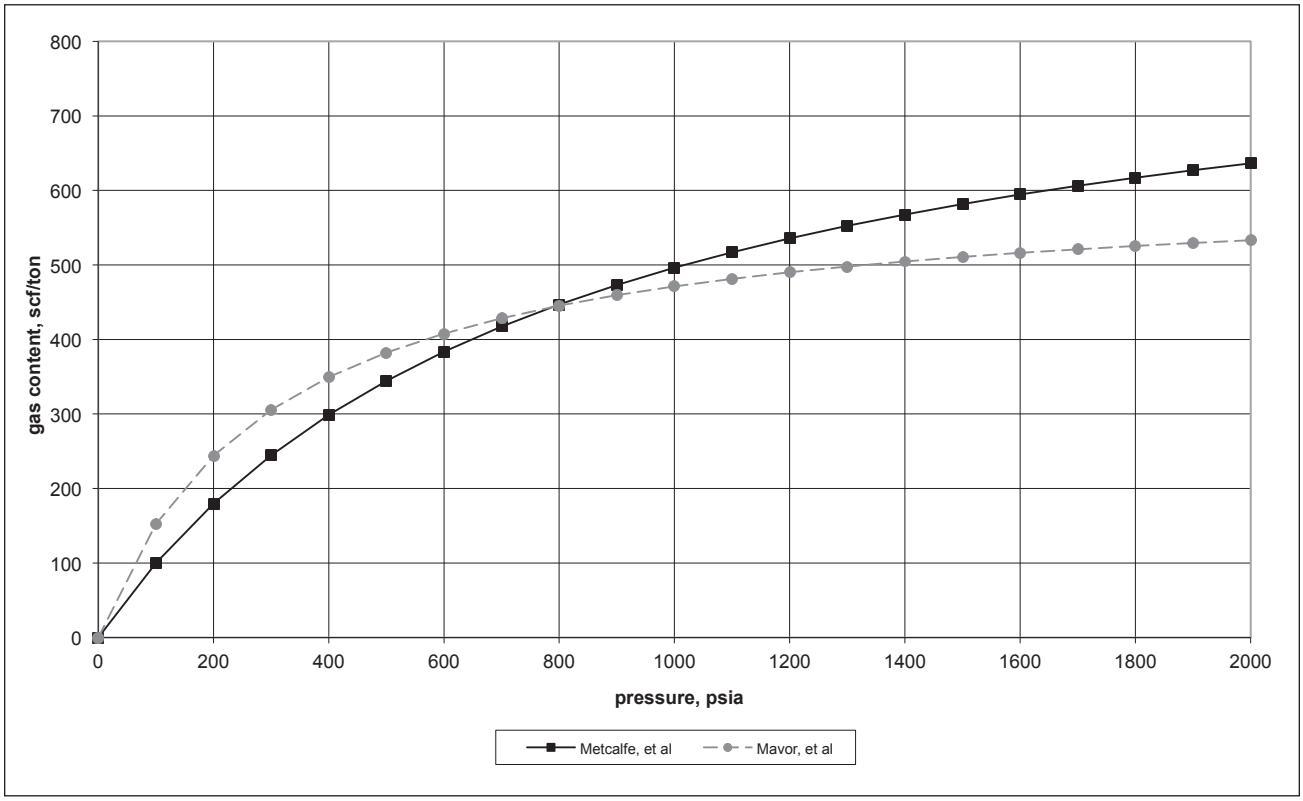



**Fig. 5–18.** Methane isotherms—Cedar Hill Field, San Juan Basin[53]

### Number of isotherms to characterize a project

The number of isotherms necessary to characterize a project depends on its geologic complexity. As an example of a single-seam project, consider the Cedar Hill Field in San Juan County, New Mexico, where the basal Fruitland coal is being produced. As noted above, Metcalfe et al. reported three dmmf isotherms for this field, and all three collapsed to the same daf isotherm.[54] The Hamilton #3 well, studied by Mavor et al., is also from this field.[55] The Metcalfe isotherm and average Hamilton isotherm are plotted in figure 5–18. At initial reservoir pressure, 1,600 psia, gas content of the Metcalfe et al. isotherm is 15% higher than that of the Mavor et al. isotherm. Gas contents of the two isotherms are nearly equal when reservoir pressure has been halved to 800 psia. At 200 psia, current reservoir pressure of many San Juan fairway wells, gas content of the Mavor isotherm is 36% higher than that of the Metcalfe isotherm. The Cedar Hill Field has been studied extensively, and great care was taken in measuring the isotherms reported here. The wells were separated by two to three miles, and differences in the daf isotherms are ascribed to lateral variation across the coal deposit. Dry, ash-free isotherms for a given project often vary by 25% to 30%, and volumetric gas in place, recovery factor, and estimated ultimate recovery calculations should reflect this variation.

A project with multiple coals seams, complicated structure, or rank and coal quality variations will require substantially more than the five isotherms measured for the basal Fruitland coal of the San Juan Basin discussed above. Conversely, measurement of only a few isotherms from exploration wildcats probing a complicated coal deposit can provide bewildering results. To reflect the uncertainty in the gas resource of such a prospect, bounding calculations for maximum and minimum gas in place or through Monte Carlo simulations are often useful.

### Number of isotherms to characterize a basin

Isotherms vary a great deal over any given basin, reflecting coal deposit heterogeneity. Attempts to characterize an entire basin with a single isotherm are as foolhardy as they are frequent. However, rank exploration plays frequently have only one isotherm available for estimation of the coal gas resource. The three examples discussed below illustrate isotherm variation between formations within a basin and across a basin.

As an example of isotherm variation between formations, consider coals of the Raton Basin, which occur primarily in the Raton and Vermejo formations. Coals in both formations were formed from deposits in floodplains and swamps following a retreating sea.[56] Coals of the overlying Raton Formation are relatively thinner and less laterally extensive than the older, more thermally mature Vermejo coals. Hydrologies, and hence reservoir pressures, are distinctly different in the two formations. Currently, most commercial coal wells in the basin are completed in Vermejo coals. Generic in-situ isotherms for coals of both formations are shown in figure 5–19.[57] Note that at 1,000 psia, a Vermejo coal sorbs 50% more gas than does a Raton coal, illustrating the need for separate isotherms for separate formations.

Coals of the Powder River Basin were laid down in a fluvial environment in Paleocene time and are nearly all subbituminous in rank. An average Powder River coal isotherm was calculated by Crockett and Meyer for the east-central Powder River Basin.[58] Individual isotherms used to construct the average isotherm were not identified, but high and low isotherms that were "one standard deviation" off the average were also calculated. All three isotherms are plotted in figure 5–20. The high and low isotherms differ from the average isotherm at any given pressure by roughly 30%. Although these three isotherms were developed for the eastern margin of the Powder River play, current indications are that for reservoir engineering purposes, they can be used for many seams across the basin in the absence of specific isotherms.

The majority of coal gas produced in the United States has been produced from the San Juan Basin, and many public domain sorption isotherms are available for the Fruitland coals of this basin. Eleven in-situ methane isotherms reported for San Juan Fruitland coals are collected in figure 5–21, with location and isotherm details given in table 5–3. This collection is not meant to be exhaustive but rather illustrative of the variation of Fruitland coal sorption characteristics across the basin. Coal rank and quality variations across the basin are reflected in the fourfold difference in sorption capacity of the Fruitland coal.

As a general rule, for a basin of even moderate complexity, over a dozen isotherms are required to adequately capture basinwide sorption behavior.

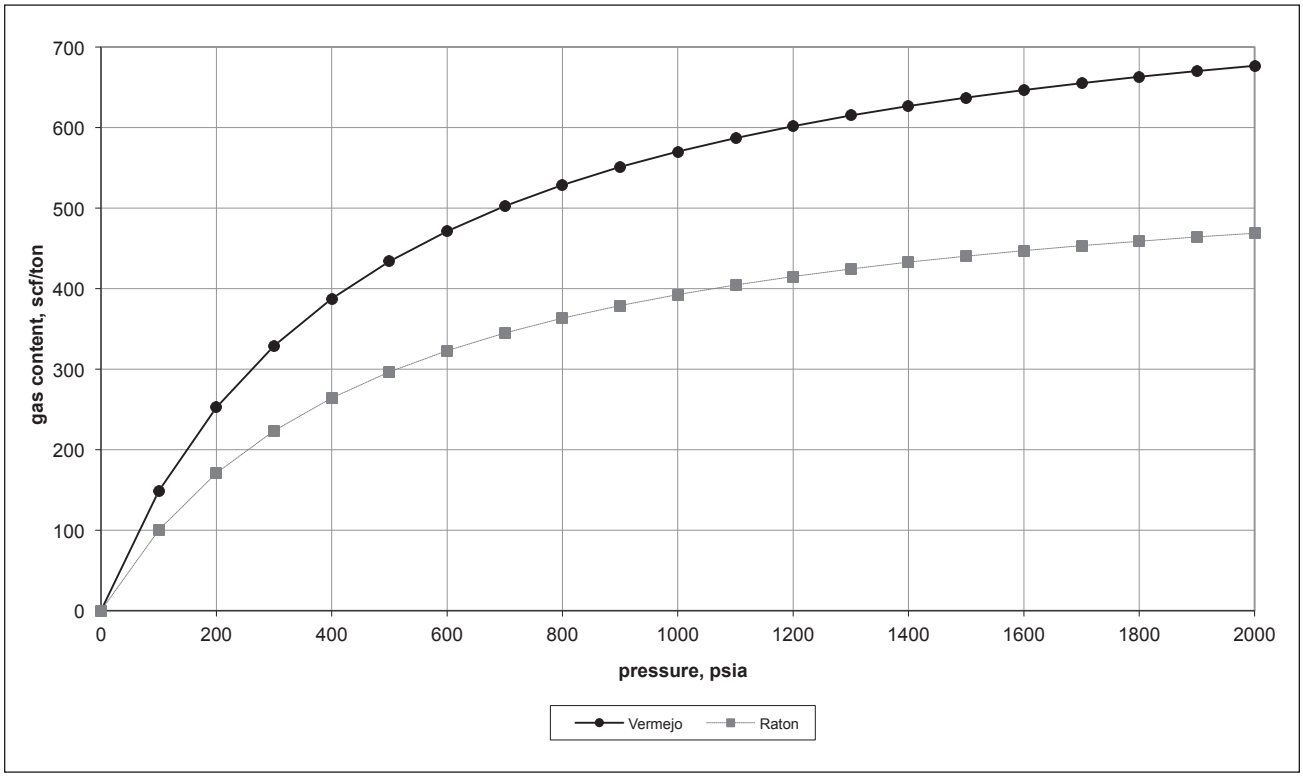



**Fig. 5–19.** Isotherm variation between Vermejo and Raton formations—Raton Basin[59]

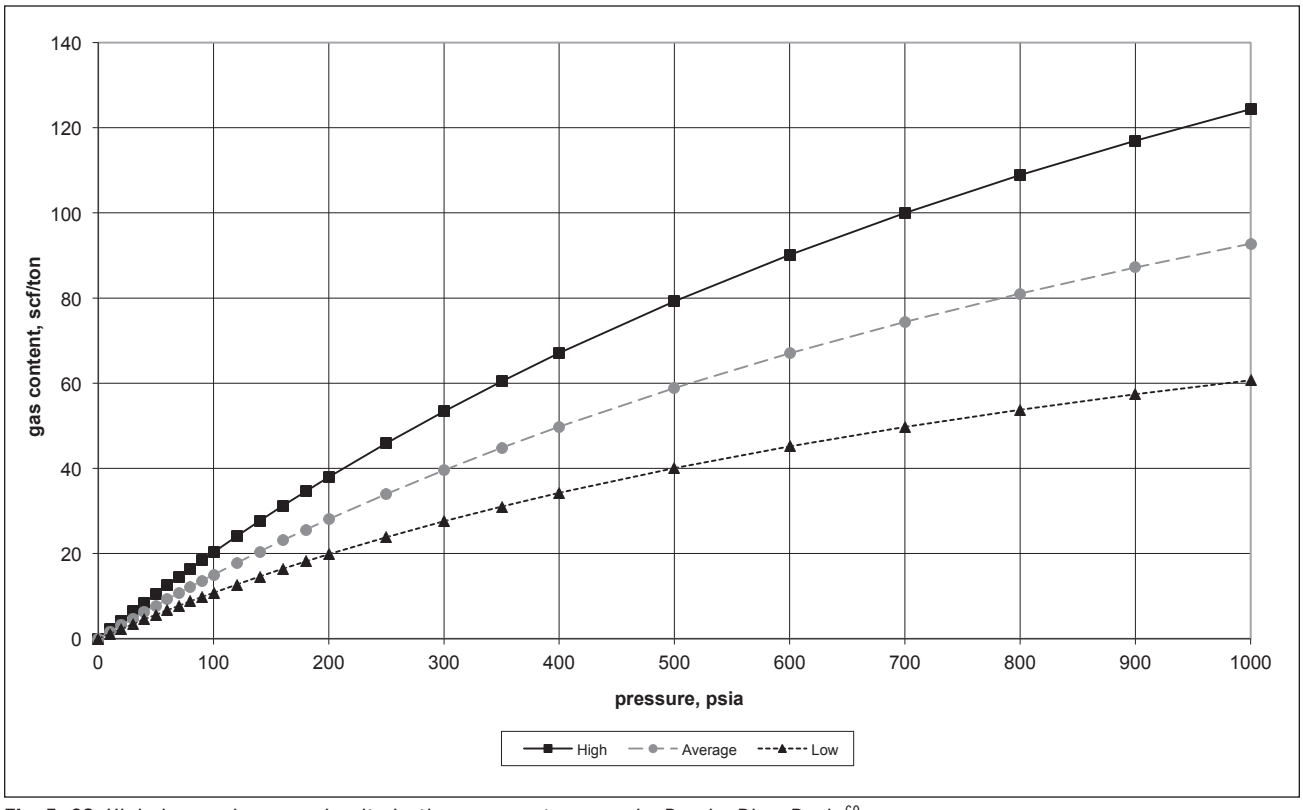



**Fig. 5–20.** High, low, and average in-situ isotherms—eastern margin, Powder River Basin[60]

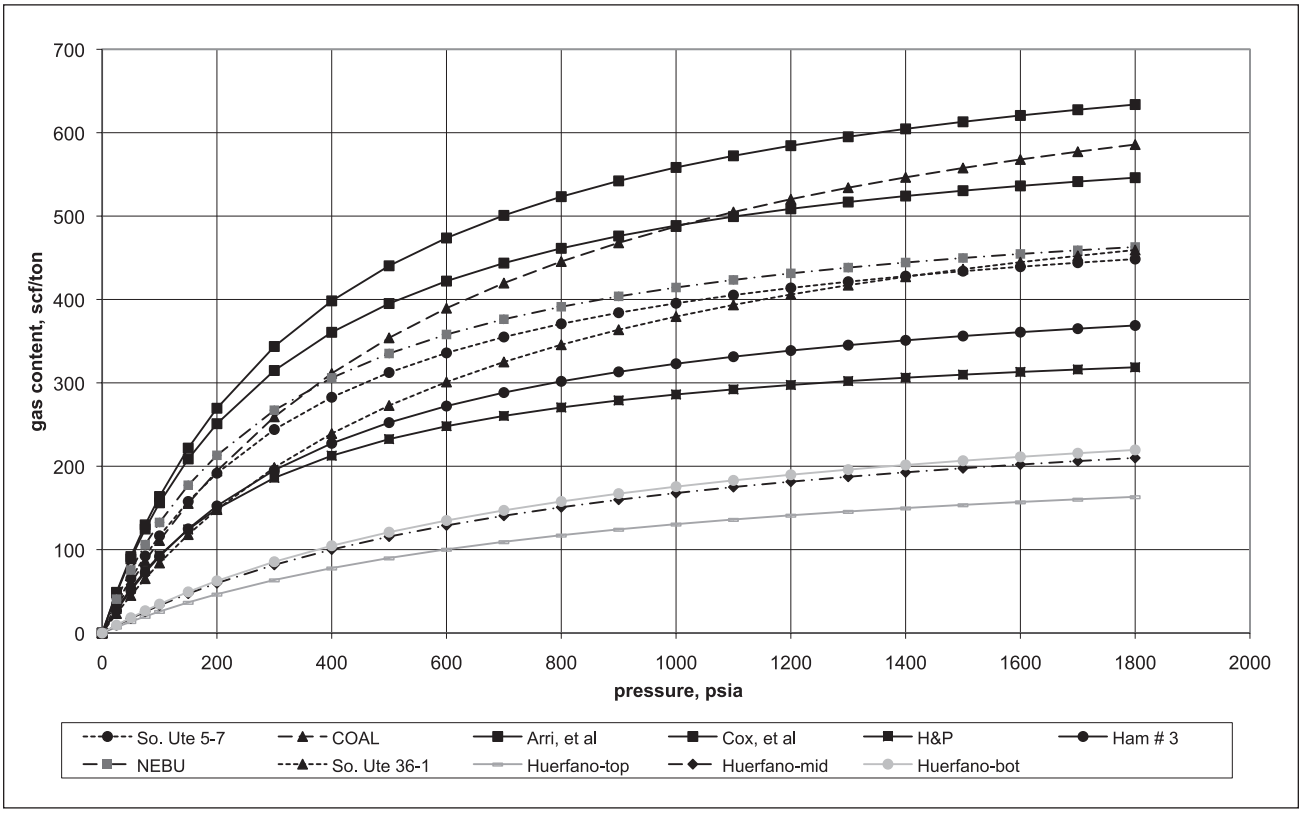



**Fig. 5–21.** In-situ methane isotherms—Fruitland coal, San Juan Basin

**Table 5–3.** Isotherm data—San Juan Basin, Fruitland coal

| Seq no. | Isotherm ID | $V_{L\,is}$, scf/ton | $p_L$, psia | Ash, % | Moisture, % | Rank | Temp, °F | Sec | T | R |
|---|---|---|---|---|---|---|---|---|---|---|
| 1[a] | So Ute 5-7 | 538.7 | 362.2 | 21.00 | 1.91 | na | 108 | 7 | 32N | 11W |
| 2[b] | COAL | 783 | 606 | na | na | na | 120 | 17 | 32N | 11W |
| 3[c] | Arri, et al. | 762.6 | 365.8 | 18.12 | 2.27 | mv | 115 | na | na | na |
| 4[d] | Cox, et al. | 640.1 | 310 | na | na | na | na | na | na | na |
| 5[e] | H&P | 371.6 | 299 | na | na | na | 112 | na | na | na |
| 6[f] | Ham # 3 | 611 | 388.5 | 21.71 | 4.90 | hvA | 115 | 30 | 32N | 10W |
| 7[g] | NEBU | 756.4 | 309 | 23.49 | 4.80 | hvA | 110 | 9 | 30N | 7W |
| 8[h] | So. Ute 36-1 | 623.1 | 641.8 | 8.57 | 7.41 | mv | 125 | 36 | 34N | 10W |
| 9[j] | Huerfano-top | 238 | 823 | na | na | na | na | 36 | 27N | 10W |
| 10[j] | Huerfano-mid | 306 | 823 | na | na | na | na | 36 | 27N | 10W |
| 11[k] | Huerfano-bot | 320 | 823 | na | na | na | na | 36 | 27N | 10W |

*na = not available*

[a]Mavor, M. J., et al. 1995. [b]Young, G. B. C., Kelso, B. S., and Paul, G. W. 1994. *Understanding Cavity Well Performance*. Paper SPE 28579. Presented at the Annual Technical Conference and Exhibition of the Society of Petroleum Engineers, New Orleans, Louisiana, September 25–28. [c]Arri, L. E., et al. 1992. [d]Cox, D. O., Young, G. B. C., and Bell, M. J., 1995, "Well Testing in Coalbed Methane (CBM) Wells: An Environmental Remediation Case history," SPE 30578, presented at the Annual Technical Conference and Exhibition of the Society of Petroleum Engineers, Dallas, Texas, October 22–25. [e]Harpalani, S., and Pariti, U. M. 1993. [f]Mavor, M. J., et al. 1990. [g]Ibid. [h]Ibid. [i]Clarkson, C. R., and McGovern, J. M. 2005. Optimization of coalbed-methane reservoir exploration and development strategies through integration of simulation and economics. *Society of Petroleum Engineers Reservoir Evaluation and Engineering*. V. 8 (no. 6/December). p. 502. [j]Ibid. [k] Ibid.

## Undersaturation

An in-situ sorption isotherm gives the maximum amount of gas a given coal can hold at current reservoir pressure and temperature. For a variety of geological reasons, many coal deposits hold less gas than their maximum amount and are therefore said to be undersaturated. Undersaturated coals are commercially challenging in that they require dewatering prior to gas production. The pressure at which gas is released from the coal, termed desorption pressure, can be calculated from the Langmuir isotherm as

$$p_d = p_L \frac{V}{V_{Lis} + V}$$

where

$p_d$ = desorption pressure, psia or MPa,
$p_L$ = Langmuir pressure constant, psia or MPa,
$V_{Lis}$ = in-situ Langmuir volume constant, scf/ton or cm$^3$/g, and
$V$ = gas content measured by desorption testing, scf/ton or cm$^3$/g.

An undersaturated coal from the Northeast Blanco Unit (NEBU) in the San Juan Basin was reported by Mavor et al.[61] Both the in-situ isotherm and measured gas contents are depicted in figure 5–22. Measured gas content was 355 scf/ton and initial reservoir pressure was 1,620 psia. Moving vertically upward on the figure from the reported gas content and initial pressure, the isotherm is intersected at a gas content of 456 scf/ton, making this coal undersaturated in gas by almost exactly 100 scf/ton. The relative amount of gas stored in the coal is 355/456 or 78%. Moving horizontally to the left from the reported gas content, the isotherm is intersected at a pressure of 585 psia, which is the desorption pressure. Thus, pressure would have to be reduced by 1,620 – 585 = 1,035 psia prior to any gas being released. The coal is said to be undersaturated in pressure by 1,035 psia. On a relative basis, the desorption pressure is 1,035/1,620, or 64% of initial reservoir pressure.

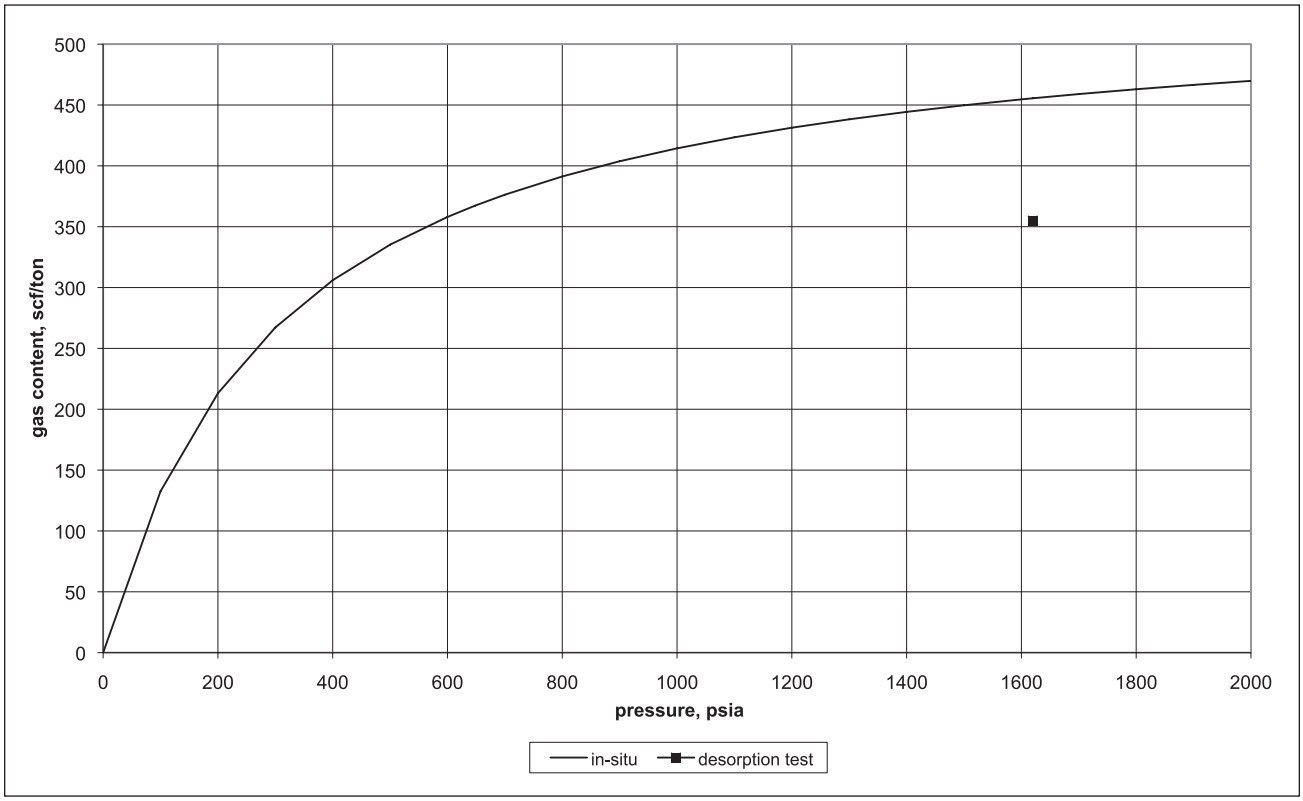



**Fig. 5–22.** Undersaturated coal—NEBU 403 well, San Juan Basin[62]

Undersaturation can be caused by a variety of geological factors and cannot be predicted with current CBM technology. At this time, the only way to quantify undersaturation is comparison of measured gas contents from desorption tests with calculated gas contents using a laboratory isotherm and current reservoir pressure. Well production tests that produce water and no gas help to confirm the hypothesis of undersaturation. The degree of saturation can vary stratigraphically, with some coals fully saturated and others undersaturated. Within a coal seam, the degree of saturation can vary laterally due to pressure compartments within the seam.

## Sorption Isotherms for $CO_2$, Nitrogen, and Other Gases

Gas held in coal deposits is composed primarily of methane but can contain significant amounts of other gases, most notably $CO_2$, nitrogen, and ethane. Coals are currently being investigated for sequestration of $CO_2$ and $H_2S$. Consequently, isotherms are often measured for gases other than methane. Sorption of these gases on coals at commonly found temperatures and pressures are described by Langmuir's equation. Sorption affinity of the various gases is related to their atmospheric pressure boiling point, allowing ranking of selected gases as He, $H_2$, $N_2$, CO, Ar, $O_2$, $CH_4$, NO, Xe, $C_2H_6$, $CO_2$, $SF_6$, $H_2S$, $C_3H_8$, $SO_2$, $NO_2$, $SO_3$.[63]

Methane, $CO_2$, and nitrogen daf isotherms for a Fruitland coal sample from the San Juan basin, reported by Arri et al., are presented in figure 5–23.[64] Associated methane, $CO_2$, and nitrogen Langmuir volume constants are 908.4 scf/ton, 1,350.1 scf/ton, and 737.3 scf/ton, respectively, in agreement with the ranking of Pratt and Baez mentioned above. Methane, $CO_2$, and nitrogen Langmuir pressure constants are 362.3 psia, 204.5 psia, and 1,457.7 psia, respectively. At this time, there is no known pattern for Langmuir pressure constants of different gas isotherms, nor any general rule for predicting them from coal properties. Variation of in-situ $CO_2$ isotherms from the San Juan Basin is illustrated in figure 5–24 with isotherms from Arri et al., Harpalani and Pariti, and Mavor et al.[65] The in-situ $CO_2$ gas content variation of a factor of two is ascribed to differences in sample rank and quality.

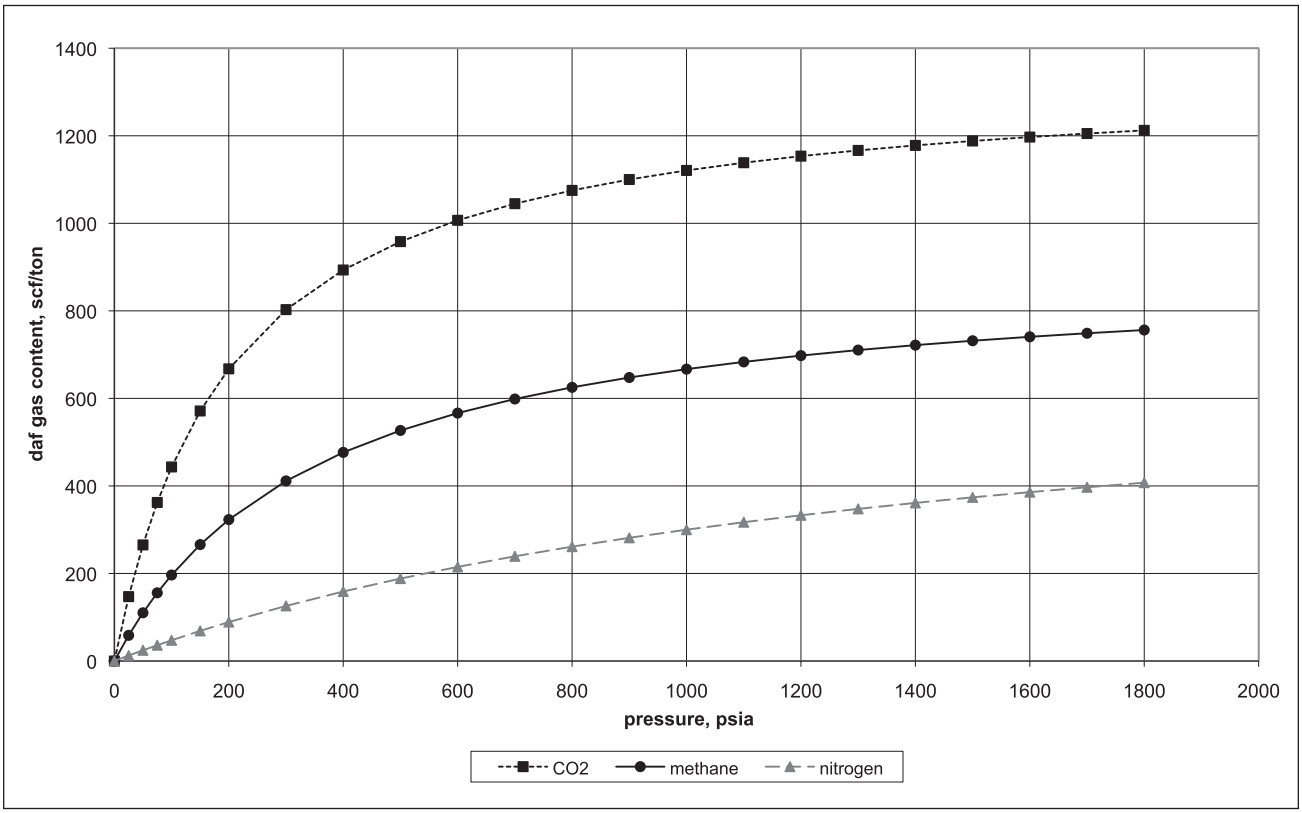



**Fig. 5–23.** Methane, nitrogen, and $CO_2$ daf isotherms—Fruitland coal, San Juan Basin[66]

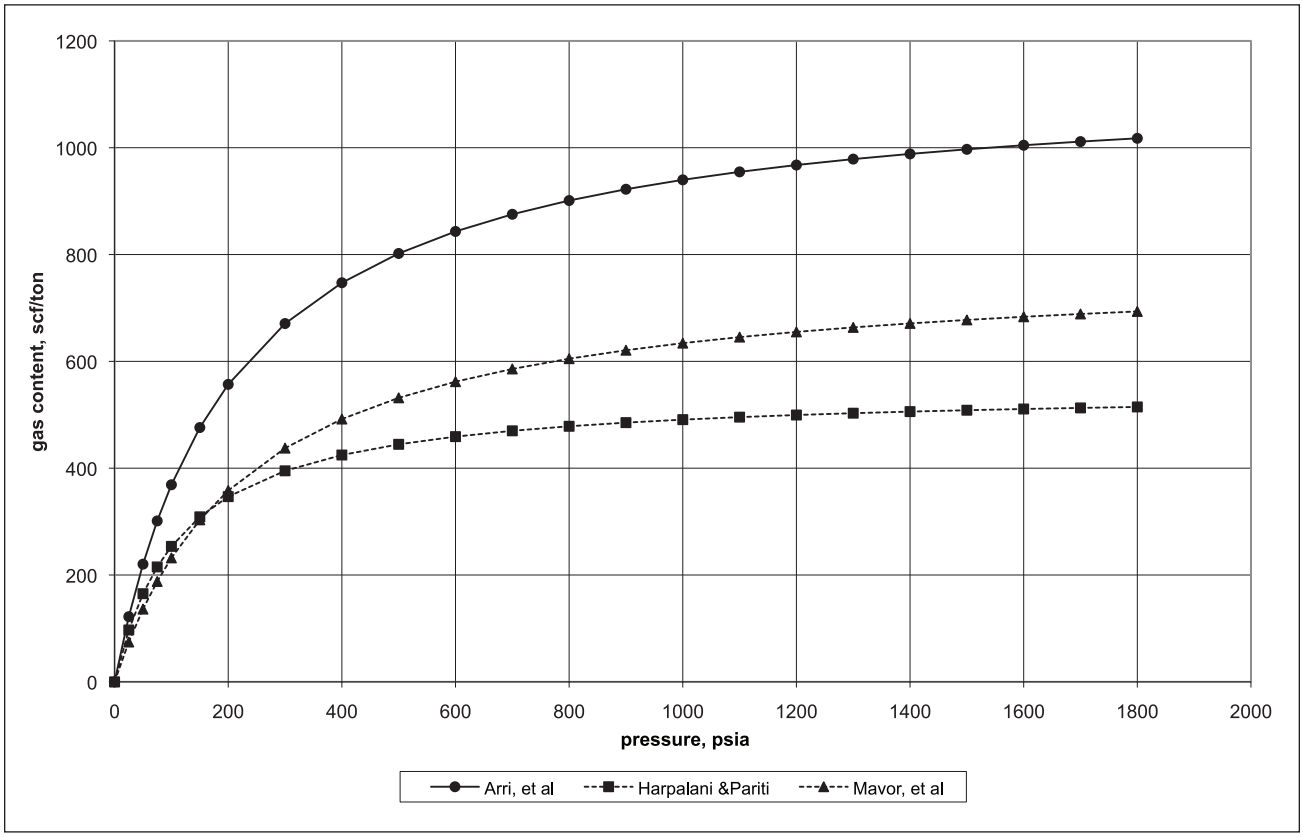



**Fig. 5–24.** In-situ $CO_2$ isotherms—Fruitland coal, San Juan Basin[67]

## Multicomponent Langmuir Isotherms

Most coal deposits contain a mixture of gases, but mathematical description of the gas content is often simplified by assuming the gas to be only methane. For reservoir engineering purposes, adsorption of gas mixtures on coals can be described with a modified form of Langmuir's equation termed the *multicomponent* (or *extended*) *Langmuir isotherm equation*:

$$V_j = V_{Lj} \frac{\frac{py_j}{p_{Lj}}}{1+\sum_{k=1}^{nc} \frac{py_k}{p_{Lk}}} \tag{5.7}$$

where

$V_j$ = component $j$ gas content, scf/ton or cm³/g,
$V_{Lj}$ = component $j$ Langmuir volume constant, scf/ton or cm³/g,
$p_{Lj}$ = component $j$ Langmuir pressure constant, psia or MPa,
$y_j$ = component $j$ free gas mole fraction, and
$p$ = pressure, psia or MPa.

Total gas content of the coal is the sum of individual gas contents, $V_j$s, over the number of components, $nc$:

$$V = \sum_{k=1}^{nc} V_K$$

As an example, consider the San Juan Basin daf methane and $CO_2$ isotherms reported by Arri et al., discussed above.[68] Assume initial coal seam pressure is 1,500 psia and initial $CO_2$ concentration in the produced gas stream is 10%, typical of the San Juan Basin. Using equation (5.7), the daf methane gas content is 620.0 scf/ton, and the daf $CO_2$ gas content is 181.4 scf/ton. Adding these two gas contents together gives a total daf gas content of 801.4 scf/ton, making the $CO_2$ fraction of the initial gas in place approximately 23%. As the coal sorbs $CO_2$ more strongly than it does methane, the sorbed gas contains significantly more $CO_2$ than does the free gas, 23% versus 10%. Composition of both the sorbed and free gas must be taken into account when calculating coal gas reserves. Variation of produced gas stream composition during depletion and recovery factors for different components is addressed in chapter 10.

As a second example, also from the San Juan Basin, Mavor et al. reported daf methane and $CO_2$ isotherms for the Southern Ute 5-7 well.[69] Langmuir volume constants on a daf basis for methane and $CO_2$ were 538.7 and 1,019.0 scf/ton, respectively. Langmuir pressure constants for methane and $CO_2$ were 362.2 and 238.5 psia, respectively. Initial coal seam pressure was 620 psia, and initial $CO_2$ concentration was 17.5%. The extended Langmuir equation gives daf methane and $CO_2$ gas contents of 265.3 and 161.7 scf/ton, respectively. Total daf gas content is 427.0 scf/ton, and the initial $CO_2$ loading is 38%.

## Apparent Oversaturation

Sometimes measured gas contents are higher than those calculated from an isotherm and initial reservoir pressure, resulting in apparent oversaturation of the coal. It is physically impossible for a coal deposit to be oversaturated with gas but quite possible to have an erroneous conception of gas storage in the coal. Slight degrees of apparent oversaturation are not all that rare in practice and are usually due to routine errors in desorption tests and/or laboratory measurements. Significant apparent oversaturation, on the order of 10% or more of the total gas content, is usually due to the presence of strongly sorbing gases, such as ethane or $CO_2$, in the gas mixture sorbed on the coal.

An example of apparent oversaturation is shown in figure 5–25, based on data from Mavor et al.[70] Measured gas content and the methane isotherm are on a daf basis, and the coal appears to contain roughly 50% more gas than would be expected from the isotherm. However, the produced gas included significant $CO_2$. When the daf $CO_2$ isotherm is included, as seen in figure 5–26, the apparent oversaturation is understood to be simply sorption of a two-component gas mixture. The isotherms and gas content are from the Southern Ute 5-7 example discussed above, and the sorbed gas contains nearly 40% $CO_2$.

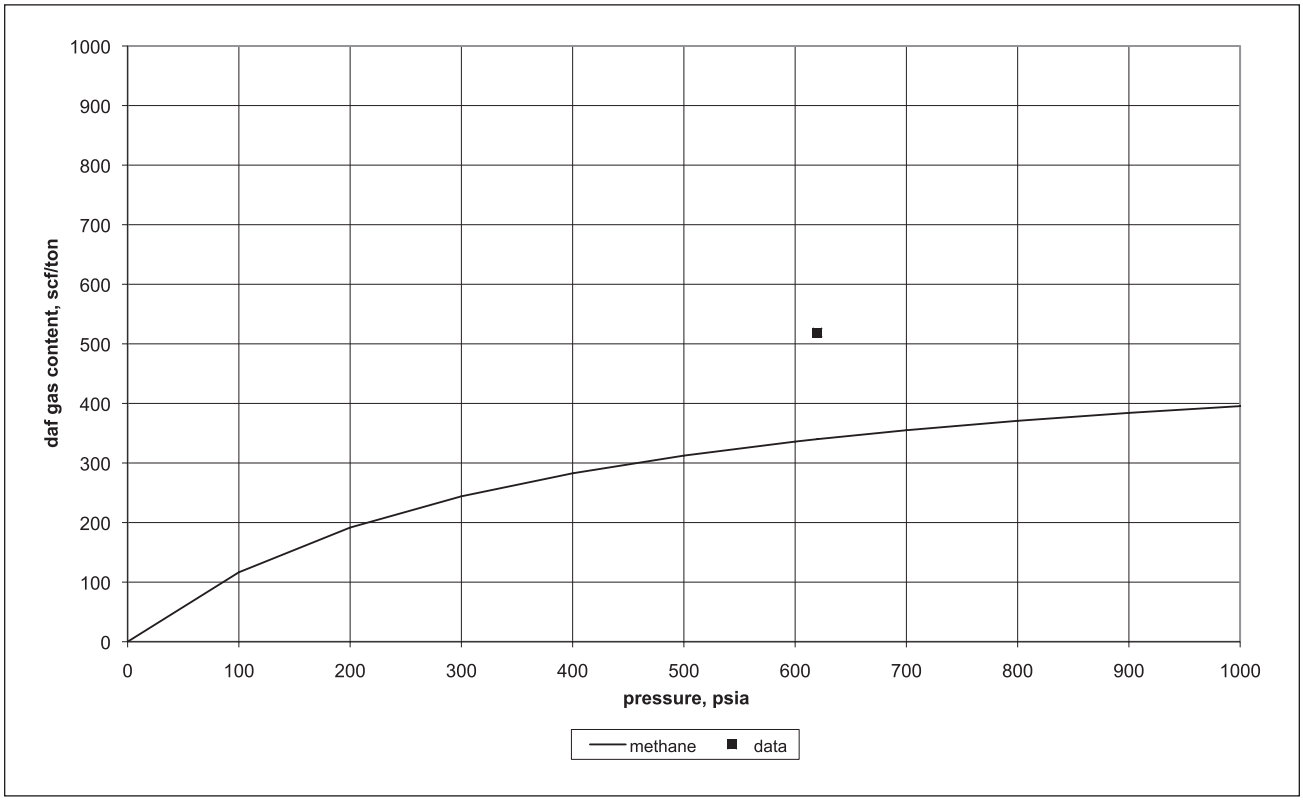



**Fig. 5–25.** Apparent oversaturation—San Juan Basin[71]

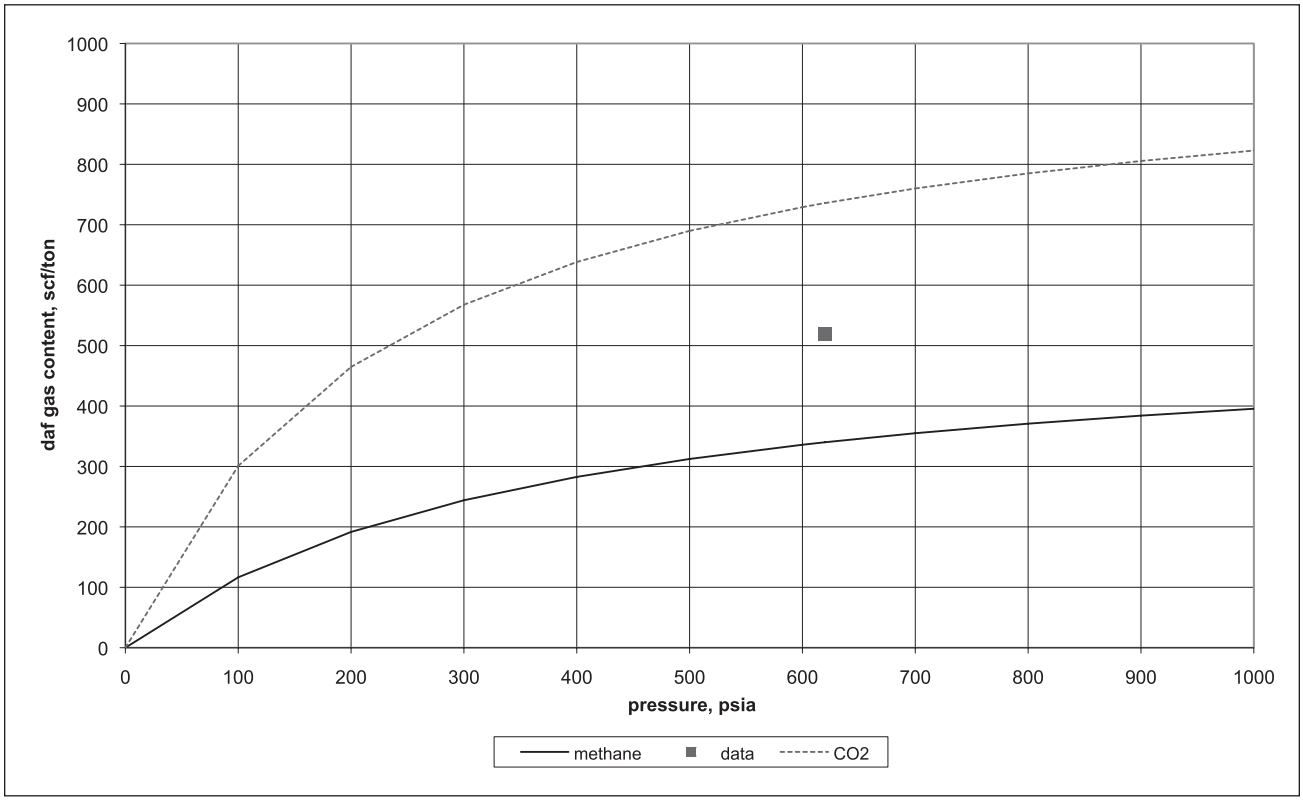



**Fig. 5–26.** Apparent oversaturation, $CO_2$ and methane isotherms—San Juan Basin

# Nomenclature

$a$ = ash mass fraction
$b$ = alternative Langmuir pressure constant, psia$^{-1}$ or MPa$^{-1}$
$B_{gi}$ = the initial gas formation volume factor, ft$^3$/scf
$E$ = characteristic energy, psi-ft$^3$/lb-mole
$n$ = a small integer, typically between 1 and 4
$nc$ = number of component gases in gas mixture
$p$ = pressure, psia, MPa, or atm
$p_c$ = critical pressure, atm
$p_d$ = desorption pressure, psia or MPa
$p_i$ = initial reservoir pressure, psia
$p_L$ = Langmuir pressure constant, psia or MPa
$p_{Lj}$ = component j Langmuir pressure constant, psia or MPa
$p_s$ = saturation vapor pressure, atm
$R$ = universal gas constant, psi-ft$^3$/lb-mole-deg-R
$S_{gi}$ = initial gas saturation, decimal
$T$ = temperature, deg R
$T_c$ = critical temperature, deg R
$T_{nbp}$ = normal boiling point temperature, deg R
$V$ = gas content, scf/ton or cc/gm
$V_j$ = component j gas content, scf/ton or cc/gm
$V_L$ = Langmuir volume constant, scf/ton or cc/gm
$V_{Ldaf}$ = dry, ash-free Langmuir volume constant, scf/ton or cc/gm
$V_{Lis}$ = in-situ Langmuir volume constant, scf/ton or cc/gm
$V_{Lj}$ = component j Langmuir volume constant, scf/ton or cc/gm
$w$ = equilibrium moisture mass fraction
$W$ = sorbed gas volume, cc/gm
$W_0$ = volume of micropores, cc/gm
$y_j$ = component j free gas mole fraction

## Greek

$\beta$ = sorbate affinitiy coefficient, dimensionless
$\phi_{eq}$ = equivalent sandstone porosity, decimal
$\rho_B$ = bulk coalbed density, gm/cc

## References


1. Testa, S. M., and Pratt, T. J. 2003. Sample preparation for coal and shale gas resource assessment. Paper 0356. In *Proceedings of the 2003 International Coalbed Methane Symposium*. May 5–9. Tuscaloosa: University of Alabama; and Pratt, T. J., and Baez, L. R. G. 2003. Critical data requirements for coal and gas shale resource assessment. Paper 0367. In *Proceedings of the 2003 International Coalbed Methane Symposium*. May 5–9. Tuscaloosa: University of Alabama.
2. Mavor, M. J., Owen, L. B., and Pratt, T. J. 1990. *Measurement and Evaluation of Coal Sorption Isotherm Data*. Paper SPE 20728. Presented at the 65th Annual Technical Conference and Exhibition of the Society of Petroleum Engineers, New Orleans, Louisiana, September 23–26; Arri, L. E., Yee, D., Morgan, W. D., and Jeansonne, M. W. 1992. *Modeling Coalbed Methane Production with Binary Gas Sorption*. Paper SPE 24363. Presented at the SPE Rocky Mountain Regional Meeting, Casper, Wyoming, May 18–21; and Greaves, K. H., Owen, L. B., McLennan, J. D., and Olszewski, A. 1993. Multi-component gas adsorption-desorption behavior of coal. Paper 9353. In *Proceedings of the 1993 International Coalbed Methane Symposium*. Tuscaloosa: University of Alabama.
3. Arri, L. E., et al. 1992.
4. Ibid.
5. Hall, F. E., Zhou, C., Gasem, K. A. M., Robinson, Jr., R. L., and Yee, D. 1994. *Adsorption of Pure Methane, Nitrogen, and Carbon Dioxide and Their Binary Mixtures on Wet Fruitland Coal*. Paper SPE 29194. Presented at the SPE Eastern Regional Conference & Exhibition, Charleston, West Virginia, November 8–10.
6. Yee, D., Seidle, J. P., and Hanson, W. B. 1993. Gas sorption on coal and measurement of gas content. Chapter 9 in *Hydrocarbons from Coal, AAPG Studies in Geology #38*. Law, B. E., and Rice, D. D., eds. Tulsa: American Association of Petroleum Geologists.
7. Hall, F. E., et al. 1994.
8. Hall, F. E., et al. 1994.
9. Ibid.
10. Ibid.
11. Levine, J. R. 1993. Coalification: The evolution of coal as source rock and reservoir rock for oil and gas. In *Hydrocarbons from Coal, AAPG Studies in Geology #38*. Law, B. E., and Rice, D. D. eds. Tulsa: American Association of Petroleum Geologists.
12. Testa, S. M., and Pratt, T. J. 2003.
13. Joubert, J. I., Grein, C. T., and Beinstock, D. 1973. Sorption of methane in moist coal. *Fuel*. V. 52. pp. 181–195; and Joubert, J. I., Grein, C. T., and Beinstock, D. 1974. Effect of moisture on the methane capacity of American coals. *Fuel*. V. 53. pp. 186–191.
14. Joubert, J. I., et al. 1974.
15. Yee, D., et al. 1993.
16. Joubert, J. I., et al. 1974.
17. Yee, D., et al. 1993.
18. Hall, F. E., et al. 1994.
19. Metcalfe, R. S., Yee, D., Seidle, J. P., and Puri, R. 1991. *Review of Research Efforts in Coalbed Methane Recovery*. Paper SPE 23025. Presented at the SPE Asia-Pacific Conference, Perth, Western Australia, November 4–7.
20. Hall, F. E., et al. 1994.
21. Metcalfe, R. S., et al. 1991.
22. Gan, H., Nandi S. P., and Walker, P. L., Jr. 1972. Nature of the porosity in American coals. *Fuel*. V. 51. p. 272–277; and Bustin, R. M., and Clarkson, C. R. 1999. Free gas storage in matrix porosity: A potentially significant coalbed resource in low rank coals. Paper 9956 in *Proceedings of the 1999 International Coalbed Methane Symposium*. May. Tuscaloosa: University of Alabama.
23. Mavor, M. J., et al. 1990.
24. Mavor, M. J., et al. 1990; Arri, L. E., et al. 1992; and Hall, F. E., et al. 1994.
25. Levine, J. R. 1993.
26. Mavor, M. J., et al. 1990; Arri, L. E., et al. 1992; and Hall, F. E., et al. 1994.
27. Bustin, R. M., and Downey, R. A. 2002. *Gas-in-place in the Powder River Basin: Coal Cores—Why Do Them? Some Field Results, Comparisons, and Suggestions*. Rocky Mountain Association of Geologists 2002 Coalbed Methane Symposium, Denver, June 19.
28. Boxho, J., Stassen, P., Mücke, G., Noack, K., Jeger, C., Lescher, L., Browning, E., Dunmore, R., and Morris, I. 1980. *Firedamp Drainage Handbook for the Coal Mining Industry in the European Community*. Coal Directorate of the Commission of the European Communities. Essen: Verlag Glückauf GmbH. pp. 28–30.
29. Hofer, L. J. E., Bayer, J., and Anderson, R. B. 1966. *Rates of Adsorption of Methane on Pocahontas and Pittsburgh Seam Coals*. U.S. Bureau of Mines Report of Investigation 6750.
30. Bustin, R. M., and Downey, R. A. 2002.
31. Ettinger, I. L., Lidin, G. D., Dimitiev, A. M., and Shaupachina, E. S. 1958. *Systematic Handbook for the Determination of the Methane Content of Coal Seams from the Seam Pressure of the Gas and the Methane Capacity of Coal*. Moscow: National Coal Board. Translation No. A1606/SEH.
32. Yee, D., et al. 1993.
33. Hofer, L. J. E., et al. 1966.
34. Clarkson, C. R., Bustin, R. M., and Levy, J. H. 1997. Application of the mono/multilayer and adsorption potential theories to coal methane adsorption isotherms at elevated temperature and pressure. *Carbon*. V. 35 (no. 12). p. 1,689.
35. Agarwal, R. K., and Schwarz, J. A. 1988. Analysis of high pressure adsorption of gases on activated carbon by potential theory. *Carbon*. V. 26 (no. 6). p. 873.

36. Kapoor, A., Ritter, J. A., and Yang, R. T. 1989. On the Dubinin-Radushkevich equation for adsorption in microporous solids in the Henry's law region. *Langmuir*. V. 5. p. 1,118.
37. Bustin, R. M., and Downey, R. A. 2002.
38. Ibid.
39. Earlougher, R. C., Jr. 1977. *Advances in Well Test Analysis*. Society of Petroleum Engineers Monograph 5. Dallas: Society of Petroleum Engineers.
40. Bustin, R. M., and Downey, R. A. 2002.
41. Ibid.
42. Ibid.
43. Metcalfe, R. S., et al. 1991.
44. Mavor, M. J., et al. 1990.
45. Nelson, C. R., Hill, D. G., and Pratt, T. J. 2000. *Properties of Paleocene Fort Union Formation Canyon Seam Coal at the Triton Federal Coalbed Methane Well, Campbell County, Wyoming*. Paper SPE 59786. Presented at the SPE/CERI Gas Technology Symposium, Calgary, Alberta, April 3–5.
46. Mavor, M. J., et al. 1990.
47. Nelson, C. R., et al. 2000.
48. Mavor, M. J., et al. 1990.
49. Ibid.
50. Ibid.
51. Ibid.
52. Ibid.
53. Metcalfe, R. S., et al. 1991; and Mavor, M. J., et al. 1990.
54. Metcalfe, R. S., et al. 1991.
55. Mavor, M. J., et al. 1990.
56. Rightmire, C. T., Eddy, G. E., and Kirr, J. N., eds. 1984. *Coalbed Methane Resources of the United States*. Tulsa: American Association of Petroleum Geologists.
57. Cox, D. O. 2001. Presentation to the Denver Section of the Society of Petroleum Evaluation Engineers. January 22.
58. Crockett, F., and Meyer, J. 2001. *Update and Revision of Interim Drainage Report on Coalbed Methane Development and Drainage of Federal Land in the South Gillette Area, Campbell and Converse Counties, Wyoming T. 40–50 N., R 70–75 W*. February 12. Casper: Wyoming Bureau of Land Management.
59. Cox, D. O. 2001.
60. Ibid.
61. Mavor, M. J., et al. 1990.
62. Ibid.
63. Pratt, T. J., and Baez, L. R. G. 2003.
64. Arri, L. E., et al. 1992.
65. Ibid.; Harpalani, S., and Pariti, U. M. 1993. *Study of Coal Sorption Isotherms Using a Multicomponent Gas Mixture*. Paper 9356. Presented at the International Coalbed Methane Symposium, University of Alabama, Tuscaloosa, Alabama, May 17–21; and Mavor, M. J., Pratt, T. J., and Nelson, C. R. 1995. *Quantitative Evaluation of Coal Seam Gas Content Estimate Accuracy*. Paper SPE 29577. Presented at the SPE Rocky Mountain Regional/Low-Permeability Reservoir Symposium, Denver, Colorado, March 20–22.
66. Arri, L. E., et al. 1992.
67. Ibid.; Harpalani, S., and Pariti, U. M. 1993; and Mavor, M. J., et al. 1995.
68. Arri, L. E., et al. 1992.
69. Mavor, M. J., et al. 1995.
70. Ibid.
71. Ibid.

# Coal Permeability 6

## Introduction

The ability of water and gas to flow through coal deposits varies greatly, not only from basin to basin but within a given seam and over the course of depletion. The ease with which a fluid moves through the interconnected pores and fissures of a rock is termed *permeability*. Of the various units used to quantify permeability, millidarcies is the most common for coals, just as for conventional reservoirs. The natural fractures, or cleats, running through a coal deposit are several orders of magnitude more permeable than the coal matrix (millidarcies or tens of millidarcies versus microdarcies) and control fluid movement through it. Coal seams are extremely heterogeneous reservoirs whose permeability depends not only on geological age, coal rank, and purity, but also on gas and water saturations, in-situ stresses, and sorbed gas content. Permeability of a coal deposit to gas and water depends on the interplay of these three influences.

For reservoir engineering purposes, permeability is often divided into absolute and relative permeabilities. *Absolute permeability* is a property of the coal and not the fluids flowing through it, but it does, however, depend on stress and sorbed gas content. Laboratory measurement of absolute coal permeability is difficult and often yields different values from field-derived estimates of permeability of the seam from which the laboratory sample was obtained. Most coals contain both free gas and water, with the saturations of each varying areally and over the course of depletion. Interference between the two phases affects mobility of each. *Relative permeability* of gas or water is the ratio of the permeability of that phase relative to permeability when only a single phase is present. Relative permeability of a phase depends on saturation of that phase. Coal gas-water relative permeabilities have been measured in laboratories, estimated from algebraic equations, and determined from history matching well performance with reservoir simulators.

Coals of all ages and ranks are fragile rocks, with little mechanical strength compared to conventional reservoir rocks. Even using the procedures discussed below, only the stronger samples will survive; the weaker ones will fragment. With face cleats better developed than butt cleats, coal cleat networks are visually anisotropic. Flow behavior parallel to these cleat directions as well as perpendicular to the bedding planes thus is intuitively expected to be distinct. Cores, of course, are nominally cut vertically, with the result that both permeability and gas-water relative permeabilities measured in the laboratory reflect vertical flow characteristics (perpendicular to the bedding planes) rather than horizontal (parallel to the bedding planes). Differences in vertical flow characteristics of mechanically strong laboratory samples and those of horizontal flow in in-situ deposits are to be expected.

Laboratory-measured permeability anisotropies reported by Gash et al. included a 2:1 contrast in face and butt cleats and a 100:1 contrast between face cleat and vertical permeability.[1] The same 2:1 ratio of face cleat to butt cleat permeabilities was observed in an interference test in San Juan coals.[2] Horizontal permeability anisotropy of 17:1 was reported from an interference test in the Warrior Basin on the basis of soft type curve matches.[3] Young et al. found horizontal permeability larger than vertical permeability by a factor of 42 through

simulation of coal well performance in the Great Divide (Greater Green River) Basin.[4] However, in virtually every commercial coal gas project as of the date of this writing, no operator has spaced wells based upon permeability anisotropy but upon other controls, such as structure or topography. Gas-water relative permeability data for coals are sparse, with only one study measuring relative permeabilities in the face and butt cleat directions and perpendicular to the bedding planes.[5] That study found that to within engineering accuracy, gas-water relative permeabilities of San Juan coal are the same in all three directions.

## Theoretical Absolute Coal Permeability

Coal deposits are naturally fractured reservoirs with two sets of cleats or fractures draining an organic matrix. The face cleat is the dominant fracture set composed of roughly parallel, throughgoing, extensive fractures. Perpendicular to the face cleats, the butt cleats are also roughly parallel but less well developed and often terminate at a face cleat. Both sets of cleats are nominally perpendicular to the bedding planes. Cleats appear similar at several different length scales but have not been described with self-similar parameters such as fractal dimensions. Hand samples of coal show cleat spacing on the order of millimeters or centimeters. While cleat orientation is nominally the same from layer to layer, cleat intensity is highly variable between layers of the coal deposit.

Coals, like most naturally fractured reservoirs, often exhibit a strong contrast between matrix and fracture permeability. Coal matrix permeability is on the order of microdarcies or nanodarcies, while as discussed below, coal cleat permeabilities range from 0.1 to 1,000 md.[6] However, unlike other naturally fractured reservoirs, where matrix permeability often dominates reservoir performance, especially at long times, coal matrix permeability plays an insignificant role in fluid movement in a coal because of sorption. Gas desorbs from the coal matrix in response to a concentration gradient, not a pressure gradient. Gas release from the matrix appears to be diffusive and can be described by Fick's law, not Darcy's law. While most coals are aquifers, or are at least moist, large volumes of water do not readily move between matrix and fissures. Coal matrix is generally not a water-wet material. As discussed in chapter 7, rapid gas release from the matrix implies that cleat permeability governs fluid flow through a coal seam.

Permeability of the cleat system in a coal can be calculated from equations derived for other naturally fractured reservoirs.[7] A well-cleated coal can be represented conceptually as a collection of matchsticks, as shown in figure 6–1.

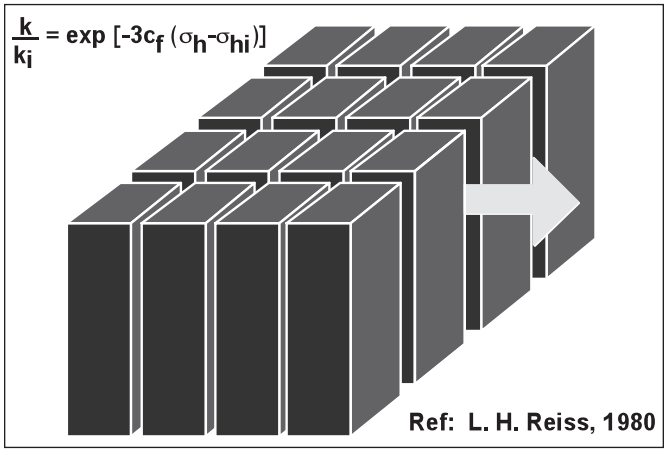



**Fig. 6–1.** Matchstick geometry

Assuming cleat aperture is much smaller than cleat spacing, porosity of a coal can be expressed as

$$\phi = \frac{2b}{a} \tag{6.1}$$

where

$\phi$ = cleat porosity,
$b$ = cleat width, and
$a$ = cleat spacing.

Expressing cleat width in microns and cleat spacing in millimeters, this equation becomes

$$\phi = \frac{b}{500a} \tag{6.2}$$

Flow down a single cleat can be described by Poiseuille's equation

$$q = \frac{b^3 l}{12\mu} \frac{\Delta p}{L}$$

where

$q$ = flow rate,
$l$ = bedding plane height,
$\mu$ = fluid viscosity, and
$\Delta p/L$ = pressure gradient.

For $n$ cleats, the total flow rate is

$$q_t = n \frac{b^3 l}{12\mu} \frac{\Delta p}{L}$$

Total flow down the cleat can also be described by Darcy's law

$$q = \frac{Ak}{\mu} \frac{\Delta p}{L}$$

where

$A$ = flow area, and
$k$ = fracture permeability.

Equating these two relations for total flow rate and solving for fracture permeability,

$$k = \frac{nb^3 l}{12A}$$

Flow area is given by

$$A = n(a + b)l$$

As cleat width, $b$, has been assumed to be much smaller than cleat spacing, $a$, permeability is approximately given by

$$k = \frac{b^3}{12a} \tag{6.3}$$

Solving (6.1) for cleat aperture, (6.3) can be written as

$$k = \frac{\phi^3 a^2}{96} \tag{6.4}$$

For permeability in millidarcies and cleat spacing in millimeters, this equation becomes

$$k = 1.0555(10)^5\, \phi^3 a^2 \tag{6.5}$$

This relation is plotted in figure 6–2 using typical values of cleat porosity and spacing.

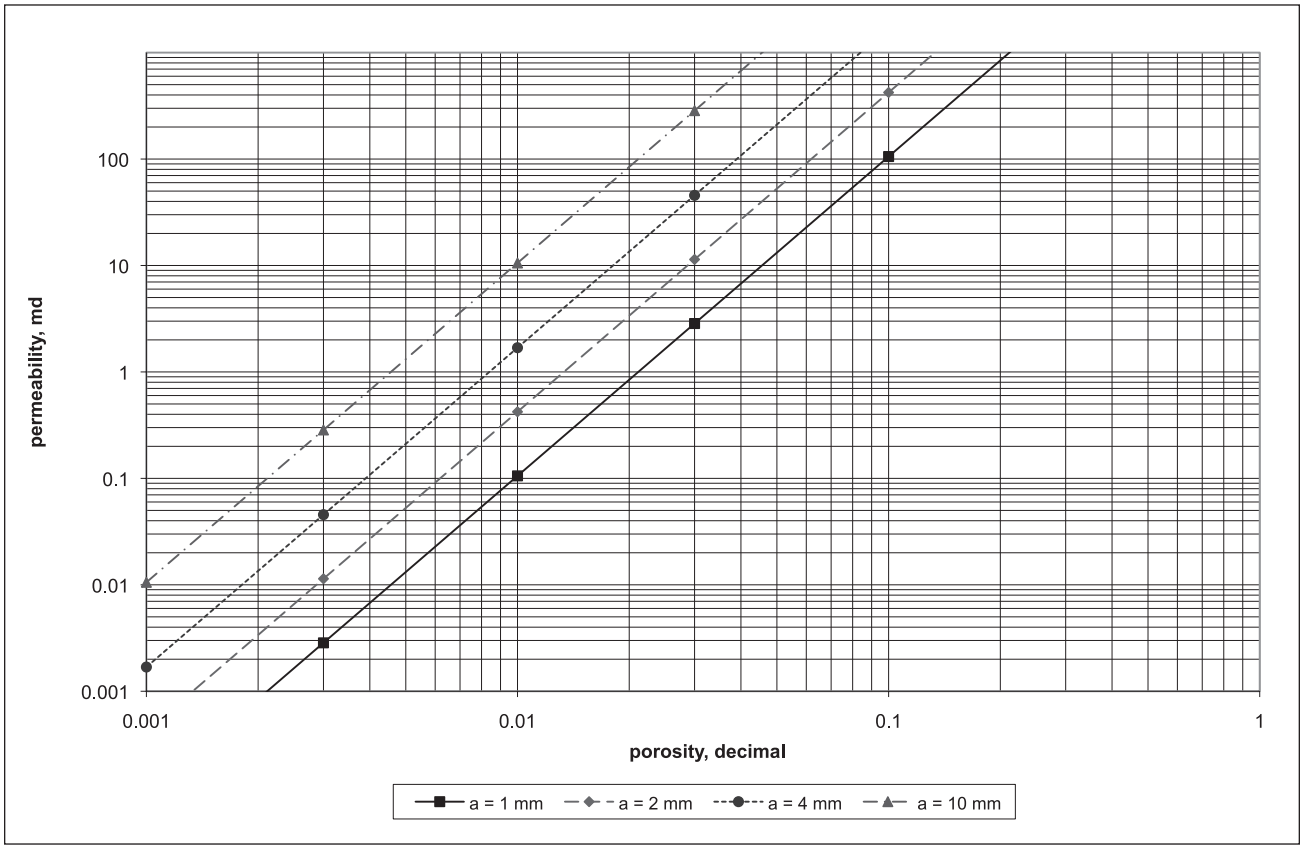



**Fig. 6–2.** Cleat permeability as a function of cleat porosity and spacing

Assuming a stiff coal matrix, cleat spacing remains constant as stress changes, and equation (6.5) leads to the following relation for porosity and permeability ratios

$$\frac{k}{k_i} = \left( \frac{\phi}{\phi_i} \right)^3 \tag{6.6}$$

Not unique to coals, this cubic relation between porosity and permeability is observed in many naturally fractured reservoirs.[8]

### Example 6.1. Hartshorne coal, Arkoma Basin—cleat permeability and porosity

Cleat properties of the Hartshorne coal of the Arkoma Basin were discussed by Cardott.[9] The No. 31-8 L. W. Stiles well (Sec. 31 T9N R25E) had an average permeability of 3.1 md, an average helium porosity of 2.3%, cleat spacing of 3 to 5 mm, and a cleat aperture of 0.2 mm at surface conditions. Using a permeability of 3 md and a cleat spacing of 4 mm in equation (6.5),

$$3 \text{ md} = 1.0555(10)^5 \phi^3 4^2 \text{ mm}^2$$

Solving for porosity,

$$\phi = 0.012$$

Thus, in-situ porosity is about one-half the reported helium porosity. This is not surprising, as helium can penetrate micropores inaccessible to methane, and laboratory conditions typically allow a rock sample to relax, increasing porosity. In-situ cleat aperture can now be calculated using equation (6.2).

$$0.012 = \frac{b}{500(4 \text{ mm})}$$

Solving for cleat aperture,

$$b = 24 \text{ μm}$$

This in-situ estimate of cleat width is almost an order of magnitude less than cleat width of the sample at surface conditions, again indicative of sample relaxation.

## Stress Dependence of Coal Permeability

Stress changes the shape of coal cleats. Alteration of cleat shape is intuitively expected to affect cleat permeability. For a given basin, stresses acting on coals increase with depth, leading to the expectation of permeability decrease with depth. For a given coal seam, stresses increase over the course of depletion, leading to the expectation of permeability decrease as gas is produced. Development of a mathematical relation between stress and permeability begins with conceptualizing a coal seam as a collection of matchsticks, a common geometrical model of naturally fractured reservoirs. For a matchstick geometry, permeability is exponentially related to stress[10]

$$\frac{k}{k_i} = \exp\left[-3c_f(\sigma_h - \sigma_{hi})\right] \quad \textbf{(6.7)}$$

where

$k$ = permeability,
$k_i$ = initial permeability,
$c_f$ = cleat compressibility,
$\sigma_h$ = hydrostatic stress, and
$\sigma_{hi}$ = initial hydrostatic stress.

This equation is useful for interpreting laboratory permeability measurements acquired in a hydrostatic stress regime. Cleat compressibility is an experimentally determined rock property, and various values reported in the literature are collected in table 6–1.

**Table 6–1.** Coal cleat compressibilities

| Basin | Seam | Cleat compressibility, psia$^{-1}$ |
|---|---|---|
| Appalachian[a] | Pittsburgh | 1.87E–03 |
| San Juan[b] | Menefee | 1.34E–03 |
| Piceance[c] | Cameo | 7.76E–04 |
| Piceance[d] | Cameo | 1.80E–03 |
| Warrior[e] | na | 1.87E–03 |
| Warrior[f] | Marylee/Blue Creek | 5.79E–04 |
| San Juan[g] | na | 9.24E–04 |
| San Juan[h] | na | 9.61E–04 |
| San Juan[i] | Fruitland | 2.00E–03 |
| San Juan[j] | Fruitland | 1.83E–03 |
| Warrior[k] | Marylee/Blue Creek | 2.50E–03 |
| San Juan[l] | Fruitland | 1.02E–03 |
| Sydney[m] | Bulli | 3.00E–04 |
| | Average | 1.37E–03 |

*na = not available*
*Sources:* [a]McKee, C. R., et al. 1988. [b]Ibid. [c]Ibid. [d]Ibid. [e]McKee, C. R., Bumb, A. C., and Koenig, R. A. 1987. Stress-dependent permeability and porosity of coal. Paper 8742 in *Proceedings of the 1987 International Coalbed Methane Symposium*. Tuscaloosa: University of Alabama. [f]Seidle, J. P., Jeansonne, M. W., and Erickson, D. J. 1992. *Application of Matchstick Geometry to Stress-Dependent Permeability in Coals*. Paper SPE 24361. Presented at the SPE Rocky Mountain Regional Meeting, Casper, Wyoming, May 18–21. [g]McKee, C. R., et al. 1987. [h]Seidle, J. P., et al. 1992. [i]Shi, J. Q., and Durucan, S. 2003. Part 1. Paper 0341; and Shi, J. Q., and Durucan, S. 2003. Part 2. Paper 0342. [j]Ibid. [k]Zuber, M. D., Sawyer, W. K., Schraufnagel, R. A., and Kuuskraa, V. A. 1987. *The Use of Simulation and History Matching to Determine Critical Coalbed Methane Reservoir Properties*. Paper SPE 16420. Presented at the Low Permeability Reservoirs Symposium, Denver, Colorado, May 18–19. [l]Gash, B. W., et al. 1993. [m]Spencer, S. J., Somers, M L., Pinczewki, W. V., and Doig, I. D. 1987. *Numerical Simulation of Gas Drainage from Coal Seams*. Paper SPE 16857. Presented at the SPE Annual Technical Conference and Exposition, Dallas, Texas, September 27–30.

Average cleat compressibility of the values reported in table 6–1 is $1.46(10)^{-3}$ psia$^{-1}$. This important rock property certainly depends on coal age, rank, purity, and other coal properties, but such effects have not been reported in the literature.

A hydrostatic stress regime was assumed by McKee to apply to in-situ coals.[11] With vertical and hydrostatic stresses equal, the variation of permeability with depth can be written

$$\frac{k}{k_i} = \exp\left[-3c_f(\sigma_v - \sigma_{vi})\right] \tag{6.8}$$

However, in-situ coal deposits are confined laterally and are therefore more closely approximated by a uniaxial strain regime. Permeability variation with seam depth in a basin or permeability behavior over depletion of a single seam can be obtained by recasting equation (6.7), assuming permeability depends on mean stress or only horizontal stress across the cleats. The constitutive equations for uniaxial strain can be written as follows, assuming a subscript *1* denotes the vertical direction

$$\varepsilon_1 = \frac{1}{E}\left(\sigma_1 - \nu(\sigma_2 + \sigma_3)\right)$$

$$\varepsilon_2 = \varepsilon_3 = 0$$

where

$\varepsilon$ = strain,
$E$ = Young's modulus,
$\sigma$ = stress, and
$\nu$ = Poisson's ratio.

Furthermore, in uniaxial strain,

$$\sigma_2 = \sigma_3$$

and

$$\sigma_1 = \sigma_v$$

where

$\sigma_v$= vertical, lithostatic stress.

As the lateral strain is defined to be zero,

$$\varepsilon_2 = 0 = \frac{1}{E}\left(\sigma_2 - \nu(\sigma_3 + \sigma_1)\right)$$

Solving for the lateral stress,

$$0 = \sigma_2 - \nu\sigma_2 - \nu\sigma_1$$

$$\sigma_2 (1 - \nu) = \nu\sigma_1$$

$$\sigma_2 = \frac{\nu}{1-\nu}\sigma_1 \qquad \textbf{(6.9)}$$

Mean stress in a uniaxial strain regime is

$$\sigma_m = \frac{1}{3}(\sigma_1 + \sigma_2 + \sigma_3)$$

$$\sigma_m = \frac{1}{3}\left(\sigma_1 + \frac{\nu}{1-\nu}\sigma_1 + \frac{\nu}{1-\nu}\sigma_1\right)$$

$$\sigma_m = \frac{1}{3}\left(\sigma_1 + \frac{2\nu}{1-\nu}\sigma_1\right)$$

As the *1* direction coincides with the local vertical direction,

$$\sigma_m = \frac{1}{3}\left(\frac{1+\nu}{1-\nu}\right)\sigma_v$$

Mean stress in a hydrostatic stress regime is

$$\sigma_m = \frac{1}{3}(\sigma_h + \sigma_h + \sigma_h)$$

$$\sigma_m = \sigma_h$$

Equating the two mean stress expressions,

$$\sigma_h = \frac{1}{3}\left(\frac{1+\nu}{1-\nu}\right)\sigma_v \qquad \textbf{(6.10)}$$

This expression allows transformation of laboratory results taken in a hydrostatic stress regime to in-situ, uniaxial strain conditions. Substitution of equation (6.10) into equation (6.7) gives

$$\frac{k}{k_i} = \exp\left[-c_f\left(\frac{1+\nu}{1-\nu}\right)(\sigma_v - \sigma_{vi})\right] \tag{6.11}$$

Alternatively, a permeability-stress relation can be derived assuming only horizontal stress affects cleats. The Imperial College model (ICM) of Shi and Durucan noted that as both face and butt cleats are usually nearly vertical, horizontal stresses across the cleats rather than vertical and horizontal stresses parallel to the cleats should control cleat permeability.[12] Assuming a uniaxial strain regime and neglecting horizontal stress parallel to the cleat, horizontal stress across the cleat is related to vertical stress by equation (6.9). Employing equation (6.9) in equation (6.7) gives

$$\frac{k}{k_i} = \exp\left[-3c_f\left(\frac{\nu}{1-\nu}\right)(\sigma_v - \sigma_{vi})\right] \tag{6.12}$$

Assumption of three different stress regimes (hydrostatic, uniaxial strain with mean stress, and uniaxial strain with horizontal stress only) leads to three equations for permeability as a function of vertical stress: equations (6.8), (6.11), and (6.12). These three equations lead to three relations for permeability decrease with depth of burial in a given basin. Vertical stress is defined here as the difference between overburden load and pore pressure,

$$\sigma_v = S - p$$

where

$S$ = overburden load, and
$p$ = pore pressure.

Assuming a lithostatic gradient of 1 psi/ft and a normally pressured basin with a pressure gradient of 0.433 psi/ft,

$$\sigma_v = (1 - 0.433)d = 0.567d \tag{6.13}$$

where

$d$ = depth, ft.

Assuming permeability is governed by mean stress in uniaxial strain, use of (6.13) in equation (6.11) yields a relation between permeability and depth,

$$\frac{k}{k_i} = \exp\left[-c_f\left(\frac{1+\nu}{1-\nu}\right)0.567(d - d_i)\right] \tag{6.14}$$

Assuming permeability is controlled by horizontal stresses in uniaxial strain, equations (6.13) and (6.12) give

$$\frac{k}{k_i} = \exp\left[-3c_f\left(\frac{\nu}{1-\nu}\right)0.567(d - d_i)\right] \tag{6.15}$$

Lastly, assuming a hydrostatic stress regime, the permeability and depth relation, from equations (6.13) and (6.12), is

$$\frac{k}{k_i} = \exp\left[-3c_f 0.567(d - d_i)\right] \tag{6.16}$$

As noted above, average coal cleat compressibility is $1.46(10)^{-3}$ psia$^{-1}$. Palmer and Mansoori reported values of Poisson's ratio for San Juan Basin coal ranging between 0.20 and 0.39.[13] The lower value was obtained from laboratory measurements on coal core, the larger value from scaling laboratory values to field scale. Shi and Durucan obtained a Poisson's ratio of 0.35 from matching San Juan Basin field data.[14] Using a cleat compressibility of $1.46(10)^{-3}$ psia$^{-1}$, a Poisson's ratio of 0.35, and a base permeability of 180 md, permeability as a function of depth as predicted by equations (6.14), (6.15), and (6.16) is plotted in figure 6–3.

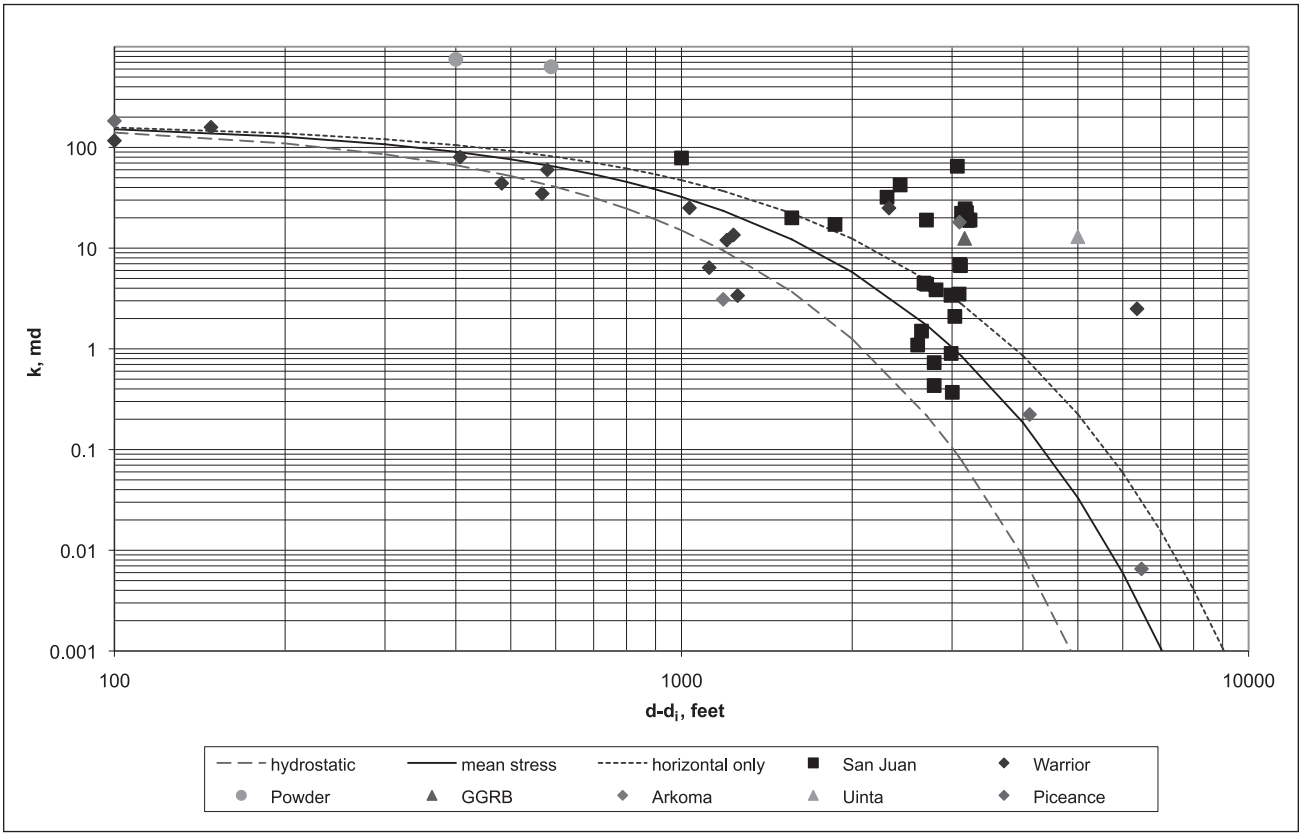



**Fig. 6–3.** Coal permeability vs. depth—data and theory

Also plotted in figure 6–3 are permeability-depth data reported in the literature and listed in table 6–2.

**Table 6–2.** Coal permeability-depth data

| Depth, ft | Perm., md | Basin | Coal | Rank |
|---|---|---|---|---|
| 3,118 | 22.2 | San Juan[a] | Fruitland | na |
| 1,184.5 | 3.1 | Arkoma[b] | Hartshorne | lo-vol. bit |
| 1,565 | 20 | San Juan[c] | Fruitland | na |
| 3,087 | 3.5 | San Juan[d] | Fruitland | med. vol. bit |
| 2,704 | 19 | San Juan[e] | Fruitland | na |
| 1,865 | 17.2 | San Juan[f] | Fruitland | na |
| 589 | 632 | Powder[g] | Canyon | subbit. C |
| 1,033 | 25.1 | Warrior[h] | ML/BC | na |
| 2,790 | 0.73 | San Juan[i] | Fruitland | na |
| 2,430 | 42.4 | San Juan[j] | Fruitland | na |
| 1,202 | 12 | Warrior[k] | na | na |
| 3,201 | 19 | San Juan[l] | Fruitland | na |
| 2,322 | 25 | Warrior[m] | Black Crk | na |
| 3,157 | 12.5 | GGRB[n] | Rock Spgs | hi-vol. B |

**Table 6–2.** Cont.

| Depth, ft | Perm., md | Basin | Coal | Rank |
|---|---|---|---|---|
| 3,065 | 65 | San Juan[o] | Fruitland | na |
| 3,164 | 24.6 | San Juan[p] | Fruitland | na |
| 3,181 | 22.5 | San Juan[q] | Fruitland | na |
| 3,227 | 19 | San Juan[r] | Fruitland | na |
| 2,989 | 0.9 | San Juan[s] | Fruitland | na |
| 3,034 | 2.1 | San Juan[t] | Fruitland | na |
| 400 | 750 | Powder[u] | Wyodak | subbit. |
| 2,650 | 1.5 | San Juan[v] | Fruitland | na |
| 2,677 | 4.5 | San Juan[w] | Fruitland | na |
| 3,094 | 6.9 | San Juan[x] | Fruitland | na |
| 3,104 | 6.7 | San Juan[y] | Fruitland | na |
| 2,987 | 3.4 | San Juan[z] | Fruitland | na |
| 2,500 | 13 | Uinta[aa] | Ferron | hi-vol. B |
| 2,609 | 1.09 | San Juan[bb] | Fruitland | hi-vol. B |
| 2,706 | 4.38 | San Juan[cc] | Fruitland | hi-vol. B |
| 3,003 | 0.37 | San Juan[dd] | Fruitland | na |
| 482 | 44 | Warrior[ee] | Pratt | na |
| 580 | 60 | Warrior[ff] | Pratt | na |
| 50 | 375.5 | Warrior[gg] | na | na |
| 79 | 888.0 | Warrior[hh] | na | na |
| 100 | 116.7 | Warrior[ii] | na | na |
| 100 | 183.4 | Piceance[jj] | na | na |
| 148 | 158.5 | Warrior[kk] | na | na |
| 407 | 80.1 | Warrior[ll] | na | na |
| 568 | 34.8 | Warrior[mm] | na | na |
| 1,000 | 78.6 | San Juan[nn] | na | na |
| 1,119 | 6.4 | Warrior[oo] | na | na |
| 1,235 | 13.5 | Warrior[pp] | na | na |
| 1,256 | 3.4 | Warrior[qq] | na | na |
| 2,304 | 32.1 | San Juan[rr] | na | na |
| 2,790 | 0.43 | San Juan[ss] | na | na |
| 2,811 | 3.9 | San Juan[tt] | na | na |
| 3,092 | 18.1 | Piceance[uu] | na | na |
| 4,110 | 0.22 | Piceance[vv] | na | na |
| 6,357 | 2.5 | Warrior[ww] | na | na |
| 6,475 | 0.007 | Piceance[xx] | na | na |

*na = not available*

*Sources:* [a]Mavor, M. J., and Robinson, J. R. 1993. [b]Cardott, B. J. 1998. [c]Cox, D. O., Young, G. B. C., and Bell, M. J. 1995. *Well Testing in Coalbed Methane (CBM) Wells: An Environmental Remediation Case History*. Paper SPE 30578. Presented at the SPE Annual Technical Conference and Exhibition, Dallas, Texas, October 22–25. [d]Jones, A. H., Ahmed, U., Bush, D. D., Holland, M. T., Kelkar, S. M., Rakop, K. C., Bowman, K. C., and Bell, G. J. 1984. *Methane Production Characteristics for a Deeply Buried Coalbed Reservoir in the San Juan Basin*. Paper SPE 12876. Presented at the Unconventional Gas Recovery Symposium, Pittsburgh, Pennsylvania, May 13–15. [e]Zahner, B. 1997. [f]Mavor, M. J., and Vaughn, J. E. 1997. [g]Mavor, M. J., Russell, B., and Pratt, T. J. 2003. *Powder River Basin Ft. Union Coal Reservoir Properties and Production Decline Analysis*. Paper SPE 84427. Presented at the SPE Annual Technical Conference and Exhibition, Denver, Colorado, October 5–8. [h]Koenig, R. A., and Stubbs, P. B. 1986. [i]Ibid. [j]Ibid. [k]Ibid. [l]Ibid. [m]Reeves, S. R., Lambert, S. W., and Zuber, M. D. 1987. A field derived inflow performance relationship for coalbed gas wells in the Black Warrior Basin. Paper 8744 in *Proceedings of the 1987 International Coalbed Methane Symposium*. Tuscaloosa: University of Alabama. [n]Young, G. B. C., et al. 1991. [o]Mavor, M. J. 1994. [p]Ibid. [q]Ibid. [r]Ibid. [s]Ibid. [t]Ibid. [u]Hower, T. L., et al. 2003. [v]Bell, G. J., et al. 1985. [w]Ramurthy, K., Marjerisson, D. M., and Daves, S. B. 2002. *Diagnostic Fracture Injection Test in Coals to Determine Pore Pressure and Permeability*. Paper SPE 75701. Presented at the SPE Gas Technology Symposium, Calgary, Alberta. April 30–May 2. [x]Vo, D. T., Ohaeri, C. U., and Montoya, G. L. 1991. *Pressure Buildup Analysis of Early-Time Data from Coalbed Methane Wells in the Rincon Unit, San Juan Basin, New Mexico*. Paper SPE 22684. Presented at the SPE Annual Technical Conference and Exhibition, Dallas, Texas, October 6–9. [y]Ibid. [z]Ibid. [aa]Burns, T. D., and Lamarre, R. A. 1997. Drunkards Wash Project: Coalbed methane production from Ferron coals in east-central Utah. Paper 9709 in *Proceedings of the 1997 International Coalbed Methane Symposium*. Tuscaloosa: University of Alabama. [bb]Ramurthy, K., et al. 2003. [cc]Ibid. [dd]Puri, R., Volz, R., and Duhrkopf, D. 1995. A micro-pilot approach to coalbed methane reservoir assessment. Paper 9556 in *Proceedings of the 1995 International Coalbed Methane Symposium*. Tuscaloosa: University of Alabama. [ee]Young, G. B. C., et al. 1991. [ff]Ibid. [gg]McKee, C. R., et al. 1988. [hh]Ibid. [ii]Ibid. [jj]Ibid. [kk]Ibid. [ll]Ibid. [mm]Ibid. [nn]Ibid. [oo]Ibid. [pp]Ibid. [qq]Ibid. [rr]Ibid. [ss]Ibid. [tt]Ibid. [uu]Ibid. [vv]Ibid. [ww]Ibid. [xx]Ibid.

All data are from single-phase tests and are therefore clear of any relative permeability effects. Reported permeabilities vary by a factor of 3,000, from 0.00653 md to 888 md, with a median value of 18 md. Depths range from 50 to 6,500 ft (15 to 1,980 m), with no data from very deep coals. All data are from North American coals of Pennsylvanian, Cretaceous, and Paleocene age. Permeabilities of coals from other areas and other geological ages may differ significantly from these reported data. The reported data exhibit such a high degree of scatter that attempts to fit a curve through them yields only a soft result, bordering on nonunique. By inspection, the best fit curve is perhaps the ICM model of Shi and Durucan, which assumes permeability is controlled by horizontal stresses.[15]

Inspection of figure 6–3 reveals permeability variation within a basin is greater than permeability variation between basins. Contributing to the variation are a host of coal properties, such as ash and moisture, degree of cleating, and rank. In addition, local stresses and tectonics will affect permeability of a coal deposit. This geological heterogeneity makes the use of a permeability-depth relation to predict sweet spots during exploration or to define a maximum coal depth during development hazardous.

As gas and water are withdrawn from a coal deposit, reservoir pressure declines and stress increases. This increase in stress decreases cleat width, reducing permeability. Assuming the vertical lithostatic load is unchanging during depletion of a coal, the change in stress is given by

$$\sigma_v - \sigma_{vi} = S - p - (S - p_i) = p_i - p$$

Assuming a hydrostatic stress regime, equation (6.8), permeability decrease during depletion is

$$\frac{k}{k_i} = \exp\left[-3c_f(p_i - p)\right] \tag{6.17}$$

The mean stress approximation, equation (6.11), yields

$$\frac{k}{k_i} = \exp\left[-c_f\left(\frac{1+\nu}{1-\nu}\right)(p_i - p)\right] \tag{6.18}$$

Assuming a uniaxial stress regime with permeability controlled by horizontal stresses, the ICM model of Shi and Durucan, equation (6.12) gives[16]

$$\frac{k}{k_i} = \exp\left[-3c_f\left(\frac{\nu}{1-\nu}\right)(p_i - p)\right] \tag{6.19}$$

Employing the values of cleat compressibility and Poisson's ratio discussed above in equations (6.17), (6.18), and (6.19) yields the permeability-depletion pressure plots shown in figure 6–4.

Inspection of this figure shows the importance of choosing the correct conceptual model, as permeabilities for a given pressure can vary by more than an order of magnitude, especially in deep depletion. The harshest permeability decline is seen under the assumption of hydrostatic stress, while the mildest permeability decline is observed under the assumption that only horizontal stresses control permeability. Permeability based upon the mean stress assumption falls between those of the other two conceptual models. Determination of which conceptual model describes a given coal seam is difficult. Even after incorporating all available geologic and engineering data, identification of the correct conceptual model is often difficult and nonunique.

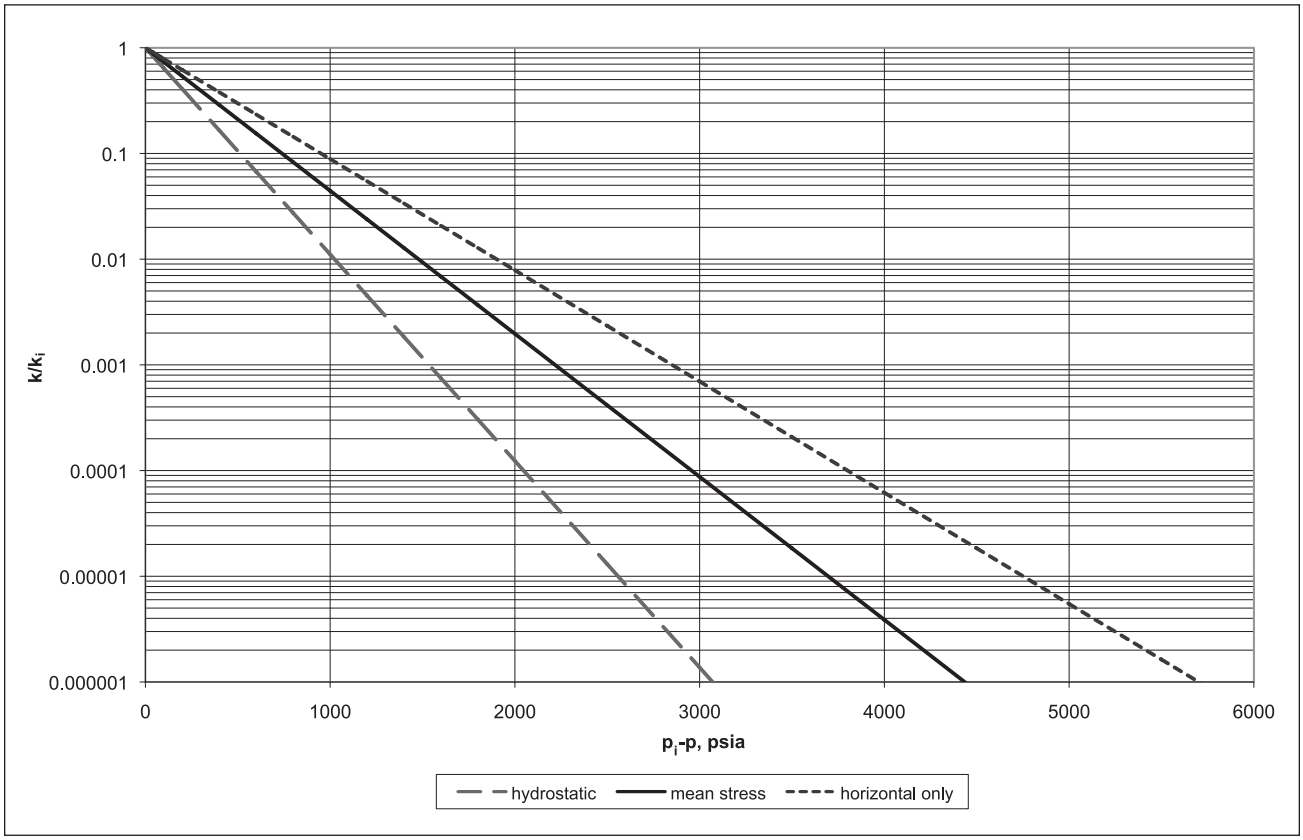



**Fig. 6–4.** Predicted coal permeability decline with depletion

## Gas-Water Relative Permeabilities in Coal

Absolute permeability of a coal is a function of the rock, not the fluids flowing through it. Effective permeability of a fluid flowing through a coal depends on fluid properties and saturations as well as absolute coal permeability. Relative permeability is the ratio of effective permeability divided by absolute permeability. As coal gas production usually involves dewatering of a coal seam, gas and water saturations in the cleats vary areally and over time. The interplay between gas and water in the cleats affects mobility of both, making gas-water relative permeabilities one of the controlling influences in coal gas production.

Similar to conventional reservoirs, gas-water relative permeability behavior in coals is difficult to predict and is therefore measured experimentally. With cleat spacing typically on the order of millimeters, the larger the sample, the more likely it is to contain a fracture network representative of the in-situ coal deposit. Consequently, coal gas-water relative permeabilities are typically measured on whole core or mine samples rather than rotary sidewall cores or core plugs. Early studies of gas-water relative permeabilities in bituminous coals encountered difficulties in adapting experimental procedures for determining relative permeabilities of fluids flowing through conventional reservoirs to coals.[17] Difficulties were encountered due to the very small coal porosities and imprecise definition of water saturation in a coal.

As discussed in chapter 2, coal porosity is comprised of phyteral porosity from relic organics and linear porosity from cleats and fractures. Coal porosity is comprised of micropores (pore diameters < 2 nm), mesopores (diameters between 2 and 50 nm), and macropores (diameters > 50 nm). The distribution of each is dependent on coal rank, purity, and other coal properties. Accessible pore volume in a coal depends on the fluid filling the pores, with $CO_2$ providing the largest microporosity. Condition of a coal sample affects measured porosity, as the more open structure of aged and dessicated samples is distinctly different than in-situ coals. Maximum values of coal porosity, on the order of 14%, are obtained from injection of helium into dried coal samples,

while minimum values, often less than 1%, are obtained by displacement of water from stressed, well-preserved samples.[18] Regardless of the experimental protocol used to measure coal porosity, determination of cleat and matrix contributions to the porosity is difficult and somewhat arbitrary. Water porosity as a function of rank was discussed by Levine.[19] Porosity was largest in subbituminous coals, up to 22%, then decreased to a minimum of 3% in semianthracites before increasing to 6% in anthracites.

Water can exist in coal as chemically-bound bed water, adsorbed to the surface of the coal, or as free water in the cleats. During depletion of a coal seam, bound bed water is static, changes in adsorbed water are minimal, and cleat water decreases enough to change gas and water mobilities by several orders of magnitude. *Water saturation* in a coal, defined as the water volume divided by the void volume, is thus more complicated than water saturation in conventional sandstone and carbonate reservoirs. A useful concept for coal gas reservoir engineering is that of *mobile water porosity*, which is defined as the water volume that will flow from a coal sample due to a pressure gradient. Measurement of mobile water porosity by various methods is discussed by Gash, with the most direct method being displacement of water from the sample with humidified helium.[20] Note that measurement of water displaced from a coal sample during stress loading can be used to determine cleat compressibility, and mobile water porosity is determined once the sample has equilibrated under the applied stresses. Mobile water porosity is used to compute original water in place for a given coal and is relevant for estimation of water disposal volumes.

Discussing selection and preparation of coal samples for relative permeability testing, Hyman et al. noted the fragile nature of coals and recommended that care be taken to keep coal samples moist and to prevent unnecessary mechanical loading, such as flexing of the core when laying down the core barrel at the surface.[21] Gash noted that many drilling mud additives can alter coal properties and recommended potassium chloride mud for coal coring operations.[22] Testa and Pratt discussed coal sample preparation necessary for reliable laboratory tests and noted that low-rank coals are even more sensitive to oxidation than high-rank coals.[23] Current practice for coal core dedicated to relative permeability and other laboratory flow tests dictates the core is not removed from the barrel at the wellsite but rather cut into pieces roughly 1 m in length, capped with rubber endcaps, and shipped to the laboratory. Note that some provision must be made to allow escape of desorbing methane gas from the samples during transport.

Upon arrival at the laboratory, the core is carefully removed from the core barrel, placed in formation water (or 2% KCl water), and gently cleaned of drilling mud and debris. Well-cleated samples are visually identified, wrapped in Teflon or jacketed with heat shrink tubing, and the ends trimmed square. Stabilization of samples by coating them with epoxy or other resins can alter coal properties and is therefore not recommended. Prepared samples are stored under water until insertion into the apparatus for relative permeability measurement.

Absolute coal permeability, necessary for calculation of relative permeabilities, declines with time during laboratory measurements and shows strong hysteresis effects.[24] This behavior is attributed to generation and migration of coal fines and irreversible stress dependence of the fracture apertures. Consequently for permeability measurements, coal samples are slowly cycled a single time, and care is taken to acquire plentiful data. Once in the flow apparatus, single-phase water flow is established and an initial permeability determined. Measurement of fluid volume expelled as the sample is stressed to test conditions allows calculation of cleat compressibility. Once at test conditions, flow is monitored for several days or a week until permeability stabilizes. Gas-water relative permeabilities are then determined by one of two methods.

Measurement of relative permeability with the steady-state method requires injection of the two fluids at constant rates or constant pressures until expelled fluid fractions are the same as injected fractions. Effective permeabilities are calculated from Darcy's law, while saturations are typically determined with tracer techniques. The low permeabilities of many coals dictate long equilibration times for this method.

The unsteady-state method for relative permeability, in which one fluid is displaced by the other, is much quicker than the steady-state method. However, it requires independent measurement of the pore volume and suffers from a lack of precision at low gas saturations, precisely the region of interest in most coal gas plays. To avoid or minimize gas sorption effects, helium or nitrogen rather than methane is employed for coal gas-water relative permeability measurements. Gash et al. suggested procedural improvements to increase accuracy of this method for low-porosity samples at low gas saturations.[25] Experimental data are analyzed with the JBN method.[26]

As noted above, coal deposits are characterized by two sets of natural fractures, the face and butt cleats. Vertical reach of a face cleat typically exceeds that of a butt cleat, but both are limited by bedding plane heterogeneity, often dying out in tough, shaley layers. Flow properties of this fracture network, such as absolute and relative permeabilities, are intuitively expected to be heterogeneous, but as discussed below, laboratory and field experience indicates the opposite.

Absolute and gas-water relative permeabilities were measured on a trio of well-cleated San Juan Fruitland coal samples by Gash et al.[27] All three samples, carefully prepared from fresh mine samples, were 3.5 in. in diameter by 4 in. long. Absolute permeability to water was determined first, followed by unsteady-state gas-water relative permeabilities. Sample porosity averaged 0.41%, and absolute permeability declined with time, probably due primarily to coal fines. Permeability in the butt cleat direction was one-half that in the face cleat direction, and vertical permeability was two orders of magnitude less than face cleat permeability. Stabilized absolute permeabilities and porosities measured at two confining pressures obeyed the cubic relation of equation (6.6). Experimental procedures to increase the accuracy of unsteady-state relative permeability measurements at low gas saturations were presented. Gas-water relative permeabilities measured in the face cleat, butt cleat, and perpendicular to the bedding planes were essentially equal, a counterintuitive result from an anisotropic fracture network.

In evaluating pressure transient tests from San Juan Basin coal wells, Mavor and Robinson investigated applicability of algebraic equations for gas and water relative permeabilities developed for conventional reservoirs to gas-water relative permeabilities of Fruitland coal measured by Gash.[28] Gas and water relative permeabilities were calculated from

$$k_{rg} = k_g^r (1 - S_w^*)^{n'} \left[ 1 - (S_w^*)^{\frac{2+\lambda}{\lambda}} \right] \tag{6.20}$$

$$k_{rw} = (S_w^*)^{\frac{2+3\lambda}{\lambda}} \tag{6.21}$$

$$S_w^* = \frac{S_w - S_{iw}}{1 - S_{iw}} \tag{6.22}$$

where

$k_{rg}$ = gas relative permeability,
$k_g^r$ = gas relative permeability at irreducible water saturation,
$k_{rw}$ = water relative permeability,
$\lambda$ = empirical coefficient,
$n'$ = empirical coefficient,
$S_w$ = water saturation, and
$S_{iw}$ = irreducible water saturation.

Mavor and Robinson reported the best fit to the Gash San Juan gas-water relative permeability data, presented in table 6–3, was obtained using

$$\lambda = 100,\ S_{iw} = 0.05,\ n' = 0.5,\ k_g^r = 0.65$$

**Table 6–3.** Gas-water relative permeabilities—San Juan Basin, Fruitland coal

| $S_w$ | $k_{rw}$ | $k_{rg}$ | $k_g/k_w$ | $S_g$ |
|---|---|---|---|---|
| 0.000 | 0.000 | 1.000 | 9999 | 1.00 |
| 0.050 | 0.000 | 0.835 | 9999 | 0.95 |
| 0.100 | 0.000 | 0.720 | 9999 | 0.90 |
| 0.150 | 0.002 | 0.627 | 314 | 0.85 |
| 0.200 | 0.007 | 0.537 | 76.7 | 0.80 |
| 0.250 | 0.015 | 0.465 | 31.0 | 0.75 |
| 0.300 | 0.024 | 0.401 | 16.7 | 0.70 |
| 0.350 | 0.035 | 0.342 | 9.77 | 0.65 |
| 0.400 | 0.049 | 0.295 | 6.02 | 0.60 |
| 0.450 | 0.067 | 0.253 | 3.78 | 0.55 |
| 0.500 | 0.088 | 0.216 | 2.45 | 0.50 |
| 0.550 | 0.116 | 0.180 | 1.55 | 0.45 |
| 0.600 | 0.154 | 0.147 | 0.955 | 0.40 |
| 0.650 | 0.200 | 0.118 | 0.590 | 0.35 |
| 0.700 | 0.250 | 0.090 | 0.360 | 0.30 |
| 0.750 | 0.312 | 0.070 | 0.224 | 0.25 |
| 0.800 | 0.392 | 0.051 | 0.130 | 0.20 |
| 0.850 | 0.490 | 0.033 | 0.067 | 0.15 |
| 0.900 | 0.601 | 0.018 | 0.030 | 0.10 |
| 0.950 | 0.731 | 0.007 | 0.010 | 0.05 |
| 0.975 | 0.814 | 0.004 | 0.004 | 0.025 |
| 1.000 | 1.000 | 0.000 | 0.000 | 0.000 |

*Source:* Gash, B. W. 1991.

Gas and water relative permeabilities measured by Gash are compared with those calculated from the Mavor and Robinson equations in figure 6–5.

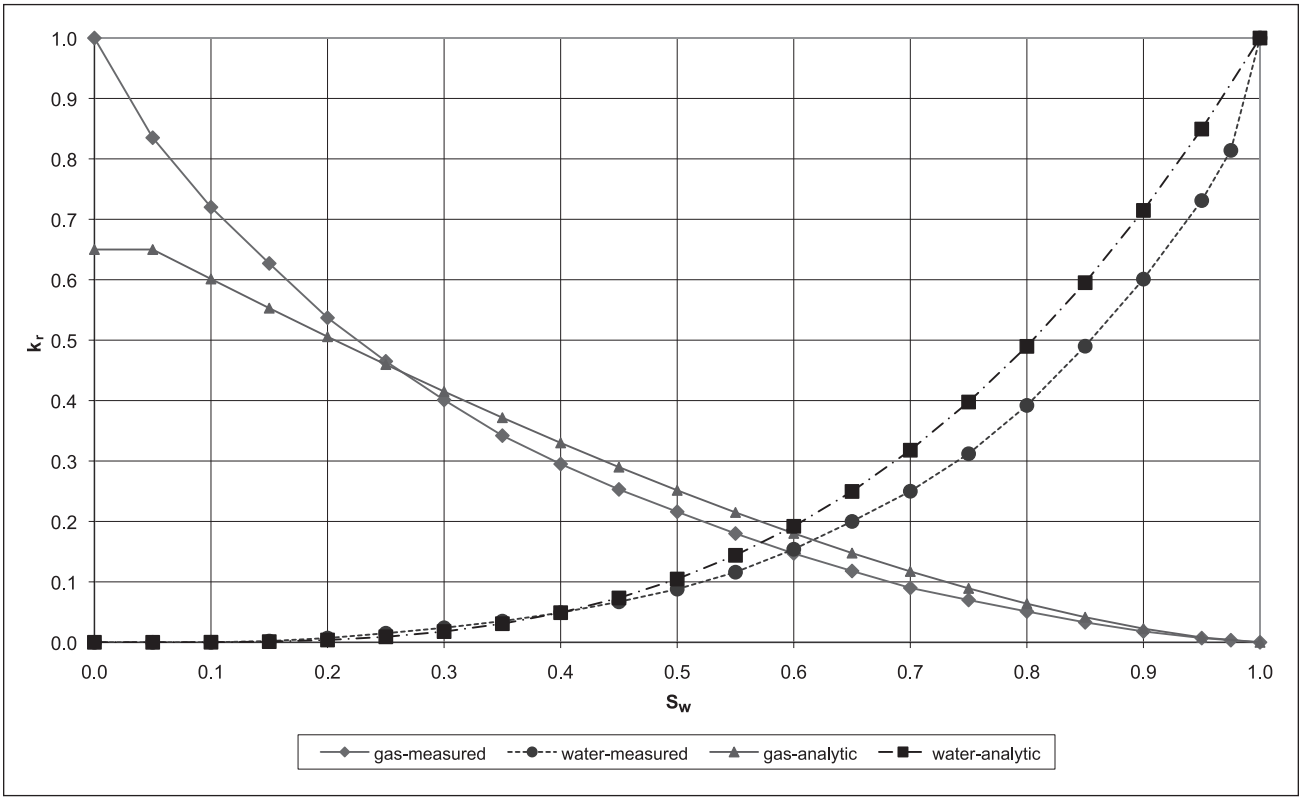



**Fig. 6–5.** Measured and calculated gas-water relative permeabilities—San Juan coal[29]

The two sets of curves are in general agreement for high water saturations, the saturations of most importance for coal gas reservoir engineering. Below water saturations of about 20%, the measured gas relative permeability is significantly larger than the analytic value. However, this is of little practical consequence, as both measured and analytic water relative permeabilities are so low here that actual coal wells may never attain such low saturations.

Gas-water relative permeabilities of the Blue Creek coal in the Warrior Basin were measured by Gash and Conway et al.[30] Gash employed a 2 in. diameter sample approximately 4 in. in length, with a base permeability of 3 md and a mobile water porosity of 1.0%. Conway et al. used a 1 in. diameter plug of unreported length and base permeability and an inferred mobile water porosity of 0.53%. Neither study reported orientation of bedding planes in the samples. Flows may have been parallel to the bedding planes (representing nominally horizontal flow in the reservoir), perpendicular to the bedding planes (representing nominally vertical flow in the coal seam), or at an angle to the bedding planes (an unlikely orientation given the difficulty in sample preparation).

The Gash and Conway et al. gas-water permeabilities, plotted in figure 6–6 and listed in tables 6–4 and 6–5, exhibit the same general shapes. The water relative permeability initially declined rapidly to a long tail, while gas relative permeability increased nearly linearly as water saturation fell.

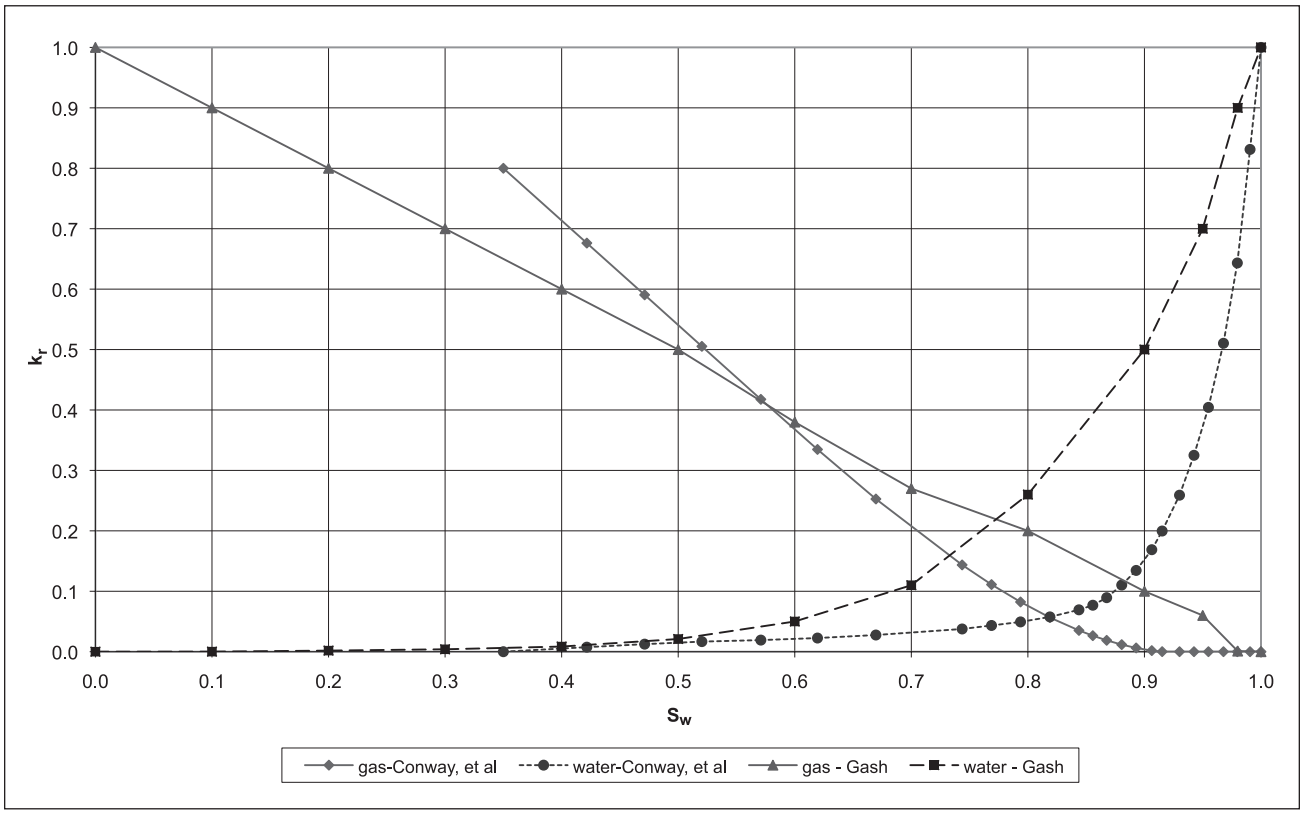



**Fig. 6–6.** Measured gas-water relative permeabilities—Marylee/Blue Creek coal[31]

The Gash data exhibit a critical gas saturation (the lowest gas saturation of nonzero gas relative permeability) of zero, in agreement with many other naturally fractured reservoirs. Gas and water relative permeabilities cross over at a value of 0.22, corresponding to a water saturation of 77%. Irreducible water saturation (the water saturation corresponding to zero relative permeability to water) is zero, as would be expected from the definition of mobile water porosity, and gas relative permeability is 1.0. The curves of Conway et al. exhibit a critical gas saturation of 7%, crossover relative permeabilities of 0.057 at a water saturation of 82%, and an irreducible water saturation of 35%, at which time gas relative permeability has risen to 0.800. Variations in the two sets of relative permeability curves are ascribed to sample heterogeneity, flow limitations of the limited fracture networks in the small coal samples, and experimental difficulties associated with extremely small porosities.

**Table 6–4.** Gas-water relative permeabilities—Warrior Basin, Blue Creek coal

| $S_w$ | $k_{rw}$ | $k_{rg}$ | $k_g/k_w$ | $S_g$ |
|---|---|---|---|---|
| 0.00 | 0.00 | 1.00 | na | 1.00 |
| 0.10 | 0.00 | 0.900 | 9000 | 0.90 |
| 0.20 | 0.00 | 0.80 | 444 | 0.80 |
| 0.30 | 0.00 | 0.70 | 175 | 0.70 |
| 0.40 | 0.01 | 0.60 | 70.6 | 0.60 |
| 0.50 | 0.02 | 0.50 | 23.8 | 0.50 |
| 0.60 | 0.05 | 0.38 | 7.60 | 0.40 |
| 0.70 | 0.110 | 0.27 | 2.45 | 0.30 |
| 0.80 | 0.260 | 0.20 | 0.769 | 0.20 |
| 0.90 | 0.500 | 0.10 | 0.200 | 0.10 |
| 0.95 | 0.700 | 0.06 | 0.086 | 0.05 |
| 0.98 | 0.900 | 0.00 | 0.001 | 0.02 |
| 1.00 | 1.00 | 0.00 | 0.000 | 0.00 |

*na = not available*
*Source:* Gash, B. W. 1991.

**Table 6–5.** Gas-water relative permeabilities—Warrior Basin, Marylee/Blue Creek coal

| $S_w$ | $k_{rw}$ | $k_{rg}$ | $k_g/k_w$ | $S_g$ |
|---|---|---|---|---|
| 0.350 | 0.000 | 0.800 | 999 | 0.650 |
| 0.422 | 0.008 | 0.676 | 90.2 | 0.578 |
| 0.471 | 0.013 | 0.591 | 47.2 | 0.529 |
| 0.520 | 0.017 | 0.505 | 30.3 | 0.480 |
| 0.571 | 0.019 | 0.418 | 21.8 | 0.429 |
| 0.620 | 0.023 | 0.335 | 14.8 | 0.381 |
| 0.670 | 0.028 | 0.253 | 9.16 | 0.330 |
| 0.744 | 0.038 | 0.144 | 3.82 | 0.256 |
| 0.769 | 0.043 | 0.111 | 2.56 | 0.231 |
| 0.794 | 0.049 | 0.082 | 1.67 | 0.206 |
| 0.819 | 0.058 | 0.057 | 0.981 | 0.181 |
| 0.844 | 0.069 | 0.035 | 0.508 | 0.156 |
| 0.856 | 0.077 | 0.027 | 0.345 | 0.144 |
| 0.868 | 0.089 | 0.019 | 0.210 | 0.132 |
| 0.881 | 0.110 | 0.012 | 0.106 | 0.120 |
| 0.893 | 0.135 | 0.006 | 0.046 | 0.107 |
| 0.906 | 0.169 | 0.002 | 0.011 | 0.094 |
| 0.915 | 0.200 | 0.000 | 0.001 | 0.085 |
| 0.930 | 0.259 | 0.000 | 0 | 0.070 |
| 0.943 | 0.325 | 0.000 | 0 | 0.058 |
| 0.946 | 0.404 | 0.000 | 0 | 0.054 |
| 0.968 | 0.510 | 0.000 | 0 | 0.032 |
| 0.980 | 0.643 | 0.000 | 0 | 0.020 |
| 0.991 | 0.831 | 0.000 | 0 | 0.009 |
| 1.000 | 1.000 | 0.000 | 0 | 0.000 |

*Source:* Conway, M. W., et al. 1995.

Similar to equation (6.21), Conway et al. fit their gas relative permeability data to

$$k_{rg} = k_g^r \left(1 - \frac{S_w - S_{iw}}{1 - (S_{iw} + S_{gc})}\right)^{n'} \left[1 - (S_w^*)^{\frac{2+\lambda}{\lambda}}\right]$$

where

$S_{gc}$ = critical gas saturation.

Note the above equation reduces to equation (6.21) for a critical gas saturation of zero. The most accurate match was obtained from

$$\lambda = 1.0,\ S_{iw} = 0.35,\ n' = 1.23,\ k_g^r = 0.8,\ S_{gc} = 0.085$$

No similar equation could be obtained for the water relative permeability.

Gas-water relative permeabilities for the Wyodak coal of the Powder River Basin were developed by Hower et al. during the history matching portion of a simulation study that included several hundred wells on the east side of the basin.[32] Performance of this highly permeable, subbituminous coal was modeled using gas-water relative permeabilities of crossed, straight lines with irreducible water and critical gas saturations of zero and different endpoint permeabilities. The endpoint values, a maximum $k_{rg}$ of 0.8 and a maximum $k_{rw}$ of 0.5, were two of the many history match parameters. Subbituminous coals are generally more porous, more permeable, and have a more open fabric than bituminous coals. Consequently, the distinctly different gas-water relative permeability curves for the different rank coals are not unexpected.

Gas-water relative permeabilities of coals from the Sydney and Bowen basins of Australia were discussed by Meany and Paterson.[33] Relative permeabilities were measured on 10 samples 2 in. in diameter and 4.75 in. long, all but one cut vertically, nominally across the bedding planes. Similar to the Warrior Basin curves discussed above, all the Australian curves exhibited crossovers at high water saturations. Meaney and Paterson attributed this behavior to viscous fingering as gas displaces water. In addition to the 10 sets of experimentally measured relative permeabilities, gas-water relative permeabilities for 6 samples were developed from history matching field performance with a reservoir simulator. Gas-water relative permeabilities were measured on two samples from the German Creek seam of the Bowen Basin. A third set was developed from history matching performance of wells draining this coal with an unspecified simulator. All three sets of gas-water relative permeabilities are plotted in figure 6–7 and collected in table 6–6.

The divergence between the three sets of German Creek curves is typical of coal seam gas-water relative permeabilities, leading to questioning the need to expend the time and money required for their laboratory measurement. For reservoir engineering purposes, this dilemma is treated two ways. First, sensitivity of a given parameter, e.g., effective permeability to water at a given saturation, can be assessed using selected sets of relative permeability curves. Secondly, gas-water relative permeability curves can be determined from simulation of well performance. Note that history-matched relative permeability curves for a coal often exhibit very different behavior from laboratory-based curves. This is because they describe not only the classical gas and water mobilities but also incorporate viscous fingering and gas buoyancy effects in this naturally fractured reservoir.

For wells completed in water-saturated coals, gas-water relative permeability curves can be approximated by first applying a decline curve to water production to determine initial water in place. Water saturation at any given time is then calculated from cumulative water and initial water in place. Absolute permeability is estimated from initial water production. Selecting times when reservoir and bottomhole flowing pressures and gas and water rates are all known, Darcy's equation yields effective permeabilities at that time. Dividing effective permeability to gas and water by initial permeability gives the respective gas and water relative permeabilities. The more the coal has been dewatered, of course, the larger the water saturation range of these field-derived relative permeabilities.

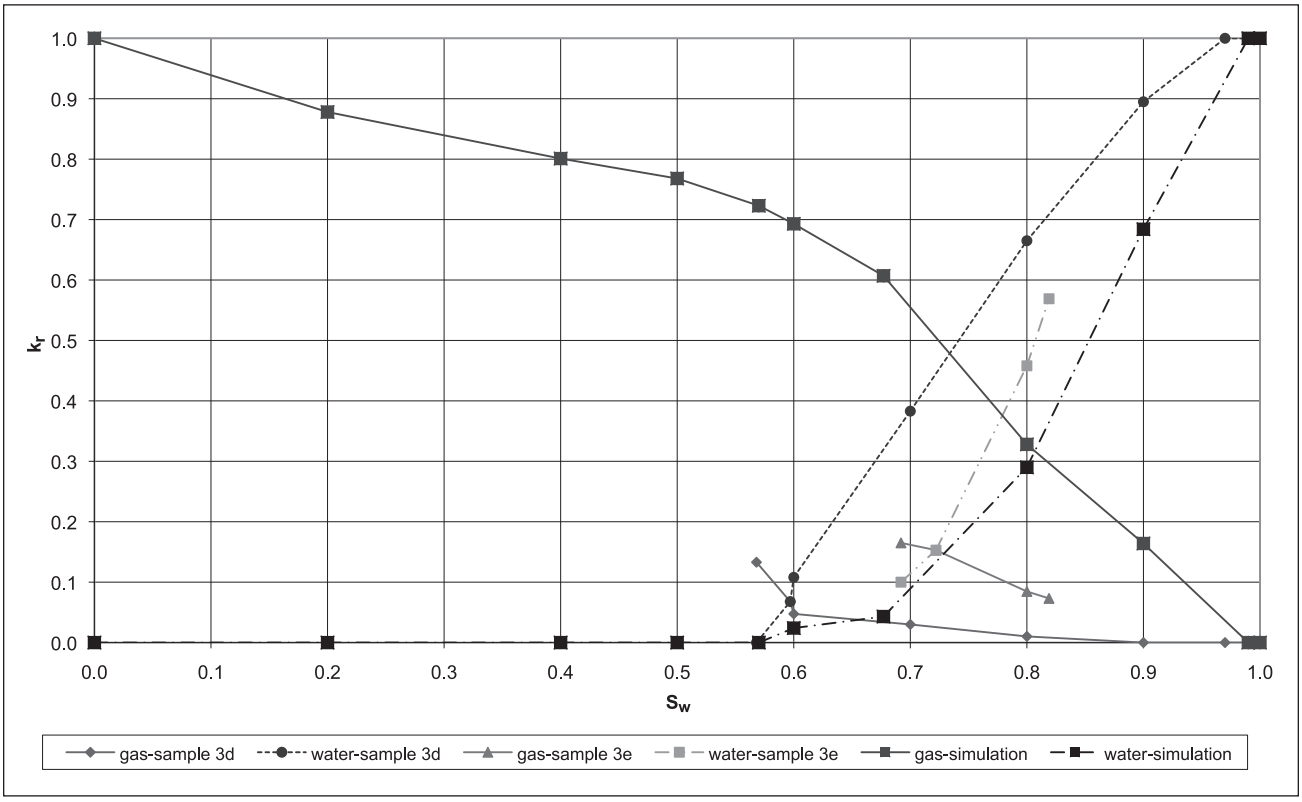



**Fig. 6–7.** Measured and history-matched gas-water relative permeabilities—Bowen Basin, Australia, German Creek seam[34]

**Table 6–6.** Gas-water relative permeabilities—Bowen Basin, Australia, German Creek seam

| | $S_w$ | $k_{rw}$ | $k_{rg}$ | $k_g/k_w$ | $S_g$ |
|---|---|---|---|---|---|
| Sample 3d | 0.568 | 0.000 | 0.133 | 999 | 0.432 |
| | 0.597 | 0.068 | 0.068 | 1.000 | 0.403 |
| | 0.600 | 0.108 | 0.048 | 0.440 | 0.400 |
| | 0.700 | 0.383 | 0.030 | 0.078 | 0.300 |
| | 0.800 | 0.665 | 0.010 | 0.015 | 0.200 |
| | 0.900 | 0.895 | 0.000 | 0.000 | 0.100 |
| | 0.970 | 1.000 | 0.000 | 0.000 | 0.030 |
| | 1.000 | 1.000 | 0.000 | 0.000 | 0.000 |
| | $S_w$ | $k_{rw}$ | $k_{rg}$ | $k_g/k_w$ | $S_g$ |
| Sample 3e | 0.692 | 0.100 | 0.165 | 1.65 | 0.308 |
| | 0.722 | 0.153 | 0.153 | 1.00 | 0.278 |
| | 0.800 | 0.458 | 0.085 | 0.185 | 0.200 |
| | 0.819 | 0.569 | 0.073 | 0.128 | 0.181 |
| | $S_w$ | $k_{rw}$ | $k_{rg}$ | $k_g/k_w$ | $S_g$ |
| Simulation | 0.000 | 0.000 | 1.000 | 999 | 1.000 |
| | 0.200 | 0.000 | 0.878 | 999 | 0.800 |
| | 0.400 | 0.000 | 0.801 | 999 | 0.600 |
| | 0.500 | 0.000 | 0.768 | 999 | 0.500 |
| | 0.570 | 0.000 | 0.723 | 999 | 0.430 |
| | 0.600 | 0.024 | 0.693 | 28.9 | 0.400 |
| | 0.677 | 0.043 | 0.607 | 14.1 | 0.323 |
| | 0.800 | 0.290 | 0.328 | 1.13 | 0.200 |
| | 0.900 | 0.684 | 0.164 | 0.240 | 0.100 |
| | 0.990 | 1.000 | 0.000 | 0.000 | 0.010 |
| | 1.000 | 1.000 | 0.000 | 0.000 | 0.000 |

*Source:* Meaney, K., and Paterson, L. 1996.

## Matrix Deformation Due to Sorption

Regardless of age, rank, or purity, coal matrix is a reactive, organic rock composed of complex hydrocarbons. Matrix "grains" or "crystals" are relatively stiff compared to the cleats, with reported compressibilities averaging $1.41(10)^{-7}$ psia$^{-1}$.[35] This average matrix compressibility is approximately four orders of magnitude smaller than the average cleat compressibility discussed above. However, the matrix swells as gas adsorbs on the surface and shrinks when the gas desorbs. Matrix shrinkage increases cleat width, increasing permeability. From equation (6.3), permeability depends on cleat width cubed. Porosities of bituminous coals are generally around 1%, implying the matrix occupies about 99% of the rock volume. If the matrix shrinks 1% during depletion, from 99% to 98%, porosity increases from 1% to 2%, and cleat width doubles. A doubling of cleat width increases permeability eight-fold. Subbituminous coals are more porous than bituminous coals, averaging about 10% porosity. For a matrix shrinkage of 1%, cleat porosity would increase from 10% to 11%, and permeability would increase by one-third. Consequently, matrix shrinkage affects higher rank coals more than low-rank coals. In addition to increasing absolute permeability, matrix shrinkage also increases gas relative permeability. As cleat volume increases, water volume does not, which decreases water saturation, leading to greater gas relative permeability.

The influences of gas composition and coal rank on matrix deformation have not been thoroughly investigated. A laboratory study of matrix shrinkage and swelling found that $CO_2$ swells coal more than does methane and noted that data relating maceral composition and ash to matrix behavior were too sparse for meaningful conclusions.[36] Laboratory-measured strains perpendicular and parallel to bedding planes were also discussed by Levine, but applicability to reservoir conditions is tenuous.[37] Several studies have measured matrix shrinkage as a function of pressure in the laboratory, and typical matrix elongation coefficients, representative but not exhaustive, are given in table 6–7.[38]

**Table 6–7.** Coal matrix strain coefficients

| Basin | Coal | Rank | Gas | Shrinkage coefficient, psia$^{-1}$ |
|---|---|---|---|---|
| na[a] | na | lo-vol. bit.–semianth. | methane | 1.70E–06 |
| na[b] | na | hi–vol. A–anth. | methane & $CO_2$ | 2.76–6.90E–6 |
| na[c] | na | bit. & anth. | na | 1.40–6.90E–6 |
| Appalachian[d] | na | na | $CO_2$ | 6.55E–05 |
| Japanese[e] | na | na | methane | 1.81E–08 |
| na[f] | na | na | methane | 2.57E–04 |
| Warrior & Piceance[g] | na | na | methane & $CO_2$ | 7.10E–06 |
| Illinois[h] | na | hi-vol. bit. | methane | 1.80E–03 |
| Illinois[i] | na | hi-vol. bit. | $CO_2$ | 5.00E–03 |

*na = not available*
*Sources:* [a]Moffat, D. H., and Weale, K. E. 1995. [b]Gunther, J. 1968. [c]Wubben, P., et al. 1986. [d]Reucroft, P. J., and Patel, H. 1986. [e]Gray, I. 1987 [f]Juntgen, H. 1987. [g]Harpalani, S., and Schraufnagel, R. A. 1990. [h]Levine, J. R. 1996. [i]Ibid.
*Note:* Average = 6.50E–4 psia$^{-1}$.

However, the degree of matrix deformation is proportional to the change in gas content, not pressure, and these coefficients have limited use for reservoir engineering purposes.[39]

As matrix deformation is proportional to gas content, Levine proposed matrix strain could be described by an equation similar to the Langmuir isotherm equation[40]

$$\varepsilon = \varepsilon_{max} \frac{p}{p + p_{50}} \tag{6.23}$$

where

$\varepsilon$ = matrix strain,
$\varepsilon_{max}$ = maximum matrix strain, and
$p_{50}$ = pressure where strain is one-half maximum strain.

Levine measured swelling of dry, Carboniferous, high-volatile bituminous coal samples from the Illinois Basin induced by sorption of methane and $CO_2$. Fitting the methane data to equation (6.23) yielded $\varepsilon_{max} = 3.46(10)^{-3}$ and $p_{50} = 697$ psia. Similarly, the $CO_2$ data gave maximum strain, $\varepsilon_{max} = 7.44(10)^{-3}$, and one-half maximum strain pressure, $p_{50} = 329$ psia. As high-rank coals typically sorb twice as much $CO_2$ as methane at any given pressure, a value of about two for the ratio of maximum strain coefficients makes intuitive sense. Seidle and Huitt measured swelling of high-volatile C bituminous coal from the San Juan Basin at reservoir temperature and humidity using both methane and $CO_2$.[41] Sufficient data were reported to convert their methane, but not $CO_2$, results to equation (6.23), resulting in Levine methane coefficients of $\varepsilon_{max} = 4.48(10)^{-4}$ and $p_{50} = 500$ psia. Similar to the Langmuir isotherm, the lower the $p_{50}$ value in equation (6.23), the steeper the Levine strain curve. With $CO_2$, $p_{50}$ value is about one-half the methane value, and the $CO_2$ strain curve rises more steeply than the methane curve. Thus for initial pressure increases, $CO_2$ swelling exceeds that of methane, which fits with laboratory comments of coals being more reactive to $CO_2$ than methane. For reservoir engineering purposes, the Langmuir pressure, $p_L$, can often be substituted for $p_{50}$ with little loss of accuracy.

## Combined Stress and Matrix Shrinkage Influences on Coal Permeability

Levine described pressure dependence of cleat width as the sum of the initial width, a term to account for stress, and a term to capture matrix deformation.[42] A similar sum was presented to describe permeability variation with pressure. During depletion, stress increases, thereby decreasing cleat width and permeability, while matrix shrinkage increases cleat width and permeability. The two effects compete with one another, and dominance depends on coal properties and reservoir pressure change. A more complete mathematical description of stress and matrix deformation physics begins with an equation for the ratio of porosity at a given pressure to initial porosity. The ratio of permeability at that pressure to initial permeability is, from equation (6.6), simply the cube of the porosity ratio.

Similar to the Levine sum for cleat width, Palmer and Mansoori described the ratio of porosity at a given pressure to initial porosity as[43]

$$\frac{\phi}{\phi_i} = 1 + \frac{c_m}{\phi_i}(p - p_i) + \frac{c_0}{\phi_i}\left(\frac{K}{M} - 1\right)\left(\frac{Bp}{1+Bp} - \frac{Bp_i}{1+Bp_i}\right) \tag{6.24}$$

where

$c_m = 1/M$, psia$^{-1}$,
$c_0$ = volumetric strain coefficient, psia$^{-1}$,
$B$ = reciprocal of Langmuir pressure, psia$^{-1}$,
$M$ = constrained axial modulus, psia, and
$K$ = bulk modulus, psia.

The constrained axial modulus, $M$, is given by

$$M = \frac{(1-\nu)E}{(1+\nu)(1-2\nu)}$$

Using the definition of $c_m$ and the relation

$$\frac{K}{M} = \frac{1}{3}\left(\frac{1+\nu}{1-\nu}\right)$$

the Palmer-Mansoori porosity relation can be written as

$$\frac{\phi}{\phi_i} = 1 + \frac{(1+\nu)(1-2\nu)}{(1-\nu)E\phi_i}(p - p_i) + \frac{c_0}{\phi_i}\frac{2(1-2\nu)}{3(1-\nu)}\left(\frac{p_i}{p_i + p_L} - \frac{p}{p + p_L}\right) \quad \textbf{(6.25)}$$

The middle term of the sum on the right-hand side of this equation describes porosity changes due to stress effects, while the last term of the sum expresses the influence of matrix shrinkage on porosity. Inspection of the equation reveals the stress term is controlled by Poisson's ratio and Young's modulus. The sorption term is controlled by Poisson's ratio, the volumetric strain coefficient, and the Langmuir pressure constant. The volumetric strain coefficient, $c_0$, is empirically determined, either from laboratory or field data, and resembles Levine's maximum matrix strain coefficient. Palmer and Mansoori obtained Poisson's ratio from laboratory or field data and Young's modulus from laboratory tests. The stress term in equation (6.25) is negative during depletion, while the sorption term is always positive. Which term dominates depends on rock mechanics properties as well as position on the sorption isotherm. From the porosity ratio of equation (6.25), Palmer and Mansoori calculated the permeability ratio with equation (6.6).

The pressure at which porosity and permeability begin to increase is defined as the *rebound pressure*. Rebound pressure is determined by setting the derivative with respect to pressure of equation (6.25) to zero, and is

$$p_c = \left[\frac{2c_0 EP_L}{3(1+\nu)}\right]^{1/2} - p_L \quad \textbf{(6.26)}$$

where

$p_c$ = rebound pressure, psia.

Coefficients determined by Palmer and Mansoori from matching San Juan coal well performance are given in table 6–8.

**Table 6–8.** Palmer–Mansoori coefficients—San Juan Basin, Fruitland coal

| | | |
|---|---|---|
| initial porosity = | 0.001–0.005 | fraction |
| initial pressure = | 1,100 | psia |
| $c_0$ = | 0.013 | $psia^{-1}$ |
| Young's modulus = | (1.24–4.45)E+5 | psia |
| Poisson's ratio = | 0.39 | |
| $p_L$ = | 625 | psia |

*Source:* Palmer, I., and Mansoori, J. 1996.

Porosity of this high-volatile bituminous coal varied from 0.001 to 0.005, much smaller than the porosity of 0.02 to 0.03 obtained from an interference test in these coals.[44] However, it was commensurate with those determined from history matching exercises with reservoir simulators (Mavor, $\phi = 0.0045$; Ramurthy, $\phi = 0.0025$).[45] Young's modulus varied from 124,000 to 445,000 psia (855 to 3068 MPa), values smaller than those reported by Bell and Jones for gassy coals.[46] The extreme sensitivity of the Palmer-Mansoori permeability ratio to rock properties is demonstrated by plotting curves resulting from the four combinations of San Juan parameters in figure 6–8.

The permeability ratio calculated with the smallest values of porosity and Young's modulus, 0.001 and 124,000 psia (855 MPa), gives physically impossible negative values, but the other three curves are credible.

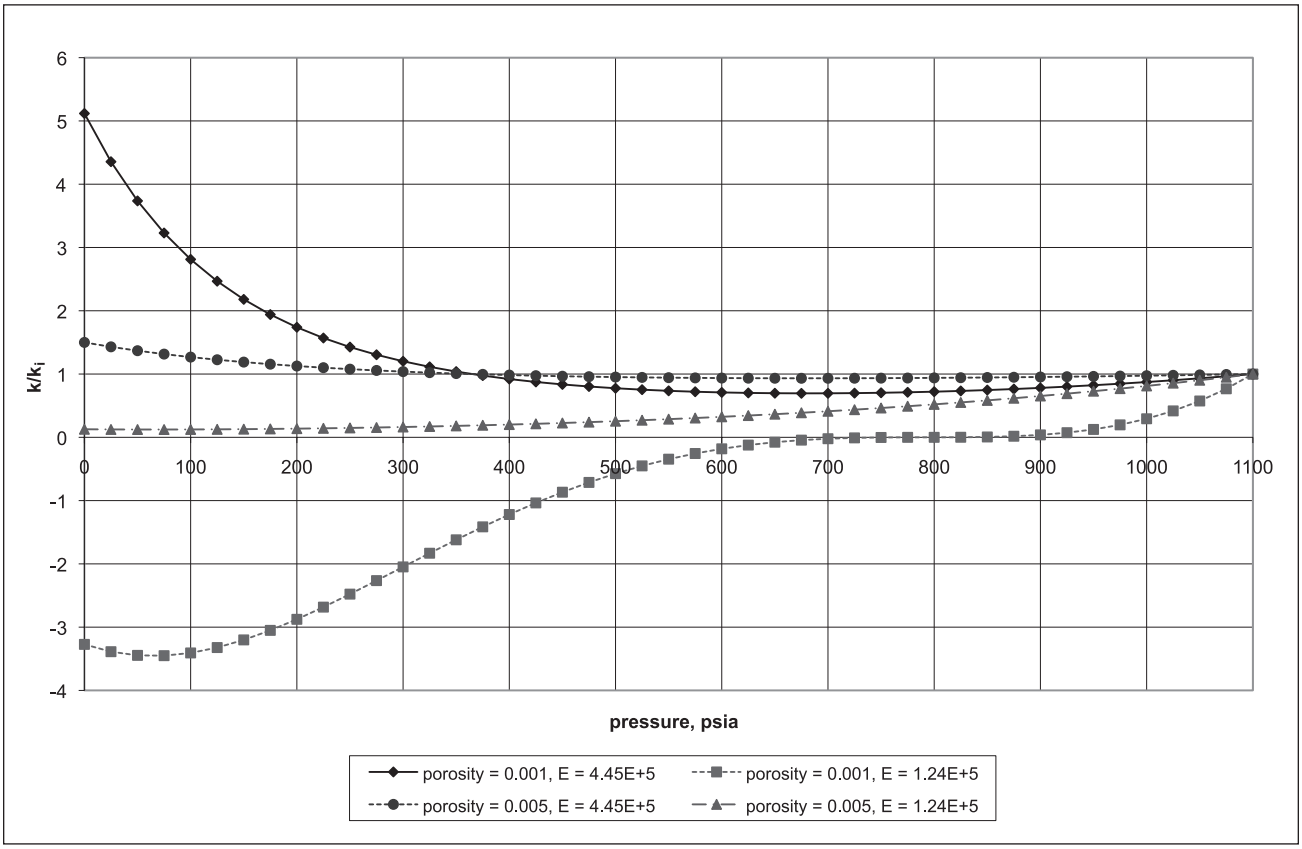



**Fig. 6–8.** Palmer-Mansoori permeability ratio—San Juan coal

Rebound pressures, calculated from equation (6.26) using the two values of Young's modulus, were 682 and 65 psia. For the more elastic coal ($E$ = 445,000 psia), stress effects dominate the first half of depletion, from 1,100 psia initial pressure down to 682 psia, then matrix shrinkage effects dominate the second half. For the stiffer coal ($E$ = 124,000 psia), stress effects dominate into deep depletion, with matrix shrinkage effects dominating stress effects only at reservoir pressures less than 65 psia.

The ICM model of Shi and Durucan for coal porosity and permeability describes stress variation during depletion as the sum of mechanical and matrix deformation terms.[47] The mechanical stress term assumes a uniaxial strain regime dominated by horizontal stress changes, while the matrix deformation term is similar to those of Levine and Palmer and Mansoori.[48] The permeability ratio is calculated from an equation similar to equation (6.7). Mathematically,

$$\sigma - \sigma_i = -\frac{\nu}{1-\nu}(p - p_i) + \frac{E\varepsilon_l}{3(1+\nu)}\left(\frac{p}{p+p_\varepsilon} - \frac{p_i}{p_i+p_\varepsilon}\right) \tag{6.27}$$

where

$\varepsilon_l$ = matrix shrinkage coefficient, psia$^{-1}$, and
$p_\varepsilon$ = matrix deformation Langmuir pressure, psia.

And the permeability ratio is given by

$$\frac{k}{k_i} = \exp\left[-3c_f(\sigma - \sigma_i)\right] \tag{6.28}$$

From equation (6.6), the porosity ratio is simply the cube root of equation (6.28). The Shi and Durucan rebound pressure, the pressure at which matrix deformation effects begin to dominate stress effects, is given by

$$p_{rb} = \left[ \frac{E\varepsilon_l p_\varepsilon}{3\nu} \right]^{1/2} - p_\varepsilon \tag{6.29}$$

where

$p_{rb}$ = rebound pressure, psia.

*Recovery pressure*, defined by Shi and Durucan as the pressure at which permeability is equal to initial permeability, is calculated from

$$p_{rc} = \frac{\mathrm{E}\varepsilon_l p\varepsilon}{3\nu(p_i + p_\varepsilon)} - p_\varepsilon \tag{6.30}$$

where

$p_{rc}$ = recovery pressure, psia.

Shi and Durucan identified five different scenarios of the stress behavior during pressure depletion that depend on the relative magnitudes of rock properties and initial pressure. They noted their model predicts larger recovery and rebound pressures than does the Palmer-Mansoori model. Shi and Durucan employed San Juan data from Palmer and Mansoori and Mavor and Vaughn to determine the coefficients in equations (6.27) and (6.28).[49] Coefficients for the Valencia Canyon 32-1 well are collected in table 6–9, and the resulting permeability and porosity ratios plotted in figure 6–9.

**Table 6–9.** ICM model stress-permeability coefficients—San Juan Basin

| | | |
|---|---|---|
| Young's modulus = | 421,000 | psia |
| Poisson's ratio = | 0.35 | |
| Initial pressure = | 957 | psia |
| Max vol strain = | 0.01266 | |
| Half strain pressure = | 625 | psia |
| Cleat compressibility = | 0.002 | $psia^{-1}$ |

*Sources:* Shi, J. Q., and Durucan, S. 2003. Part I. Paper 0341; and Shi, J. Q., and Durucan, S. 2003. Part II. Paper 0342.

As seen in this figure, the ICM model predicts steadily increasing permeability and porosity ratios throughout depletion. Both rebound and recovery pressures are above initial pressure.

Average San Juan coal parameters developed by Palmer and Mansoori and Shi and Durucan are collected in table 6–10, and the resulting permeability and porosity ratios plotted in figures 6–10 and 6–11, respectively.[50]

**Table 6–10.** Physical constants for Palmer-Mansoori and ICM comparison

| | | |
|---|---|---|
| Initial porosity = | 0.003 | fraction |
| Initial pressure = | 1,000 | psia |
| $c_0$ = | 0.013 | $psia^{-1}$ |
| Young's modulus = | 400,000 | psia |
| Poisson's ratio = | 0.37 | |
| $p_L$ = | 625 | psia |
| Max vol strain = | 0.01266 | |
| Cleat compressibility = | 0.00146 | $psia^{-1}$ |

*Sources:* Shi, J. Q., and Durucan, S. 2003. Part 1. Paper 0341; and Shi, J. Q., and Durucan, S. 2003. Part 2. Paper 0342; and Palmer, I., and Mansoori, J. 1996.

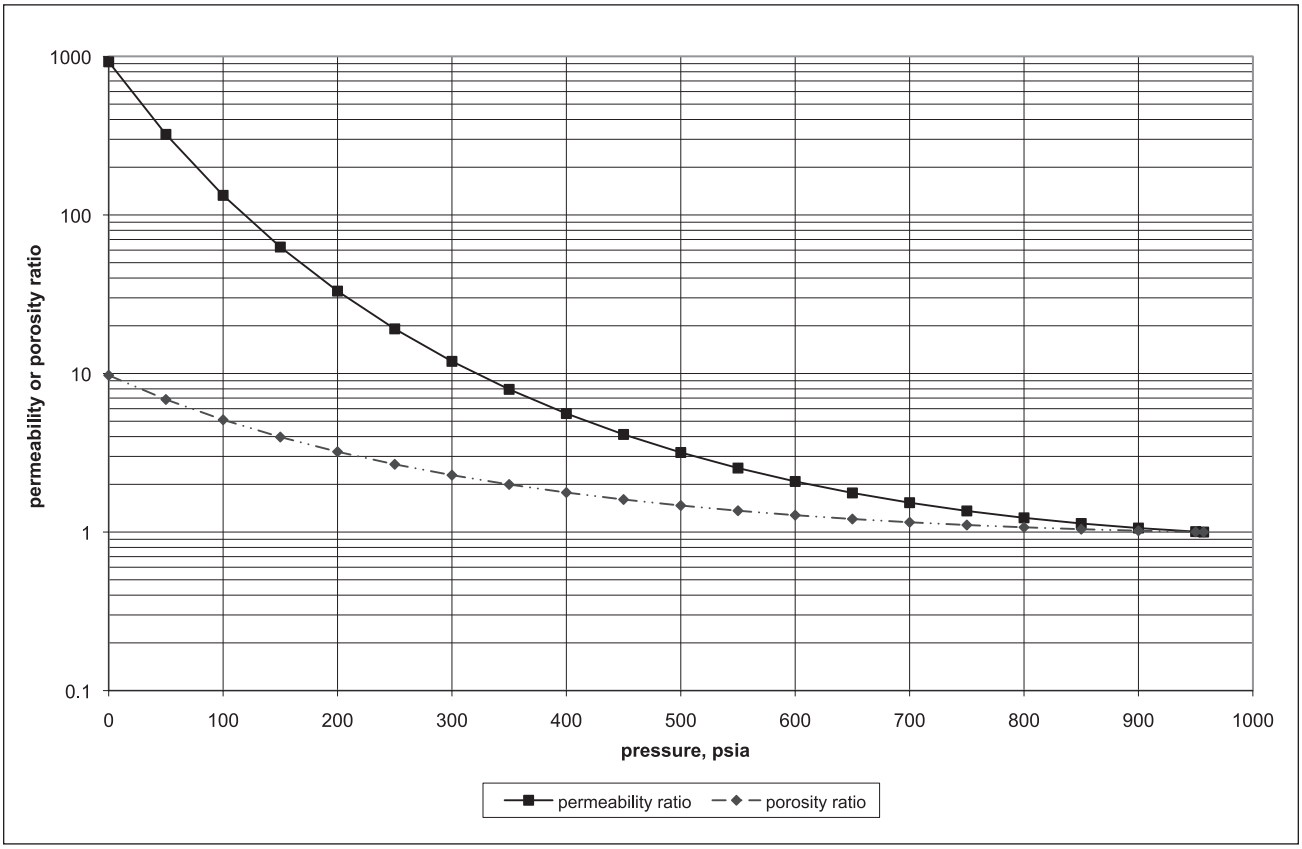



**Fig. 6–9.** ICM model permeability and porosity ratios—San Juan Basin

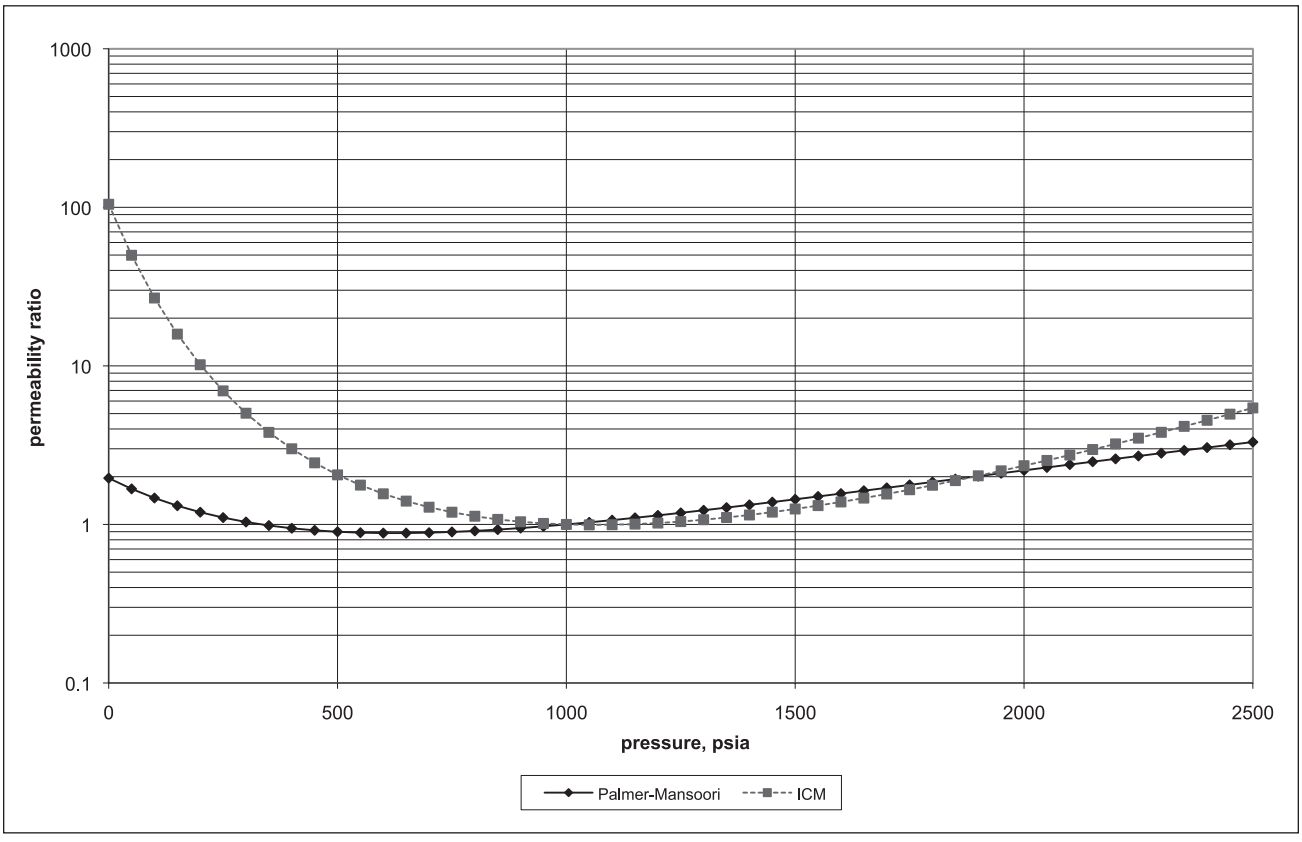



**Fig. 6–10.** Comparison of Palmer-Mansoori and ICM permeability ratios

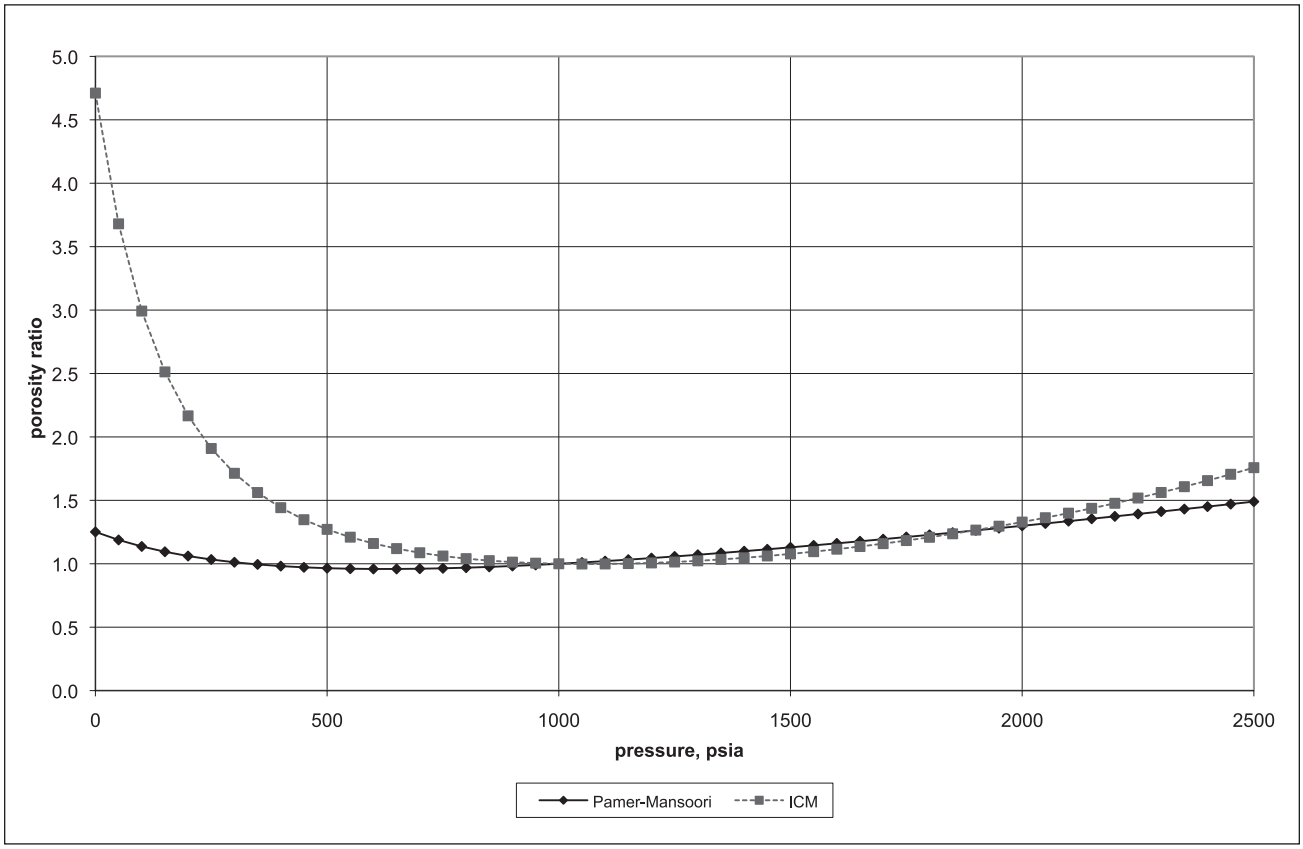



**Fig. 6–11.** Comparison of Palmer-Mansoori and ICM porosity ratios

From the initial pressure of 1,000 psia, the Palmer-Mansoori theory predicts a shallow decline in both permeability and porosity until the rebound pressure of 623 psia is reached. At rebound pressure, permeability has decreased by 12% and porosity has declined by 4%. At complete depletion, zero psia, permeability has doubled, while porosity has increased by 25% over the initial value. If methane were to be injected into the coal deposit, doubling the initial pressure, this theory yields a steady increase in both permeability and porosity. At 2,000 psia, porosity has increased by 30%, and permeability has doubled.

In contrast, the ICM theory predicts a steady increase in both porosity and permeability throughout depletion of the coal. At zero psia, porosity has increased by a factor of 4.7, and permeability by a factor of 105. Injecting methane would cause both porosity and permeability to decrease slightly before increasing. At rebound pressure, 1,064 psia, both have decreased by a fraction of a percent. *Recovery pressure*, the pressure at which porosity and permeability return to their initial values, is 1,130 psia. When reservoir pressure reaches 2,000 psia, porosity has increased by one-third and permeability by a factor of 2.3.

Unfortunately, very little field data currently exist to test theories of porosity and permeability changes due to matrix deformation from stress and sorption. Field evidence of increasing coal permeability with depletion has been reported only in the San Juan Basin. Mavor and Vaughn reported permeability increases in some Valencia Canyon wells by a factor of three to seven.[51] From a set of four pressure buildup tests on a single dry coal well, Zahner reported exponentially increasing permeability with depletion.[52] A reduction in reservoir pressure of 1,200 psia increased permeability by a factor of 2.

# Nomenclature

| | |
|---|---|
| $a$ | Cleat spacing |
| $A$ | Flow area |
| $b$ | Cleat width |
| $B$ | Reciprocal of Langmuir pressure, psia$^{-1}$ |
| $c_f$ | Cleat compressibility, psia$^{-1}$ |
| $c_m$ | Palmer-Mansoori coefficient = $1/M$, psia$^{-1}$ |
| $c_0$ | Palmer-Mansoori volumetric strain coefficient, psia$^{-1}$ |
| $d$ | Depth, ft |
| $E$ | Young's modulus, psia |
| $k$ | Cleat permeability |
| K | Bulk modulus, psia |
| $k_i$ | Initial permeability |
| $k_{rg}$ | Gas relative permeability |
| $k_{rg}$ | Gas relative permeability at irreducible water saturation |
| $k_{rw}$ | Water relative permeability |
| $l$ | Bedding plane height |
| $M$ | Constrained axial modulus, psia |
| $n$ | Number of cleats |
| $n'$ | Empirical coefficient, equation (6.20) |
| $p$ | Pressure, psia |
| $p_c$ | Palmer-Mansoori rebound pressure, psia, equation (6.28) |
| $p_i$ | Initial pressure, psia |
| $p_{rb}$ | Shi and Durucan rebound pressure, psia, equation (6.29) |
| $p_{rc}$ | Shi and Durucan recovery pressure, psia, equation (6.30) |
| $p_{50}$ | Levine pressure, where strain is one-half maximum strain, psia |
| $\Delta p/L$ | Pressure gradient |
| $q$ | Flow rate |
| $q_t$ | Flow rate through $n$ cleats |
| $S$ | Overburden load, psia |
| $S_{gc}$ | Critical gas saturation |
| $S_{iw}$ | Irreducible water saturation |
| $S_w$ | Water saturation |
| $S_w^*$ | Normalized water saturation, equation (6.22) |

## Greek

| | |
|---|---|
| $\varepsilon$ | Strain or matrix strain |
| $\varepsilon_{max}$ | Levine maximum matrix strain coefficient |
| $\lambda$ | Empirical coefficient, equation (6.20) |
| $\mu$ | Fluid viscosity |
| $\nu$ | Poisson's ratio |
| $\sigma$ | Stress |
| $\sigma_h$ | Hydrostatic stress, psia |
| $\sigma_{hi}$ | Initial hydrostatic stress, psia |
| $\phi$ | Cleat porosity |

# References


1. Gash, B. W., Volz, R. F., Potter, G., and Corgan, J. M. 1993. The effects of cleat orientation and confining pressure on cleat porosity, permeability and relative permeability in coal. Paper 9321 in *Proceedings of the 1993 International Coalbed Methane Symposium*. Tuscaloosa: University of Alabama.
2. Mavor, M. J., and Robinson, J. R. 1993. *Analysis of Coal Gas Reservoir Interference and Cavity Well Tests*. Paper SPE 25860. Presented at the Joint Rocky Mountain Regional and Low Permeability Reservoirs Symposium, Denver, Colorado, April 26–28; and Gas Research Institute. 1996. *A Guide to Coalbed Methane Reservoir Engineering*. GRI-94/0397. Chicago: Gas Research Institute.
3. Koenig, R. A., and Stubbs, P. B. 1986. *Interference Testing of a Coalbed Methane Reservoir*. Paper SPE 15225. Presented at the SPE Unconventional Gas Technology Symposium, Louisville, Kentucky, May 18–21.
4. Young, G. B. C., McElhiney, J. E., Dhir, R., Mavor, M. J., and Anbouba, I. K. A. 1991. *Coalbed Methane Production Potential of the Rock Springs Formation, Great Divide Basin, Sweetwater County, Wyoming*. Paper SPE 21487. Presented at the SPE Gas Technology Symposium, Houston, Texas, January 23–25.
5. Gash, B. W., et al. 1993.
6. Gas Research Institute. 1996; and Bell, G. J., Seccombe, J. C., Rakop, K. C., and Jones, A. H. 1985. *Laboratory Characterization of Deeply Buried Coal Seams in the Western U.S.* Paper SPE 14445. Presented at the SPE Annual Technical Conference and Exhibition, Las Vegas, Nevada, September 22–25.
7. Reiss, L. H. 1980. *The Reservoir Engineering Aspects of Fractured Reservoirs*. Paris: Gulf Publishing Company.
8. Ibid.
9. Cardott, B. J. 1998. Coal as gas-source rock and reservoir, Hartshorne Formation, Oklahoma. In *The Hartshorne Play in Southeastern Oklahoma: Regional and Detailed Sandstone Reservoir Analysis and Coalbed-Methane Resources*. Andrews, R. D., Cardott, B. J., and Storm, T. Oklahoma Geological Survey Special Publication 98-7. Norman: University of Oklahoma.
10. Reiss, L. H. 1980; and McKee, C. R., Bumb, A. C., and Koenig, R. A. 1988. Stress-dependent permeability and porosity of coal and other geologic formations. *Society of Petroleum Engineers Formation Evaluation*. V. 3 (no. 1). p. 81.
11. McKee, C. R., et al. 1988.
12. Shi, J. Q., and Durucan, S. 2003. Changes in permeability of coalbeds during primary recovery. Part 1. Model formulation and analysis. Paper 0341 in *Proceedings of the 2003 International Coalbed Methane Symposium*. Tuscaloosa: University of Alabama.
13. Palmer, I., and Mansoori, J. 1996. *How Permeability Depends on Stress and Pore Pressure in Coalbeds: A New Model*. Paper SPE 36737. Presented at the SPE Annual Technical Conference and Exhibition, Denver, Colorado, October 6–9.
14. Shi, J. Q., and Durucan, S. 2003. Changes in permeability of coalbeds during primary recovery. Part 2. Model validation and field application. Paper 0342 in *Proceedings of the 2003 International Coalbed Methane Symposium*. Tuscaloosa: University of Alabama.
15. Shi, J. Q., and Durucan, S. 2003. Part 1. Paper 0341.
16. Ibid.
17. Reznik, A. A., Dabbous, M. K., Fulton, P. F., and Taber, J. J. 1974. Air-water relative permeability studies of Pittsburgh and Pocohontas coals. *Society of Petroleum Engineers Journal*. V. 6 (December). p. 556; and Puri, R., Evanoff, J. C., and Brugler, M. L. 1991. *Measurement of Coal Cleat Porosity and Relative Permeability Characteristics*. Paper SPE 21491. Presented at the SPE Gas Technology Symposium, Houston, Texas, January 23–25.
18. Bustin, R. M., and Clarkson, C. R. 1999. Free gas storage in matrix porosity: A potentially significant coalbed resource in low rank coals. Paper 9956 in *Proceedings of the 1999 International Coalbed Methane Symposium*. Tuscaloosa: University of Alabama; and Gash, B. W. 1991. *Measurement of "Rock Properties" in Coal for Coalbed Methane Production*. Paper SPE 22909. Presented at the SPE Annual Technical Conference and Exhibition, Dallas, Texas, October 6–9.
19. Levine, J. R. 1993. Coalification: The evolution of coal as source rock and reservoir rock for oil and gas. In *Hydrocarbons from Coal, AAPG Studies in Geology #38*. Law, B. E., and Rice, D. D., eds. Tulsa: American Association of Petroleum Geologists. p. 39.
20. Gash, B. W. 1991.
21. Hyman, L., Ohen, H. A., Amaefule, J. O., and Danehjou, D. 1991. Simultaneous determination of capillary pressure and relative permeability in coal-bed methane reservoirs. Paper 9118 in *Proceedings of the 1991 International Coalbed Methane Symposium*. Tuscaloosa: University of Alabama.
22. Gash, B. W. 1991.
23. Testa, S. M., and Pratt, T. J. 2003. Sample preparation for coal and shale gas resource assessment. Paper 0356 in P*roceedings of the 2003 International Coalbed Methane Symposium*. Tuscaloosa: University of Alabama.
24. Gash, B. W. 1991; Paterson, L. 1990. Laboratory measurement of coal permeability. In *Methane Drainage from Coal*. Paterson, L., ed. Syndal, Victoria: CSIRO Division of Geomechanics; and Gash, B. W., et al. 1993.
25. Gash, B. W., et al. 1993.
26. Johnson, E. F., Bossler, D. P., and Naumann, V. O. 1959. Calculation of relative permeability from displacement experiment. *Transactions*. AIME. V. 216. p. 370.
27. Gash, B. W., et al. 1993.
28. Mavor, M. J., and Robinson, J. R. 1993; Burdine, N. T. 1953. Relative permeability calculations from pore size distribution data. *Transactions*. AIME. V. 198. p. 71; Brooks, R. H., and Corey, A. T. 1966. Properties of porous media affecting fluid flow. *Journal of the Irrigation and Drainage Division, Proceedings of the ASCE*. V. 92 (June). p. 61; and Gash, B. W. 1991.
29. Mavor, M. J., and Robinson, J. R. 1993; and Gash, B. W. 1991.

30. Gash, B. W. 1991; and Conway, M. W., Mavor, M . J., Saulsberry, J., Barree, R. B., and Schraufnagel, R. A. 1995. *Multi-Phase Flow Properties for Coalbed Methane Wells: A Laboratory and Field Study*. Paper SPE 29576. Presented at the Joint Rocky Mountain Regional Meeting and Low-Permeability Reservoirs Symposium, Denver, Colorado, March 20–22.
31. Ibid.
32. Hower, T. L., Jones, J. E., Goldstein, D. M., and Harbridge, W. 2003. *Development of the Wyodak Coalbed Methane Resource in the Powder River Basin*. Paper SPE 84428. Presented at the SPE Annual Technical Conference and Exhibition, Denver, Colorado, October 5–8.
33. Meaney, K., and Paterson, L. 1996. *Relative Permeability in Coal*. Paper SPE 36986. Presented at the SPE Asia Pacific Oil and Gas Conference, Adelaide, Australia, October 28–31.
34. Ibid.
35. Harpalani, S., and Schraufnagel, R. A. 1990. *Influence of Matrix Shrinkage and Compressibility on Gas Production from Coalbed Methane Reservoirs*. Paper SPE 20729. Presented at the SPE Annual Technical Conference and Exhibition, New Orleans, Louisiana, September 23–26; Harpalani, S. and Chen, G. 1995. Estimation of changes in fracture porosity of coal with gas emission. *Fuel*. V. 74 (no. 10). p. 1,491; and Seidle, J. P., and Huitt, L. G. 1995. *Experimental Measurement of Coal Matrix Shrinkage Due to Gas Desorption and Implications for Cleat Permeability Increases*. Paper SPE 30010. Presented at the International Meeting on Petroleum Engineering, Beijing, China, November 14–17.
36. Levine, J. R. 1996. Model study of the influence of matrix shrinkage on absolute permeability of coal bed reservoirs. *Coalbed Methane and Coal Geology, Special Publication No. 109*. Gayer, R. A., and Harris, I. A., eds. London: Geological Society. p. 197.
37. Ibid.
38. Harpalani, S., and Schraufnagel, R. A. 1990; Seidle, J. P., and Huitt, L. G. 1995; Levine, J. R. 1996; Moffat, D. H., and Weale, K. E. 1955. Sorption by coal of methane at high pressures. *Fuel*. V. 34 (no. 4). p. 449; Gunther, J. 1968. Investigation of the gas-coal bond. *Revue de l'Industrie Minérale*. V. 47 (October). p. 693. Wubben, P., Seewald, H., and Jurgen, K. 1986. Permeation and sorption behavior of gas and water in coal. *Proceedings of the Twelfth Annual Underground Coal Gasification Symposium*. August 24–28. DOE/FE/60922-H1. Washington, DC: Department of Energy; Reucroft, P. J., and Patel, H. 1986. Gas-induced swelling in coal. *Fuel*. V. 65 (no. 6). p. 816; Gray, I. 1987. Reservoir engineering in coal seams. Part 1. The physical process of gas storage and movement in coal seams. SPE 12514. *Society of Petroleum Engineers Reservoir Engineering*. V. 2 (no. 1). p. 28; Juntgen, H. 1987. Research for future in situ conversion of coal. *Fuel*. V. 66 (no. 4). p. 443.
39. Harpalani, S., and Schraufnagel, R. A. 1990.
40. Levine, J. R. 1996.
41. Seidle, J. R., and Huitt, L. G. 1995.
42. Levine, J. R. 1996.
43. Palmer, I., and Mansoori, J. 1996.
44. Mavor, M. J., and Robinson, J. R. 1993.
45. Mavor, M. J. 1994. *Coal Gas Openhole Well Performance*. Paper SPE 27993. Presented at the University of Tulsa Centennial Petroleum Engineering Symposium, Tulsa, Oklahoma, August 29–31; and Ramurthy, K., Young, G. B. C., Daves, S. B., and Witsell, F. 2003. *Case History: Reservoir Analysis of the Fruitland Coals Results in Optimizing Coalbed Methane Completions in the Tiffany Area of the San Juan Basin*. Paper SPE 84426. Presented at the SPE Annual Technical Conference and Exhibition, Denver, Colorado, October 5–8.
46. Bell, G. J., and Jones, A. H. 1989. Variation in mechanical strength with rank of gassy coals. Paper 8924 in *Proceedings of the 1989 International Coalbed Methane Symposium*. Tuscaloosa: University of Alabama.
47. Shi, J. Q., and Durucan, S. 2003. Part 1. Paper 0341; and Shi, J. Q., and Durucan, S. Part 2. Paper 0342.
48. Levine, J. R. 1996; and Palmer, I., and Mansoori, J. 1996.
49. Palmer, I., and Mansoori, J. 1996; and Mavor, M. J., and Vaughn, J. E. 1997. Increasing absolute permeability in the San Juan Basin Fruitland Formation. Paper 9738 in *Proceedings of the 1997 International Coalbed Methane Symposium*. Tuscaloosa: University of Alabama.
50. Palmer, I., and Mansoori, J. 1996; Shi, J. Q., and Durucan, S. 2003. Part 1. Paper 0341; and Shi, J. Q., and Durucan, S. Part 2. Paper 0342.
51. Mavor, M. J., and Vaughn, J. E. 1997.
52. Zahner, B. 1997. *Application of Material Balance to Determine Ultimate Recovery of a San Juan Fruitland Coal Well*. Paper SPE 38858. Presented at the SPE Annual Technical Conference and Exhibition, San Antonio, Texas, October 5–8.

# Coal Well Pressure Transient Tests 7

## Introduction

For more than half a century, reservoir permeability and pressure and wellbore condition have been determined in conventional wells from the observed pressure response resulting from a change in production rate. More recently, these techniques also have been used in coal wells. Many of the basic principles of conventional well testing can be employed to analyze coal well tests with little or no modification. Coal deposits are often aquifers with little, if any, free gas present. Consequently, initial attempts to characterize the reservoir often involve injection of water into or production of water from the coal. Well tests of producing wells often consider both gas and water flow. Well tests in coals include injection/falloffs, drillstem tests, tank tests, slug tests, diagnostic fracture injection tests, drawdown and buildup tests, interference tests, and micropilot injectivity tests.

## Injection/Falloff Tests

Historically, injection/falloff tests (or pressure falloff tests) have been used to characterize new coals and new coal wells. Adapted from falloff testing of waterflood injectors, injection/falloff tests work well in water-saturated coals but are complicated by relative permeability effects if any free gas is present. Zuber et al. studied injection/falloff tests in Warrior Basin coals using both simulation and actual field tests and developed the following general test design for cased hole completions.[1]

- Perforate target seam(s) with four to eight shots per foot.
- Break down target seam(s) with breakdown/ballout treatments.
- Isolate test interval with a bridge plug and packer assembly.
- Hang pressure bombs below packer.
- Inject water into formation at 1 to 2 gal/min (0.02 to 0.05 bbl/min) for 12 to 18 hr. Bottomhole injection pressure should not exceed 80% of frac parting pressure.
- Shut in well and monitor pressure falloff for 24 to 36 hr.

Analysis of falloff tests in liquid-filled reservoirs as discussed by Earlougher is directly applicable to injection/falloff testing of coal wells.[2] Theoretical considerations of falloff tests in new coal wells and San Juan field examples were presented by Seidle et al.[3] As with most other transient well tests, the first step in analysis of injection/falloff tests in coals is identification of wellbore storage. This can be done from unit slope behavior of the data

on a log-log plot of the change in shut-in bottomhole pressure versus shut-in time. Alternatively, time to the beginning of radial flow can be estimated from

$$t_{bsl} = \frac{170{,}000C \exp(0.14s)}{(kh/\mu_w)} \tag{7.1}$$

where

$t_{bsl}$ = time to beginning of the semilog straight line, hr,
$s$ = wellbore skin, dimensionless,
$k$ = coal permeability, md,
$h$ = net thickness of the tested interval, ft, and
$\mu_w$ = water viscosity, cp.

Permeability is determined from the slope of the radial flow data portion of a semilog plot of shut-in bottomhole pressure as a function of Horner time,

$$t_H = \frac{(t_i + \Delta t)}{\Delta t} \tag{7.2}$$

where

$t_H$ = Horner time, dimensionless,
$t_i$ = injection time, hr, and
$\Delta t$ = shut-in time, hr.

As injection and shut-in times in coal well injection/falloff tests are roughly equal, it can be argued the correct time function for analysis of these tests is not Horner time but equivalent time, defined by Agarwal as[4]

$$\Delta t_e = \frac{t_i \Delta t}{t_i + \Delta t} \tag{7.3}$$

where

$\Delta t_e$ = Agarwal equivalent time, hr.

In practice, permeability estimates obtained with Horner time and Agarwal equivalent time are often equal for reservoir engineering purposes. A semilog plot of shut-in bottomhole pressure as a function of the selected time function yields a straight line, the slope of which is used to calculate permeability[5]

$$k = -\frac{162.6 q_w B_w \mu_w}{mh} \tag{7.4}$$

where

$q_w$ = water injection rate, bpd,
$B_w$ = water formation volume factor, reservoir bbl/stb, and
$m$ = slope of the semilog straight line, psi/cycle.

Note that as water is being injected into a water-saturated coal, permeability determined by this test is absolute permeability.

Wellbore skin factor is determined from a relation given by Earlougher[6]

$$s = 1.1513 \left[ \frac{p_{1hr} - p_{wsi}}{m} - \log\left( \frac{k}{\phi \mu_w c_t r_w^2} \right) + 3.2275 \right] \tag{7.5}$$

where

$p_{1hr}$ = extrapolated pressure at 1 hr after shut-in, psia,
$p_{wsi}$ = pressure at shut-in, psia,
$\phi$ = coal porosity, fraction,
$c_t$ = system compressibility, psia$^{-1}$, and
$r_w$ = wellbore radius, ft.

Extrapolation of pressure data to infinite time (a Horner time of 1 or an Agarwal equivalent time of $t_i$) yields a value of $p^*$. Both Zuber et al. and Seidle et al. report that $p^*$ values from injection/falloffs in new coal wells are equal to initial reservoir pressure.[7] Interpretation of the $p^*$ value from an injection/falloff test done on a producing coal well has not been addressed in the literature at this time.

The radius of investigation of an injection/falloff test can be calculated from[8]

$$r_i = 0.029\sqrt{\frac{kt}{\phi\mu_w c_t}} \tag{7.6}$$

where

$r_i$ = the radius of investigation, ft.

Note that if free gas is present, gas saturation will decrease in response to pressure increases due to water injection. In the extreme case that injection pressure is greater than desorption pressure, gas may resorb entirely, complicating test analysis through changing relative permeability and compressibility effects.

Injection/falloff tests should not be employed in coals with no moveable water, as the test can seriously reduce gas productivity due to the high water saturation left near the wellbore. Unfortunately, knowledge of fluid saturations in the cleats is often not known at the time of testing, and the first indication of a gas-filled coal comes from the falloff test. In a gas-filled coal, falloff data indicate a composite reservoir with a high-permeability (to water) inner zone and a very low permeability (to water) far-field permeability.

### Example 7.1. Coal well prefrac falloff test

A prefrac pressure falloff test of a San Juan Basin coal well was discussed by Seidle et al.[9] The well was completed in 42 ft of water-saturated Fruitland coal, and the wellbore radius was 0.2 ft. Water formation volume factor was 1.0 rb/stb, and viscosity was 0.5 cp. Coal porosity was 0.01, and compressibility was 9.24E–4 psia$^{-1}$. The test consisted of water injection at a rate of 360 bpd for 12 hr, followed by a shut-in of 28 hr. Pressure at shut-in was 1,856.00 psia. Test data and various time functions are collected in table 7–1.

Test analysis begins with a plot of pressure data (fig. 7–1). Pressure data initially decline rapidly and then asymptotically approach reservoir pressure at late time, with a total pressure change of about 500 psia. The log-log plot (fig. 7–2) contains both the pressure and derivative traces. The derivative was calculated as described by Bourdet et al.[10] The first few points may be colored by wellbore storage as they appear to fall on a unit slope line. However, such effects rapidly die out, leaving data reflective of wellbore condition and formation properties. The derivative trace exhibits the noise typical of numerical derivatives yet allows some conclusions to be drawn. Absence of a pronounced hump in the derivative at early time implies only modest wellbore damage, while flattening of the derivative at late time indicates the test reached radial flow. Consequently, permeability and skin can be calculated using both Horner time and equivalent time.

**Table 7–1.** Prefrac PFOT data

| Point no. | Δ *t*, hr | Pressure, psia | Horner time, hr | Equivalent time, hr | Δ pressure, psia | Bourdet τ | ddp/dτ, psia/hr |
|---|---|---|---|---|---|---|---|
| 1 | 0.004057 | 1,788.51 | 2,959 | 0.004055 | 67.49 | 5.508 | |
| 2 | 0.008208 | 1,719.46 | 1,463 | 0.008203 | 136.54 | 4.803 | 98.02 |
| 3 | 0.01248 | 1,693.27 | 962.9 | 0.01246 | 162.73 | 4.385 | 62.62 |
| 4 | 0.01661 | 1,669.46 | 723.3 | 0.01659 | 186.54 | 4.099 | 83.20 |
| 5 | 0.02080 | 1,645.65 | 577.8 | 0.02077 | 210.35 | 3.874 | 106.04 |
| 6 | 0.02504 | 1,633.75 | 480.3 | 0.02499 | 222.25 | 3.689 | 64.38 |
| 7 | 0.02909 | 1,621.84 | 413.5 | 0.02902 | 234.16 | 3.540 | 79.53 |
| 8 | 0.03351 | 1,614.70 | 359.2 | 0.03341 | 241.30 | 3.399 | 50.70 |
| 9 | 0.03758 | 1,609.94 | 320.3 | 0.03746 | 246.06 | 3.284 | 41.60 |
| 10 | 0.04197 | 1,605.18 | 286.9 | 0.04182 | 250.82 | 3.174 | 43.26 |
| 11 | 0.05008 | 1,586.13 | 240.6 | 0.04988 | 269.87 | 2.998 | 108.16 |
| 12 | 0.05847 | 1,576.60 | 206.2 | 0.05819 | 279.40 | 2.844 | 61.81 |
| 13 | 0.06677 | 1,567.08 | 180.7 | 0.06640 | 288.92 | 2.712 | 72.11 |
| 14 | 0.07459 | 1,562.32 | 161.9 | 0.07413 | 293.68 | 2.602 | 43.26 |
| 15 | 0.08333 | 1,550.41 | 145.0 | 0.08275 | 305.59 | 2.492 | 108.16 |
| 16 | 0.09106 | 1,543.27 | 132.8 | 0.09037 | 312.73 | 2.404 | 81.12 |
| 17 | 0.1008 | 1,538.51 | 120.0 | 0.1000 | 317.49 | 2.303 | 47.03 |
| 18 | 0.1255 | 1,523.83 | 96.62 | 0.1242 | 332.17 | 2.086 | 67.75 |
| 19 | 0.1479 | 1,513.62 | 82.12 | 0.1461 | 342.38 | 1.923 | 62.82 |
| 20 | 0.1744 | 1,507.32 | 69.81 | 0.1719 | 348.68 | 1.761 | 38.72 |
| 21 | 0.2001 | 1,500.90 | 60.96 | 0.1968 | 355.10 | 1.625 | 47.42 |
| 22 | 0.2496 | 1,484.26 | 49.08 | 0.2445 | 371.74 | 1.409 | 76.79 |
| 23 | 0.3013 | 1,478.52 | 40.83 | 0.2939 | 377.48 | 1.224 | 31.15 |
| 24 | 0.3482 | 1,470.32 | 35.46 | 0.3384 | 385.68 | 1.084 | 58.20 |
| 25 | 0.4479 | 1,457.04 | 27.79 | 0.4318 | 398.96 | 0.840 | 54.48 |
| 26 | 0.5457 | 1,450.83 | 22.99 | 0.5220 | 405.17 | 0.650 | 32.72 |
| 27 | 0.6853 | 1,444.52 | 18.51 | 0.6483 | 411.48 | 0.433 | 29.12 |
| 28 | 0.8885 | 1,431.58 | 14.51 | 0.8273 | 424.42 | 0.190 | 53.10 |
| 29 | 1.229 | 1,418.19 | 10.77 | 1.114 | 437.81 | –0.108 | 44.94 |
| 30 | 1.777 | 1,408.61 | 7.753 | 1.548 | 447.39 | –0.437 | 29.15 |
| 31 | 2.064 | 1,403.83 | 6.814 | 1.761 | 452.17 | –0.566 | 37.04 |
| 32 | 2.526 | 1,397.57 | 5.751 | 2.087 | 458.43 | –0.736 | 36.90 |
| 33 | 3.044 | 1,393.89 | 4.942 | 2.428 | 462.11 | –0.887 | 24.29 |
| 34 | 3.538 | 1,390.20 | 4.392 | 2.732 | 465.80 | –1.005 | 31.20 |
| 35 | 4.027 | 1,385.05 | 3.980 | 3.015 | 470.95 | –1.104 | 52.33 |
| 36 | 4.569 | 1,382.84 | 3.627 | 3.309 | 473.16 | –1.197 | 23.78 |
| 37 | 5.093 | 1,379.16 | 3.356 | 3.576 | 476.84 | –1.274 | 47.47 |
| 38 | 5.595 | 1,376.58 | 3.145 | 3.816 | 479.42 | –1.339 | 39.65 |
| 39 | 6.066 | 1,374.37 | 2.978 | 4.029 | 481.63 | –1.394 | 40.58 |
| 40 | 7.089 | 1,371.79 | 2.693 | 4.456 | 484.21 | –1.494 | 25.59 |
| 41 | 8.083 | 1,368.11 | 2.485 | 4.830 | 487.89 | –1.575 | 45.74 |
| 42 | 9.039 | 1,366.27 | 2.328 | 5.155 | 489.73 | –1.640 | 28.22 |
| 43 | 12.02 | 1,360.75 | 1.999 | 6.004 | 495.25 | –1.792 | 36.25 |
| 44 | 16.18 | 1,356.33 | 1.742 | 6.890 | 499.67 | –1.930 | 32.10 |
| 45 | 20.10 | 1,353.39 | 1.597 | 7.514 | 502.61 | –2.017 | 33.95 |
| 46 | 27.53 | 1,348.97 | 1.436 | 8.358 | 507.03 | –2.123 | 41.54 |

*Source:* Seidle, J. P., et al. 1991.
*Note:* $t_i = 12$ hours; $p_{wsi} = 1{,}856.00$ psia.

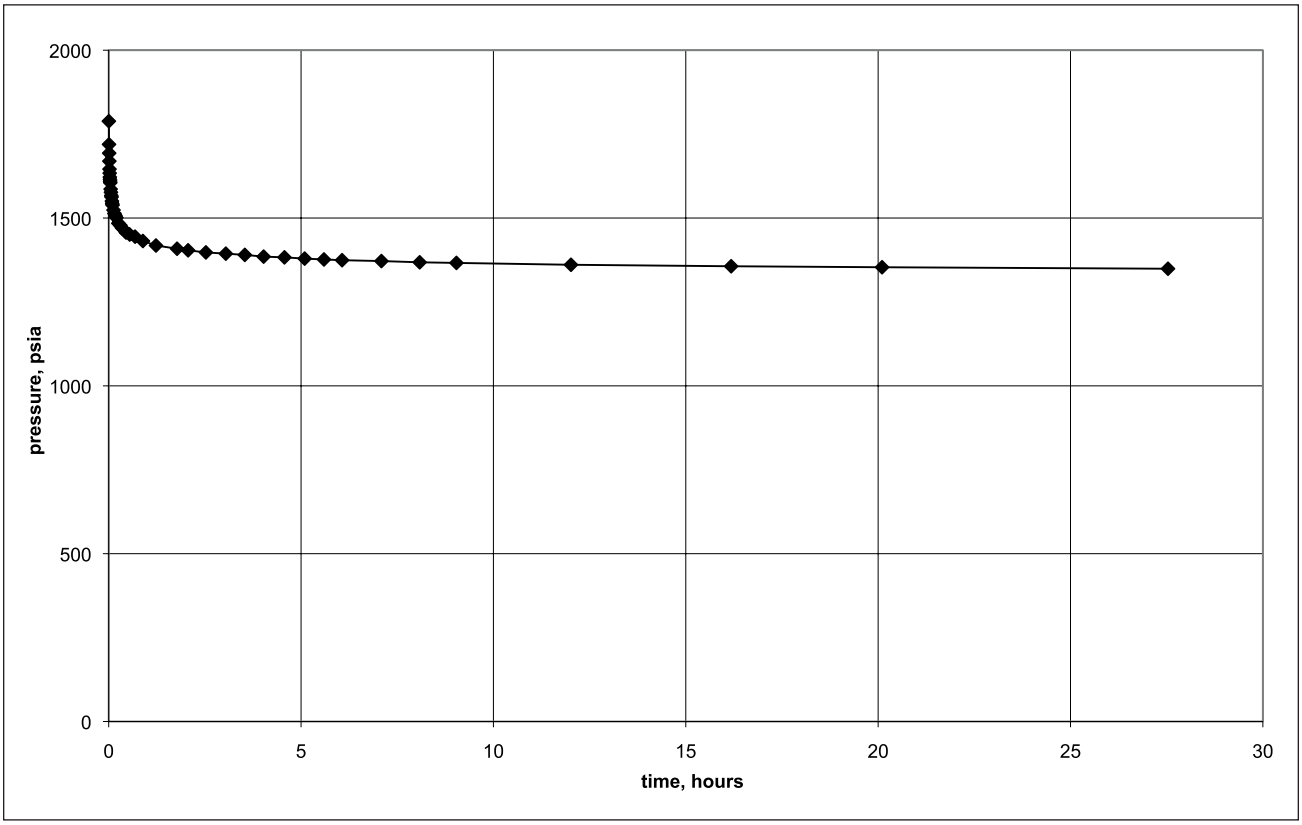



**Fig. 7–1.** Well A, prefrac PFOT—Cartesian plot

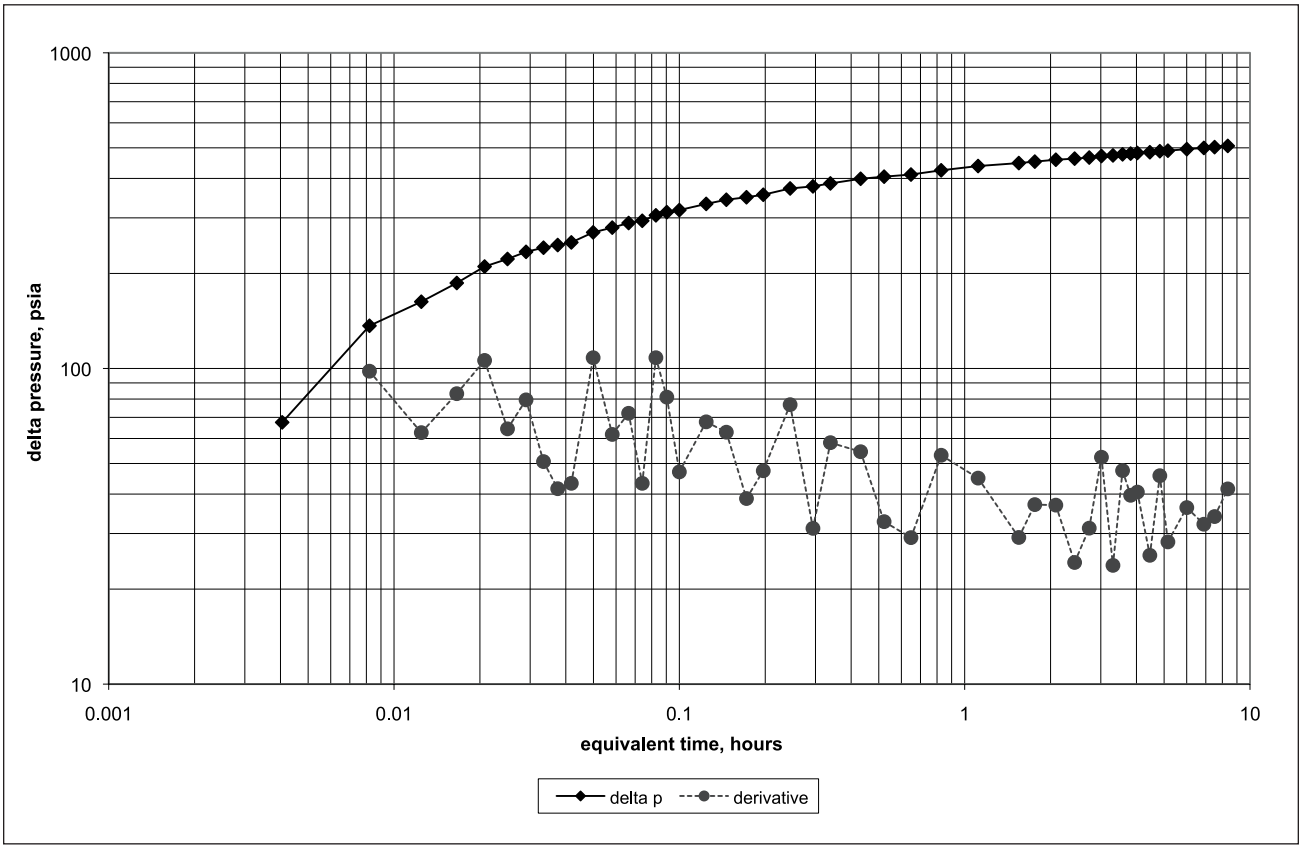



**Fig. 7–2.** Well A, prefrac PFOT—log-log plot

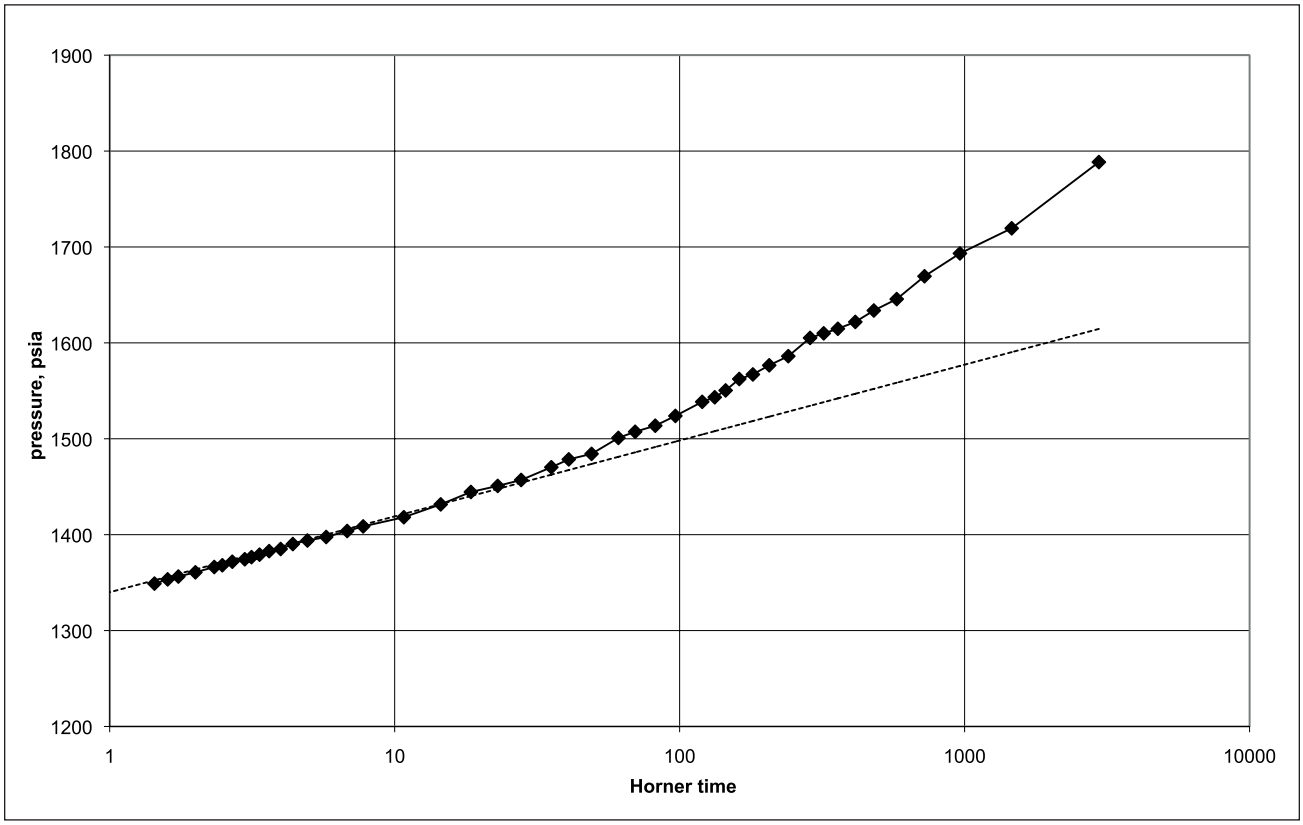



**Fig. 7–3.** Well A, prefrac PFOT—semilog plot, Horner time

Analysis using Horner time begins with a semilog plot, figure 7–3, and calculation of the late-time slope. Using points 29 and 46,

$$m = \frac{1{,}348.97 - 1{,}418.19 \text{ psia}}{\log(1.436) - \log(10.77)} = -79.10 \text{ psia/cycle}$$

From equation (7.4), permeability is

$$k = -\frac{162.6(360 \text{ bpd})(1.0 \text{ rb/stb})(0.50 \text{ cp})}{-79.10 \text{ psia/cycle } (42 \text{ ft})} = 8.8 \text{ md}$$

From the semilog straight line, $p_{1hr} = 1{,}428.1$ psia. Thus, wellbore skin calculated from equation (7.5) is

$$s = 1.1513\left[\frac{1{,}428.1 - 1{,}856.0 \text{ psia}}{-79.10 \text{ psia/cycle}} - \log\left(\frac{8.8 \text{ md}}{0.01(0.5\text{cp})(9.24\text{E} - 4 \text{ psia}^{-1})(0.20 \text{ ft})^2}\right) + 3.2275\right]$$

$$s = +1.1$$

Extrapolating to infinite time, the Horner time approaches 1, and from the semilog plot, $p^*$, initial reservoir pressure, is 1,338 psia.

Repeating the analysis using Agarwal equivalent time, a semilog plot is shown in figure 7–4. Again using points 29 and 46 to calculate the late-time slope,

$$m = \frac{1{,}348.97 - 1{,}418.19 \text{ psia}}{\log(8.358) - \log(1.114)} = -79.09 \text{ psia/cycle}$$

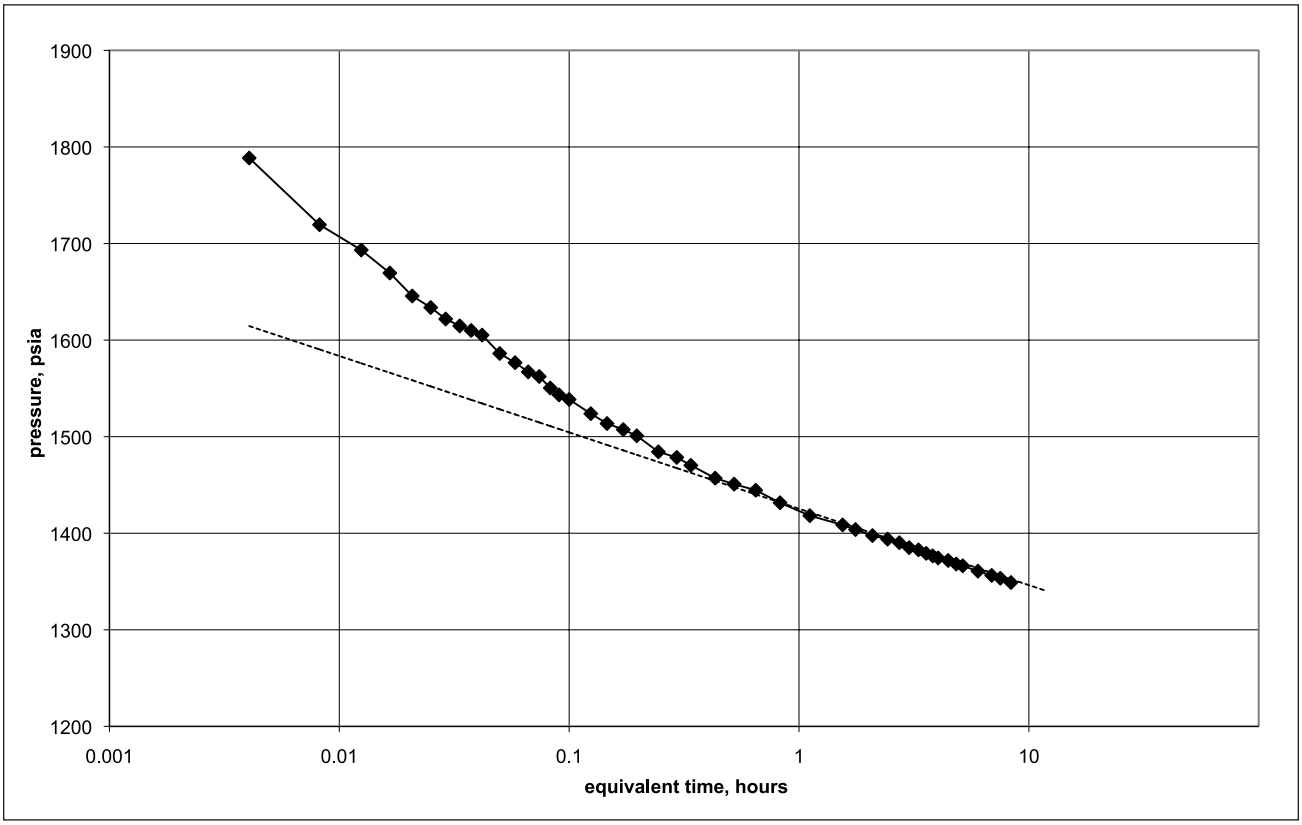



**Fig. 7–4.** Well A, prefrac PFOT—semilog plot, equivalent time

From equation (7.4), permeability is

$$k = -\frac{162.6(360\text{ bpd})(1.0\text{ rb/stb})(0.50\text{ cp})}{-79.09\text{ psia/cycle (42 ft)}} = 8.8\text{ md}$$

From the semilog straight line, $p_{1hr}$ = 1,428.1 psia, just as before. Thus, wellbore skin calculated from equation (7.5) is

$$s = 1.1513\left[\frac{1{,}428.1 - 1{,}856.0\text{ psia}}{-79.09\text{ psia/cycle}} - \log\left(\frac{8.8\text{ md}}{0.01(0.5\text{cp})(9.24\text{E} - 4\text{ psia}^{-1})(0.20\text{ ft})^2}\right) + 3.2275\right]$$

$$s = +1.1$$

The radius of investigation for this test is figured from equation (7.6).

$$r_i = 0.029\sqrt{\frac{8.8\text{ md }12\text{ hr}}{0.01(0.5\text{ cp})\ 9.24\text{E} - 4\text{ psia}^{-1}}} = 139\text{ ft} \qquad \textbf{(7.6)}$$

As time grows without bound, Agarwal equivalent time approaches $t_i$, the injection time, or 12 hr, and initial reservoir pressure, $p^*$, estimated from the semilog plot, is 1,340 psia.

Permeability determined with Horner time and equivalent time are virtually identical and in good agreement with the 8.2 md reported by Seidle et al., which was obtained from semilog analysis and refined by history matching the test with a simulator.[11] The wellbore skin factor of +1.1, indicative of modest wellbore damage and

typical of a new, unstimulated coal well, is nominally larger than the +0.7 skin factor determined by Seidle et al. Initial reservoir pressure determined using Horner time was 1,338 psia, 2 psia lower than that determined using equivalent time. Both are in good agreement with the 1,340 psia initial pressure reported by Seidle et al.

Postfrac injection/falloffs can be used to determine fracture parameters such as fracture half-length, *xf*, and fracture conductivity, *FCD*, thereby gauging effectiveness of the stimulation treatment. Stimulations in some coals deteriorate with time due to fines migration, proppant embedment, gel residue contamination of the sand pack, or a variety of other reasons. Injection/falloff tests done promptly after the treatment can provide baseline fracture parameters.

## Drillstem Tests

Both openhole and cased-hole drillstems tests (DSTs) have been employed in coals to determine permeability, pressure, and wellbore condition. Similar to DSTs in conventional wells, drillstem tests in coals isolate the zone of interest with a packer or straddle packers. Pressure and temperature are measured during a short flow period, a short shut-in period, a longer flow period, and a longer shut-in period. Design and interpretation of DSTs for coal wells is nearly identical to DSTs in conventional wells. Earlougher discussed DST tool operation, showed diagnostic plots illustrating various DST pressure trace behaviors, and presented relevant equations for DST analysis.[12] Coal well drillstem test design and procedures were detailed by GRI.[13] In addition, GRI addressed downhole and surface equipment requirements and presented an example test design.

The initial flow period is to reduce mud pressure against the formation, while the initial shut-in allows pressure in the tool to approach formation pressure. The second flow period may provide fluid samples and should be long enough to allow flow stabilization. The final shut-in should be long enough to provide sufficient data to determine formation and wellbore properties, an admittedly subjective requirement. Recommended flow and shut-in times from Earlougher are reproduced here as table 7–2.[14] For coal well DSTs, GRI recommends an initial flow period of 5 to 30 min, an initial shut-in duration of 4 to 8 times the initial flow period, roughly 20 min to 2 hr, a final flow period of 3 to 8 hr, and a final shut-in period at least 1.5 times the length of the final flow period.[15]

**Table 7–2.** Recommended DST flow and shut-in times when experience is not available

| Test period | Situation during test | Recommended time | Minimum time, min |
|---|---|---|---|
| Initial flow | All | Short—release hydrostatic mud pressure | 3 to 5 |
| Initial shut-in | All | 60 min unless total test time is too short—45 min then | 30 |
| Final flow | Strong, continuing blow | 60 min | 60 |
| | Blow dies | Shut-in when blow dies | 60 |
| | Reservoir fluid produced at surface | 60 min; longer to gauge flow rates if time is available | 60 |
| Final shut-in | Strong, continuous blow during final period | Shut-in time equal to flow time | 45 |
| | Blow dies during final period | Minimum shut-in time of twice flow time | Two times flow time |
| | Reservoir fluid produced at surface during flow period | Shut-in time equal to one-half flow time | 30 |

*Source:* Earlougher, R. C., Jr. 1977.

If the well produces water during the flow period, the rate will be continually decreasing as backpressure from the column of produced water steadily increases bottomhole pressure. This behavior is usually neglected, and an average rate is employed in test analysis. Although Agarwal equivalent time is arguably more theoretically correct, Horner time is used to analyze the buildup portion of the data. Permeability can be determined from equation (7.4). As production and shut-in times are roughly equal, the above equation for the skin factor, equation (7.5), is modified to be

$$s = 1.1513\left[\frac{p_{1hr} - p_{si}}{m} + \log\left(\frac{t_p + 1}{t_p}\right) - \log\left(\frac{k}{\phi\mu_w c_t r_w^2}\right) + 3.2275\right] \quad \textbf{(7.7)}$$

where

$t_p$ = duration of the flow period, hr.

In practice, drillstem tests are often problematic in coals due to the production of gas and coal fines. If a coal produces both gas and water during a DST, the above analysis provides effective permeability to water. To obtain absolute permeability, gas-water relative permeabilities and fluid saturations are required, data that are often not available at the time of testing. Coal fines are frequently produced during drillstem tests, especially openhole DSTs. Production of even a small amount of coal fines can interfere with tool operation, complicating test interpretation.

## Tank Tests

*Tank tests* are essentially constant rate injection tests for underpressured, highly permeable coal deposits. In these tests, water from a tank at atmospheric pressure is allowed to drain into a wellbore, approximating a constant injection rate. A schematic of the test apparatus is shown in figure 7–5. Design of tank tests is discussed by GRI, and an example test design is presented.[16] As tank tests are characterized by a falling liquid level, wellbore storage effects can be significant. Consequently, small diameter tubing strings are preferred over large diameter well casing for tank tests, and these tests are more amenable to shallow rather than deep coals.

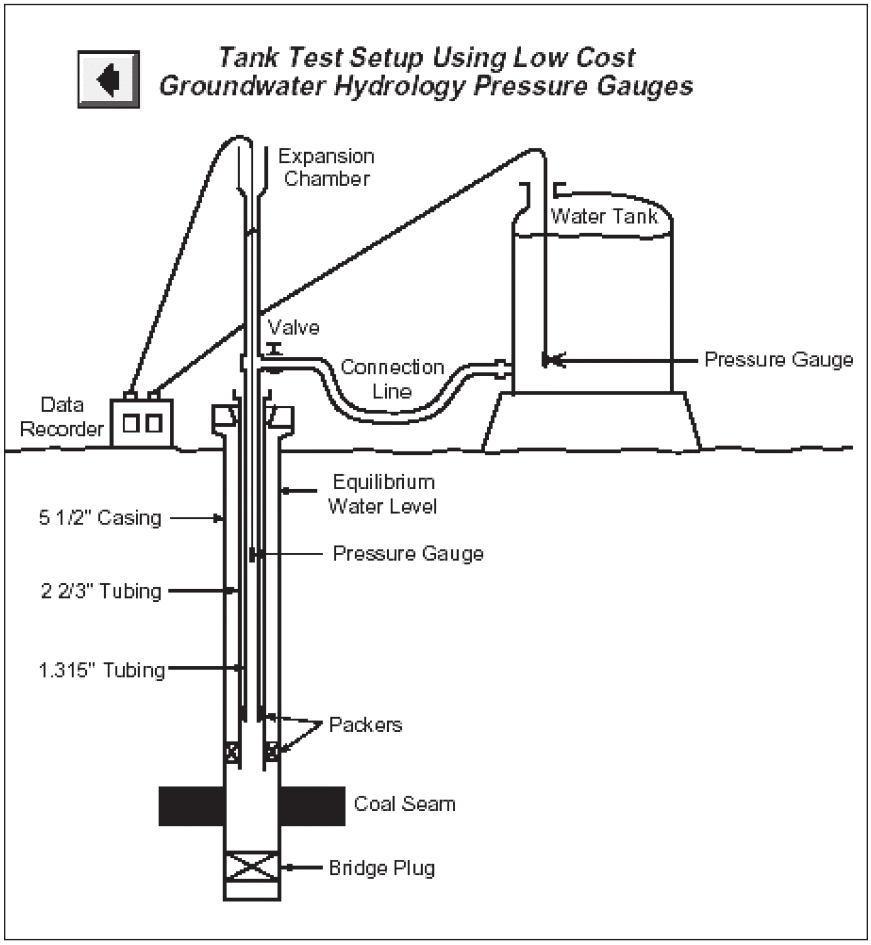



**Fig. 7–5.** GRI tank test schematic[17]

The GRI procedure specifies calculation of a falling liquid level wellbore storage coefficient based upon tubing diameter. Time for cessation of wellbore storage effects is calculated using equation (7.1). Injection duration is typically five times longer than this minimum time. Required water volumes are estimated from the van Everdingen and Hurst dimensionless time and cumulative volume solution, initial formation pressure, and the flowing bottomhole pressure during injection.[18] Shut-in time is equal to injection time, and analysis employs equations (7.4) and (7.5) to calculate permeability and skin factor, respectively.

Because of their restriction to shallow, underpressured, highly permeable coals, tank tests have seen limited application outside the Warrior Basin where they were developed.

## Slug Tests

*Slug tests* involve rapid addition or withdrawal of fluid from a well followed by observation of the subsequent bottomhole pressure change as the fluid level returns to equilibrium. Because of the possibility of gas desorption due to fluid withdrawal, slug tests in coals usually involve addition of fluid to the wellbore. These tests are relatively simple and inexpensive in coal wells but can require excessively long test times in low-permeability coals. They have a small radius of investigation and often lead to ambiguous, nonunique results.

Both theoretical and practical aspects of analysis of slug tests and DSTs were discussed by Ramey et al.[19] Dimensionless pressure was presented as a function of dimensionless time and a wellbore storage coefficient to facilitate type curve matching of slug tests. Test duration was discussed, and dependence of permeability on the square of the wellbore radius noted. In practice, accurate determination of permeability depends on knowledge of the wellbore configuration, and wellbore radius is often the crucial element in slug test interpretation. Ramey et al. found the radius of investigation of a slug test is approximately 100 times the wellbore radius. For example, a well completed with 5½ in., J-55, 15.5 lb/ft casing has an inside diameter (ID) of 4.950 in., and a slug test in this well would have a radius of investigation of roughly 21 ft.

Use of slug tests in coal wells was proposed by Koenig and Schraufnagel and further refined by GRI.[20] These workers noted for best results, a well must be stabilized prior to a slug test, which can require between a day and several weeks. Analysis of the test is simplified if the initial fluid level, and hence initial pressure, are measured after the well has stabilized and before addition of the slug of fluid. Test duration can be estimated from

$$t_{st} = \frac{43{,}700\ \mu_w r_c^2}{kh} \tag{7.8}$$

where

$t_{st}$ = slug test duration, hr, and
$r_c$ = radius of the tubing or casing in which the fluid level is rising or falling, ft.

Using well and coal properties from example 7.1 above, slug test duration in this well is calculated to be

$$t_{st} = \frac{43{,}700\ (0.5\ \text{cp})\ 0.2^2\ \text{ft}^2}{8.8\ \text{md}\ (42\ \text{ft})} = 2.4\ \text{hr}$$

Note this test time is much shorter than the 12 hr injection and 28 hr shut-in of the injection/falloff test of example 7.1.

Difficulties and limitations of slug tests in Warrior Basin coal wells were presented by Conway et al.[21] Applying the method of Ramey et al. to four sets of high-quality data repeatedly taken from the same unstimulated well, these workers found slug tests were unable to uniquely determine reservoir permeability and wellbore skin.[22] Permeabilities ranged from 0.3 to 52 md, and wellbore skin factors varied from +3 to +40. Reasons for such variations were ascribed to the nonunique nature of slug test analysis, even with use of pressure derivatives, and short testing times, often limiting the test to the damaged zone surrounding the unstimulated wellbore.

## Diagnostic Fracture Injection Tests

Use of pressure falloff data from fracture calibration tests in moderate and high-permeability formations was developed by Mayerhofer et al. and modified by Valko and Economides.[23] Application of such tests, termed *diagnostic fracture injection tests (DFITs)* or *G-function tests* (after the time transform used in their analysis), to coals was presented by Ramurthy et al.[24] This study incorporated the G-function derivative analysis of Barree and Mukherjee and identified four distinct signatures seen in coal well DFITs.[25] The four different test responses, shown in figure 7–6, include normal leakoff, pressure dependent leakoff, fracture-tip extension, and fracture height recession.

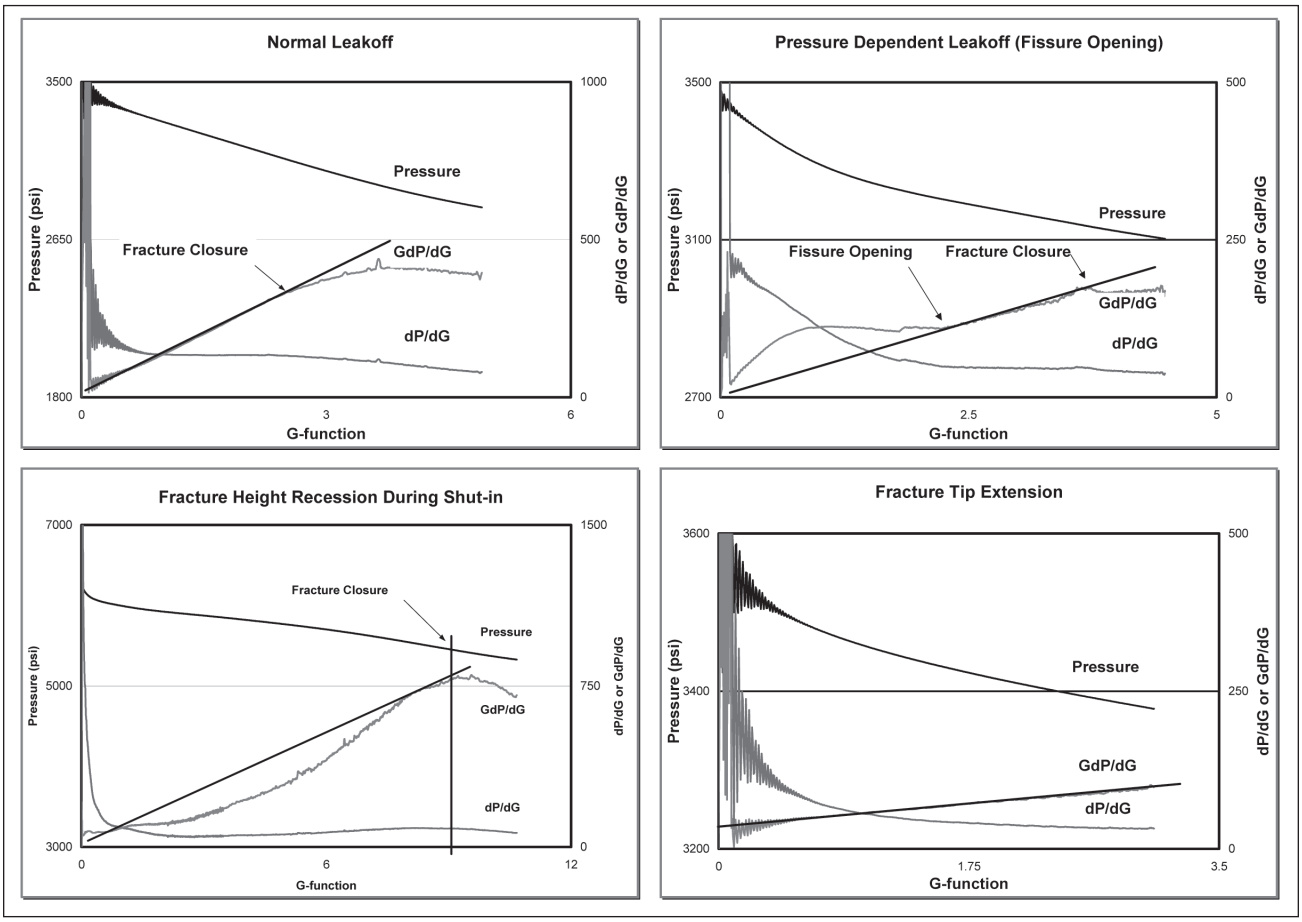



**Fig. 7–6.** Coal well diagnostic fracture injection test signatures[26]

Normal leakoff, which occurs from a constant area fracture in a homogeneous formation, was reported to occur in approximately 1% of all coal well DFITs. Pressure-dependent leakoff was the predominant response seen in coal well DFITs, occurring in 75% of all tests studied. This signature is seen in tests with multiple fractures and is intuitively what would be expected from cleated coals. Ramurthy et al. noted that permeability determined from this test signature will depend on the time interval analyzed.[27] Analysis of early-time data will yield a permeability representative of dilated cleats, while analysis of late-time data, after fracture closure, will result in a permeability closer to that prevailing during depletion. Consequently, care should be taken to assure that late-time data, also known as *radial flow data* or *after-closure data*, are selected for analysis. Fracture tip extension type behavior was seen in 10% of coals tested, primarily in the deep Piceance Basin. This signature is seen in tests of low-leakoff, tight rock in which sufficient fluid energy remains after shut-in to drive the fracture further into the formation. The fourth type of behavior, fracture height recession, was seen in only 14% of coal well DFITs and occurs when in-situ stresses are sufficient to heal the top and/or bottom of the fracture during the shut-in.

Ramurthy et al. reported DFITs in coals typically employ 1,000 gal (24 bbl) of fluid pumped at rates of 3 to 10 bpm.[28] Thus, injection time for such tests is on the order of 2 to 10 min. Shut-ins range from an hour to overnight. These tests are especially useful for characterizing permeabilities in wells with multizone completions. A full day of testing followed by an overnight shut-in of the final zone can characterize up to half a dozen individual seams penetrated by a single wellbore.

DFITs currently have several limitations. Interpretation of before-closure data depends on rock properties. Consequently, in practice, these data are often history matched using after-closure permeability and pressure to determine rock properties. Because of their short test cycle, the radius of investigation of these tests can be quite small. As DFITs employ injection pressures above fracture parting pressure and actually drive a small fracture into the reservoir, they are currently employed only in unstimulated zones and are not used to assess fracture stimulation parameters. At this time, development of DFITs for stimulated coals is being actively pursued by several workers but has not been publicly reported.

DFITs are difficult to interpret in coals with free gas present due to complications from relative permeability effects. As with injection/falloff tests, the injected water serves to sweep gas from the near-wellbore region and drive any trapped gas back onto the coal surface. In coals with little, if any, moveable water, such as the coals of the Arkoma basins, the Horseshoe Canyon coals of the Alberta plains, and some coals in the Appalachian basins, DFITs leave a ring of water around the wellbore, similar to a condensate ring in a retrograde reservoir. Near-wellbore gas mobility is low due to this water ring and may not clean up with time, permanently impairing well productivity. A nitrogen slug test for determination of shale permeability and pressure and unstimulated wellbore condition was developed by Jochen et al.[29] Similar to a DFIT, a slug of nitrogen is quickly injected into the formation and the subsequent pressure decline recorded. Developed for wells penetrating multiple shale layers, nitrogen slug testing time is similar to a DFIT, enabling rapid characterization of the zone but with limited radii of investigation. Analysis of a nitrogen slug test typically begins with matching the pressure decay on the type curves of Ramey et al. and terminates with computer simulation of the entire test response.[30] At the time of this writing, service companies are fusing this methodology with the mathematics of the more recent DFIT to develop a diagnostic injection test for low-permeability, gas-saturated sands, shales, and coals but are not yet offering it commercially.

## Drawdown and Buildup Tests

Drawdown and buildup tests in coal wells producing water, or wells with gas-water ratios on the order of one or less, can be analyzed with semilog methods developed for slightly compressible fluids. Following Lee and Wattenbarger, drawdown test analysis begins with a semilog plot of bottomhole flowing pressure versus time.[31] Effective permeability to water is calculated from

$$k_w = \frac{162.6 q_w B_w \mu_w}{mh} \tag{7.9}$$

where

$k_w$ = effective permeability to water, md, and
$q_w$ = water production rate, bpd.

Wellbore skin factor is determined from

$$s = 1.1513 \left[ \frac{p_i - p_{1hr}}{m} - \log \left( \frac{k_w}{\phi \mu_w c_t r_w^2} \right) + 3.2275 \right] \tag{7.10}$$

where

$p_i$ = initial reservoir pressure, psia.

Again drawing on Lee and Wattenbarger, analysis of a buildup test from a coal well producing only water begins with a plot of bottomhole shut-in pressure versus Horner time, and effective permeability to water is calculated using equation (7.9).[32] Wellbore skin is determined from

$$s = 1.11513\left[\frac{p_{1hr} - p_{wsi}}{m} - \log\left(\frac{k_w}{\phi\mu_w c_t r_w^2}\right) + 3.2275\right] \tag{7.11}$$

where

$p_{wsi}$ = bottomhole flowing pressure at the time of shut-in, psia.

Extrapolation of the semilog straight line to infinite time (a Horner time of 1) yields a false pressure, $p^*$. Average reservoir pressure can be determined from $p^*$ using the Matthews-Brons-Hazebroek (MBH) method.[33] A dimensionless time based on drainage area, $A$, and production time, $t_p$, is given by

$$t_{DA} = \frac{0.0002637\, kt_p}{\phi\mu_w c_t A} \tag{7.12}$$

For dimensionless times less than 0.1, the MBH dimensionless pressure function is written by Reynolds et al. as[34]

$$p_{MBHD} = 4\pi t_{DA} \tag{7.13}$$

For dimensionless times greater than 0.1, the MBH dimensionless pressure function is defined as

$$p_{MBHD} = \ln(C_A t_{DA}) \tag{7.14}$$

where

$C_A$ = the shape factor for the well drainage area, dimensionless.

The shape factor for a circular drainage area is 31.62, that of a square drainage area is 30.8828, and other drainage areas are given in Earlougher.[35] Once $p_{MBHD}$ is known, average reservoir pressure is calculated from

$$\overline{p} = p^* - \frac{m}{2.3025}\, p_{MBHD}\,(t_{DA}) \tag{7.15}$$

Development of well test techniques for coal wells producing only gas began by assuming single-phase gas flow in coals, neglecting relative permeability effects and saturation gradients. Bayles and Reznik simulated constant gas production rate drawdown tests of a coal well.[36] Gas sorption in the matrix was modeled with a Langmuir isotherm, and gas release from the matrix into the cleat was assumed to be instantaneous. Gas flow was described with a radial diffusivity equation using the real gas pseudopressure function

$$m(p) = 2\int \frac{p}{\mu_g Z}\, dp \tag{7.16}$$

where

$m(p)$ = the real gas pseudopressure, psia$^2$/cp, and

$Z$ = the gas deviation factor, dimensionless.

With the addition of a term to account for the effects of sorption in the radial diffusivity equation for gas flow, Bayles and Reznik demonstrated their numerical solutions were close analogs of those obtained from conventional gas well testing. Permeability was determined with a semilog straight line applied to pressure data from the transient flow period. Drainage area was determined with data from the boundary-dominated flow period. Quantification of wellbore skin was not addressed in this study. When gas transfer from the matrix to cleat was negated, the solutions collapsed back to those of conventional gas wells, as expected.

Bumb and McKee presented an approximate analytical solution for constant rate drawdown tests in coals and Devonian shales, assuming instantaneous desorption and gas storage according to a Langmuir isotherm. Gas flow was described using the real gas pseudopressure.[37] A step-by-step procedure for analysis of drawdown tests was presented, and sensitivity of pressure response to various reservoir parameters was investigated using Piceance Basin coal properties. These authors were the first to note that desorption effects are manifested in well tests as increased system compressibility.

An analytical solution that assumed time-dependent gas release from the coal matrix was presented by Ertekin and Sung.[38] Gas storage in the matrix was described with Henry's law, and gas flow in the cleats was modeled with the p-squared formulation of Darcy's law. Pressure responses from two well tests, one from the Warrior Basin, one from the Piceance Basin, were matched using the analytical solution. However, equations for determination of coal permeability and wellbore skin were not presented. Effects of sorption compressibility on coal well test interpretation were not discussed.

Design and analysis of drawdown and buildup tests in coal wells were treated by GRI.[39] Determination of effective permeability to gas, wellbore skin factor, and average reservoir pressure for coal wells is quite similar to the same exercise for a conventional dry gas well. Test analysis can be based upon real gas pseudopressure, pressure squared, or pressure methods as outlined in Lee and Wattenbarger.[40] Regardless of the pressure function employed, test interpretation begins with a plot of pressure data versus time, followed by log-log and semilog plots. Once the straight-line portion of the data on the semilog plot has been identified, permeability is determined from the slope of that line. Wellbore skin factor is determined from the 1 hr pressure point and various well and reservoir parameters, just as is done for conventional gas wells. Average reservoir pressure is calculated from the extrapolated false pressure, $p^*$, and the Matthews-Brons-Hazebroek method.

The real gas pseudopressure method is the most robust method for interpretation of coal well drawdown and buildup tests. After a Cartesian plot of the data indicates a sound test and a log-log plot reveals the radial flow portion of the data, the slopes of the corresponding data on the semilog plot are used to calculate effective permeability to gas using[41]

$$k_g = \frac{1{,}637 q_g T}{mh} \tag{7.17}$$

where

$k_g$ = effective permeability to gas, md,
$q_g$ = gas production rate, mcfd,
$T$ = reservoir temperature, °R, and
$m$ = slope of the semilog straight line, psia$^2$/cp-cycle.

Wellbore skin is determined from[42]

$$s = 1.1513\left[\frac{m(\bar{p}) - m(p_{1hr})}{m} - \log\left(\frac{k_g}{\phi \bar{\mu}_g \bar{c}_t r_w^2}\right) + 3.2275\right] \tag{7.18}$$

where

$m(\bar{p})$ = real gas pseudopressure of average reservoir pressure, psia$^2$/cp-cycle,
$m(p_{1hr})$ = real gas pseudopressure of pressure at 1 hr, psia$^2$/cp-cycle,
$\bar{\mu}_g$ = average gas viscosity, cp, and
$\bar{c}_t$ = average total compressibility, psia$^{-1}$.

Analysis of a buildup test using the $m(p)$ formulation employs a plot of real gas pseudopressure versus Horner time. Effective permeability to gas is calculated with equation (7.17), and wellbore skin is determined from

$$s = 1.1513\left[\frac{m(p_{1hr}) - m(p_{wsi})}{m} - \log\left(\frac{k_g}{\phi\bar{\mu}_g\bar{c}_t r_w^2}\right) + 3.2275\right] \tag{7.19}$$

where

$m(p_{wsi})$ = real gas pseudopressure of bottomhole flowing pressure at the instant of shut-in, psia$^2$/cp-cycle.

Average pressure is determined from the dimensionless MBH pressure function, equations (7.13) and (7.14), from the dimensionless time, equation (7.12), and

$$m(\bar{p}) = m(p^*) - \frac{m}{2.3025}\,p_{MBHD}\,(t_{DA}) \tag{7.20}$$

Similarly, for interpretation of a drawdown test using the p-squared formulation, a plot of the square of bottomhole flowing pressure, $p_{wf}^2$, versus time is constructed. Effective permeability to gas is determined from the straight-line portion of the data using

$$k_g = \frac{1{,}637 q_g T\bar{Z}\bar{\mu}_g}{mh} \tag{7.21}$$

where

$\bar{Z}$ = average gas deviation factor, dimensionless.

The skin factor is calculated from

$$s = 1.1513\left[\frac{\bar{p}^2 - p_{1hr}^2}{m} - \log\left(\frac{k_g}{\phi\bar{\mu}_g\bar{c}_t r_w^2}\right) + 3.2275\right] \tag{7.22}$$

Calculation of permeability from a buildup test using the pressure-squared method commences with a plot of the square of bottomhole shut-in pressure as a function of Horner time and identification of the semilog straight-line portion of the data. Effective permeability to gas is calculated using equation (7.21), and skin is determined using

$$s = 1.1513\left[\frac{p_{1hr}^2 - p_{wf}^2}{m} - \log\left(\frac{k_g}{\phi\bar{\mu}_g\bar{c}_t r_w^2}\right) + 3.2275\right] \tag{7.23}$$

Average pressure determination using the pressure-squared formulation again begins with calculation of dimensionless production time, equation (7.12), which is then used in either equation (7.13) or (7.14) to calculate $p_{MBHD}$. Average reservoir pressure is given by

$$\bar{p}^2 = p^{*2} - \frac{m}{2.3025}\,p_{MBHD}\,(t_{DA}) \tag{7.24}$$

If the pressure variable is simply pressure, permeability is calculated from

$$k_g = \frac{162.6 q_g \bar{B}_g \bar{\mu}_g}{mh} \tag{7.25}$$

where

$\bar{B}_g$ = average gas formation volume factor, rb/mcf.

Skin factor is calculated from

$$s = 1.1513\left[\frac{\bar{p} - p_{1hr}}{m} - \log\left(\frac{k_g}{\phi\bar{\mu}_g\bar{c}_t r_w^2}\right) + 3.2275\right] \quad \textbf{(7.26)}$$

where

$\bar{p}$ = average reservoir pressure, psia.

Calculation of permeability from a buildup test using the pressure formulation begins with a plot of shut-in bottomhole pressure versus Horner time. Effective permeability to gas is determined using equation (7.25). Skin factor is calculated with

$$s = 1.1513\left[\frac{p_{1hr} - p_{wf}}{m} - \log\left(\frac{k_g}{\phi\bar{\mu}_g\bar{c}_t r_w^2}\right) + 3.2275\right] \quad \textbf{(7.27)}$$

Average reservoir pressure in the drainage volume can be estimated with the MBH method outlined above. Dimensionless time is calculated according to equation (7.12), $p_{MBHD}$ from either equation (7.13) or (7.14), and $\bar{p}$ from equation (7.15).

### Example 7.2. Coal well pressure buildup test

Pressure buildup tests from coal wells in the Rincon Unit of the San Juan Basin were discussed by Vo et al.[43] These fracture-stimulated wells drain the dry, underpressured coals of the southern portion of the basin. At the time of testing, Well 1 had been flowing 117 mcfd for 924.9 hr. Bottomhole pressure at shut-in was 151.8 psia. Pertinent data for this well are given below, while pressure data are collected in table 7–3 and gas properties in table 7–4.

$p_i$ = 400 psia
$T$ = 110°F
$\gamma_g$ = 0.65
$\phi$ = 0.01
$r_w$ = 0.31 ft
$h$ = 40 ft
$A$ = 320 ac

**Table 7–3.** Example 7.2 pressure buildup test data

| Point no. | Δ t, hr | Bottomhole shut-in pressure, psia |
|---|---|---|
| 1 | 0.020 | 153.056 |
| 2 | 0.050 | 156.177 |
| 3 | 0.100 | 159.298 |
| 4 | 0.207 | 166.476 |
| 5 | 0.332 | 171.782 |
| 6 | 0.516 | 179.584 |
| 7 | 1.032 | 195.189 |
| 8 | 1.710 | 212.484 |
| 9 | 2.659 | 229.649 |
| 10 | 3.833 | 243.693 |
| 11 | 5.255 | 256.177 |
| 12 | 7.203 | 263.979 |
| 13 | 9.690 | 271.782 |
| 14 | 11.370 | 276.860 |
| 15 | 14.315 | 283.471 |
| 16 | 18.767 | 292.355 |
| 17 | 23.425 | 299.587 |
| 18 | 29.932 | 307.231 |
| 19 | 37.055 | 313.017 |
| 20 | 44.110 | 316.529 |
| 21 | 50.959 | 318.802 |
| 22 | 58.151 | 321.694 |
| 23 | 65.342 | 323.760 |
| 24 | 73.014 | 325.413 |
| 25 | 80.685 | 327.893 |
| 26 | 85.890 | 330.785 |
| 27 | 93.699 | 330.992 |

*Source:* Vo, D. T., et al. 1991.

**Table 7–4.** Example 7.2 pressure buildup test–gas properties

| Pressure, psia | Z factor | $B_g$, ft³/scf | $c_g$, psia$^{-1}$ | Visc., cp | $m(p)$, psia²/cp |
|---|---|---|---|---|---|
| 14.7 | 0.9981 | 1.091383829 | 0.068157118 | 0.0115 | 0 |
| 20 | 0.9974 | 0.801614816 | 0.050130194 | 0.0115 | 15967.51801 |
| 40 | 0.9948 | 0.399763332 | 0.025130405 | 0.0116 | 120263.7745 |
| 60 | 0.9922 | 0.265814779 | 0.016797132 | 0.0116 | 294285.8568 |
| 80 | 0.9896 | 0.198841277 | 0.012630606 | 0.0116 | 538165.8624 |
| 100 | 0.9870 | 0.158657829 | 0.010130737 | 0.0116 | 852013.1686 |
| 120 | 0.9845 | 0.131869434 | 0.008464191 | 0.0116 | 1235918.334 |
| 140 | 0.9819 | 0.11273538 | 0.007273825 | 0.0117 | 1689955.466 |
| 160 | 0.9793 | 0.098385311 | 0.006381066 | 0.0117 | 2214183.789 |
| 180 | 0.9768 | 0.087224584 | 0.005686709 | 0.0117 | 2808648.746 |
| 200 | 0.9742 | 0.078296416 | 0.005131228 | 0.0117 | 3473382.82 |
| 220 | 0.9716 | 0.070991943 | 0.004676745 | 0.0118 | 4208406.148 |
| 240 | 0.9691 | 0.064905258 | 0.004298007 | 0.0118 | 5013727.001 |
| 260 | 0.9666 | 0.059755348 | 0.003977531 | 0.0118 | 5889342.161 |
| 280 | 0.9640 | 0.055341489 | 0.003702993 | 0.0118 | 6835237.215 |
| 300 | 0.9615 | 0.051516486 | 0.003464913 | 0.0119 | 7851386.792 |
| 320 | 0.9590 | 0.04816994 | 0.003256581 | 0.0119 | 8937754.751 |
| 340 | 0.9564 | 0.045217431 | 0.003072744 | 0.0119 | 10094294.33 |
| 360 | 0.9539 | 0.042593299 | 0.002909316 | 0.0120 | 11320948.25 |
| 380 | 0.9514 | 0.040245705 | 0.002763072 | 0.0120 | 12617648.82 |
| 400 | 0.9489 | 0.038133182 | 0.002631432 | 0.0120 | 13984317.99 |
| 420 | 0.9465 | 0.036222158 | 0.002512306 | 0.0121 | 15420867.42 |
| 440 | 0.9440 | 0.034485167 | 0.002403985 | 0.0121 | 16927198.46 |
| 460 | 0.9415 | 0.032899521 | 0.002305057 | 0.0121 | 18503202.25 |
| 480 | 0.9390 | 0.031446311 | 0.002214345 | 0.0122 | 20148759.64 |
| 500 | 0.9366 | 0.030109656 | 0.00213086 | 0.0122 | 21863741.25 |
| 520 | 0.9342 | 0.028876116 | 0.002053766 | 0.0122 | 23648007.42 |
| 540 | 0.9317 | 0.027734245 | 0.00198235 | 0.0123 | 25501408.23 |
| 560 | 0.9293 | 0.026674231 | 0.001916 | 0.0123 | 27423783.43 |
| 580 | 0.9269 | 0.025687615 | 0.001854191 | 0.0124 | 29414962.45 |
| 600 | 0.9245 | 0.024767067 | 0.001796464 | 0.0124 | 31474764.34 |
| 620 | 0.9221 | 0.023906203 | 0.001742424 | 0.0124 | 33602997.75 |
| 640 | 0.9197 | 0.023099436 | 0.00169172 | 0.0125 | 35799460.89 |
| 660 | 0.9174 | 0.022341857 | 0.001644048 | 0.0125 | 38063941.5 |
| 680 | 0.9150 | 0.021629136 | 0.001599136 | 0.0126 | 40396216.79 |
| 700 | 0.9127 | 0.020957436 | 0.001556747 | 0.0126 | 42796053.4 |

This test will be analyzed with the three methods described above, beginning with real gas pseudopressure. A Cartesian plot of the test data (fig. 7–7) shows a smooth and steadily rising pressure trace, indicative of a sound test. A log-log plot of the *real gas pseudopressure difference*, defined as pseudopressure at time *t* minus the pseudopressure at shut-in, and the pressure derivative, calculated as described by Bourdet et al., are depicted in figure 7–8.[44] At early time, the pressure difference and pressure derivative traces give the signature of a fractured well with little wellbore storage and little, if any, damage. Minimal wellbore storage effects are evident in this test, as the first few points lie close to a unit slope line. However, after about 0.2 hr, the data fall away from the line yet never descend to the half-slope line often seen in fractured wells at early time. About 2 hr after shut-in, the derivative flattens and remains so throughout the remainder of the test, indicative of radial flow. The derivative spikes at late time are numerical artifacts and are not related to reservoir boundaries.

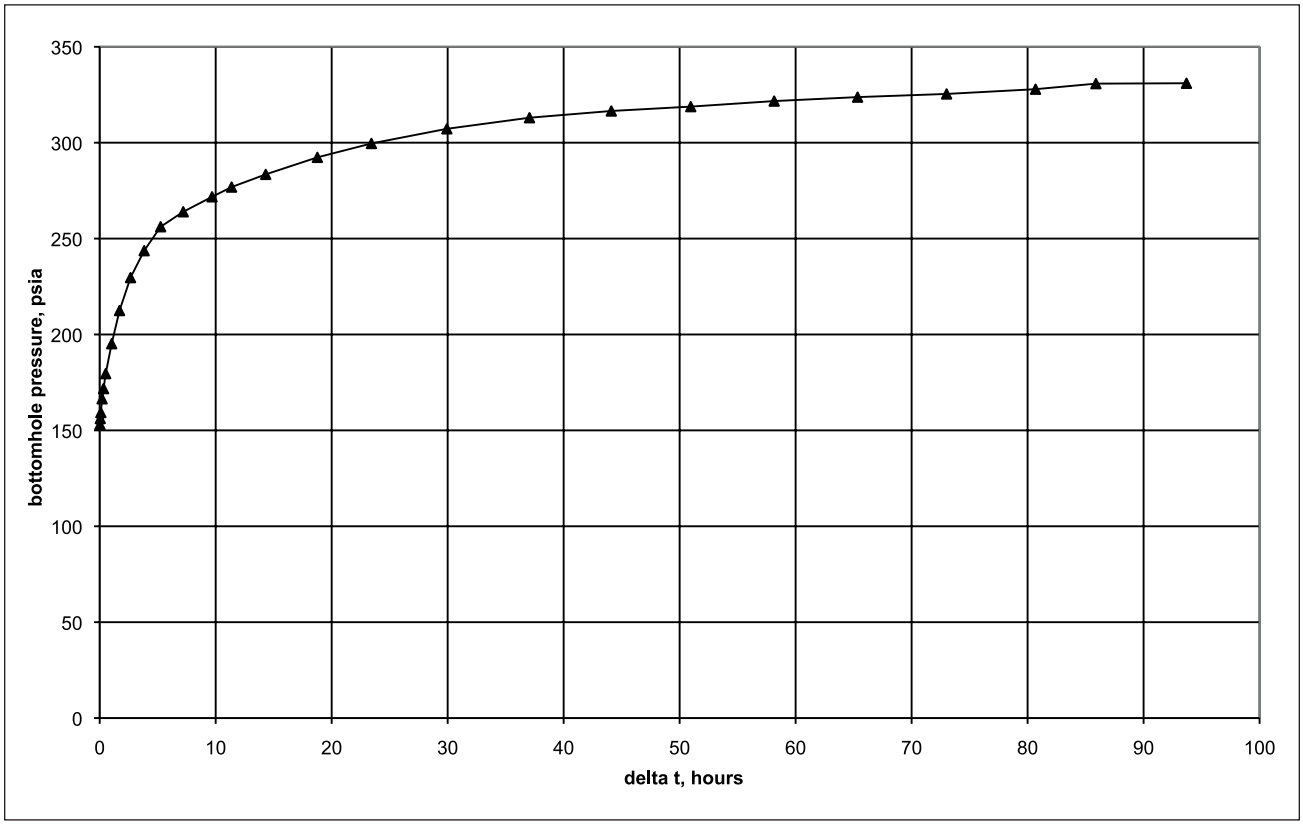



**Fig. 7–7.** Example 7.2 pressure buildup test—Cartesian plot

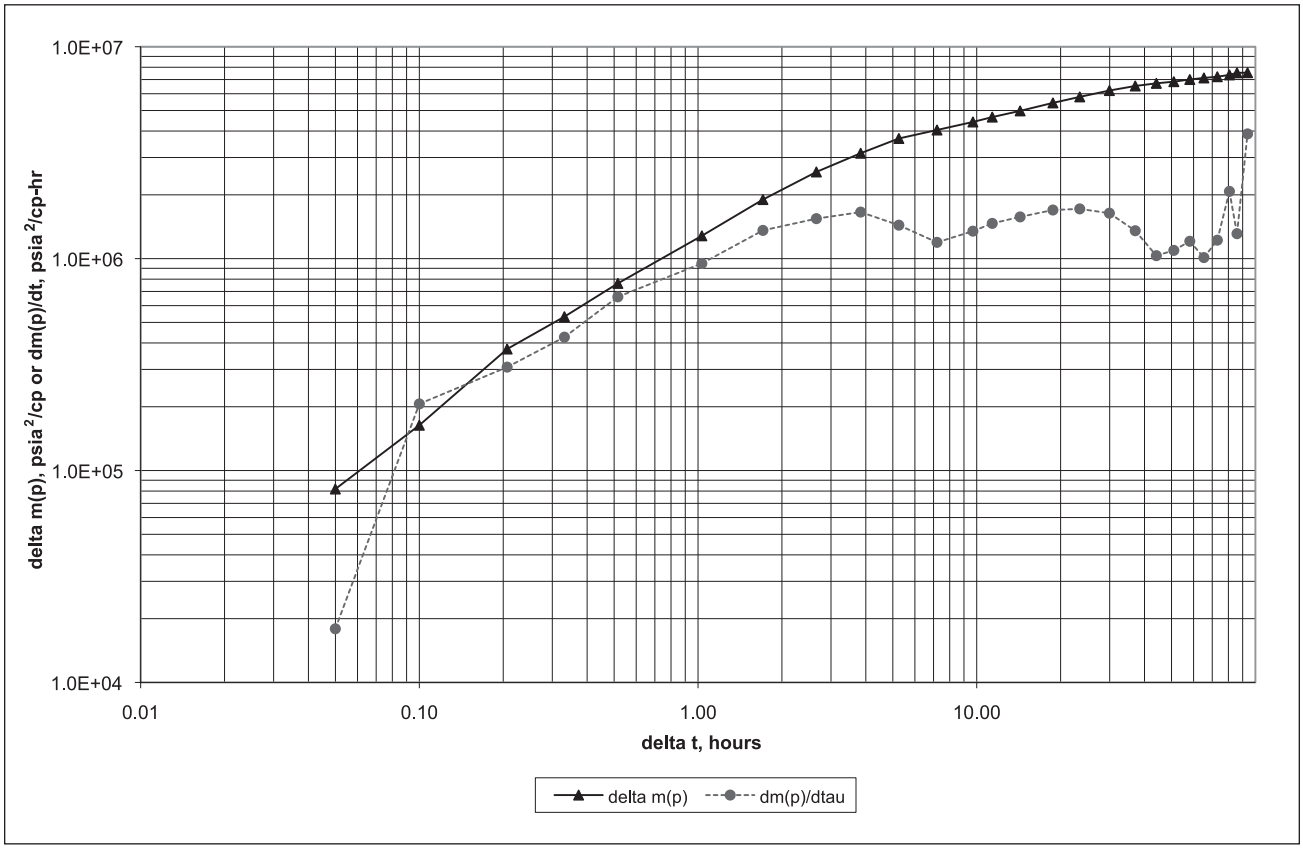



**Fig. 7–8.** Example 7.2 pressure buildup test—log-log plot

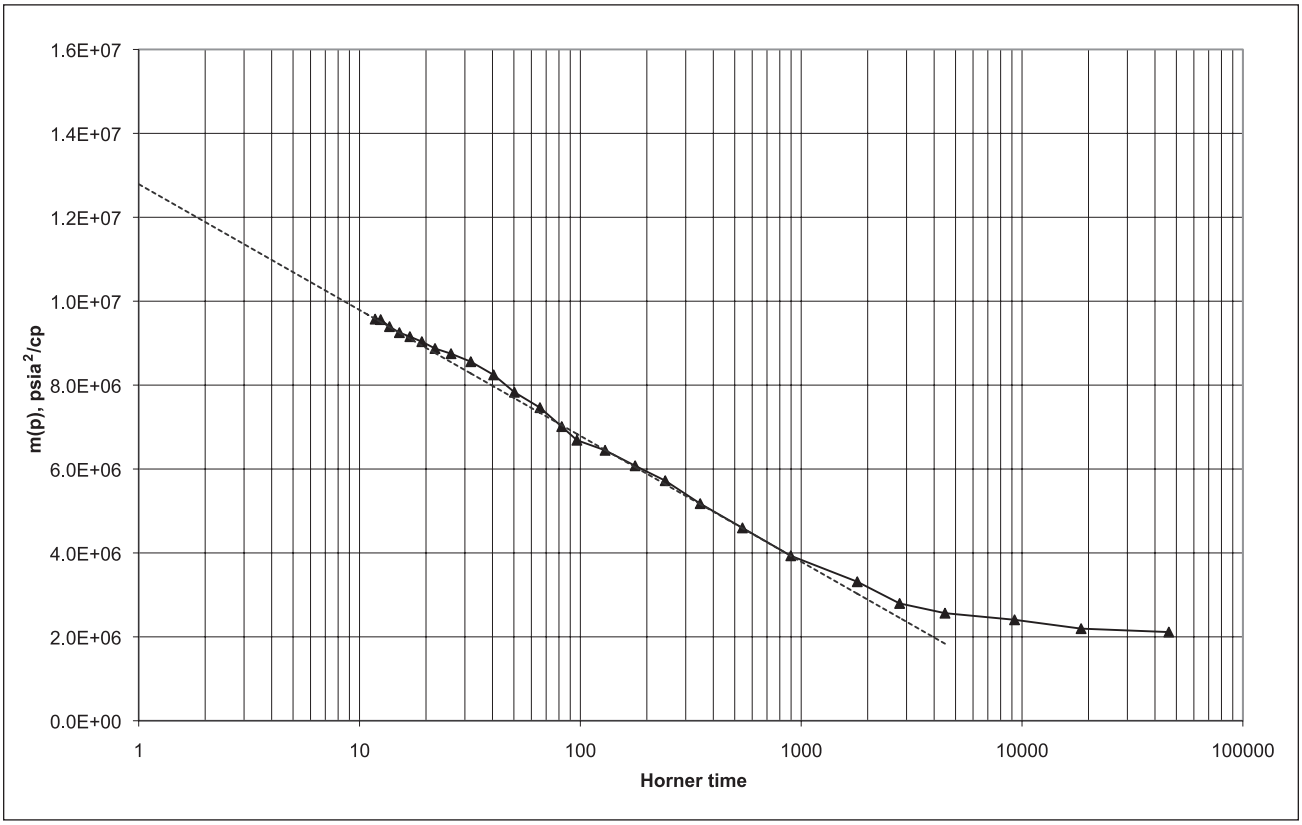



**Fig. 7–9.** Example 7.2 pressure buildup test—semilog plot

As seen in figure 7–9, the semilog, or Horner, plot of the test data exhibit straight-line behavior at late time. Slope of the semilog straight line is –2.9999E+6 psia$^2$/cp-cycle and $m(p^*)$ is 1.2790E+7 psia$^2$/cp. From equation (7.17),

$$k_g = \frac{1{,}637(117 \text{ mcfd})(460 + 110)°\text{R}}{2.9999\text{E} + 6 \text{ psia}^2/\text{cp} - \text{cycle}(40 \text{ ft})} = 0.91 \text{ md}$$

This effective permeability to gas is 6% higher than the 0.8 md reported by Vo et al., which was obtained from Horner semilog analysis and refined by history matching the test with a simulator.

Wellbore skin factor is calculated next. From the Horner semilog straight line, pseudopressure at 1 hr is 3.8906(10)$^6$ psia$^2$/cp. The skin factor calculated with equation (7.19) is

$$s = 1.1513\left[\frac{(3.8906 - 1.9993)\text{E} + 6 \text{ psia}^2/\text{cp}}{2.9999\text{E} + 6 \text{ psia}^2/\text{cp} - \text{cycle}} - \log\left(\frac{0.91 \text{ md}}{0.01(0.0119 \text{ cp})(3.1830\text{E} - 3 \text{ psia}^{-1})(0.31 \text{ ft})^2}\right) + 3.2275\right]$$

where gas compressibility has been used for total system compressibility. The resulting skin factor is

$$s = -4.1$$

Vo et al. reported a skin factor of –4.7 and obtained a fracture half-length of 95 ft from matching the test response with uniform-flux fracture type curves. From Earlougher, fracture half-length of a uniform-flux fracture can be estimated with[45]

$$x_f = r_w e^{-s}/0.37 \qquad \textbf{(7.28)}$$

Thus,

$$x_f = 0.31 \text{ ft } (e^{+4.1})/0.37 = 51 \text{ ft}$$

Repeating the calculation with the –4.7 skin factor reported by Vo et al. yields a fracture half-length of 92 ft. Thus, the difference in fracture half-lengths is attributed to small differences in the very negative skin factors.

Determination of average reservoir pressure begins with calculation of dimensionless producing time, equation (7.12)

$$t_{DA} = \frac{0.0002637\ (0.91 \text{ md})\ 924.9 \text{ hr}}{0.01(0.0119 \text{ cp})(3.1830\text{E} - 3 \text{ psia}^{-1})\ 320 \text{ ac}(43{,}560 \text{ ft}^2/\text{ac})}$$

$$t_{DA} = 4.2036(10)^{-2}$$

Using this in equation (7.13) yields a dimensionless MBH pressure, $p_{MBHD}$, of 0.528. Pseudopressure corresponding to average reservoir pressure, determined from equation (7.20) with this value of $p_{MBHD}$ and the slope and $m(p^*)$ values discussed above, is

$$m(\bar{p}) = 1.2102\text{E} + 7 \text{ psia}^2/\text{cp}$$

Interpolating from table 7–4 yields an average pressure,

$$\bar{p} = 372.1 \text{ psia}$$

This average reservoir pressure is 43 psia (13%) above the 328.8 psia value reported by Vo et al.

Repeating the analysis using the pressure-squared formulation, slope of the semilog straight line is –3.7662E+4 psia$^2$/cycle, and the intercept is 1.4656E+5 psia$^2$. Permeability calculated from equation (7.21) is 0.83 md. From the slope and intercept, pressure squared at 1 hr is 3.4833E+4 psia$^2$. Skin factor from equation (7.23) is –4.5, and the corresponding fracture half-length, from equation (7.28), is 72 ft. Average reservoir pressure, from equations (7.12), (7.13), and (7.24), is 371.2 psia.

Lastly, this test is analyzed with the pressure formulation. Slope of the semilog straight line –42.886 psia/cycle and the intercept, $p^*$, is 372.73 psia. Permeability calculated from equation (7.25) is 1.00 md. From the slope and intercept, pressure at 1 hr is 245.51 psia. Skin factor from equation (7.27) is –2.4, and the corresponding fracture half-length, from equation (7.28), is only 9 ft. Average reservoir pressure, from equations (7.12), (7.13), and (7.15), is 360.9 psia.

Permeabilities, skin factors, fracture half-lengths, and average reservoir pressures calculated with all three methods are compared with values published by Vo et al. in table 7–5. Both the real gas pseudopressure and pressure-squared formulations yield results sufficiently accurate for most reservoir engineering purposes. Clearly, the pressure formulation should not be used for analysis of this test. Superiority of the real gas pseudopressure analysis over the pressure formulation was noted by GRI for interpretation of a pressure buildup test of a Warrior Basin coal well, but no comparison was made with the pressure-squared method.[46]

**Table 7–5.** Example 7.2 pressure buildup test—summary of analyses

| Parameter | Real gas pseudopressure | Pressure squared | Pressure | Vo, et al. |
|---|---|---|---|---|
| Permeability to gas, md | 0.91 | 0.83 | 1.00 | 0.86 |
| Skin factor | –4.1 | –4.5 | –2.4 | –4.7 |
| Fracture half length, ft | 49 | 72 | 9 | 95 |
| Average pressure, psia | 372.1 | 370.8 | 360.9 | 328.8 |

## Sorption Compressibility

Sorption of gas on coal (or shale) results in a highly compressible reservoir/fluid system. Total system compressibility for a coal reservoir is given by[47]

$$c_t = c_f + S_w c_w + S_g c_g + c_s \tag{7.29}$$

where

$c_f$ = formation compressibility, also called *cleat volume compressibility*, in psia$^{-1}$,
$S_w$ = water saturation, fraction,
$S_g$ = gas saturation, fraction,
$c_s$ = sorption compressibility, psia$^{-1}$, and is defined as[48]

$$c_s = \frac{B_g \rho_c V_{Ldaf} (1 - a - w) p_L}{5{,}706 (p_L + p)^2 \phi} \tag{7.30}$$

where

$B_g$ = gas formation volume factor, rb/mcf,
$\rho_c$ = coal bulk density, g/cm$^3$,
$V_{Ldaf}$ = the dry, ash-free Langmuir volume constant, scf/ton,
$a$ = ash, fraction,
$w$ = equilibrium moisture, fraction, and
$p_L$ = the Langmuir pressure constant, psia.

Example calculations using coal properties from the Illinois and Powder River basins will demonstrate that sorption compressibility can be either greater or less than methane compressibility. As a result, making generalizations is difficult, and it is necessary to calculate gas, sorption, and total system compressibilities for practical coal well test interpretation. In-situ Langmuir volume and pressure constants for an Illinois Basin high-volatile B bituminous coal, computed from laboratory sorption data reported by Joubert et al., were 541.6 scf/ton and 1,293.3 psia, respectively.[49] Neglecting formation and water compressibilities and assuming a porosity of 1%, a gas saturation of 100%, and a bulk density of 1.65 g/cm$^3$, sorption, gas, and total compressibilities are plotted in figure 7–10 as functions of pressure. As seen in the figure, sorption compressibility behaves quite similarly to gas compressibility but is roughly an order of magnitude larger. Consequently, total compressibility in this instance is only slightly larger than sorption compressibility for the coal.

Composite sorption isotherms for Powder River Basin coals were published by Crockett and Meyer.[50] Approximately two dozen laboratory isotherms measured on coals from this basin were combined to yield an average in-situ isotherm as well as high and low in-situ isotherms, which differed from the average by one standard deviation. Langmuir constants for the average in-situ isotherm, 218.4 scf/ton and 1,355.3 psia, were used with a bulk density of 1.3 g/cm$^3$ and a porosity of 10% to calculate the gas, sorption, and total compressibilities shown in figure 7–11. Again, both the gas and sorption compressibility curves exhibit similar shapes. At low pressures, gas and sorption compressibilities are nearly equal. As pressure increases, gas compressibility is increasingly larger than sorption compressibility, until at 1,000 psia, it is nearly four times larger.

As a component of total system compressibility, sorption compressibility does not enter into permeability calculations [equations (7.17), (7.21), and (7.25)] in well test analysis. However, it does influence wellbore skin factors [equations (7.18), (7.22) and (7.26)], radius of investigation [equation (7.6)], and distance to a fault or other flow boundary. Type curve matches employing dimensionless times incorporate sorption compressibility through equation (7.29). Popular time transforms, such as Agarwal real gas pseudotime, require system compressibility, and therefore, use of such time transforms in well test analysis requires sorption compressibilities.[51]

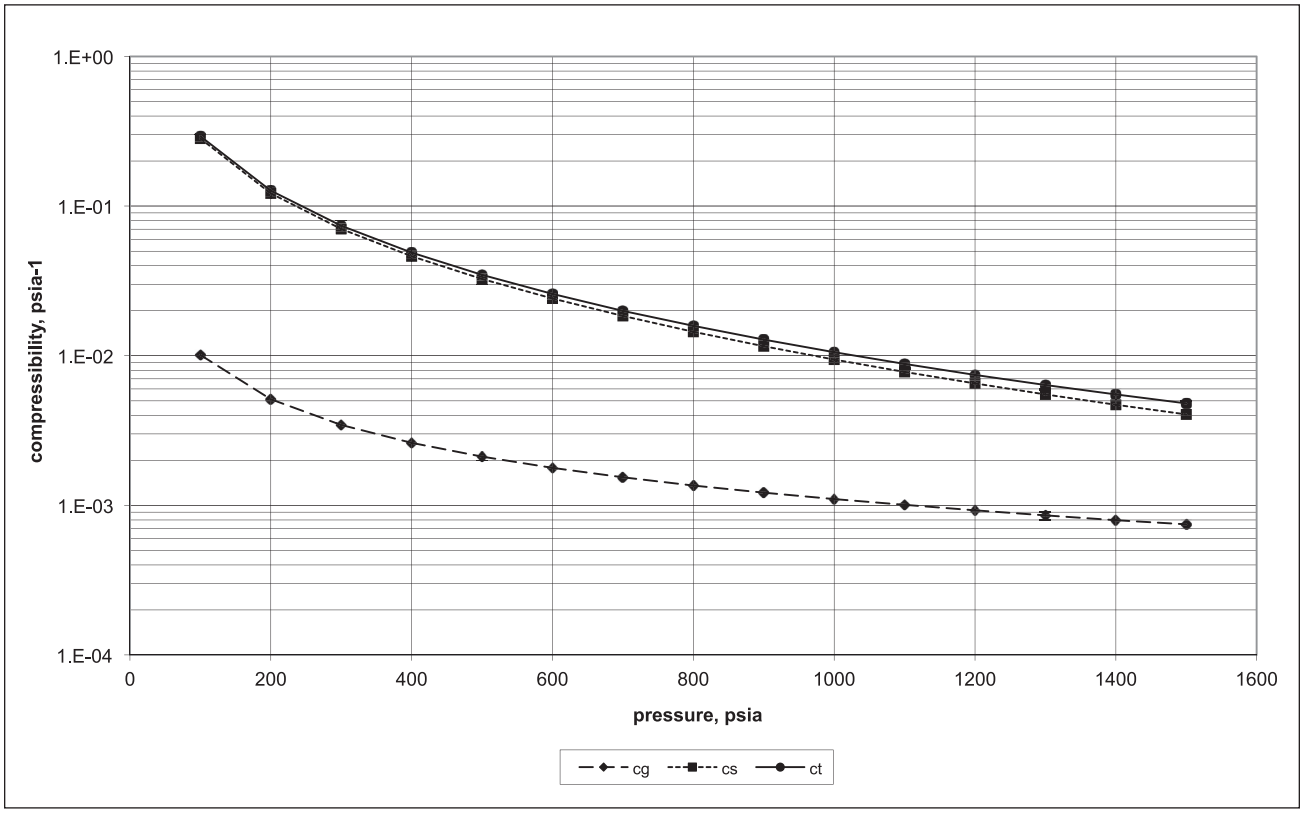



**Fig. 7–10.** Gas and sorption compressibilities—Illinois Basin coal[52]

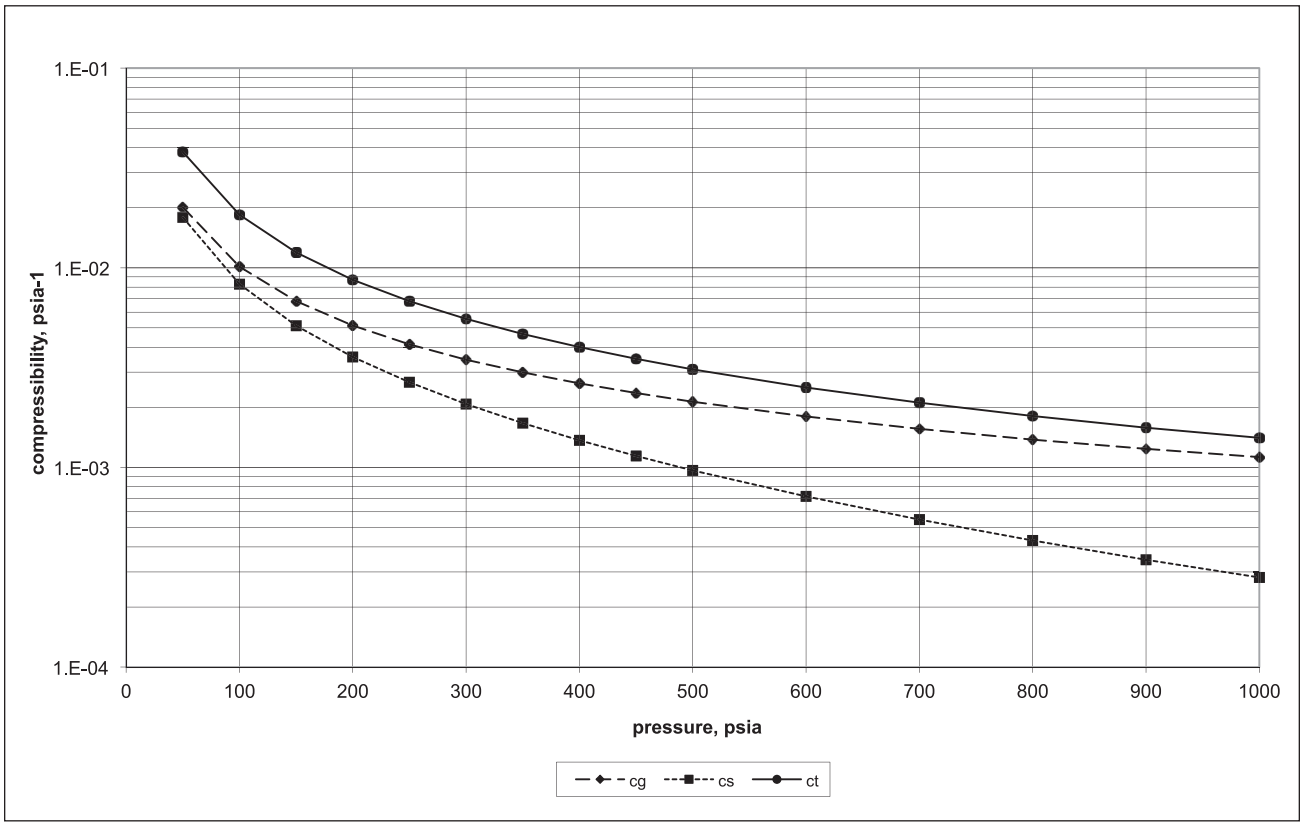



**Fig. 7–11.** Gas and sorption compressibilities—Powder River Basin coal[53]

Sorption compressibility affects only the wellbore completion portion of coal well test interpretation. Inclusion of sorption compressibility in the analysis typically changes the skin factor by one unit. When an isotherm is not available, a practical correction to a coal well skin factor calculated from conventional compressibility is to simply add one. For example, no isotherm was reported for the pressure buildup test from the Rincon Unit of the San Juan Basin discussed above in example 7.2. Thus, an approximate correction for sorption compressibility is a skin factor change from –4.1 to –3.1. Fracture half-length, calculated from equation (7.28), drops from 51 to 18 ft. If wellbore completion is a primary goal of the test, an accurate sorption isotherm should be used in the analysis.

## Two-Phase Pseudopressures

The drawdown and buildup test analysis methods described above determine effective permeability to gas or water but not absolute permeability of the coal deposit. For wells completed either in water-saturated coals or dry coals, effective permeability from a drawdown or buildup test is often sufficiently close to absolute formation permeability for many reservoir engineering calculations. In other cases, however, where a well makes substantial volumes of both gas and water, effective permeabilities to both phases can be significantly lower than the absolute permeability.

A method to overcome this limitation and also determine wellbore skin and reservoir pressure was proposed by Kamal and Six.[54] Two critical assumptions in development of this method were the following:

1. Gas is rapidly desorbed from the matrix into the cleats compared to gas flow in the cleats.
2. The fluids are in equilibrium and travel together from their initial location through the reservoir to the wellbore.

This second assumption, analogous to steady-state flow in gas condensate reservoirs, is expressed mathematically as

$$\frac{q_w}{q_g} = \frac{v_w}{v_g} \tag{7.31}$$

where $v_w$, the water volume, is related to coal volume, $v_c$, by

$$v_w = \phi v_c$$

and $v_g$, the gas volume, is given by

$$v_g = 8.8239(10)^{-4}\, v_c \rho_c (V_i - V)\frac{ZT}{p}$$

where

$V_i$ = initial gas content, scf/ton.

Rewriting equation (7.31) to link relative permeabilities and gas and water volumes,

$$\frac{k_{rw}}{k_{rg}} = \frac{v_w}{v_g}\,\frac{\mu_w}{\mu_g}$$

allowed Kamal and Six to define a two-phase coal degasification pseudopressure as

$$m_{cd}(p) = 2\int \left( \frac{k_{rg}}{\mu_g Z} + \frac{k_{rw}}{\mu_w Z_w} \right) p\,dp$$

Kamal and Six presented a detailed eight-step procedure for calculating the coal degasification pseudopressure. Note that this requires both gas-water relative permeability curves and an in-situ sorption isotherm. Pressure transient tests are frequently performed in coal wells where neither of these is known, limiting utility of the method. Kamal and Six validated their method against numerical simulations and presented field examples from San Juan Basin coal wells.

In addition to conventional, single-phase analyses of San Juan coal well tests discussed above, Vo et al. used the Kamal and Six pseudopressure to determine absolute formation permeability.[55] Absolute permeabilities were about an order of magnitude larger than effective permeabilities to gas, but no other absolute permeability estimates were available for comparison.

Jochen et al. tested the equilibrium assumption of Kamal and Six, equation (7.31), through simulations and found that it is not generally valid in coals.[56] Consequently, two-phase pseudopressure methods for analysis of coal well pressure transient tests have largely fallen out of use at the time of this writing.

## Why Dual Porosity Behavior Is Not Apparent in Coal Well Tests

Coal deposits are often regarded as naturally fractured reservoirs containing both gas and water. Therefore, well tests in coals would be expected to exhibit the dual porosity behavior seen in other naturally fractured reservoirs. First, consider water production from coals. Most of the moveable water in a coal resides in the cleats, with little, if any, transfer between matrix and cleats. Coal is a single porosity reservoir to water. Pressure transient tests of coal wells producing only water, or at low gas-water ratios, would intuitively respond as single porosity reservoirs. The injection/falloff test discussed in example 7.1 above showed no evidence of dual porosity behavior. In contrast, gas is present in both the matrix and the fractures of a coal. Coal matrix is essentially impermeable; consequently, all fluid flow in a coal deposit is through the cleats.[57] Most of the gas is sorbed on the low-permeability matrix, while most of the flow capacity is provided by the low-porosity cleats. Consequently, coal is a dual porosity reservoir to gas, and transient tests of wells draining gas from coals might be expected to reflect this.

Mathematics of the pressure response of a naturally fractured reservoir due to fluid withdrawal was first developed by Warren and Root.[58] Two dimensionless parameters were used to characterize the reservoir. The interporosity flow parameter, $\lambda$, is defined as

$$\lambda = \alpha r_w^2 \frac{k_m}{k_f} \tag{7.32}$$

where

$k_m$ = matrix permeability, md,
$k_f$ = fracture permeability, md, and
$\alpha$ = the block shape parameter, $ft^{-2}$, given by

$$\alpha = \frac{4n(n+2)}{l^2} \tag{7.33}$$

where

$n$ = the number of normal sets of planes defining the matrix ($n = 1$ for a multilayered reservoir, $n = 2$ for a coal with well-developed face and butt cleats, and $n = 3$ for a well-cleated coal with bedding plane fractures), and
$l$ = the characteristic matrix dimension, ft.

A typical matrix dimension of well-cleated coal is 1 cm (0.033 ft) or less, thus

$$\alpha = \frac{4(2)(2+2)}{0.033^2\ \text{ft}^2} = 29{,}385\ \text{ft}^{-2}$$

Assuming the well is completed with 5½ in. casing in a coal with matrix and cleat permeabilities of 0.010 and 5 md, respectively,

$$\lambda = 29{,}385\ \text{ft}^{-2}\ 0.208^2\ \text{ft}^2\ \frac{0.010\ \text{md}}{5\ \text{md}} = 2.5$$

Storativity, $\omega$, is defined as

$$\omega = \frac{\phi_f c_{tf}}{\phi_{m+f} c_{t(m+f)}}$$

Porosity in coals is distinctly different than the ideal fracture and matrix porosities assumed by Warren and Root. Fracture porosities in bituminous coals are approximately 1%, and total porosities, determined by helium or mercury injection, are typically on the order of 7%. Fracture and matrix compressibilities of a coal, different from the idealized compressibilities of Warren and Root, are essentially equal. Thus,

$$\omega = \frac{0.01}{0.07} = 0.143$$

Warren and Root discovered that the semilog plot of a drawdown or buildup test from a well completed in a naturally fractured reservoir exhibited two parallel straight lines. The first straight line is controlled by the fractures, the second by the total system. Transition time from the first to the second line depends on the interporosity flow coefficient, while separation of the two lines is a function of the storativity. Gringarten provided a survey of developments in pressure transient methods for dual porosity reservoirs in the two decades following the seminal work by Warren and Root.[59] Time to full system response, $t_2$, in a drawdown test is determined from

$$t_2 = \frac{(\phi c_t)_{m+f}\ \mu_g r_w^2}{4.6968(10)^{-4}\ k_f \lambda}$$

Substitution of (7.32) and (7.33) into the above equation and simplifying yields

$$t_2 = \frac{(\phi c_t)_{m+f}\ \mu_g l^2}{1.879(10)^{-3}\ n(n+2)k_m} \tag{7.34}$$

where

$l$ = cleat spacing, cm.

Gringarten also provided an equation for time to full system response in a buildup test. The time variable is equivalent time, which for small shut-in times is approximately equal to shut-in time, and equation (7.34) can also be applied to coal well buildup tests.

Two example calculations will illustrate the very short time to full system response typical of a coal well test. As coal matrix is essentially impermeable and no reliable measurements have been reported, these two examples assume a value of 0.010 md. Bustin and Clarkson report porosity of Powder River Basin coals is on the order of 12%.[60] Assuming the coals are fully saturated with methane gas at 65°F and 200 psia, system compressibility, equation (7.29), is approximately given by

$$c_t = S_g c_g + c_s = 1.0 \times 5.134(10)^{-3}\ \text{psia}^{-1} + 3.579(10)^{-3}\ \text{psia}^{-1} = 8.713(10)^{-3}\ \text{psia}^{-1}$$

where the sorption compressibility, $c_s$, has been taken from above. The coal was assumed to be well cleated, thus $n = 2$, with an arbitrary cleat spacing of 1 cm (0.0328 ft). From equation (7.34), the time to total system response is

$$t_2 = \frac{(0.12)8.713(10)^{-3}\ \text{psia}^{-1}\ 0.0113\ \text{cp}\ 0.0328^2\ \text{ft}^2}{1.879(10)^{-3}\ (2)(2+2)0.010\ \text{md}} = 8.456(10)^{-5}\ \text{hr} = 0.3\ \text{sec}$$

For a second example, response time of the matrix and fracture system of an Illinois Basin coal saturated with methane gas at 86°F and 800 psia is calculated. Porosity was assumed to be 1%, typical of high-volatile A bituminous coals. System compressibility, from above, is

$$c_t = S_g c_g + c_s = 1.0 \times 1.359(10)^{-3}\ \text{psia}^{-1} + 1.446(10)^{-2}\ \text{psia}^{-1} = 1.582(10)^{-2}\ \text{psia}^{-1}$$

Assuming a well-cleated coal with 1 cm (0.0328 ft) fracture spacing, time to total system response is

$$t_2 = \frac{(0.01)1.582(10)^{-2}\ \text{psia}^{-1}\ 0.0127\ \text{cp}\ 0.0328^2\ \text{ft}^2}{1.879(10)^{-3}\ (2)(2+2)0.010\ \text{md}} = 1.438(10)^{-5}\ \text{hr} = 0.05\ \text{sec}$$

Note that these times may be upper bounds, as many coals have cleat spacings much less than 1 cm. In spite of a large system compressibility (due to low-pressure, low-temperature methane and sorption compressibility) and tight matrix, the small fracture spacing of coal deposits implies that dual porosity behavior will probably not be seen in any coal well pressure transient tests.

## Interference Tests

Interference tests have long been used in conventional oil and gas reservoirs to determine interwell properties. They require at least one active well and one observation well and typically investigate a larger reservoir volume than a single well test. Rate variation of the active well produces pressure perturbations that are monitored at one or more observation wells, with the objectives of determining permeability and the porosity-compressibility product. The theory of interference testing in homogeneous reservoirs was treated by Earlougher, and several analysis techniques and examples were presented.[61] A brief theory of interference testing in such reservoirs was also presented by Lee.[62] Kazemi et al. developed the mathematical foundations of interference testing in naturally fractured reservoirs assuming a uniform fracture distribution.[63] These authors report that methods developed for homogeneous reservoirs were inadequate to describe early-time behavior of interference tests in naturally fractured reservoirs. However, they worked well for interpretation of late-time responses, especially for large well spacings and interporosity flow parameters larger than $10^{-6}$. A typical interporosity flow parameter for coal, as calculated previously, is several orders of magnitude larger than this value, implying that interference tests in coals can be analyzed using homogeneous reservoir methods.

The Pratt A and B coals of the Warrior Basin behaved as a homogeneous reservoir in a two-step interference test reported by Koenig and Stubbs.[64] Water was injected into a central well and pressure monitored at three observation wells located 100 to 200 ft distant. The first portion of the test utilized straddle packers to isolate the Pratt A seam, and water was injected at a rate of 1.4 bpd for 8 days. Type curve matching of observation well pressure responses yielded nearly equal permeabilities in all three wells, with an average permeability of 59 md. Test data were interpreted as indicating permeability anisotropy ranging from 1:3 to 1:17, with the major permeability axis aligned with the face cleat direction. As the area was believed to be free of faults and joints, the permeability anisotropy was attributed to the coal fabric. The second portion of the test involved injection into both the A and B seams of the active well at a rate of 4.5 bpd for 19 days. Type curve matches of data from this portion of the test yielded permeabilities of 27, 74, and 84 md at the observation wells. Lack of permeability anisotropy in the dual zone interference test was ascribed to reservoir heterogeneities, including variation in net

coal thickness. Values of the porosity-compressibility product varied from 15 to $190(10)^{-6}$ psia–1 and averaged $60(10)^{-6}$ $psia^{-1}$. Test interpretation was complicated by noisy data, inaccuracies inherent in type curve matching, and the lack of a computer simulation of the test.

Because of the complexities inherent in interference tests, interpretation of these tests is easier, and the results more credible, when only a single phase is present in the coal deposit. In practice, coal interference tests are easier to interpret when water is injected into a water-saturated coal prior to any production or by shutting in a producing well after the coal has been dewatered and the wells can be considered as gas wells.

## Micropilot Injectivity Tests

A test to assess the viability of enhanced coalbed methane recovery in coal deposits was discussed by Puri et al.[65] This test is also useful for determining suitability of a coal for $CO_2$ sequestration. A micropilot test is comprised of three stages, all of approximately three weeks' duration. Actual test time will, of course, depend on permeability of the target coal as well as aboveground considerations, such as nitrogen supply and test cost. In the first stage of a micropilot test, either nitrogen or air is injected into the subject coal. Recommended data acquisition during this first stage includes wellhead pressures and temperatures, injected gas volumes, and downhole pressures and temperatures.

After the injection period, the well is shut in to allow injected gases to soak into the coal, possibly displacing some native methane, and pressures to equilibrate. Wellhead and downhole pressures are recorded during the shut-in.

In the third and final stage of a micropilot test, the well is put on production. Gas and water production rates are recorded, along with wellhead and downhole pressures and temperatures. In addition, multiple, even daily, gas samples are taken for analysis.

History matching all three phases of a micropilot test with a computer simulator calibrates the model, enabling its use as a planning tool for full-field enhanced recovery or $CO_2$ sequestration projects.

Puri et al. discussed interpretation of a micropilot injectivity test in a San Juan Basin coal well. Located in the New Mexico portion of the basin, the well was completed in two seams with a net coal thickness of 55 ft and had produced 63.9 mmcf and no reported water at the time of testing. The well was shut in for approximately three weeks to configure the well for micropilot test and to allow the reservoir to equilibrate. The first stage of the micropilot test began with air injection at a rate of 800 mcfd. After five days, the rate was increased to 1.4 mmcfd for 17 days. Cumulative injected air volume was 27.6 mmcf, approximately 43% of the pretest cumulative production. Pressure falloff was monitored during the 30-day shut-in comprising the second stage of the test. Analysis of this data yielded a reservoir permeability of 0.37 md and a fracture half-length of 95 ft. The well was then returned to production and wellhead pressure and gas composition measured for three months.

The micropilot test was simulated assuming a single-layer reservoir and infinitely fast adsorption and desorption of gas off the coal matrix. Model gas rate was specified and bottomhole pressure and flowback gas composition matched. A reasonable match of bottomhole pressure was obtained by incorporating a pressure-dependent permeability, which was also thought to reflect relative permeability effects in addition to stress effects, even though this well produced minimal water. When use of published stress-permeability relations in the simulation failed to match well performance, the pressure-permeability curve was treated as a history match parameter. The resulting permeability ratio varied from 0.55 to 0.35 with significant hysteresis. Flowback gas composition in the model was qualitatively correct, but the nitrogen fraction was overpredicted. Because of the infinitely fast sorption in the simulator, predicted initial nitrogen fraction was 100%, while actual nitrogen concentration was 70%. This difference of approximately 30% in nitrogen cut was observed throughout the flowback period, illustrating the necessity of incorporating sorption kinetics into simulation of micropilot tests.

Puri et al. noted that analysis of the produced gas stream aids in understanding the type of formation in which the well is completed. As coal is a known oxygen scavenger, a flowback gas composition devoid of oxygen indicates the well is completed in a coal, whereas if injection is into a sandstone, flowback gas composition will be close to atmospheric.

# Nomenclature

| | |
|---|---|
| $a$ | Ash fraction |
| $A$ | Area, ac |
| $B_g$ | Gas formation volume factor, rb/mcf |
| $\overline{B}_g$ | Gas formation volume factor, rb/mcf |
| $B_w$ | Water formation volume factor, rb/stb |
| $C$ | Wellbore storage coefficient, bbl/psia |
| $C_A$ | Well drainage shape factor, dimensionless |
| $c_f$ | Cleat volume compressibility, psia$^{-1}$ |
| $c_g$ | Gas compressibility, psia$^{-1}$ |
| $c_s$ | Sorption compressibility, psia$^{-1}$ |
| $c_t$ | Total compressibility, psia$^{-1}$ |
| $\overline{c}_t$ | Average total compressibility, psia$^{-1}$ |
| $c_{tf}$ | Total compressibility of the fracture and the fluids it contains |
| $C_{t(m+f)}$ | Total compressibility of the entire system, matrix plus fracture, and the fluids they contain |
| $c_w$ | Water compressibility, psia$^{-1}$ |
| $h$ | Net coal thickness, ft |
| $k$ | Permeability, md |
| $k_f$ | Facture permeability, md |
| $k_g$ | Effective permeability to gas, md |
| $k_m$ | Matrix permeability, md |
| $k_r$ | Relative permeability, fraction |
| $k_w$ | Effective permeability to water, md |
| $l$ | Cleat spacing, ft |
| $m$ | Semilog straight-line slope, psia/cycle, psia$^2$/cycle, or psia$^2$/cp-cycle |
| $m_{cd}(p)$ | Kamal and Six two-phase pseudopressure, psia$^2$/cp |
| $m(p)$ | Real gas pseudopressure, psia$^2$/cp |
| $m(\overline{p})$ | Real gas pseudopressure of average reservoir pressure, psia$^2$/cp-cycle |
| $n$ | Number of normal sets of planes defining the matrix |
| $p$ | Pressure, psia |
| $\overline{p}$ | Average reservoir pressure, psia |
| $p^\star$ | False pressure, psia |
| $p_{1hr}$ | Extrapolated pressure at 1 hr, psia |
| $p_i$ | Initial reservoir pressure, psia |
| $p_L$ | Langmuir pressure constant, psia |
| $p_{MBHD}$ | Dimensionless Matthews-Brons-Hazebroek pressure function |
| $p_{wsi}$ | Bottomhole pressure at shut-in, psia |
| $q_g$ | Gas flow rate, mcfd |
| $q_w$ | Water injection or production rate, bpd |
| $r_c$ | Radius of tubing or casing in which fluid level is rising or falling in a slug test, ft |
| $r_i$ | Radius of investigation, ft |
| $r_w$ | Wellbore radius, ft |
| $s$ | Skin factor |
| $S_g$ | Gas saturation, fraction |
| $S_w$ | Water saturation, fraction |
| $t$ | Time, hr |
| $T$ | Temperature, °R |
| $t_2$ | Time to full system response in well test in dual porosity reservoir, hr |
| $t_{bsl}$ | Time to beginning of semilog straight line, hr |

| | |
|---|---|
| $t_{DA}$ | Dimensionless time based on area |
| $t_H$ | Horner time |
| $t_i$ | Injection time, hr |
| $t_p$ | Production or flow time, hr |
| $t_{st}$ | Slug test duration, hr |
| $\Delta t$ | Time since well was shut-in, hr |
| $\Delta t_e$ | Equivalent time, hr |
| $V$ | Gas content, scf/ton |
| $v_c$ | Coal volume, $ft^3$ |
| $v_g$ | Gas volume, $ft^3$ |
| $V_i$ | Initial gas content, scf/ton |
| $V_{Ldaf}$ | Dry, ash-free Langmuir volume constant, scf/ton |
| $v_w$ | Water volume, $ft^3$ |
| $w$ | Equilibrium moisture, fraction |
| $xf$ | Fracture half-length, ft |
| $Z$ | Gas deviation factor |
| $\overline{Z}$ | Average gas deviation factor |
| $Z_w$ | Water compressibility factor, equation (7.31) |

### Greek

| | |
|---|---|
| $\alpha$ | Block shape factor, $ft^{-2}$ |
| $\lambda$ | Interporosity flow parameter |
| $\mu_g$ | Gas viscosity, cp |
| $\overline{\mu}_g$ | Average gas viscosity, cp |
| $u_w$ | Water viscosity, cp |
| $\rho_c$ | Coal bulk density, $g/cm^3$ |
| $\varphi$ | Porosity, fraction |
| $\varphi_f$ | Fracture porosity, fraction |
| $\varphi_m$ | Matrix porosity, fraction |
| $\omega$ | Storativity |

# References


1. Zuber, M. D., Sparks, D. P., and Lee, W. J. 1990. *Design and Interpretation of Injection/Falloff Tests for Coalbed Methane Wells*. Paper SPE 20569. Presented at the 65th Annual Technical Conference and Exhibition of the Society of Petroleum Engineers, New Orleans, Louisiana, September 23–26.
2. Earlougher, R. C., Jr. 1977. *Advances in Well Test Analysis*. SPE Monograph 5. Richardson, Texas: Society of Petroleum Engineers.
3. Seidle, J. P., Kutas, G. M., and Krase, L. D. 1991. *Pressure Falloff Tests of New Coal Wells*. Paper SPE 21809. Presented at the SPE Rocky Mountain Regional Meeting and Low Permeability Reservoirs Symposium, Denver, Colorado, April 15–17.
4. Agarwal, R. G. 1980. *A New Method to Account for Producing Time Effects When Drawdown Type Curves Are Used to Analyze Pressure Buildup and Other Test Data*. Paper SPE 9289. Presented at the Annual Technical Conference and Exhibition, Dallas, Texas, September 21–24.
5. Earlougher, R. C., Jr. 1977.
6. Ibid.
7. Zuber, M. D., et al. 1990; and Seidle, J. P., et al. 1991.
8. Earlougher, R. C., Jr. 1977.
9. Seidle, J. P., et al. 1991.
10. Bourdet, D., Ayoub, J. A., and Pirard, Y. M. 1984. *Use of Pressure Derivative in Well Test Interpretation*. Paper SPE 12777. Presented at the California Regional Meeting, Long Beach, California, April 11–13.
11. Seidle, J. P., et al. 1991.
12. Earlougher, R. C., Jr. 1977.
13. Gas Research Institute. 1996. *A Guide to Coalbed Methane Reservoir Engineering*. GRI-94/0397. Chicago: Gas Research Institute.
14. Earlougher, R. C., Jr. 1977.
15. Gas Research Institute. 1996.
16. Ibid.
17. Ibid.
18. Van Everdingen, A. F., and Hurst, W. 1949. The application of the Laplace transformation to flow problems in reservoirs. *Transactions*. AIME. V. 186. p. 305.
19. Ramey, H. J., Jr., Agarwal, R. G., and Martin, I. 1975. Analysis of 'slug test' or DST flow period data. *Journal of Canadian Petroleum Technology*. July–September. p. 37.
20. Koenig, R. A., and Schraufnagel, R. A. 1987. Application of the slug test in coalbed methane testing. Paper 8743 in *Proceedings of the 1987 International Coalbed Methane Symposium*. Tuscaloosa: University of Alabama; and Gas Research Institute. 1996.
21. Conway, M. W., Mavor, M .J., Saulsberry, J., Barree, R. B., and Schraufnagel, R. A. 1995. *Multi-Phase Flow Properties for Coalbed Methane Wells: A Laboratory and Field Study*. Paper SPE 29576. Presented at the Joint Rocky Mountain Regional Meeting and Low-Permeability Reservoirs Symposium, Denver, Colorado, March 20–22.
22. Ramey, H. J., Jr., et al. 1975.
23. Mayerhofer, M. J., Ehlig-Economides, C. A., and Economides, M. J. 1995. Pressure-transient analysis of fracture-calibration tests. *Journal of Petroleum Technology*. V. 47 (no. 3). p. 229; and Valko, P. P., and Economides, M. J. 1999. Fluid-leakoff delineation in high permeability fracturing. *Society of Petroleum Engineers Production and Facilities*. V. 14 (no. 2). p. 110.
24. Ramurthy, M., Marjerrison, D. M., and Daves, S. B. 2002. *Diagnostic Fracture Injection Tests in Coals to Determine Pore Pressure and Permeability*. Paper SPE 75701. Presented at the SPE Gas Technology Symposium, Calgary, Alberta, April 30–May 2.
25. Barree, R. D., and Mukherjee, H. 1996. *Determination of Pressure-dependent Leakoff and Its Effects on Fracture Geometry*. Paper SPE 36424. Presented at the SPE Annual Technical Conference and Exhibition, Denver, Colorado, October 6–9.
26. Ramurthy, M., et al. 2002.
27. Ibid.
28. Ibid.
29. Jochen, J. E., Hopkins, C. W., and Frantz, J. H., Jr. 1993. *Quantifying Layered Reservoir Properties with a Novel Permeability Test*. Paper SPE 25864. Presented at the SPE Rocky Mountain Regional/Low Permeability Reservoirs Symposium, Denver, Colorado, April 12–14.
30. Ramey, H. J., Jr. 1975.
31. Lee, J. and Wattenbarger, R. A. 1996. *Gas Reservoir Engineering*. Richardson, Texas: Society of Petroleum Engineers.
32. Ibid.
33. Earlougher, R. C., Jr. 1977.
34. Reynolds, A. C., Bratvold, R. B., and Ding, W. 1987. Semilog analysis of gas well drawdown and buildup data. *Society of Petroleum Engineers Formation Evaluation*. V. 2 (no. 4). p. 657.
35. Earlougher, R. C., Jr. 1977.
36. Bayles, G. A. and Reznik, A. A. 1986. *Pressure Transient Analysis of Methane Production from Coal Beds: An Analytical Approach*. Paper SPE 15226. Presented at the SPE Unconventional Gas Technology Symposium, Louisville, Kentucky, May 18–21.
37. Bumb, A. C., and McKee, C. R. 1986. *Gas-Well Testing in the Presence of Desorption for Coalbed Methane and Devonian Shale*. Paper SPE 15227. Presented at the SPE Unconventional Gas Technology Symposium, Louisville, Kentucky, May 18–21.
38. Ertekin, T., and Sung, W. 1989. *Pressure Transient Analysis of Coal Seams in the Presence of Multi-Mechanistic Flow and Sorption Phenomena*. Paper SPE 19102. Presented at the SPE Gas Technology Symposium, Dallas, Texas, June 7–9.
39. Gas Research Institute. 1996.

40. Lee, J., and Wattenbarger, R. A. 1996.
41. Ibid.
42. Ibid.
43. Vo, D. T., Ohaeri, C. U., and Montoya, G. L. 1991. *Pressure Buildup Analysis of Early-Time Data from Coalbed Methane Wells in the Rincon Unit, San Juan Basin, New Mexico*. Paper SPE 22684. Presented at the Annual Technical Conference and Exhibition, Dallas, Texas, October 6–9.
44. Bourdet, D., et al. 1984.
45. Earlougher, R. C., Jr. 1977.
46. Gas Research Institute. 1996.
47. Bourdet, D., et al. 1984.
48. Ibid.
49. Joubert, J. I., Grein, C. T., and Beinstock, D. 1974. Effect of moisture on the methane capacity of American coals. *Fuel*. V. 53 (no. 3). p. 186.
50. Crockett, F., and Meyer, J. 2001. *Update and Revision of Interim Drainage Report on Coalbed Methane Development and Drainage of Federal Land in the South Gillette Area, Campbell and Converse Counties, Wyoming T. 40–50 N, R 70–75 W*. February 12. Casper: Wyoming Bureau of Land Management.
51. Agarwal, R. G. 1979. *Real Gas Pseudo-Time—A New Function for Pressure Buildup Analysis of Gas Wells*. Paper SPE 8279. Presented at the SPE Annual Technical Conference and Exhibition, Las Vegas, Nevada, September 23–26.
52. Joubert, J. I., Grein, C. T., and Beinstock, D. 1974.
53. Crockett, F., and Meyer, J. 2001.
54. Kamal, M. M., and Six, J. L. 1989. *Pressure Transient Testing of Methane Producing Coalbeds*. Paper SPE 19789. Presented at the SPE Annual Technical Conference and Exhibition, San Antonio, October 8–11.
55. Vo, D. T., et al. 1991.
56. Jochen, V. A., Lee, W. J., and Semmelbeck, M. E. 1994. *Determining Permeability in Coalbed Methane Reservoirs*. Paper SPE 28584. Presented at the Annual Technical Conference and Exhibition, New Orleans, Louisiana, September 25–28.
57. Paterson, L. I. 1990. Laboratory measurement of coal permeability. In *Methane Drainage from Coal*. Peterson, L. I., ed. Syndal, Victoria: CSIRO Division of Geomechanics. p. 33; Puri, R., King, G. E., and Palmer, I. D. 1991. *Damage to Coal Permeability during Hydraulic Fracturing*. Paper SPE 21813. Presented at the Rocky Mountain Regional Meeting and Low-Permeability Reservoirs Symposium, Denver, Colorado, April 15–17; and Cui, X., and Bustin, R. M. 2005. Volumetric strain associated with methane desorption and its impact on coalbed gas production from deep coals seams. *AAPG Bulletin*. V. 89 (no. 9). p. 1,181.
58. Warren, J. E., and Root, P. J. 1963. The behavior of naturally fractured reservoirs. *Society of Petroleum Engineers Journal*. V. 3 (no. 3). p. 245.
59. Gringarten, A. C. 1984. Interpretation of tests in fissured and multilayered reservoirs with double-porosity behavior: Theory and practice. *Journal of Petroleum Technology*. V. 36 (no. 4). p. 549.
60. Bustin, R. M., and Clarkson, C. R. 1999. Free gas storage in matrix porosity: A potentially significant coalbed resource in low rank coals. Paper 9956 in *Proceedings of the 1999 International Coalbed Methane Symposium*. Tuscaloosa: University of Alabama.
61. Earlougher, R. C., Jr. 1977.
62. Lee, J. 1982. *Well Testing*. SPE Textbook Series No. 1. Richardson, Texas: Society of Petroleum Engineers.
63. Kazemi, H., Seth, M. S, and Thomas, G. W. 1969. The interpretation of interference tests in naturally fractured reservoirs with uniform fracture distribution. *Society of Petroleum Engineers Journal*. V. 9 (no. 4). p. 463.
64. Koenig, R. A., and Stubbs, P. B. 1986. *Interference Testing of a Coalbed Methane Reservoir*. Paper SPE 15225. Presented at the SPE Unconventional Gas Technology Symposium, Louisville, Kentucky, May 18–21.
65. Puri, R., Volz, R., and Duhrkopf, D. 1995. A micro-pilot approach to coalbed methane reservoir assessment. Paper 9556 in *Proceedings of the 1995 International Coalbed Methane Symposium*. Tuscaloosa: University of Alabama.

# Gas and Water Mass Balances in Coals

# 8

## Coal Gas Mass Balance Equation

Mass balance equations have historically been used by the petroleum industry to estimate original hydrocarbons in place, original reservoir pressure, expected ultimate recovery, and remaining reserves for a given reservoir. Derivation of a coal gas mass balance equation begins with the following assumptions:

- The coal and gas are nonreactive.
- Isothermal depletion.
- Gas-saturated coal matrix.
- No gas influx.
- Single-component gas.

Conceptually, the produced gas volume from a coal is the difference between initial gas in place and gas remaining in the coal. As coals hold gas both adsorbed on the surface of the coal matrix and as free gas in the cleats, the gas mass balance can be expressed mathematically as

$$G_p = G_i - G_r$$

$$G_p = G_i - 1.3597(10)^{-3} Ah\rho_B V_{Ldaf}(1 - a - w)\frac{p}{p + p_L} - 0.04356\, Ah\phi(1 - S_w)\frac{1}{B_g} \quad \textbf{(8.1)}$$

where

$G_p$ = produced gas, mmcf,
$G_i$ = initial gas in place, mmcf,
$G_r$ = remaining gas, mmcf,
$A$ = drainage area, ac,
$h$ = coal thickness, ft,
$\rho_B$ = average bulk density, g/cm$^3$,
$V_{Ldaf}$ = dry, ash-free Langmuir volume constant, scf/ton,
$a$ = average ash fraction, decimal,
$w$ = average equilibrium moisture, decimal,
$p$ = current reservoir pressure, psia,
$p_L$ = Langmuir pressure constant, psia,
$\phi$ = porosity, decimal,
$S_w$ = current average water saturation, decimal,
$B_g$ = gas formation volume factor, ft$^3$/scf.

The initial gas in place is the sum of initial sorbed and free gas volumes,

$$G_p = 1.3597(10)^{-3} Ah\rho_B V_{Ldaf}(1-a-w)\frac{p_i}{p_i+p_L} - 0.04356\,Ah\phi_i(1-S_{wi})\frac{1}{B_g} \tag{8.2}$$

where

$p_i$ = initial reservoir pressure, psia,
$\phi_i$ = initial porosity, decimal,
$S_{wi}$ = initial average water saturation, decimal,
$B_{gi}$ = initial gas formation volume factor, ft³/scf.

Coal is a compressible rock, allowing porosity to decrease with depletion. Such variation can be expressed as

$$\frac{\phi}{\phi_i} = \exp\left[-c_f(p_i - p)\right] \tag{8.3}$$

where

$c_f$ = cleat volume compressibility, psia$^{-1}$.

Coal cleat volume compressibility is on the order of 1 to 2(10)$^{-3}$ psia$^{-1}$, and the above equation can be approximated as[1]

$$\frac{\phi}{\phi_i} = 1 - c_f(p_i - p)] \tag{8.4}$$

for pressure changes on the order of 100 to 200 psia. To maintain generality, equation (8.3) will be employed here.

Conceptually, remaining water volume in a coal is original water volume plus influxed water less produced water. Mathematically,

$$7{,}758.4Ah\phi S_w\frac{1}{B_w} = 7{,}758.4Ah\phi_i S_{wi}\left[1 + c_w(p_i - p)\right]\frac{1}{B_w} + W_e - W_p$$

where

$B_w$ = water formation volume factor, rb/stb,
$B_{wi}$ = initial water formation volume factor, rb/stb,
$c_w$ = water compressibility, psia$^{-1}$,
$W_e$ = water influx, stb, and
$W_p$ = water produced, stb.

Dividing through by $7{,}758.4Ah\phi_i$,

$$\frac{\phi}{\phi_i}S_w\frac{1}{B_w} = S_{wi}\left[1 + c_w(p_i - p)\right]\frac{1}{B_w} + \frac{W_e - W_p}{7{,}758.4Ah\phi_i}$$

Then solving for current water saturation,

$$S_w = \frac{B_w}{\dfrac{\phi}{\phi_i}}\left(S_{wi}\left[1 + c_w(p_i - p)\right]\frac{1}{B_w} + \frac{W_e - W_p}{7{,}758.4\,Ah\phi_i}\right) \tag{8.5}$$

Substituting from equation (8.3) and simplifying,

$$S_w = \frac{S_{wi}[1 + c_w(p_i - p)] + \dfrac{B_w(W_e - W_p)}{7{,}758.4\,Ah\phi_i}}{\exp[-c_f(p_i - p)]} \tag{8.6}$$

Assume coal gas can be described by the real gas law,

$$pv = ZnRT$$

where

$v$ = gas volume, ft$^3$,
$Z$ = gas deviation factor,
$n$ = number of moles,
$R$ = universal gas constant, psia-ft$^3$/lb-mol-°R, and
$T$ = temperature, °R.

Then the gas formation volume factor can be written as

$$B_g = \frac{\dfrac{ZnRT}{p}}{\dfrac{Z_{sc}nRT_{sc}}{p_{sc}}}$$

Simplifying,

$$B_g = \frac{ZTp_{sc}}{pZ_{sc}T_{sc}} \tag{8.7}$$

Substitution of equations (8.2), (8.6), and (8.7) into (8.1) yields the complete mass balance equation for gas in a coal.

$$G_p = 1.3597(10)^{-3}Ah\rho_B V_{Ldaf}(1 - a - w)\frac{p_i}{p_i + p_L} + 0.04356\,Ah\phi_i(1 - S_{wi})\frac{p_i Z_{sc}T_{sc}}{p_{sc}Z_i T} \tag{8.8}$$

$$- 1.3597(10)^{-3}Ah\rho_B V_{Ldaf}(1 - a - w)\frac{p}{p + p_L} - 0.04356\,Ah\phi\left(1 - \frac{S_{wi}[1 + c_w(p_i - p)] + \dfrac{B_w(W_e - W_p)}{7758.4\,Ah\phi_i}}{\exp[-c_f(p_i - p)]}\right)\frac{pZ_{sc}T_{sc}}{p_{sc}ZT}$$

This full mass balance equation can be used to describe depletion of a coal deposit similar to depletion of a conventional gas reservoir.

Note that if no gas is sorbed and the coal is dry and incompressible, equation (8.8) reduces to

$$G_p = 0.04356Ah\phi\,\frac{p_i Z_{sc}T_{sc}}{p_{sc}Z_i T} - 0.04356Ah\phi\,\frac{pZ_{sc}T_{sc}}{p_{sc}ZT} \tag{8.9}$$

Initial gas in place for this case is

$$G_i = 0.04356Ah\phi \frac{p_i Z_{sc} T_{sc}}{p_{sc} Z_i T}$$

Thus,

$$G_p = G_i - 0.04356Ah\phi \frac{Z_{sc} T_{sc}}{p_{sc} T} \frac{p}{Z} \tag{8.10}$$

Solving equation (8.9) for $p/Z$,

$$\frac{p}{Z} = \frac{p_i}{Z_i} - \frac{p_{sc} T}{0.04356Ah\phi Z_{sc} T_{sc}} G_p \tag{8.11}$$

Using the expression for initial gas in place for this dry, barren, and incompressible coal,

$$\frac{p}{Z} = \frac{p_i}{Z_i}\left(1 - \frac{G_p}{G_i}\right) \tag{8.12}$$

which is the mass balance equation of a volumetric, dry gas reservoir.

The full coal gas mass balance equation, equation (8.8), was considerably simplified with the introduction of the $Z^*$ function introduced by King.[2] Returning to equation (8.1)

$$G_p = G_i - 1.3597(10)^{-3} Ah\rho_B V_{Ldaf}(1 - a - w)\frac{p}{p + p_L} - 0.04356Ah\phi(1 - S_w)\frac{pZ_{sc}T_{sc}}{p_{sc} ZT} \tag{8.13}$$

Collecting terms and using equation (8.3) for the porosity ratio,

$$G_p = G_i - 0.04356Ah\phi \frac{Z_{sc} T_{sc}}{p_{sc} T}\left[\frac{\rho_B V_{Ldaf}(1 - a - w)p_{sc} T}{32.037\phi_i Z_{sc} T_{sc}} \frac{p}{p + p_L} + (1 - S_w)\exp[-c_f(p_i - p)]\frac{p}{Z}\right] \tag{8.14}$$

Comparing the above equation to equation (8.10) intuitively led King to the define the $Z^*$ function as

$$\frac{p}{Z^*} = \frac{p}{Z}\left[\frac{\rho_B V_{Ldaf}(1 - a - w)p_{sc} TZ}{32.037\,\phi_i Z_{sc} T_{sc}} \frac{1}{p + p_L} + (1 - S_w)\exp\left[-c_f(p_i - p)\right]\right] \tag{8.15}$$

Solving for $Z^*$ explicitly,

$$Z^* = \frac{Z}{\dfrac{\rho_B V_{Ldaf}(1 - a - w)\,p_{sc} TZ}{32.037\,\phi_i Z_{sc}\, T_{sc}(p + p_L)} + (1 - S_w)\exp\left[-c_f(p_i - p)\right]} \tag{8.16}$$

The $Z^*$ function is simply the gas deviation factor divided by the sum of two terms. The first term is the ratio of sorbed gas to free gas per unit reservoir volume. Bituminous and higher rank coals can typically hold 20 to 50 times more gas by sorption than free gas in the cleats. Subbituminous coals, with less sorptive capacity and more porosity than higher rank coals, often hold equal amounts of sorbed and free gas. Thus, this first term in the $Z^*$ denominator can range from a value of 1 to 50. The second term is the product of two differences and represents the volume of free gas in the cleat per unit reservoir volume. Both range in value between 0 and 1, making their

product less than 1. Consequently, the denominator of the $Z^*$ function is frequently dominated by the first term, the ratio of sorbed to free gas per unit reservoir volume.

Depletion of a bounded coal well draining an unidentified coal was discussed by GRI.[3] Pertinent coal properties are given in table 8–1, and the resulting $Z^*$ function plotted in figure 8–1. For simplicity, a constant water saturation of 0.90 was assumed. Value of the first term in the denominator of the $Z^*$ function, equation (8.16), the ratio of sorbed gas to free gas, varies from 43 to 247, while value of the second term, the saturation term, is nearly constant at 0.1. As seen in figure 8–1, the resulting $Z^*$ function is a nearly linear function of pressure, smoothly varying from 0.005 to 0.026 over a range of 2,000 psia.

**Table 8–1.** Reservoir properties—unidentified coal

| | | |
|---|---|---|
| $V_{L\ daf}$ = | 747.7 | scf/ton |
| $p_L$ = | 371 | psia |
| Ash = | 0.11 | decimal |
| Equilibrium moisture = | 0.03 | decimal |
| Coal density = | 1.35 | g/cm$^3$ |
| Initial pressure = | 1,600 | psia |
| Temperature = | 130 | °F |
| Initial porosity = | 0.005 | decimal |
| Cleat compressibility = | 4.0E–05 | psia$^{-1}$ |
| Water saturation = | 1.00 | decimal |

*Source:* Gas Research Institute. 1996.

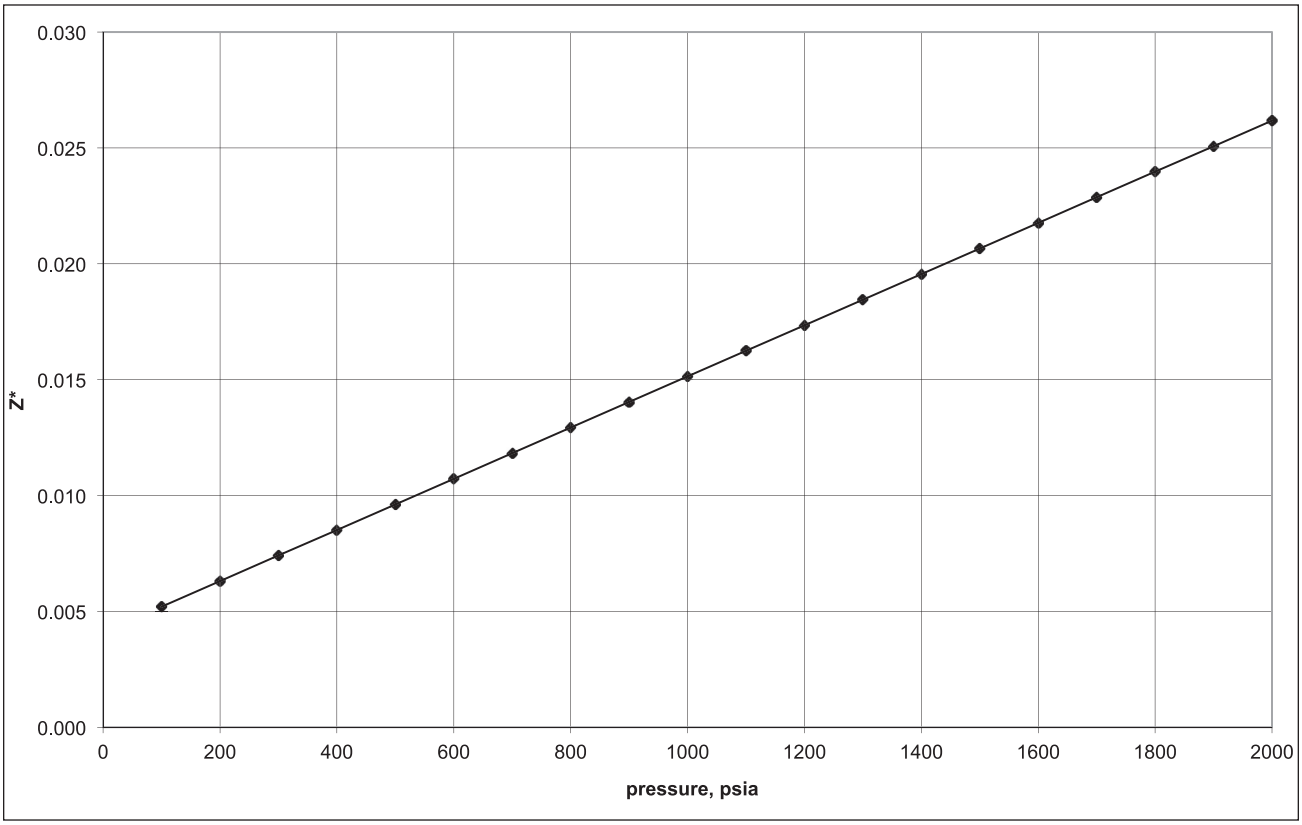



**Fig. 8–1.** King $Z^*$ function for unidentified coal[4]

Reservoir properties of the Canyon coal in the Powder River Basin of Wyoming were reported by Nelson et al.[5] Porosity characteristics of Powder River coals were discussed by Bustin and Clarkson.[6] Coal properties are collected in table 8–2, and the resulting $Z^*$ function, assuming a constant water saturation of 0.8, is plotted in

figure 8–2. For this example, the ratio of sorbed gas to free gas varied from 0.8 to 1.3, while the water saturation term was a constant 0.2. Value of the resulting $Z^*$ function varied between 0.68 and 0.96 over a pressure range of 200 psia. For engineering purposes, a $Z^*$ value of 0.8 is probably adequate.

**Table 8–2.** Reservoir properties—Powder River Basin coal

| | | |
|---|---|---|
| $V_{L\,daf}$ = | 117.2 | scf/ton |
| $p_L$ = | 394 | psia |
| Ash = | 0.0392 | decimal |
| Equilibrium moisture = | 0.2766 | decimal |
| Coal density = | 1.34 | g/cm$^3$ |
| Initial pressure = | 153 | psia |
| Temperature = | 65 | °F |
| Initial porosity = | 0.100 | decimal |
| Cleat compressibility = | 0.0E+00 | psia$^{-1}$ |
| Water saturation = | 0.80 | decimal |

*Source:* Nelson, C. R., et al. 2000; and Bustin, R. M., and Clarkson, C. R. 1999.

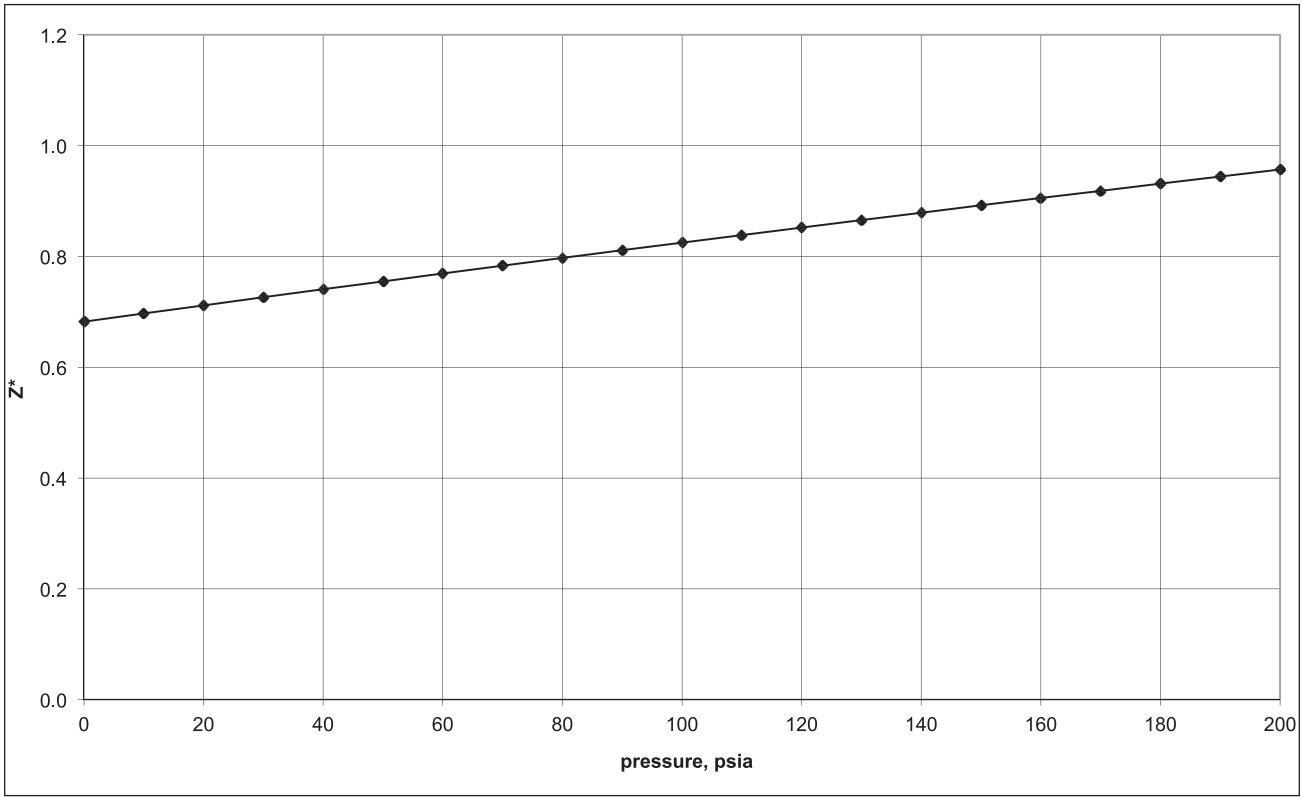



**Fig. 8–2.** King $Z^*$ function for Canyon coal—Powder River Basin[7]

Rewriting equation (8.2) for initial gas in place and using equation (8.7) for the gas formation volume factor,

$$G_i = \frac{0.04356 A h \phi_i Z_{sc} T_{sc}}{p_{sc} T} \frac{p_i}{Z_i} \left[ \frac{\rho_B V_{Ldaf} (1 - a - w)\, p_{sc} T Z_i}{32.037 \phi_i Z_{sc} T_{sc} (p_i + p_L)} + (1 - S_{wi}) \right]$$

From equation (8.15) this simplifies to

$$G_i = \frac{0.04356Ah\phi_i Z_{sc}T_{sc}}{p_{sc}T}\frac{p_i}{Z_i^\star} \tag{8.17}$$

which can be rewritten as

$$\frac{p_{sc}T}{0.04356Ah\phi_i Z_{sc}T_{sc}} = \frac{1}{G_i}\frac{p_i}{Z_i^\star} \tag{8.18}$$

Gas remaining in the coal is given by the last two terms on the right-hand side of equation (8.1)

$$G_r = 1.3597(10)^{-3}Ah\rho_B V_{Ldaf}(1-a-w)\frac{p}{p+p_L} + 0.04356Ah\phi(1-S_w)\frac{1}{B_g}$$

Substituting equation (8.3) for the porosity and equation (8.7) for the gas formation volume factor gives

$$G_r = 1.3597(10)^{-3}Ah\rho_B V_{Ldaf}(1-a-w)\frac{p}{p+p_L} + 0.04356\,Ah\phi_i \exp\left[-c_f(p_i-p)\right](1-S_w)\frac{1}{\dfrac{ZTp_{sc}}{Z_{sc}T_{sc}p}}$$

Simplifying,

$$G_r = \frac{0.04356Ah\phi_i Z_{sc}T_{sc}}{p_{sc}T}\frac{p}{Z}\left[\frac{\rho_B V_{Ldaf}(1-a-w)\,p_{sc}TZ}{32.037\phi_i Z_{sc}T_{sc}(p+p_L)} + (1-S_w)\exp[-c_f(p_i-\mathrm{p})]\right]$$

From the definition of $Z^\star$, equation (8.15),

$$G_r = \frac{0.04356Ah\phi_i Z_{sc}T_{sc}}{p_{sc}T}\frac{p}{Z^\star}$$

With the above equation and equation (8.17) for initial gas in place, the gas mass balance equation, equation (8.1), can be rewritten as

$$G_p = \frac{0.04356Ah\phi_i Z_{sc}T_{sc}}{p_{sc}T}\frac{p_i}{Z_i^\star} - \frac{0.04356Ah\phi_i Z_{sc}T_{sc}}{p_{sc}T}\frac{p}{Z^\star}$$

Solving for $p/Z^\star$,

$$\frac{p}{Z^\star} = \frac{p_i}{Z_i^\star} - \frac{p_{sc}T}{0.04356Ah\phi_i Z_{sc}T_{sc}}G_p \tag{8.19}$$

Substituting equation (8.18) into the above equation yields

$$\frac{p}{Z^\star} = \frac{p_i}{Z_i^\star} - \frac{p_i}{G_i Z_i^\star}G_p \tag{8.20}$$

or, more simply, the gas mass balance equation for a coal may be written

$$\frac{p}{Z^\star} = \frac{p_i}{Z_i^\star}\left(1-\frac{G_p}{G_i}\right) \tag{8.21}$$

which is analogous to equation (8.12), the mass balance equation for a conventional volumetric, dry gas reservoir.

## Solution of the Coal Gas Mass Balance Equation

Inspection of equation (8.21) indicates that a plot of $p/Z^*$ versus cumulative gas recovery from a coal deposit should be linear, analogous to equation (8.12) for a conventional volumetric, dry gas reservoir. The vertical intercept of a $p/Z^*$ plot leads to an estimate of initial reservoir pressure, while the horizontal intercept yields original gas in place. Construction of a $p/Z$ plot for a conventional reservoir is straightforward, as $Z$ is solely a function of gas composition and pressure. Construction of a $p/Z^*$ plot for a coal is more difficult, as the $Z^*$ function depends not only on gas composition and pressure but also on reservoir properties, necessitating an iterative solution.

The $Z^*$ function, equation (8.16), contains a water saturation term in the denominator. The water saturation, equation (8.6), in turn, is a function of several variables, including drainage area. Drainage area, determined from the slope of the $p/Z^*$ line given by equation (8.19), is

$$A = \frac{p_{sc}T}{0.04356mh\phi_i Z_{sc}T_{sc}} \tag{8.22}$$

where

$m$ = slope of $p/Z^*$ plot, psia/mmcf.

Thus, solution of the general coal gas mass balance equation, equation (8.21), is an iterative procedure beginning with an assumed drainage area. Water saturations and $Z^*$ values are then calculated for each cumulative production point using equations (8.6) and (8.16), respectively. The slope of the resulting plot of $p/Z^*$ versus cumulative gas production is employed in equation (8.22) to determine a new value of drainage area. This process is repeated with the new drainage area until it converges.

Note that the original King method plot of cumulative production and $p/Z^*$ is the opposite of conventional gas reservoir depletion plots. That is, the King method plots $p/Z^*$ on the horizontal axis and cumulative production on the vertical axis. This is in contrast to the established practice for gas reservoirs, in which cumulative production is plotted on the horizontal axis and $p/Z$ on the vertical axis. For simplicity, this work follows the usual convention of plotting cumulative gas production on the horizontal axis and the pressure function, $p/Z$ or $p/Z^*$, on the vertical axis.

From the $p/Z^*$ plot of the final iteration and equation (8.20), original gas in place (OGIP) is the intercept divided by the slope, and the value so obtained can be compared with the volumetric OGIP calculated from the inputs required by this method. For any given abandonment pressure, the associated water saturation is not known, thus estimated ultimate recovery (EUR) cannot be calculated with this method. However, as noted above, the $Z^*$ function is often weakly affected by the water saturation term in the denominator. Thus, a reasonable approximation of EUR can often be obtained using the water saturation calculated from the last reported production data.

### Example 8.1. Coal gas reserves—King method—GRI well

This example from a well completed in an unidentified coal was presented by GRI and uses reservoir parameters collected in table 8–1 with the exception of water saturation.[8] Initial water saturation for the GRI example was 100%, not the arbitrary and constant 90% used in table 8–1 to calculate the $Z^*$ function. In addition to the initial point, cumulative gas and water production at two reservoir pressures are presented in table 8–3, along with additional reservoir parameters. The well was bounded, with no water influx.

**Table 8–3.** Gas and water production—unidentified coal

| | | | | |
|---|---|---|---|---|
| Pressure = | 1,600 | 900 | 490 | psia |
| Cumulative gas production = | 0 | 455 | 1,162 | mmcf |
| Cumulative water production = | 0 | 21,400 | 93,500 | stb |
| Water influx = | 0 | 0 | 0 | stb |
| Initial water saturation = | 1.00 | | | decimal |
| Net coal thickness = | 27 | | | feet |
| Water compressibility = | 3.20E–06 | | | $psia^{-1}$ |
| Water formation volume factor = | 1.00 | | | rb/stb |

*Source:* Gas Research Institute. 1996.

Following the GRI assumption of a drainage area of 119 ac, water saturation after the coal had been depleted to 900 psia, calculated from equation (8.6), is

$$S_w = \frac{1.0\left[1 + 3.2(10)^{-6}\,\text{psia}^{-1}(1600 - 900)\ \text{psia}\right] + \dfrac{1.0\ \dfrac{\text{rb}}{\text{stb}}\,(0 - 21{,}400)\,\text{stb}}{7{,}758.4\,(119\ \text{ac})\,27\ \text{ft}\ 0.005}}{\exp\left[-4(10)^{-5}\ \text{psia}^{-1}\ (1{,}600 - 900)\ \text{psia}\right]}$$

$$S_w = 0.8541$$

The associated $Z^*$ value, from equation (8.16), is

$$Z^* = \frac{0.9276}{\dfrac{1.35\,\dfrac{\text{g}}{\text{cm}^3}\,747.7\,\dfrac{\text{scf}}{\text{ton}}(1-0.11-0.03)\,14.7\,\text{psia}(460+130)^\circ\text{R}(0.9276)}{32.037(0.005)0.9980(460+60)^\circ\text{R}(900+371)\text{psia}} + (1-0.8541)\exp\left[-4(10)^{-5}\text{psia}(1{,}600-900)\text{psia}\right]}$$

$$Z^* = 0.01400$$

Making

$$\frac{p}{Z^*} = 64{,}269\ \text{psia}$$

After depletion to 490 psia, water saturation from equation (8.6) is 0.2649, $Z^*$ from equation (8.16) is 0.00944, and the resulting $p/Z^*$ value is 51,902 psia. The initial $p/Z^*$ plot is shown in figure 8–3. As the method converges quite rapidly, the initial and final points are nearly superimposed. The slope of a line fit through the three initial points is –18.508 psia/mmcf, and from equation (8.19), the associated drainage area is

$$A = -\frac{14.7\ \text{psia}\ (460 + 130)\ ^\circ\text{R}}{0.04356\ (-18.508\ \text{psia/mmcf})\ 27\ \text{ft}\ (0.005)\ 0.9980\ (460 + 60)\ ^\circ\text{R}} = 153.6\ \text{ac}$$

Repeating the calculations with this new estimate of drainage area, 153.6 ac, water saturation at 900 psia is 0.8939, $Z^*$ is 0.01401, and $p/Z^*$ is 64,231 psia. After depletion to 490 psia, water saturation is 0.4414, $Z^*$ is 0.00946, and $p/Z^*$ is 51,816 psia. From the $p/Z^*$ plot slope of –18.582 psia/mmcf, drainage area is 152.9 ac.

The third iteration assumed a drainage area of 152.9 ac. At 900 psia, water saturation is 0.8933, $Z^*$ is 0.01401, and $p/Z^*$ is 64,232 psia. After depletion to 490 psia, water saturation is 0.4389, $Z^*$ is 0.00946, and $p/Z^*$ is 51,817 psia. The $p/Z^*$ plot slope of –18.581 psia/mmcf yields a drainage area of 153.0 ac, essentially the same as the previous iteration, indicating the method has converged. All calculations are summarized in table 8–4.

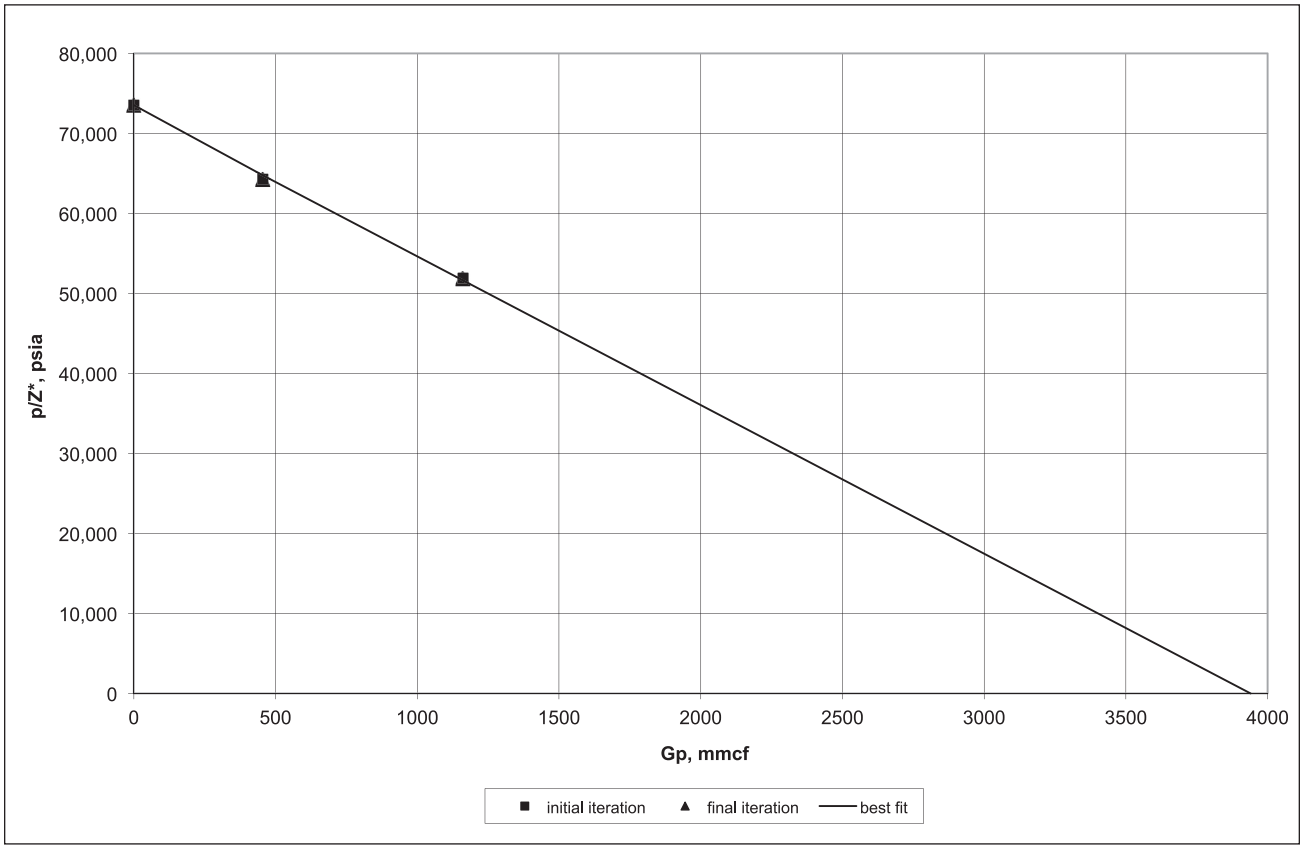



**Fig. 8–3.** *p*/*Z** plot—GRI coal well

**Table 8–4.** King iterative solution—GRI coal well

| | | Initial | 1 | 2 |
|---|---|---|---|---|
| Iteration 1 | $S_w$ = | 1.00 | 0.8541 | 0.2649 |
| | $Z^*$ = | 0.02176 | 0.01400 | 0.00944 |
| | $p/Z^*$ = | 73,520 | 64,269 | 51,902 |
| | Slope = | -18.508 | psia/mmcf | |
| | $A$ = | 153.6 | ac | |
| Iteration 2 | $S_w$ = | 1.00 | 0.8939 | 0.4414 |
| | $Z^*$ = | 0.02176 | 0.01401 | 0.00946 |
| | $p/Z^*$ = | 73,520 | 64,231 | 51,816 |
| | Slope = | -18.582 | psia/mmcf | |
| | $A$ = | 152.9 | acres | |
| Iteration 3 | $S_w$ = | 1.00 | 0.8933 | 0.4389 |
| | $Z^*$ = | 0.02176 | 0.01401 | 0.00946 |
| | $p/Z^*$ = | 73,520 | 64,232 | 51,817 |
| | Slope = | -18.581 | psia/mmcf | |
| | $A$ = | 153.0 | ac | |

The $p/Z^*$ plot for the final iteration, shown in figure 8–3, yields an original gas in place of 3.940 bcf. This volume is 0.5% lower than the volumetric OGIP of 3.957 bcf calculated from parameters given in tables 8–1 and 8–3. Assuming an abandonment pressure of 100 psia and using the water saturation of the final production point, $S_w$ = 0.4389, the EUR is 2.902 bcf, and the recovery factor is 0.737. Remaining reserves from the last reported production point are 1.740 bcf. The results are collected in table 8–5.

**Table 8–5.** King iterative solution—GRI coal well, estimated ultimate recovery and remaining reserves

| | | |
|---|---|---|
| $A$ = | 153.0 | acres |
| Volumetric OGIP = | 3.957 | bcf |
| King OGIP = | 3.940 | bcf |
| EUR = | 2.902 | bcf |
| Remaining reserves = | 1.740 | bcf |
| Recovery factor = | 0.737 | |

## Example 8.2. Coal gas reserves—King method—Canyon coal, Powder River Basin

Gas and water production from a bounded Canyon coal well in the Powder River Basin were simulated using reservoir properties given above in table 8–2, except the initial water saturation was 0.95.[9] Additional data and simulated cumulative gas and water production and reservoir pressures at 180 and 600 days are in table 8–6. As shown in table 8–7, the method converged in three iterations to a drainage area of 80.7 ac. The $p/Z^*$ plot for the final iteration, (fig. 8–4), yielded an OGIP of 223.2 mmcf, which is 0.15% higher than the volumetric OGIP of 222.9 mmcf. Estimated ultimate recovery, calculated with an assumed abandonment pressure of 35 psia and the water saturation from the final production point, $S_w$ = 0.9286, is 156.6 mmcf. The corresponding recovery factor is 0.702, and remaining reserves from the last data point are 105.0 mmcf. Table 8–8 summarizes all these results.

**Table 8–6.** Powder River coal well—simulated production data

| | | | | |
|---|---|---|---|---|
| Time = | 0 | 180 | 600 | days |
| Pressure = | 153 | 138.1 | 103.1 | psia |
| Cumulative gas production = | 0.000 | 14.321 | 51.603 | mmcf |
| Cumulative water production = | 0.000 | 54.000 | 180.000 | mstb |
| Water influx = | 0.000 | 0.000 | 0.000 | mstb |
| Initial water saturation = | 0.95 | | | decimal |
| Net coal thickness = | 64 | | | ft |
| Water compressibility = | 3.20E–06 | | | $psia^{-1}$ |
| Water formation volume factor = | 1.00 | | | rb/stb |

**Table 8–7.** King iterative solution—Canyon coal well

| | | Initial | 1 | 2 |
|---|---|---|---|---|
| Iteration 1 | $S_w$ = | 0.95 | 0.9380 | 0.9099 |
| | $Z^*$ = | 1.03857 | 0.999440 | 0.91346 |
| | $p/Z^*$ = | 147 | 138 | 113 |
| | Slope = | –0.670 | psia/mmcf | |
| | $A$ = | 79.6 | acres | |
| Iteration 2 | $S_w$ = | 0.95 | 0.9364 | 0.9046 |
| | $Z^*$ = | 1.03857 | 0.99784 | 0.90904 |
| | $p/Z^*$ = | 147 | 138 | 113 |
| | Slope = | –0.660 | psia/mmcf | |
| | $A$ = | 80.9 | acres | |
| Iteration 3 | $S_w$ = | 0.95 | 0.9366 | 0.9053 |
| | $Z^*$ = | 1.03857 | 0.99806 | 0.90963 |
| | $p/Z^*$ = | 147 | 138 | 113 |
| | Slope = | –0.661 | psia/mmcf | |
| | $A$ = | 80.7 | acres | |

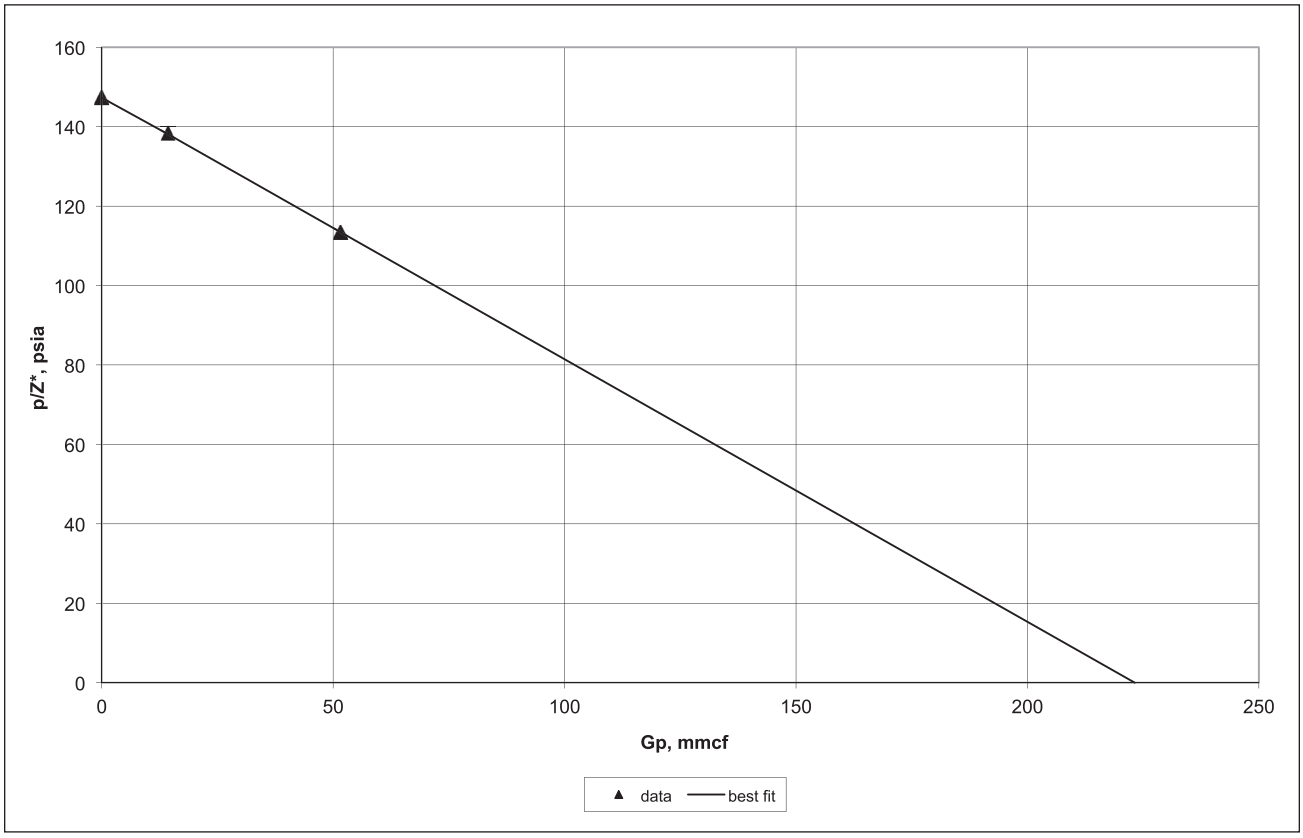



**Fig. 8–4.** *p/Z** plot for final iteration in King solution—Canyon coal well

**Table 8–8.** King iterative solution—Canyon coal well estimated ultimate recovery and remaining reserves

| | | |
|---|---|---|
| *A* = | 80.7 | ac |
| Volumetric OGIP = | 222.9 | mmcf |
| King OGIP = | 223.2 | mmcf |
| EUR = | 156.6 | mmcf |
| Remaining reserves = | 105.0 | mmcf |
| Recovery factor = | 0.702 | |

## Modified King Method

When the iterative King method is applied to actual production data, it often converges to unrealistic values of initial pressure and gas in place.[10] Selective elimination of noisy data points did not improve the estimates. The weakness of the method was traced to the denominator of the $Z^*$ function. As noted above, the ratio of sorbed gas to free gas in the denominator of equation (8.16) is often much larger than the water saturation term. Thus, the value of $Z^*$ is relatively insensitive to changes in average water saturation, and iterations on drainage area had minimal effect on the value of $Z^*$, allowing convergence to erroneous values.

The modified method assumes a constant water saturation over time. King's original method employs a water saturation averaged over the drainage area. Assuming the water saturation is also constant over time is not as unrealistic as it first appears. Water saturations in a coal deposit change very slowly, on the order of years, as the gas is produced. Seidle reported saturation changes on the order of 0.35 in a 10-year simulation. While saturations are important for calculating gas and water mobilities and production rates at any specific time,

changes in the saturations do not strongly influence the denominator of the $Z^*$ function when it is dominated by the ratio of sorbed gas to free gas.

Assumption of an average water saturation eliminates the iterative solution of the original King method and allows direct calculation of initial gas in place, estimated ultimate recovery, and remaining reserves. Clearly, the chosen water saturation must lie between zero and one. However, a more realistic saturation can be obtained from the initial gas-water ratio and gas-water relative permeability curves or, perhaps, reservoir simulation. Seidle verified the modified King method with simulated production and found it worked well when used against the production data that were problematic for the original King method.

### Example 8.3. Coal gas reserves—modified King method—GRI coal well

Original gas in place, EUR, and remaining reserves were calculated for the unidentified coal well of example 8.1 using the modified King method, assuming an average water saturation of 0.7. Coal and reservoir properties are given in tables 8–1 and 8–3. The resulting $p/Z^*$ plot is shown in figure 8–5. Original gas in place is estimated to be 3.850 bcf, some 3% lower than the volumetric OGIP of 3.957 bcf. Estimated ultimate recovery is 2.849 bcf, remaining reserves are 1.687 bcf, and drainage area is 148.5 ac. The recovery factor is 0.740. Comparing results from the modified method with those from the original method in table 8–9, it is seen that modified method gas volumes are typically 2% or 3% lower than those determined with the original iterative method.

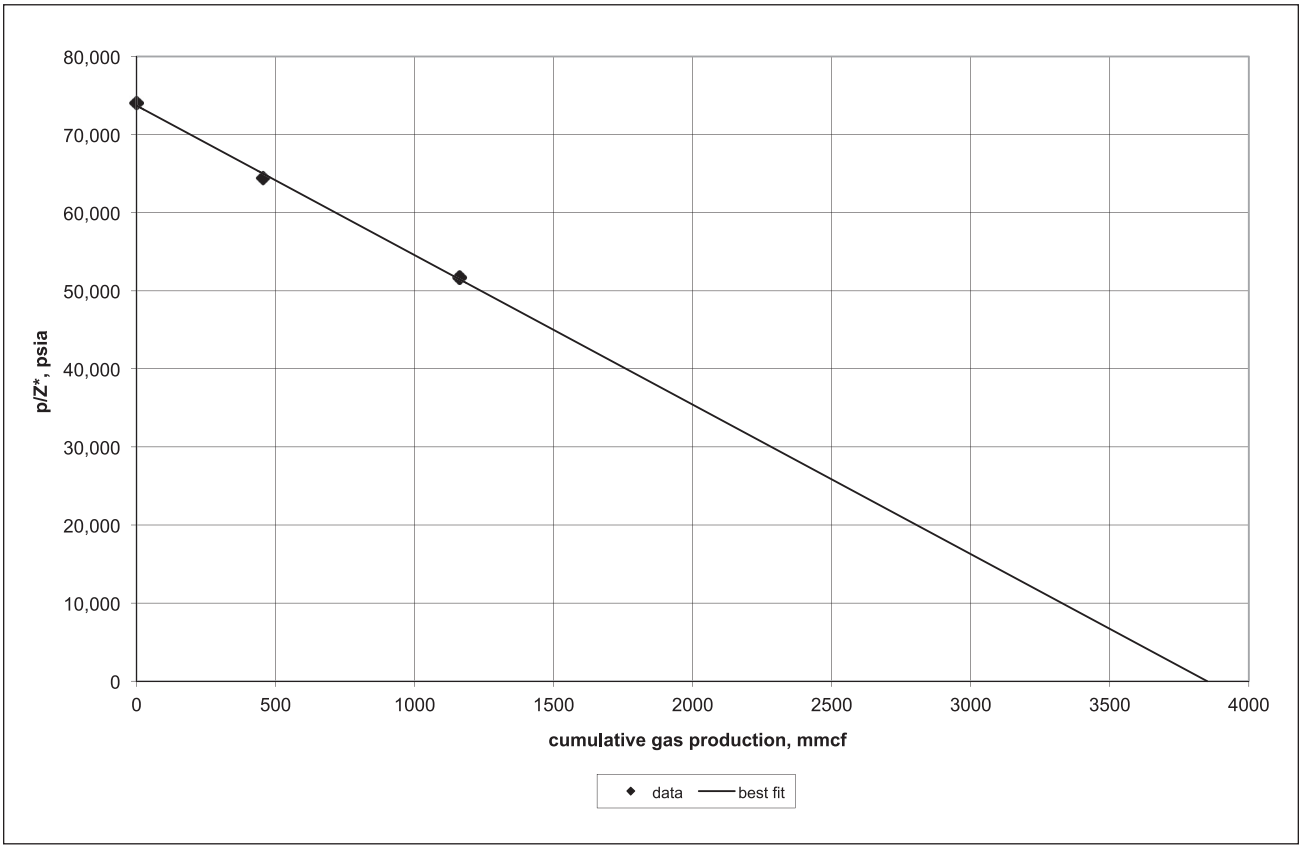



**Fig. 8–5.** Modified King method $p/Z^*$ plot—unidentified well[11]

**Table 8–9.** Comparison of gas volumes—unidentified GRI well, original and modified King methods

| | | | |
|---|---|---|---|
| Volumetric OGIP = | 3.957 | bcf | |
| | **original King** | **modified King** | |
| *A* = | 153.0 | 148.5 | ac |
| OGIP = | 3.940 | 3.850 | bcf |
| EUR = | 2.902 | 2.849 | bcf |
| Remaining reserves = | 1.740 | 1.687 | bcf |
| Recovery factor = | 0.737 | 0.740 | |

## Example 8.4. Coal gas reserves—modified King method—Canyon coal well

Simulated production data from the Canyon coal well discussed in example 8.2 were analyzed with the modified King method using the average water saturation of 0.9393. The three points comprising the $p/Z^*$ plot, shown in figure 8–6, appear quite linear and yield an original gas in place of 196.2 bcf, 12% lower than the volumetric OGIP of the simulator. As seen in table 8–10, EUR predicted with the modified method was 11% less than that of the original method (139.9 bcf vs. 156.6 bcf), and remaining reserves were 16% less (88.3 bcf vs. 105.0 bcf). The recovery factor of 0.713 was essentially that of the original King method, 0.702.

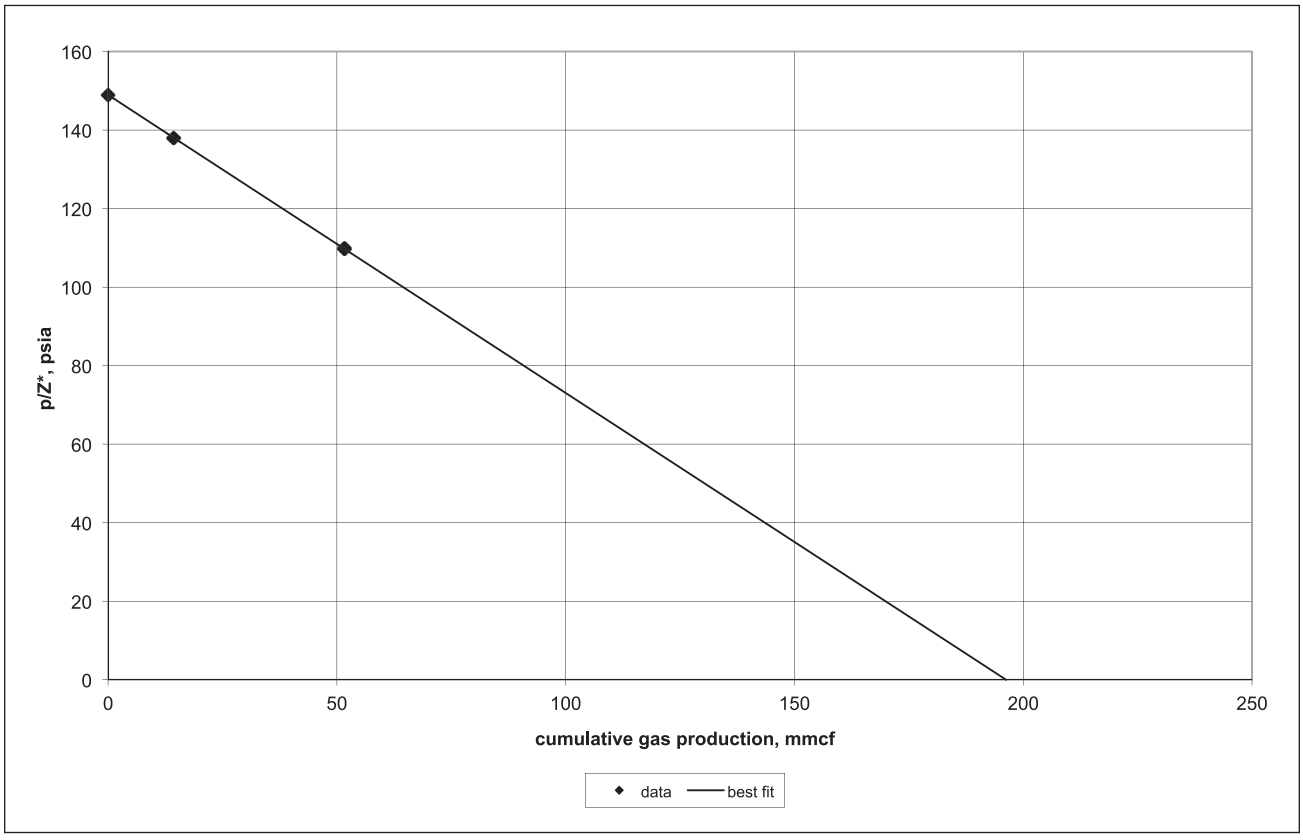



**Fig. 8–6.** Canyon coal well—modified King method, $p/Z^*$ plot

**Table 8–10.** Comparison of gas volumes—Canyon coal well, original and modified King methods

| Volumetric OGIP = | 222.9 | bcf |
|---|---|---|
| | **original King** | **modified King** |
| *A* = | 80.7 | 70.3 |
| OGIP = | 223.2 | 196.2 |
| EUR = | 156.6 | 139.9 |
| Remaining reserves = | 105.0 | 88.3 |
| Recovery factor = | 0.702 | 0.713 |

Gas volumes are underpredicted in this example because the assumption that the water saturation variation can be neglected is no longer valid. From the denominator of the definition of the $Z^*$ function, equation (8.16), the ratio of sorbed to free gas, given by

$$\frac{\rho_B V_{Ldaf}(1-a-w)\,p_{sc}TZ}{32.037\phi_i Z_{sc}T_{sc}\,(p+p_L)}$$

is on the order of one. Water saturations are also on the order of one and thus cannot be neglected. A practical test of when the modified method may be in error is comparison of $Z$ and $Z^*$ values. When the two values are approximately equal, the method may be underpredicting gas volumes and the full, iterative King method should be employed.

## Jensen and Smith Modified Material Balance

A modified material balance method was developed by Jensen and Smith for coals that hold most of their gas by sorption.[12] This method neglects not only water but also free gas in the fractures. Consequently, equation (8.16) for the $Z^*$ function becomes

$$Z^* = \frac{Z}{\dfrac{\rho_B V_{Ldaf}(1-a-w)\,p_{sc}TZ}{32.037\,\phi_i Z_{sc}T_{sc}\,(p+p_L)}}$$

And the gas mass balance equation, equation (8.8), simplifies to

$$\frac{p}{p+p_L} = \frac{p_i}{p_i+p_L}\left(1-\frac{G_p}{G_i}\right) \qquad \textbf{(8.23)}$$

As this method requires only the Langmuir pressure, $p_L$, reservoir pressures, and cumulative gas production data, it is extremely practical. Knowledge of abandonment pressure allows rapid calculation of estimated ultimate recovery and remaining reserves. Note that no estimate of drainage area is available with this method.

### Example 8.5. Coal gas reserves—Jensen and Smith method—GRI coal well

Returning to the unidentified coal well of example 8.1, Langmuir pressure is 371 psia. From table 8–3, reservoir pressure had fallen from 1,600 psia to 900 psia after production of 455 mmcf, then to 490 psia after a cumulative production of 1,162 mmcf. Using these data in equation (8.23) yields the Jensen and Smith plot shown in figure 8–7. Original gas in place is 3.890 bcf, lower than the volumetric gas in place by 2%. Estimated ultimate recovery is 2.869 bcf and recovery factor is 0.737. As seen in table 8–11, gas volumes obtained with the Jensen and Smith method are roughly 1% below those from the original and modified King methods.

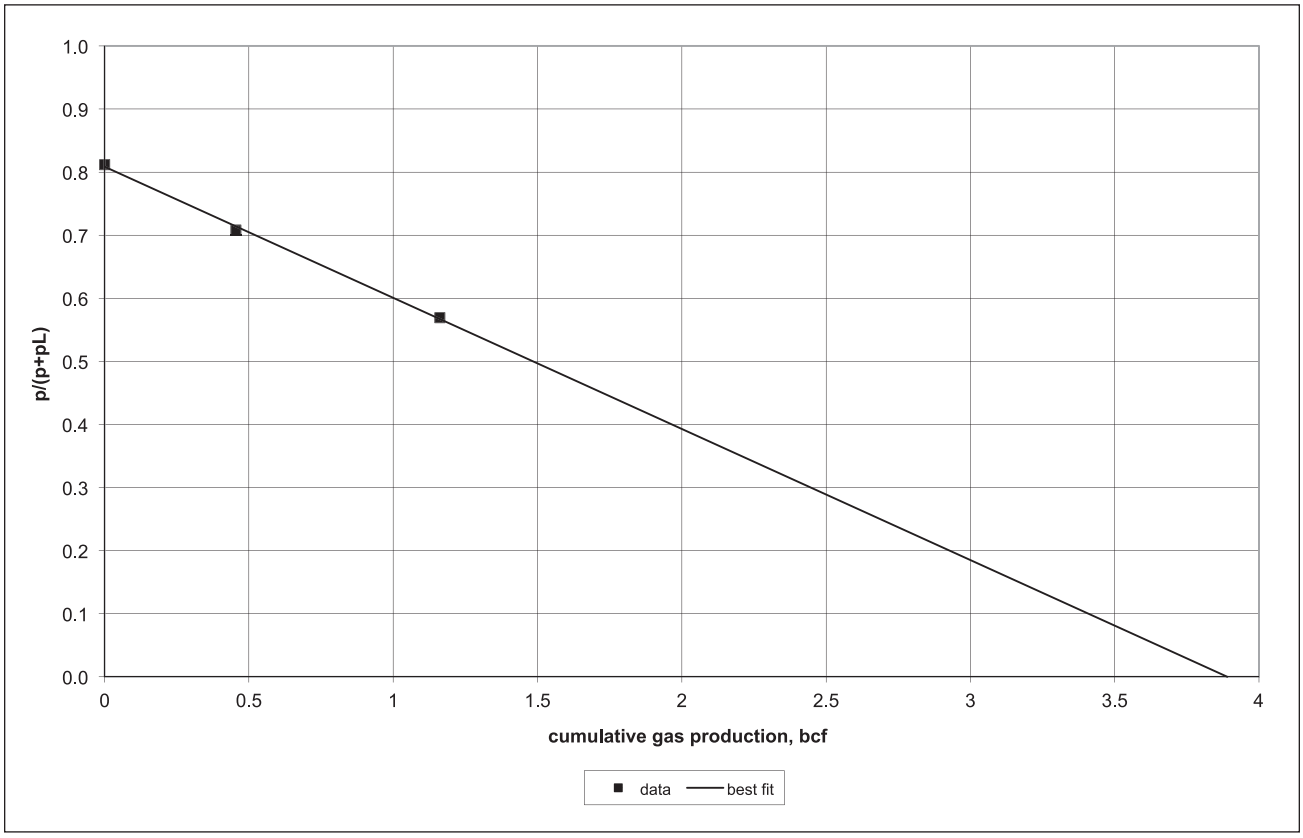



**Fig. 8–7.** Jensen and Smith plot—GRI coal well

**Table 8–11.** Comparison of gas volumes—unidentified GRI well, Jensen and Smith method, plus original and modified King methods

| Volumetric OGIP = | 3.957 | bcf | | |
|---|---|---|---|---|
| | **original King** | **modified King** | **J&S method** | |
| *A* = | 153.0 | 148.5 | na | ac |
| OGIP = | 3.940 | 3.850 | 3.890 | bcf |
| EUR = | 2.902 | 2.849 | 2.869 | bcf |
| Remaining reserves = | 1.740 | 1.687 | 1.707 | bcf |
| Recovery factor = | 0.737 | 0.740 | 0.737 | |

## Example 8.6. Coal gas reserves—Jensen and Smith method—Canyon coal well

Langmuir pressure for the Powder River Basin coal well discussed in example 8.2 was 394 psia. Original pressure was 153 psia. As seen in table 8–6, after 180 days of simulated production, reservoir pressure had fallen to 138.1 psia and cumulative gas production was 14.321 mmcf. After 600 days, reservoir pressure had declined to 103.1 psia with a cumulative gas production of 51.603 mmcf. The resulting Jensen and Smith plot is depicted in figure 8–8, and gas volumes predicted with the Jensen and Smith method are compared with those from the original and modified King methods in table 8–12. The Jensen and Smith method yields gas volumes similar to those of the modified King method, yet all are low compared to the original King method. Original gas in place is 199.7 mmcf (12% low), EUR is 141.4 mmcf (10% low), and remaining reserves are 89.8 mmcf (16% low). Recovery factor was 0.708, very similar to those calculated by the original and modified King methods. As with the modified method, the Jensen and Smith method underpredicts gas volumes through neglect of gas and water in the cleats. Unlike the modified method, there is no practical test to determine when the Jensen and Smith method fails.

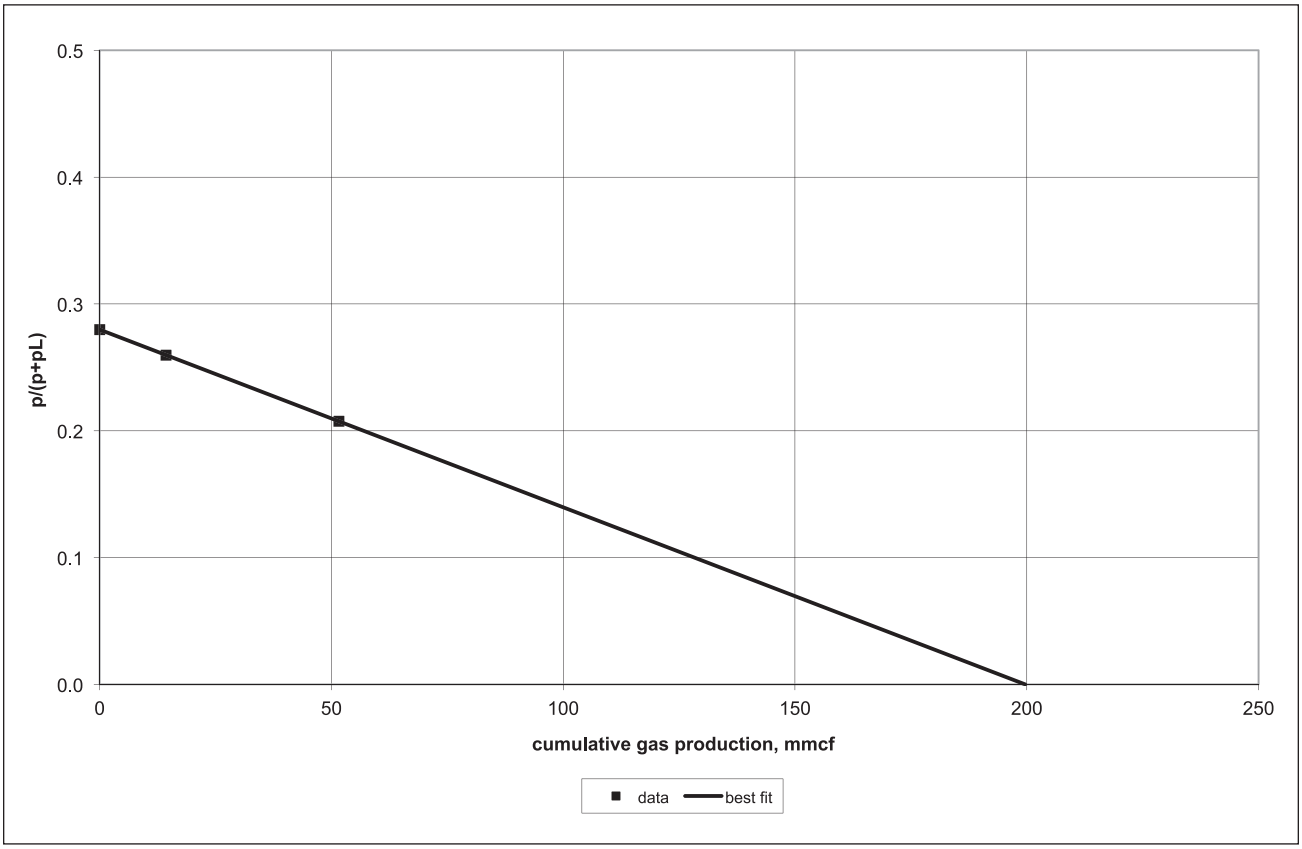



**Fig. 8–8.** Jensen and Smith plot—Canyon coal well

**Table 8–12.** Comparison of gas volumes—Canyon coal well, Jensen and Smith method, plus original and modified King methods

| | | | | |
|---|---|---|---|---|
| Volumetric OGIP = | 222.9 | bcf | | |
| | **original King** | **modified King** | **J&S method** | |
| *A* = | 80.7 | 70.3 | na | ac |
| OGIP = | 223.2 | 196.2 | 199.7 | mmcf |
| EUR = | 156.6 | 139.9 | 141.4 | mmcf |
| Remaining reserves = | 105.0 | 88.3 | 89.8 | mmcf |
| Recovery factor = | 0.702 | 0.713 | 0.708 | |

*na=not available*

## Coal Gas Recovery Factor

The recovery factor for a reservoir fluid is defined as

$$\text{recovery factor} = \frac{\text{fluid recovered}}{\text{original fluid in place}} = \frac{\text{original fluid in place} - \text{remaining fluid}}{\text{original fluid in place}}$$

Mathematically, the gas recovery factor is

$$r = \frac{G_p}{G_i} = \frac{G_i - G_r}{G_i} = 1 - \frac{G_r}{G_i}$$

where

$r$ = recovery factor, decimal, and
$G_r$ = remaining gas, mmcf.

Original gas in place is given by equation (8.2), while remaining gas can be expressed as

$$G_r = 1.3597(10)^{-3} Ah\rho_B V_{Ldaf}(1-a-w)\frac{p}{p+p_L} + 0.04356Ah\phi(1-S_w)\frac{1}{B_g}$$

Using equation (8.7) for the gas formation volume factor, $B_g$, the equation for recovery factor can be written as

$$r = 1 - \frac{1.3597\,(10)^{-3}\,Ah\rho_B V_{Ldaf}(1-a-w)\dfrac{p}{p+p_L} + 0.04356\,Ah\phi(1-S_w)\dfrac{pZ_{sc}T_{sc}}{p_{sc}ZT}}{1.3597\,(10)^{-3}\,Ah\rho_B V_{Ldaf}(1-a-w)\dfrac{p_i}{p_i+p_L} + 0.04356\,Ah\phi_i(1-S_{wi})\dfrac{p_i Z_{sc}T_{sc}}{p_{sc}Z_i T}}$$

Rewriting both numerator and denominator and using equation (8.3) for porosity,

$$r = 1 - \frac{\dfrac{0.04356\,Ah\phi_i Z_{sc}T_{sc}}{p_{sc}T}\dfrac{p}{Z}\left[\dfrac{\rho_B V_{Ldaf}(1-a-w)p_{sc}TZ}{32.037\phi_i Z_{sc}T_{sc}(p+p_L)} + (1-S_w)\exp\left[-c_f(p_i-p)\right]\right]}{\dfrac{0.04356\,Ah\phi_i Z_{sc}T_{sc}}{p_{sc}T}\dfrac{p_i}{Z_i}\left[\dfrac{\rho_B V_{Ldaf}(1-a-w)p_{sc}TZ_i}{32.037\phi_i Z_{sc}T_{sc}(p_i+p_L)} + (1-S_{wi})\right]}$$

Employing equation (8.15),

$$r = 1 - \frac{\dfrac{p}{Z^*}}{\dfrac{p_i}{Z_i^*}} = 1 - \frac{pZ_i^*}{p_i Z^*}$$

Alternatively, on a unit reservoir volume basis, the ratio of free gas to sorbed gas, defined as $\alpha$, is

$$\alpha = \frac{\phi(1-S_w)\dfrac{pZ_{sc}T_{sc}}{p_{sc}ZT}}{\dfrac{1}{32.037}\rho_B V_{Ldaf}(1-a-w)\dfrac{p}{p+p_L}}$$

Simplifying,

$$\alpha = \frac{32.037\phi(1-S_w)Z_{sc}T_{sc}(p+p_L)}{\rho_B V_{Ldsf}(1-a-w)p_{sc}ZT} \qquad \textbf{(8.24)}$$

The equation for recovery factor can now be written as

$$r = 1 - \frac{1.3597\,(10)^{-3}\rho_B V_{Ldaf}(1-a-w)\dfrac{p}{p+p_L}(1+\alpha)}{1.3597\,(10)^{-3}\rho_B V_{Ldaf}(1-a-w)\dfrac{p_i}{p_i+p_L}(1+\alpha_i)}$$

which reduces to

$$r = 1 - \frac{p}{p_i}\frac{p_i + p_L}{p + p_L}\frac{(1+\alpha)}{(1+\alpha_i)} \tag{8.25}$$

High-rank coals often have small cleat porosities and hold substantial gas volumes in the matrix, making the ratio of free to sorbed gas much less than one. In this case, the recovery factor simplifies further to

$$r = 1 - \frac{p}{p_i}\frac{p_i + p_L}{p + p_L} \tag{8.26}$$

Gas storage in coals is described by the Langmuir isotherm, even in coals with substantial cleat porosity. Thus, intuitively, the recovery factor resembles the inverted isotherm. This behavior is seen in the following two examples.

### Example 8.7. Gas recovery factor—unidentified GRI well

Recovery factor for the unidentified GRI well can be calculated using values from table 8–1. As the initial water saturation is 100%, the ratio of free to sorbed gas at initial conditions is zero. To better understand the influence of free gas on recovery factor, its value will be maximized by assuming no porosity reduction during depletion, as described by equation (8.3), and a completely dry coal seam at abandonment, making the final water saturation zero. Use of these two assumptions and an abandonment pressure of 100 psia in equation (8.24) gives

$$\alpha = \frac{32.037(0.005)(1-0)0.9980(460+60)\,^{\circ}\mathrm{R}(100+371)\,\mathrm{psia}}{1.35\frac{\mathrm{g}}{\mathrm{cm}^3}\,747.7\,\frac{\mathrm{scf}}{\mathrm{ton}}\,(1-0.11-0.03)\,14.7\,\mathrm{psia}\,0.9911(460+130)\,^{\circ}\mathrm{R}}$$

Working through the algebra,

$$\alpha = 0.0052 = \frac{1}{191}$$

Thus, at an abandonment pressure of 100 psia, the coal holds almost 200 times more gas by sorption than as free gas in the cleats. This is a maximum bound of the value of $\alpha$; inclusion of porosity reduction and a nonzero water saturation gives smaller values. Consequently, for many practical situations, the approximate recovery factor given by equation (8.26) is quite adequate. The full recovery factor, from equation (8.25), is

$$r = 1 - \frac{100\ \mathrm{psia}}{1{,}600\ \mathrm{psia}}\frac{1{,}600 + 371\ \mathrm{psia}}{100 + 371\ \mathrm{psia}}\frac{(1+0.0052)}{(1+0)}$$

$$r = 0.737$$

And the simplified recovery factor of equation (8.26) is

$$r = 1 - \frac{100\ \mathrm{psia}}{1{,}600\ \mathrm{psia}}\frac{1{,}600 + 371\ \mathrm{psia}}{100 + 371\ \mathrm{psia}}$$

$$r = 0.738$$

These recovery factors are nearly identical to the recovery factors calculated in examples 8.1, 8.3, and 8.5 above.

Note that at an abandonment pressure roughly 6% of initial pressure, three-fourths of the initial gas in the coal has been recovered, leaving 25% remaining. In actuality, water saturation steadily decreases, and the gas deviation factor varies over the course of depletion. However, for purposes of illustration, assume a constant water saturation of 0.6 and a constant Z factor of 0.96. The resulting full recovery factor of equation (8.25) and approximate recovery factor of equation (8.26) are plotted as functions of pressure in figure 8–9. The proximity of the two curves demonstrates the validity of the approximate recovery factor given by equation (8.26) for most practical situations.

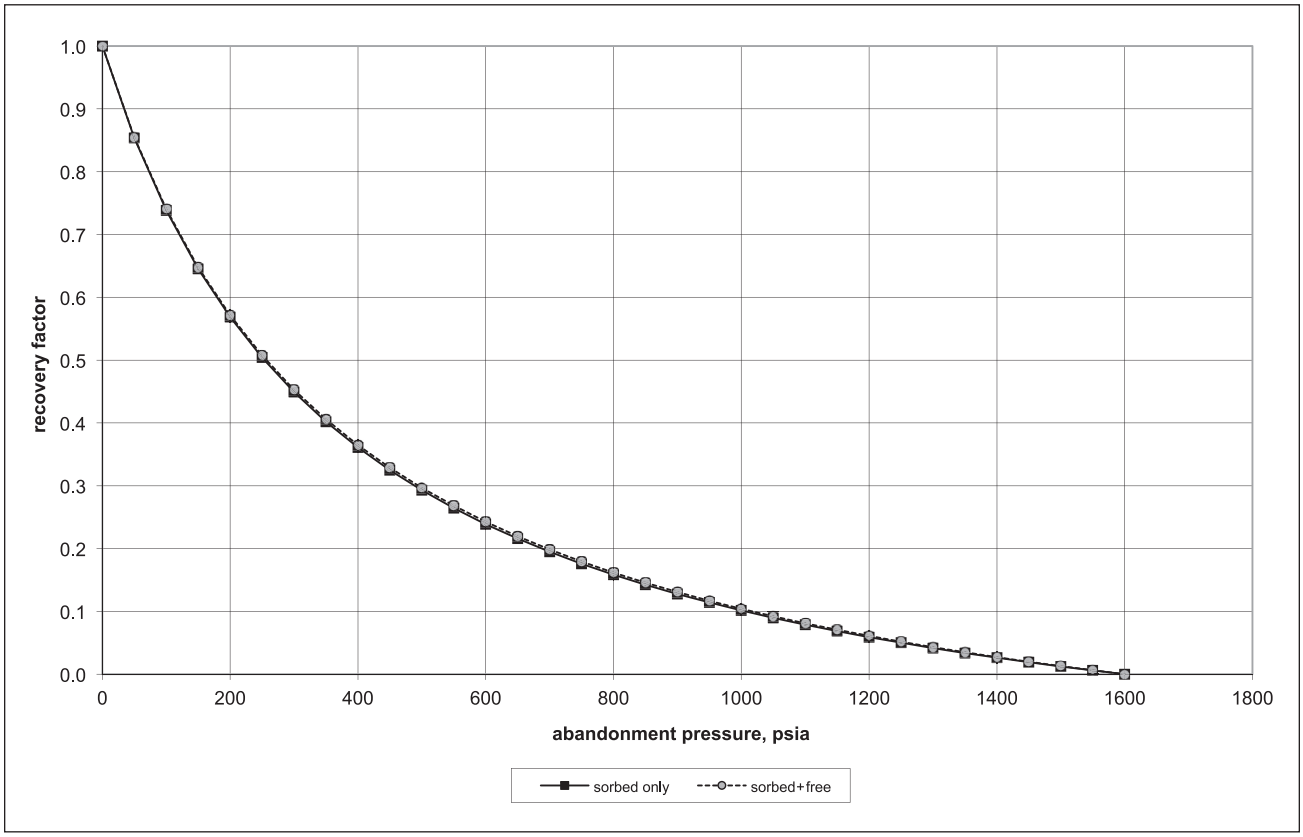



**Fig. 8–9.** Coalbed methane recovery factors—unidentified GRI well

## Example 8.8. Gas recovery factor—Canyon coal well

As a second example of coal gas recovery factor, consider the Canyon coal well of example 8.2, with coal properties given in table 8–2 and an initial water saturation of 0.95. At initial conditions, equation (8.24) gives the ratio of free to sorbed gas as

$$\alpha_i = \frac{32.037(0.1)(1-0.95)0.9980(460+60)\ ^\circ\text{R}(153+394)\ \text{psia}}{1.34\frac{\text{g}}{\text{cm}^3}117.2\frac{\text{scf}}{\text{ton}}(1-0.0392-0.2766)14.7\ \text{psia}\ 0.9799(460+65)\ ^\circ\text{R}} = 0.0560 = \frac{1}{17.9}$$

Thus, at initial conditions, the sorbed gas volume is almost 18 times larger than the free gas volume. At an abandonment pressure of 35 psia, the water saturation is 0.8116 and the ratio of free to sorbed gas is 0.1688,

implying the coal now holds 6 times as much gas by sorption as it stores in the cleats. From equation (8.25), the recovery factor at an abandonment pressure of 35 psia is

$$r = 1 \frac{35 \text{ psia}}{153 \text{ psia}} \frac{153 + 394 \text{ psia } (1 + 0.1688)}{35 + 394 \text{ psia } (1 + 0.0563)} = 0.677$$

Neglecting free gas, the simplified recovery factor of equation (8.26) is

$$r = 1 - \frac{35 \text{ psia}}{153 \text{ psia}} \frac{153 + 394 \text{ psia}}{35 + 394 \text{ psia}} = 0.708$$

These recovery factors are 1% to 2% higher than that obtained in examples 8.2, 8.4, and 8.6 above.

As in the previous example, considerable gas yet remains in the coal. At an abandonment pressure roughly one-fifth of initial pressure, over one-fourth of the gas remains in place. Both the full and approximate recovery factors for this example, calculated with the average water saturation of 0.8808, are plotted in figure 8–10. Again, the proximity of the two recovery factor curves indicates the approximate recovery factor of equation (8.26) is adequate for most practical situations. The linear behavior of the recovery factors seen in this example is due to the low pressures relative to the Langmuir pressure. Initial reservoir pressure, 153 psia, is less than one-half the Langmuir pressure, 394 psia, implying that depletion occurs over the relatively steep, nearly linear region of the sorption isotherm.

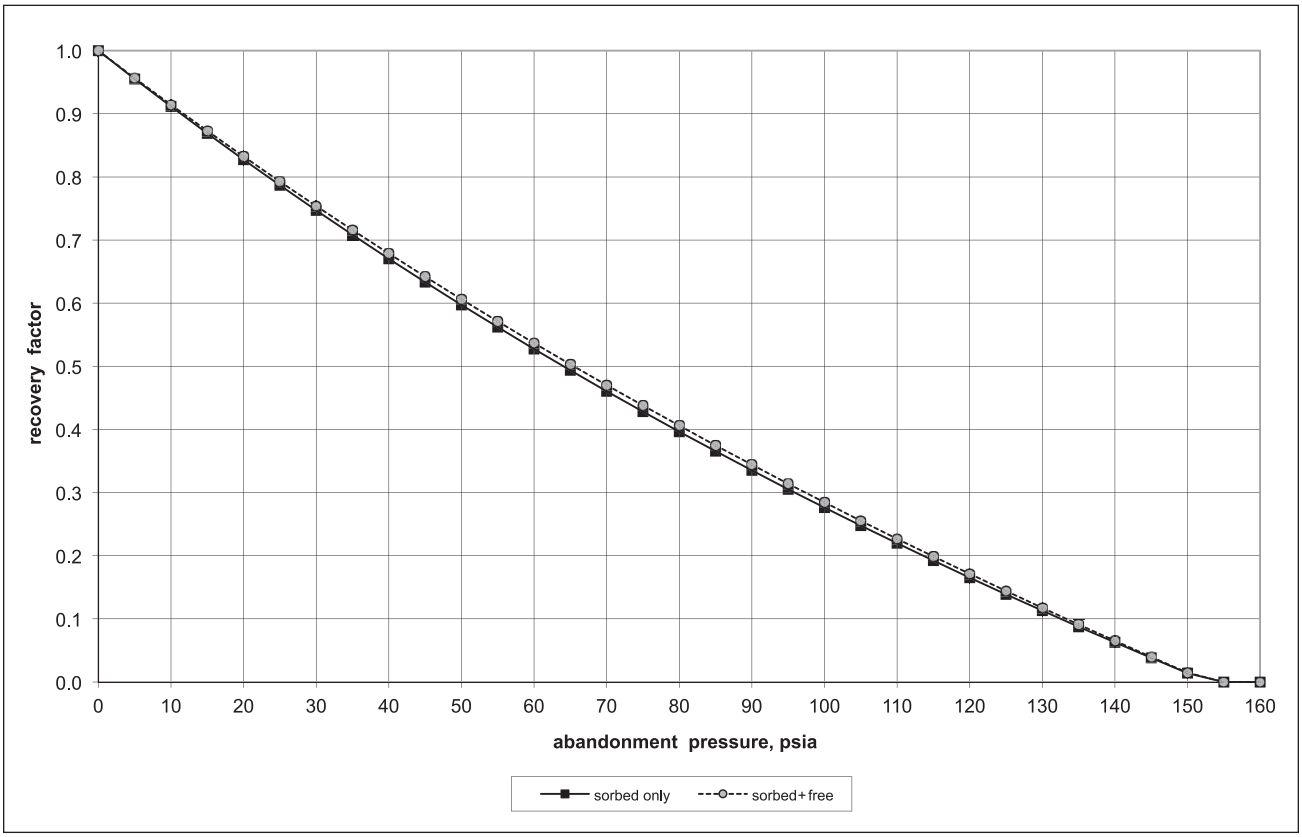



**Fig. 8–10.** Coalbed methane recovery factors—Canyon coal well

## Gas Mass Balance Equation for Undersaturated Coals

An undersaturated coal holds less gas than physically possible at current reservoir pressure and temperature. The cleats are filled with water, and reservoir pressure must be reduced by removal of water from the cleats before gas will be released from the coal matrix. The pressure at which gas begins to desorb from the coal and appear as free gas is defined as the desorption pressure, denoted as $p_d$. Desorption pressure is calculated from measured in-situ gas content, ash and equilibrium moisture, and the Langmuir isotherm constants with

$$p_d = p_L \frac{V_i}{V_{Ldaf}(1 - a - w) - V_i}$$

Free gas cannot exist in undersaturated coals. Any free gas that appears in the cleats of an undersaturated coal, for instance, biogenic gas generated by methanogens, is taken up by the matrix. Only when the matrix is saturated (at current reservoir temperature and pressure) with gas can free gas exist in the fractures. This absence of free gas complicates gas mass balance calculations in undersaturated coal deposits. Knowing the desorption pressure, original gas in place is calculated from a revised form of equation (8.2)

$$G_i = 1.3597(10)^{-3} Ah\rho_B V_{Ldaf}(1 - a - w)\frac{p_d}{p_d + p_L}$$

The mass balance equation depends on both the desorption pressure (to address sorbed gas) and initial pressure (to account for porosity changes). Once pressure in the coal deposit falls below the desorption pressure, the gas mass balance equation, equation (8.8) now becomes

$$G_p = 1.3597(10)^{-3} Ah\rho_B V_{Ldaf}(1 - a - w)\frac{p_d}{p_d + p_L} - 1.3597(10)^{-3} Ah\rho_B V_{Ldaf}(1 - a - w)\frac{p}{p + p_L} - 0.04356\, Ah\phi\left(1 - \frac{\frac{B_w(W_e - W_p)}{7758.4\, Ah\phi_i}}{\exp[-c_f(p_i - p)]}\right)\frac{pZ_{sc}T_{sc}}{p_{sc}ZT}$$

The $Z^\star$ function, equation (8.16), is defined mathematically for all pressures but only makes physical sense for pressures less than or equal to desorption pressure. Similar to fully gas saturated coals, depletion of an undersaturated coal can be described by a $p/Z^\star$ plot, which reflects the undersaturation. Equation (8.21) becomes

$$\frac{p}{Z^\star} = \frac{p_d}{Z^\star_d}\left(1 - \frac{G_p}{G_i}\right)$$

Depletion of undersaturated coals with porosities on the order of 1% can be described using the original and modified King methods, as well as that of Jensen and Smith. Equation (8.23) is now written as

$$\frac{p}{p + p_L} = \frac{p_d}{p_d + p_L}\left(1 - \frac{G_p}{G_i}\right)$$

As undersaturated coals have no free gas, the initial ratio of free gas to sorbed gas, equation (8.24), is zero. Once reservoir pressure drops below desorption pressure, gas production commences and the gas recovery factor, equation (8.25), becomes

$$r = 1 - \frac{p}{p_d}\frac{p_d + p_L}{p + p_L}(1+\alpha)$$

as the initial ratio of free to sorbed gas is zero. The approximate recovery factor of equation (8.26) becomes

$$r = 1 - \frac{p}{p_d}\frac{p_d + p_L}{p + p_L}$$

## Gas Mass Balance Equation for Multicomponent Gases

Gas held by a coal is often a mixture of several components, each with their individual sorption strength. Weakly sorbed gases are more readily released from the coal than strongly held gases, causing compositions of the free and sorbed gas mixtures to change over depletion. The volume of component $k$ sorbed onto the matrix depends on the partial pressure of that component in the free gas and is characterized by Langmuir constants $V_{Ldafk}$ and $p_{Lk}$, which are determined from laboratory sorption measurements with pure gases. Gas content of component $k$ is calculated with the extended or multicomponent Langmuir equation,

$$V_k = V_{Ldafk}(1 - a - w)\frac{\frac{py_k}{p_{Lk}}}{1 + \sum_m \frac{py_m}{p_{Lm}}} \tag{8.27}$$

where

$y_k$ = free gas mole fraction of component $k$, and
$m$ = total number of components.

Total gas content of the coal is the sum of the individual component gas contents

$$V = \sum_k V_k \tag{8.28}$$

Consequently, mass balance calculations for multicomponent systems require knowledge of free gas composition. For engineering purposes, composition of the produced gas stream is often reasonably close to the free gas composition in the reservoir and is therefore used in the above calculations without correction.

The general mass balance equation for a single component gas, equation (8.8), is readily adapted for multicomponent gas by substitution of the extended Langmuir isotherm. For a multicomponent gas, the $Z^*$ function defined by equation (8.16) becomes

$$Z^* = \frac{Z}{\frac{\rho_B(1-a-w)p_{sc}TZ}{32.037\phi_i Z_{sc}T_{sc}}\sum_k V_{Ldafk}\frac{\frac{py_k}{p_{Lk}}}{1+\sum_m \frac{py_m}{p_{Lm}}} + (1-S_w)\exp[-c_f(p_i - p)]}$$

The relation between $p/Z^*$ and produced multicomponent gas volume, equation (8.21), remains unchanged from its single-component form, allowing use of both the original, iterative King method or modified method to determine original gas in place, estimated ultimate recovery, and remaining reserves. The $Z^*$ function for a coal that holds most of the multicomponent gas by sorption as compared to free gas in the cleats is

$$Z^* = \frac{1}{\dfrac{\rho_B(1-a-w)p_{sc}T}{32.037\phi_i Z_{sc}T_{sc}}\displaystyle\sum_k V_{Ldafk}\frac{\dfrac{py_k}{p_{Lk}}}{1+\displaystyle\sum_m \frac{py_m}{p_{Lm}}}}$$

Thus, the basic equation of the Jensen and Smith modified material balance method, equation (8.23), becomes

$$\sum_k V_{Ldafk}\frac{\dfrac{py_k}{p_{Lk}}}{1+\displaystyle\sum_m \frac{py_m}{p_{Lm}}} = \sum_k V_{Ldafk}\frac{\dfrac{p_i y_{ki}}{p_{Lk}}}{1+\displaystyle\sum_m \frac{p_i y_{mi}}{p_{Lm}}}\left(1-\frac{G_p}{G_i}\right)$$

For a single-component gas, the Jensen and Smith method requires only the Langmuir pressure. In contrast, for a multicomponent gas, the method requires both the Langmuir volume and pressure constants for every component gas, as well as produced gas composition at each cumulative production point, causing the method to lose some of its practical utility.

Recovery factor for a multicomponent gas can be written

$$r = 1 - \frac{1.3597\,(10)^{-3}Ah\rho_B(1-a-w)\displaystyle\sum_k V_{Ldafk}\frac{\dfrac{py_k}{p_{Lk}}}{1+\displaystyle\sum_m \frac{py_m}{p_{Lm}}} + 0.04356\,Ah\phi(1-S_w)\dfrac{pZ_{sc}T_{sc}}{p_{sc}ZT}}{1.3597\,(10)^{-3}Ah\rho_B(1-a-w)\displaystyle\sum_k V_{Ldafk}\frac{\dfrac{p_i y_{ki}}{p_{Lk}}}{1+\displaystyle\sum_m \frac{p_i y_{mi}}{p_{Lm}}} + 0.04356\,Ah\phi_i(1-S_{wi})\dfrac{p_i Z_{sc}T_{sc}}{p_{sc}Z_i T}}$$

As with the single component recovery factor, this expression can be simplified using the multicomponent $Z^*$ function to

$$r = 1 - \frac{pZ_i^*}{p_i Z^*}$$

The ratio of free to sorbed gas, $\alpha$, for a multicomponent gas is

$$\alpha = \frac{\phi(1-S_w)\dfrac{pZ_{sc}T_{sc}}{p_{sc}ZT}}{\dfrac{1}{32.037}\rho_B(1-a-w)\displaystyle\sum_k V_{Ldafk}\frac{\dfrac{py_k}{p_{Lk}}}{1+\displaystyle\sum_m \frac{py_m}{p_{Lm}}}}$$

Simplifying,

$$\alpha = \frac{32.037\phi(1-S_w)pZ_{sc}T_{sc}}{\rho_B(1-a-w)p_{sc}ZT\sum_k V_{Ldafk}\dfrac{\dfrac{py_k}{p_{Lk}}}{1+\sum_m \dfrac{py_m}{p_{Lm}}}} \tag{8.29}$$

For an individual component *j*, this ratio is

$$\alpha_j = \frac{32.037\phi(1-S_w)pZ_{sc}T_{sc}p_{Lk}\left(1+\sum_m \dfrac{py_m}{p_{Lm}}\right)}{\rho_B(1-a-w)p_{sc}ZTV_{Ldafj}py_k} \tag{8.30}$$

Concise recovery factor equations for multicomponent gases, similar to equations (8.25) and (8.26), are based upon the extended Langmuir equation. As noted above, coals sorb some gases more strongly than others. Consequently, at a given stage of depletion, recoveries of individual species will vary. Recovery of component *j*, like sorption, depends on partial pressure. The recovery factor for species *j* can be defined as

$$r_j = 1 - \frac{G_{rj}}{G_{ij}}$$

where

$r_j$ = recovery factor of species *j*,
$G_{rj}$ = remaining species *j* gas volume, and
$G_{ri}$ = initial species *j* gas volume.

Including both sorbed and free gas terms, the full recovery factor for species *j* can be written as

$$r = 1 - \frac{1.3597\,(10)^{-3}Ah\rho_B(1-a-w)V_{Ldafj}\dfrac{\dfrac{py_j}{p_{Lj}}}{1+\sum_m \dfrac{py_m}{p_{Lm}}} + 0.04356\,Ah\phi(1-S_w)\dfrac{py_jZ_{jsc}T_{sc}}{p_{sc}Z_jT}}{1.3597\,(10)^{-3}Ah\rho_B(1-a-w)V_{Ldafj}\dfrac{\dfrac{p_i\,y_{ji}}{p_{Lj}}}{1+\sum_m \dfrac{p_iy_{mi}}{p_{Lm}}} + 0.04356\,Ah\phi_i(1-S_{wi})\dfrac{p_iy_{ji}Z_{jsc}T_{sc}}{p_{sc}Z_{ji}T}}$$

Dividing numerator and denominator by their respective sorption terms and simplifying,

$$r = 1 - \frac{\dfrac{\dfrac{py_j}{p_{Lj}}}{1+\sum_m \dfrac{py_m}{p_{Lm}}}\left(1+\dfrac{32.037\phi(1-S_w)p_{Lj}Z_{jsc}T_{sc}\left[1+\sum_m \dfrac{py_m}{p_{Lm}}\right]}{\rho_B V_{Ldafj}(1-a-w)p_{sc}Z_jT}\right)}{\dfrac{\dfrac{p_i y_{ji}}{p_{Lj}}}{1+\sum_m \dfrac{p_i y_{mi}}{p_{Lm}}}\left(1+\dfrac{32.037\phi_i(1-S_{wi})p_{Lj}Z_{jsc}T_{sc}\left[1+\sum_m \dfrac{py_{mi}}{p_{Lm}}\right]}{\rho_B V_{Ldafj}(1-a-w)p_{sc}Z_{ji}T}\right)}$$

Employing equation (8.30),

$$r = 1 - \frac{py_j}{p_i y_{ji}} \frac{\left[1+\sum_m \dfrac{py_{mi}}{p_{Lm}}\right]}{\left[1+\sum_m \dfrac{py_m}{p_{Lm}}\right]} \frac{1+\alpha_j}{1+\alpha_{ji}}$$

A more practical approach to multicomponent recovery factors is based upon gas contents alone. The recovery factor for total gas or for a specific component can be expressed as

$$r_j = 1 - \frac{V_j}{V_{ji}} \tag{8.31}$$

## Example 8.9. Multicomponent gas recovery

Reservoir properties of San Juan coal wells discussed by Zahner are collected in table 8–13.[13] Methane and $CO_2$ isotherms for San Juan Fruitland coal were reported by Arri et al., and Langmuir constants from that work are also in table 8–13.[14] Assume the initial produced gas stream from the well contains 10% $CO_2$. The multicomponent Langmuir isotherm, equation (8.27), is used to calculate initial gas content of the coal, beginning with methane.

**Table 8–13.** Example 8.9 coal properties

| | | |
|---|---|---|
| Drainage area = | 320 | ac |
| Coal thickness = | 50 | ft |
| Porosity = | 0.005 | fraction |
| Coal density = | 1.40 | g/cm$^3$ |
| Initial pressure = | 1600 | psia |
| Coal temperature = | 108 | °F |
| Ash = | 0.23 | fraction |
| Moisture = | 0.02 | fraction |
| Initial $CO_2$ in free gas = | 0.1 | fraction |
| Methane $V_{Ldaf}$ = | 908.4 | scf/ton |
| Methane $p_L$ = | 362.3 | psia |
| $CO_2$ $V_{Ldaf}$ = | 1,350.1 | scf/ton |
| $CO_2$ $p_L$ = | 204.5 | psia |

*Source:* Zahner, R. 1997; and Arri, L. E., et al. 1992.

$$V_k = V_{Ldafk}(1 - a - w)\frac{\frac{py_k}{p_{Lk}}}{1 + \sum_m \frac{py_m}{p_{Lm}}}$$

$$V_{meth} = 908.4\,\frac{\text{scf}}{\text{ton}}(1 - 0.23 - 0.02)\frac{\frac{1{,}600\text{ psia}\,(0.9)}{362.3\text{ psia}}}{1 + \frac{1{,}600\text{ psia}\,(0.9)}{362.3\text{ psia}} + \frac{1{,}600\text{ psia}\,(0.1)}{204.5\text{ psia}}}$$

$$V_{meth} = 470.4\,\frac{\text{scf}}{\text{ton}}$$

Similarly for $CO_2$,

$$V_{CO_2} = 1{,}350.1\,\frac{\text{scf}}{\text{ton}}(1 - 0.23 - 0.02)\frac{\frac{1{,}600\text{ psia}\,(0.1)}{204.5\text{ psia}}}{1 + \frac{1{,}600\text{ psia}\,(0.9)}{362.3\text{ psia}} + \frac{1{,}600\text{ psia}\,(0.1)}{204.5\text{ psia}}}$$

$$V_{CO_2} = 137.6\,\frac{\text{scf}}{\text{ton}}$$

Using equation (8.28) for total gas content

$$V = \sum_k V_k = 470.4 + 137.6\,\frac{\text{scf}}{\text{ton}} = 608.0\,\frac{\text{scf}}{\text{ton}}$$

Note that although the initial $CO_2$ fraction in the free gas is 10%, the initial $CO_2$ sorbed fraction is 23%. Initial gas in place for this well is 18.517 bcf, with 14.326 bcf methane and 4.191 bcf $CO_2$.

These isotherms are used in example 10.7 to illustrate gas composition variation over depletion. Detailed free and sorbed gas compositions are discussed there. From that example, after reservoir pressure is halved to 800 psia, methane and $CO_2$ gas contents are 394 and 129 scf/ton, respectively, making total gas content 523 scf/ton. The total gas recovery, from equation (8.30), is

$$r_{total} = 1 - \frac{523\,\frac{\text{scf}}{\text{ton}}}{608\,\frac{\text{scf}}{\text{ton}}} = 0.140$$

As coal sorbs $CO_2$ more strongly than it does methane, intuitively methane recovery should initially be higher than that of $CO_2$. Calculating component recovery factors,

$$r_{meth} = 1 - \frac{394.0 \frac{scf}{ton}}{470.4 \frac{scf}{ton}} = 0.162$$

$$r_{CO_2} = 1 - \frac{129 \frac{scf}{ton}}{137.6 \frac{scf}{ton}} = 0.063$$

These calculations indicate that when reservoir pressure is one-half depleted, methane recovery is roughly three times that of $CO_2$.

When one-half the initial gas in place has been recovered, reservoir pressure has fallen to 213 psia. Of the 304 scf/ton sorbed gas remaining, 204 scf/ton is methane and 100 scf/ton is $CO_2$. Individual component recovery factors are

$$r_{meth} = 1 - \frac{204 \frac{scf}{ton}}{470.4 \frac{scf}{ton}} = 0.566$$

$$r_{CO_2} = 1 - \frac{100 \frac{scf}{ton}}{137.6 \frac{scf}{ton}} = 0.273$$

Thus, over one-half the initial methane in place has been recovered, but only one-fourth of the $CO_2$ has been produced. Current sorbed gas is only two-thirds methane (204/304 = 0.671), and although remaining gas in place for this well is 9.259 bcf, remaining methane reserves are 6.213 bcf.

Estimation of reserve volumes should include compositional effects. As discussed above, initial gas in place for this well is 18.5 bcf, but only 14.3 bcf is methane, a difference of 4.2 bcf. Anecdotal evidence suggests many San Juan wells such as the one discussed in this example are currently being produced at very low reservoir pressures, perhaps 100 psia or less. For the purposes of this example, assume an abandonment pressure of 100 psia. Total gas content at abandonment is 192 scf/ton, of which 112 scf/ton is methane and 80 scf/ton is $CO_2$. Abandoned total gas in place is 5.8 bcf, and abandoned methane is 3.4 bcf. Estimated ultimate recovery for this well is therefore 18.5 bcf – 5.8 bcf = 12.7 bcf. Methane EUR of this well is 14.3 bcf – 3.4 bcf = 10.9 bcf, a difference of 12.7 bcf – 10.9 bcf = 1.8 bcf. At the time of this writing, in-ground reserves were being valued at \$1/mcf. Assuming the gas volumes in this example are proved reserves, the 1.8 bcf difference between total and methane EURs is approximately \$1.8 million.

From above, when one-half the gas has been recovered and reservoir pressure drops to 213 psia, current total gas in place is 9.3 bcf, with 6.2 bcf being methane. Again assuming an abandonment pressure of 100 psia, this well would be expected to produce an additional 9.3 bcf – 5.8 bcf = 3.5 bcf, and the methane EUR would be 6.2 bcf – 3.4 bcf = 2.8 bcf, which is 0.7 bcf less. Using the valuation rule-of-thumb of \$1/mcf for in-ground reserves, value of the remaining reserves falls by roughly \$700,000.

# Nomenclature

| | |
|---|---|
| $A$ | Drainage area, ac |
| $a$ | Ash fraction, decimal |
| $B_g$ | Gas formation volume factor, ft$^3$/scf |
| $B_w$ | Water formation volume factor, bbl/stb |
| $c_f$ | Cleat volume compressibility, psia$^{-1}$ |
| $c_w$ | Water compressibility, psia$^{-1}$ |
| $G_i$ | Initial gas in place, mmcf |
| $G_p$ | Produced gas, mmcf |
| $G_r$ | Remaining gas, mmcf |
| $h$ | Coal thickness, ft |
| $m$ | Slope of $p/Z^\star$ plot, psia/mmcf |
| $n$ | Number of moles |
| $p$ | Pressure, psia |
| $p_d$ | Desorption pressure, psia |
| $p_L$ | Langmuir pressure constant, psia |
| $r$ | Recovery factor, decimal |
| $R$ | Universal gas constant, psia-ft$^3$/(lb-mol-°R) |
| $T$ | Temperature, °R |
| $S_w$ | Water saturation, decimal |
| $v$ | Gas volume in ft$^3$ |
| $V$ | Sorbed gas volume in scf/ton |
| $V_{Ldaf}$ | Dry, ash-free Langmuir volume constant, scf/ton |
| $w$ | Equilibrium moisture, decimal |
| $W_e$ | Water influx, stb |
| $W_p$ | Produced water, stb |
| $Z$ | Gas deviation factor |
| $Z^\star$ | King $Z^\star$ function, equation (8.16), dimensionless |

## Greek

| | |
|---|---|
| $\alpha$ | Ratio of free gas to sorbed gas, equation (8.24), dimensionless |
| $\rho_B$ | Bulk density, g/cm$^3$ |
| $\phi$ | Porosity, decimal |

## Subscripts

| | |
|---|---|
| $i$ | Initial |
| $sc$ | Standard conditions |

# References


1. McKee, C. R., Bumb, A. C., and Koenig, R. A. 1988. Stress-dependent permeability and porosity of coal and other geologic formations. *Society of Petroleum Engineers Formation Evaluation*. March. p. 81.
2. King, G. R. 1990. *Material Balance Techniques for Coal Seam and Devonian Shale Gas Reservoirs*. Paper SPE 20730. Presented at the 65th Annual Technical Conference and Exhibition, New Orleans, Louisiana, September 23–26.
3. Gas Research Institute. 1996. *A Guide to Coalbed Methane Reservoir Engineering*. GRI Reference No. GRI-94/0397. Chicago: Gas Research Institute.
4. Ibid.
5. Nelson, C. R., Hill, D. G., and Pratt, T. J. 2000. *Properties of Paleocene Fort Union Formation Canyon Seam Coal at the Triton Federal Coalbed Methane Well, Campbell County, Wyomin*g. Paper SPE 59786. Presented at the SPE/CERI Gas Technology Conference, Calgary, AB, April 3–5.
6. Bustin, R. M., and Clarkson, C. R. 1999. *Free Gas Storage in Matrix Porosity: A Potentially Significant Coalbed Resource in Low Rank Coals*. Paper 9956. Presented at the International Coalbed Methane Symposium, University of Alabama, Tuscaloosa, Alabama, May.
7. Nelson, C. R., et al. 2000; and Bustin, R. M, and Clarkson, C. R. 1999.
8. Gas Research Institute. 1996.
9. Nelson, C. R., et al. 2000; and Bustin, R. M, and Clarkson, C. R. 1999.
10. Seidle, J. P. 1999. *A Modified p/Z Method for Coal Wells*. Paper SPE 55605. Presented at the SPE Rocky Mountain Regional Meeting, Gillette, Wyoming, May 15–18.
11. Gas Research Institute. 1996.
12. Jensen, D., and Smith, L. K. 1997. *A Practical Approach to Coalbed Methane Reservoir Prediction Using a Modified Material Balance Technique*. Paper 9765. Proceedings of the 1997 International Coalbed Methane Symposium, The University of Alabama, Tuscaloosa, Alabama, pp. 105–113.
13. Zahner, R. 1997. *Application of Material Balance to Determine Ultimate Recovery of a San Juan Fruitland Coal Well*. Paper SPE 38858. Presented at the Annual Technical Conference and Exhibition, San Antonio, Texas, October 5–8.
14. Arri, L. E., Yee, D., Morgan, W. D., and Jeansonne, M. W. 1992. *Modeling Coalbed Methane Production with Binary Gas Sorption*. Paper SPE 24363. Presented at the SPE Rocky Mountain Regional Meeting, Casper, Wyoming, May 18–21.

# Gas and Water Flow in Coals 9

## Introduction

Most coal deposits contain both free gas and water. Many coals are aquifers, and wells completed in them initially produce substantial amounts of water and very little gas. This is especially true of undersaturated coals. As production continues, gas and water saturations in the coal change continuously until, ultimately, the deposit is dewatered and the wells often produce at high gas-water ratios. Fluid flow in coal deposits is a two-phase phenomenon. However, at a given instant during depletion, insight into gas and water production can be obtained from single-phase, classical Darcy's law flow rate equations due to slowly varying gas and water saturations over time and space. Beginning with derivation of a general equation for gas flow in coal, traditional constant gas rate solutions for bottomhole pressure in infinite and bounded gas-filled coal are presented. Similar equations for water flow are given.

## Gas Flow in Coal Seams

Gas flow in coal cleats can be described by the real gas pseudopressure developed by Al-Hussainy et al. for dry, volumetric gas reservoirs.[1] Following the development of Seidle, consider a coal deposit at irreducible water saturation.[2] The continuity equation for gas flow in the cleats of a unit volume of coal can be written as

$$\rho F + \nabla \bullet [\rho v] = -\phi_f \frac{\partial \rho}{\partial t} \tag{9.1}$$

where

$\rho$ = gas density,
$F$ = the rate of gas flux out of the matrix into the cleat,
$\nabla$ = Laplacian or gradient operator,
$v$ = gas velocity vector,
$\phi_f$ = cleat porosity, and
$t$ = time.

Darcy's law relates gas velocity and the gradient of pressure as

$$v = -\frac{k_g}{\mu_g} \nabla p$$

where

$k_g$ = effective permeability to gas, and
$\mu_g$ = gas viscosity.

Thus equation (9.1) becomes

$$\nabla\bullet\left[p(-\frac{k_g}{\mu_g}\nabla p)\right] = -\phi_f\frac{\partial\rho}{\partial t} - \rho q \tag{9.2}$$

Assuming the coal is filled with a real gas,

$$\rho = \frac{M}{RT}\left(\frac{p}{Z}\right)$$

where

$M$ = molecular weight,
$R$ = the universal gas constant,
$T$ = absolute temperature, and
$Z$ = gas deviation factor.

Substituting for density in equation (9.2) yields

$$\nabla\bullet\left[\frac{M}{RT}\frac{p}{Z}\left(-\frac{k_g}{\mu_g}\nabla p\right)\right] = -\phi_f\frac{\partial}{\partial t}\left(\frac{M}{RT}\frac{p}{Z}\right) - \rho F$$

Assuming an isothermal coal seam with constant effective permeability to gas, this simplifies to

$$-\frac{M}{RT}k_g\nabla\bullet\left[\frac{p}{\mu_g Z}\nabla p\right] = -\frac{M}{RT}\phi_f\frac{\partial}{\partial t}\left(\frac{p}{Z}\right) - \rho F \tag{9.3}$$

Using Langmuir's equation, gas sorbed per unit volume of coal can be expressed as

$$V = V_{Lis}\frac{p}{p + p_L}\rho_B \tag{9.4}$$

where

$V$ = gas content of the coal,
$V_{Lis}$ = in-situ Langmuir volume constant,
$p_L$ = Langmuir pressure constant, and
$\rho_B$ = bulk coal density.

The in-situ Langmuir volume constant is related to the dry, ash-free volume constant by

$$V_{Lis} = V_{Ldaf}(1 - a - w)$$

where

$V_{Ldaf}$ = dry, ash-free Langmuir volume constant, scf/ton,
$a$ = ash fraction, and
$w$ = equilibrium moisture fraction.

Gas flux from matrix to cleat, at standard temperature and pressure, is

$$F_{sc} = \frac{\partial V}{\partial t} = \frac{\partial V}{\partial p}\frac{\partial p}{\partial t}$$

where

$F_{sc}$ = gas flux at standard conditions.

Substitution of (9.4) into this equation yields

$$F_{sc} = \rho_B V_{Lis} \frac{p_L}{(p + p_L)^2}\frac{\partial p}{\partial t} \tag{9.5}$$

From the real gas law in the form

$$pV_g = ZnRT$$

where

$V_g$ = gas volume,

matrix gas flux at reservoir and standard conditions is related by

$$\frac{pF}{ZT} = \frac{p_{sc}F_{sc}}{Z_{sc}T_{sc}}$$

or

$$F = \frac{p_{sc}ZT}{pZ_{sc}T_{sc}}F_{sc}$$

Substitution of equation (9.5) into the above yields

$$F = \frac{p_{sc}ZT}{pZ_{sc}T_{sc}}\rho_B V_{Lis}\frac{p_L}{(p + p_L)^2}\frac{\partial p}{\partial t}$$

Using this equation for gas flux from matrix to cleat and the real gas law for density in equation (9.3) gives

$$-\frac{M}{RT}k_g \nabla\bullet\left[\frac{p}{\mu_g Z}\nabla p\right] = -\frac{M}{RT}\phi_f\frac{\partial}{\partial t}\left(\frac{p}{Z}\right) - \frac{M}{RT}\frac{p}{Z}\frac{p_{sc}ZT}{pZ_{sc}T_{sc}}\rho_B V_{Lis}\frac{p_L}{(p + p_L)^2}\frac{\partial p}{\partial t}$$

Simplifying,

$$k_g \nabla\bullet\left[\frac{p}{\mu_g Z}\nabla p\right] = \phi_f\frac{\partial}{\partial t}\left(\frac{p}{Z}\right) + \frac{p_{sc}T}{Z_{sc}T_{sc}}\rho_B V_{Lis}\frac{p_L}{(p + p_L)^2}\frac{\partial p}{\partial t} \tag{9.6}$$

This expression can be simplified further beginning with the definition of isothermal gas compressibility

$$c_g = \frac{1}{\rho}\frac{\partial \rho}{\partial p}$$

where

$c_g$ = isothermal gas compressibility.

As coal gas has been assumed to behave as a real gas,

$$c_g = \frac{1}{\frac{M}{RT}\frac{p}{Z}} \frac{\partial}{\partial p}\left(\frac{M}{RT}\frac{p}{Z}\right) = \frac{1}{\frac{p}{Z}} \frac{\partial}{\partial p}\left(\frac{p}{Z}\right)$$

Rearranging,

$$c_g \frac{p}{Z} = \frac{\partial}{\partial p}\left(\frac{p}{Z}\right) \tag{9.7}$$

Using the chain rule to evaluate the derivative,

$$\frac{\partial}{\partial t}\left(\frac{p}{Z}\right) = \frac{\partial}{\partial p}\left(\frac{p}{Z}\right)\frac{\partial p}{\partial t}$$

or, from equation (9.7),

$$\frac{\partial}{\partial t}\left(\frac{p}{Z}\right) = c_g\left(\frac{p}{Z}\right)\frac{\partial p}{\partial t}$$

Substituting this in the first term on the right-hand side of equation (9.6)

$$k_g \nabla \bullet \left[\frac{p}{\mu_g Z}\nabla p\right] = \phi_f c_g \left(\frac{p}{Z}\right)\frac{\partial p}{\partial t} + \frac{p_{sc}T}{Z_{sc}T_{sc}}\rho_B V_{Lis}\frac{p_L}{(p+p_L)^2}\frac{\partial p}{\partial t} \tag{9.8}$$

Real gas pseudopressure was defined by Al-Hussainy et al. as[3]

$$m(p) = 2\int_{p_b}^{p}\frac{p}{\mu_g Z}\,dp$$

where

$m(p)$ = real gas pseudopressure, and
$p_b$ = an arbitrary base pressure.

Differentiating with respect to time using the chain rule gives

$$\frac{\partial m(p)}{\partial t} = \frac{\partial m(p)}{\partial p}\frac{\partial p}{\partial t} = \frac{2p}{\mu_g Z}\frac{\partial p}{\partial t}$$

And equation (9.8) can be written as

$$k_g \nabla \bullet \left[\frac{1}{2}\nabla m(p)\right] = \frac{1}{2}\phi_f c_g \mu_g \frac{\partial m(p)}{\partial t} + \frac{p_{sc}T}{Z_{sc}T_{sc}}\rho_B V_{Lis}\frac{p_L}{(p+p_L)^2}\frac{\mu_g Z}{2p}\frac{\partial m(p)}{\partial t}$$

which simplifies to

$$\nabla^2 m(p) = \frac{\phi_f \mu_g}{k_g}\left[c_g + \frac{p_{sc}TZ}{pZ_{sc}T_{sc}}\frac{\rho_B V_{Lis}}{\phi_f}\frac{p_L}{(p+p_L)^2}\right]\frac{\partial m(p)}{\partial t} \tag{9.9}$$

For a real gas, the gas formation volume factor can be expressed as

$$B_g = \frac{p_{sc} Z T}{p Z_{sc} T_{sc}}$$

where

$B_g$ = gas formation volume factor.

Substitution of this expression into equation (9.9) yields

$$\nabla^2 m(p) = \frac{\phi_f \mu_g}{k_g} \left[ c_g + \frac{B_g \rho_B V_{Lis}}{\phi_f} \frac{p_L}{(p + p_L)^2} \right] \frac{\partial m(p)}{\partial t}$$

This equation is similar to that of Al-Hussainy et al. for describing real gas flow in conventional reservoirs.[4] The extra term added to gas compressibility represents an apparent compressibility due to sorption of gas by the coal. Defining sorption compressibility, $c_s$, as

$$c_s = \frac{B_g V_{Lis} \rho_B p_L}{\phi_f (p + p_L)^2} \tag{9.10}$$

the basic equation for gas flow in a coal can be expressed as

$$\nabla^2 m(p) = \frac{\phi_f \mu_g}{k_g} [c_g + c_s] \frac{\partial m(p)}{\partial t} \tag{9.11}$$

Seidle demonstrated the equivalence of this pseudopressure formulation for coal gas flow and the classical liquid flow solution using the results of a Warrior Basin simulation.[5] Definition of dimensionless time, $t_D$, included sorption compressibility:

$$t_D = \frac{2.637(10)^{-3} k_g t}{\phi_f \mu_g (c_g + c_s) r_w^2} \tag{9.12}$$

where

$k_g$ = permeability, md,
$t$ = time, hr,
$\mu_g$ = gas viscosity, cp,
$c_g$ = gas compressibility, psia$^{-1}$,
$c_s$ = sorption compressibility, psia$^{-1}$, and
$r_w$ = wellbore radius, ft.

In metric units, this dimensionless time is

$$t_D = \frac{0.4117(10)^{-3} k_g t}{\phi_f \mu_g (c_g + c_s) r_w^2}$$

where

$k_g$ = permeability, md,
$t$ = time, hr,
$\mu_g$ = gas viscosity, cp,
$c_g$ = gas compressibility, MPa$^{-1}$,
$c_s$ = sorption compressibility, MPa$^{-1}$, and
$r_w$ = wellbore radius, m.

Gas flow rate was calculated from

$$q_g = \frac{k_g h\left(m(p_R) - m(p_{wf})\right)}{1422\,T\left[\ln\frac{r_e}{r_w} - 0.75 + s\right]} \tag{9.13}$$

where

$q_g$ = gas flow rate, mcfd,
$h$ = coal seam thickness, ft,
$p_R$ = average reservoir pressure, psia,
$p_{wf}$ = bottomhole flowing pressure, psia,
$T$ = coal seam temperature, °R,
$r_e$ = external radius, ft, and
$s$ = wellbore skin factor, dimensionless.

In metric units, the gas flow equation is

$$q_g = \frac{k_g h\left(m(p_R) - m(p_{wf})\right)}{1.310\,T\left[\ln\frac{r_e}{r_w} - 0.75 + s\right]}$$

where

$q_g$ = gas flow rate, $E^3m^3$/day,
$h$ = coal seam thickness, m,
$p_R$ = average reservoir pressure, MPa,
$p_{wf}$ = bottomhole flowing pressure, MPa,
$T$ = coal seam temperature, K,
$r_e$ = external radius, m,
$r_w$ = wellbore radius, m, and
$s$ = wellbore skin factor, dimensionless.

Similar to the results of Al-Hussainy et al. and Al-Hussainy and Ramey for conventional gas reservoirs, equation (9.13) does not represent an exact solution to the flow of gas through a coal deposit but is a useful engineering approximation for many practical situations.[6]

As discussed in chapter 7, sorption compressibility can be quite large compared to coal, water, and gas compressibilities, often dominating system compressibility. Consequently, pressure perturbations travel more slowly through a coal deposit than a conventional gas reservoir. Earlougher discussed time required for a well to respond to such a perturbation and to establish (or reestablish) boundary-dominated or pseudosteady-state flow in terms of a dimensionless time based on drainage area defined as[7]

$$t_{DA} = \frac{2.637(10)^{-4}\,k_g t}{\phi\mu_g c_g \pi r_e^2} = \frac{2.637(10)^{-4}\,k_g t}{\phi_f \mu_g c_g\, 43{,}560A}$$

where

$A$ = drainage area, ac.

Pseudosteady-state flow, also called *boundary-dominated flow*, occurs only in bounded wells and commences at a dimensionless time of approximately 0.1 for circular and square drainage areas and often much longer for other drainage areas.[8] For coal wells, influenced by sorption compressibility, this equation becomes

$$t_{DA} = \frac{2.637(10)^{-4}\, k_g t}{\phi_f \mu_g (c_g + c_s)43{,}560A}$$

Assuming $t_{DA} = 0.1$ and solving for time required to reach boundary-dominated flow,

$$t_{pss} = \frac{0.1\phi_f \mu_g (c_g + c_s)43{,}560A}{2.637(10)^{-4}\, k_g} = 1.652(10)^7 \frac{\phi_f \mu_g (c_g + c_s)A}{k_g} \quad \textbf{(9.14)}$$

As seen in the following examples, sorption compressibility significantly increases time required for a coal well to reach pseudosteady-state flow compared to a conventional gas well.

## Example 9.1. Time to pseudosteady-state flow

Time to reach pseudosteady-state flow ($t_{pss}$) for wells completed in coals from the San Juan, Warrior, and Powder River basins will be calculated assuming each well is completed in a single, homogeneous coal seam. Reservoir properties of San Juan, Warrior, and Powder River coal wells are collected in table 9–1.[9]

**Table 9–1.** Example 9.1—coal properties and time to reach pseudosteady-state flow—San Juan, Warrior, and Powder River basins

| | San Juan | Warrior | Powder River |
|---|---|---|---|
| Drainage area, ac = | 320 | 40 | 80 |
| Porosity, fraction = | 0.02 | 0.019 | 0.03 |
| Assumed coal density, g/cm$^3$ = | 1.75 | 1.50 | 1.34 |
| Permeability to gas, md = | 1.2 | 1 | 300 |
| Reservoir pressure, psia = | 1,537 | 440 | 153 |
| Coal temperature, °F = | 120 | 70 | 65 |
| $V_L$ in-situ, scf/ton = | 783 | 616 | 80.2 |
| $p_L$, psia = | 606 | 147 | 394 |
| $B_g$, ft$^3$/scf = | 9.41E–03 | 3.21E–02 | 9.48E–02 |
| Gas viscosity, cp = | 0.0148 | 0.0118 | 0.0113 |
| $c_g$, psia$^{-1}$ = | 7.03E–04 | 2.40E–03 | 6.67E–03 |
| $c_s$, psia$^{-1}$ = | 2.66E–03 | 2.08E–02 | 1.40E–02 |
| $c_t$, psia$^{-1}$ = | 3.36E–03 | 2.32E–02 | 2.06E–02 |
| $t_{pss}$, hr = | 4,382 | 3,424 | 30.7 |
| $t_{pss}$, days = | 183 | 143 | 1.3 |

*Source:* Mavor, M. J., and Robinson, J. R. 1993; GRI 1996; Zuber, M. D., et al. 1989; Nelson, C. R., et al. 2000; and Hower, T. L., et al. 2003.

The San Juan coal properties were acquired as part of a research effort to understand cavity completions at the COAL site.[10] Interference testing of the wells was reported by Mavor and Robinson.[11] From properties listed in table 9–1, where a density of 1.75 g/cm$^3$ was assumed, and equation (9.10), sorption compressibility for the San Juan coal is

$$c_s = \frac{B_g V_{Lis} \rho_B p_L}{\phi_f (p + p_L)^2}$$

$$c_s = \frac{9.41(10)^{-3}\,\frac{\text{ft}^3}{\text{scf}}\,783\,\frac{\text{scf}}{\text{ton}}\,1.75\,\frac{\text{g}}{\text{cm}^3}\,606\text{ psia}}{32.037\,\frac{\text{g}-\text{ft}^3}{\text{ton}-\text{cm}^3}\,(0.02)(1{,}537+606)^2\text{ psia}^2} = 2.66(10)^{-3}\text{ psia}^{-1}$$

Note that sorption compressibility is nearly four times larger than gas compressibility for this example. From equation (9.14),

$$t_{pss} = 1.652(10)^7\,\frac{\phi_f \mu_g (c_g + c_s) A}{k_g}$$

$$t_{pss} = 1.652(10)^7\,\frac{0.02(0.0148\text{cp})(7.03(10)^{-4} + 2.66(10)^{-3})\text{psia}^{-1}\ 320\text{ ac}}{1.2\text{ md}}$$

$$t_{pss} = 4{,}385\text{ hr} = 183\text{ days}$$

Thus, it takes six months for this well to reach boundary-dominated flow after a perturbation such as a rate change or shut-in. If this was a conventional gas reservoir, sorption compressibility would vanish and time to reach pseudosteady-state flow would be 917 hr, about 38 days, shorter by a factor of about five, approximately the ratio of sorption to gas compressibilities.

Coal well performance at the Rock Creek Project in the Warrior Basin of Alabama was discussed by Zuber et al.[12] A multiwell, multilayer simulation model, calibrated with early-time production data, was used to investigate long-term production behavior and well interference. Using reservoir properties presented in table 9–1, where a coal density of 1.50 g/cm$^3$ was assumed, sorption compressibility for this coal is

$$c_s = \frac{3.21(10)^{-2}\,\frac{\text{ft}^3}{\text{scf}}\,616\,\frac{\text{scf}}{\text{ton}}\,1.5\,\frac{\text{g}}{\text{cm}^3}\,147\text{ psia}}{32.037\,\frac{\text{g}-\text{ft}^3}{\text{ton}-\text{cm}^3}\,(0.019)(440+147)^2\text{ psia}^2} = 2.08(10)^{-2}\text{ psia}^{-1}$$

Absolute permeability of this coal was 10 md, but neither Zuber et al. nor GRI discussed effective permeability to gas in this project.[13] From Warrior Basin coal gas-water relative permeability curves measured by Gash and water saturation estimates from Zuber and GRI of 0.1, a reasonable gas relative permeability for these wells is 0.1.[14] Thus, time to reach pseudosteady-state flow is

$$t_{pss} = 1.652(10)^7\,\frac{0.019(0.0118\text{ cp})(2.4(10)^{-3} + 2.08(10)^{-2})\text{psia}^{-1}\ 40\text{ ac}}{10\text{ md }0.1}$$

$$t_{pss} = 3{,}437\text{ hr} = 143\text{ days}$$

That is, time to reach boundary-dominated flow is five months. If this were a conventional gas reservoir, without sorption, time to reach pseudosteady-state would be 355 hr, quicker by almost an order of magnitude.

Using coal properties from Nelson et al. and Hower et al., time required for a Powder River Basin well to reach pseudosteady-state flow is 31 hr, less than 1.5 days.[15] Neglecting sorption compressibility, pseudosteady-state flow commences at 10 hr. These times are much smaller than those of San Juan and Warrior wells due to much larger permeability and smaller drainage area.

## Characteristic Times for Sorption and Darcy Flow

Production of gas from a coal deposit is a two-step process. Desorption of gas from the matrix into the cleat is followed by Darcy flow of gas in the cleats to the wellbore. The slower of these two processes will control coal well performance. Gas desorption from coal matrix is often described mathematically by diffusion equations, as was done in chapters 2 and 4. The rapidity of gas release from a coal in response to a pressure change is quantified by the diffusivity, defined as the diffusion coefficient divided by the square of the particle radius, or the sorption time. Utilizing results from chapter 2, time required to desorb 95% of the gas in response to a pressure perturbation is given by

$$t_{95} = \frac{0.253118}{\frac{D}{r_p^2}}$$

where

$t_{95}$ = time required to desorb 95% of the gas, hr,
$D$ = gas diffusion constant, ft$^2$/hr, and
$r_p$ = coal particle radius, ft.

Alternatively, time required to desorb 95% of the gas and sorption time, defined in chapter 2 as the time required to desorb 63.2% of the gas, are related by

$$t_{95} = 4.54\tau \tag{9.15}$$

where

$\tau$ = sorption time, hr.

Sorption time at the COAL site in the San Juan Basin was 4 hr.[16] Consequently, time to desorb 95% of the gas is

$$t_{95} = 4.54(4 \text{ hr}) = 18.16 \text{ hr}$$

After any change in well operating conditions, such as a shut-in, desorption from the matrix reaches equilibrium in 18 hr, whereas Darcy flow in the cleat requires 4,385 hr to attain boundary-dominated flow. Darcy flow, almost 250 times slower than the sorption in this example, will control well behavior.

Sorption time of Warrior Basin coals at the Rock Creek site was initially reported to be 60 days but was later reduced to 10 days.[17] Using this latter value, time required for desorption to reach 95% of equilibrium is

$$t_{95} = 4.54(10 \text{ days}) = 45.4 \text{ days} = 1{,}090 \text{ hr}$$

This time is about one-third the time required for the well to reach pseudosteady-state flow, implying production behavior of this well is controlled by Darcy flow of gas in the cleats rather than desorption of gas off the matrix.

Both Nelson et al. and Hower et al. report sorption time of Powder River coal to be 50 hr.[18] Thus, time required for the matrix to equilibrate to a pressure disturbance is

$$t_{95} = 4.54(50 \text{ hr}) = 227 \text{ hr}$$

This time is longer by a factor of seven than the 32 hr required to reach pseudosteady-state flow. Curiously, gas production from Powder River coal wells is adequately described by Darcy's law, implying desorption does not control well performance, contradicting the above calculation.

Simulation studies have investigated the influence of sorption time on coal well performance. Remner et al. matched gas and water production from a single well draining an unidentified coal seam.[19] The model assumed a constant flowing bottomhole pressure, a no-flow external boundary, and quasisteady-state desorption. Time for the well to attain boundary-dominated flow, calculated from equation (9.14), was 20 days. Sorption times employed by Remner et al. ranged from $0.5(10)^7$ to $8(10)^7$ sec.[20] Corresponding times for 95% gas desorption are 263 to 4,204 days, longer than the time to reach boundary-dominated flow by an order of magnitude. Although the limiting case of infinitely fast desorption was not addressed, the gas production profile was relatively unaffected by sorption time. Only at very large values of sorption times, corresponding to 95% desorption times of three years or greater, was gas production noticeably suppressed.

Sawyer et al. simulated performance of single, bounded coal wells draining Warrior and San Juan coals to identify controls on gas production.[21] The Warrior Basin well drained 80 ac and, from equation (9.14), required 34 days to reach pseudosteady-state flow. Gas production from this well was simulated using sorption times of 30, 100, and 300 days (95% desorption times were 136, 454, and 1,362 days, respectively). As intuitively expected, the sorption times, being longer than pseudosteady-state time by a factor of four or more, controlled the gas production rate. The longer sorption times completely suppressed the "negative decline" behavior at early time.

Hower investigated the effect of sorption time on simulated gas production from a French coal well.[22] Although insufficient information was provided to calculate time to boundary-dominated flow for this well, reported sorption time was 72 hr. Gas production profiles for infinitely fast desorption (a sorption time of 0) and a sorption time of 720 hr (an order of magnitude larger than actual) were virtually identical except at very early time.

Based on these simulation studies, coal well behavior is usually controlled by Darcy flow in the cleats. However, prudence suggests comparing time to boundary-dominated flow, equation (9.14), and 95% desorption time, equation (9.15), when in doubt. These calculations are especially helpful in understanding early-time production behavior of a well and early-time controls in drawdown and buildup tests.

## Bottomhole Pressure—Constant Rate Gas Production—Infinite Coal

The basic equation for gas flow in coals developed above, equation (9.11), must be solved under a variety of boundary conditions in order to be useful for coal reservoir engineering purposes. The real gas pseudopressure formulation, equation (9.13), is not, as noted above, a strict solution to equation (9.11). Similarly, the real gas pseudopressure formulation of the gas flow rate presented by Al-Hussainy et al. and Al-Hussainy and Ramey is not an exact solution for gas flow in conventional reservoirs.[23] However, it is sufficiently accurate for many coal gas reservoir engineering problems.

Building on that analogy, the basic equations for dimensionless flow in the drainage area of a conventional gas well can be extended to coal wells. Similar to those conventional solutions, the following assumptions are made:

- Homogeneous, isotropic coal
- Isothermal, incompressible, constant porosity coal
- Negligible gravitational effects
- Single-phase gas flow
- Laminar flow

Similar to the conventional flow solutions, inner boundary conditions of interest include constant rate and constant pressure solutions at the coalface and outer boundary conditions of infinite reservoirs and no-flow or constant pressure boundaries for finite reservoirs. The initial condition is one of uniform pressure throughout the coal deposit.

Solutions of the gas flow equation subject to the above and other boundary conditions have been presented by several authors.[24] Because of the complexity of the various solutions and the tedious calculations required, many approximate solutions have been developed for gas and liquid flows in reservoirs. Bottomhole flowing pressure due to constant rate gas production of a coal well completed in an infinite coal seam, or simply a coal well that has not yet felt boundaries, can be approximated as

$$m(p_i) - m(p_{wf}) = \frac{1{,}422Tq_{sc}}{k_g h}\frac{1}{2}\left(\ln\left[\frac{2.637(10)^{-4}\,k_g t}{\phi\mu_{gi}(c_{gi}+c_{si})r_w^2}\right] + 0.80907 + 2s\right) \tag{9.16}$$

The approximate solution of equation (9.16) is valid for dimensionless times greater than 25. Mathematically,

$$25 < t_D$$

Solving for time,

$$\frac{25\phi\mu_{gi}\,(c_{gi}+c_{si})r_w^2}{2.637(10)^{-4}\,k_g} < t \tag{9.17}$$

For pressures less than about 2,000 psia, the product of gas viscosity and $Z$ factor is nearly constant, allowing another solution for the gas flow rate, termed the *pressure-squared solution*, written as[25]

$$p_i^2 - p_{wf}^2 = \frac{1{,}422Tq_{sc}\overline{Z}\,\overline{\mu}_g}{k_g h}\frac{1}{2}\left(\ln\left[\frac{2.637(10)^{-4}\,k_g t}{\phi\mu_{gi}(c_{gi}+c_{si})r_w^2}\right] + 0.80907 + 2s\right) \tag{9.18}$$

### Example 9.2. Bottomhole flowing pressure for a Warrior Basin coal well

Bottomhole flowing pressure for a Warrior Basin coal well produced at a constant rate of 20 mcfd for 3,400 hr can be calculated with both the real gas pseudopressure and pressure-squared methods. Necessary reservoir and well properties are taken from Zuber et al.[26] In addition to the Warrior Basin properties collected in table 9–1, coal seam thickness was 6.8 ft, wellbore radius was 0.5 ft, and the skin factor was –1. The gas was assumed to be pure methane, and the resulting real gas pseudopressure function is in table 9–2. Solving equation (9.16) for the bottomhole flowing pressure,

$$m(p_{wf}) = m(p_i) - \frac{1{,}422Tq_{sc}}{k_g h}\frac{1}{2}\left(\ln\left[\frac{2.637(10)^{-4}\,k_g t}{\phi\mu_{gi}\,(c_{gi}+c_{si})r_w^2}\right] + 0.80907 + 2s\right)$$

$$m(p_{wf}) = 1.7398(10)^7\,\frac{\text{psia}^2}{\text{cp}} - \frac{1{,}422(460+70)\ ^\circ\text{R}(20\ \text{mcfd})}{1\ \text{md}\ (6.8\ \text{ft})}\frac{1}{2}$$

$$\left(\ln\left[\frac{2.637(10)^{-4}(1\ \text{md})t\ \text{hr}}{0.019(0.0118\text{cp})(2.40(10)^{-3}+2.08(10)^{-2})\,\text{psia}^{-1}(0.5)^2\,\text{ft}^2}\right] + 0.80907 + 2(-1)\right)$$

$$m(p_{wf}) = 1.8718(10)^7 - 1.1083(10)^6\,(\ln[2.0292(10)^2\,t])$$

**Table 9–2.** Warrior Basin coal gas properties and real gas pseudopressure

| Pressure, psia | Z factor | $B_g$, ft$^3$/scf | $c_g$, psia$^{-1}$ | Viscosity, cp | $m(p)$, psia$^2$/cp |
|---|---|---|---|---|---|
| 14.7 | 0.9981 | 1.0148E+00 | 6.8155E–02 | 0.0112 | 0.0000E+00 |
| 20 | 0.9974 | 7.4539E–01 | 5.0128E–02 | 0.0112 | 1.6418E+04 |
| 30 | 0.9962 | 4.9629E–01 | 3.3462E–02 | 0.0112 | 6.1077E+04 |
| 40 | 0.9949 | 3.7174E–01 | 2.5128E–02 | 0.0112 | 1.2364E+05 |
| 50 | 0.9936 | 2.9701E–01 | 2.0128E–02 | 0.0113 | 2.0412E+05 |
| 60 | 0.9923 | 2.4719E–01 | 1.6795E–02 | 0.0113 | 3.0253E+05 |
| 70 | 0.9911 | 2.1161E–01 | 1.4414E–02 | 0.0113 | 4.1889E+05 |
| 80 | 0.9898 | 1.8492E–01 | 1.2629E–02 | 0.0113 | 5.5322E+05 |
| 90 | 0.9885 | 1.6416E–01 | 1.1240E–02 | 0.0113 | 7.0553E+05 |
| 100 | 0.9872 | 1.4755E–01 | 1.0129E–02 | 0.0113 | 8.7582E+05 |
| 120 | 0.9847 | 1.2264E–01 | 8.4622E–03 | 0.0113 | 1.2704E+06 |
| 140 | 0.9822 | 1.0485E–01 | 7.2719E–03 | 0.0113 | 1.7371E+06 |
| 160 | 0.9796 | 9.1510E–02 | 6.3791E–03 | 0.0114 | 2.2758E+06 |
| 180 | 0.9771 | 8.1132E–02 | 5.6848E–03 | 0.0114 | 2.8867E+06 |
| 200 | 0.9746 | 7.2831E–02 | 5.1294E–03 | 0.0114 | 3.5699E+06 |
| 220 | 0.9721 | 6.6039E–02 | 4.6749E–03 | 0.0114 | 4.3252E+06 |
| 240 | 0.9696 | 6.0379E–02 | 4.2962E–03 | 0.0115 | 5.1527E+06 |
| 260 | 0.9670 | 5.5590E–02 | 3.9757E–03 | 0.0115 | 6.0525E+06 |
| 280 | 0.9645 | 5.1486E–02 | 3.7011E–03 | 0.0115 | 7.0245E+06 |
| 300 | 0.9621 | 4.7929E–02 | 3.4630E–03 | 0.0115 | 8.0686E+06 |
| 320 | 0.9596 | 4.4818E–02 | 3.2547E–03 | 0.0116 | 9.1849E+06 |
| 340 | 0.9571 | 4.2072E–02 | 3.0708E–03 | 0.0116 | 1.0373E+07 |
| 360 | 0.9546 | 3.9632E–02 | 2.9074E–03 | 0.0116 | 1.1634E+07 |
| 380 | 0.9521 | 3.7449E–02 | 2.7612E–03 | 0.0117 | 1.2966E+07 |
| 400 | 0.9497 | 3.5485E–02 | 2.6296E–03 | 0.0117 | 1.4371E+07 |
| 420 | 0.9472 | 3.3708E–02 | 2.5105E–03 | 0.0117 | 1.5847E+07 |
| 440 | 0.9448 | 3.2092E–02 | 2.4021E–03 | 0.0118 | 1.7395E+07 |
| 460 | 0.9423 | 3.0618E–02 | 2.3032E–03 | 0.0118 | 1.9014E+07 |
| 480 | 0.9399 | 2.9267E–02 | 2.2125E–03 | 0.0118 | 2.0706E+07 |
| 500 | 0.9375 | 2.8024E–02 | 2.1291E–03 | 0.0119 | 2.2468E+07 |
| 520 | 0.9351 | 2.6876E–02 | 2.0520E–03 | 0.0119 | 2.4302E+07 |
| 540 | 0.9327 | 2.5814E–02 | 1.9806E–03 | 0.0119 | 2.6207E+07 |
| 560 | 0.9303 | 2.4829E–02 | 1.9143E–03 | 0.0120 | 2.8183E+07 |
| 580 | 0.9279 | 2.3911E–02 | 1.8525E–03 | 0.0120 | 3.0230E+07 |
| 600 | 0.9255 | 2.3055E–02 | 1.7948E–03 | 0.0120 | 3.2348E+07 |
| 620 | 0.9232 | 2.2254E–02 | 1.7408E–03 | 0.0121 | 3.4536E+07 |

*Source:* Zuber, M. D., et al. 1989.

For any given time, real gas pseudopressure is calculated from the above equation, and then the corresponding bottomhole pressure is interpolated from table 9–2. This solution is valid for times that satisfy the inequality of equation (9.17),

$$\frac{25(0.019)(0.0118\text{ cp})(2.4\,(10)^{-3} + (2.08)10^{-2})\text{ psia}^{-1}\,(0.5)^2\text{ ft}^2}{2.637(10)^{-4}\,(1\text{ md})} < t$$

$$0.123\text{ hr} < t$$

That is, the bottomhole pressure solution is valid for times longer than approximately 8 min.

Calculation of bottomhole flowing pressure with the pressure-squared method begins with solving equation (9.18) for $p_{wf}^2$

$$p_{wf}^2 = p_i^2 - \frac{1{,}422 T q_{sc} \overline{Z}\overline{\mu}_g}{k_g h} \frac{1}{2}\left(\ln\left[\frac{2.637(10)^{-4} k_g t}{\phi \mu_{gi}(c_{gi} + c_{si}) r_w^2}\right] + 0.80907 + 2s\right)$$

The solution depends on average fluid properties that, in turn, depend on average pressure, requiring an iterative solution for bottomhole flowing pressure. As most coals are shallow, cool, and predominantly filled with methane, the average Z factor and viscosity terms in the above equation can be evaluated using the arithmetic average of initial and final pressures, and the solution rapidly converges. Average pressure for this example, calculated from initial and final bottomhole flowing pressures, was 323.4 psia, leading to

$$\overline{Z} = 0.9591, \overline{\mu}_g = 0.0116 \text{ cp}$$

Thus, the final equation for bottomhole flowing pressure is

$$p_{wf}^2 = 440^2 \text{ psia}^2 - \frac{1{,}422(460 + 70)°\text{R}(20 \text{ mcfd})0.9591(0.0116 \text{ cp})}{1 \text{ md}(6.8 \text{ ft})} \frac{1}{2}\left(\ln\left[\,2.0292(10)^2\, t \text{ hrs}\,\right] + 0.80907 + 2(-1)\right)$$

$$p_{wf}^2 = 2.0829(10)^5 \text{ psia}^2 - 1.2331(10)^4 \left(\ln[2.0292(10)^2\, t]\right)\text{psia}^2$$

This solution, subject to the same inequality as is the real gas pseudopressure solution, is valid only for times longer than 8 min. Bottomhole flowing pressures, calculated with both the real gas pseudopressure and pressure-squared solutions, are plotted in figure 9–1. The example terminates at 3,400 hr, the onset of pseudosteady-state flow calculated above. The excellent agreement between the two methods is attributed to the low reservoir pressure, a common feature of many coal deposits.

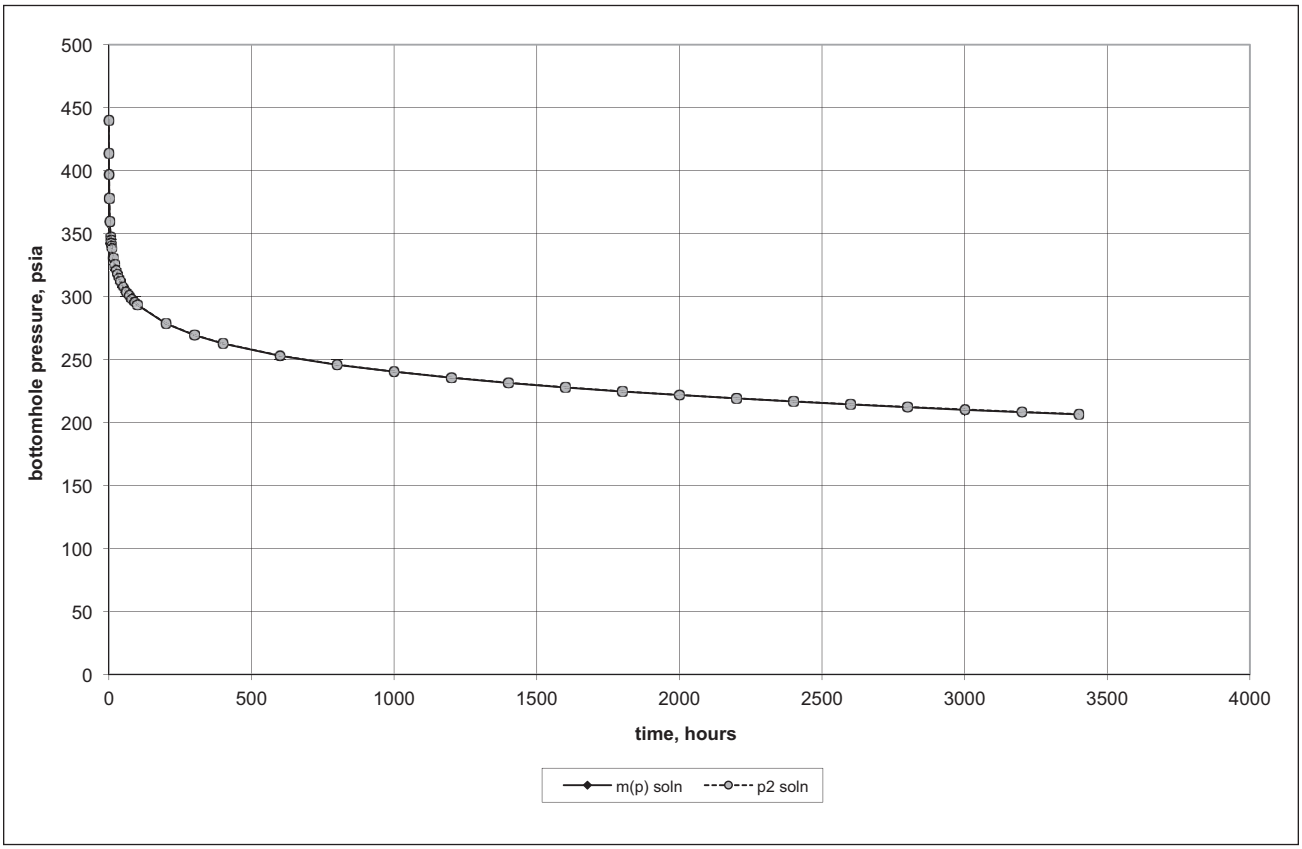



**Fig. 9–1.** Bottomhole pressure—constant rate production—infinite reservoir—Warrior Basin coal well[27]

## Bottomhole Pressure—Constant Rate Gas Production—Bounded Drainage

Pressure solutions for a bounded well produced at constant rate are discussed by Govier et al., Matthews and Russell, and Lee.[28] These authors present detailed solutions for pressure across the drainage area throughout all times, and interested readers are referred to those studies, as this work is concerned only with pressure at the coalface. The two basic solutions of most interest in practical coal well reservoir engineering are no-flow and constant-pressure outer boundaries.

Assuming a no-flow outer boundary and a drainage radius much larger than the wellbore radius, flowing bottomhole pressure can be approximated as[29]

$$m(p_i) - m(p_{wf}) = \frac{1{,}422Tq_{sc}}{k_g h}\left(2\pi t_{DA} + \ln\left[\frac{r_e}{r_w}\right] - \frac{3}{4} + s\right) \tag{9.19}$$

or

$$p_i^2 - p_{wf}^2 = \frac{1{,}422Tq_{sc}\overline{Z}\overline{\mu}_g}{k_g h}\left(2\pi t_{DA} + \ln\left[\frac{r_e}{r_w}\right] - \frac{3}{4} + s\right) \tag{9.20}$$

Both approximate solutions are valid if the inequality of equation (9.21) is satisfied.

$$\frac{1}{4\pi} < t_{DA} \tag{9.21}$$

Assuming a constant-pressure outer boundary and a drainage radius much larger than the wellbore radius, flowing bottomhole pressure can be approximated as[30]

$$m(p_i) - m(p_{wf}) = \frac{1{,}422Tq_{sc}}{k_g h}\left(\ln\left[\frac{r_e}{r_w}\right] + s\right) \tag{9.22}$$

or

$$p_i^2 - p_{wf}^2 = \frac{1{,}422Tq_{sc}\overline{Z}\overline{\mu}_g}{k_g h}\left(\ln\left[\frac{r_e}{r_w}\right] + s\right) \tag{9.23}$$

provided

$$\frac{1}{\pi} < t_{DA} \tag{9.24}$$

### Example 9.3. Bottomhole flowing pressure for an Arkoma Basin coal well

The low-volatile bituminous coals of the Arkoma Basin are dry and were initially exploited with vertical wellbores on 80 ac spacing. Arkoma coal and well parameters from Andrews et al. are shown in table 9–3.[31] Bottomhole flowing pressure for the first 325 days of 80 mcfd constant rate methane production from an Arkoma Basin coal well with a no-flow outer boundary was calculated using both the real gas pseudopressure and pressure-squared formulations, equations (9.19) and (9.20), respectively. As the pressure-squared equation requires fluid properties evaluated at average reservoir pressure, a few iterations were required using the arithmetic average of initial and final bottomhole flowing pressures. The resulting pressure traces are plotted in figure 9–2. From equation (9.21), the solutions are valid for times greater than 3,037 hr, about 127 days. However, both solutions are smooth after the first day, implying sufficient validity for engineering purposes much sooner than the time of mathematical certainty predicted from equation (9.21). The excellent agreement between the two methods is again attributed to the low reservoir pressure.

**Table 9–3.** Example 9.3—Arkoma Basin coal and well properties

| | | |
|---|---|---|
| Permeability = | 3 | md |
| Porosity = | 0.02 | fraction |
| Thickness = | 6.8 | feet |
| Initial pressure = | 550 | psia |
| temperature = | 70 | °F |
| Gas production rate = | 80 | mcfd |
| $r_w$ = | 0.5 | feet |
| $s$ = | –2.0 | |
| $A$ = | 80 | acres |
| $V_{Lis}$ = | 1,321.8 | scf/ton |
| $p_L$ = | 489.7 | psia |
| Coal density = | 1.45 | g/cm$^3$ |
| $m(p_i)$ = | 2.72E+07 | psia$^2$/cp |
| $Z_i$ = | 0.9315 | |
| $B_{gi}$ = | 2.53E–02 | ft$^3$/scf |
| Initial viscosity = | 0.0120 | cp |
| $c_{gi}$ = | 1.95E–03 | psia$^{-1}$ |
| $c_{si}$ = | 3.43E–02 | psia$^{-1}$ |
| $c_{ti}$ = | 3.62E–02 | psia$^{-1}$ |
| Average pressure = | 432.6 | psia |
| Average $Z$ = | 0.9457 | |
| Average viscosity = | 0.0117 | cp |

*Source:* Cardott, B. J. 1998.

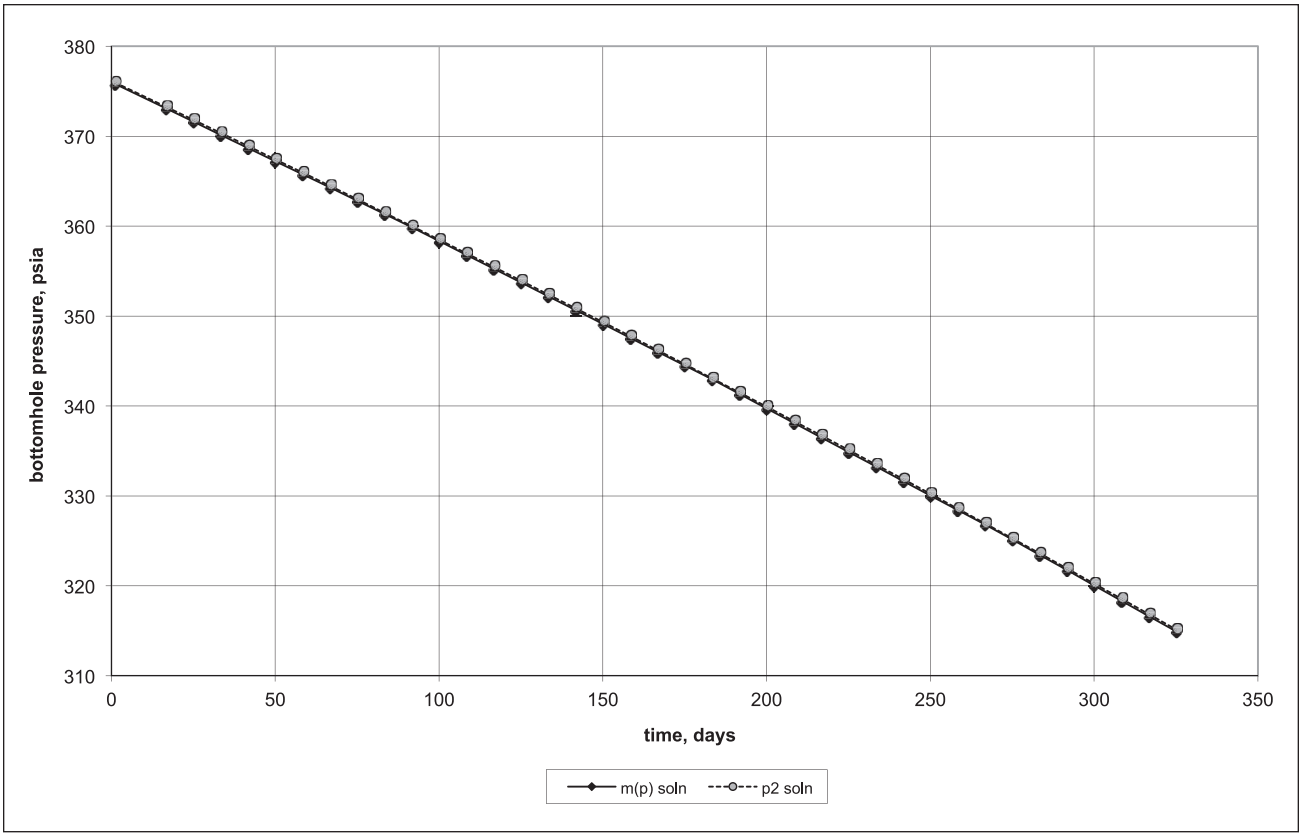



**Fig. 9–2.** Bottomhole pressure—constant rate production—no flow at outer boundary—Arkoma Basin coal well[32]

Assuming a constant pressure outer boundary, bottomhole flowing pressures for this well were calculated using equations (9.22) and (9.23). The real gas pseudopressure method yielded a bottomhole flowing pressure of 341.7 psia. The pressure-squared formulation required three iterations to converge on a bottomhole flowing pressure of 341.1 psia. From equation (9.24), the solutions are valid for times greater than 12,198 hr or about 1.4 years.

## Gas Production Rate—Pseudosteady State

After the boundary begins to influence well performance, the gas production rate transitions to pseudosteady-state flow. Once the well has attained pseudosteady-state flow, gas production rate can be written as a function of average reservoir pressure rather than initial reservoir pressure[33]

$$m(p_R) - m(p_{wf}) = \frac{1{,}422Tq_{sc}}{k_g h}\left(\ln\left[\frac{r_e}{r_w}\right] - 0.75 + s\right) \tag{9.25}$$

where

$m(p_R)$ = real gas pseudopressure for average reservoir pressure, psia$^2$/cp.

The pressure-squared formulation of pseudosteady state is

$$p_R^2 - p_{wf}^2 = \frac{1{,}422Tq_{sc}\overline{Z}\overline{\mu}_g}{k_g h}\left(\ln\left[\frac{r_e}{r_w}\right] - 0.75 + s\right) \tag{9.26}$$

Note that these pseudosteady-state equations are valid for times that satisfy

$$\frac{1}{4\pi} < t_{DA} \tag{9.27}$$

## Gas Production Rate—Constant Bottomhole Pressure—Bounded Drainage

Coal wells are often operated with a stable fluid level, usually close to the top of the seam, and constant wellhead pressures, making the idealized case one of constant bottomhole pressure. Solution of this problem, with either no-flow or constant-pressure boundaries, is much more difficult than the constant rate problems discussed above. It is usually cast as a series of tables of dimensionless time and cumulative gas production with drainage radius as a parameter.[34] Transient flow gives way to steady-state flow when[35]

$$\frac{1}{\pi r_{eD}} < t_{DA}$$

Assuming a wellbore radius of 0.5 ft for the San Juan coal well in example 9.1, steady-state flow commences at

$$\frac{1}{\pi \dfrac{2{,}106.4 \text{ ft}}{0.5 \text{ ft}}} < \frac{2.637(10)^{-4}1.2 \text{ md } (t \text{ hr})}{0.02(0.0148 \text{ cp})3.36(10)^{-3} \text{ psia } \pi \ (2{,}106.4)^2 \text{ ft}^2}$$

Solving for time,

$$3.3 \text{ hr} < t$$

That is, the steady-state approximation replaces the transient solution after just a few hours in this well. Given the tabular nature and short time frame of the transient solution for constant bottomhole pressure, it is primarily of interest for coal well pressure transient problems.

## Water Flow in Coal Seams

Many coal deposits are aquifers, and the resulting hydrostatic head provides the seal to retain gas in the coal. Water is expelled from organic debris during coalification, and the resulting coals do not readily sorb water, leaving the bulk of the in-situ water in the cleats. For engineering purposes, coal deposits behave as single-porosity reservoirs to water, and equations developed by hydrologists and conventional reservoir engineers to describe water flow in aquifers apply directly to coals. Bottomhole flowing pressure of a coal well produced at constant water rate can be obtained from the classical solutions presented by Govier and Lee, respectively.[36] For infinite acting flow,

$$p_i - p_{wf} = \frac{141.2 B_w \mu_w q_w}{k_w h} \frac{1}{2} (\ln[t_D] + 0.80907 + 2s) \tag{9.28}$$

where

$B_w$ = water formation volume factor, rb/stb,
$\mu_w$ = water viscosity, cp,
$q_w$ = water production rate, bpd, and
$k_w$ = effective permeability to water, md.

Dimensionless time is defined as

$$t_D = \frac{2.637(10)^{-4} k_w t}{\phi \mu_w (c_f + c_w) r_w^2} \tag{9.29}$$

where

$c_f$ = cleat compressibility, psia$^{-1}$, and
$c_w$ = water compressibility, psia$^{-1}$.

This solution is valid for times that satisfy

$$25 < t_D \tag{9.30}$$

Bottomhole flowing pressure in a well produced at constant rate with a no-flow outer boundary and $r_e >> r_w$ is given by

$$p_i - p_{wf} = \frac{141.2 B_w \mu_w q_w}{k_w h} \left( 2\pi t_{DA} + \ln \left[ \frac{r_e}{r_w} \right] - \frac{3}{4\text{ss}} + s \right)$$

where

$t_{DA}$ = dimensionless time based upon drainage area, defined as

$$t_{DA} = \frac{2.637(10)^{-4} k_w t}{\phi_f \mu_w (c_f + c_w) \pi r_e^2}$$

and the following inequality is satisfied

$$\frac{1}{4\pi} < t_{DA}$$

Bottomhole flowing pressure in a well produced at a constant rate with a constant pressure boundary is given by

$$p_i - p_{wf} = \frac{141.2 B_w \mu_w q_w}{k_w h} \left( \ln \left[ \frac{r_e}{r_w} \right] + s \right) \tag{9.31}$$

for dimensionless times that satisfy

$$\frac{1}{\pi} < t_{DA} \tag{9.32}$$

### Example 9.4. Bottomhole flowing pressure of a well in an undersaturated coal

The above equations lend insight into a single well production test of a well completed in an undersaturated coal. Properties of the Canyon coal seam of the Powder River Basin were measured by Nelson et al., and development of the Wyodak coal seam in this basin was simulated by Hower et al.[37] Pertinent coal and well properties from these studies are presented in table 9–4. With an initial pressure in the Canyon coal seam of 150 psia and a desorption pressure of 135 psia, dewatering time until gas production commences is an important question to any operator.

**Table 9–4.** Example 9.4—Undersaturated Powder River coal and well properties

| | | |
|---|---|---|
| Water production rate = | 300 | bpd |
| Permeability = | 350 | md |
| Thickness = | 64 | feet |
| Porosity = | 0.03 | fraction |
| Initial pressure = | 150 | psia |
| Desorption pressure = | 135 | psia |
| Wellbore radius = | 0.5 | ft |
| Skin factor = | 0 | |
| Well spacing = | 80 | ac |
| $B_w$ = | 1.00 | rb/stb |
| Water viscosity = | 1.05 | cp |
| Temperature = | 65 | °F |
| $c_f$ = | 1.00E–03 | $psia^{-1}$ |
| $c_w$ = | 1.00E–06 | $psia^{-1}$ |

*Source:* Nelson, C. R., et al. 2000; and Hower, T. L., et al. 2003.

Assuming this well is produced at a constant water rate and drains an infinite, uniform coal deposit, equation (9.28) can be solved for time until bottomhole pressure is reduced to desorption pressure.

$$\ln[t_D] = \frac{(p_i - p_{wf})2k_w h}{141.2 B_w \mu_w q_w} - 0.80907 - 2s$$

$$\ln[t_D] = \frac{(150 - 135)\text{ psia } 2(350\text{ md})64\text{ ft}}{141.2\left(1.0\dfrac{\text{rb}}{\text{stb}}\right)1.05\text{ cp } 300\text{ bpd}} - 0.80907 - 2(0) = 14.300$$

Bottomhole flowing pressure will drop to desorption pressure at a dimensionless time of

$$t_D = 1.62(10)^6$$

Solving equation (9.29) for time and using the above result

$$t = \frac{t_D \phi \mu_w (c_f + c_w) r_w^2}{2.637(10)^{-4}\, k_w}$$

$$t = \frac{1.62(10)^6(0.03)(1.05\text{ cp})(1.0(10)^{-3} + 3.0(10)^{-6})\text{psia}^{-1}\, 0.5^2\text{ ft}^2}{2.637(10)^{-4}\,(350\text{ md})}$$

$$t = 139\text{ hr} \approx 6\text{ days}$$

From equations (9.29) and (9.30), this solution is valid for times that satisfy

$$t_D = \frac{2.637(10)^{-4}\, k_w t}{\phi \mu_w (c_f + c_w) r_w^2} > 25$$

$$t > \frac{25 \phi \mu_w (c_f + c_w) r_w^2}{2.637(10)^{-4}\, k_w}$$

$$t > \frac{25(0.03)(1.05\text{ cp})(1.0(10)^{-3} + 3.0(10)^{-6})\text{psia}^{-1}\, 0.5^2\text{ ft}^2}{2.637(10)^{-4}\,(350\text{ md})} = 2.14(10)^{-3}\text{ hr}$$

$$t > \approx 8\text{ sec}$$

Thus, this bottomhole pressure will reach desorption pressure after about six days of production. Pressure in the near-wellbore region will fall to desorption pressure soon after, liberating the first gas. Note that this exercise does not predict time to first gas production but simply time to reach desorption pressure. Once gas is liberated into the coal cleats, multiphase flow effects and near-wellbore heterogeneities will control gas production.

This single-well production test in a highly permeable coal could also be conceptualized as having a constant pressure boundary. The assumption of a constant pressure boundary implies a steady pressure drop, unchanging with time. Thus, this approach yields a bounding value of desorption pressure rather than a time to reach that pressure. Solving equation (9.31) for the bounding desorption pressure,

$$p_{des} = p_{wf} = p_i - \frac{141.2 B_w \mu_w q_w}{k_w h}\left(\ln\left[\frac{r_e}{r_w}\right] + s\right)$$

$$p_{des} = 150 \text{ psia} - \frac{141.2\left(1.0\,\frac{\text{rb}}{\text{stb}}\right)1.05 \text{ cp } 300 \text{ bpd}}{350 \text{ md } 64 \text{ ft}}\left(\ln\left[\frac{1{,}053.2 \text{ ft}}{0.5 \text{ ft}}\right] + 0\right)$$

$$p_{des} = 134.8 \text{ psia}$$

As this bounding desorption pressure is almost exactly the reported desorption pressure, this single-well production test may never sufficiently decrease reservoir pressure for gas to desorb from the coal. Note, from equation (9.32), this solution is valid for times greater than

$$\frac{1}{\pi} < t_{DA} = \frac{2.637(10)^{-4} k_w t}{\phi \mu_w (c_f + c_w) A}$$

$$t > \frac{\phi \mu_w (c_f + c_w) A}{\pi 2.637(10)^{-4} k_w h}$$

$$t > \frac{0.03(1.05 \text{ cp})(1.0(10)^{-3} + 3.0(10)^{-6})\text{psia}^{-1}\, 80 \text{ ac } 43{,}560\,\frac{\text{ft}^2}{\text{ac}}}{\pi 2.637(10)^{-4}\,(350 \text{ md})}$$

$$t = 380 \text{ hr} \approx 16 \text{ days}$$

Repeating these calculations with reasonable variations of coal and well properties by the interested reader will indicate not only credibility of the conclusion that this single well test may never yield gas but also the futility of using such a test to determine desorption pressure of an undersaturated coal.

# Nomenclature

| | |
|---|---|
| $a$ | Average ash fraction, decimal |
| $A$ | Drainage area, ac |
| $B_g$ | Gas formation volume factor, $ft^3/scf$ |
| $c_g$ | Gas compressibility, $psia^{-1}$ |
| $c_s$ | Sorption compressibility, $psia^{-1}$ |
| $c_t$ | Total compressibility, $psia^{-1}$ |
| $F$ | Gas flux from matrix to cleat |
| $G_i$ | Initial gas in place, mmcf |
| $G_p$ | Produced gas, mmcf |
| $h$ | Coal thickness, ft |
| $k$ | Permeability, md |
| $M$ | Gas molecular weight |
| $m(p)$ | Real gas pseudopressure |
| $n$ | Number of moles |
| $p$ | Current reservoir pressure, psia |
| $p_b$ | Base pressure in real gas pseudopressure definition |
| $p_L$ | Langmuir pressure constant, psia |
| $p_R$ | Average reservoir pressure, psia |
| $p_{wf}$ | Bottomhole flowing pressure |
| $q_g$ | Gas flow rate, mcfd |
| $R$ | Universal gas constant, 10.732 $psia\text{-}ft^3\text{-}lb\text{-}mol^{-1}\text{-}°R^{-1}$ |
| $r_e$ | External radius |
| $r_w$ | Wellbore radius |
| $s$ | Wellbore skin factor, dimensionless |
| $S_w$ | Current average water saturation, decimal |
| $t$ | Time |
| $T$ | Absolute temperature, °R |
| $t_{90}$ | Time required for a coal to desorb 90% of its sorbed gas |
| $t_{95}$ | Time required for a coal to desorb 95% of its sorbed gas |
| $v$ | Gas velocity vector |
| $V$ | Coalbed gas content, scf/ton |
| $V_g$ | Gas volume |
| $V_{Ldaf}$ | Dry, ash-free Langmuir volume constant, scf/ton |
| $V_{Lis}$ | In-situ Langmuir volume constant, scf/ton |
| $w$ | Average equilibrium moisture, decimal |
| $Z$ | Gas deviation factor |

## Greek

| | |
|---|---|
| $\mu_g$ | Gas viscosity, cp |
| $\rho$ | Gas density |
| $\rho_B$ | Coal bulk density, $g/cm^3$ |
| $\varphi$ | Porosity, decimal |

## Subscripts

| | |
|---|---|
| $f$ | Final |
| $g$ | Gas |
| $i$ | Initial |

*pss* Pseudosteady-state or boundary dominated flow
*sc* Standard conditions
*w* Water

## References


1. Al-Hussainy, R., Ramey, H. J., and Crawford, P. B. 1966. The flow of real gases through porous media. *Journal of Petroleum Technology*. V. 18. p. 624.
2. Seidle, J. P. 1991. *Long Term Gas Deliverability of a Dewatered Coalbed*. Paper SPE 21488. Presented at the SPE Gas Technology Symposium, Houston, Texas, January 23–25.
3. Al-Hussainy, R., et al. 1966.
4. Ibid.
5. Seidle, J. P. 1991.
6. Al-Hussainy, R., et al. 1966; and Al-Hussainy, R., and Ramey, H. J. 1966. Application of real gas flow theory to well testing and deliverability forecasting. *Journal of Petroleum Technology*. V. 18. p. 637.
7. Earlougher, R. C., Jr. 1977. *Advances in Well Test Analysis*. Society of Petroleum Engineers Monograph 5. Dallas: Society of Petroleum Engineers.
8. Ibid.
9. Gas Research Institute. 1996. *A Guide to Coalbed Methane Reservoir Engineering*. GRI Reference No. GRI-94/0397. Chicago: Gas Research Institute; Mavor, M. J., and Robinson, J. R. 1993. *Analysis of Coal Gas Reservoir Interference and Cavity Well Tests*. Paper SPE 25860. Presented at the Joint Rocky Mountain Regional and Low Permeability Reservoirs Symposium, Denver, Colorado, April 26–28; Zuber, M. D., Boyer, C. M., Schraufnagel, R. A., and Saulsberry, J. 1989. *Insights and Analysis from the Rock Creek Project: A Reservoir Engineering Approach*. Paper SPE 19057. Presented at the SPE Gas Technology Symposium, Dallas, Texas, June 7–9; Nelson, C. R., Hill, D. G., and Pratt, T. J. 2000. *Properties of Paleocene Fort Union Formation Canyon Seam Coal at the Triton Federal Coalbed Methane Well, Campbell County, Wyoming*. Paper SPE 59786. Presented at the SPE/CERI Gas Technology Conference, Calgary, Alberta, April 3–5; and Hower, T. L., Jones, J. E., Goldstein, D. M., and Harbridge, W. 2003. *Development of the Wyodak Coalbed Methane Resource in the Powder River Basin*. Paper SPE 84428. Presented at the Annual Technical Conference and Exhibition, Denver, Colorado, October 5–8.
10. Gas Research Institute. 1996.
11. Mavor, M. J., and Robinson, J. R. 1993.
12. Zuber, M. D., et al. 1989.
13. Zuber, M. D., et al. 1989; and Gas Research Institute. 1996.
14. Gash, B. W. 1991. *Measurement of "Rock Properties" in Coal for Coalbed Methane Production*. Paper SPE 22909. Presented at the Annual Technical Conference and Exhibition, Dallas, Texas, October 6–9.
15. Nelson, C. R., et al. 2000; and Hower, T. L., et al. 2003.
16. Gas Research Institute. 1996.
17. Zuber, M. D., et al. 1989; and Gas Research Institute. 1996.
18. Nelson, C. R., et al. 2000; and Hower, T. L., et al. 2003.
19. Remner, D. J., Ertekin, T., Sung, W., and King, G. R. 1986. A parametric study of the effects of coal seam properties on gas drainage efficiency. *Society of Petroleum Engineers Reservoir Engineering*. November. p. 633.
20. Ibid.
21. Sawyer, W. K., Zuber, M. D., Kuuskraa, V. A., and Horner, D. M. 1987. *Using Reservoir Simulation and Field Data to Define Mechanisms Controlling Coalbed Methane Production*. Paper 8763. Presented at the Coalbed Methane Symposium, Tuscaloosa, Alabama, November 16–19.
22. Hower, T. L. 2003. *Coalbed Methane Simulation: An Evolving Science*. Paper SPE 84424. Presented at the Annual Technical Conference and Exhibition, Denver, Colorado, October 5–8.
23. Al-Hussainy, R., et al. 1966; and Al-Hussainy, R., and Ramey, H. J. 1966.
24. Govier, G. W. 1975. *Theory and Practice of the Testing of Gas Wells*. Calgary, Alberta: Energy Resources Conservation Board; Matthews, C. S., and Russell, D. G. 1967. *Pressure Buildup and Flow Tests in Wells*. Richardson, Texas: Society of Petroleum Engineers; and Lee, J. 1982. *Well Testing*. Richardson, Texas: Society of Petroleum Engineers.
25. Govier, G. W. 1975.
26. Zuber, M. D., et al. 1989.
27. Govier, G. W. 1975; Zuber, M. D., et al. 1989.
28. Govier, G. W. 1975; Matthews, C. S., and Russell, D. G. 1967; and Lee, J. 1982.
29. Govier, G. W. 1975; and Lee, J. 1982.
30. Ibid.
31. Cardott, B. J., 1998, "Part II. Coal as a Gas-source Rock and Reservoir, Hartshorne Formation, Oklahoma." *The Hartshorne Play in Southeastern Oklahoma: Regional and Detailed Sandstone Reservoir Analysis and Coalbed-Methane Resources*. Andrews, R. D., Cardott, B. J., and Storm, T. Special Publication 98-7. Norman: Oklahoma Geological Survey.

32. Govier, G. W. 1975; Nelson, et al. 2000; Kissell, F. N., C. M. McCulloch, and C. H. Elder. "The Direct Method of Determining Methane Content of Coalbeds for Ventilation Designs." *US Bureau of Mines Report of Investigations*, RI 7767. 1973; Cardot, B J., 1998.
33. Govier, G. W. 1975.
34. Lee, J. 1982.
35. Ibid.
36. Govier, G. W. 1975; and Lee, J. 1982.
37. Nelson, C. R., et al. 2000; Hower, T. L., et al. 2003.

# Depletion of Gas and Water in Coals

# 10

## Introduction

Most coal deposits contain both gas and water. Many coals are aquifers, with the hydrostatic water column providing the seal to keep gas sorbed to the coal matrix. Production of coal gas requires dewatering the coalbed, and initial gas rates are often low. As dewatering progresses, additional gas desorbs from the matrix into the cleat, increasing gas saturation and gas mobility, thus causing gas rates to steadily increase. This rising gas production is termed *negative decline*, and an example from the Drunkard's Wash Field in the Uinta Basin is shown in figure 10–1. Gas production eventually peaks and begins to fall. The initial water production rate can be several hundred barrels per day but declines as water saturation and thus water mobility decrease due to gas desorbing into the cleat.

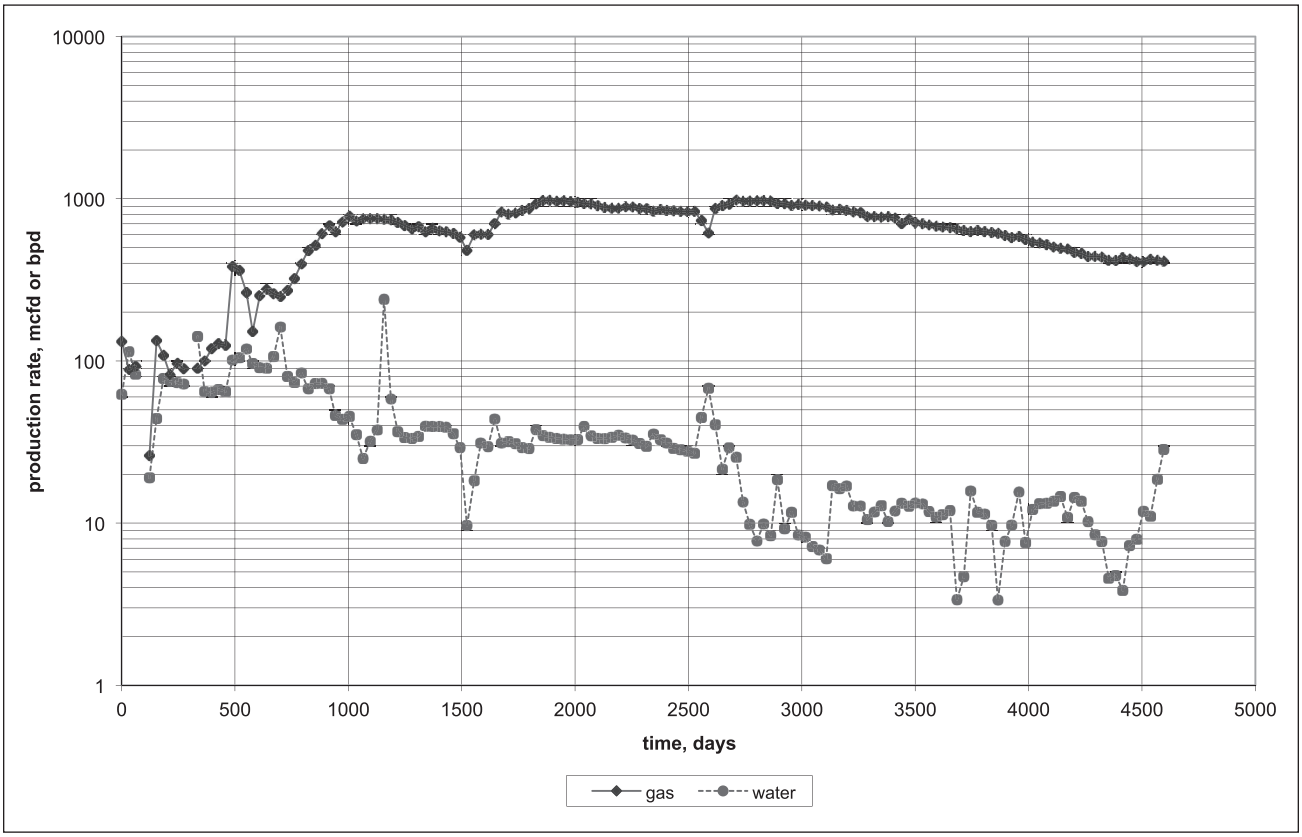



**Fig. 10–1.** Example of coal well negative decline—Utah #25-7-6 production history

This unique behavior is due to the interplay between dewatering and depressuring of the coal deposit. The magnitude and timing of the peak in gas rate as well as the water decline behavior are dictated by gas-water relative permeabilities, the sorption isotherm, and initial pressure. However, this striking behavior does not occur in all coals wells. A good rule of thumb is that negative decline will be observed in only about one-third of the wells in any given field. One-third of the wells will exhibit declines similar to conventional gas wells due to being located on the periphery of the field, drilled late in the development program, or completed in structurally higher coals containing substantial amounts of free gas. The final one-third of the wells will have a wellbore history so complicated it masks reservoir response. These are wells subjected to frequent pump changes, refracs, and opening of additional pay and variable surface operating conditions.

Undersaturated coals require that reservoir pressure be reduced to desorption pressure before gas production commences. While the coal deposit is above desorption pressure, water mobility is constant, with no relative permeability effects due to free gas. Once desorption pressure is reached, well behavior is similar to that of a saturated coal, with gas rate exhibiting negative decline, a peak, and a subsequent decline. Water production from these wells is analogous to production of undersaturated oil, with the desorption pressure corresponding to the bubblepoint.

Wells completed in coals with little moveable water require no dewatering and do not show negative decline. Gas production in these wells declines from the initial rate, similar to conventional gas wells.

Gas sorbed on a coal is often a mixture of gases, and composition of the produced gas varies over the course of depletion. For instance, coal holding a mixture of methane and $CO_2$ will preferentially release the more loosely sorbed gas, methane, over the more strongly held gas, $CO_2$, as the pressure is reduced. Consequently, the produced gas stream becomes increasingly leaner in methane and richer in $CO_2$ over depletion.

Coal is an organic, reactive rock, and the permeability can vary over depletion. As discussed in chapter 6, permeability of coal depends on stress and gas content. Increased stress due to pressure depletion acts to decrease permeability, while matrix shrinkage due to gas desorption serves to increase permeability. The interplay of these two effects leads to a dynamic permeability over depletion.

## Tank-Type Model of Coal Depletion

A tank-type model for gas and water production from a bounded coal well can be constructed by assuming gas and water mobilities are controlled by water in the cleats and pressure is controlled by gas in the matrix. Depletion of a coal is described with seven parameters—gas and water rates, cumulative gas and water production, gas and water saturations, and pressure—coupled through mass balance and flow equations.

Production rates are calculated with Darcy's pseudosteady-state equations. As discussed in chapter 9, gas rate can be calculated with either the real gas pseudopressure formulation or the pressure-squared formation. The real gas pseudopressure calculation is shown in equation (10.1).[1]

$$m(p_R) - m(p_{wf}) = \frac{1{,}422Tq_g}{k_g h}\left(\ln\left[\frac{r_e}{r_w}\right] - 0.75 + s\right) \quad \textbf{(10.1)}$$

where

$m(p_R)$ = real gas pseudopressure for average reservoir pressure, psia$^2$/cp,
$m(p_{wf})$ = real gas pseudopressure for bottomhole flowing pressure, psia$^2$/cp,
$T$ = reservoir temperature, °R,
$q_g$ = gas flow rate, mcfd,
$k_g$ = effective permeability to gas, md,
$h$ = net coal thickness, ft,
$r_e$ = drainage radius, ft,
$r_w$ = wellbore radius, ft, and
$s$ = wellbore skin factor.

The pressure-squared formulation for pseudosteady state gas flow is shown in equation (10.2).[2]

$$p_R^2 - p_{wf}^2 = \frac{1{,}422 T q_g \overline{Z} \overline{\mu}_g}{k_g h} \left( \ln \left[ \frac{r_e}{r_w} \right] - 0.75 + s \right) \tag{10.2}$$

where

$\overline{Z}$ = average gas deviation factor, and
$\overline{\mu}_g$ = average gas viscosity, cp.

Also from chapter 9, water production rate is calculated from the liquid pseudosteady-state equation[3]

$$\overline{p} - p_{wf} = \frac{141.2 B_w \mu_w q_w}{k_w h} \left( \ln \left[ \frac{r_e}{r_w} \right] - 0.75 + s \right) \tag{10.3}$$

where

$B_w$ = water formation volume factor, rb/stb,
$\mu_w$ = water viscosity, cp,
$q_w$ = water production rate, bpd, and
$k_w$ = effective permeability to water, md.

Time required to reach pseudosteady-state flow, as discussed in chapter 9, is given by

$$t_{pss} = 1.652(10)^7 \frac{\phi_f \mu_g (c_g + c_s) A}{k_g} \tag{10.4}$$

where

$k_g$ = gas permeability, md,
$t_{pss}$ = time to reach pseudosteady-state flow, hr,
$\mu_g$ = gas viscosity, cp,
$c_g$ = gas compressibility, psia$^{-1}$,
$c_s$ = sorption compressibility, psia$^{-1}$,
$\phi$ = cleat porosity, decimal, and
$A$ = drainage area, ac.

Cumulative gas production from a tank-type model can be approximated as

$$G_p = 0.001 \int q_g \, dt \cong 0.001 \sum_j q_{gj} \Delta t_j \tag{10.5}$$

where

$G_p$ = cumulative gas production, mmcf.

Similarly for cumulative water production

$$W_p = \int q_w \, dt \cong \sum_j q_{wj} \Delta t_j \tag{10.6}$$

where

$W_p$ = cumulative water production, stb.

With only two phases present, gas saturation is given by

$$S_g = 1 - S_w$$

Water saturation is calculated from the water mass balance equation of chapter 8. For this bounded coal well, water influx is zero. Neglecting water and formation compressibilities, equation (8.6) becomes

$$S_w = S_{wi}\frac{B_w}{B_{wi}} - \frac{B_w}{7758.4Ah\phi}W_p$$

Assuming a constant water formation volume factor

$$S_w = S_{wi}\frac{B_w}{7758.4Ah\phi}W_p \tag{10.7}$$

From chapter 8, the gas mass balance equation can be written as

$$\frac{p}{Z^*} = \frac{p_i}{Z_i^*}\left(1 - \frac{G_p}{G_i}\right) \tag{10.8}$$

where

$G_i$ = initial gas in place, mmcf.

And the $Z^*$ function, discussed in chapter 8, for this case is defined as

$$Z^* = \frac{Z}{\dfrac{\rho_B V_{Ldaf}(1-a-w)p_{sc}TZ}{32.037\,\phi Z_{sc}T_{sc}(p+p_L)} + (1-S_w)} \tag{10.9}$$

where

$\rho_B$ = coal density, g/cm$^3$,
$V_{Ldaf}$ = dry, ash-free Langmuir volume constant, scf/ton,
$a$ = ash fraction,
$w$ = equilibrium moisture fraction,
$S_w$ = water saturation,
$\phi$ = porosity, decimal, and
$Z$ = gas deviation factor.

Depletion of the coal well can be modeled as a series of discrete time steps using the above equations. At any given time, gas and water rates are calculated from current pressures and relative permeabilities. Multiplication of these rates by a small but arbitrary time step gives incremental production of gas and water volumes for updating cumulatives. Water saturation at this next time is calculated from new cumulative water production, and $p/Z^*$ is calculated from the updated cumulative gas production. As pressure and water saturation change at each step, an iterative procedure is used to calculate the new pressure. New gas and water relative permeabilities are determined from the revised water saturation. Calculation of new gas and water rates begins the mathematics of the following step. Depletion of a single coal well is described in the example below.

### Example 10.1. Depletion of Utah #25-7-6, Drunkard's Wash Field, Uinta Basin

Geology of the Drunkard's Wash Field, located in Carbon and Emery counties, Utah, was discussed by Montgomery et al. and Lamarre and Pratt.[4] Production behavior of the wells completed in the Ferron coals and additional geologic information were presented by Lamarre and Burns and Burns and Lamarre, respectively.[5] Gas and water production from one of the first wells in the field, the Utah #25-7-6 well, were calculated using the real gas pseudopressure formulation, equation (10.1), and equation (10.3), respectively. Saturations and mass balances were calculated from equations (10.5) through (10.9). Reservoir and well parameters are collected in table 10–1. Note only the in-situ Langmuir volume constant was reported, which is already corrected for the (unreported) ash and moisture fractions. The in-situ sorption isotherm is shown in figure 10–2.[6] The gas-water relative permeabilities are in figure 10–3.[7] These relative permeabilities were measured on Fruitland coal from the San Juan Basin, which is roughly analogous to the Ferron coals on a geological and rank basis. Original gas in place (OGIP) in the 160 ac drainage area was 4.589 bcf; original water in place (OWIP) was 339.6 mstb.

**Table 10–1.** Example 10.1. Reservoir and well properties—Utah #25-7-6

| | | |
|---|---|---|
| Drainage area = | 160 | ac |
| Coal thickness = | 24 | ft |
| $V_L$ is = | 920.8 | scf/ton |
| $p_L$ = | 759.3 | psia |
| Bulk density = | 1.560 | g/cm$^3$ |
| Cleat porosity = | 0.012 | fraction |
| Initial pressure = | 1,191 | psia |
| Initial water saturation = | 0.95 | |
| Coalbed temperature = | 70 | °F |
| Permeability = | 12 | md |
| Cleat compressibility = | 1.46E–03 | psia$^{-1}$ |
| Bottomhole press = | 100 | psia |
| $r_w$ = | 0.210 | ft |
| Skin = | –2.0 | |
| $B_w$ = | 1.0 | rb/stb |
| $\mu_w$ = | 1.00 | cp |
| Time step = | 30 | days |
| Water production rate = | 80 | bpd |

*Sources:* Montgomery, S. L., et al. 2001; Lamarre, R. A., and Pratt, T. J. 2002; Lamarre, R. A., and Burns, T. D. 1997; and Burns, T. D., and Lamarre, R. A. 1997.

Gas and water production for the first 4,000 days of production were calculated using the iterative scheme discussed above. A water rate of 80 bpd was specified, and permeability and porosity were adjusted to obtain the match. When the model could no longer support the specified water rate, it defaulted to a flowing bottomhole pressure of 100 psia. Step-by-step calculations for the first 870 days of production are in table 10–2. Calculated gas and water rates are compared with actual rates in figure 10–4, while calculated and actual cumulatives are given in figure 10–5. Calculated reservoir pressure, gas saturation, and gas relative permeability over time are plotted in figure 10–6. No reported pressures or saturations were available for comparison.

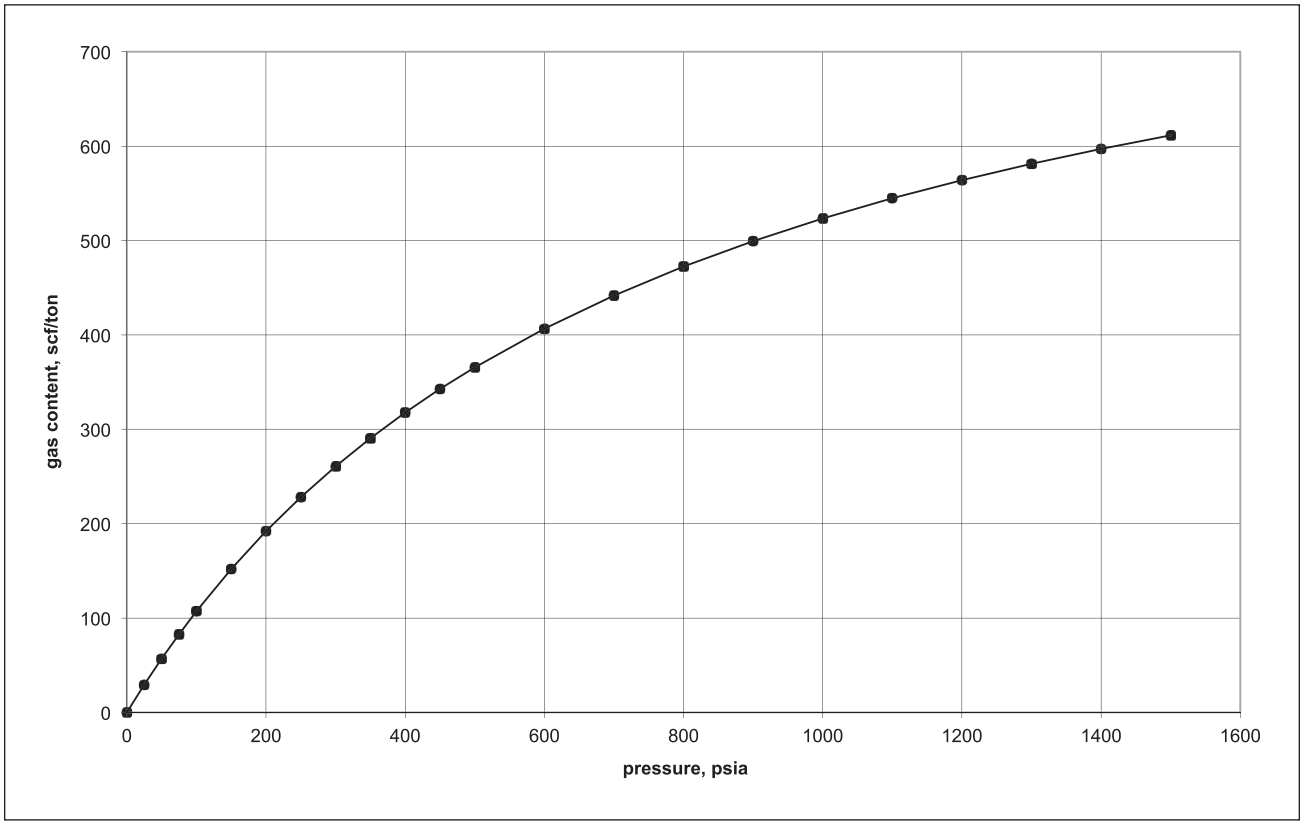



**Fig. 10–2.** Drunkard's Wash in-situ sorption isotherm—Uinta Basin, Ferron coal[8]

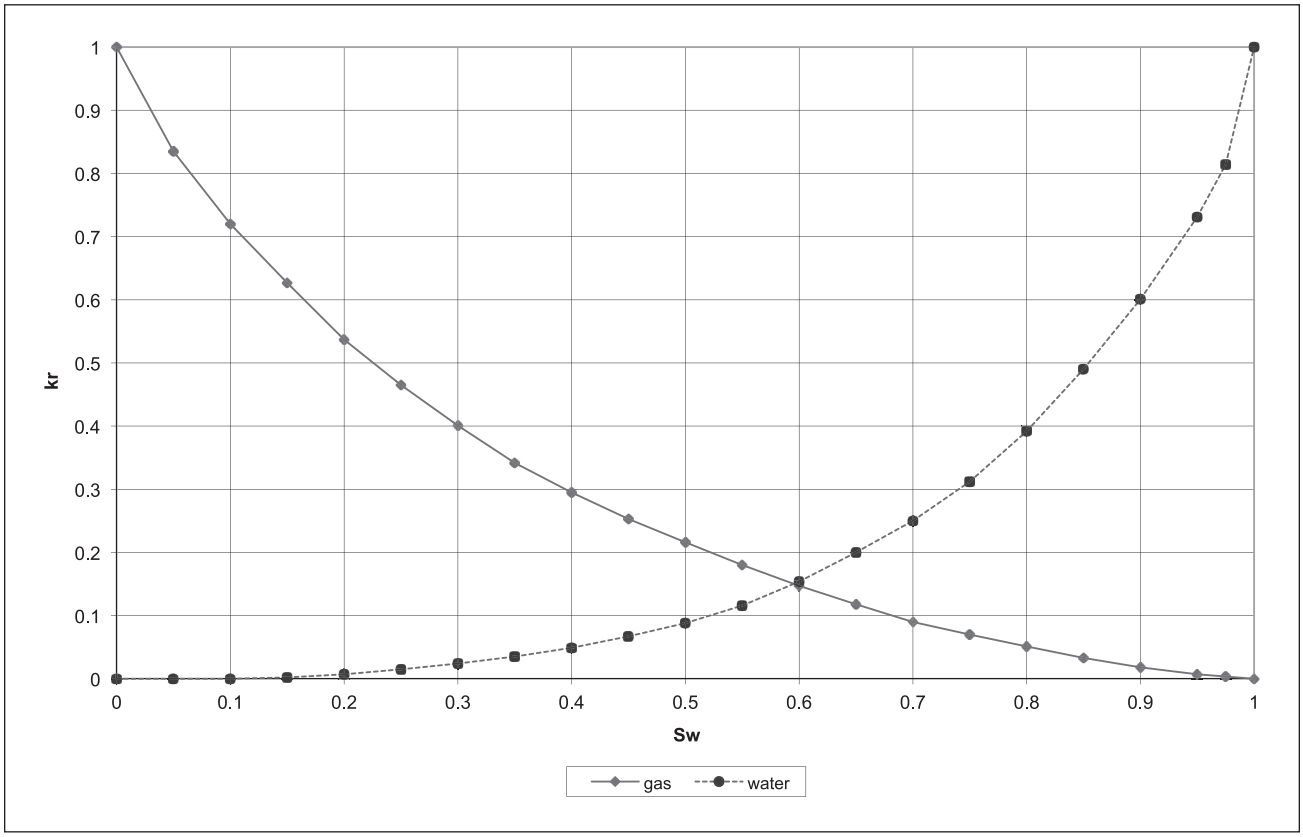



**Fig. 10–3.** Example 10.1 gas-water relative permeabilities[9]

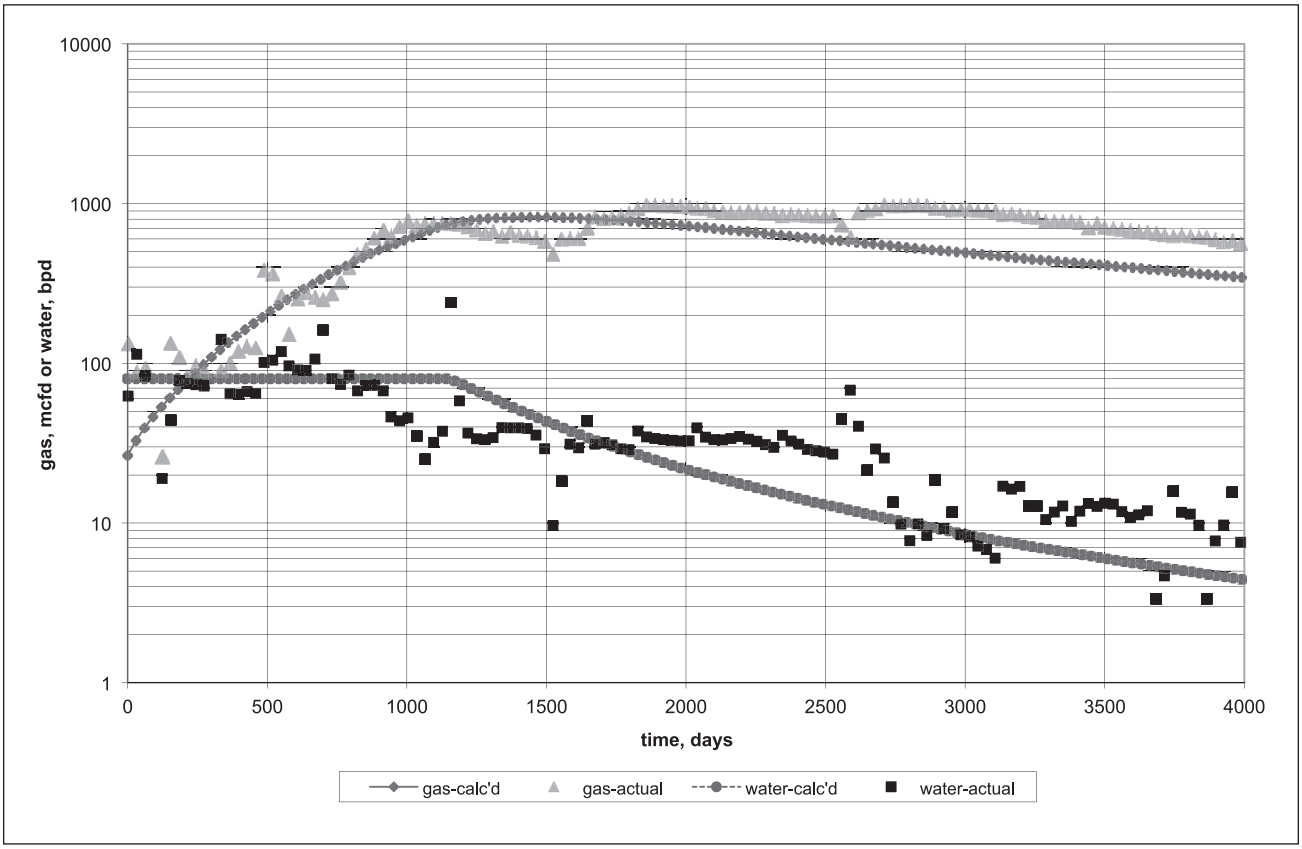



**Fig. 10–4.** Example 10.1 Utah #25-7-6 gas and water production rates

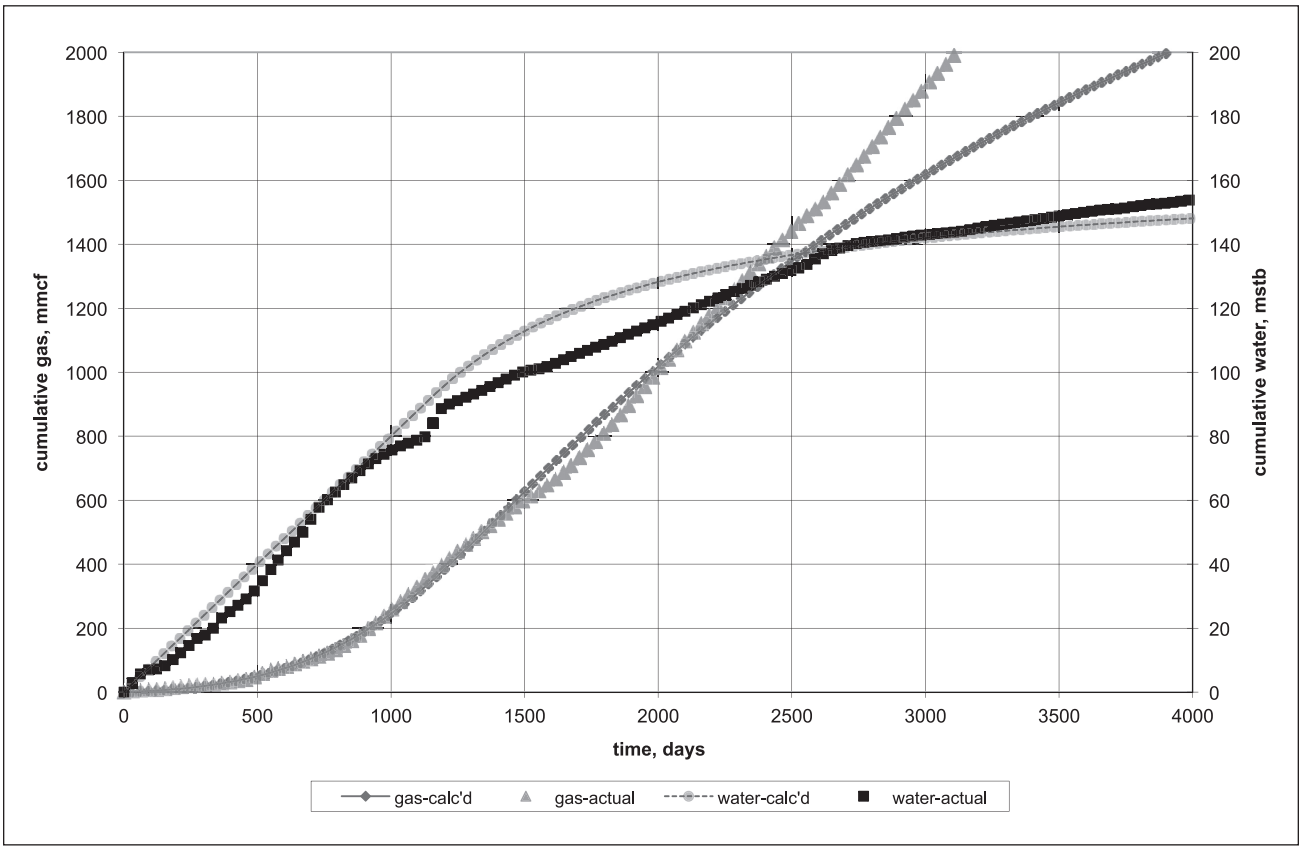



**Fig. 10–5.** Example 10.1 Utah #25-7-6 gas and water cumulative production

**Table 10–2.** Example 10.1—Utah #25-7-6 step-by-step calculation

| Time, days | $S_w$ | $k_{rw}$ | $k_{rg}$ | $p_{wf}$, psia | $q_w$, bpd | $\Delta W_p$, mstb | $W_p$, mstb | $m(p_{wf})$, psia$^2$/cp | $m(p_{bar})$, psia$^2$/cp | $q_g$, mcfd | $\Delta G_p$, mmcf |
|---|---|---|---|---|---|---|---|---|---|---|---|
| 0 | 0.9500 | 0.731 | 0.007 | 928.4 | 80.0 | 0.000 | 0.000 | 7.71E+07 | 1.26E+08 | 26.6 | 0.000 |
| 30 | 0.9433 | 0.714 | 0.008 | 922.0 | 80.0 | 2.400 | 2.400 | 7.60E+07 | 1.26E+08 | 32.9 | 0.891 |
| 60 | 0.9366 | 0.696 | 0.010 | 914.7 | 80.0 | 2.400 | 4.800 | 7.48E+07 | 1.26E+08 | 39.4 | 1.084 |
| 90 | 0.9298 | 0.679 | 0.011 | 906.7 | 80.0 | 2.400 | 7.200 | 7.36E+07 | 1.25E+08 | 46.2 | 1.285 |
| 120 | 0.9231 | 0.661 | 0.013 | 897.9 | 80.0 | 2.400 | 9.600 | 7.22E+07 | 1.25E+08 | 53.4 | 1.494 |
| 150 | 0.9163 | 0.644 | 0.014 | 888.6 | 80.0 | 2.400 | 12.000 | 7.07E+07 | 1.25E+08 | 60.8 | 1.712 |
| 180 | 0.9096 | 0.626 | 0.016 | 878.6 | 80.0 | 2.400 | 14.400 | 6.91E+07 | 1.24E+08 | 68.6 | 1.942 |
| 210 | 0.9028 | 0.608 | 0.017 | 867.9 | 80.0 | 2.400 | 16.800 | 6.75E+07 | 1.24E+08 | 76.9 | 2.182 |
| 240 | 0.8960 | 0.592 | 0.019 | 857.3 | 80.0 | 2.400 | 19.200 | 6.58E+07 | 1.24E+08 | 86.8 | 2.454 |
| 270 | 0.8892 | 0.577 | 0.021 | 846.6 | 80.0 | 2.400 | 21.600 | 6.42E+07 | 1.23E+08 | 97.9 | 2.770 |
| 300 | 0.8823 | 0.562 | 0.023 | 835.3 | 80.0 | 2.400 | 24.000 | 6.26E+07 | 1.23E+08 | 109.6 | 3.112 |
| 330 | 0.8754 | 0.546 | 0.025 | 823.3 | 80.0 | 2.400 | 26.400 | 6.08E+07 | 1.22E+08 | 121.8 | 3.470 |
| 360 | 0.8685 | 0.531 | 0.027 | 810.5 | 80.0 | 2.400 | 28.800 | 5.89E+07 | 1.22E+08 | 134.6 | 3.845 |
| 390 | 0.8616 | 0.516 | 0.030 | 796.8 | 80.0 | 2.400 | 31.200 | 5.69E+07 | 1.21E+08 | 148.1 | 4.240 |
| 420 | 0.8546 | 0.500 | 0.032 | 782.2 | 80.0 | 2.400 | 33.600 | 5.49E+07 | 1.21E+08 | 162.0 | 4.652 |
| 450 | 0.8476 | 0.485 | 0.034 | 767.1 | 80.0 | 2.400 | 36.000 | 5.29E+07 | 1.20E+08 | 177.2 | 5.088 |
| 480 | 0.8406 | 0.472 | 0.036 | 752.0 | 80.0 | 2.400 | 38.400 | 5.08E+07 | 1.19E+08 | 194.2 | 5.571 |
| 510 | 0.8335 | 0.458 | 0.039 | 735.8 | 80.0 | 2.400 | 40.800 | 4.86E+07 | 1.18E+08 | 212.2 | 6.096 |
| 540 | 0.8264 | 0.444 | 0.041 | 718.5 | 80.0 | 2.400 | 43.200 | 4.64E+07 | 1.18E+08 | 230.8 | 6.644 |
| 570 | 0.8192 | 0.430 | 0.044 | 700.0 | 80.0 | 2.400 | 45.600 | 4.41E+07 | 1.17E+08 | 250.0 | 7.211 |
| 600 | 0.8120 | 0.416 | 0.047 | 680.1 | 80.0 | 2.400 | 48.000 | 4.16E+07 | 1.16E+08 | 270.3 | 7.805 |
| 630 | 0.8048 | 0.401 | 0.049 | 658.7 | 80.0 | 2.400 | 50.400 | 3.90E+07 | 1.15E+08 | 291.7 | 8.430 |
| 660 | 0.7974 | 0.388 | 0.052 | 636.9 | 80.0 | 2.400 | 52.800 | 3.65E+07 | 1.14E+08 | 313.3 | 9.075 |
| 690 | 0.7901 | 0.376 | 0.055 | 615.7 | 80.0 | 2.400 | 55.200 | 3.41E+07 | 1.13E+08 | 335.7 | 9.735 |
| 720 | 0.7826 | 0.364 | 0.058 | 593.0 | 80.0 | 2.400 | 57.600 | 3.16E+07 | 1.11E+08 | 358.9 | 10.418 |
| 750 | 0.7751 | 0.352 | 0.060 | 568.7 | 80.0 | 2.400 | 60.000 | 2.92E+07 | 1.10E+08 | 382.5 | 11.121 |
| 780 | 0.7675 | 0.340 | 0.063 | 542.5 | 80.0 | 2.400 | 62.400 | 2.65E+07 | 1.09E+08 | 407.6 | 11.852 |
| 810 | 0.7598 | 0.328 | 0.066 | 514.4 | 80.0 | 2.400 | 64.800 | 2.39E+07 | 1.08E+08 | 433.2 | 12.612 |
| 840 | 0.7521 | 0.315 | 0.069 | 483.9 | 80.0 | 2.400 | 67.200 | 2.11E+07 | 1.06E+08 | 459.7 | 13.393 |
| 870 | 0.7443 | 0.305 | 0.072 | 455.3 | 80.0 | 2.400 | 69.600 | 1.87E+07 | 1.05E+08 | 485.7 | 14.180 |

Inspection of figure 10–4 shows that although calculated and actual gas rates are in general agreement, they do not match for the first 500 days of production, and calculated gas rate is below actual rate after about 2,500 days. Initial production from a coal well is transient flow, and the above rate equations, equations (10.1), (10.2), and (10.3), are valid only after the well reaches pseudosteady-state flow. Time to reach pseudosteady-state flow can be calculated with equation (10.4) using reservoir properties from table 10–1. From table 10–2, the average gas relative permeability for the first 510 days of production is 0.021. Gas properties, calculated with standard correlations, and sorption compressibility, from equation (7.30), are the following:

$$c_g = 9.48(10)^{-4} \text{ psia}^{-1}$$

$$\mu_g = 0.0134 \text{ cp}$$

$$c_s = 8.07(10)^{-3} \text{ psia}^{-1}$$

| | | Iterate 3 times for new average pressure | | | | | | | | |
|---|---|---|---|---|---|---|---|---|---|---|
| | | Iteration 1 | | | Iteration 2 | | | Iteration 3 | | |
| $G_p$, mmcf | p/Z* | Z | Z* | $p_{bar}$, psia | Z | Z* | $p_{bar}$, psia | Z | Z* | $p_{bar}$, psia |
| 0.000 | | 0.8619 | 3.47E–02 | 1,191.0 | | | | | | 1,191.0 |
| 0.891 | | 0.8619 | 3.47E–02 | 1,190.4 | 0.8620 | 3.47E–02 | 1,190.4 | 0.8620 | 3.47E–02 | 1,190.4 |
| 1.976 | | 0.8620 | 3.47E–02 | 1,189.5 | 0.8620 | 3.47E–02 | 1,189.5 | 0.8620 | 3.47E–02 | 1,189.5 |
| 3.261 | 3.43E+04 | 0.8620 | 3.46E–02 | 1,188.3 | 0.8622 | 3.46E–02 | 1,188.3 | 0.8622 | 3.46E–02 | 1,188.3 |
| 4.754 | 3.43E+04 | 0.8622 | 3.46E–02 | 1,186.8 | 0.8623 | 3.46E–02 | 1,186.8 | 0.8623 | 3.46E–02 | 1,186.8 |
| 6.467 | 3.43E+04 | 0.8623 | 3.46E–02 | 1,185.2 | 0.8625 | 3.46E–02 | 1,185.2 | 0.8625 | 3.46E–02 | 1,185.2 |
| 8.408 | 3.43E+04 | 0.8625 | 3.45E–02 | 1,183.4 | 0.8626 | 3.45E–02 | 1,183.4 | 0.8626 | 3.45E–02 | 1,183.4 |
| 10.590 | 3.42E+04 | 0.8626 | 3.45E–02 | 1,181.5 | 0.8628 | 3.45E–02 | 1,181.5 | 0.8628 | 3.45E–02 | 1,181.5 |
| 13.045 | 3.43E+04 | 0.8628 | 3.45E–02 | 1,179.3 | 0.8630 | 3.45E–02 | 1,179.3 | 0.8630 | 3.45E–02 | 1,179.3 |
| 15.815 | 3.43E+04 | 0.8630 | 3.44E–02 | 1,177.0 | 0.8632 | 3.44E–02 | 1,177.0 | 0.8632 | 3.44E–02 | 1,177.0 |
| 18.927 | 3.43E+04 | 0.8632 | 3.44E–02 | 1,174.6 | 0.8635 | 3.44E–02 | 1,174.6 | 0.8635 | 3.44E–02 | 1,174.6 |
| 22.397 | 3.42E+04 | 0.8635 | 3.43E–02 | 1,171.9 | 0.8637 | 3.43E–02 | 1,171.9 | 0.8637 | 3.43E–02 | 1,171.9 |
| 26.242 | 3.41E+04 | 0.8637 | 3.43E–02 | 1,169.0 | 0.8640 | 3.43E–02 | 1,169.0 | 0.8640 | 3.43E–02 | 1,169.0 |
| 30.482 | 3.41E+04 | 0.8640 | 3.42E–02 | 1,165.9 | 0.8643 | 3.42E–02 | 1,165.9 | 0.8643 | 3.42E–02 | 1,165.9 |
| 35.133 | 3.41E+04 | 0.8643 | 3.41E–02 | 1,162.5 | 0.8646 | 3.41E–02 | 1,162.5 | 0.8646 | 3.41E–02 | 1,162.5 |
| 40.222 | 3.40E+04 | 0.8646 | 3.41E–02 | 1,159.0 | 0.8649 | 3.41E–02 | 1,159.0 | 0.8649 | 3.41E–02 | 1,159.0 |
| 45.793 | 3.40E+04 | 0.8649 | 3.40E–02 | 1,155.1 | 0.8653 | 3.40E–02 | 1,155.1 | 0.8653 | 3.40E–02 | 1,155.1 |
| 51.889 | 3.39E+04 | 0.8653 | 3.39E–02 | 1,151.0 | 0.8657 | 3.39E–02 | 1,151.0 | 0.8657 | 3.39E–02 | 1,151.0 |
| 58.533 | 3.39E+04 | 0.8657 | 3.38E–02 | 1,146.7 | 0.8661 | 3.38E–02 | 1,146.7 | 0.8661 | 3.38E–02 | 1,146.7 |
| 65.744 | 3.38E+04 | 0.8661 | 3.38E–02 | 1,142.0 | 0.8666 | 3.38E–02 | 1,142.0 | 0.8666 | 3.38E–02 | 1,142.0 |
| 73.549 | 3.38E+04 | 0.8666 | 3.37E–02 | 1,137.0 | 0.8671 | 3.37E–02 | 1,137.0 | 0.8671 | 3.37E–02 | 1,137.0 |
| 81.979 | 3.37E+04 | 0.8671 | 3.36E–02 | 1,131.7 | 0.8676 | 3.36E–02 | 1,131.7 | 0.8676 | 3.36E–02 | 1,131.7 |
| 91.055 | 3.36E+04 | 0.8676 | 3.35E–02 | 1,126.0 | 0.8681 | 3.35E–02 | 1,126.0 | 0.8681 | 3.35E–02 | 1,126.0 |
| 100.789 | 3.36E+04 | 0.8681 | 3.34E–02 | 1,120.0 | 0.8687 | 3.34E–02 | 1,120.0 | 0.8687 | 3.34E–02 | 1,120.0 |
| 111.208 | 3.35E+04 | 0.8687 | 3.33E–02 | 1,113.7 | 0.8693 | 3.33E–02 | 1,113.7 | 0.8693 | 3.33E–02 | 1,113.7 |
| 122.329 | 3.34E+04 | 0.8693 | 3.31E–02 | 1,107.0 | 0.8700 | 3.31E–02 | 1,107.0 | 0.8700 | 3.31E–02 | 1,107.0 |
| 134.181 | 3.33E+04 | 0.8700 | 3.30E–02 | 1,100.0 | 0.8707 | 3.30E–02 | 1,100.0 | 0.8707 | 3.30E–02 | 1,100.0 |
| 146.793 | 3.32E+04 | 0.8707 | 3.29E–02 | 1,092.6 | 0.8714 | 3.29E–02 | 1,092.6 | 0.8714 | 3.29E–02 | 1,092.6 |
| 160.186 | 3.31E+04 | 0.8714 | 3.27E–02 | 1,084.8 | 0.8722 | 3.27E–02 | 1,084.8 | 0.8722 | 3.27E–02 | 1,084.8 |
| 174.366 | 3.30E+04 | 0.8722 | 3.26E–02 | 1,076.7 | 0.8730 | 3.26E–02 | 1,076.7 | 0.8730 | 3.26E–02 | 1,076.7 |

Calculating time to reach boundary-dominated flow,

$$t_{pss} = 1.652(10)^7 \frac{0.012(0.0134 \text{ cp})(9.48(10)^{-4} + 8.07(10)^{-3}) \text{ psia } 160 \text{ ac}}{15 \text{ md } (0.021)}$$

$$t_{pss} = 12{,}168 \text{ hr} = 507 \text{ days}$$

Consequently, the disagreement between early-time calculated and actual rates is not unexpected.

Calculated gas rate peaks at about 820 mcfd after 1,500 days of production. Cumulative production at this time is 0.602 bcf and 111.5 mstb, about 13% of OGIP and 33% of OWIP. Occurrence of the actual peak in gas production is difficult to determine due to noisy data but appears to occur later, perhaps as late as 1,800 days, and has a magnitude of about 950 mcfd.

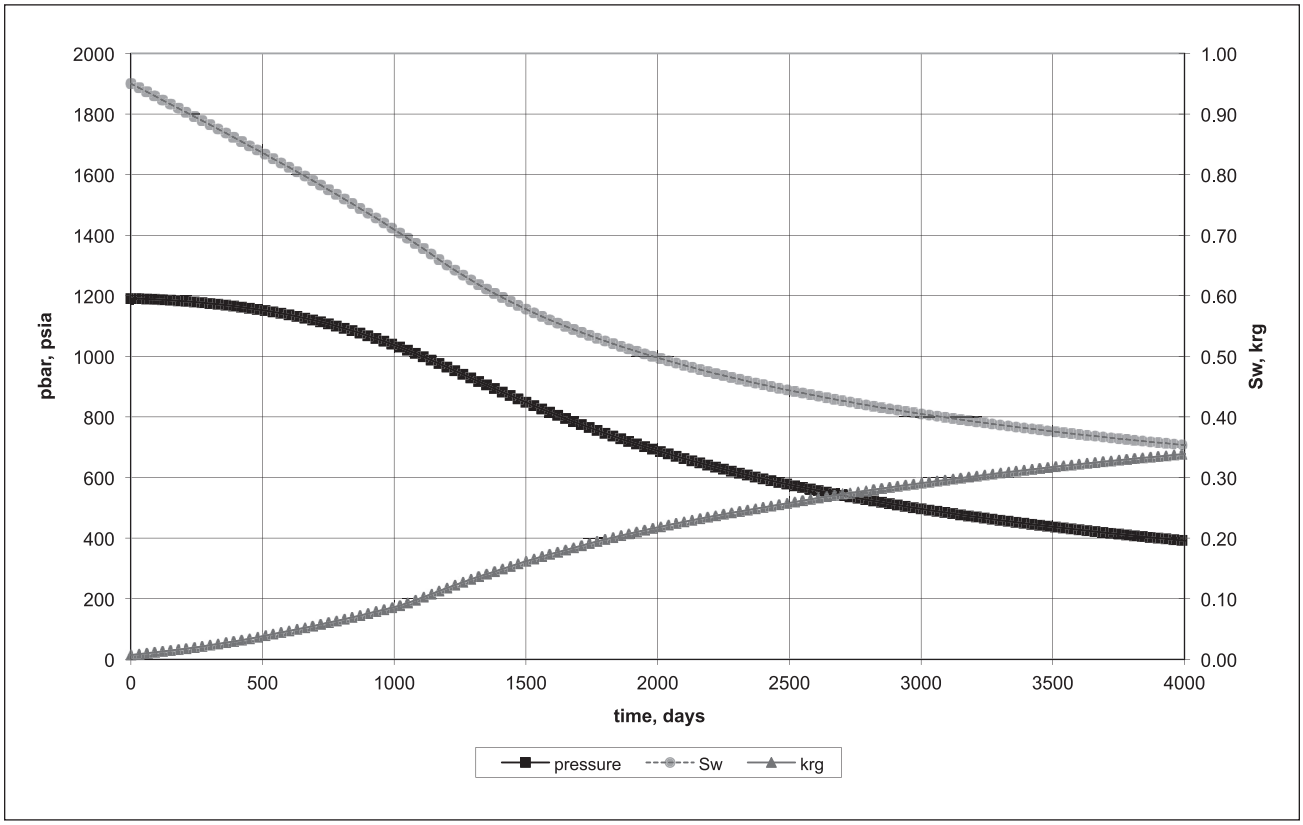



**Fig. 10–6.** Utah #25-7-6 tank model—average pressure, water saturation, and gas relative permeability

Figure 10–4 shows that after approximately 2,500 days, calculated gas rate consistently falls below actual rate. Inspection of figure 10–5 indicates calculated and actual water cumulatives, 148.1 mstb and 154.1 mstb (44% and 45% of OWIP, respectively), are in good agreement throughout the 4,000 day history. However, because of the underprediction of gas rate at late time, calculated cumulative gas production of 2.037 bcf (44% of OGIP) is below the actual cumulative of 2.629 bcf (57% of OGIP). As the early gas production rate, water rate, and water cumulative are all matched fairly well, drainage volume appears correct. The late-time gas production could be explained by gas influx from a dry source. Lamarre and Pratt, investigating gas sorbed by different density rocks of the Drunkard's Wash Field, found significant gas in rocks with densities in excess of 2.0 g/cm$^3$.[10] For instance, a gas content of 100 scf/ton was measured in a sample with a bulk density of 2.3 g/cm$^3$. The reservoir thickness and in-situ isotherm volume constant (and hence OGIP) reported above were based upon a bulk density pay cutoff of 1.75 g/cm$^3$. Lamarre and Pratt calculated that opening up the pay cutoff from 1.75 g/cm$^3$ to 2.40 g/cm$^3$ increased original gas in place of the Birkinshaw No. 18-149 well by 80%. Gas influx from high-density rocks would perhaps explain the difference of 2.629 – 2.037 bcf = 0.592 bcf in cumulative gas production from the Utah #25-7-6 well.

Assuming an economic limit of 3 mcfd, this well has a 105 year well life, with estimated ultimate gas and water recoveries of 3.686 bcf and 161.3 mstb, respectively. Gas recovery is 80% of OGIP, while water recovery is 48% of OWIP.

In summary, using a tank-type model to calculate 4,000 days of gas and water production from this Drunkard's Wash well demonstrated that early-time behavior could not be described accurately due to violation of the assumption of pseudosteady-state flow. However, late-time calculations indicated additional gas is being recovered from high-density rocks, supporting the conclusions of Lamarre and Pratt. Although the tank model cannot predict variation of pressure and saturations over the drainage volume, the calculated gas and water profiles are often sufficiently accurate for driving economic calculations. Note that accurate depletion simulations

require detailed coal and well data, plus substantial production history. Use of tank models, or any other type of model, to predict well behavior in a new coal play requires sufficient data to constrain the model(s).

Depletion behavior of a coal deposit depends on the interplay of degasifying and dewatering. Position on the isotherm (high on the plateau or below the knee) and water saturation (cleats filled with water or with gas) lead to distinct rate signatures. Using a tank model to calculate gas and water profiles for four hypothetical depletion scenarios will demonstrate the variety seen in coal well performance. Consider a single well operated at constant bottomhole pressure draining a bounded, single, flat, homogeneous coal seam with the arbitrary coal and well parameters given in table 10–3. Gas-water relative permeabilities are those measured by Conway et al. for the Marylee/Blue Creek seam in the Warrior Basin.[11] Scenario A assumes an initial gas content high on the isotherm plateau (fig. 10–7), and a high initial water saturation poised to descend the water relative permeability curve (fig. 10–8). Changes in gas content and saturations over the first 250 days of production are also noted on the figures. During this production period, the coal experiences minimal degasification as gas content drops only 1 scf/ton from the initial value of 562.7 scf/ton. Reservoir pressure decreases 20 psia from the initial 1,200 psia pressure. In contrast, water saturation falls 11%, from 0.99 to 0.88, during the 250 day production interval. This 11% reduction in water saturation decreases water relative permeability from 0.82 to 0.11, while that of gas increases from 0 to 0.012. Gas and water production rates for this scenario, depicted in figure 10–9, change dramatically in response to the rapid dewatering of the coal. Gas rate increases three orders of magnitude, while water rate drops by one. The gas-water ratio rises from 0 to more than 2 mcf/stb during the 250 days of production.

**Table 10–3.** Coal and well parameters for isotherm and relative permeability sensitivities

| | | A | B | C | D |
|---|---|---|---|---|---|
| Drainage area, ac = | 160 | | | | |
| Coal thickness, ft = | 20 | | | | |
| $V_{L\,is}$, scf/ton = | | 634 | 2,355 | 634 | 2,355 |
| $p_L$, psia = | | 152 | 3,797 | 152 | 3,797 |
| Bulk density, gm/cc = | 1.800 | | | | |
| Cleat porosity, fraction = | 0.010 | | | | |
| Initial pressure, psia = | 1,200 | | | | |
| Initial water saturation, fraction = | | 0.99 | 0.99 | 0.88 | 0.88 |
| Coalbed temperature, °F = | 70 | | | | |
| Permeability, md = | 15 | | | | |
| Cleat compressibility, psia = | 1.46E–03 | | | | |
| Bottomhole pressure, psia = | 100 | | | | |
| Wellbore radius, feet = | 0.210 | | | | |
| skin = | –2.0 | | | | |
| $B_w$, rb/stb = | 1.0 | | | | |
| water viscosity, cp | 1.00 | | | | |

Scenario B, like scenario A, assumes the same initial water saturation, 0.99, and gas content, 562.7 scf/ton, with isotherm constants chosen to place this gas content on the nearly linear portion of the isotherm below the knee. The sorption isotherm and initial and final gas contents are plotted in figure 10–10. Water saturation changes over 250 days of production, identical to those of scenario A, are shown in figure 10–8. As degasification and dewatering of the coal seam are similar in the two scenarios, the similarity of scenario B gas and water rates, given in figure 10–11, with those of scenario A are not surprising.

Scenario C returns to the isotherm plateau of scenario A and assumes a coal with an initial water saturation of 0.88. The same degree of dewatering, that is, removal of 11% of water in place, now requires 1,063 days, and reservoir pressure drops from 1,200 psia to 753 psia. Isotherm and relative permeability traverses are depicted in figures 10–12 and 10–13, respectively. Gas production rate, plotted in figure 10–14, shows negative decline, a peak, and then relaxes to a gentle decline, while water rate declines exponentially (linearly on a semilog plot) by almost an order of magnitude.

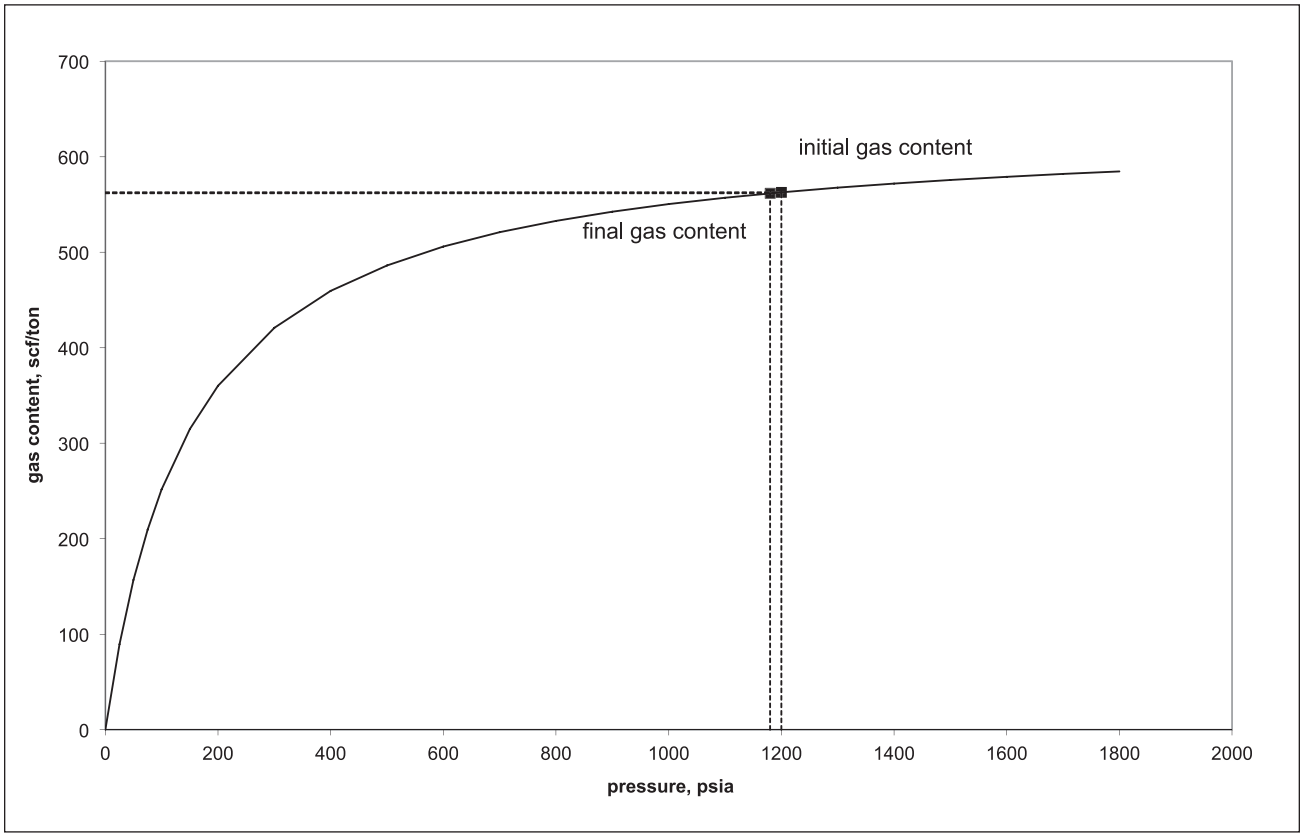



**Fig. 10–7.** Scenario A isotherm traverse

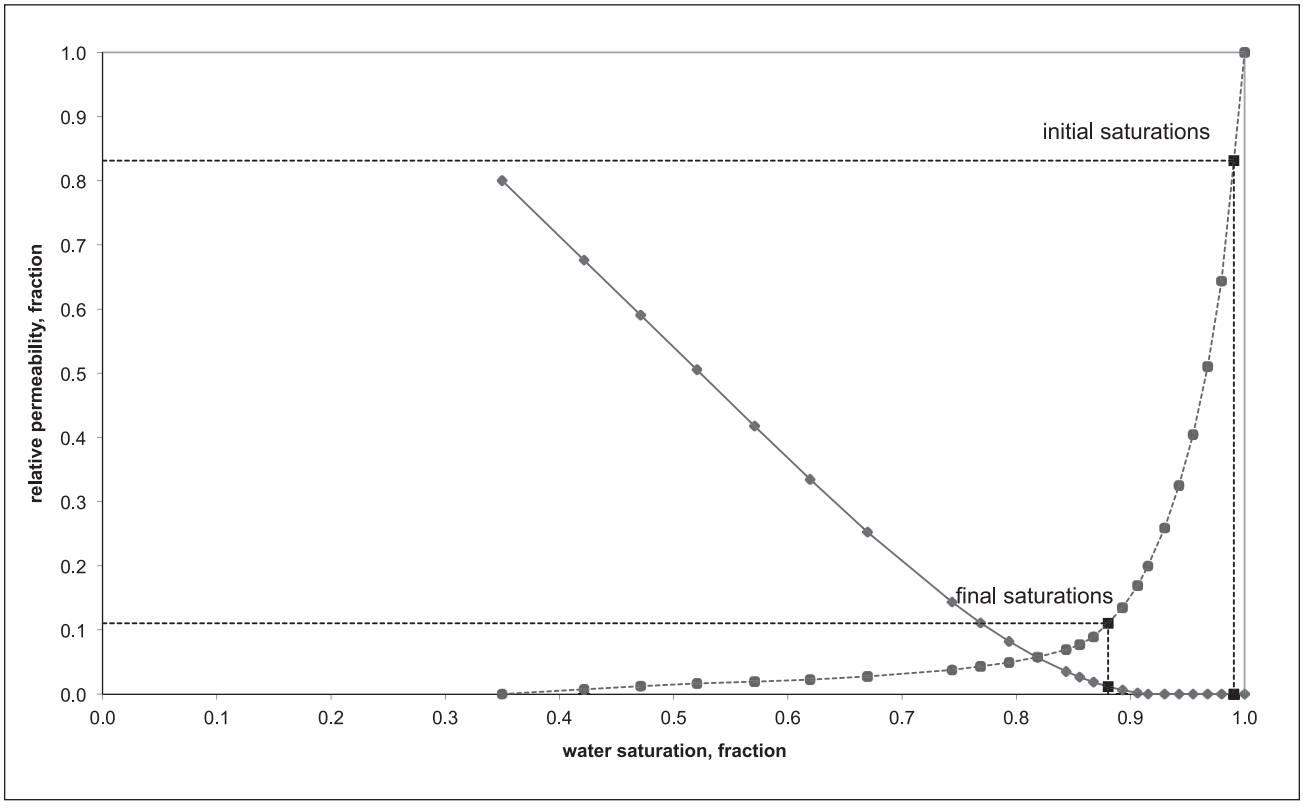



**Fig. 10–8.** Scenarios A and B relative permeabilities traverse[12]

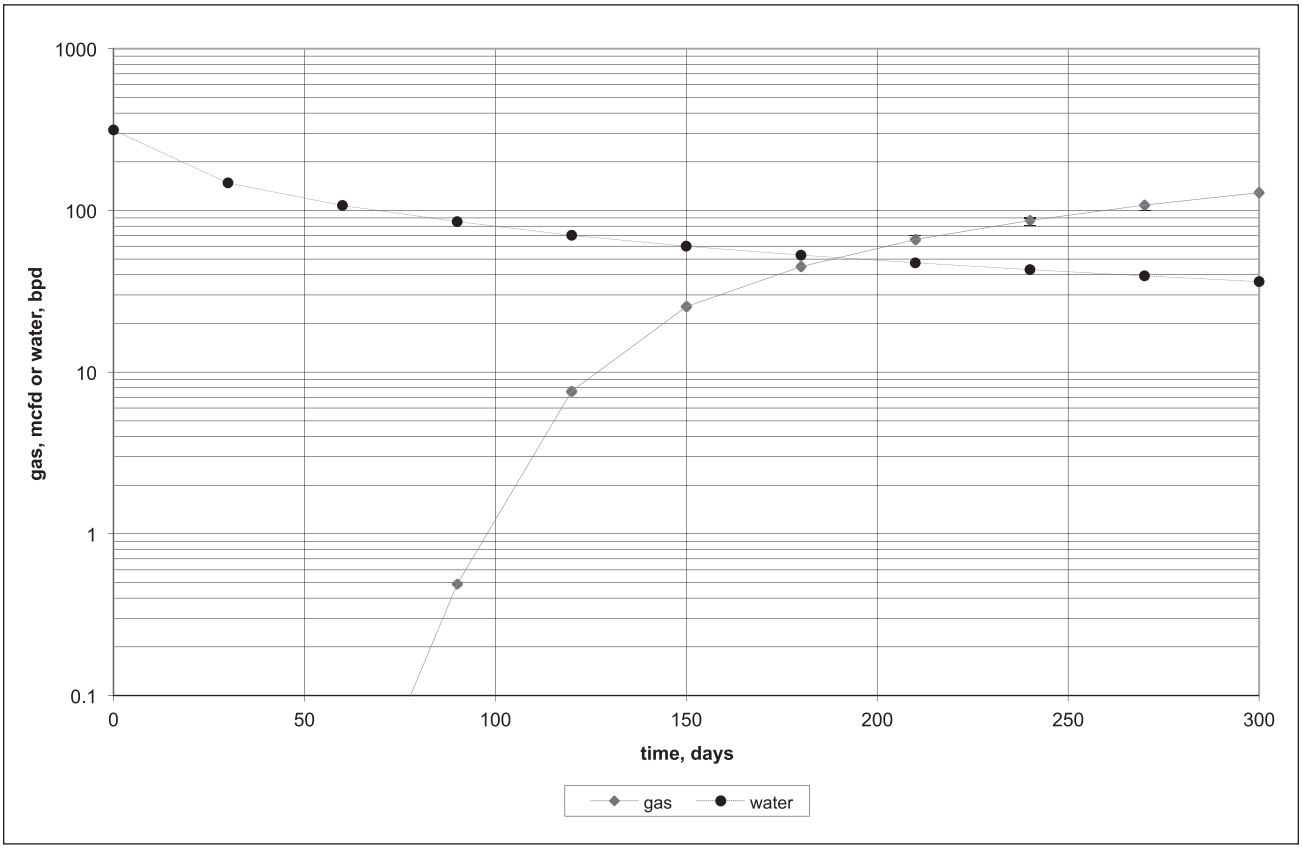



**Fig. 10–9.** Scenario A gas and water production rates

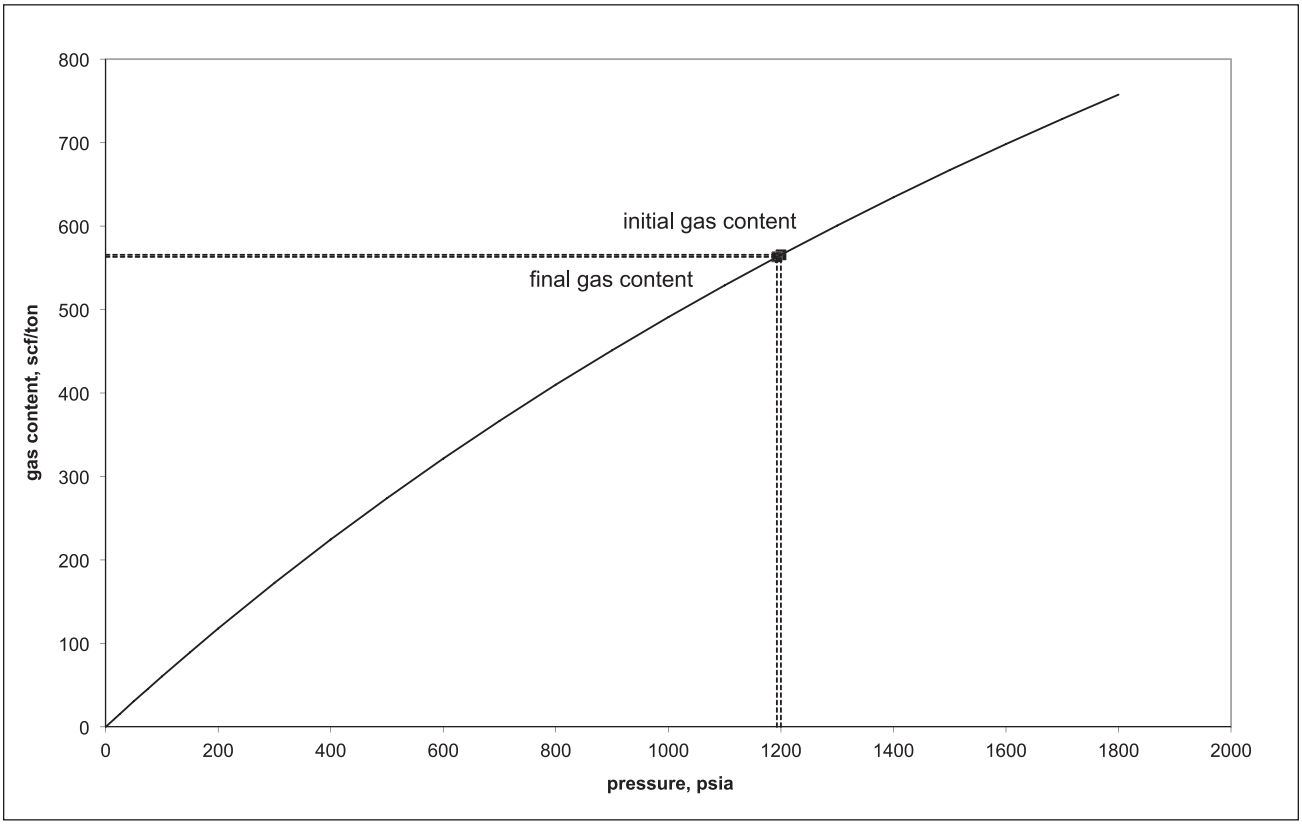



**Fig. 10–10.** Scenario B isotherm traverse

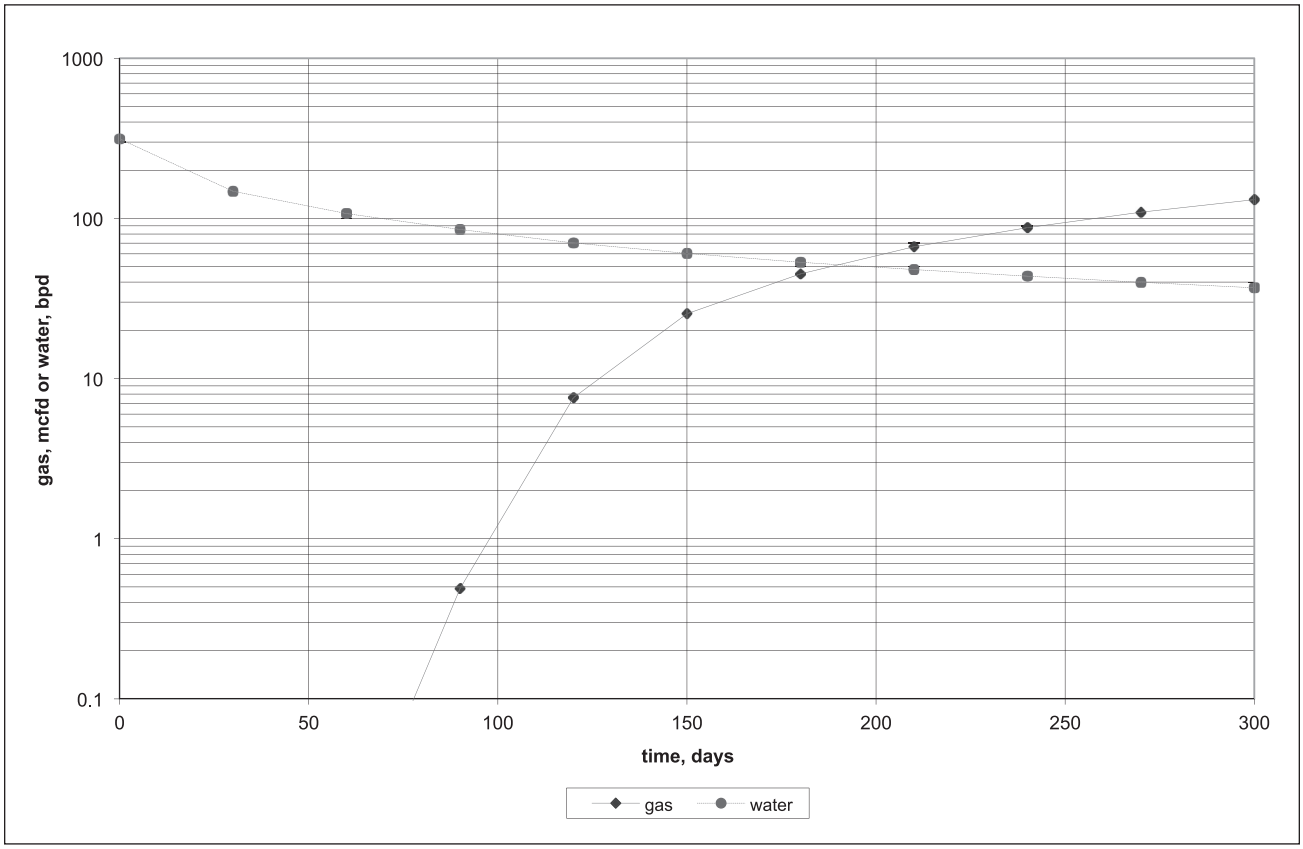



**Fig. 10–11.** Scenario B gas and water production rates

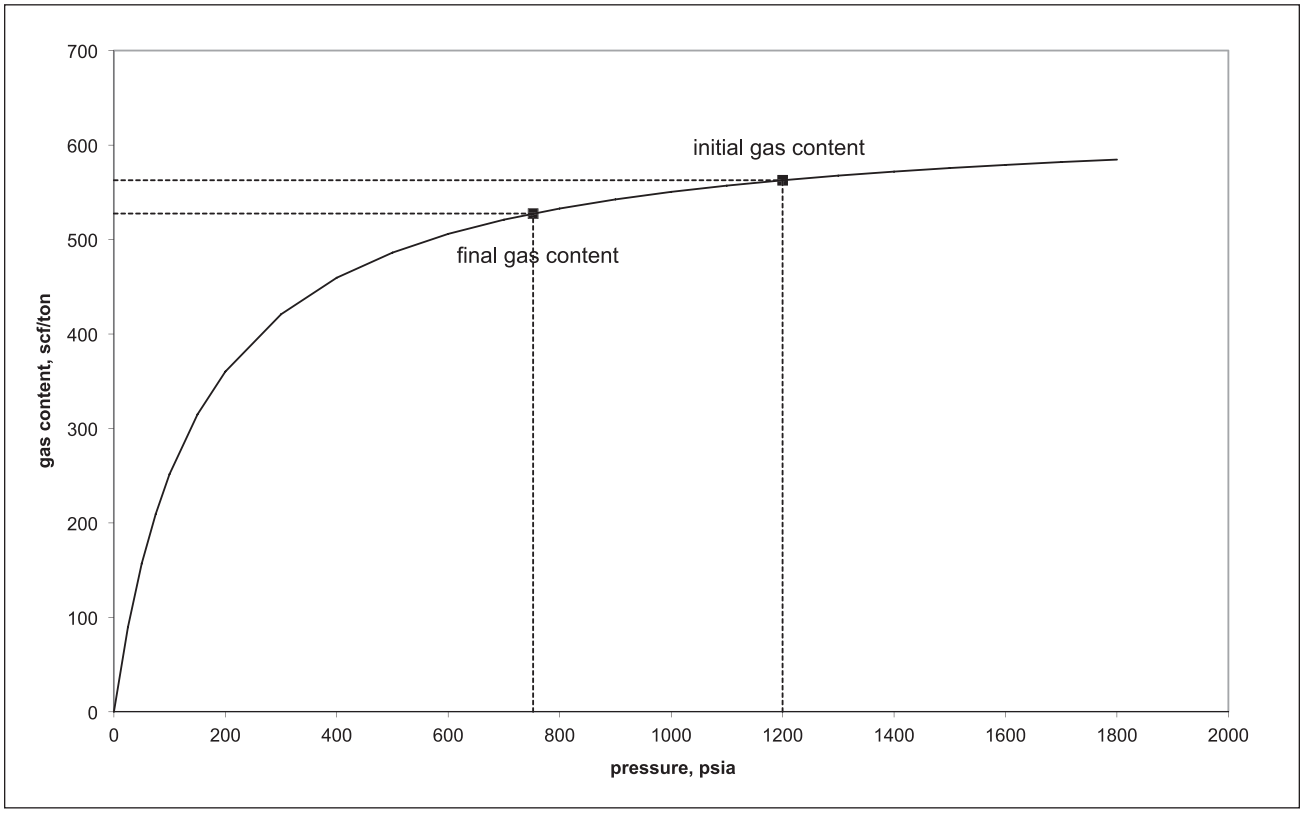



**Fig. 10–12.** Scenario C isotherm traverse

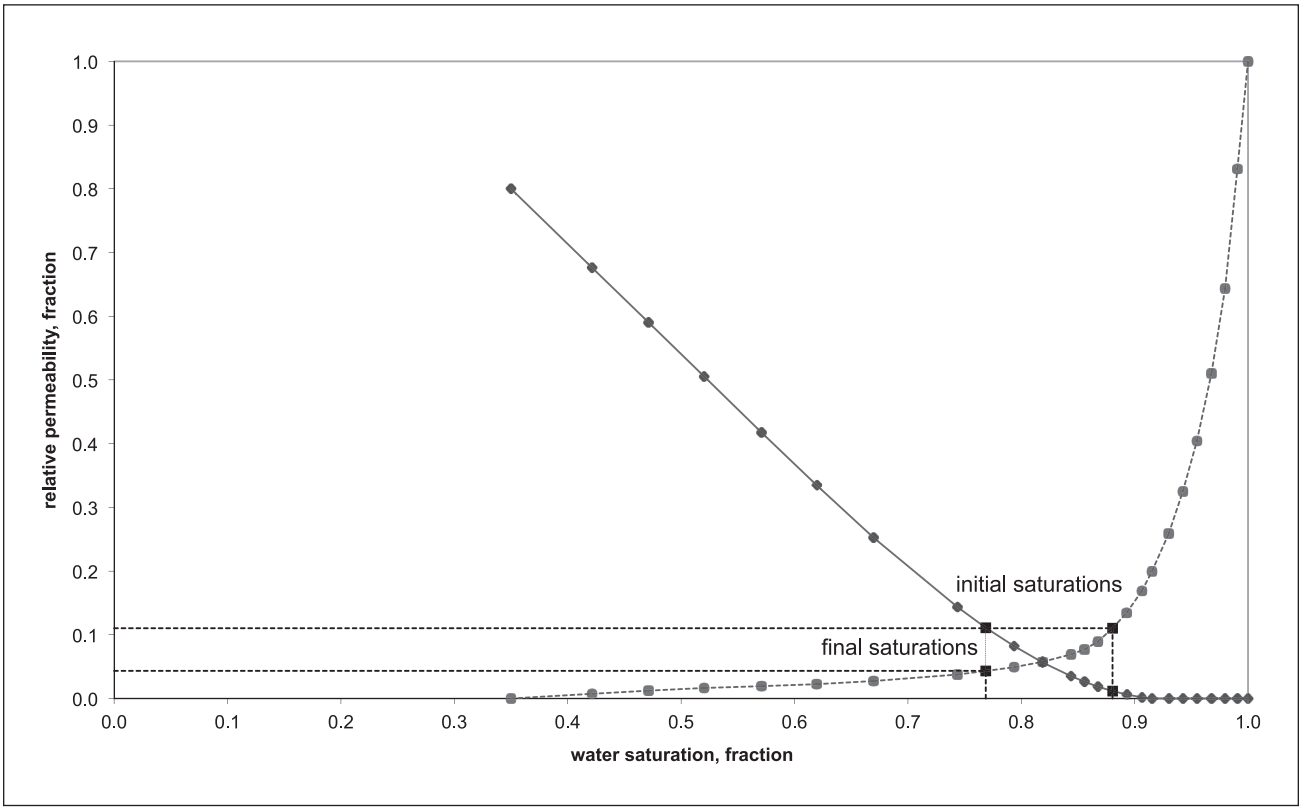



**Fig. 10–13.** Scenarios C and D gas-water relative permeabilities traverse[13]

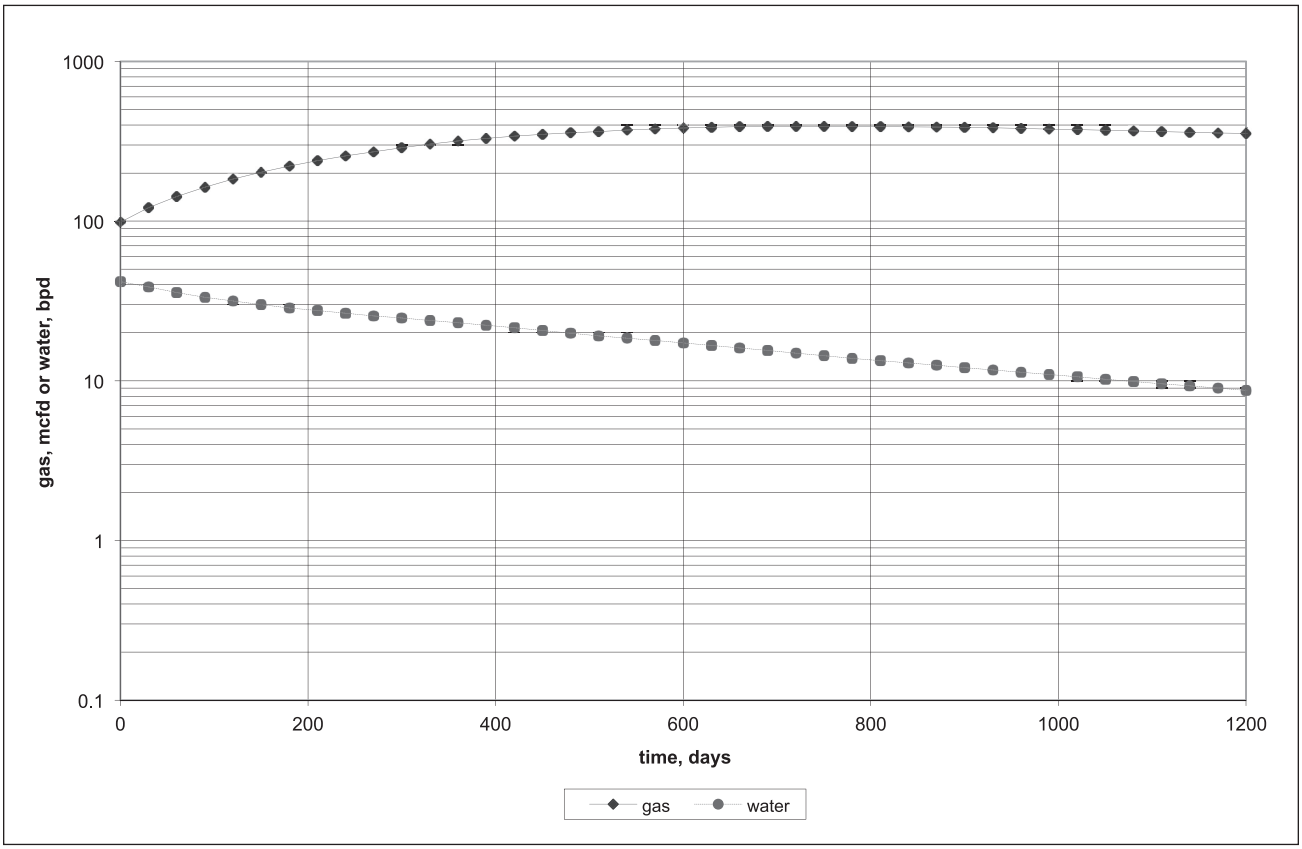



**Fig. 10–14.** Scenario C gas and water production rates

Scenario D utilizes the isotherm of scenario B, placing the initial gas content below the knee of the isotherm, and the water saturation of scenario C, representing a coal with substantial free gas in the cleats. Removal of 11% of the water requires 1,119 days. Reservoir pressure drops to 1,033 psia, reducing gas content by 62 scf/ton to 504 scf/ton. The isotherm traverse is shown in figure 10–15; the relative permeability traverse, shown in figure 10–13, is identical to that of scenario C. Gas production rate, plotted in figure 10–16, rises steadily throughout the production period, while water rate, same figure, declines almost exponentially.

While these four scenarios are highly idealized and by no means exhaustive, they do indicate the diverse signatures seen in gas and water production profiles due to the interaction of dewatering and degasifying a coal seam. Of course, actual coal well performance will be complicated by reservoir complexity and wellbore operations. Reservoir properties of coal deposits vary laterally and stratigraphically. Regardless of whether a coal well is completed in a single seam or in multiple seams, it will drain a reservoir with highly variable thickness, gas content, permeability, and other properties. Coal wells, like conventional wells, are not operated at a constant bottomhole pressure or a constant rate. Mechanical condition of the wellbore can change over time due to deterioration of the frac job, scale deposits, or pump failure and repair or replacement. Surface conditions such as pipeline constraints or water disposal limitations can influence well behavior.

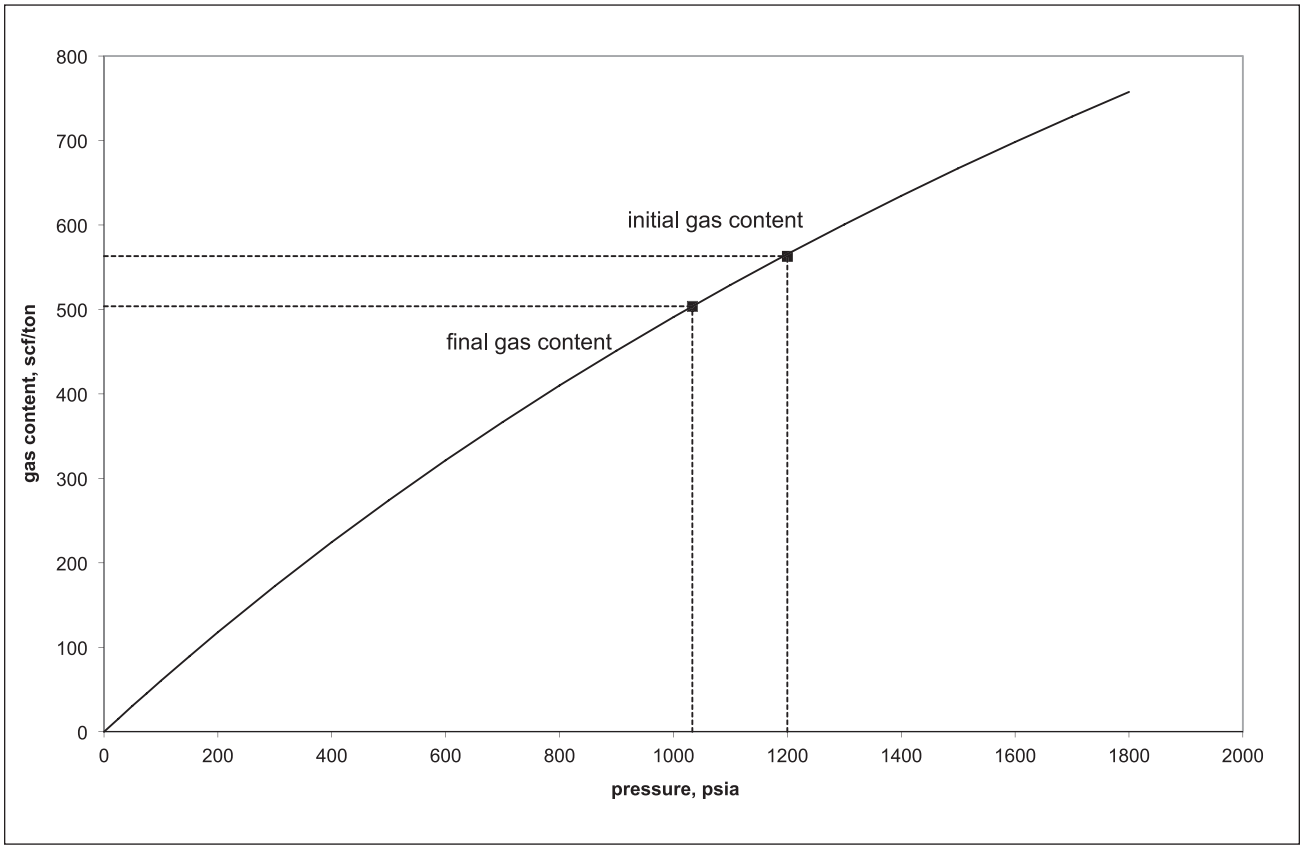



**Fig. 10–15.** Scenario D isotherm depletion traverse

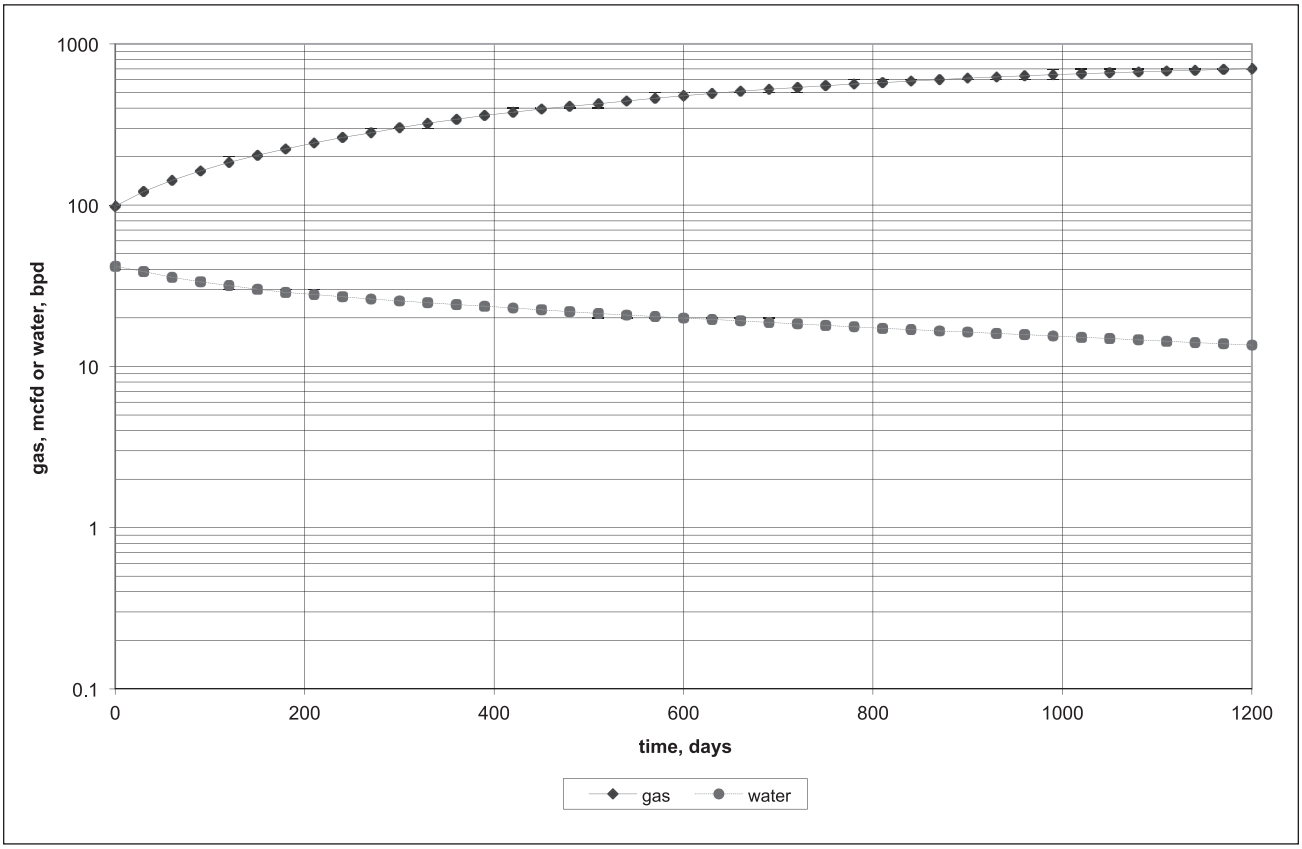



**Fig. 10–16.** Scenario D gas and water production rates

## Gas Production from Dry Coals

Some coal deposits have little, if any, moveable water. Wells completed in the Horseshoe Canyon coals of Alberta, the south San Juan Basin of New Mexico, and the Arkoma Basin of Oklahoma produce gas and almost no water. With no dewatering required, gas production from these wells steadily declines from the initial rate. Calculation of the gas profile requires only a gas rate equation, such as equation (10.1) or (10.2) above, the gas cumulative approximation, equation (10.5), the gas mass balance equation, equation (10.8), and the $Z^*$ relation equation (10.9). Behavior of a dewatered coal using this approach was discussed by Seidle.[14]

The $Z^*$ function for a dry or dewatered coal requires a constant but difficult-to-determine water saturation. Arbitrarily assuming gas relative permeability in a dry coal to be an order of magnitude greater than water relative permeability, inspection of the San Juan gas-water relative permeabilities shown in figure 10–3 yields a water saturation of 0.35. The denominator of the $Z^*$ function is the sum of two terms. One is the ratio of sorbed to free gas per unit volume of coal, and the second is the gas saturation. For many coals, the first term is much larger than the second, allowing the latter to be neglected or simply assumed to be a reasonable value, such as 0.5.

### Example 10.2. Depletion of two Arkoma Basin coal wells

Coals of the Arkoma Basin in eastern Oklahoma are Paleozoic in age and low-volatile bituminous in rank.[15] Occurring as a thin, laterally extensive seam, the primary coal gas target is the Hartshorne coal, which is a dry coal. Geology of the Hartshorne coal and its reservoir properties were discussed by Cardott.[16] The Hartshorne was initially exploited with vertical wells stimulated with cross-linked gel and sand. Resulting well productivity was poor, and a superior stimulation was developed using fresh water (typically 3,500 bbl) and sand (typically 60,000 lb of 20/40 and/or 12/20 mesh). Gas production from two wells in section 35 of T9N R25E was matched

using the real gas pseudopressure formulation, equation (10.1), and the reservoir properties enumerated in table 10–4.

**Table 10–4.** Example 10.2 Franklin and Spiro well and coal properties

| | | |
|---|---|---|
| $V_{L\ daf}$ = | 1,321.8 | scf/ton |
| $p_L$ = | 489.7 | psia |
| Bulk density = | 1.450 | g/cm$^3$ |
| Cleat porosity = | 0.010 | fraction |
| Ash = | 0.0562 | fraction |
| Moisture = | 0.0143 | fraction |
| Initial pressure = | 550 | psia |
| Irreducible water saturation = | 0.5 | |
| Coalbed temperature = | 70 | °F |
| Cleat compressibility = | 1.46E–03 | psia$^{-1}$ |
| Minimum bottomhole press = | 50 | psia |
| $r_w$ = | 0.210 | ft |
| Time step = | 30 | days |

| | Methane gas properties | | |
|---|---|---|---|
| | Franklin 35-2 | Town of Spiro 35-10 | |
| Drainage area = | 40 | 27 | ac |
| Coal thickness = | 4 | 5 | ft |
| Effective permeability to gas = | 5 | 4 | md |
| Skin = | –1.5 | –2.5 | |

*Source:* Cardott, B. J. 1988.

Calculated and actual gas production rates and cumulative production for the Franklin 35-2 are plotted in figures 10–17 and 10–18, respectively. Gas rates agree well for the first 1,000 days, but after this time, the actual gas rate increases, perhaps due to a restimulation or a change in surface operating conditions, neither of which is reflected in the math. Calculated and actual cumulative gas production are in good agreement through about 1,300 days, then actual cumulative rises above calculated due the noted increase in gas rate. Estimated ultimate recovery (EUR) predicted from the tank model will therefore be less than actual. Assuming an economic limit of 3 mcfd, the EUR for this well is 140 mmcf, a recovery of 68% of original gas in place, and well life is 25.8 years.

Calculated and actual gas rates and cumulatives for the Town of Spiro 35-10 well are compared in figures 10–19 and 10–20. Both the gas rate and cumulative production are well matched throughout the 1,600 days of production. Assuming an economic limit of 3 mcfd, estimated ultimate recovery for this well is 122.6 mcf, about 70% of the original gas in place. Well lifetime is 20.6 years.

Drainage areas for the Franklin 35-2 and the Town of Spiro 35-10 wells appear to be 40 ac and 27 ac, respectively, considerably less than the nominal 80 ac spacing for vertical Arkoma coal wells.

The gas flow rate equation assumes pseudosteady-state flow. Time to reach boundary-dominated flow, calculated from equation (10.4), for these two wells is 35 to 45 days. Thus, the 30 day time step employed in the calculations is reasonable.

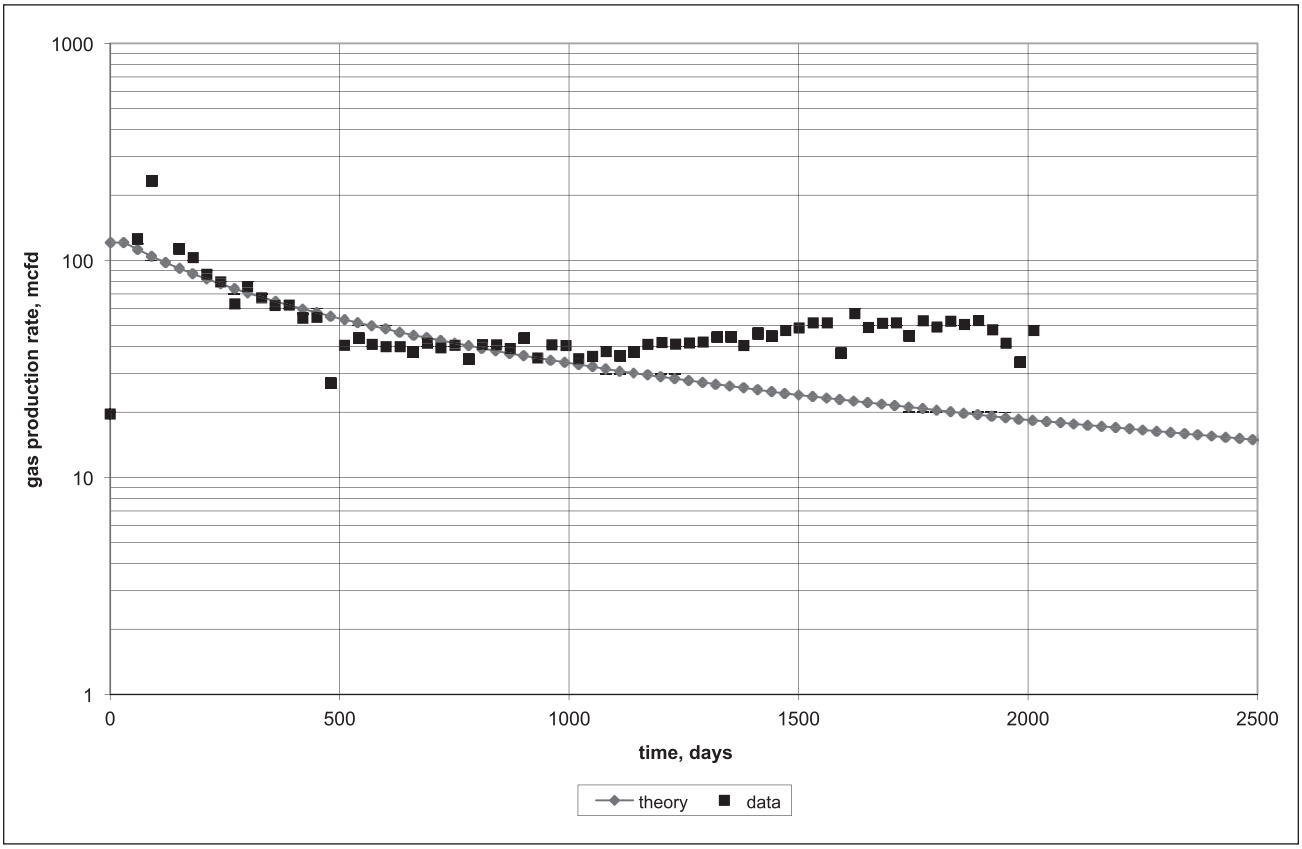



**Fig. 10–17.** Example 10.2 Franklin 35-2 gas production rate

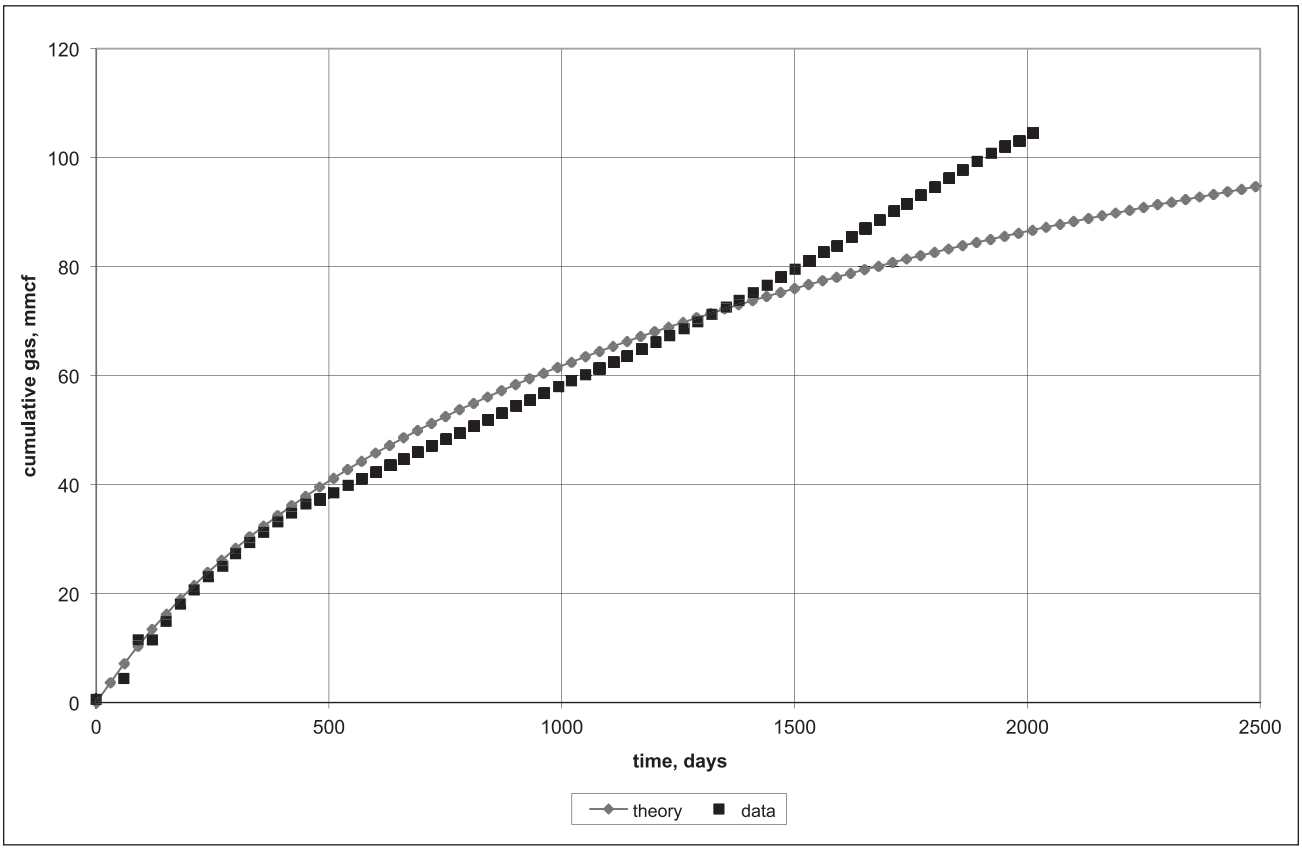



**Fig. 10–18.** Example 10.2 Franklin 35-2 cumulative production

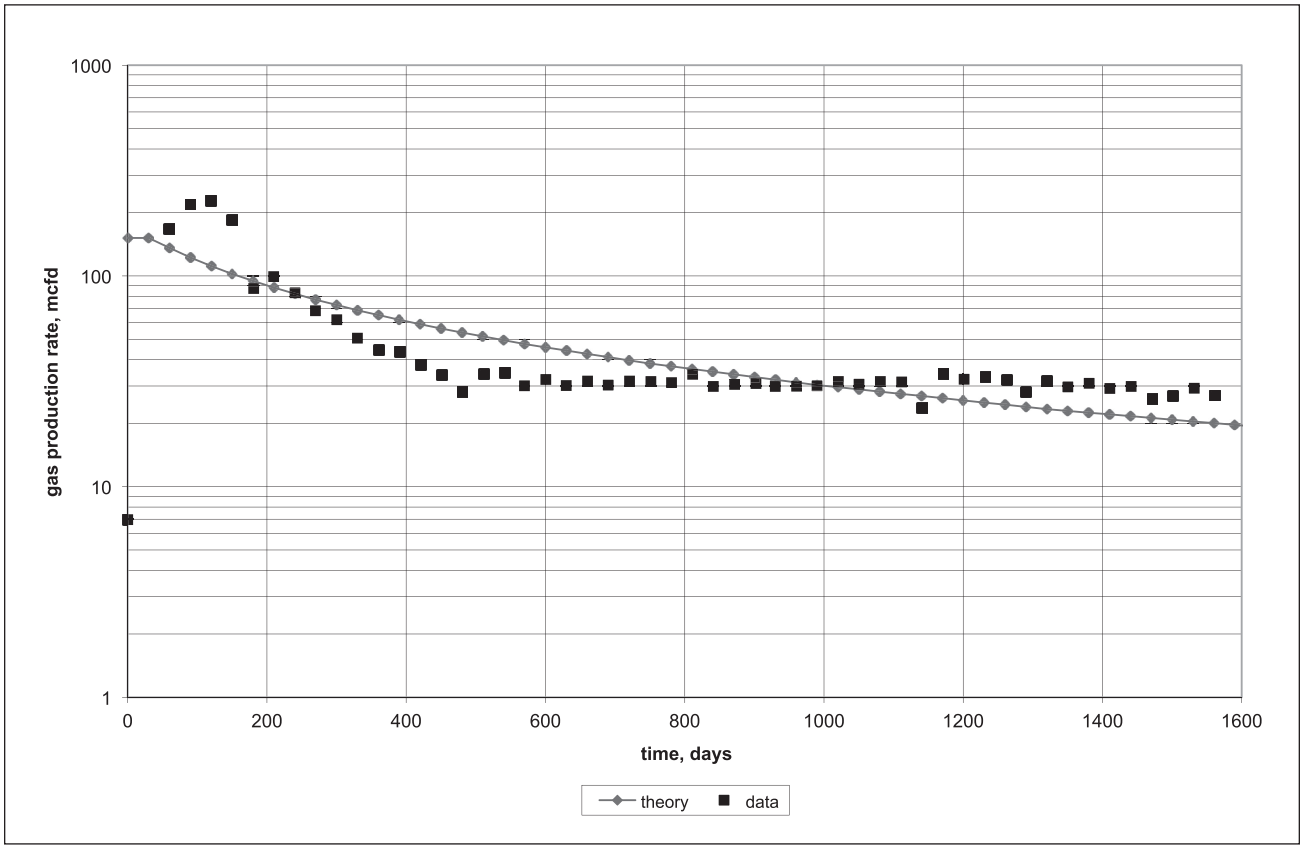



**Fig. 10–19.** Example 10.2 Spiro 35-10 gas production rate

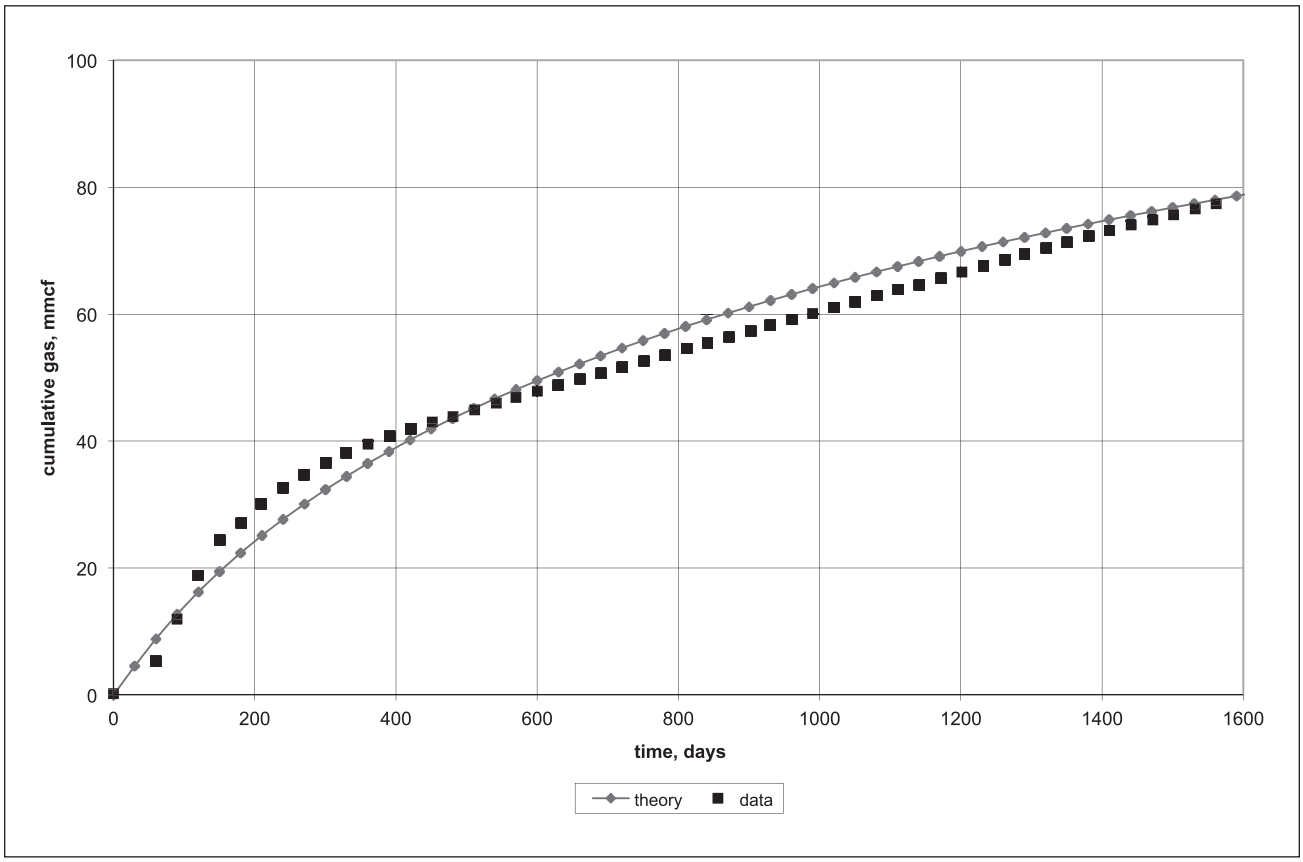



**Fig. 10–20.** Example 10.2 Spiro 35-10 cumulative production

## Depletion of Undersaturated Coals

The amount of gas a coal can sorb depends on temperature and pressure. A coal with a gas content equal to that calculated from the sorption isotherm and current reservoir pressure is said to be *fully saturated*, or simply *saturated*. Coals with less gas currently sorbed than predicted from the sorption isotherm and reservoir pressure are said to be *undersaturated*. The pressure at which gas is first released from the coal is defined as the *desorption pressure*. While a slight degree of undersaturation is not uncommon in many coals, deep undersaturation of a coal deposit is relatively rare. Undersaturated coals require sustained dewatering before any gas is liberated. Consequently, even a modest degree of undersaturation stresses commerciality of a coalbed methane play due to excessive water production and disposal costs before any revenue from gas sales is realized.

The Marylee coal in the Rock Creek Project in the Warrior Basin of Alabama is undersaturated in some areas. Langmuir constants, initial pressure, and desorption pressure for this coal are collected in table 10–5.[17] Actual gas content is calculated as

$$V_i = V_{Lis}\frac{p_d}{p_d + p_L}$$

where

$V_i$ = initial gas content, scf/ton,
$V_{Lis}$ = in-situ Langmuir volume constant, scf/ton,
$p_d$ = desorption pressure, psia, and
$p_L$ = Langmuir pressure constant, psia.

**Table 10–5.** Marylee coal, Rock Creek Project, Warrior Basin, Alabama—Langmuir constants and pressures

| | | |
|---|---|---|
| $V_{Lis}$ = | 561 | scf/ton |
| $p_L$ = | 145 | psia |
| $p_i$ = | 472 | g/cm$^3$ |
| $p_d$ = | 346 | fraction |

*Source:* Gas Research Institute. 1996.

Using table 10–5,

$$V_i = 561\frac{\text{scf}}{\text{ton}}\frac{346\text{ psia}}{(346+145)\text{ psia}} = 395.3\frac{\text{scf}}{\text{ton}}$$

If the coal was fully saturated, it could contain

$$V_{fs} = V_{Lis}\frac{p_i}{p_i + p_L}$$

$$V_{fs} = 561\frac{\text{scf}}{\text{ton}}\frac{472\text{ psia}}{(472+145)\text{ psia}} = 429.2\frac{\text{scf}}{\text{ton}}$$

where

$V_{fs}$ = fully saturated gas content, scf/ton, and
$p_i$ = initial pressure, psia.

The degree of undersaturation can be expressed in terms of gas content or pressure. At this location, the Marylee coal is undersaturated by

$$429.2\ \frac{\text{scf}}{\text{ton}} - 395.3\ \frac{\text{scf}}{\text{ton}} = 33.9\ \frac{\text{scf}}{\text{ton}}$$

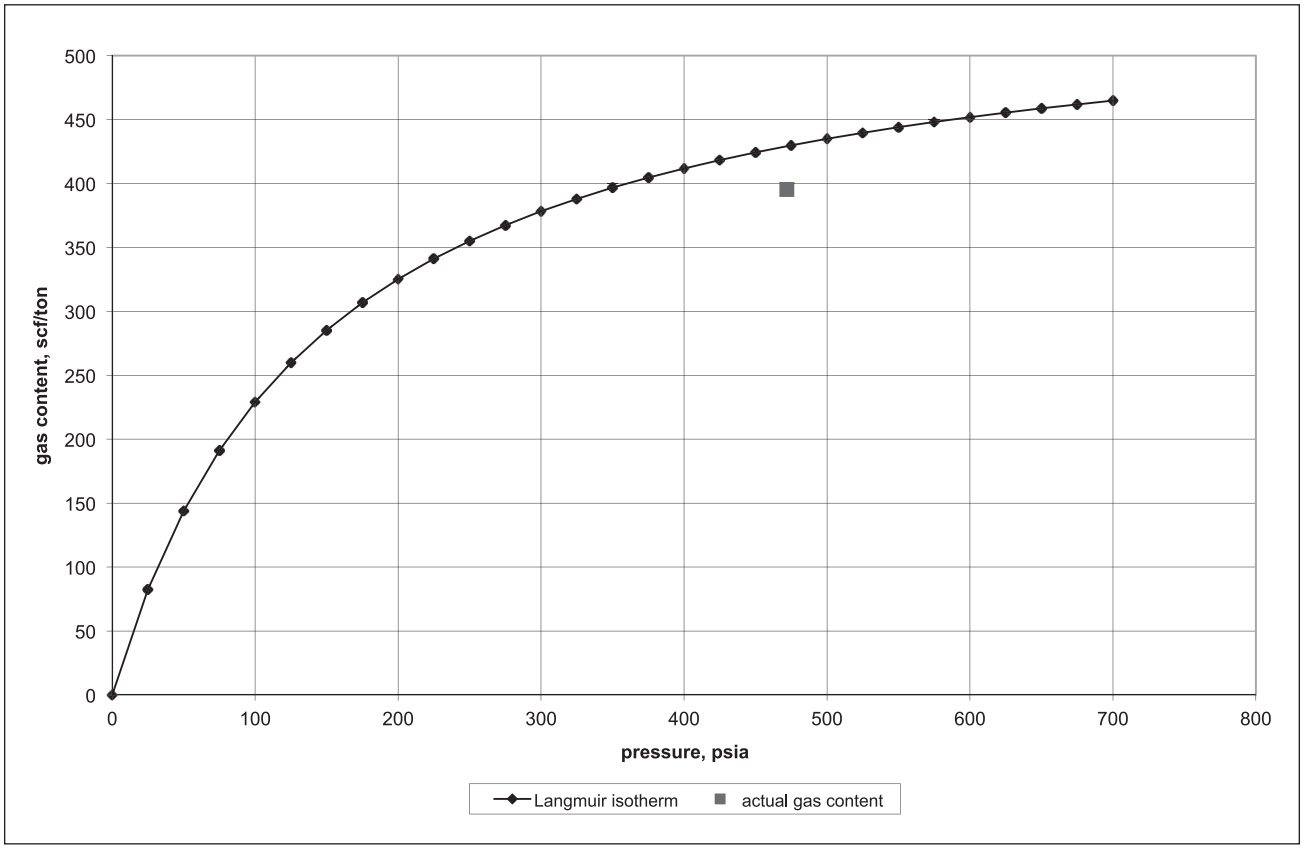
The degree of undersaturation in gas is

$$\frac{V_{fc} - V_i}{V_{fs}} = \frac{429.2\ \frac{\text{scf}}{\text{ton}} - 395.3\ \frac{\text{scf}}{\text{ton}}}{429.2\ \frac{\text{scf}}{\text{ton}}} = 0.079 \approx 8\%$$

The difference between initial and desorption pressures is 472 psia – 346 psia = 126 psia. The degree of undersaturation in pressure is

$$\frac{p_i - p_d}{p_i} = \frac{472\ \text{psia} - 346\ \text{psia}}{472\ \text{psia}} = 0.267 \approx 27\%$$

The isotherm and actual gas content are plotted in figure 10–21. Thus this coal seam is said to be 8% undersaturated in gas and 27% undersaturated in pressure.




**FFig. 10–21.** Sorption isotherm and gas content for Marylee coal, Warrior Basin

With no free gas in the fractures, water production from an undersaturated coal is controlled by cleat, or formation, compressibility. The general equation for compressibility of a coal deposit can be written

$$c_t = c_f + S_w c_w + S_g c_g + c_s$$

where

$c_t$ = total compressibility, psia$^{-1}$,
$c_f$ = cleat compressibility, psia$^{-1}$,
$S_w$ = water saturation, fraction,
$c_w$ = water compressibility, psia$^{-1}$,
$S_g$ = gas saturation, fraction,
$c_g$ = gas compressibility, psia$^{-1}$, and
$c_s$ = sorption compressibility, psia$^{-1}$.

With no free gas present, this equation becomes

$$c_t = c_f + c_w \approx c_f$$

because cleat compressibility is two or three orders of magnitude larger than water compressibility. Cleat compressibility can be written as

$$c_f = -\frac{1}{V}\left(\frac{\partial V}{\partial p}\right)_T$$

The amount of water that must be produced to reduce pressure in the coal seam down to desorption pressure is approximately

$$c_f = -\frac{1}{Ah\phi}\left(\frac{W_p}{p_d - p_i}\right)$$

where

$p_i$ = initial reservoir pressure, psia.

Solving for cumulative water production,

$$W_p = Ah\phi c_f (p_i - p_d)$$

If water is produced at a constant rate, time to reach desorption pressure is

$$t_{des} = \frac{7{,}758.4Ah\phi c_f}{q_w}(p_i - p_d) \qquad \textbf{(10.10)}$$

where

$t_{des}$ = time to reach desorption pressure, days, and
$q_w$ = water production rate, bpd.

After coal seam pressure has fallen to desorption pressure, depletion is described by the same equations as a fully saturated coal.

### Example 10.3. Depletion of a Marylee coal well, Rock Creek Project, Warrior Basin

The Marylee coal was one of the first seams to be exploited for coal gas in the Warrior Basin of Alabama. Initial efforts to mine this seam sought to extract gas ahead of longwall mining. An early description of the reservoir engineering aspects of gas extraction from the Marylee seam in the Rock Creek Project was presented by Zuber et al.[18] A full-field simulation study of the Rock Creek Project was discussed by GRI.[19] Langmuir isotherm constants and initial and desorption pressures are in table 10–5. Other necessary reservoir and well parameters to describe depletion of an 80 ac well draining this coal are collected in table 10–6.

**Table 10–6.** Coal and well properties—Marylee coal, Rock Creek Project, Warrior Basin

| | | |
|---|---|---|
| Drainage area = | 40 | ac |
| Coal thickness = | 6.8 | ft |
| Bulk density = | 1.750 | g/cm$^3$ |
| Cleat porosity = | 0.011 | fraction |
| Coalbed temperature = | 75 | °F |
| Permeability = | 17 | md |
| Cleat compressibility = | 4.00E–04 | psia$^{-1}$ |
| Bottomhole press = | 50 | psia |
| $r_w$ = | 0.210 | ft |
| Skin = | –2.0 | |
| $B_w$ = | 1.0 | rb/stb |
| $\mu_w$ = | 0.90 | cp |
| Time step = | 30 | days |
| Water production rate = | 20 | bpd |

*Source:* Zuber, M. D., et al. 1989.

Depletion of this coal can be divided into two segments defined by the desorption pressure. Above this pressure, constant rate water production steadily reduces coal seam pressure. Below this pressure, gas and water production can be described by the equations employed to describe depletion of a saturated coal in example 10.1. Time to reach desorption pressure, equation (10.10), is

$$t_{des} = \frac{7{,}758.4(40 \text{ ac})\ 6.8 \text{ ft}\ (0.011)4(10)^{-4}\ \text{psia}^{-1}}{20 \text{ bpd}} (472 \text{ psia} - 346 \text{ psia})$$

$$t_{des} = 58.5 \text{ days} \approx 2 \text{ months}$$

Gas and water production rates, plotted in figure 10–22, show this two-month depressurization period followed by steadily rising gas production up to a peak of 56 mcfd after a year. Production rates then slowly decline to 20 mcfd after 2,000 days. Water production, a constant 20 bpd when reservoir pressure is above desorption pressure, steadily declines below it to a final rate of about 1 bpd. Cumulative gas and water production are depicted in figure 10–23. After 2,000 days on production, this well has produced 69.075 mmcf of gas, 27% of original gas in place, and 10.043 mstb of water, which is 43% of original water in place. Cumulative water production required to depressure the coal down to desorption pressure is approximately 1.2 mstb. This volume is only 5% of initial water in place and 12% of cumulative water production through 2,000 days.

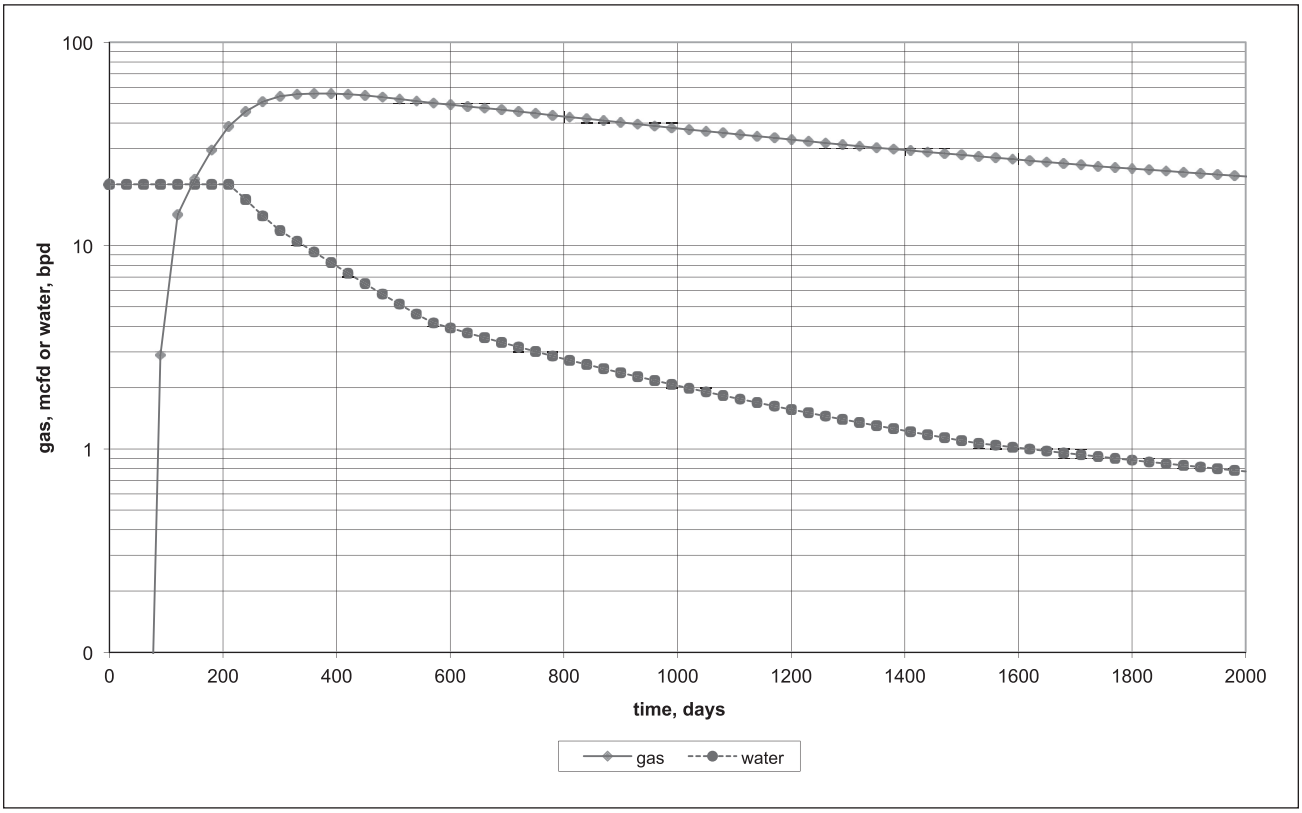



**Fig. 10–22.** Marylee coal, Rock Creek Project, Warrior Basin—gas and water production rates

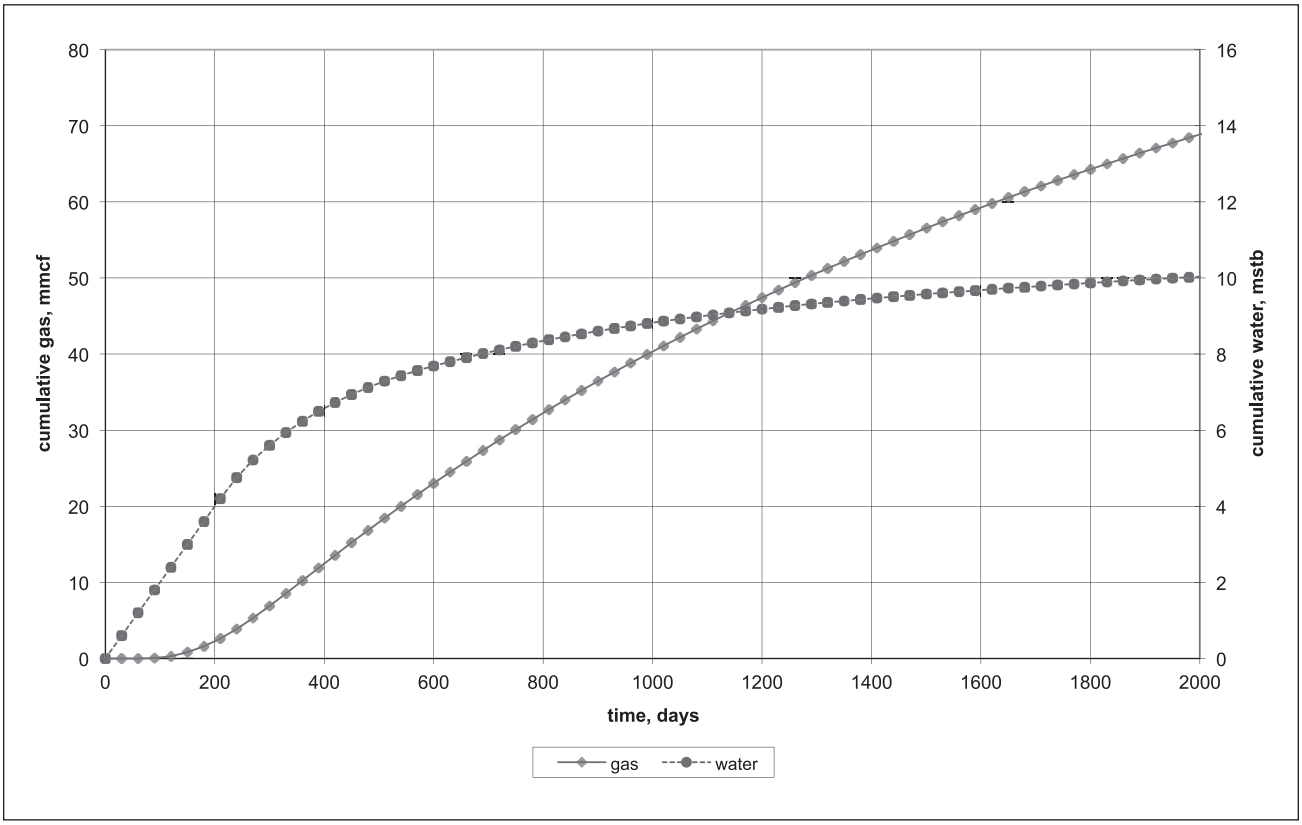



**Fig. 10–23.** Marylee coal, Rock Creek Project, Warrior Basin—cumulative gas and water production

## Coal Well Decline Curves

After more than a century of study, decline curve behavior of oil and gas wells has evolved into a semiempirical, simple, and accurate tool to forecast future production from a well or a field. Early studies of oil well production declines were discussed by Arps using a blend of theoretical arguments and empirical observations.[20] The assumptions underlying these type curves are the following:

- Constant bottomhole flowing pressure
- Constant drainage area with no-flow boundaries
- Constant permeability and wellbore condition
- Boundary-dominated flow

Three basic decline behaviors were recognized: exponential, hyperbolic, and harmonic. The simplest and easiest to use is exponential decline, which is mathematically described by

$$q = q_i e^{-Dt} \tag{10.11}$$

where

$q$ = production rate, bpd or mcfd,
$q_i$ = initial production rate, bpd or mcfd,
$D$ = exponential or nominal decline rate, month$^{-1}$ or year$^{-1}$, and
$t$ = time, month or year.

Any convenient time units can be used in equation (10.11) provided they are consistent, leaving the product $Dt$ dimensionless. Cumulative production at any time $t$, obtained by integrating equation (10.11), is

$$X_p(t) = \frac{q_i - q(t)}{D} f \tag{10.12}$$

where

$X_p$ = cumulative production, stb or mcf, and
$f$ = time factor to cancel units, such as 365 days/year.

Economic lifetime of a well experiencing exponential decline is given by

$$t_{el} = \frac{1}{D} \ln \left[ \frac{q_{el}}{q_i} \right] \tag{10.13}$$

where

$t_{el}$ = economic lifetime, months or years, and
$q_{el}$ = economic rate limit, bpd or mcfd.

The most common type of decline seen in conventional oil and gas wells, hyperbolic, is given by

$$q = \frac{q_i}{(1 + bD_i t)^{1/b}} \tag{10.14}$$

where

$D_i$ = initial nominal decline rate, month$^{-1}$ or year$^{-1}$, and
$b$ = Arps decline curve exponent.

Cumulative production under hyperbolic decline is given by Thompson and Wright[21]

$$X_p(t) = \frac{q_i^b}{D_i(1-b)}[q_i^{1-b} - q^{1-b}]f \tag{10.15}$$

A well experiencing hyperbolic decline will have an economic lifetime given by

$$t_{el} = \frac{\left(\frac{q_{el}}{q_i}\right)^{-b} - 1}{bD_i} \tag{10.16}$$

The third type of decline, harmonic, is described by

$$q = \frac{q_i}{1 + bD_i t}$$

with cumulative production given by

$$X_p(t) = \frac{q_i}{D_i} \ln \frac{q_i}{q} f$$

and well lifetime by

$$t_{el} = \frac{\left(\frac{q_{el}}{q_i}\right)^{-1} - 1}{D_i}$$

Arps noted that exponential and harmonic declines were special cases of hyperbolic decline with $b = 0$ and 1, respectively. Although lacking any theoretical basis, these special cases came to be regarded as bounding cases, and even today, $b$ values outside this range are often regarded with suspicion.

Fetkovich supplied theoretical foundations for Arps curves and joined them with transient solutions to form type curves for rate predictions.[22] Early-time transient data are used to determine reservoir flow capacity and wellbore skin, while late-time boundary-dominated flow data are utilized to calculate drainage area and to estimate recoverable reserves. Several authors have discussed the Arp $b$ values associated with various conventional reservoir and fluid combinations. Thompson and Wright, Fetkovich et al., and Laustsen noted that the mistaken use of transient data instead of boundary-dominated data yields apparent $b$ values higher than actual.[23] Value of these erroneous $b$ constants could exceed one. The philosophical question of the possible existence of a reservoir and fluid combination such that wells draining it would have a $b$ value greater than one was not addressed.

Although the $b$ value associated with a given oil well or field is constant, the $b$ value for a gas well decline can vary with the degree of drawdown and over the life of the well.[24] For small drawdowns, gas well decline is described by a $b$ value of zero (exponential decline). As the degree of drawdown increases, the $b$ value also increases. Fraim and Wattenbarger noted that gas well declines plotted against real time are not matched by exponential, harmonic, or hyperbolic type curves.[25] To overcome these deficiencies, various time transforms have been introduced for gas well decline type curves , such as those of Agarwal, Carter, Fraim and Wattenbarger, Blasingame and Lee, and Palacio and Blasingame.[26] Most of these time transforms are difficult to use in practice as they require initial gas in place, which must be determined iteratively.

Decline type curves for two-phase coal wells were developed by Ertekin and Mohaghegh and compared to simulated depletions but not actual production.[27] Matches from the simulated examples yielded permeability

errors up to 13% and porosity errors up to 65%. These type curves do not reduce to the classical type curves of Fetkovich, preventing comparison with them or other type curves derived from them.

In practice, more useful results are obtained from describing coal well declines not with dimensionless type curves but with the equations of Arps. Similar to conventional gas wells, this practice requires minimal reservoir information and leads directly to results that are readily utilized in economics. Coal well decline behavior, like that of conventional wells, can vary from well to well but often shows the same type of behavior (exponential, hyperbolic, or harmonic) in the same field or perhaps the same basin. Theoretical Arps *b* values for coal wells have not yet been established but appear to range between zero and one, similar to conventional gas wells.

Gas declines of Warrior Basin coal wells were reported by Hanby and Richardson et al. to be exponential.[28] Hanby reported annual average gas decline coefficients of 22.8%, 17.3%, and 31.4% for wells in the Cedar Cove, Deerlick Creek, and Oak Grove fields, respectively. Water rate decline was not addressed in either study. Seidle observed that coal well gas and water declines were almost always exponential and derived theoretical expressions for gas and water decline coefficients.[29] Comparison with gas decline coefficients from actual Warrior Basin wells and simulated Powder River and San Juan coal wells indicated the theoretical decline coefficients were always conservative. Comparison with water decline coefficients from simulated Powder River Basin and actual Uinta Basin coal wells was complicated by uncertainty in water saturations and noise in the water production data. Decline behavior of Powder River Basin coal wells was investigated by Mavor et al.[30] Simulation studies, analytical derivations, and production decline analysis of more than 8,000 coal wells all indicated gas and water declines of Powder River coal wells are exponential.

### Example 10.4. Decline curve analysis of Utah #25-7-6, Drunkard's Wash Field, Utah

Returning to the Utah #25-7-6 well in the Drunkard's Wash Field of the Uinta Basin, gas production, shown in figure 10–24, exhibits exponential decline after about 2,800 days. The decline curve can be shifted to the right by modifying equation (10.11) to be

$$q = q_i \exp\left[-D\frac{(t - t_0)}{365}\right]$$

where

$t_0$ = offset time, days.

Gas decline in this well can be described with $q_i$ = 1,003.4 mcfd, $D$ = 0.1865 yr$^{-1}$, and $t_0$ = 2,811 days. The resulting semilog straight line is the solid line in figure 10–24. Combining cumulative production at 2,800 days with that predicted from equation (10.12) assuming an economic limit of 3 mcfd gives an estimated ultimate recovery of 3.633 bcf or about 80% of the original gas in place of 4.589 bcf. This estimated ultimate recovery is slightly less than the 3.686 bcf obtained from the tank-type mass balance approach in example 10.1. Decline curve economic lifetime of the well is 38.8 years, about one-third the mass balance lifetime. Calculated late-time rates are very sensitive to decline curve parameters, and the difference in lifetimes is ascribed to mathematics rather than a flaw in either method.

Water production rate, plotted in figure 10–24, is nearly constant during the initial transient period and then exhibits hyperbolic decline throughout the remainder of the well history. Water rate decline, shown as the dashed line in figure 10–24, was calculated from a modified form of equation (10.14)

$$q = \frac{q_i}{\left(1 + bD_i\dfrac{(t - t_0)}{365}\right)^{1/b}}$$

with

$q_i$ = 109.0 bpd,
$b$ = 0.8377,
$D_i$ = 0.6533 $yr^{-1}$, and
$t_0$ = 601 days.

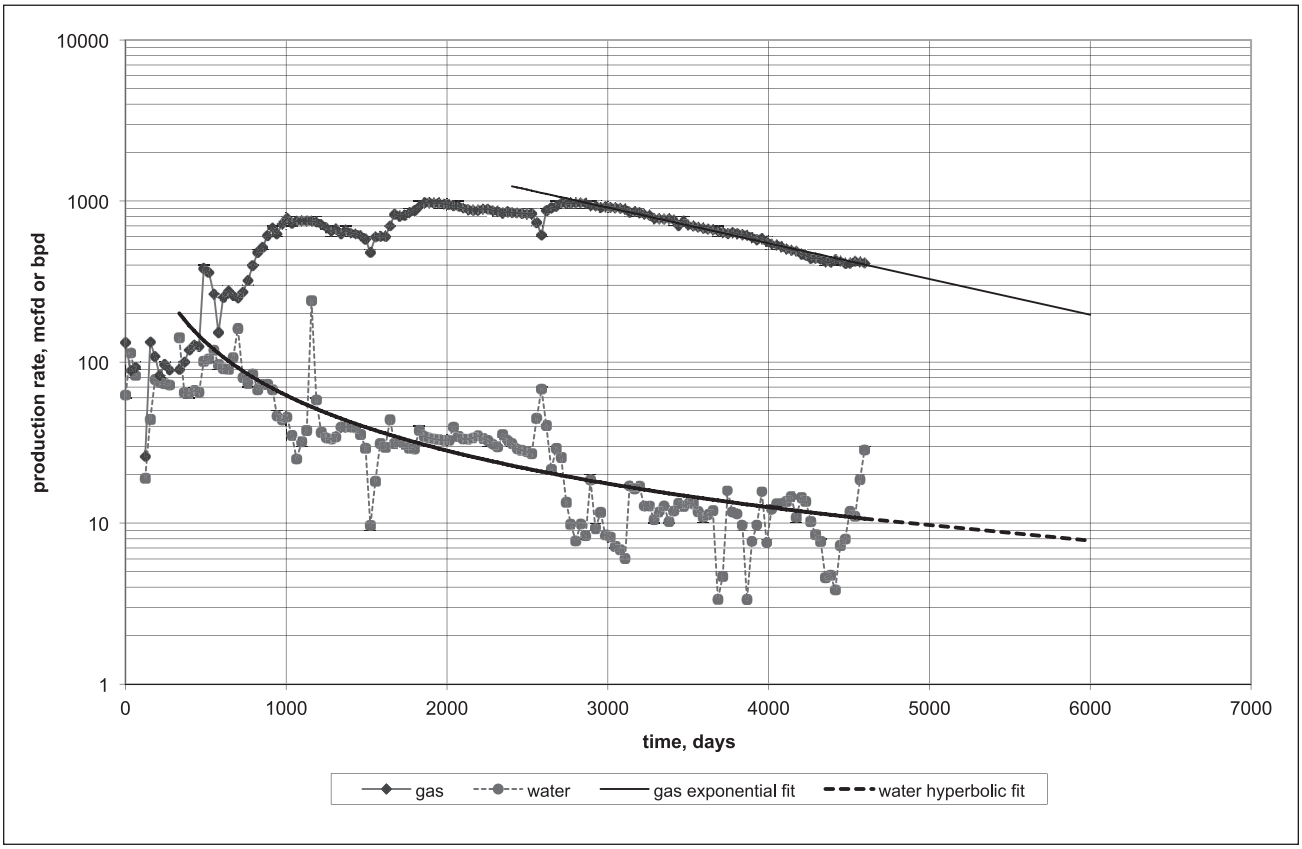



**Fig. 10–24.** Utah #25-6-7 gas and water declines

When gas production falls to the economic limit, the corresponding water production rate is 2.82 bpd. Cumulative water production during the transient flow period plus that predicted from equation (10.15) give an estimated ultimate recovery of 167.4 mstb, about 49% of the 339.6 mstb of water originally in place. Estimated ultimate water recovery from the tank-type mass balance of example 10.1 was 161.3 mstb, approximately 4% less than the decline curve EUR.

## Example 10.5. Decline curve analysis of two Arkoma Basin coal wells

Gas production from wells draining dry coals steadily declines from the initial rate, allowing application of decline curves to all production history. The hyperbolic decline equation, equation (10.14), was fit to production data from the two Arkoma Basin coal wells discussed above. The resulting matches, shown in figures 10–25 and 10–26, were obtained with the coefficients in table 10–7.

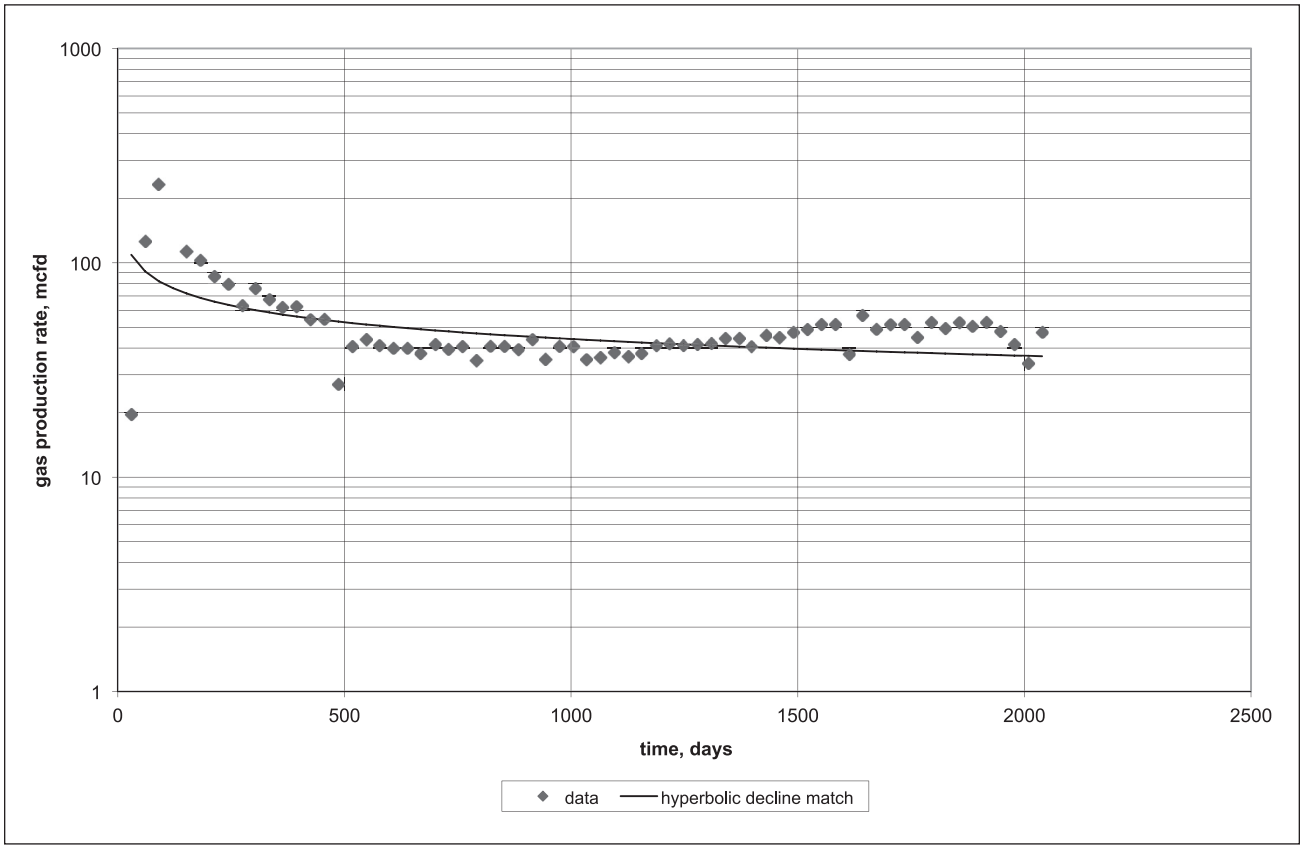



**Fig. 10–25.** Franklin 35-2 hyperbolic decline match

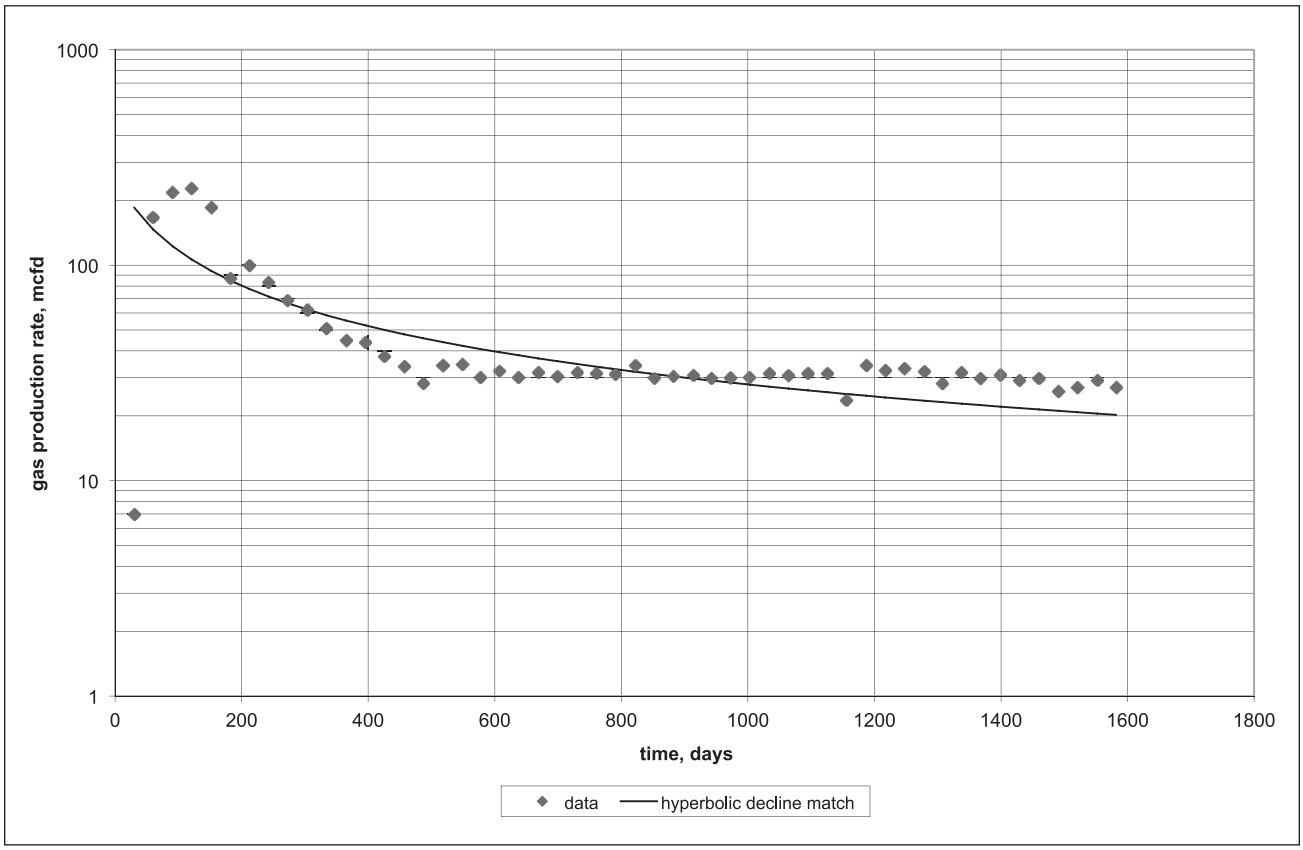



**Fig. 10–26.** Spiro 35-10 hyperbolic decline match

**Table 10–7.** Hyperbolic decline coefficients for two Arkoma Basin coal wells

| | Franklin 35-2 | Spiro 35-10 |
|---|---|---|
| $q_i$, mcf/day = | 317 | 262 |
| $b$ = | 3.847 | 1.357 |
| $D_i$, mon$^{-1}$ = | 15.598 | 0.445 |

Gas production from the Franklin 35-2 is fairly well described by the hyperbolic equation. The exception, as noted above, is the late-time behavior of this well, which appears to be influenced by lower permeability layers or a change in wellhead conditions, neither of which is accounted for in equation (10.14). However, this agreement at early time is deceptive. With an economic limit of 3 mcfd, estimated ultimate recovery, from equation (10.15), is 125 bcf. Well lifetime, from equation (10.16), is 85,000 years. Both of these unrealistically large values are due to the large $b$ factor of 3.847. While no theoretical reason exists for coal well $b$ values to fall between 0 and 1, use of values greater than 1 leads to erroneously large recoveries and lengthy well lives, similar to conventional gas wells. This large $b$ value implies cumulative gas production reaches original gas in place (206.399 mmcf) after 15 years of production. For comparison, the tank model of example 10.2 gives a 15 year recovery of 122.072 mmcf, 59% of OGIP.

The apparent match of Town of Spiro 35-10 gas production with hyperbolic decline is also somewhat deceptive. With a $b$ value of 1.357, estimated ultimate recovery from this well is 197.121 mmcf after a lifetime of 59 years. However, cumulative production equals gas in place (174.149 mmcf) after 41 years of production. For comparison, the tank model of example 10.2 gives an EUR of 122.564 mmcf and a lifetime of 21 years.

## Gas Composition during Depletion

Coal gas is predominantly methane with minor amounts of $CO_2$, nitrogen, and higher hydrocarbons. Produced gas composition will vary as a coal deposit is depleted due to differing sorption strengths of the component gases. Gases that are sorbed more loosely than methane, such nitrogen, will be preferentially released over methane for a given pressure drop. Conversely, gases that are more strongly sorbed than methane, such as $CO_2$ and ethane, will be preferentially retained over methane for a given pressure drop. Note these are equilibrium states, free of any time constraints, depending solely on pressure depletion of the coal seam. Analytical expressions for free and sorbed gas compositions during depletion of a coal containing methane and $CO_2$ can be developed beginning with a mental exercise concerning one ton of dry coal.

Imagine all free gas is instantaneously removed from the pore volume of the sample. In response to this voidage, methane and $CO_2$ will be released from the matrix, charging the cleat to a new pressure. Description of the new state of the system requires five parameters—pressure of the free gas mixture and free and sorbed mole fractions of methane and $CO_2$. As shown below, only four equations are available to describe the state of the system, requiring an iterative solution. These expressions can be readily modified to describe other two-component depletions, such as methane and nitrogen.

Development of these analytical expressions begins with the assumption of a coal with no water in the cleats. Free methane per ton of coal can be written as

$$32.037 \frac{\text{g} - \text{ft}^3}{\text{ton} - \text{cm}^3} \frac{\phi}{\rho_B \frac{\text{g}}{\text{cm}^3} B_{g1} \frac{\text{res ft}^3}{\text{scf}}}$$

Assuming an ideal gas, the methane formation volume factor is

$$B_{g1} = \frac{p_{sc}T}{p_1 T_{sc}}$$

where
subscript *1* = methane, and
$p_1$ = methane partial pressure.

Free methane per ton of coal can now be written as

$$32.037 \frac{\phi}{\rho_B \dfrac{p_{sc}T}{p_1 T_{sc}}} \frac{\text{scf}}{\text{ton}} = 32.037 \frac{\phi p_1 T_{sc}}{\rho_B p_{sc} T} \frac{\text{scf}}{\text{ton}}$$

With subscript *2* denoting $CO_2$, free gas mole fractions, $y_j$s, sum to one, as shown in equation (10.17).

$$1 = y_1 + y_2 \tag{10.17}$$

The sorbed gas mole fractions, $x_j$s, also sum to one, as shown in equation (10.18).

$$1 = x_1 + x_2 \tag{10.18}$$

Relating methane partial pressure to total pressure using the mole fraction of $CO_2$ in the free gas and simplifying gives

$$32.037 \frac{\phi p(1 - y_2)T_{sc}}{\rho_B p_{sc} T} \frac{\text{scf}}{\text{ton}}$$

Similarly, free $CO_2$ per ton of coal is

$$32.037 \frac{\phi p y_2 T_{sc}}{\rho_B p_{sc} T} \frac{\text{scf}}{\text{ton}}$$

Sorbed volumes of methane and $CO_2$ per ton of coal can be calculated from the multicomponent Langmuir equation.

$$V_1 = V_{Lis1} \frac{(1 - y_2)\dfrac{p}{p_{L1}}}{1 + (1 - y_2)\dfrac{p}{p_{L1}} + y_2 \dfrac{p}{p_{L2}}} \frac{\text{scf}}{\text{ton}}$$

$$V_2 = V_{Lis2} \frac{y_2 \dfrac{p}{p_{L2}}}{1 + (1 - y_2)\dfrac{p}{p_{L1}} + y_2 \dfrac{p}{p_{L2}}} \frac{\text{scf}}{\text{ton}}$$

where
subscript *2* = $CO_2$.

Sorbed gas mole fractions are

$$x_1 = \frac{V_1}{V_1 + V_2}$$

$$x_2 = \frac{V_2}{V_1 + V_2}$$

If all free gas is instantaneously removed from the cleats and the system is allowed to come to equilibrium, gas that was sorbed at the initial pressure will now be split between sorbed gas and free gas at a new pressure. Mathematically,

Old sorbed methane, scf/ton = new sorbed methane, scf/ton + new free methane, scf/ton

$$V_{Lis1} \frac{(1 - y_{2i}) \dfrac{p_i}{p_{L1}}}{1 + (1 - y_{2i}) \dfrac{p_i}{p_{L1}} + y_{2i} \dfrac{p_i}{p_{L2}}}$$

$$= V_{Lis1} \frac{(1 - y_2) \dfrac{p}{p_{L1}}}{1 + (1 - y_2) \dfrac{p}{p_{L1}} + y_2 \dfrac{p}{p_{L2}}} + 32.037 \frac{\phi p (1 - y_2) T_{sc}}{\rho_B p_{sc} T}$$

Define sorbed methane at the initial pressure as

$$G_1 = V_{Lis1} \frac{(1 - y_{2i}) \dfrac{p_i}{p_{L1}}}{1 + (1 - y_{2i}) \dfrac{p_i}{p_{L1}} + y_{2i} \dfrac{p_i}{p_{L2}}}$$

Define a new constant from the collection of constants in the free gas expression as

$$E = 32.037 \frac{\phi T_{sc}}{\rho_B p_{sc} T} \tag{10.19}$$

The methane balance can now be expressed as

$$G_1 = V_{Lis1} \frac{(1 - y_2) \dfrac{p}{p_{L1}}}{1 + (1 - y_2) \dfrac{p}{p_{L1}} + y_2 \dfrac{p}{p_{L2}}} + Ep(1 - y_2) \tag{10.20}$$

Similarly, the $CO_2$ mass balance can be written as

Old sorbed $CO_2$, scf/ton = new sorbed $CO_2$, scf/ton + new free $CO_2$, scf/ton

$$V_{Lis2}\frac{y_{2i}\dfrac{p_i}{p_{L2}}}{1+(1-y_{2i})\dfrac{p_i}{p_{L1}}+y_{2i}\dfrac{p_i}{p_{L2}}}=V_{Lis2}\frac{y_2\dfrac{p}{p_{L2}}}{1+(1-y_2)\dfrac{p}{p_{L1}}+y_2\dfrac{p}{p_{L2}}}+32.037\frac{\phi p y_2 T_{sc}}{\rho_B p_{sc} T}$$

Define sorbed $CO_2$ at the initial pressure as

$$G_2=V_{Lis2}\frac{y_{2i}\dfrac{p_i}{p_{L2}}}{1+(1-y_{2i})\dfrac{p_i}{p_{L1}}+y_{2i}\dfrac{p_i}{p_{L2}}}$$

The $CO_2$ balance can now be expressed as, using the above expression and equation (10.19),

$$G_2=V_{Lis2}\frac{y_2\dfrac{p}{p_{L2}}}{1+(1-y_2)\dfrac{p}{p_{L1}}+y_2\dfrac{p}{p_{L2}}}+apy_2 \tag{10.21}$$

As noted above, the new state of the system is described by five variables, pressure and methane and $CO_2$ free and sorbed gas fractions, yet only four equations are available for mathematical behavior of the new state, equations (10.17), (10.18), (10.20), and (10.21). Consequently, an iterative solution is required and will be facilitated by defining methane and $CO_2$ differentials as

$$D_1=V_{Lis1}\frac{(1-y_2)\dfrac{p}{p_{L1}}}{1+(1-y_2)\dfrac{p}{p_{L1}}+y_2\dfrac{p}{p_{L2}}}+Ep(1-y_2)-G_1 \tag{10.22}$$

$$D_2=V_{Lis2}\frac{y_2\dfrac{p}{p_{L2}}}{1+(1-y_2)\dfrac{p}{p_{L1}}+y_2\dfrac{p}{p_{L2}}}+Epy_2-G_2 \tag{10.23}$$

The condition that both these differentials be zero at equilibrium leads to two quadratic equations for the free $CO_2$ mole fraction, $y_2$. From the methane mass balance,

$$0=A_1y_{2meth}^2+B_1y_{2meth}+C_1 \tag{10.24}$$

where

$$A_1=Ep^2\left(\frac{1}{p_{L1}}-\frac{1}{p_{L2}}\right)$$

$$B_1=Ep^2\left(\frac{1}{p_{L2}}-\frac{1}{p_{L1}}\right)-Ep\left(1+\frac{p}{p_{L1}}\right)-V_{Lis1}\frac{p}{p_{L1}}+G_1p\left(\frac{1}{p_{L1}}-\frac{1}{p_{L2}}\right)$$

$$C_1=V_{Lis1}\frac{p}{p_{L1}}+Ep\left(1+\frac{p}{p_{L1}}\right)-G_1\left(1+\frac{p}{p_{L1}}\right)$$

And from the $CO_2$ mass balance

$$0 = A_2 y_{2CO2}^2 + B_2 y_{2CO2} + C_2 \tag{10.25}$$

where

$$A_2 = Ep^2\left(\frac{1}{p_{L2}} - \frac{1}{p_{L1}}\right)$$

$$B_2 = Ep\left(1 + \frac{p}{p_{L1}}\right) + V_{Lis2}\frac{p}{p_{L2}} + G_2 p\left(\frac{1}{p_{L1}} - \frac{1}{p_{L2}}\right)$$

$$C_2 = -G_2\left(1 + \frac{p}{p_{L1}}\right)$$

Equations (10.24) and (10.25) can be solved using the quadratic formula,

$$y_2 = \frac{-B \pm \sqrt{B^2 - 4AC}}{2A}$$

The new system pressure is that which gives the same value of free $CO_2$ mole fraction calculated from equations (10.24) and (10.25).

### Example 10.6. Gas composition during laboratory depletion

Gas contents during adsorption and desorption of selected mixtures of methane and $CO_2$ on a coal sample from the Sewickley seam, located in Pennsylvania, were reported by Greaves et al.[31] Single-component isotherms were also determined. Measured gas contents during depletion of one of the mixtures and the pure component Langmuir isotherm constants are given in table 10–8. Gas compositions were not reported but can be calculated from the selectivity factor

$$\alpha = \frac{V_{Lis1} p_{L2}}{V_{Lis2} p_{L1}} = \frac{x_1 y_2}{x_2 y_1}$$

The initial free $CO_2$ fraction is calculated by first determining the selectivity factor

$$\alpha = \frac{447\,\frac{\text{scf}}{\text{ton}}\ 151\ \text{psia}}{705\,\frac{\text{scf}}{\text{ton}}\ 297\ \text{psia}} = 0.3224$$

Initial sorbed gas fractions are calculated from initial gas contents

$$x_1 = \frac{V_1}{V_1 + V_2} = \frac{149\,\frac{\text{scf}}{\text{ton}}}{523\,\frac{\text{scf}}{\text{ton}}} = 0.2849$$

$$x_2 = \frac{V_2}{V_1 + V_2} = \frac{374\,\frac{\text{scf}}{\text{ton}}}{523\,\frac{\text{scf}}{\text{ton}}} = 0.7151$$

The initial $CO_2$ fraction in the free gas can now be calculated from

$$\alpha = \frac{x_1 y_2}{x_2(1 - y_2)}$$

$$0.3224 = \frac{0.2849 y_2}{0.7151(1 - y_2)}$$

$$y_2 = 0.4473$$

And from equation (10.17),

$$y_1 = 1 - y_2 = 0.5527$$

**Table 10–8.** Reported depletion gas contents and Langmuir isotherms

| | | Langmuir constants | |
|---|---|---|---|
| | | **Methane** | **$CO_2$** |
| | $V_L$, scf/ton = | 447 | 705 |
| | $p_L$, psia = | 297 | 151 |
| **Reported gas contents** | | | |
| **Pressure, psia** | **Total gas content, scf/ton** | **$CH_4$ gas content, scf/ton** | **$CO_2$ gas content, scf/ton** |
| 1,023 | 523 | 149 | 374 |
| 836 | 498 | 141 | 357 |
| 634 | 471 | 128 | 343 |
| 525 | 456 | 120 | 336 |
| 425 | 433 | 109 | 324 |
| 322 | 407 | 92 | 315 |
| 217 | 366 | 60 | 306 |
| 134 | 323 | 28 | 295 |
| 91 | 295 | 10 | 285 |
| 12 | 128 | 9 | 119 |

*Source:* Greaves, K. H., et al. 1993.

Constants in the two quadratics can be evaluated by assuming a coal density of 1.65 g/cm$^3$ and a porosity of 0.01. Beginning with equation (10.19),

$$E = 32.037\frac{\phi T_{sc}}{\rho_B p_{sc} T} = 32.037\frac{\text{g} - \text{scf}}{\text{ton} - \text{cm}^3}\frac{0.01(460 + 60)\,^\circ\text{R}}{1.65\dfrac{\text{g}}{\text{cm}^3}\,14.7\text{ psia}\,(460 + 73)\,^\circ\text{R}}$$

$$E = 0.01289\,\frac{\text{scf}}{\text{ton} - \text{psia}}$$

Initial gas contents are given in table 10–8 but will be calculated here to demonstrate application of the method. Sorbed methane is

$$G_1 = V_{Lis1} \frac{y_{1i} \dfrac{p_i}{p_{L1}}}{1 + y_{1i} \dfrac{p_i}{p_{L1}} + y_{2i} \dfrac{p_i}{p_{L2}}}$$

Evaluating the denominator,

$$1 + y_{1i} \frac{p_i}{p_{L1}} + y_{2i} \frac{p_i}{p_{L2}} = 1 + 0.5527 \frac{1{,}023 \text{ psia}}{297 \text{ psia}} + 0.4473 \frac{1{,}023 \text{ psia}}{151 \text{ psia}} = 5.9341$$

Thus,

$$G_1 = 447 \frac{\text{scf}}{\text{ton}} \frac{0.5527 \dfrac{1{,}023 \text{ psia}}{297 \text{ psia}}}{5.9341} = 143.4 \frac{\text{scf}}{\text{ton}}$$

which compares favorably with the measured value of 149 scf/ton. Similarly, initial sorbed $CO_2$ is

$$G_2 = V_{Lis2} \frac{y_{2i} \dfrac{p_i}{p_{L2}}}{1 + y_{1i} \dfrac{p_i}{p_{L1}} + y_{2i} \dfrac{p_i}{p_{L2}}}$$

$$G_2 = 705 \frac{\text{scf}}{\text{ton}} \frac{0.4473 \dfrac{1{,}023 \text{ psia}}{151 \text{ psia}}}{5.9341} = 360.0 \frac{\text{scf}}{\text{ton}}$$

The reported initial $CO_2$ gas content is slightly higher, 374 scf/ton.

Coefficients in the two quadratics depend on the new pressure value. Assuming as a first guess that the new pressure is 972 psia, or 95% of the initial pressure, the methane mass balance gives

$$A_1 = Ep^2 \left( \frac{1}{p_{L1}} - \frac{1}{p_{L2}} \right)$$

$$A_1 = 0.01289 \frac{\text{scf}}{\text{ton} - \text{psia}} 972^2 \text{ psia}^2 \left( \frac{1}{297 \text{ psia}} - \frac{1}{151 \text{ psia}} \right) = -39.65 \frac{\text{scf}}{\text{ton}}$$

$$B_1 = Ep^2 \left( \frac{1}{p_{L2}} - \frac{1}{p_{L1}} \right) - Ep \left( 1 + \frac{p}{p_{L1}} \right) - V_{Lis1} \frac{p}{p_{L1}} + G_1 p \left( \frac{1}{p_{L1}} - \frac{1}{p_{L2}} \right)$$

$$B_1 = 0.01289\,\frac{\text{scf}}{\text{ton} - \text{psia}}\,972^2\ \text{psia}^2\left(\frac{1}{151\ \text{psia}} - \frac{1}{297\ \text{psia}}\right) - 0.01289\,\frac{\text{scf}}{\text{ton} - \text{psia}}\,972\ \text{psia}\left(1 + \frac{972\ \text{psia}}{297\ \text{psia}}\right)$$

$$- 447\,\frac{\text{scf}}{\text{ton}}\frac{972\ \text{psia}}{297\ \text{psia}} + 143.4\,\frac{\text{scf}}{\text{ton}}\,972\ \text{psia}\left(\frac{1}{297\ \text{psia}} - \frac{1}{151\ \text{psia}}\right)$$

$$B_1 = -1{,}930.56\,\frac{\text{scf}}{\text{ton}}$$

$$C_1 = V_{Lis1}\,\frac{p}{P_{L1}} + EP\left(1 + \frac{p}{P_{L1}}\right) - G_1\left(1 + \frac{p}{P_{L1}}\right)$$

$$C_1 = 447\,\frac{\text{scf}}{\text{ton}}\,\frac{972\ \text{psia}}{297\ \text{psia}} + 0.01289\,\frac{\text{scf}}{\text{ton} - \text{psia}}\,972\ \text{psia}\left(1 + \frac{972\ \text{psia}}{297\ \text{psia}}\right) - 143.4\,\frac{\text{scf}}{\text{ton}}\left(1 + \frac{972\ \text{psia}}{297\ \text{psia}}\right)$$

$$C_1 = 903.73\,\frac{\text{scf}}{\text{ton}}$$

The solution of the methane quadratic is

$$y_{2meth} = \frac{-B_1 \pm \sqrt{B_1^2 - 4A_1C_1}}{2A_1}$$

$$y_{2meth} = \frac{-\left(-1{,}930.56\,\frac{\text{scf}}{\text{ton}}\right) \pm \sqrt{\left(-1{,}930.56\,\frac{\text{scf}}{\text{ton}}\right)^2 - 4\left(-39.65\,\frac{\text{scf}}{\text{ton}}\right)903.73\,\frac{\text{scf}}{\text{ton}}}}{2\left(-39.65\,\frac{\text{scf}}{\text{ton}}\right)}$$

$$y_{2meth} = 0.4637 \text{ and } -49.1537$$

Similarly the $CO_2$ mass balance quadratic gives

$$A_2 = 39.63\,\frac{\text{scf}}{\text{ton}}$$

$$B_2 = 3{,}452.42\,\frac{\text{scf}}{\text{ton}}$$

$$C_2 = -1{,}538.28\,\frac{\text{scf}}{\text{ton}}$$

$$y_{2CO2} = 0.4433 \text{ and } -87.5596$$

Comparing the two physically meaningful solutions, free $CO_2$ fractions of 0.4637 and 0.4433, indicates another iteration is required. Assuming the new pressure is 90% of initial pressure, 921 psia, gives

$$y_{2meth} = 0.4588$$

and

$$y_{2CO2} = 0.4494$$

Assuming a linear relationship between pressure and free $CO_2$ fractions for subsequent iterations quickly yields

$$p = 881.3 \text{ psia}$$

$$y_2 = 0.4547$$

Repeating this exercise for entire depletion yields the free gas composition curves shown in figure 10–27. Also posted on the figure are free gas compositions calculated from the data of Greaves et al. Compositions derived from the data of Greaves et al. are in good agreement with those calculated with the above method throughout most of the depletion. The scattered experimental compositions at low pressure are nearly bisected by the calculated composition curves.

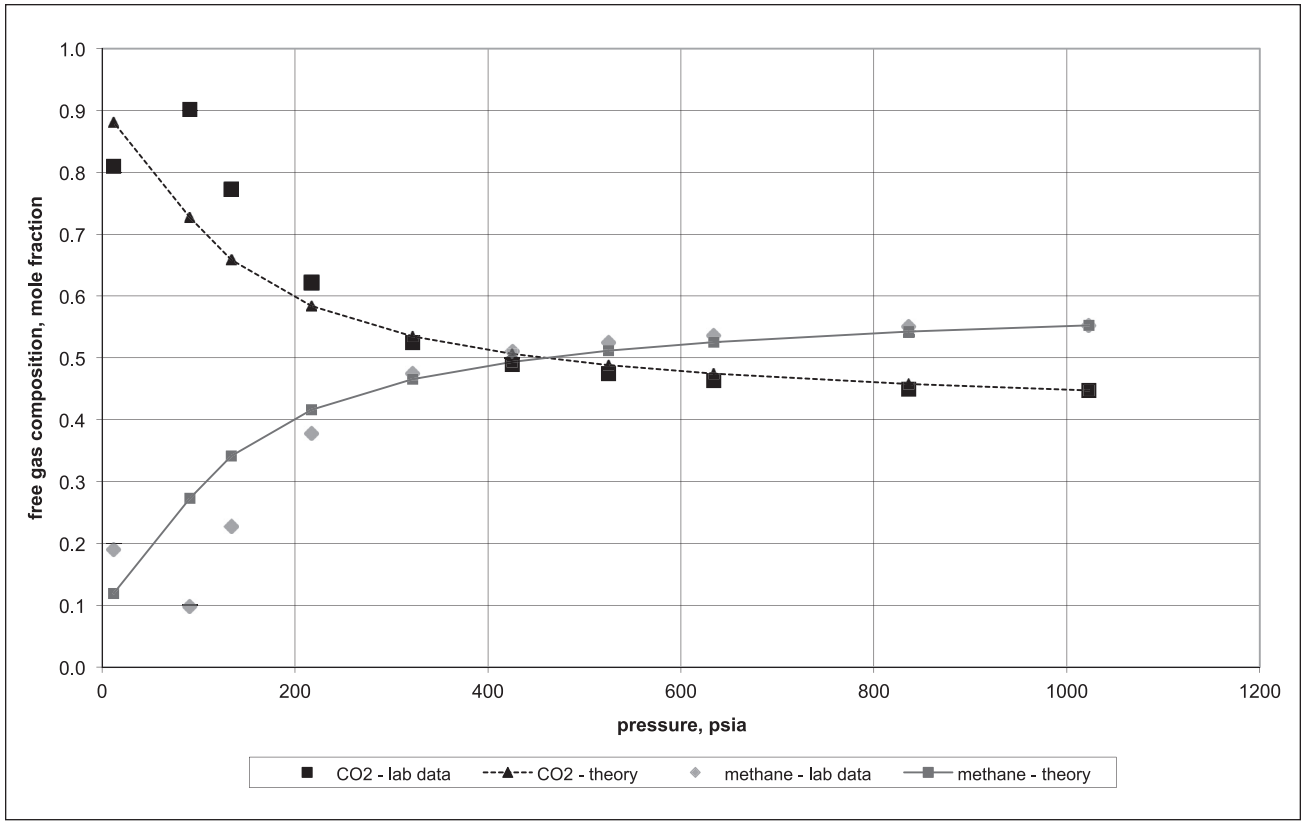



**Fig. 10–27.** Free gas composition during depletion[32]

## Example 10.7. Gas composition during depletion of a San Juan coal well

Fruitland coals of the San Juan Basin typically contain both $CO_2$ and methane. Studying completions in the NEBU #403R well, Mavor reported an initial $CO_2$ fraction of 11% in gas produced from a coal seam at 1,432 psia.[33] Methane and $CO_2$ isotherms of Fruitland coals were reported by Arri et al.[34] Pertinent properties from these two studies are collected in table 10–9.

**Table 10–9.** Example 10.7 coal properties

| | | |
|---|---|---|
| Initial free $CO_2$ fraction = | 0.1100 | |
| Initial reservoir pressure = | 1,432 | psia |
| Methane $V_{L,\,daf}$ = | 957.9 | scf/ton |
| Methane $p_L$ = | 365.8 | psia |
| $CO_2$ $V_{L,\,daf}$ = | 1,425.7 | scf/ton |
| $CO_2$ $p_L$ = | 207.6 | psia |
| Reservoir temp = | 116 | °F |
| Ash fraction = | 0.3075 | |
| Moisture fraction = | 0.0100 | |
| Bulk density = | 1.500 | g/cm$^3$ |

*Sources:* Mavor, M. J., 1994; and Arri, L. E., et al. 1992.

Produced gas composition was calculated as described above, and the free gas composition over depletion was plotted in figure 10–28. Inspection of the figure reveals that the fraction of $CO_2$ in the produced gas stream initially increases slowly with depletion. $CO_2$ in the produced gas stream increases by one-half, to 16.5%, when reservoir pressure falls by 1,200 psia to 232 psia. A doubling of $CO_2$ in the free gas requires reservoir pressure be reduced to 110 psia. Reservoir pressure in many San Juan fairway wells had fallen to near this level in 2003.[35] The assumed abandonment pressure of 80 psia for these wells implies a produced gas stream with 25% $CO_2$.[36]

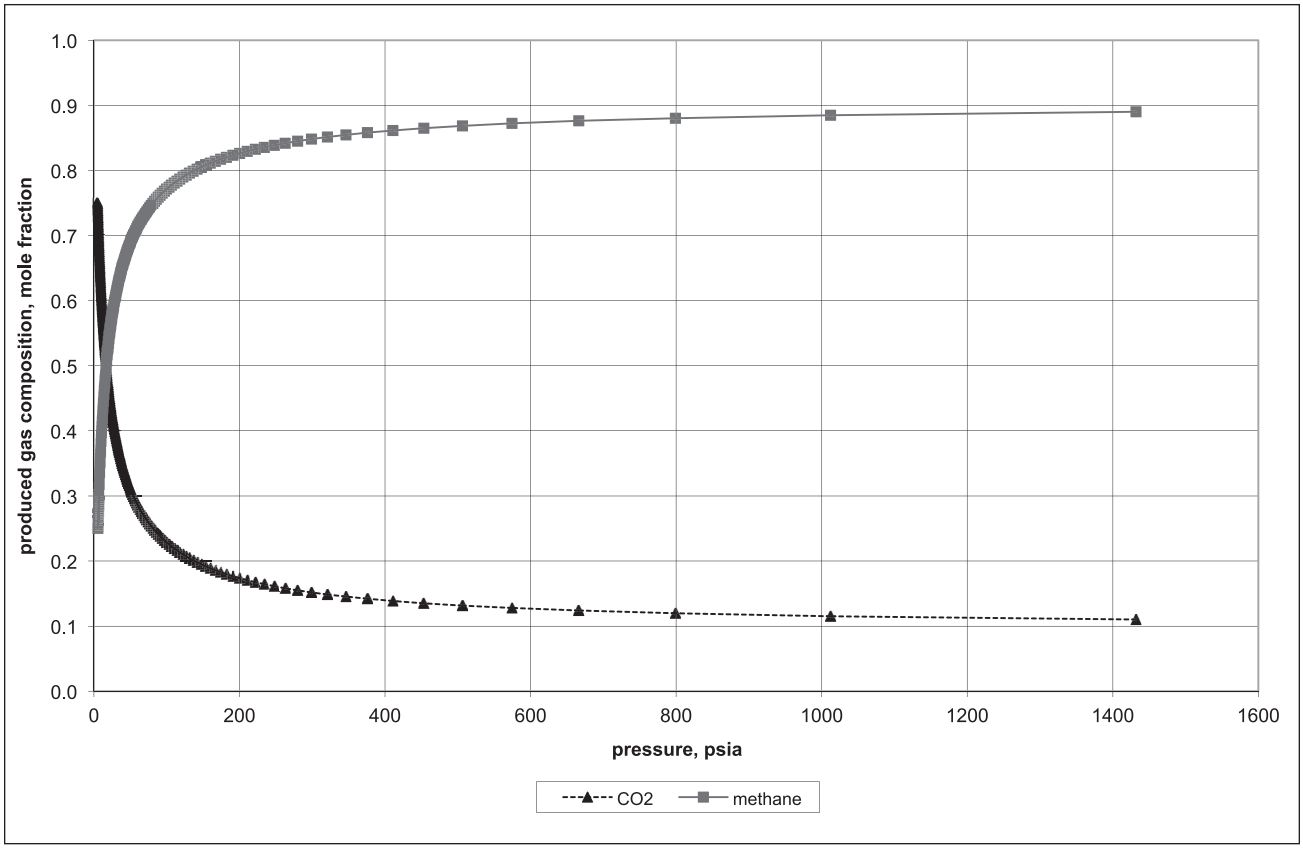



**Fig. 10–28.** San Juan coal well—free gas composition during depletion

Neglecting any free gas in the coal cleats, recovery factors for total gas, methane, and $CO_2$ from this coal are plotted in figure 10–29. As $CO_2$ is more strongly sorbed than methane, methane is preferentially released from the coal, leading to a higher recovery factor at a given abandonment pressure. The total gas recovery factor lies between that of methane and $CO_2$. When the $CO_2$ cut in the produced gas stream has doubled, the total recovery factor is 66%. Note that although two-thirds of the gas in place has been recovered, nearly three-fourths of the methane has been produced (74%), but less than one-half the $CO_2$ has been removed (40%). Thus, abandonment of wells draining coals holding a mixture of methane and $CO_2$ is a function of both reservoir pressure and produced gas composition. Produced gas composition, recovery factors, and $CO_2$ treating economics are used to determine remaining reserves and the economic limit of a given well.

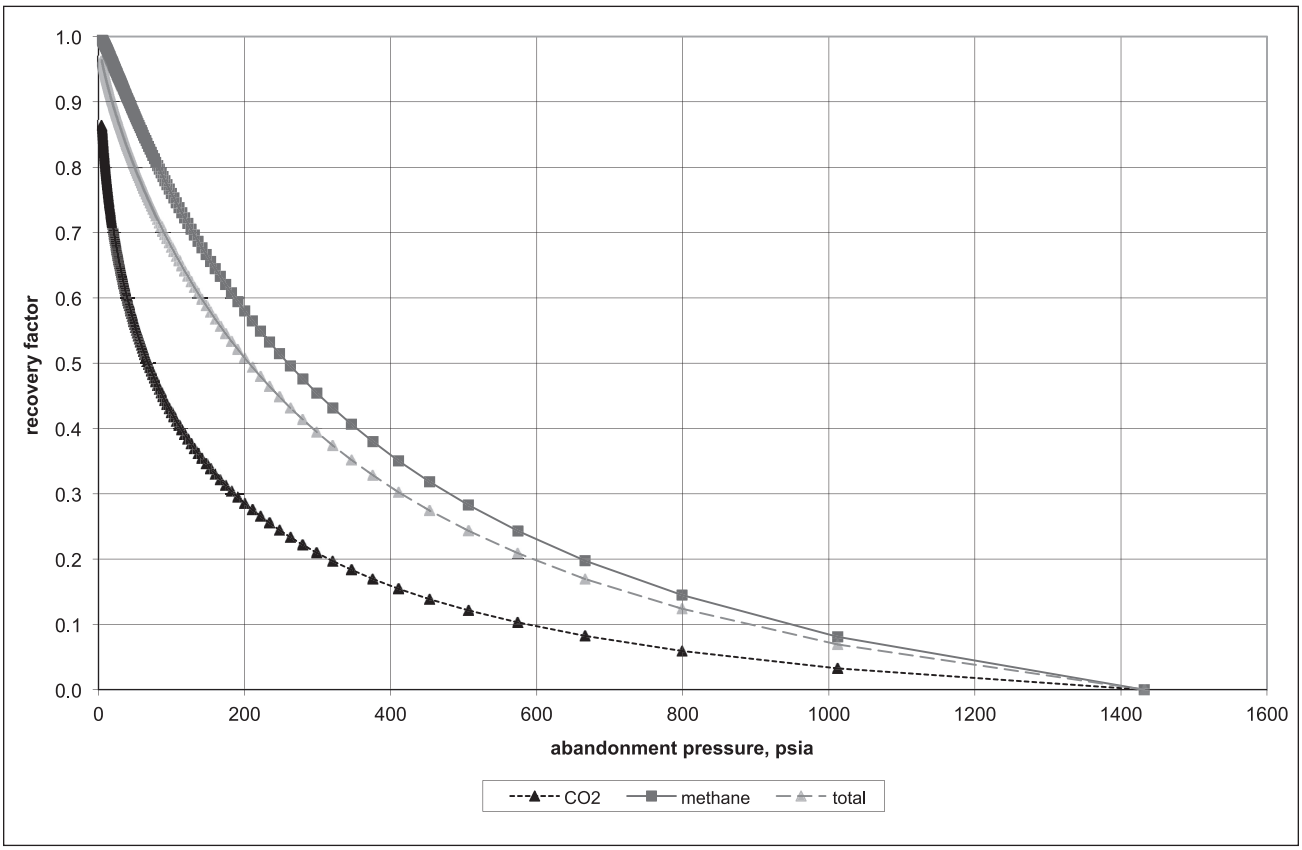



**Fig. 10–29.** San Juan Basin coal well—recovery factors vs. abandonment pressure

## Depletion of Variable Permeability Coal

Coal permeability can vary with stress and gas content. As stress increases over the course of depletion, the cleats close and permeability decreases. As gas is desorbed from the coal matrix during depletion, the matrix shrinks, increasing cleat width and, hence, permeability. Various theories for predicting coal permeability with depletion were discussed in chapter 6. The influence of variable permeability can be seen by coupling the tank model discussed above with the desired permeability function. While simulation of detailed permeability variation over time and space requires a full-scale numerical model, the tank model provides some grounding calculations for this sometimes baffling permeability behavior.

Productivity of coal wells draining the San Juan fairway was discussed by Simpson and Kutas.[37] These wells dewater quickly, on the order of a month, and are characterized by low, nearly constant gas-water ratios ranging from 80 to 700 mcf/stb. Consequently, performance of these wells is not strongly affected by gas-water relative

permeabilities, making them good candidates for observing changes in absolute permeability due to stress and/or matrix shrinkage. Coal and well properties of the NEBU 403R well reported by Mavor and rock mechanics coefficients from the Palmer and Mansoori study of San Juan coals are collected in table 10–10.[38] The resulting gas rate profile is compared with that from a constant permeability coal in figure 10–30. In contrast to the increased well productivity reported by Simpson and Kutas, the Palmer-Mansoori theory predicts a modest decrease in gas rate throughout the decade of production.[39] This behavior is attributed to use of inappropriate rock mechanics parameters in the Palmer-Mansoori equations. These constants are determined empirically and therefore must be tuned for each area to reflect different coal properties. Adjusting the Palmer-Mansoori coefficients to match actual coal well performance is a required first step in developing a permeability function for use in detailed reservoir simulations.

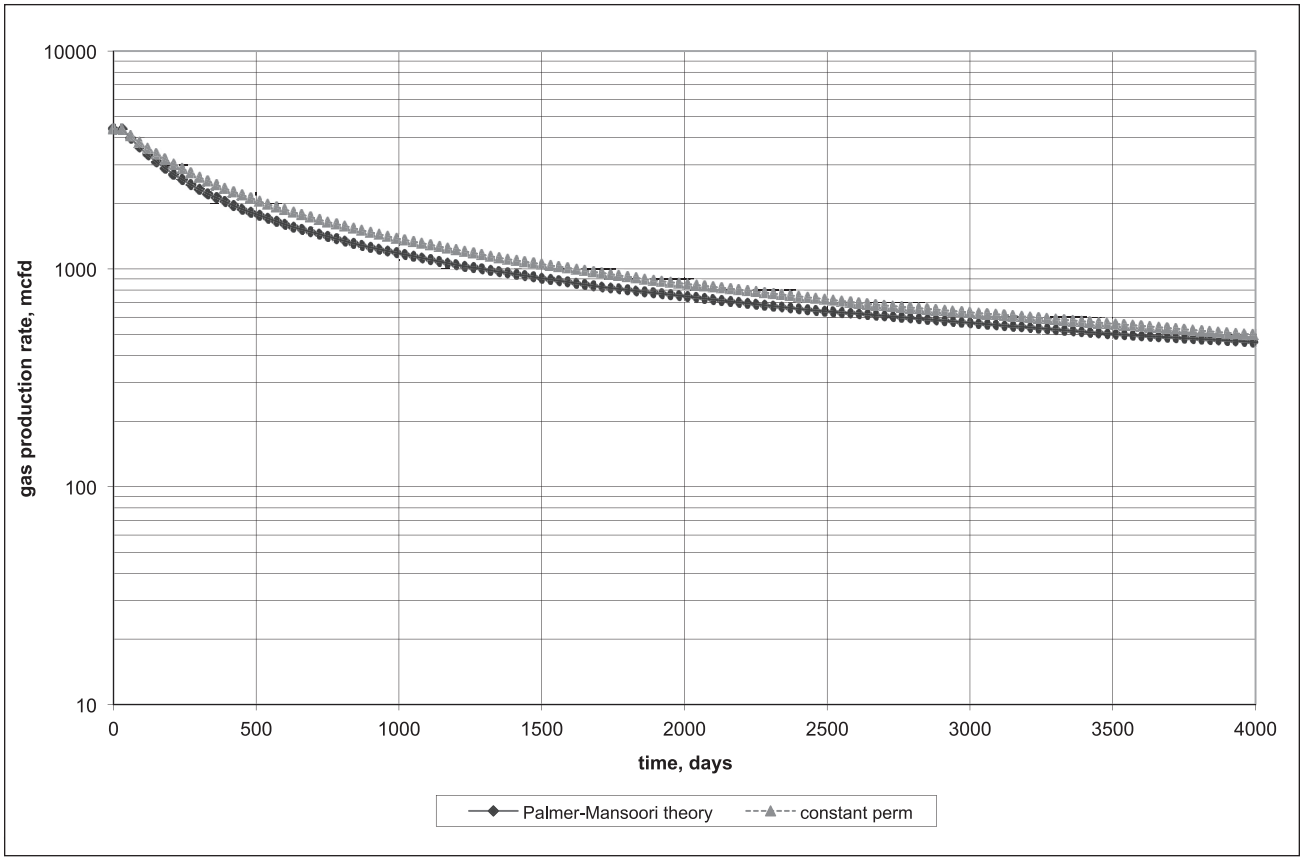



**Fig. 10–30.** San Juan Basin coal well gas profiles[40]

**Table 10–10.** San Juan Basin coal and well properties

| | | |
|---|---|---|
| Drainage area = | 320 | ac |
| Coal thickness = | 50.6 | ft |
| $V_{Ldaf}$ = | 932.0 | scf/ton |
| $p_L$ = | 303.3 | psia |
| Bulk density = | 1.529 | g/cm$^3$ |
| Cleat porosity = | 0.0045 | fraction |
| Ash = | 0.3075 | fraction |
| Moisture = | 0.0100 | fraction |
| Initial pressure = | 1,432 | psia |
| Irreducible water saturation = | 0.5 | |
| Coalbed temperature = | 116 | °F |
| Effective permeability to gas = | 3 | md |
| Cleat compressibility = | 1.46E–03 | psia$^{-1}$ |
| Specified gas rate = | 5,000 | mcfd |
| Minimum bottomhole pressure = | 50 | psia |
| $r_w$ = | 0.210 | ft |
| Skin = | –1.5 | |
| $c_0$ = | 0.0128 | psia$^{-1}$ |
| Young's modulus = | 4.45E+05 | psia |
| Poisson's ratio = | 0.39 | |

*Sources:* Mavor, M. J. 1994; and Palmer, I., and Mansoori, J. 1996.

## Nomenclature

| | |
|---|---|
| $a$ | Average ash fraction, decimal |
| $A$ | Drainage area, ac |
| $A_1$, $A_2$ | Constants in depletion composition equations |
| $b$ | Arps decline curve exponent |
| $B_1$, $B_2$ | Constants in depletion composition equations |
| $B_g$ | Gas formation volume factor, ft$^3$/scf |
| $B_w$ | Water formation volume factor, rb/stb |
| $C_1$, $C_2$ | Constants in depletion composition equations |
| $c_f$ | Formation compressibility, psia$^{-1}$ |
| $c_g$ | Gas compressibility, psia$^{-1}$ |
| $c_s$ | Sorption compressibility, psia$^{-1}$ |
| $c_t$ | Total compressibility, psia$^{-1}$ |
| $c_w$ | Water compressibility, psia$^{-1}$ |
| $D$ | Exponential or nominal decline rate, month$^{-1}$ or year$^{-1}$ |
| $D_1$, $D_2$ | Constants in depletion composition equations |
| $D_i$ | Initial nominal decline rate, month$^{-1}$ or year$^{-1}$ |
| $E$ | Constant in depletion composition equations |
| $f$ | Decline curve time factor to cancel units, such as 365 days/year |
| $G_1$ | Sorbed methane at initial pressure, scf/ton |
| $G_2$ | Sorbed $CO_2$ at initial pressure, scf/ton |
| $G_i$ | Initial gas in place, mmcf |
| $G_p$ | Produced gas, mmcf |
| $h$ | Coal thickness, ft |
| $k$ | Permeability, md |
| $m(p)$ | Real gas pseudopressure, psia$^2$/cp |
| $p$ | Current reservoir pressure, psia |
| $p_d$ | Desorption pressure, psia |
| $p_i$ | Initial reservoir pressure, psia |
| $p_L$ | Langmuir pressure constant, psia |
| $p_R$ | Average reservoir pressure, psia |
| $p_{wf}$ | Wellbore flowing pressure, psia |
| $q$ | Production rate, mcfd or bpd |
| $q_{el}$ | Economic rate limit, bpd or mcfd |
| $q_g$ | Gas production rate, mcfd |
| $q_i$ | Initial production rate, mcfd or bpd |
| $q_w$ | Water production rate, bpd |
| $r_e$ | External radius, ft |
| $r_w$ | Wellbore radius, ft |
| $s$ | Wellbore skin factor, dimensionless |
| $S_g$ | Gas saturation, decimal |
| $S_w$ | Current average water saturation, decimal |
| $S_{wi}$ | Initial water saturation, decimal |
| $t$ | Time, month or year |
| $t_{des}$ | Time to reach desorption pressure, days |
| $t_{el}$ | Economic lifetime, months or years |
| $t_{pss}$ | Time to reach pseudosteady-state flow, days |
| $T$ | Absolute temperature, °R |
| $V_i$ | Initial gas content, scf/ton |

| | |
|---|---|
| $V_{Ldaf}$ | Dry, ash-free Langmuir volume constant, scf/ton |
| $V_{Lis}$ | In-situ Langmuir volume constant, scf/ton |
| $w$ | Average equilibrium moisture, decimal |
| $W_p$ | Cumulative water production, stb |
| $x_j$ | Component *j* sorbed gas fraction |
| $X_p$ | Decline curve cumulative production, stb or mcf |
| $y_{2CO2}$ | $CO_2$ free gas fraction from $CO_2$ quadratic |
| $y_{2meth}$ | $CO_2$ free gas fraction from methane quadratic |
| $y_j$ | Component *j* free gas fraction |
| $Z$ | Gas deviation factor |
| $Z^*$ | King $Z^*$ function |

## Greek

| | |
|---|---|
| $\alpha$ | Sorption selectivity factor, dimensionless |
| $\mu_g$ | Gas viscosity, cp |
| $\mu_w$ | Water viscosity, cp |
| $\rho_B$ | Coal bulk density, g/cm$^3$ |
| $\phi$ | Porosity, decimal |

## Subscripts

| | |
|---|---|
| *1* | Methane component for binary depletion calculations |
| *2* | CO component for binary depletion calculations |
| *I* | Initial |
| *f* | Cleats |
| *fs* | Fully saturated |
| *g* | Gas |
| *sc* | Standard conditions |
| *w* | Water |

# References


1. Govier, G. W. 1975. *Theory and Practice of the Testing of Gas Wells*. Calgary, Alberta: Energy Resources Conservation Board.
2. Ibid.
3. Ibid.
4. Montgomery, S. L., Tabet, D. E., and Barker, C. E. 2001. Upper Cretaceous Ferron Sandstone: Major coalbed methane play in central Utah. *AAPG Bulletin*. V. 85 (no. 2–February). p. 199; and Lamarre, R. A. and Pratt, T. J. 2002. Reservoir characterization study: Calculation of gas-in-place in Ferron coals at Drunkard's Wash Unit, Carbon and Emery counties, Utah. 2002. *The Mountain Geologist*. V. 39 (no. 2–April). p. 41.
5. Lamarre, R. A. and Burns, T. D. 1997. Drunkard's Wash project: Coalbed methane production from Ferron coals in east-central Utah. In *Innovative Applications of Petroleum Technology Guidebook*. Rocky Mountain Association of Geologists. p. 47; and Burns, T. D., and Lamarre, R. A. 1997. Drunkard's Wash project: Coalbed methane production from Ferron coals in east-central Utah. Paper 9709 in *Proceedings of the International Coalbed Methane Symposium*. Tuscaloosa: University of Alabama.
6. Montgomery, S. L., et al. 2001.
7. Gash, B. W. 1991. *Measurement of "Rock Properties" in Coal for Coalbed Methane Production*. Paper SPE 22909. Presented at the Annual Technical Conference and Exhibition, Dallas, Texas, October 6–9.
8. Montgomery, S. L., et al. 2001.
9. Gash, B. W. 1991.
10. Lamarre, R. A., and Pratt, T. J. 2002.
11. Conway, M. W., Mavor, M. J., Saulsberry, J., Barree, R. B., and Schraufnagel, R. A. 1995. *Multi-Phase Flow Properties for Coalbed Methane Wells: A Laboratory and Field Study*. Paper SPE 29576. Presented at the Joint Rocky Mountain Regional Meeting and Low-Permeability Reservoirs Symposium, Denver, Colorado, March 20–22.
12. Ibid.
13. Ibid.
14. Seidle, J. P. 1991. *Long Term Gas Deliverability of a Dewatered Coalbed*. Paper SPE 21488. Presented at the SPE Gas Technology Symposium, Houston, Texas, January 23–25.
15. Rightmire, C. T., Eddy, G. E., and Kirr, J. N., eds. 1984. *Coalbed Methane Resources of the United States, AAPG Studies in Geology #17*. Tulsa: American Association of Petroleum Geologists.
16. Cardott, B. J. 1998. Coal as a gas-source rock and reservoir, Hartshorne Formation, Oklahoma. In *The Hartshorne Play in Southeastern Oklahoma: Regional and Detailed Sandstone Reservoir Analysis and Coalbed-Methane Resources*. Andrews, R. D., Cardott, B. J., and Storm, T. Special Publication 98-7. Oklahoma Geological Survey. Norman: University of Oklahoma.
17. Gas Research Institute. 1996. *A Guide to Coalbed Methane Reservoir Engineering*. GRI Reference No. GRI-94/0397. Chicago: Gas Research Institute.
18. Zuber, M. D., Boyer, C. M., Schraufnagel, R. A., and Saulsberry, J. 1989. *Insights and Analysis from the Rock Creek Project: A Reservoir Engineering Approach*. Paper SPE 19057. Presented at the SPE Gas Technology Symposium, Dallas, Texas, June 7–9.
19. Gas Research Institute. 1996.
20. Arps, J. J. 1945. Analysis of decline curves. *Transactions*. AIME. V. 160. p. 228.
21. Thompson, R. S., and Wright, J. D. 1984. *Oil Property Evaluation*. Golden, Colorado: Thompson-Wright Associates.
22. Fetkovich, M. J. 1973. *Decline Curve Analysis Using Type Curves*. Paper SPE 4629. Presented at the SPE Annual Technical Conference and Exhibition, Las Vegas, Nevada, September 30–October 3.
23. Thompson, R. S., and Wright, J. D. 1984; Fetkovich, M. J., Bradley, M. D., Works, A. M., and Thrasher, T. S. 1988. *Depletion Performance of Layered Reservoirs without Crossflow*. Paper SPE 18266. Presented at the SPE Annual Technical Conference and Exhibition, Houston, Texas, October 2–5; and Fetkovich, M. J., Fetkovich, E. J., and Fetkovich, M. D. 1994. *Useful Concepts for Decline Curve Forecasting, Reserve Estimation, and Analysis*. Paper SPE 28628. Presented at the SPE Annual Technical Conference and Exhibition, New Orleans, Louisiana, September 25–28; Laustsen, D. 1996. Practical decline analysis. Part 1. Uses and misuses. *Journal of Canadian Petroleum Technology*. V. 35 (no. 9/November). p. 34; and Laustsen, D. 1996. Practical decline analysis. Part 2. Identification and quantification of development opportunities. *Journal of Canadian Petroleum Technology*. V. 35 (no. 10/December). p. 14.
24. Fetkovich, M. J. 1973; and Fetkovich, M. J., Vienot, M. E., Bradley, M. D., and Kiesow, U. G. 1987. Decline-curve analysis using type curves—case histories. *Society of Petroleum Engineers Formation Evaluation*. December. p. 637.
25. Fraim, M. L., and Wattenbarger, R. A. 1987. Gas reservoir decline-curve analysis using type curves with real gas pseudopressure and normalized time. *Society of Petroleum Engineers Formation Evaluation*. December. p. 671.
26. Agarwal, R. G. 1979. *'Real Gas Pseudo-Time'—A New Function for Pressure Buildup Analysis of Gas Wells*. Paper SPE 8279. Presented at the SPE Annual Technical Conference and Exhibition, Las Vegas, Nevada, September 23–26; Carter, R. D. 1984. *Type Curves for Finite Radial and Linear Gas-Flow Systems: Constant Terminal Pressure Case*. Paper SPE 12917. Presented at the SPE Rocky Mountain Regional Meeting, Casper, Wyoming, May 21–23; Fraim, M. L., and Wattenbarger, R. A. 1987; Blasingame, T. A., and Lee, W. J. 1988. *The Variable-Rate Reservoir Limits Testing of Gas Wells*. Paper SPE 17708. Presented at the SPE Gas Technology Symposium, Dallas, Texas, June 13–15; and Palacio, J. C., and Blasingame, T. A. 1993. *Decline-Curve Analysis Using Type Curves-Analysis of Gas Well Production Data*. Paper SPE 25909. Presented at the SPE Joint Rocky Mountain Regional and Low Permeability Reservoirs Symposium, Denver, Colorado, April 26–28.
27. Ertekin, T., and Mohaghegh, S. 1991. *A Type-Curve Solution for Coal Seam Degasification Wells Producing under Two-Phase Flow Conditions*. Paper SPE 22673. Presented at the SPE Annual Technical Conference and Exhibition, Dallas, Texas, October 6–9.

28. Hanby, K. P. 1991. The use of production profiles for coalbed methane valuations. Paper 9117 in *Proceedings of the 1991 Coalbed Methane Symposium*. Tuscaloosa, Alabama, May 13–16; and Richardson, J. S., Sparks, D. P., and Burkett, W. C. 1991. The TEAM project reserve analysis: A comprehensive evaluation to predict ultimate recovery of coalbed methane. Paper 9105 in *Proceedings of the 1991 Coalbed Methane Symposium*, Tuscaloosa, Alabama, 13–16 May.
29. Seidle, J. P. 2002. *Coal Well Decline Behavior and Drainage Areas: Theory and Practice*. Paper SPE 75519. Presented at the SPE Gas Technology Symposium, Calgary Alberta, April 30–May 2.
30. Mavor, M. J., Russell, B., and Pratt, T. J. 2003. *Powder River Basin Ft. Union Coal Reservoir Properties and Production Decline Analysis*. Paper SPE 84427. Presented at the Annual Technical Conference and Exhibition, Denver, Colorado, October 5–9.
31. Greaves, K. H., Owen, L. B., McLennan, J. D., and Olszewski, A. 1993. Multi-component gas adsorption—desorption behavior of coal. Paper 9353 in *Proceedings of the 1993 International Coalbed Methane Symposium*, Tuscaloosa, Alabama, May 17–21.
32. Ibid.
33. Mavor, M. J. 1994. *Coal Gas Openhole Well Performance*. Paper SPE 27993. Presented at the University of Tulsa Centennial Petroleum Engineering Symposium, Tulsa, Oklahoma, August 29–31.
34. Arri, L. E., Yee, D., Morgan, W. D., and Jeansonne, M. W. 1992. *Modeling Coalbed Methane Production with Binary Gas Sorption*. Paper SPE 24363. Presented at the SPE Rocky Mountain Regional Meeting, Casper, Wyoming, May 18–21.
35. Simpson, D., and Kutas, M. 2003. *Producing Coalbed Methane at High Rates at Low Pressures*. Paper SPE 84509. Presented at the SPE Annual Technical Conference and Exhibition, Denver, Colorado, October 5–8.
36. Ibid.
37. Ibid.
38. Mavor, M. J. 1994; and Palmer, I., and Mansoori, J. 1996. *How Permeability Depends on Stress and Pore Pressure in Coalbeds: A New Model*. Paper SPE 36737. Presented at the SPE Annual Technical Conference and Exhibition, Denver, Colorado, October 6–9.
39. Simpson, D., and Kutas, M. 2003.
40. Palmer, I., and Mansoori, J. 1996.

# Simulation of Coal Well Performance

# 11

## Introduction

Simulation of hydrocarbon production from conventional reservoirs has become routine over the last half century. Insights from such numerical models have prompted development of coalbed methane simulators over the last 25 years. Coal deposits have been modeled as single-, double-, and triple-porosity systems. Some early coal gas simulators modeled gas transport in the matrix with Fick's law, while others neglected matrix flow by assuming sorption kinetics are fast compared to Darcy flow in the cleats. Modern coal gas simulators generally treat gas release from the matrix as a pseudosteady-state process.

Numerical models used to forecast actual coal well behavior are similar to conventional simulators in that they must be tuned using performance data. Given the unique dewatering behavior of water-bearing coals, calibration of coal simulators is both frustrating and necessary. Negative decline in gas production, the hallmark of coal wells, is difficult to predict accurately with numerical simulators. The time required to collect all necessary simulator inputs and tune the model often approaches the time required to dewater the wells. More useful for engineering purposes is a history match of pilot project performance through the gas production peak and into decline. The tuned model can then be employed to investigate different development scenarios.

Analytical solutions for some of the more complex facets of coal reservoirs such as variable absolute permeability, injection and production of multicomponent gases, and horizontal wells are extremely limited. Computational algorithms of current simulators are sufficiently fast and stable to allow numerical experiments for insight into the unique physics of coal reservoirs. Simulation can yield valuable insights for development of coal reservoirs, just as for conventional reservoirs.

## Development of Coalbed Methane Simulators

The common conceptual model of a coal deposit as solid matrix penetrated by a regular network of cleats leads intuitively to dual-porosity simulation models. Coal gas reservoir simulators have drawn heavily on the dual-porosity model of Warren and Root.[1] Assumptions of these early simulators that remain valid for many coal deposits are gas resided in the coal matrix and cleat, whereas water was present only in the cleats. Storage of gas in the matrix was usually described by Langmuir isotherms, with transport from matrix to cleat described by unsteady-state or pseudosteady-state equations. Storage of fluids in the fractures was by compression, and transport was described by Darcy's law.

The regularity of face and butt cleats in a coal led early workers such as Ancell et al. and King et al. to consider the matrix as slabs, cylinders, cubes, or spheres.[2] Regardless of the geometry, modeling gas transport in the matrix with a mesh greatly increases the number of nodes in a problem. A 3-D simulation of a conventional reservoir requires $N_x N_y N_z$ nodes, where $N_j$ is the number of nodes in the $j$-direction. Modeling gas transport

in a coal matrix element (slab, cylinder, cube, or sphere) with $N_r$ nodes increases the number of nodes (and equations to be solved at each time step) to $N_x N_y N_z N_r$. While spatial distribution of gas with a matrix element at a given time is perhaps interesting, such a high resolution of gas distribution in the coal is computationally expensive. Furthermore, for engineering purposes, gas flow out of the matrix is usually more important than the gas distribution within it.

Consequently, coal gas simulators rapidly evolved to represent the matrix as a single node in which gas storage is described with a Langmuir isotherm and a matrix pressure. Gas flow out of the matrix into the cleat is modeled either as an unsteady-state phenomenon based upon Fick's law of diffusion or the pseudosteady-state process of Warren and Root.[3]

The desorbed gas fraction for Fickian diffusion out of a spherical coal particle can be written as Smith and Williams[4]

$$\frac{G}{G_t} = 1 - \frac{6}{\pi^2} \sum_{n=1}^{\infty} \frac{1}{n^2} \exp\left(-n^2 \pi^2 \frac{D}{r_p^2} t\right) \tag{11.1}$$

where

$G$ = desorbed gas volume, cm$^3$,
$G_t$ = total desorbed gas volume, cm$^3$,
$D$ = diffusion coefficient, cm/sec,
$t$ = time, sec, and
$r_p$ = particle radius, cm.

The ratio $D/r_p^2$ is termed the diffusivity, has dimensions of sec$^{-1}$, and is determined from canister desorption tests.

Pseudosteady-state gas flow out of the coal matrix is mathematically expressed as

$$\frac{\partial V(p_m)}{\partial t} = -\frac{1}{\tau} \left(V(p_m) - V(p_c)\right) \tag{11.2}$$

where

$V$ = gas content of the matrix, scf/ton or cm$^3$/g,
$p$ = pressure, psia or MPaa,
subscript $m$ = matrix,
$c$ = cleat,
$t$ = time, and
$\tau$ = characteristic time.

The characteristic time, $\tau$, has the same dimensions as the time variable and includes both the matrix shape factor and resistance to flow in the matrix.

Imagine a small piece of coal initially at equilibrium, with cleat and matrix pressures equal, in which cleat pressure is instantaneously dropped, initiating gas flow out of the matrix. For a constant cleat pressure, $p_c$, equation (11.2) can be rewritten as

$$\frac{\partial \left(V(p_m) - V(p_c)\right)}{\partial t} = \frac{1}{\tau} \left(V(p_m) - V(p_c)\right)$$

This equation is readily solved by separation of variables to yield

$$\frac{V(p_m) - V(p_c)}{V_i - V(p_c)} = \exp\left[-\frac{t}{\tau}\right]$$

where

$V_i$ = initial gas content of the matrix, scf/ton or $cm^3/g$.

When time $t$ equals the characteristic time $\tau$, gas remaining in the matrix is given by

$$\frac{V(p_m) - V(p_c)}{V_i - V(p_c)} = \exp[-1] = 0.368$$

The volume of gas that has been desorbed from this piece of coal is 1 – 0.368 = 0.632. Thus $\tau$ is often referred to as the *characteristic (de)sorption time* and is readily determined from canister desorption tests as that time at which 63.2% of the gas has been desorbed.

The relation between diffusivity and characteristic desorption time comes from equation (11.1). As discussed in chapter 2, time required to diffuse 63.2% of the gas out of a sphere is given by

$$\frac{D}{r_p^2}\tau = 0.055767 \tag{11.3}$$

Solutions for the diffusion equation are infinite series that converge slowly, especially at small times, making them computationally expensive to implement. Thus, coal gas simulators typically employ a pseudosteady-state description of gas release from matrix to cleat. The gas flow equation is similar to that of Warren and Root, where gas flux into the cleat is represented by a source term, while that of water is unchanged from single-porosity flow. Simulation of unsteady-state gas flow through cylindrical and spherical coal elements by Kolesar and Ertekin with a single-phase gas, 1-D model indicated gas flow rates approached the pseudosteady-state gas rate after only a few months.[5] Early simulation studies that considered the effect of sorption time on well performance include Remner et al., Spencer et al., and Sawyer et al.[6] All three studies found that long-term well performance is affected by sorption for sorption times greater than about 100 days. Young et al. found that variation of sorption time from 1 to 100 days had a negligible effect on gas and water rates.[7] For most reservoir engineering purposes, coal well production can be described with Darcy's law for coals with sorption times less than three digits.

Surveys by King and Ertekin discussed a total of 52 models for coalbed methane simulation.[8] Some models assumed gas diffusion was sufficiently rapid that matrix and cleat are in equilibrium, while other models described gas transfer between matrix and cleat as a pseudosteady-state process or an unsteady-state process. Models were applicable to coal cores and cuttings, single-well simulations, and full-field studies. Many of them were also applicable to gas production from shales. All models except one from Collings assumed a single-component gas and a single sorption isotherm, precluding investigation of compositional effects.[9] Fully 3-D coal gas simulators with pseudosteady-state matrix to cleat gas flow were developed and validated by Sawyer et al. and Paul et al.[10] A triple-porosity, dual-permeability coal gas simulator was developed by Reeves and Pekot.[11] Similar to a conventional dual-porosity model with the addition of a sorbed gas capability, this model requires matrix permeability and gas-water relative permeabilities in addition to those of the cleat.

Equilibrium models assume desorption of gas from the matrix is very rapid compared to gas flow in the cleats, desorption kinetics are unimportant, and well behavior is controlled by Darcy flow in the cleats. With this assumption of instantaneous gas release from a coal, Seidle and Arri employed a black oil simulator for coalbed methane simulations.[12] Gas sorbed on the coal was modeled as gas dissolved in an immobile oil. The solution gas-oil ratio was calculated from the sorption isotherm constants. Oil saturation was assumed to be small, on the order of 1% to 10%, and the gas-water relative permeability curves were normalized to account for the oil. The oil phase was immobilized with a high viscosity and low relative permeability at all saturations.

Concurrent with coalbed methane simulator development, vigorous worldwide coal gas exploration and development efforts provided ample opportunities to apply the new simulators and spurred further development. Simulators were used to investigate production performance of specific coal seams, to optimize well completions and full-field developments, and for numerical experiments to gain insight into coal reservoir physics. The diverse nature of coal well behaviors was first realized from simulation studies of specific coals. A representative, not exhaustive, collection of early simulation studies of specific coal seams is given in table 11–1. Beginning with single-layer simulations of bituminous coals, these early studies soon branched out to cover gas production from coals of various ranks, reservoir architectures, and completions.

**Table 11–1.** Early coal seam simulation studies

| Basin | Coal | Year | Comments |
|---|---|---|---|
| Warrior[a] | Marylee | 1980 | Single-seam, 17-well pattern ahead of mining |
| Warrior[b] | Marylee | 1983 | 31 wells, same area as Ancell et al. |
| Warrior[c] | Marylee | 1987 | Single-well, single-seam matches |
| Powder River[d] | Wyodak | 1992 | 5-well, single-seam Betop pilot |
| Great Divide[e] | Rock Springs | 1991 | Single well, two layers, coal and sand |
| San Juan[f] | Fruitland | 1991 | Cedar Hill Field, anisotropic permeability |
| Sydney[g] | Bulli | 1987 | Horizontal well in multiseam Westcliff mine |
| San Juan[h] | Fruitland | 1993 | Single well, anisotropic permeability |

*Sources:* [a]Ancell, K. L., et al. 1980. [b]Dunn, W. W. 1983. *Coal as a "Conventional" Source of Methane: A Review and Analysis of a 31-Well Production Area in the Mary Lee Coal Seam in Tuscaloosa County, Alabama*. Paper SPE 12186. Presented at the SPE Annual Technical Conference and Exhibition, San Francisco, California, October 5–8. [c]Zuber, M. D., et al. 1989. [d]Reid, G. W., et al. 1992. [e]Young, G. C. B., McElhiney, J. E., Dhir, R., Mavor, M. J., and Anbouba, I. K. A. 1991. *Coalbed Methane Production Potential of the Rock Springs Formation, Great Divide Basin, Sweetwater County, Wyoming*. Paper SPE 21487. Presented at the SPE Gas Technology Symposium, Houston, Texas, January 23–25. [f]Young, G. C. B., McElhiney, J. E., Paul, G. W., and McBane, R. A. 1991. *An Analysis of Fruitland Coalbed Methane Production, Cedar Hill Field, Northern San Juan Basin*. Paper SPE 22913. Presented at the SPE Annual Technical Conference and Exhibition, Dallas, Texas, October 6–9. [g]Young, G. C. B., et al. 1992. [h]Mavor, M. J., and Robinson, J. R. 1993. *Analysis of Coal Gas Reservoir Interference and Cavity Well Tests*. Paper SPE 25890. Presented at the Joint Rocky Mountain Regional and Low Permeability Reservoir Symposium, Denver, Colorado, April 26–28.

With origins in the coal mining industry, coalbed methane has long been associated with horizontal wells. Early simulation studies compared horizontal and vertical wells draining thin, shallow coals and investigated horizontal well performance as a function of alignment with cleats and vertical placement within a seam.[13] Gas drainage by horizontal wells drilled in a single seam of a multiple seam play was simulated by Spencer et al.[14] The 3-D simulation indicated 60% of the "removable gas" would be recovered in 400 days. Simulators, often in conjunction with economics, were used to optimize individual well completions and full-field developments.[15]

## Simulation Insights into Coal Reservoir Physics

With robust simulation capability, a variety of numerical studies were published investigating unique aspects of coal gas production. Numerical models capture the interplay between desorption, dewatering, and depressuring of a coal seam, yielding insights into coal reservoir physics that cannot be obtained from laboratory experiments or field data. For example, the benefits of well interference in establishing coal gas production were discussed by Remner et al. and Young et al.[16] These simulations demonstrated that contrary to experience in conventional reservoirs, interference between young coal wells accelerates dewatering in the interwell region, promoting gas desorption and thereby increasing the gas saturation and gas mobility.

Coal permeability decreases with increased stress and increases due to matrix shrinkage from gas desorption. Permeability reduction due to increased stress during depletion of Warrior and San Juan coals was simulated by Sawyer et al., and combined stress and shrinkage effects during depletion of a Warrior Basin coal were simulated by Zuber et al.[17] As discussed in chapter 6, a variety of theoretical models have been proposed to describe coal permeability during depletion, such as those of Palmer and Mansoori, Shi and Durucan, and Cui and Bustin.[18] Equations from several of these theories have been incorporated into modern simulators. In addition, most coal and conventional reservoir simulators permit tabular entry of permeability as a function of pressure.

Coal well performance depends on gas-water relative permeabilities in a functional rather than a discrete manner. That is, well performance depends on the shape of the relative permeability curves rather than on relative permeability at a single saturation. Simulators are ideal for investigating the role of relative permeabilities in coal well performance. Unlike actual coal seams, all other pertinent parameters can be held constant. Using three sets of gas-water relative permeability curves in simulations of a single well draining an unspecified coal, Remner et al. observed variations in gas and water rates but little influence on the timing of peak gas production.[19] The strong influence of gas-water relative permeabilities on coal well performance was demonstrated by simulations of north San Juan coal wells by Young et al., employing four sets of Fruitland coal gas-water relative permeability curves.[20] Developed from field simulations or measured in the laboratory, all four sets of relative permeabilities were credible yet led to very different well behaviors. Magnitude of gas and water peak rates varied by a factor of roughly three, while timing of peak gas rate varied by two. Gas recovery factors after 25 years of production ranged from 38% to 63%, while water recoveries, inversely related to gas recoveries, varied between 33% and 52%. The shape of the $k_g/k_w$ curve impacted well performance more strongly at early times than at late times, and higher gas recoveries were associated with steeper slopes of the $k_g/k_w$ curve. Simulations by Gash et al. demonstrated that 10% increases in relative permeabilities around the crossover point of laboratory-measured San Juan relative permeabilities increased peak gas rate by 70%, and time to peak gas was halved.[21]

Undersaturation strongly affects coal well performance and economics and has, therefore, been the subject of numerous simulation studies. Sensitivity of gas production rate and recovery to the degree of undersaturation in a San Juan Fruitland coal was investigated as part of a simulation study by Young et al.[22] Initial reservoir pressure was sufficiently high to place the fully saturated coal up on the plateau of the sorption isotherm, and a small degree of undersaturation implied a desorption pressure substantially less than initial pressure. Assuming the coal was 14% undersaturated in gas, that is, actual gas content was 14% less than predicted from the isotherm and initial reservoir pressure, resulted in a desorption pressure approximately one-half the initial reservoir pressure. Peak gas rate was reduced by 60%. Numerical complications and model instabilities arising when grid block pressure drops to desorption pressure were discussed by Kohler and Ertekin.[23] The simulations exhibited oscillations in gas production rate and block pressures when more than one block pore volume of gas was flowed through a gridblock in a time step.

Another example of simulation providing insight into unique coal reservoir physics comes from the Powder River Basin of Wyoming. Production of large volumes of water from wells completed in the coals of this basin is often necessary to establish commercial gas production. Simulation studies by Reid et al. and Hower et al. matched production behavior assuming this water comes from the laterally extensive, highly permeable, subbituminous coal seams.[24] An alternative explanation offered by Onsager and Cox and based upon single-well, single-coal simulations is water influx from bounding beds.[25] Assuming bounding bed horizontal and vertical permeabilities ranged from 0 to 0.03 md yielded simulated gas and water profiles similar to some Powder River coal wells. The gas and water signatures associated with water influx from bounding beds were not unique, i.e., similar behavior could be obtained assuming a single coal with certain properties bounded by impermeable beds. However, the insights afforded by numerical simulation led to a recommendation to characterize permeability and porosity of bounding beds.

## Probabilistic Coal Well Simulations

While probabilistic simulations obviously require substantially more time and effort than do deterministic simulations, they provide a much richer set of results. In contrast to the single case resulting from deterministic models, probabilistic simulation results can be sorted according to peak gas rate, cumulative production, or any desired parameter and percentile ranges ascertained. One of the most common and confusing descriptions employs the 10th, 50th, and 90th percentiles, termed *P10*, *P50*, and *P90*. While the P50 case is always the median (not necessarily the average) case, confusion arises with the P90 and P10 definitions. Some workers designate the bottom 10% with P10, but others use P90 for this same cutoff with the understanding that 90% of the cases will lie above it. For instance, sorting of peak gas rates yields a value that is greater than 10% of all peak rates and,

conversely, is lower than 90% of all peak gas rates. Thus this value is sometimes designated as P10 and sometimes as P90. Conversely, a sort of cumulative gas production yields a value greater than 90% and less than 10% of all gas recoveries, leading some workers to define this value as P90, others as P10. As of the time of this writing, no consensus has yet evolved, leaving the reader to interpret each study.

Measurement of coal seam properties, like measurement of conventional reservoir properties, always entails some error. To understand the impact of these errors on Warrior and San Juan Basin coal well performance, Zuber and Olszewski employed different model data sets of Sawyer et al. to investigate the influence of a 1% change in key reservoir properties and for Monte Carlo simulations.[26] The parametric study of 1% variation in a variable (while holding all other variables constant) showed gas production rate to be most sensitive to, in order of descending importance, coalbed gas content, Langmuir volume, and initial water saturation. Curiously, permeability was fourth on the list. The Monte Carlo simulations employed triangle distributions for key reservoir properties. In addition, Latin hypercube sampling was used to ensure the resulting 700 simulations of well performance in each basin were statistically valid. The 90% confidence interval (representing 90% of all possible outcomes) for 20-year cumulative gas production varied from 118 to 363 mmcf, a factor of three. Such variation due to measurement errors in key coal reservoir parameters illustrates the importance of quality data and highlights the importance of calibrating simulators to past well performance.

Coal heterogeneity is characterized by a length scale sufficiently small that production behavior of adjacent wells can differ by an order of magnitude. Dewatering and subsequent gas production from coal deposits requires interference among several wells. Consequently, coal well performance is often best understood statistically. Purvis et al. employed Monte Carlo methods to generate input parameters for finite difference simulations of stacked sands, coal mine methane, and coalbed methane projects.[27] Production profiles were simulated employing Latin hypercube sampling to minimize the number of simulations while still capturing reservoir uncertainty. All three studies were performed prior to initial production, precluding calibration of the simulators against actual performance and highlighting the importance of the input distributions. These workers noted that although many reservoir parameters exhibit normal or log normal distributions, in practice, many times insufficient data are available to construct such distributions. Thus, their recommendation is to approximate them with triangular or uniform distributions. Use of maximum and minimum data values to define a triangular distribution results in a distribution that is too narrow, as the endpoints have zero probability. A more realistic distribution is obtained by extending endpoints of the triangle beyond the extreme data values or truncating the triangle at the extreme points. Alternatively, a uniform distribution is appropriate when knowledge of the parameter distribution is lacking but absolute limits are known.

A reservoir simulator was developed by Jalali and Mohaghegh for independent producers who lack the funds and expertise required for commercial simulators.[28] The simulator described production of a single-component gas from a single coal by a single well using radial coordinates, or for a hydraulically fractured well, elliptical coordinates. Gas-water relative permeability curves were calculated analytically, precluding use of laboratory-measured values or adjustment of the curves during a history matching exercise. Monte Carlo simulations employed parameter distributions defined by minimum, maximum, and most likely values.

A spreadsheet-based tank model developed by Clarkson and McGovern was first validated against a gridded commercial model before coupling it with various engineering and economic tools.[29] The model assumed three layers, each an independent tank with uniform properties throughout, with one layer describing a wet coal, a second layer simulating a dry coal, and a third modeling production from a conventional gas reservoir. Other model attributes included two-component gas sorption and variation of absolute permeability due to stress and sorption effects. A commercial spreadsheet add-in Monte Carlo package, with a variety of distribution functions to describe coal well parameters, was coupled with the tank model for probabilistic simulations. Key profiles (such as P90, P50, and P10 cases) and economic parameters were input to financial modules to generate various metrics such as likely capital requirements, net present values, and chances of economic success.

A large set of Monte Carlo simulations by Roadifer et al. sought to identify reservoir and wellbore parameters controlling production from coals and coals in conjunction with sands.[30] Coals ranged from dry to water-saturated with fully gas-saturated matrix to 50% undersaturated in gas. Sands varied from water filled with no free gas to irreducible water saturation with a gas resource similar to that of the associated coal. Thirty primary

parameters (such as permeability, net coal thickness, and sand porosity) and 62 combination parameters (such as the permeability-thickness product) were identified as possible controls on well performance. Uniform distributions were chosen for the great majority of the parameters, with $\log_{10}$ distributions employed for a few selected parameters. A total of 100,000 Monte Carlo simulations of 25 years of production from a single, bounded well were analyzed using the Spearman rank correlation. Permeability was found to be the most important parameter controlling coal-only well performance, while the free gas saturation was the most important parameter influencing coal plus sand wells. As the input parameters were described with uniform distributions rather than actual distributions, no meaningful P10/P50/P90 rankings of the results were possible.

Construction, calibration, and application of a probabilistic simulator for Horseshoe Canyon, Alberta coals were presented by Bastian et al.[31] Laid down in coastal plain swamps subject to sea-level fluctuations, the resulting Horseshoe Canyon coals are encountered as a series of multiple, thin, shallow coals. Subbituminous in rank, the coals are generally underpressured and dry. Consequently, no dewatering is required, and the wells decline from an initial rate following clean up from stimulation. Geological heterogeneity of Horseshoe Canyon coals was captured by constructing distributions of key reservoir parameters using data obtained from coal cores, pressure transient tests, and production logs. Data distributions were generally characterized by a mean or median, standard deviation, and minimum and maximum values. Reservoir properties for a given simulation were obtained either by sampling actual distributions or distributions constructed from mean values and standard deviations. The single-well bounded model for a given area was calibrated by altering reservoir parameter distributions to match the original gas in place distribution and the average production performance in the project area. Once calibrated, a series of Monte Carlo simulations was used to calculate distribution of original gas in place for the project, optimum well spacing, and to generate P10, P50, and P90 gas profiles for reserves bookings.

## Simulation of Enhanced Coalbed Methane Recovery and $CO_2$ Sequestration

Flooding of a coal deposit with nitrogen gas to increase coal gas recovery, proposed by Puri and Yee and termed *enhanced coalbed methane recovery (ECBM)*, spurred further development of coal gas simulators.[32] The ECBM concept was quickly expanded to include other inert gases, such as $CO_2$. The process was initially modeled by assuming instantaneous transfer of gases between matrix and cleat and describing sorbed gas volumes with the binary Langmuir equation.[33] The models accurately described laboratory displacement of methane with nitrogen or $CO_2$, but no field data were yet available for model verification.

Puri et al. reported development of an air injection test to determine ECBM viability of a coal deposit and provided data from a field test of a San Juan Basin coal well.[34] The test, termed a *micropilot test*, involves air injection, shut-in, and subsequent production of a given well. Each portion of the test lasts one to three weeks, making total test time approximately two months. An integral part of test interpretation is simulation of well performance throughout the test. Gas production rate and bottomhole pressures from the San Juan field example were matched reasonably well throughout the test. However, nitrogen composition during flowback was consistently overestimated. This inability to match composition was attributed to use of a simulator with infinitely fast sorption kinetics to describe a process with a sorption time approximately equal to the shut-in time.[35]

A fully compositional model with pseudosteady-state gas flow between matrix and cleat, suitable for simulation of multicomponent coal gas production as well as ECBM, was developed by Manik et al. and verified against other simulators.[36] Pseudosteady-state transfer of gas between matrix and cleat was described with a single sorption time, regardless of gas composition. Thus, this model is capable of describing compositional behavior during periods of sorption limited behavior, such as flowback during a micropilot test or early-time response of a coal well drawdown test. Several commercial coal gas simulators now have ECBM capability, often based upon the assumption of pseudosteady-state transfer of gases between matrix and cleat, a single sorption time, and the extended Langmuir equation.

At the time of this writing, the only two field-scale ECBM projects in operation are the $CO_2$ flood of the Allison Unit and the nitrogen flood of the Tiffany Unit, both located in the northern portion of the San Juan

Basin. Performance of these two ECBM projects has been studied by Reeves and Oudinot.[37] The ability to strongly sorb large volumes of $CO_2$ makes coal deposits attractive formations for $CO_2$ sequestration. Compositional simulators developed for ECBM can be employed to model this process. A comparative numerical study by Law et al. of a micropilot test and a "huff-n-puff" pilot in an inverted five spot assumed infinitely fast sorption kinetics and an isothermal coal with constant permeability.[38] Both problems assumed $CO_2$ injection into a coal containing both free and sorbed methane. Rates, recoveries, and compositions predicted by all five simulators were within engineering accuracy.

Simulations studies have been conducted of $CO_2$ sequestration and the resulting increased methane production from vertical and horizontal wells completed in Appalachian-type coals, Appalachian Basin and Warrior Basin coals, and a generic coal.[39] These simulations studies investigated various injection pressures, horizontal well lengths and orientations, and coal permeability anisotropy ratios. All coals were assumed saturated with methane, and no stress or matrix shrinkage influences on permeability were considered. One interesting conclusion of these parametric studies was the identification of optimal horizontal injector length for selected permeability anisotropy and coal sorption time. Another interesting conclusion was a monotonic decrease in the volume of methane produced as $CO_2$ injection pressure increased. No explanation of either result was provided.

Injection of $CO_2$ above frac parting pressure in swelling coals was modeled by van der Meer and Fokker using a simulator calibrated to field data from an Alberta ECBM pilot test.[40] As coal swells upon $CO_2$ uptake, permeability and hence injectivity can be reduced, sometimes dramatically. This study proposed the novel concept of maintaining $CO_2$ injectivity by injection at increasingly higher pressures to steadily drive the induced fracture through the constantly growing zone of reduced permeability out into the native coal seam.

ECBM and $CO_2$ sequestration models are now sufficiently mature that simulation of these processes is considered routine, and modeling is an integral part of both efforts.[41]

## Required Inputs

Accurate simulation of hydrocarbon production from conventional reservoirs requires information about both the formations and the wells draining them. Simulation of gas and water production from a coal deposit requires the same information plus three additional coal properties: sorption isotherms, coalbed gas contents, and sorption time.

Coal deposit architecture is described by thickness, depth, and structure of each productive seam. Rock properties such as porosity, permeability, and relative permeability curves are necessary to describe fluid storage and movement in the cleats. These properties often vary areally as well as stratigraphically. Fluid properties of the coal gas and water must be specified for different reservoir temperatures and pressure. Completion histories (perforation and stimulation of specific intervals, pump changes, gathering system pressure changes, etc.) and operating constraints (wellhead or bottomhole pressure and/or limiting rates of fluid production) must be specified for each well in the simulation. Coal gas simulators typically require single-component sorption isotherms (methane, nitrogen, $CO_2$, etc.) and employ the multicomponent Langmuir equation to describe sorption of the gas mixture. Coalbed gas contents define current gas storage and, in conjunction with sorption isotherms and reservoir pressure, dictate the degree of undersaturation in a coal seam. Sorption time characterizes the rate of gas transfer between matrix and cleat and is obtained from desorption tests or calculated from cleat spacing and the diffusion constant with equation (11.3).

Given the difficulty of measuring both effective porosity (sometimes called *mobile water porosity*) and gas-water relative permeabilities in the laboratory, these two parameters are frequently adjusted or even determined during the history matching process.

## History Matching

Confidence in predicted gas and water production from coals is increased when the model has been calibrated against actual well performance, similar to conventional reservoir simulation studies. Necessary production data for history matching include gas and water production rates and wellhead pressures and fluid levels. Driving the model by specifying one fluid production rate (gas or water), model parameters are adjusted to match the other. Bottomhole flowing pressures, important for matching skin factor, can be calculated from wellbore configuration and wellhead pressures. Reservoir pressures from observation wells or from shut-ins of producing wells are necessary for material balance calculations.

The rule of thumb from conventional reservoir simulations that a model can predict one to one and one-half times as much future performance as can be matched also applies to coal well simulations. Thus, if two years of field history is matched with a simulator, it is anticipated that the next two or three years of performance can be accurately predicted. And, similar to conventional simulations, history matching of past coal well performance is often a tedious, time-consuming exercise.

The history matching procedure described by Mattax and Dalton for conventional reservoir simulation is also applicable to coal simulations.[42] Paul and Young focused specifically on history matching of coal well simulations.[43] Both of these studies emphasize that the reservoir description obtained from matching performance is not unique and that the least well-characterized variables should be the first to be modified to obtain a match. Some reservoir simulations seek to match production rates, while others seek to match fluid ratios (gas-oil ratio, water-oil ratio, etc.) and gas and water arrival times. Thus, objectives of a history match exercise should be clearly stated before the task commences.

Regardless of history match objectives, a fundamental match parameter is reservoir pressure. The primary variables for obtaining that match are absolute permeability, relative permeability, and thickness. Mattax and Dalton recommend use of the single-phase, transient flow equation for estimating permeability:

$$p = p_i + 70.6 \frac{q_w \mu_w B_w}{kh} Ei\left(-\frac{1}{4t_D}\right) \tag{11.4}$$

where

$p$ = pressure at radius $r$ from the producing well, psia,
$p_i$ = initial reservoir pressure, psia,
$q_w$ = water production rate, bpd,
$k$ = permeability, md,
$\mu_w$ = water viscosity, cp,
$B_w$ = water formation volume factor, rb/stb,
$h$ = coal thickness, ft,
$Ei$ = exponential integral function, and
$t_D$ = dimensionless time, calculated from

$$t_D = 0.00632 \frac{kt}{\phi \mu c_t r^2} \tag{11.5}$$

where

$t$ = time, days,
$\phi$ = porosity, fraction,
$c_t$ = system compressibility, psia$^{-1}$, and
$r$ = radius from producing well, ft.

From equation (11.5) it can be seen that the time at which a permeability discontinuity affects the pressure response is proportional to the square of the distance of the heterogeneity from the wellbore. Thus, if a well was known to be near a sealing fault, distance to that fault could be estimated from equation (11.5).

A variety of pressure data are typically available for a simulation study. Reservoir pressures obtained from periodic well shut-ins or pressure transient tests and initial reservoir pressures are employed for material balance calculations. Long-term shut-ins that reach current reservoir pressure or allow extrapolation to it are preferable to short-term shut-ins. Pressures from individual wells are used to determine wellbore skin factors. Bottomhole pressures are preferable to wellhead pressures, as the latter require knowledge of a fluid level to calculate the former.

Relative permeability curves for conventional reservoirs are easier to measure in the laboratory and are more representative of the whole reservoir than are coal relative permeabilities. Relative permeabilities are fourth on a list of variables presented by Mattax and Dalton to be changed in history matching, behind changes in aquifer transmissibility, aquifer storage, and reservoir transmissibility.[44] In contrast, Paul and Young consider coal gas-water relative permeabilities to be one of the primary variables to be adjusted during a performance matching exercise, especially if the curves were measured in the laboratory.

In general, gas and water mobilities are governed by relative permeability curves, not wellbore condition. Changes in the skin factor will change pressures but not the gas-water ratio of a given well. However, wellbore condition can affect gas and water production rates from a coal similar to production from conventional black oil reservoirs near the bubblepoint. Pressure always drops across wellbore damage. For a given bottomhole pressure, reservoir pressure in the near-wellbore region around a damaged well is higher than around a similar, undamaged well. The pressure drop across severe damage may be so large as to maintain reservoir pressure above the coal desorption pressure, similar to maintaining reservoir pressure above the oil bubblepoint. Consequently, wellbore skin factor specified in a simulation can indirectly influence the gas-water ratio of a well.

Coal porosity is heterogeneous and difficult to measure in the laboratory, and the distinction between cleat and matrix porosity is often arbitrary. Water resides in both cleat and matrix porosity, with the majority of the moveable water in the cleats. Thus, model cleat porosity is frequently adjusted to obtain a match of water production. Model porosity describes not only physical coal porosity but also reflects errors in endpoints of gas and water relative permeability curves, and in single-layer simulations, the effect of neglecting gravity. Consequently, history match porosities often seem unrealistically small. Young et al. employed porosities ranging from 0.05% to 0.80% to match San Juan coal well performance.[45] Robinson et al. used a porosity of 0.80% to match performance of a micropilot injectivity test in anthracitic coals of the Qinshui Basin of China.[46]

The impact of data available for simulator calibration on predictions of future performance can be illustrated with two modeling studies of wells draining the Wyodak coal of the Powder River Basin in Wyoming. The Betop pilot in section 20, T51N, R72W was one of the first installed in this basin. Measurement of key reservoir parameters such as coalbed gas contents, sorption isotherms, and permeability of these coals had just begun and were all highly uncertain. Reid et al. calibrated their simulator employing the best available reservoir properties and most of the coal well production data from the basin at that time, which was slightly more than two years of production history from five Betop wells.[47] Their assumption of free gas in the cleats and undersaturated coal in the matrix is now known to be physically impossible but at the time was thought to be realistic.

Reasonable matches of gas and water production were obtained for all five wells. Typical matches are shown in figures 11–1 and 11–2. Sensitivity analyses using the calibrated data set indicated the parameters most influential in coal well performance are, in order of decreasing importance, permeability, desorption pressure, and drainage area. From these sensitivity runs, three cases (average, worst, and best) were constructed for field development simulations and preliminary economics. These simulations indicated an average well completed in the Wyodak coal would have a peak rate on the order of 600 mcfd, an estimated ultimate recovery (EUR) of 1.1 bcf per 40 ac location, and a well life of at least 20 years.

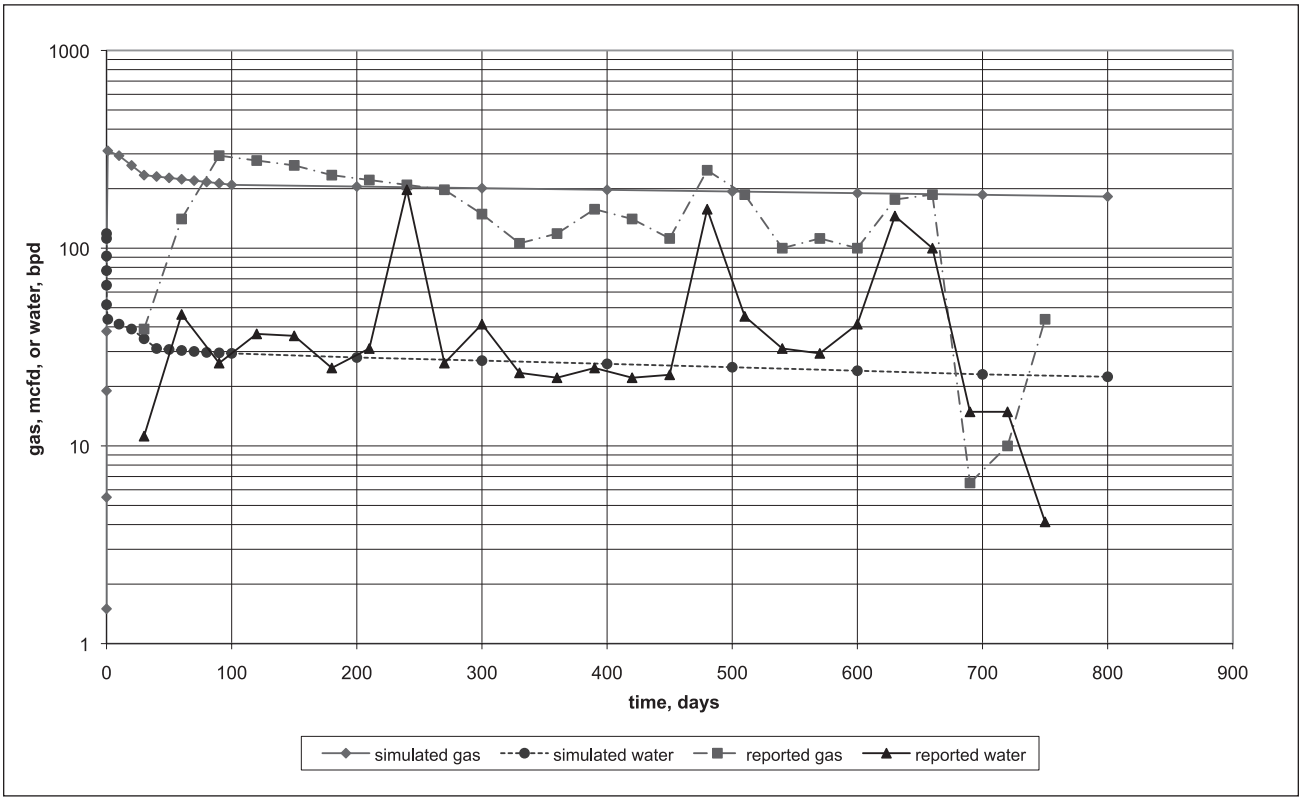



**Fig. 11–1.** Comparison of simulated and actual production—Well 3-20[48]

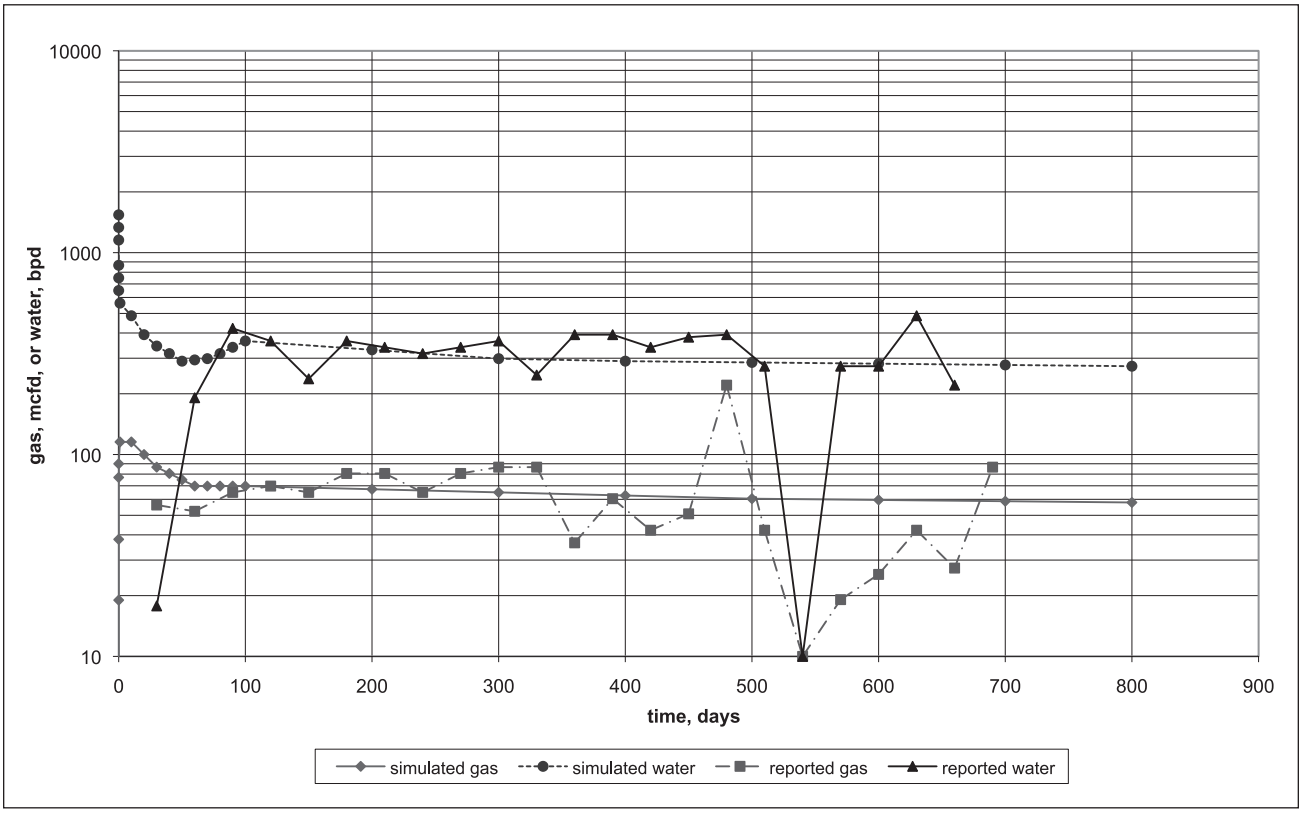



**Fig. 11–2.** Comparison of simulated and actual production—Well 7–20[49]

The second Wyodak simulation, performed by Hower a decade after that of Reid et al., matched nine years of production history from more than 1,300 wells in 136 sections in T47–49N R71–74W.[50] As was suspected from geological evidence, simulations with the calibrated data set indicated the Wyodak is an extensive, permeable coal deposit. The final model grid was not a closed system but incorporated downdip water influx and updip gas migration. With the resulting open, dynamic reservoir, the model could match well behavior without resorting to water flow from bounding beds as hypothesized by Onsager and Cox.[51] The calibrated model was used to investigate Wyodak well spacing and developed type curves for wells on 40 and 80 ac. A typical well draining 40 ac had a peak gas rate of 500 mcfd, EUR of 0.154 bcf, and a lifetime of three years.

Simulated and reported gas profiles for the 3-20 and 7-20 wells from Reid et al. and the generic 40 ac gas profile from Hower et al. are compared in figure 11–3.[52] Gas profiles from these two studies had roughly the same peak rate, 500 to 600 mcfd, but EURs and well lifetimes varied by an order of magnitude. Consideration of calibration and prediction times helps understand this variation. Reid et al. had two years of production data, during which time the wells reached peak rate and started on decline. Thus, the simulator could be calibrated to peak rates but not to any full well histories prior to being employed to generate a 20-year performance prediction. The prediction interval was, of necessity, 10 times longer than the history match period. In contrast, production data available to Hower et al. for simulator calibration not only included peak gas rates, but many early wells were nearing their economic limits, permitting more accurate simulator calibration using full well lifetimes.[53]

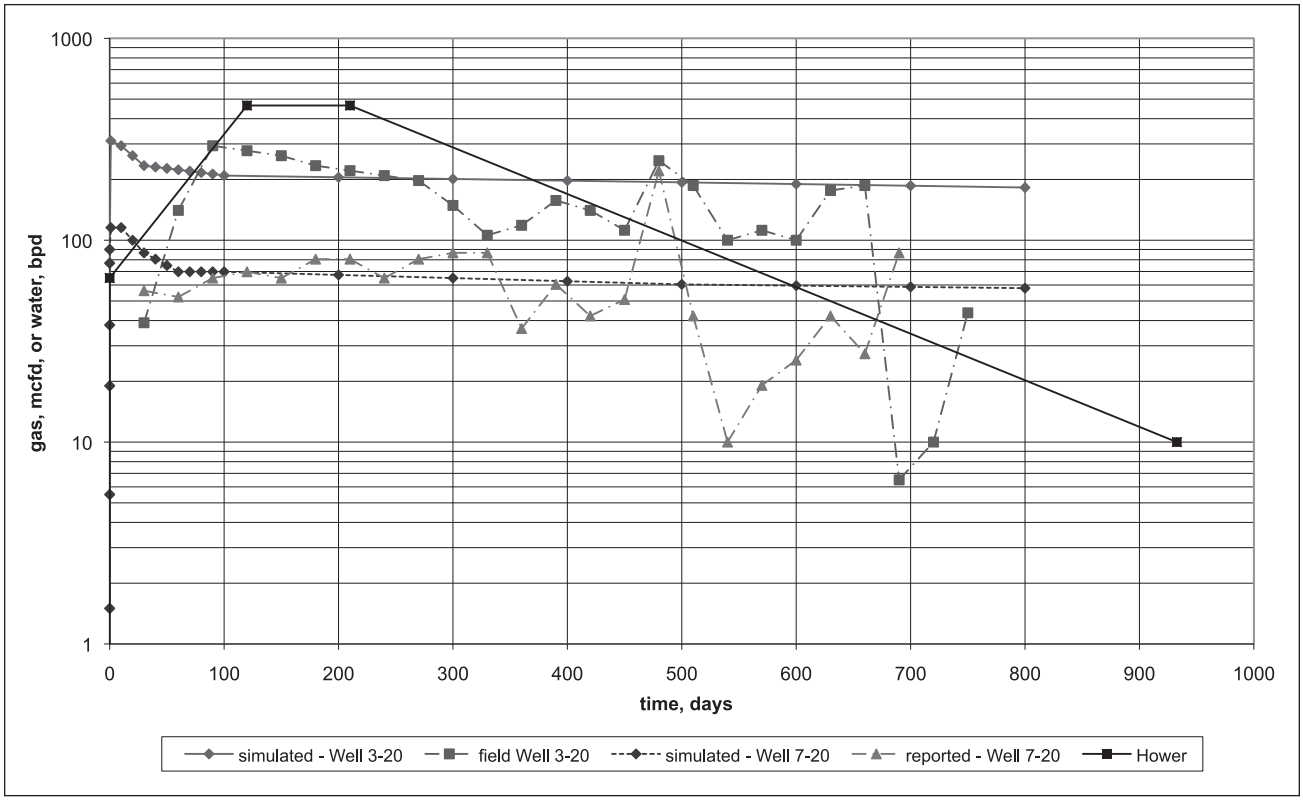



**Fig. 11–3.** Simulated and reported gas profiles for 3-20 and 7-20 wells[54]

The sorption isotherm of Reid et al. yielded an initial coalbed gas content of 176 scf/ton, more than seven times the 23 scf/ton from the isotherm of Hower et al.[55] The resulting larger initial gas in place volume of the Reid simulation contributed to the predicted longer well lives. Precise measurement of in-situ gas contents and sorption isotherms of Powder River Basin coals in the decade between the two simulations served to better constrain the latter simulation.[56]

Three aspects of coal gas production that can be better understood through simulation include undersaturation and the time to first gas production, the role of cleat compressibility in fluid production from undersaturated coals, and the interplay between sorption time and permeability.

### Example 11.1. Simulation of undersaturated coal with tank and gridded models

Typical reservoir and well parameters for the Big George coal of the Powder River Basin of Wyoming are collected in table 11–2. Gas storage in the matrix was described with the average Powder River Basin sorption isotherm of Crockett and Meyer, and gas-water relative permeabilities were crossed, straight lines.[57] With an initial reservoir pressure of 500 psia and a desorption pressure of 300 psia, gas content of this coal seam is 58.9 scf/ton, making it undersaturated in gas by 33%. Initial fluids in place were 581.349 mmcf of gas and 6,206.694 mstb of water. A decade of production from a single well draining 80 ac of constant-thickness, flat, homogeneous Big George coal was modeled with a tank model and a gridded simulator. The well was controlled by specifying a water rate of 500 bpd, and when that could no longer be sustained, a bottomhole pressure of 20 psia.

**Table 11–2.** Typical reservoir and well parameters—Big George coal, Powder River Basin

| | | |
|---|---|---|
| Area = | 80 | ac |
| $h$ = | 100 | ft |
| $V_{Lis}$ = | 218.4 | scf/ton |
| $p_L$ = | 1355 | psia |
| Density = | 1.35 | g/cm$^3$ |
| Initial pressure = | 500 | psia |
| Desorption pressure = | 300 | psia |
| Porosity = | 0.10 | |
| $S_{gi}$ = | 0.00 | |
| Permeability = | 100 | md |
| Temperature = | 65 | °F |
| Coal compressibility = | 0.0001 | psia$^{-1}$ |
| Cleat spacing = | 10 | mm |
| Sorption time = | 5 | days |
| $r_w$ = | 0.50 | ft |
| $s$ = | 0.00 | |
| Bottomhole pressure, min. = | 20 | psia |

The tank model, described in detail previously in the text, couples pseudosteady-state Darcy equations for gas and water flow rates with mass balance equations. For this exercise, gas flow rate was calculated with the real gas pseudopressure formulation. Due to the assumption of pseudosteady state (or boundary-dominated) flow, transient behavior cannot be described with this approach. Assuming boundary-dominated flow begins at a dimensionless time of 0.1 and a water-saturated coal with no free gas, time for this well to reach pseudosteady-state flow is 5.5 days. Assuming a gas relative permeability of 0.5 when desorption pressure is reached, time to reach pseudosteady state flow is 7.1 days. Consequently, a 30-day time step in the tank model is acceptable.

To test for grid effects, the gridded model employed three 2-D areal grids with increasingly finer blocks. The coarsest grid was 5 by 5 blocks, the intermediate grid was 13 by 13 blocks, and the finest grid 21 by 21 blocks. The well was always located in the center gridblock.

Gas and water production rates are depicted in figure 11–4. First gas production occurred at the same time in all three gridded models, 274 days, compared to 300 days for the tank model. The slightly earlier gas production in the gridded model is attributed to its ability to describe the cone of depressuring around the wellbore and consequent near-wellbore gas desorption. In contrast, gas release in the tank model commences only when average pressure in the 80 ac drainage falls below desorption pressure. The water production rate is constant during

depressurization down to desorption pressure and beyond. Thus, time to first gas production is approximately time to reach desorption pressure and can be estimated from the definition of system compressibility

$$c_t = -\frac{1}{V_p}\frac{dV_p}{dp}$$

where

$V_p$ = pore volume, ft³.

Neglecting water compressibility, this can be approximated as

$$c_f = \frac{1}{Ah\phi}\frac{q_w t_{des} B_w}{(p_i - p_d)}$$

where

$c_f$ = formation compressibility, psia$^{-1}$,
$A$ = drainage area, ac,
$t_{des}$ = time to reach desorption pressure, days, and
$p_d$ = desorption pressure, psia.

Solving for time to reach desorption pressure,

$$t_{des} = \frac{Ah\phi c_f}{q_w B_w}(p_i - p_d)$$

$$t_{des} = \frac{80\text{ ac}\,100\text{ ft}(0.10)(10^{-4})\text{ psia}^{-1}\,43{,}560\,\frac{\text{ft}^2}{\text{ac}}\,0.1781076\,\frac{\text{rb}}{\text{ft}^3}}{500\,\frac{\text{stb}}{\text{day}}\,1.0\,\frac{\text{rb}}{\text{stb}}}(500-300)\text{psia}$$

$$t_{des} = 248 \text{ days}$$

This approximate desorption time is slightly earlier than those of both the tank and gridded models. Once gas production is established, gas rates in the two models were in excellent agreement throughout the remainder of the decade of production. Rates in the gridded model exhibited little sensitivity to grid size, with differences between the coarse and fine grids averaging 1% or less.

Water production in the gridded model began to decline from the specified rate of 500 bpd after 2,130 days compared to 2,280 days for the tank model. The difference of 150 days is attributed to the ability of the gridded model to represent saturation and pressure distributions, which the tank model cannot. As the near-wellbore region of the gridded model had a higher than average gas saturation and a lower than average pressure, water production decline occurred sooner in this model than in the tank model. Water production began to decline in the gridded model at a cumulative water production of 1,065 mstb and in the tank model at a cumulative water production of 1,140 mstb. These represent 17% and 18% of original water in place, respectively. Onset of water rate decline at a recovery of 17% of OWIP implies an average water saturation of 83% in the coal at that time. This simple numerical experiment demonstrates that the process of "dewatering" a coal does not imply all moveable water has been removed from a coal seam.

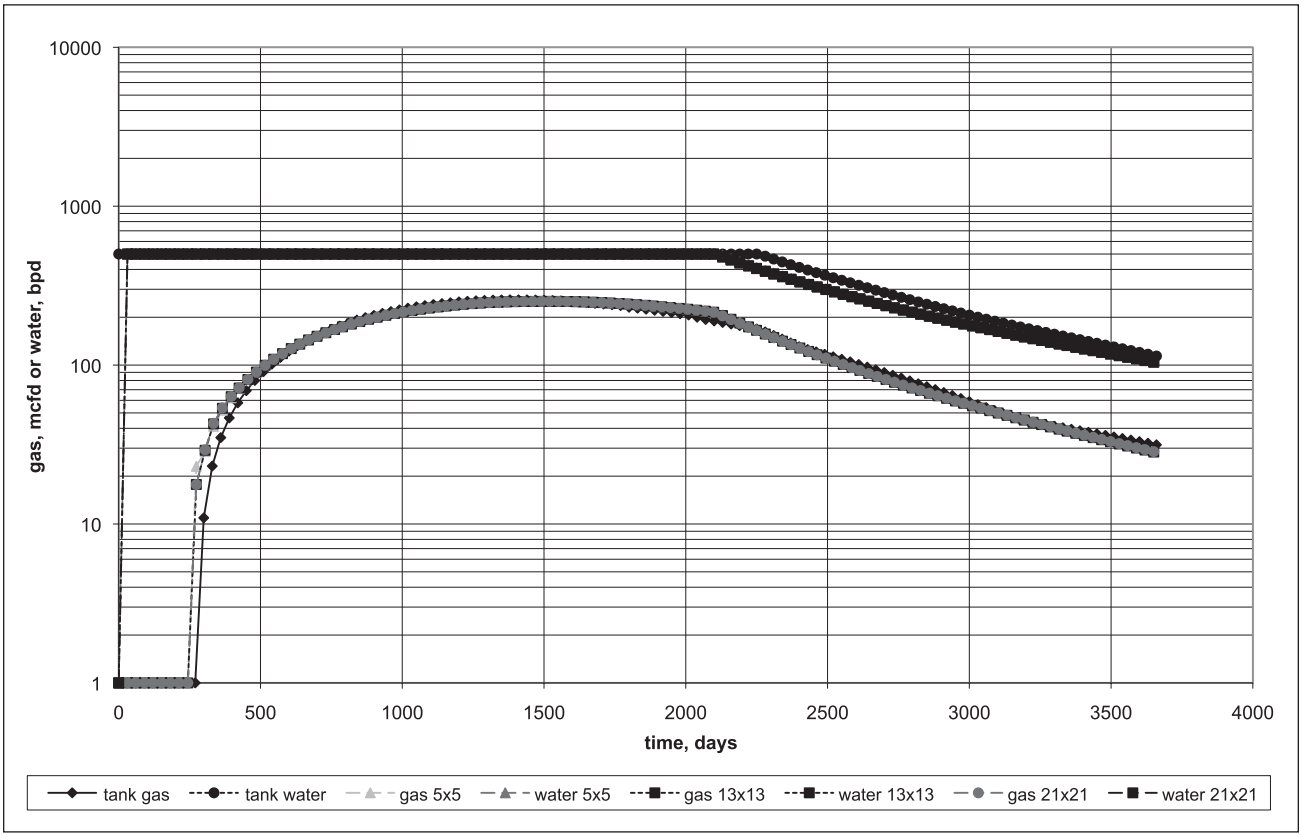



**Fig. 11–4.** Simulated gas and water rates, gridded and tank models

Cumulative gas and water production for both models is plotted in figure 11–5. Cumulative gas production from the two models was in excellent agreement throughout the decade of production, while the cumulative water production curves exhibit an offset due to the additional 150 days of water production at a constant 500 bpd from the tank model. After a decade, cumulative gas production was 485.883 mmcf (83.58% of OGIP) and 486.266 mmcf (83.64% of OGIP) from the tank and gridded models, respectively. Cumulative water production at that time was 1,471.818 mstb (23.71% of OWIP) and 1,403.179 mstb (22.61% of OWIP) from the tank and gridded models, respectively. Cumulative volumes were not a strong function of grid size, as the maximum difference between coarse and fine grids was less the 0.2% for both gas and water.

The excellent agreement in gas and water rates and cumulatives predicted by the three grids demonstrates the robust solution algorithms of current coal gas simulators. Differences between the gridded and tank models are ascribed to the use of average saturations and pressures in the latter.

Average reservoir pressures for the models, plotted in figure 11–6, initially decline linearly and exhibit a notch of approximately 20 psia when desorption pressure is reached and gas is first released. Once gas is present, pressure in the tank model is at worst one-half an atmosphere higher, or alternatively, lags the gridded model by at most about two months. During the second half of the decade, average pressures in the two models are in excellent agreement.

Average water saturations in the models are shown in figure 11–7. Initially in agreement, water saturation in the tank model falls below that of the gridded model after 2,130 days due to an additional 150 days of constant water production at 500 bpd. After a decade of production, average water saturation of the tank model, 0.7761, is lower than that of the gridded model, 0.8110, reflecting the 69 mstb difference in cumulative water productions.

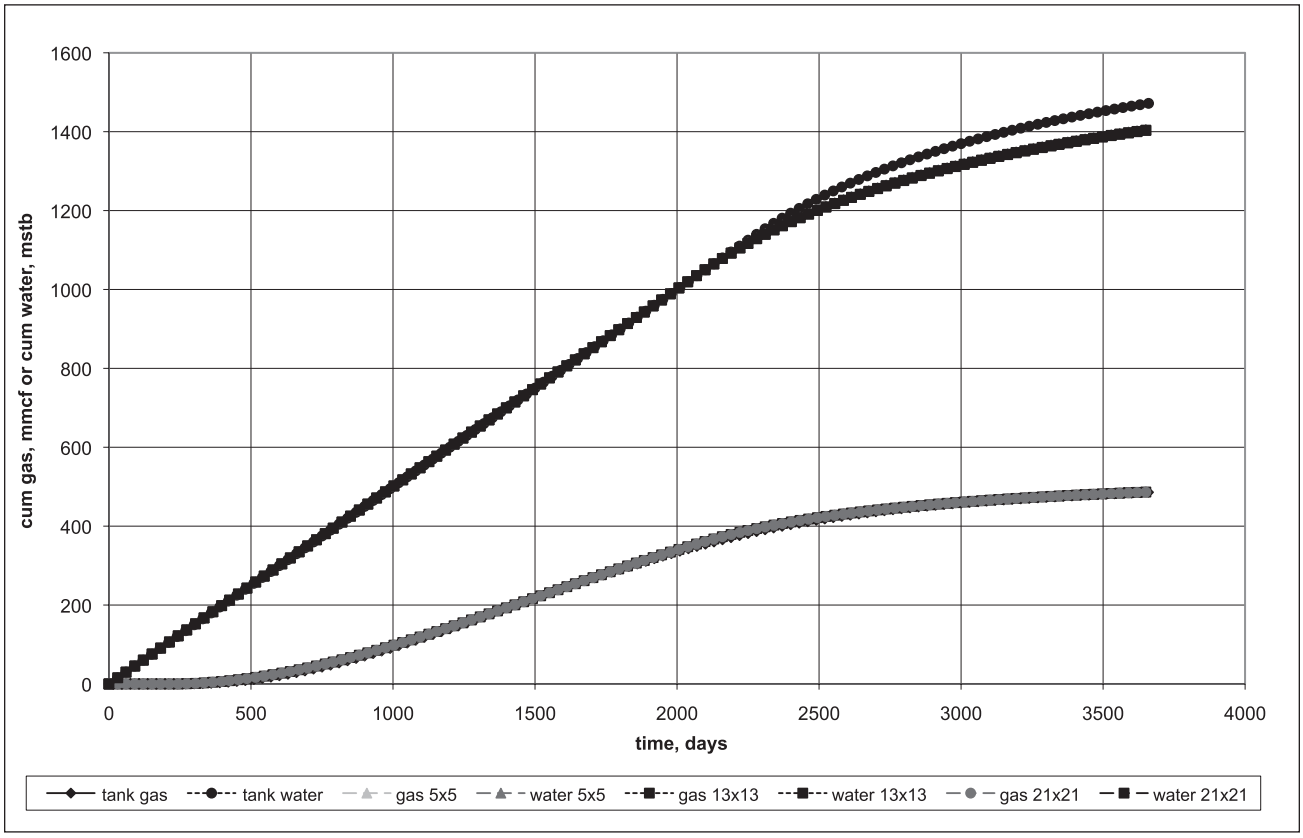



**Fig. 11–5.** Cumulative gas and water production, gridded and tank models

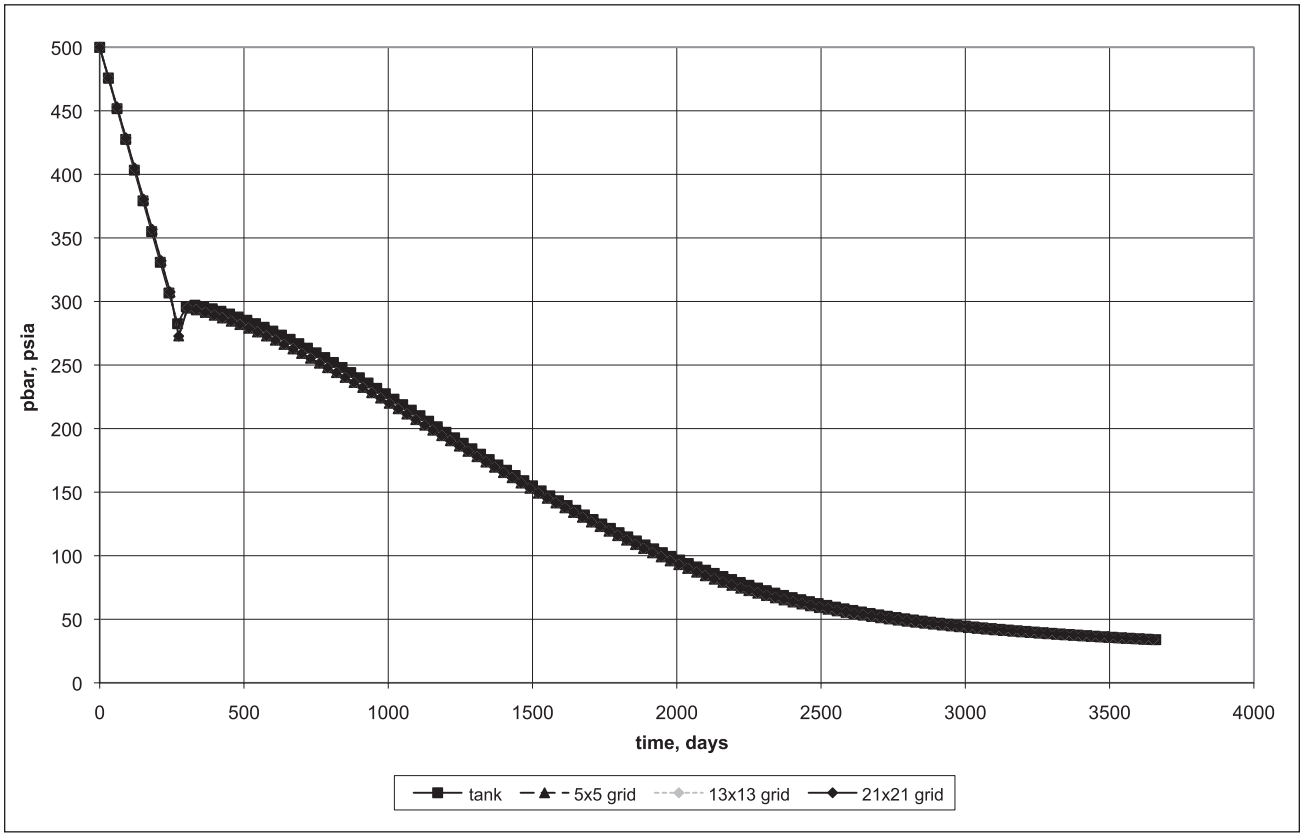



**Fig. 11–6.** Average reservoir pressures, gridded and tank models

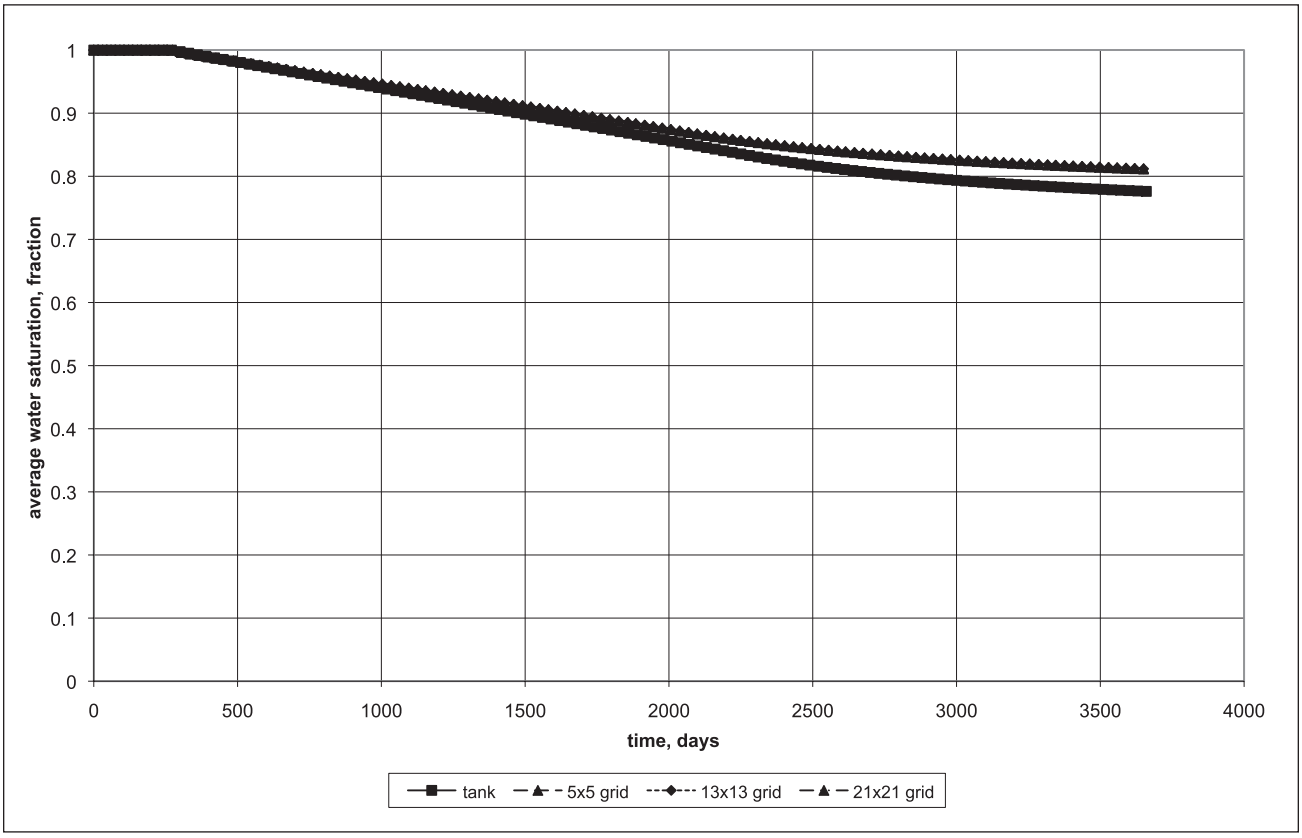



**Fig. 11–7.** Average water saturations, gridded and tank models

## Example 11.2. Cleat compressibility effects in undersaturated coal

Coal is a compressible rock, often exhibiting cleat compressibilities an order of magnitude or more greater than conventional reservoirs. This compressibility provides reservoir energy and affects performance of wells draining the coal seam. System compressibility of a coal deposit can be expressed as

$$c_t = c_f + S_w c_w + S_g c_g + c_s$$

where

$c_t$ = system compressibility, psia$^{-1}$,
$S_w$ = water saturation, fraction,
$c_w$ = water compressibility, psia$^{-1}$,
$S_g$ = gas saturation, fraction,
$c_g$ = gas compressibility, psia$^{-1}$, and
$c_s$ = sorption compressibility, psia$^{-1}$.

Sorption compressibility, which accounts for gas storage on the surface of the coal, affects system compressibility only when gas is present. Above the desorption pressure, both gas and sorption compressibilities are undefined, the cleats are water filled, and system compressibility is given by

$$c_t = c_f + c_w$$

Assuming a water compressibility of $3(10)^{-6}$ $psia^{-1}$ or 3 microsips, the tank model of example 11.1 was run with selected values of cleat compressibility. In addition to the cleat compressibility of 100 microsips employed by Hower et al. to simulate Powder River Basin coals, a decade of well performance was simulated assuming cleat compressibilities of 3, 30, and 300 microsips.

As shown in figure 11–8, increasing cleat compressibility increases both time to reach desorption pressure and time to onset of water rate decline. After a year of production, gas rates ranged from 0 mcfd in the most elastic coal (300 microsips) to 122 mcfd in the stiffest coal (3 microsips). The specified water rate of 500 bpd began to decline first in the stiffest coal (5.6 years) and last in the most elastic (7.4 years). In a financial light, the stiffest coal shows earliest gas production and earliest onset of water rate decline, making it the most economic of the four cases. The most elastic coal begins to produce gas after 2.1 years and maintains a constant water production for another five years, making it the least economic of the four cases. The sensitivity of economics to cleat compressibility is matched by the difficulty in measuring this parameter. While estimates of cleat compressibility can be obtained from the slope of laboratory-measured stress-permeability curves or from multiwell interference tests, it is most accurately determined from field data such as history matching well performance with a simulator.

Cumulative gas and water production, depicted in figure 11–9, exhibit opposite sensitivities to cleat compressibility. Cumulative gas production is most influenced by cleat compressibility in the early years, and after a decade of production, cumulative gas volumes ranged from 470 to 489 mmcf, a variation of only 4%. In contrast, cumulative water curves were identical in the early years, as intuitively expected from specification of a constant rate, and diverged in later years to vary from 1,393 to 1,624 mstb, a difference of 14%. Average reservoir pressures, plotted in figure 11–10, were most strongly influenced by cleat compressibility early in the life of the well and converged at late time. Average water saturation, shown in figure 11–11, was most strongly influenced by cleat compressibility at middle times, with all four simulations converging to a final value of 78%.

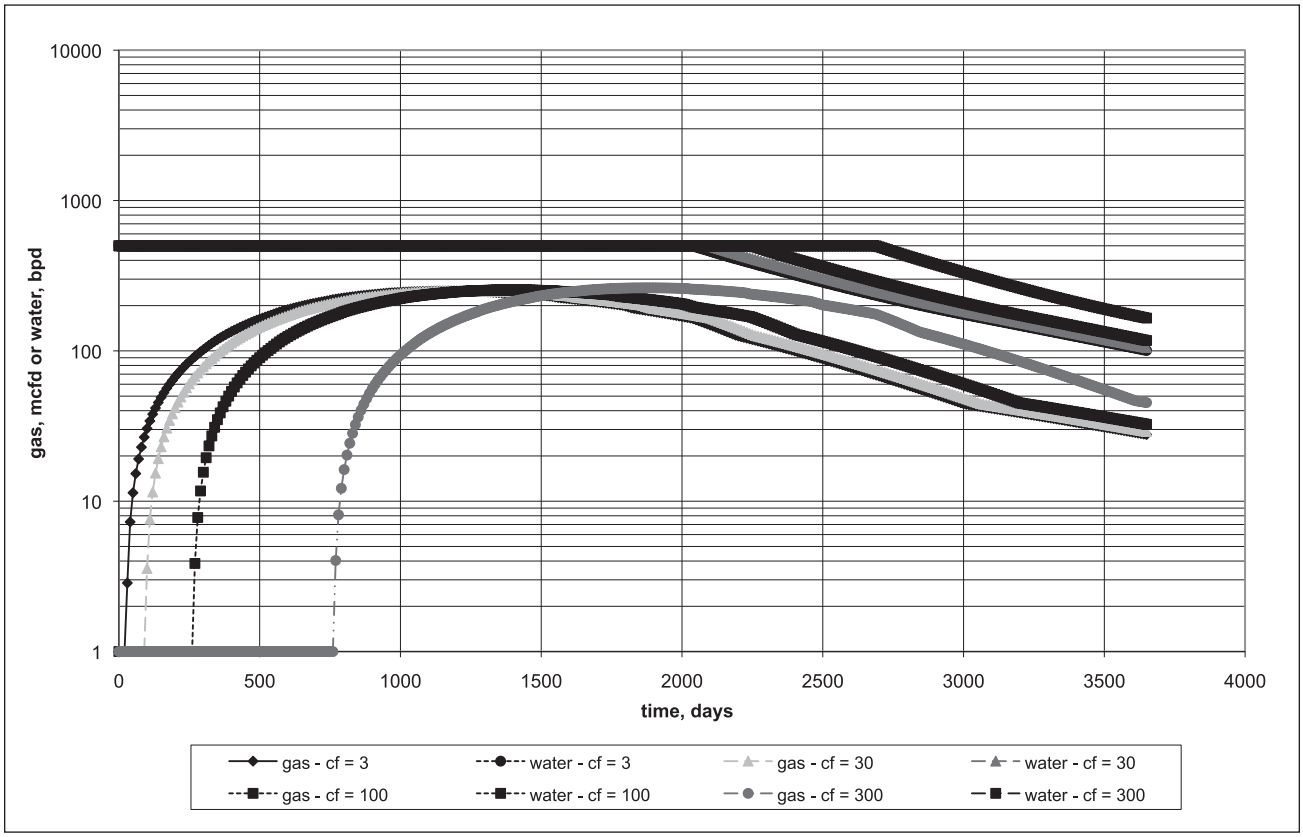



**Fig. 11–8.** Effect of cleat compressibility on Big George coal well rates

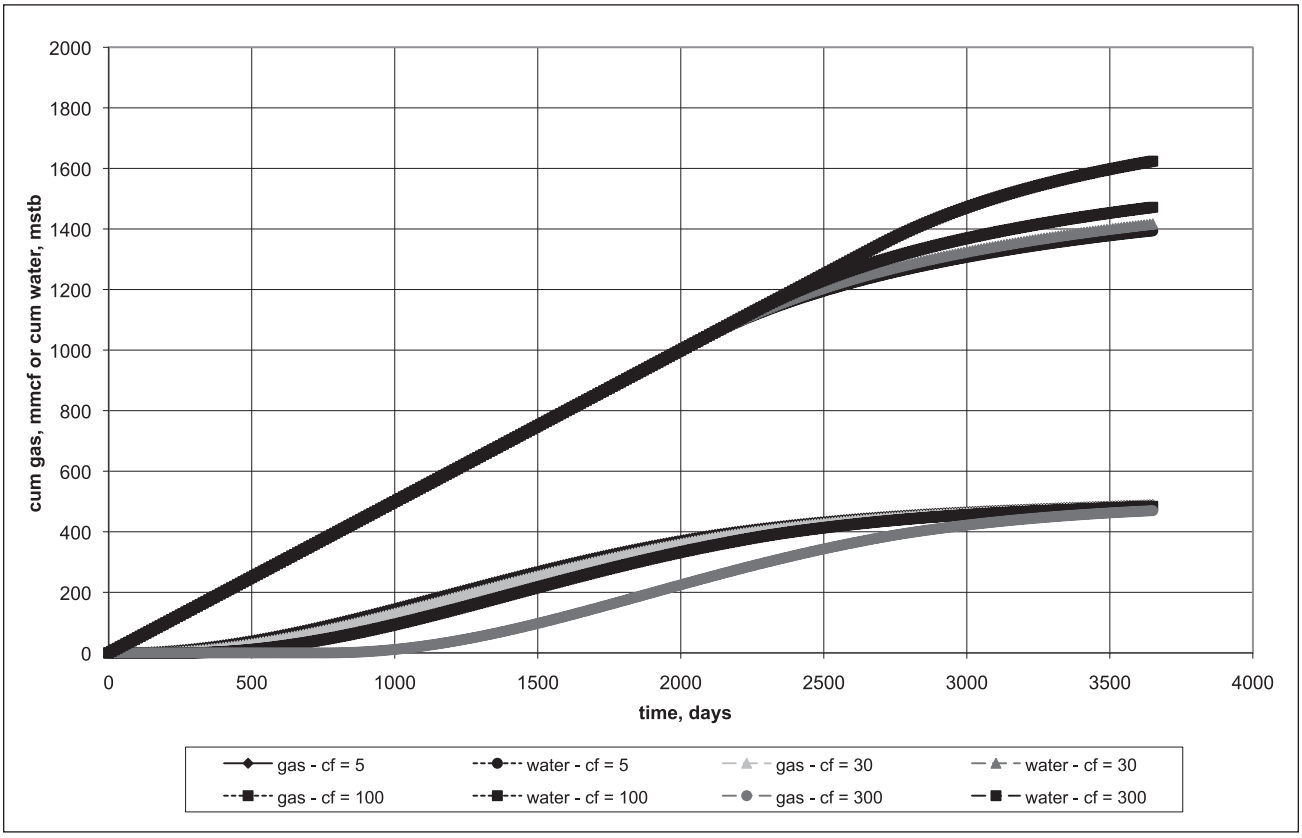



**Fig. 11–9.** Effect of cleat compressibility on Big George coal well cumulative production

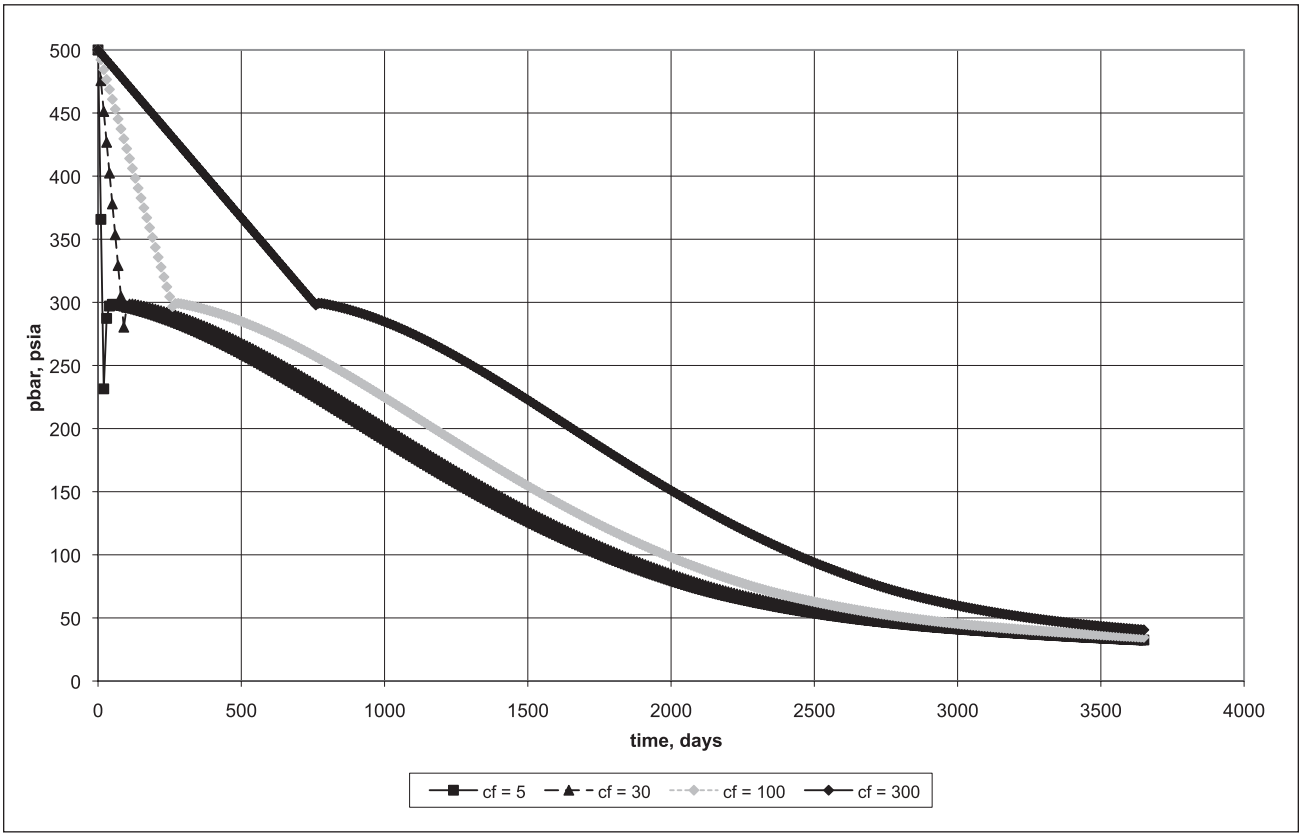



**Fig. 11–10.** Effect of cleat compressibility on Big George coal well average reservoir pressure

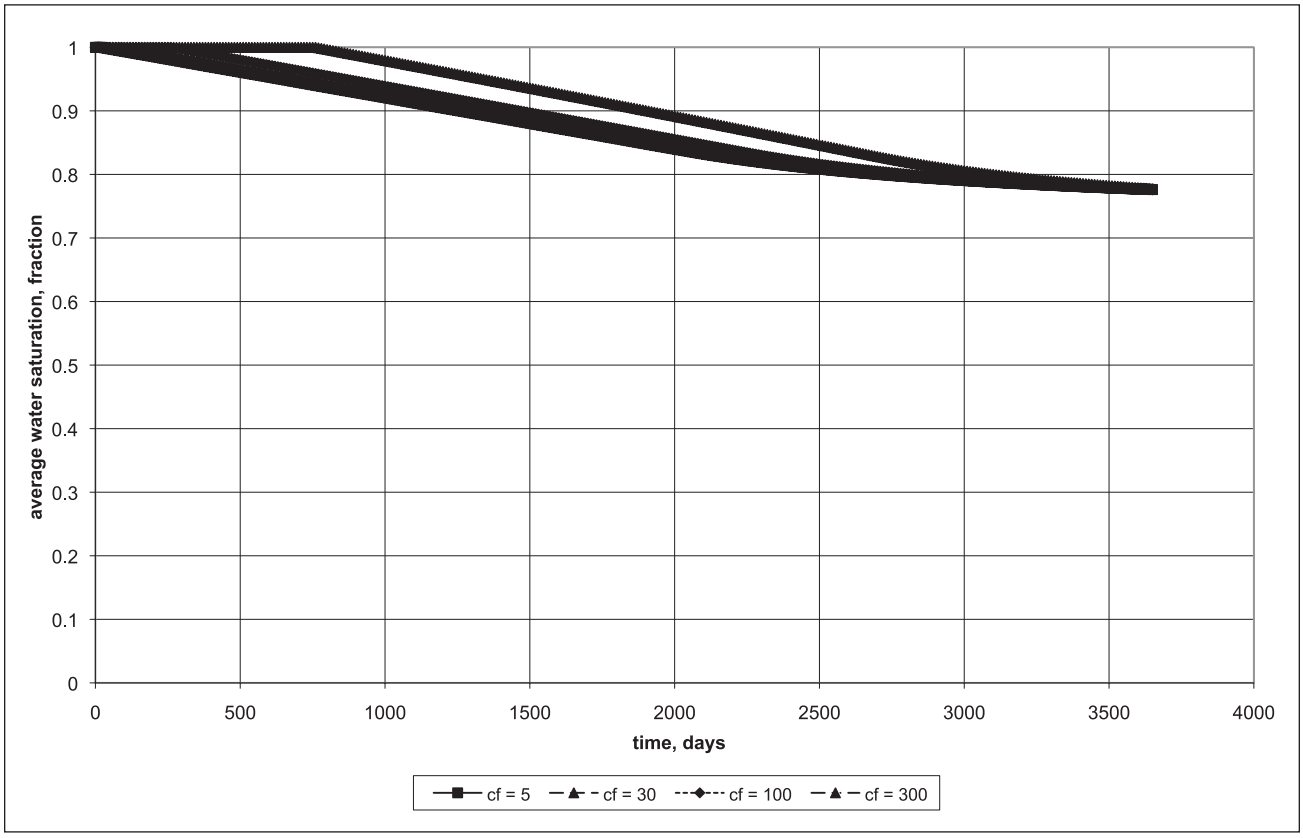



**Fig. 11–11.** Effect of cleat compressibility on Big George coal well average water saturation

## Example 11.3. Effect of sorption time on coal well performance

Production of gas from a coal seam is a two-step process beginning with desorption of gas from the coal matrix and terminating with the flow of gas through the coal cleats to the wellbore. The slower of these two processes will control well behavior. To illustrate the effect of sorption time on coal well behavior, the tank and gridded (21-block) models of the Big George coal of example 11.1 were employed. For a clearer understanding of the role of sorption time, the coal was assumed to be fully saturated. Gas and water rates and cumulatives from the tank model, which assumes instantaneous gas release from the matrix, were compared with those predicted by the gridded model with a typical Powder River sorption time of 1 day, followed by progressively larger sorption times of 10, 100, and 1,000 days.

Gas and water rates from the five simulations are plotted in figure 11–12. Timing and magnitude of peak gas production, time to onset of water rate decline, and 10-year cumulative production volumes are collected in table 11–3. Gas and water rates are relatively unaffected for sorption times less than 100 days. Sorption times of 100 days and longer reduce peak gas rates up to 75% and shorten time to peak gas up to 20%. Similarly, sorption time has little influence on time to onset of water decline up to 100 days. Longer sorption times result in earlier onset of water decline, reducing it by over one-half for a sorption time of 1,000 days.

**Table 11–3.** Example 11.3 well data

| Sorption time, days | Peak gas rate, mcfd | Time to peak gas rate, days | Time to onset of water decline, days | 10-year cumulative gas, mmcf | Fraction of OGIP | 10-year cumulative water, mstb | Fraction of OWIP |
|---|---|---|---|---|---|---|---|
| 0 | 401.0 | 1,080 | 2,280 | 768.874 | 0.889 | 1,461.028 | 0.235 |
| 1 | 405.6 | 1,126 | 2,038 | 771.959 | 0.893 | 1,341.305 | 0.216 |
| 10 | 399.6 | 1,126 | 2,038 | 769.774 | 0.890 | 1,348.965 | 0.217 |
| 100 | 315.0 | 1,215 | 1,946 | 713.306 | 0.825 | 1,429.148 | 0.230 |
| 1,000 | 99.3 | 881 | 911 | 299.123 | 0.346 | 1,228.974 | 0.198 |

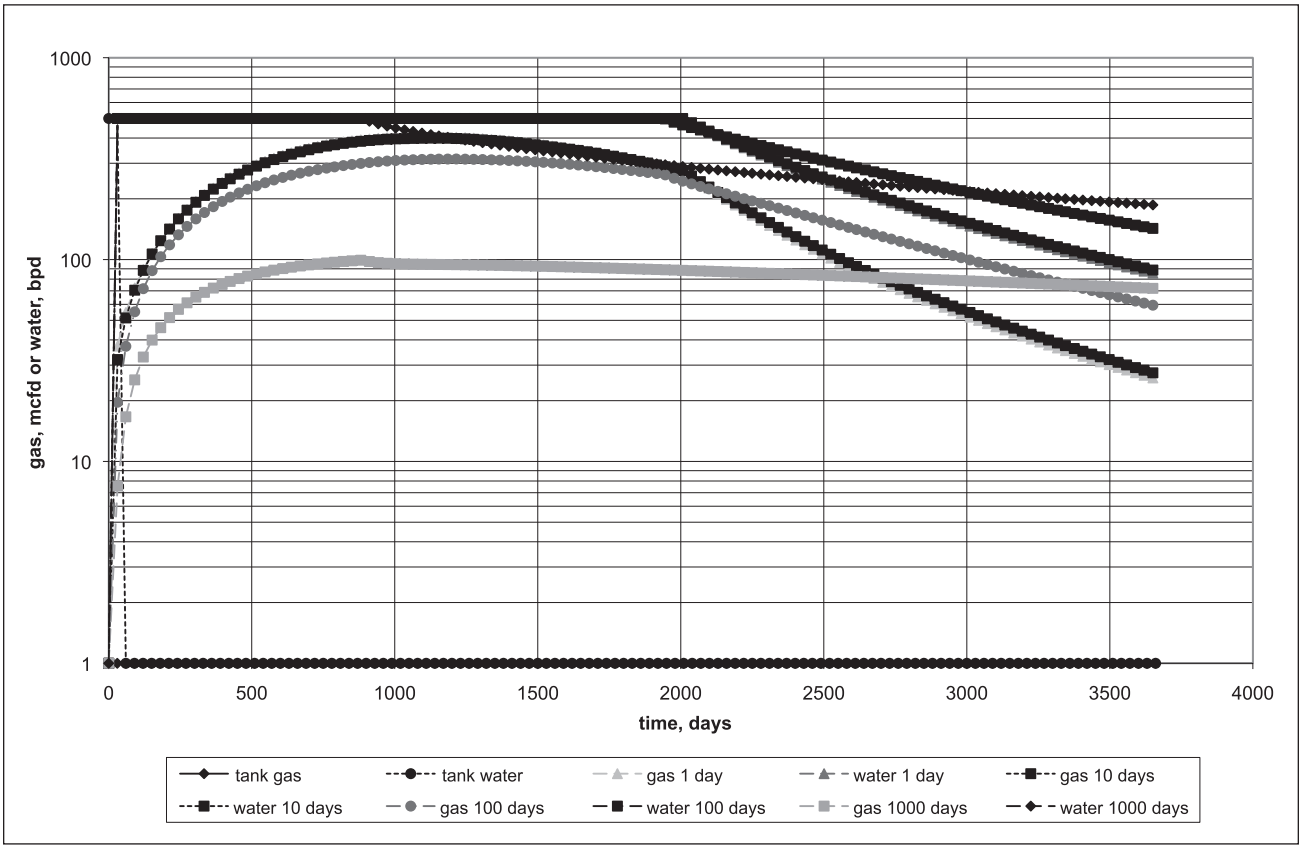



**Fig. 11–12.** Effect of sorption time on gas and water production rates

Cumulative gas and water volumes after 10 years of production are shown in figure 11–13 and are summarized in table 11–3. Both cumulative gas and water production decrease as sorption time increases, but this effect is significant only for sorption times of 100 days or longer. Fast sorption times lead to production of about 90% of original gas in place after 10 years, whereas the slowest sorption time of 1,000 days recovers only one-third of the OGIP in a decade. The effect of sorption time on cumulative water production is less profound with 10-year recoveries, dropping steadily from 24% to 20% as sorption time grows by three orders of magnitude.

The effect of sorption time on average reservoir pressure and water saturation is shown in figures 11–14 and 11–15, respectively. Average reservoir pressure is only slightly affected by fast sorption times but drops more rapidly as sorption time grows. Longer sorption times reduce gas flux into the matrix, preventing pressure support and throttling reservoir energy. In the latter one-third of the simulation, average pressures converge as total gas release from the slower coals approaches that of the rapid coals. After a decade of production, average reservoir pressures of fast sorption cases is about 32 psia, while that of slow sorption cases is an atmosphere higher, 46 psia. Average water saturation is less sensitive to sorption time than is average pressure, varying by only 4% after a decade, and higher values being associated with longer sorption times.

The reduction in well productivity with increasing sorption time is due to a slower release of reservoir energy from matrix to cleat as sorption, rather than Darcy flow, comes to control well performance. Some effects of increasing sorption time seen in this example, such as decreased times to peak gas rate and onset of water rate decline, are also influenced by other reservoir parameters, such as cleat compressibility and gas-water relative permeabilities. Generalization of results from these simulations to other coals is difficult.

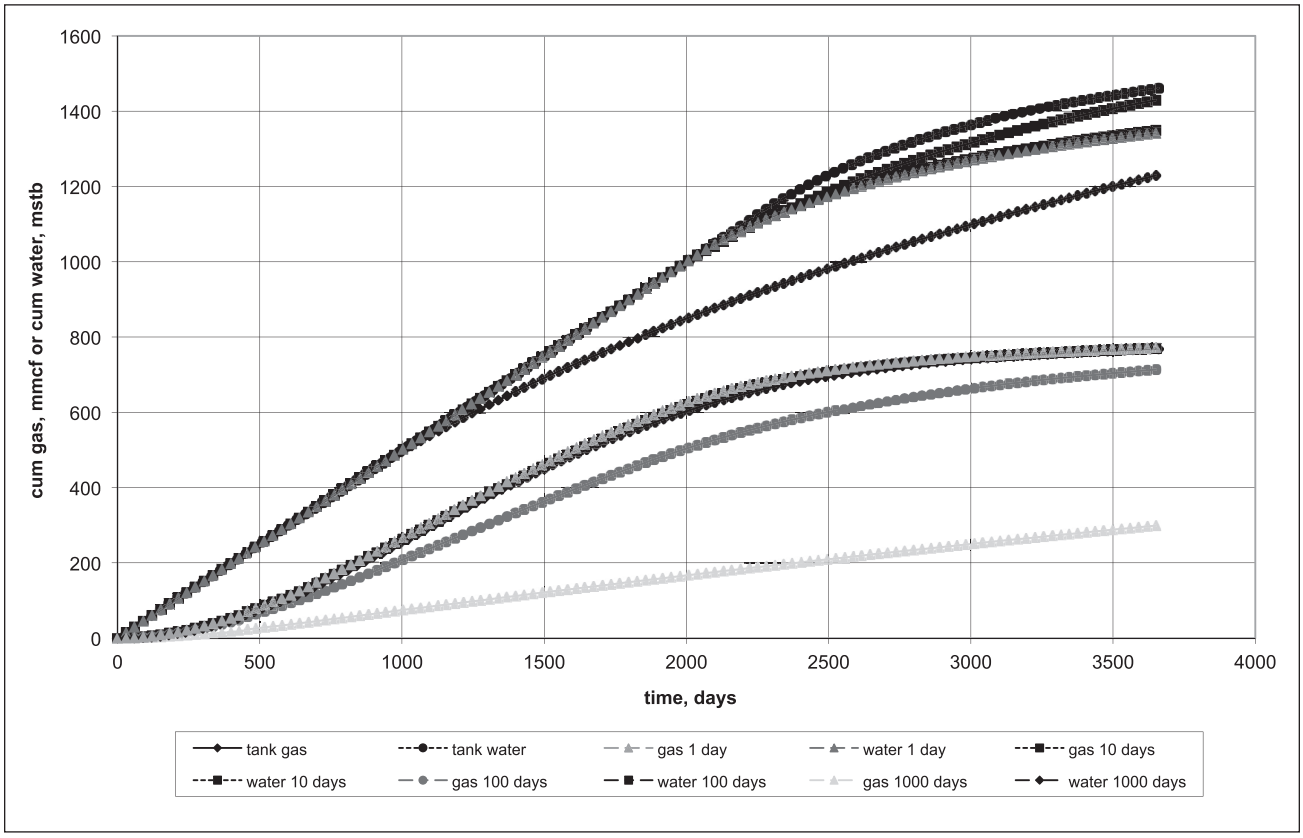



**Fig. 11–13.** Effect of sorption time on cumulative gas and water production

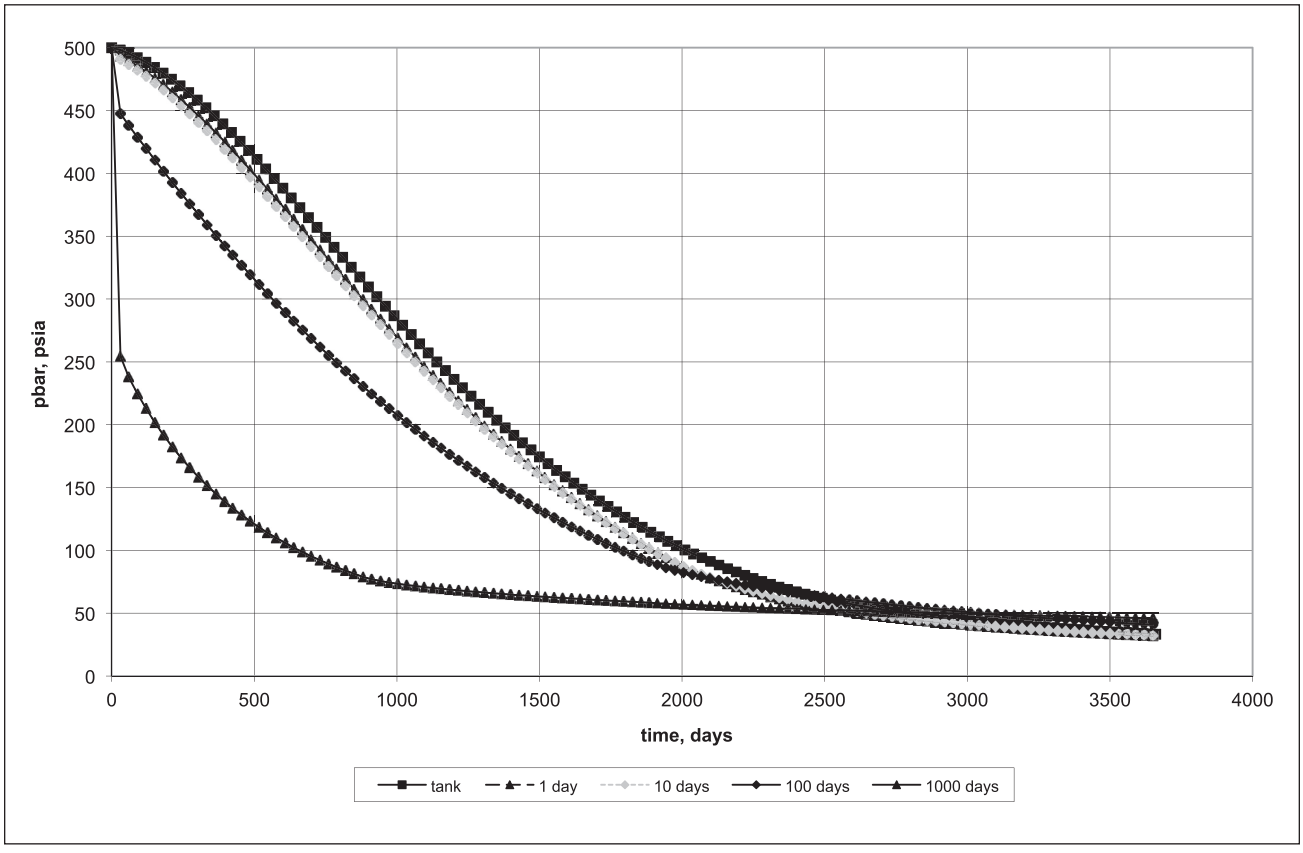



**Fig. 11–14.** Effect of sorption time on average reservoir pressure

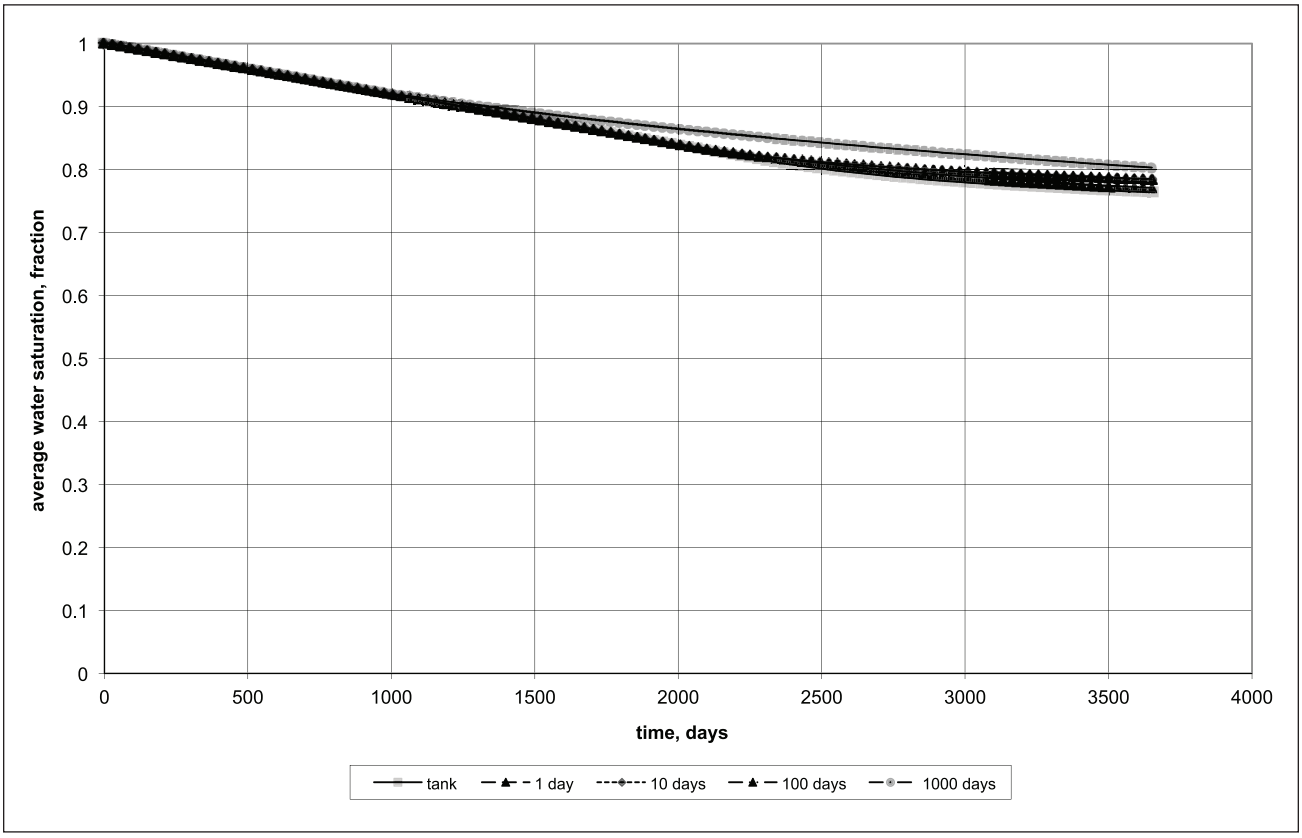



**Fig. 11–15.** Effect of sorption time on average water saturation

Competition between desorption and Darcy flow for control of well behavior can be illustrated by comparing characteristic times. As discussed in chapter 2, desorption of gas from the matrix in response to a pressure change in the cleats can be described mathematically with an infinite series of exponentially decreasing terms. Time required to desorb 95% of the gas in response to a pressure perturbation, such as that due to putting a well on production, is given by

$$t_{95} = 4.54\tau$$

where

$t_{95}$ = time for gas desorption to be 95% complete, days, and
$\tau$ = sorption time, days.

Table 11–4 shows time required for desorption to be 95% complete for each sorption time considered here.

**Table 11–4.** Time to pseudosteady-state flow

| | | Time to pss | |
|---|---|---|---|
| Sorption time, days | $t_{95}$, days | 1 yr of production | 10 yr of production |
| 0 | 0.0 | 79 | 152 |
| 1 | 4.5 | 82 | 171 |
| 10 | 45.4 | 83 | 165 |
| 100 | 454.0 | 103 | 127 |
| 1,000 | 4,540.0 | 269 | 129 |

Darcy flow can be characterized by the time to reach pseudosteady-state (boundary-dominated) flow after the well is put on production or subjected to a pressure perturbation. Times to pseudosteady-state flow assuming a dimensionless time of 0.1 and utilizing reservoir conditions after 1 year and 10 years of production are presented in table 11–4. For instantaneous desorption and sorption times of 1 and 10 days, time to reach boundary-dominated flow is always larger than sorption time. Therefore, the well is controlled by Darcy flow in the cleats. For sorption times of 100 and 1,000 days, time for release of the gas is longer than time to reach pseudosteady state, and the well is controlled by sorption. For engineering purposes, sorption strongly influences then begins to control coal well behavior as sorption time equals and then exceeds pseudosteady-state time.

Sorption and pseudosteady state times for simulation studies cited in this chapter are collected in figure 11–16. Also shown in the figure is the isochronal line of equal sorption and pseudosteady-state times. In studies with substantial changes in cleat gas saturation, such as those simulating full well life, time to reach boundary-dominated flow varies throughout the simulation. These studies would be more accurately represented by a vertical line, not a single point, in the figure. However, all parameters required for calculation of times to pseudosteady-state flow were often not published. In these cases, the crossover point on the relative permeability curves was used as a proxy for gas saturation and gas relative permeability to calculate time to pseudosteady-state flow. While this assumption is not entirely correct, it does allow the general conclusion from figure 11–16 that for reservoir engineering purposes, a coal well is controlled by release of gas from the matrix when sorption time is greater than 100 days.

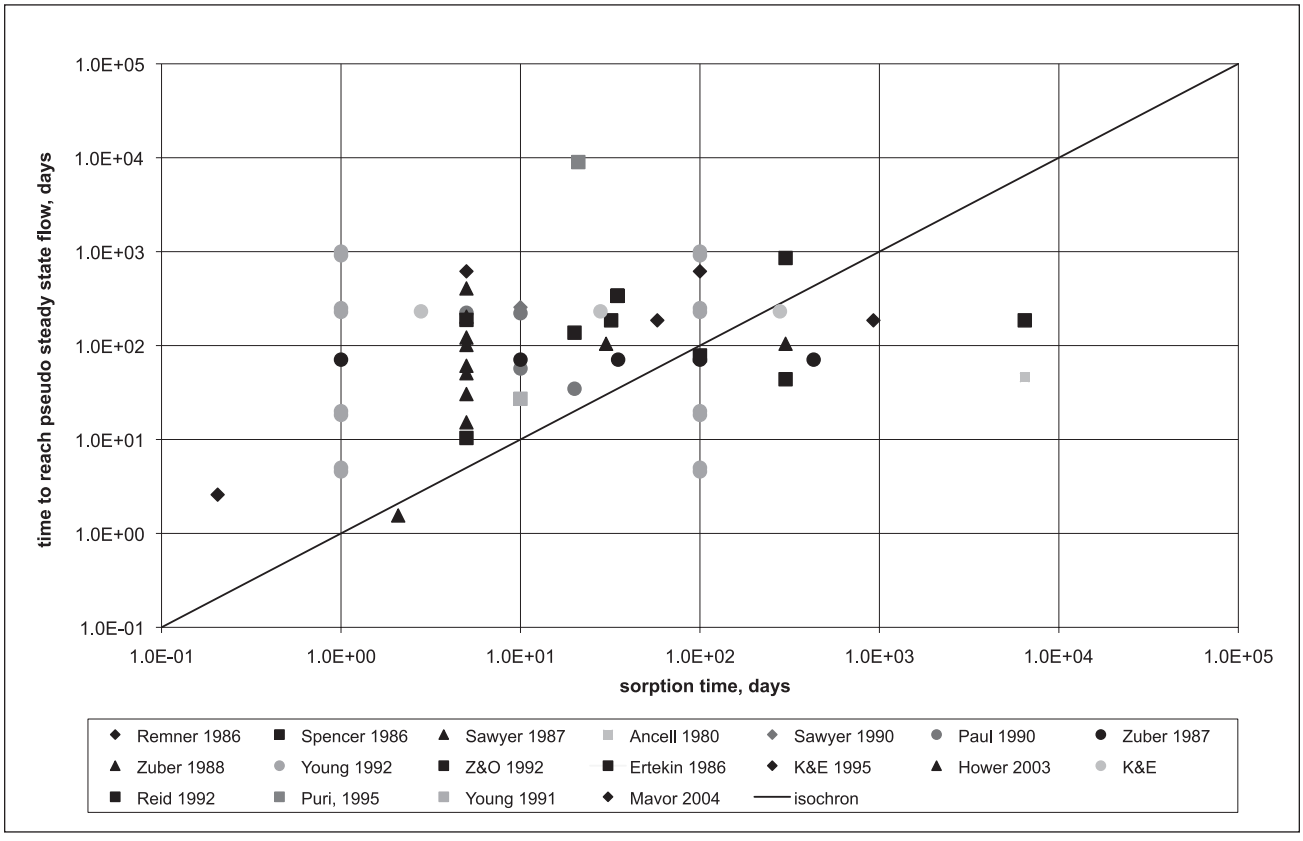



**Fig. 11–16.** Sorption and pseudosteady-state times for selected simulation studies

# Nomenclature

| | |
|---|---|
| $A$ | Drainage area, ac |
| $B_w$ | Water formation volume factor, rb/stb |
| $c_f$ | Formation or cleat compressibility, psia$^{-1}$ |
| $c_g$ | Gas compressibility, psia$^{-1}$ |
| $c_s$ | Sorption compressibility, psia$^{-1}$ |
| $c_t$ | System compressibility, psia$^{-1}$ |
| $c_w$ | Water compressibility, psia$^{-1}$ |
| $D$ | Diffusion coefficient, cm/sec |
| $G$ | Desorbed gas volume, cm$^3$ or scf |
| $G_t$ | Total desorbed gas volume, cm$^3$ or scf |
| $h$ | Coal thickness, ft |
| $k$ | Permeability, md |
| $p$ | Pressure, psia or MPaa |
| $p_c$ | Gas pressure in the cleat, psia or MPaa |
| $p_d$ | Desorption pressure, psia |
| $p_i$ | Initial reservoir pressure, psia or MPaa |
| $p_m$ | Gas pressure in the matrix, psia or MPaa |
| $q_w$ | Water production rate, bpd |
| $r$ | Radius from producing well, ft |
| $r_p$ | Particle radius, cm |
| $S_g$ | Gas saturation, fraction |
| $S_w$ | Water saturation, fraction |
| $t$ | Time |
| $t_D$ | Dimensionless time |
| $t_{des}$ | Time to reach desorption pressure, days |
| $V$ | Coalbed gas content, scf/ton |
| $V_{Ldaf}$ | Dry, ash-free Langmuir volume constant, scf/ton |
| $V_p$ | Pore volume, ft$^3$ |
| $w$ | Equilibrium moisture, fraction |

## Greek

| | |
|---|---|
| $\mu_w$ | Water viscosity, cp |
| $\tau$ | Characteristic desorption time |
| $\phi$ | Porosity, fraction |

## Subscripts

| | |
|---|---|
| $i$ | Initial |

# References


1. Warren, J. E., and Root, P. J. 1963. The behavior of naturally fractured reservoirs. *Society of Petroleum Engineers Journal*. V. 3 (no. 3/September). p. 245.
2. Ancell, K. L., Lambert, S. L., and Johnson, F. S. 1980. Analysis of the coalbed degasification process at a seventeen well pattern in the Warrior Basin of Alabama. SPE/DOE 8971. Pittsburgh, Pennsylvania, May 18–21. In *Proceedings of the SPE Unconventional Gas Recovery Symposium*. p. 391; and King, G. R., Ertekin, T., and Schwerer, F. C. 1986. Numerical simulation of the transient behavior of coal-seam degasification wells. *Society of Petroleum Engineers Formation Evaluation*. V. 1 (April). p. 165.
3. Warren, J. E., and Root, P. J. 1963.
4. Smith, D. M., and Williams, F. L. 1984. Diffusional effects in the recovery of methane from coalbeds. *Society of Petroleum Engineers Journal*. October. p. 529.
5. Kolesar, J. E., and Ertekin, T. 1986. *The Unsteady-State Nature of Sorption and Diffusion Phenomena in the Micropore Structure of Coal*. Paper SPE 15233. Presented at the SPE Unconventional Gas Technology Symposium, Louisville, Kentucky, May 18–21.
6. Remner, D. J., Ertekin, T., Sung, W., and King, G. R. 1986. A parametric study of the effects of coal seam properties on gas drainage efficiency. *Society of Petroleum Engineers Reservoir Engineering*. November. p. 633; Spencer, S. J., Somers, M. L., Pinczewski, W. V., and Doig, I. D. 1987. *Numerical Simulation of Gas Drainage from Coal Seams*. Paper SPE 16857. Presented at the SPE Annual Technical Conference and Exhibition, Dallas, Texas, September 27–30; and Sawyer, W. K., Zuber, M. D., Kuuskraa, V. A., and Horner, D. M. 1987. Using reservoir simulation and field data to define mechanisms controlling coalbed methane production. Paper 8763 in *Proceedings of the 1987 Coalbed Methane Symposium*. Tuscaloosa: University of Alabama.
7. Young, G. C. B., Paul, G. W., McElhiney, J. E., and McBane, R. A. 1992. *A Parametric Analysis of Fruitland Coalbed Methane Reservoir Producibility*. Paper SPE 24903. Presented at the SPE Annual Technical Meeting and Conference, Washington, DC, October 4–7.
8. King, G. R., and Ertekin, T. 1989. A survey of mathematical models related to methane production from coal seams. Part I: Empirical and equilibrium sorption models. Paper 8950 in *Proceedings of the 1989 Coalbed Methane Symposium*. Tuscaloosa: University of Alabama; King, G. R., and Ertekin, T. 1989. A survey of mathematical models related to methane production from coal seams. Part II: Non-equilibrium sorption models. Paper 8951 in *Proceedings of the 1989 Coalbed Methane Symposium*. Tuscaloosa: University of Alabama; and King, G. R., and Ertekin, T. 1995. *State-of-the-Art Modeling for Unconventional Gas Recovery. Part II: Recent Developments (1989–1994)*. Paper SPE 29575. Presented at the SPE Rocky Mountain Regional/Low Permeability Reservoirs Symposium, Denver, Colorado, March 20–22.
9. Collings, R. C. 1982. *The Feasibility of Enhanced Recovery of Methane from Coalbeds through Inert Gas Injection*. Thesis. University of Texas at Austin. December.
10. Sawyer, W. K., Paul, G. W., and Schraufnagel, R. A. 1990. *Development and Application of a 3D Coalbed Simulator*. Paper CIM/SPE 90-119. Presented at the International Technical Meeting hosted by the Petroleum Society of CIM and the Society of Petroleum Engineers, Calgary, Alberta, June 10–13; and Paul, G. W., Sawyer, W. K., and Dean, R. H. 1990. *Validation of 3D Coalbed Simulators*. Paper SPE 20733. Presented at the Annual Technical Conference and Exhibition, New Orleans, Louisiana, September 23–26.
11. Reeves, S., and Pekot, L. 2001. Advanced Reservoir Modeling in Desorption-Controlled Reservoirs. Paper SPE 71090. Presented at the SPE Rocky Mountain Petroleum Technology Conference, Keystone, Colorado, May 21–23.
12. Seidle, J. P., and Arri, L. E. 1990. *Use of Conventional Reservoir Models for Coalbed Methane Simulation*. Paper CIM/SPE 90-118. Presented at the International Technical Meeting hosted by the Petroleum Society of CIM and the Society of Petroleum Engineers, Calgary, Alberta, June 10–13.
13. King, G. R., and Ertekin, T. 1984. *A Comparative Evaluation of Vertical and Horizontal Drainage Wells for the Degasification of Coal Seams*. Paper SPE 13091. Presented at the SPE Annual Technical Conference and Exhibition, Houston, Texas, September 16–19; and Ertekin, T., Sung, W., and Schwerer, F. C. 1986. *Production Performance Analysis of Horizontal Drainage Wells for the Degasification of Coal Seams*. Paper SPE 15453. Presented at the SPE Annual Technical Conference and Exhibition, New Orleans, October 5–8.
14. Spencer, S. J., et al. 1987.
15. Zuber, M. D., Kuuskraa, V. A., and Saywer, W. K. 1989. *Optimizing Well Spacing and Hydraulic Fracture Design for Economic Recovery of Coalbed Methane*. Paper SPE 17726. Presented at the SPE Gas Technology Symposium, Dallas, Texas, June 13–15; and Sung, W., and Ertekin, T. 1987. *An Analysis of Field Development Strategies for Methane Production from Coal Seams*. Paper SPE 16858. Presented at the SPE Annual Technical Conference and Exhibition, Dallas, Texas, September 27–30.
16. Remner, D. J., et al. 1986; and Young, G. C. B., McElhiney, J. E., Paul, G. W., and McBane, R. A. 1991. *An Analysis of Fruitland Coalbed Methane Production, Cedar Hill Field, Northern San Juan Basin*. Paper SPE 22913. Presented at the SPE Annual Technical Conference and Exhibition, Dallas, Texas, October 6–9.
17. Sawyer, W. K., et al. 1987; and Zuber, M. D., Sawyer, W. K., Schraufnagel, R. A., and Kuuskraa, V. A. 1987. *The Use of Simulation and History Matching to Determine Critical Coalbed Methane Reservoir Properties*. Paper SPE/DOE 16420. Presented at the SPE/DOE Low Permeability Reservoirs Symposium, Denver, Colorado, May 18–19.
18. Palmer, I., and Mansoori, J. 1996. *How Permeability Depends on Stress and Pore Pressure in Coalbeds: A New Model*. Paper SPE 36737. Presented at the SPE Annual Technical Conference and Exhibition, Denver, Colorado, October 6–9; and Shi, J. Q., and Durucan, S. 2003. *Changes in Permeability of Coalbeds during Primary Recovery. Part 1: Model Formulation and Analysis*. Paper 0341. Presented at the 2003 International Coalbed Methane Symposium, Tuscaloosa, Alabama, May 5–9; Shi, J. Q., and Durucan, S. 2003. *Changes in Permeability of Coalbeds during Primary Recovery. Part 2: Model Validation and Field Application*.

Paper 0342. Presented at the 2003 International Coalbed Methane Symposium, Tuscaloosa, Alabama, May 5–9; and Cui, X., and Bustin, R. M. 2005. Volumetric strain associated with methane desorption and its impact on coalbed gas production from deep coal seams. *AAPG Bulletin*. V. 89 (no. 9/September). p. 1,181.

19. Remner, D. J., et al. 1986.
20. Young, G. B. C., et al. 1992.
21. Gash, B. W., Volz, R. F., Potter, G., and Corgan, J. M. 1993. The effects of cleat orientation and confining pressure on cleat porosity, permeability and relative permeability in coal. Paper 9321. In *Proceedings of the 1993 International Coalbed Methane Symposium*. Tuscaloosa: University of Alabama.
22. Young, G. C. B., et al. 1992.
23. Kohler, T. E., and Ertekin, T. 1995. *Modeling of Undersaturated Coal Seam Gas Reservoirs*. Paper SPE 29578. Presented at the SPE Rocky Mountain Regional/Low Permeability Reservoirs Symposium, Denver, Colorado, March 20–22.
24. Reid, G. W., Towler, B. F., and Harris, H. G. 1992. *Simulation and Economics of Coalbed Methane Production in the Powder River Basin*. Paper SPE 24360. Presented at the SPE Rocky Mountain Regional Meeting, Casper, Wyoming, May 18–21; and Hower, T. L., Jones, J. E., Goldstein, D. M., and Harbridge, W. 2003. *Development of the Wyodak Coalbed Methane Resource in the Powder River Basin*. Paper SPE 84428. Presented at the SPE Annual Technical Conference and Exhibition, Denver, Colorado, October 5–8.
25. Onsager, P. R., and Cox, D. O. 2000. *Aquifer Controls on Coalbed Methane Development in the Powder River Basin, Wyoming*. Paper SPE 63090. Presented at the SPE Annual Technical Conference and Exhibition, Dallas, Texas, October 1–4.
26. Zuber, M. D., and Olszewski, A. J. 1992. *The Impact of Errors in Measurements of Coalbed Methane Reservoir Properties on Well Production Forecasts*. Paper SPE 24908. Presented at the SPE Annual Technical Conference and Exhibition, Washington, DC, October 4–7; Sawyer, W. K., et al. 1987; and Sawyer, W. K., et al. 1991. History match of a multi-seam coalbed well in the Black Warrior Basin. In *Proceedings of the 1991 Coalbed Methane Symposium*. Tuscaloosa: University of Alabama. p. 403.
27. Purvis, D. C., Strickland, R. F., Alexander, R. A., and Quinn, M. A. 1997. *Coupling Probabilistic Methods and Finite Difference Simulation: Three Case Histories*. Paper SPE 38777. Presented at the Annual Technical Conference and Exhibition, San Antonio, Texas, October 5–8.
28. Jalali, J., and Mohaghegh, S. D. 2004. *A Coalbed Methane Reservoir Simulator Designed and Developed for the Independent Producers*. Paper SPE 91414. Presented at the SPE Eastern Regional Meeting, Charleston, West Virginia, September 15–17.
29. Clarkson, C. R., and McGovern, J. M. 2003. A new tool for unconventional reservoir exploration and development applications. Paper 0336. In *Proceedings of the 2003 International Coalbed Methane Symposium*. Tuscaloosa: University of Alabama; and Clarkson, C. R., and McGovern, J. M. 2005. Optimization of coalbed-methane-reservoir exploration and development strategies through integration of simulation and economics. *Society of Petroleum Engineers Reservoir Evaluation and Engineering*. December. p. 502.
30. Roadifer, R. D., Moore, T. R., Raterman, K. T., Farnan, R. A., and Crabtree, B. J. 2003. *Coalbed Methane Parametric Study: What's Really Important to Production and When?* Paper SPE 84425. Presented at the Annual Technical Conference and Exhibition, Denver, Colorado, October 5–8.
31. Bastian, P. A., Wirth, O. F. R., Wang, L., and Voneiff, G. W. 2005. *Assessment and Development of the Dry Horseshoe Canyon CBM Play in Canada*. Paper SPE 96899. Presented at the SPE Annual Technical Conference and Exhibition, Dallas, Texas, October 9–12.
32. Puri, R. and Yee, D. 1990. *Enhanced Coalbed Methane Recovery*. Paper SPE 20732. Presented at the SPE Annual Technical Conference and Exhibition, New Orleans, Louisiana, September 23–26.
33. Collings, R. C. 1982; Puri, R., and Yee, D. 1990; and Arri, L. E., Yee, D., Morgan, W. D., and Jeansonne, M. W. 1992. *Modeling Coalbed Methane Production with Binary Gas Sorption*. Paper SPE 24363. Presented at the SPE Rocky Mountain Regional Meeting, Casper, Wyoming, May 18–21.
34. Puri, R., Voltz, R., and Duhrkopf, D. 1995. *A Micro-Pilot Approach to Coalbed Methane Reservoir Assessment*. Paper 9556 in *Intergas 95 Proceedings*. Tuscaloosa: University of Alabama.
35. Chaback, J. J., Morgan, D., and Yee, D. 1996. *Sorption Irreversibilities and Mixture Compositional Behavior during Enhanced Coal Bed Methane Recovery Processes*. Paper SPE 35622. Presented at the SPE Gas Technology Conference, Calgary, Alberta, April 28–May 1.
36. Manik, J., Ertekin, T., and Kohler, T. E. 2002. Development and validation of a compositional coalbed simulator. *Journal of Canadian Petroleum Technology*. V. 41 (no. 4/April). p. 39.
37. Reeves, S., and Oudinot, A. 2005. The Allison Unit $CO_2$-ECBM pilot—a reservoir and economic analysis. Paper 0522 in *Proceedings of the 2005 International Coalbed Methane Symposium*; and Reeves, S., and Oudinot, A. 2005. The Tiffany Unit $N_2$-ECBM pilot—a reservoir and economic analysis. Paper 0523 in *Proceedings of the 2005 International Coalbed Methane Symposium*. Tuscaloosa: University of Alabama.
38. Law, D. H-S., van der Meer, L. G. H., and Gunter, W. D. 2002. *Numerical Simulator Comparison Study for Enhanced Coalbed Methane Recovery Processes. Part I: Pure Carbon Dioxide Injection*. Paper SPE 75669. Presented at the SPE Gas Technology Symposium, Calgary, Alberta, April 30–May 2.
39. Smith, D. H., Sams, W. N., Bromhal, G., Jikich, S., and Ertekin, T. 2003. *Simulating Carbon Dioxide Sequestration/ECBM Production in Coal Seams: Effects of Permeability Anisotropies and Other Coal Properties*. Paper SPE 84423. Presented at the SPE Annual Technical Conference and Exhibition, Denver, Colorado, October 5–8; Sams, W. N., Bromhal, G., Jikich, S., Odusote, O., Ertekin, T., and Smith, D. 2003. Using reservoir simulation to evaluate the effect of uncertainties in reservoir properties on the design of a pilot project for sequestration of carbon dioxide and enhanced coalbed methane production. Paper 0353 in

*Proceedings of the International Coalbed Methane Symposium*. Tuscaloosa: University of Alabama; Bromhal, G., Sams, W. N., Jikich, S., Odusote, O., Ertekin, T., and Smith, D. 2003. Reservoir simulation of the effects of anisotropy and ECBM production/$CO_2$ sequestration with horizontal wells. Paper 0352 in *Proceedings of the International Coalbed Methane Symposium*. Tuscaloosa: University of Alabama.

40. van der Meer, B., and Fokker, P. 2003. The injectivity of coalbed $CO_2$ in injection wells. Paper 0319 in *Proceedings of the International Coalbed Methane Symposium*. Tuscaloosa: University of Alabama; and Mavor, M. J., Gunter, W. D., and Robinson, J. R. 2004. *Alberta Multiwell Micro-Pilot Testing for CBM Properties, Enhanced Methane Recovery and $CO_2$ Storage Potential*. Paper SPE 90256. Presented at the Annual Technical Conference and Exhibition, Houston, Texas, September 26–29.
41. Mavor, M. J., Gunter, W. D., and Robinson, J. R. 2004; and Robinson, J., Kadatz, B., Wong, S., Gunter, W., Sangli, F., and Zhiqiang, F. 2004. *ECBM Micro-Pilot Test in the Anthracitic Coals of the Qinshui Basin, China: Field Results & Preliminary Analysis*. Presented at the Third International Workshop of Prospective Roles of $CO_2$ Sequestration in Coal Seams, Hokkaido University, Sapporo, Japan, October 5.
42. Mattax, C. C., and Dalton, R. L., eds. 1990. *Reservoir Simulation*. SPE Monograph. Chapter 8. Richardson, Texas: Society of Petroleum Engineers.
43. Paul, G. W., and Young, G. B. C. 1990. Simulating coalbed methane reservoirs. Chapter 6 in *A Guide to Coalbed Methane Reservoir Engineering*. GRI-94-0397. Chicago: Gas Research Institute.
44. Mattax, C. C., and Dalton, R. L., eds. 1990.
45. Young, G. C. B., et al. 1991.
46. Robinson, J., et al. 2004.
47. Reid, G. W., et al. 1992.
48. Ibid.
49. Ibid.
50. Hower, T. L., Jones, J. E., Goldstein, D. M., and Harbridge, W. 2003. *Development of the Wyodak Coalbed Methane Resource in the Powder River Basin*. Paper SPE 84424. Presented at the SPE Annual Technical Conference and Exhibition, Denver, Colorado, October 5–8.
51. Onsager, P. R., and Cox, D. O. 2000.
52. Reid, G. W., et al. 1992; and Hower, T. L., et al. 2003.
53. Hower, T. L., et al. 2003.
54. Reid, G. W., et al. 1992; and Hower, T. L., et al. 2003.
55. Hower, T. L., et al. 2003.
56. Pratt, T. J., Mavor, J. J., and DeBruyn, R. P. 1999. *Coal Gas Resource and Production Potential of Subbituminous Coal in the Powder River Basin*. Paper SPE 55599. Presented at the SPE Rocky Mountain Regional Meeting, Gillette, Wyoming, May 15–18; Nelson, C. R., Hill, D. R., and Pratt, T. J. 2000. *Properties of Paleocene Fort Union Formation Canyon Seam Coal at the Triton Federal Coalbed Methane Well, Campbell County, Wyoming*. Paper SPE 59786. Presented at the SPE/CERI Gas Technology Symposium, Calgary, Alberta, April 3–5; and Crockett, F., and Meyer, J. 2001. *Update and Revision of Interim Drainage Report on Coalbed Methane Development and Drainage of Federal Land in the South Gillette Area, Campbell and Converse Counties, Wyoming T40–50N, R70–75W*. Casper: Wyoming Bureau of Land Management.
57. Crockett, F., and Meyer, J. 2001.

# Enhanced Coalbed Methane Recovery and $CO_2$ Sequestration

# 12

## Introduction

Gas held in a coal deposit has historically been produced by pressure reduction. In coals with moveable water, this pressure reduction is accomplished by pumping out water. In coals with no moveable water, pressure reduction is accomplished by opening the well to flow, similar to wells draining conventional reservoirs. However, the amount of gas sorbed on the coal matrix depends on its partial pressure in the cleats, not total pressure. Thus native gas can be released from a coal deposit by reduction of partial pressure through injection of a foreign gas. To minimize costs, this injected gas should be cheap and nonsorbing. Production of coal gas by reduction of partial pressure, accomplished via single-well huff-n-puff or multiwell floods, is termed *enhanced coalbed methane (ECBM) recovery*. Possible injectants that have been given serious consideration include nitrogen, $CO_2$, and flue gas. Sequestration of $CO_2$ in coals involves many of the same concerns as ECBM, with the interesting twist that loss of the flood gas to the formation is desirable. For engineering purposes, the naturally occurring gas in a coal deposit is often considered to be only methane. And the simplest form of ECBM is injection of a single-component gas, which leads to a two-component gas mixture in the cleats and binary sorption on the matrix.

## Binary Langmuir Sorption

In a mixture of gases, each contributes to the total pressure in proportion to concentration. The fraction of the total pressure due to a given component is termed the *partial pressure* and is given by

$$p_j = p y_j \tag{12.1}$$

where

$p_j$ = partial pressure of component $j$,
$p$ = total pressure, and
$y_j$ = free gas mole fraction of component $j$.

Total pressure can be expressed as the sum of partial pressures of each component gas

$$p = \sum_{j=1}^{N} p_j$$

where

$N$ = number of component gases.

For a mixture of $N$ component gases, the sorbed gas volume of component $k$ is calculated from

$$V_k = V_{Lk} \frac{\frac{py_k}{p_{Lk}}}{1 + \sum_{j=1}^{N} \frac{py_j}{p_{Lj}}} \tag{12.2}$$

where

$V_k$ = sorbed quantity of component $k$, scf/ton or cm$^3$/g,
$V_{Lk}$ = component $k$ in-situ Langmuir volume constant, scf/ton or cm$^3$/g, and
$p_{Lk}$ = component $k$ Langmuir pressure constant, scf/ton or cm$^3$/g.

Total gas content of the coal is the sum of each individual component gas content

$$V_T = \sum_{j=1}^{N} V_j \tag{12.3}$$

where

$V_T$ = total gas content of the coal, scf/ton or cm$^3$/g.

The sorbed gas mole fraction of component $j$ is given by

$$x_j = \frac{V_j}{V_T} \tag{12.4}$$

where

$x_j$ = sorbed gas mole fraction of component $j$.

### Example 12.1. Coalbed gas contents of a two-component gas mixture

In-situ methane and nitrogen Langmuir isotherm constants for a San Juan Basin coal reported by Puri and Yee are given in the following:[1]

$V_{L1}$ = 797 scf/ton
$p_{L1}$ = 493 psia
$V_{L2}$ = 561 scf/ton
$p_{L2}$ = 1,658 psia

where

subscript *1* = methane, and
subscript *2* = nitrogen.

Both isotherms are plotted in figure 12–1. Assuming a free gas composed of 50% of each gas at 1,000 psia, the sorbed gas volume of each component and total sorbed gas can be calculated employing equations (12.2) and (12.3). Beginning with the methane,

$$V_1 = V_{L1}\frac{\dfrac{py_1}{p_{L1}}}{1+\dfrac{py_1}{p_{L1}}+\dfrac{py_2}{p_{L2}}} = 797\frac{\text{scf}}{\text{ton}}\frac{\dfrac{1{,}000\text{ psia }0.5}{493\text{ psia}}}{1+\dfrac{1{,}000\text{ psia }0.5}{493\text{ psia}}+\dfrac{1{,}000\text{ psia }0.5}{1{,}658\text{ psia}}} = 797\frac{\text{scf}}{\text{ton}}\frac{1.014}{1+1.014+0.302}$$

$$V_1 = 349.0\frac{\text{scf}}{\text{ton}}$$

Similarly for the nitrogen,

$$V_2 = V_{L2}\frac{\dfrac{py_2}{p_{L2}}}{1+\dfrac{py_1}{p_{L1}}+\dfrac{py_2}{p_{L2}}} = 561\frac{\text{scf}}{\text{ton}}\frac{\dfrac{1{,}000\text{ psia }0.5}{1{,}658\text{ psia}}}{1+\dfrac{1{,}000\text{ psia }0.5}{493\text{ psia}}+\dfrac{1{,}000\text{ psia }0.5}{1{,}658\text{ psia}}} = 561\frac{\text{scf}}{\text{ton}}\frac{0.302}{1+1.014+0.302}$$

$$V_2 = 73.1\frac{\text{scf}}{\text{ton}}$$

Total sorbed gas is therefore

$$V_T = \sum_{j=1}^{N} V_j = 349.0 + 73.1\frac{\text{scf}}{\text{ton}}$$

$$V_T = 422.1\frac{\text{scf}}{\text{ton}}$$

Sorbed gas mole fractions determined from equation (12.4) are

$$x_j = \frac{V_j}{V_T}$$

$$x_1 = \frac{349.0\dfrac{\text{scf}}{\text{ton}}}{422.1\dfrac{\text{scf}}{\text{ton}}} = 0.827$$

$$x_2 = \frac{73.0\dfrac{\text{scf}}{\text{ton}}}{422.1\dfrac{\text{scf}}{\text{ton}}} = 0.173$$

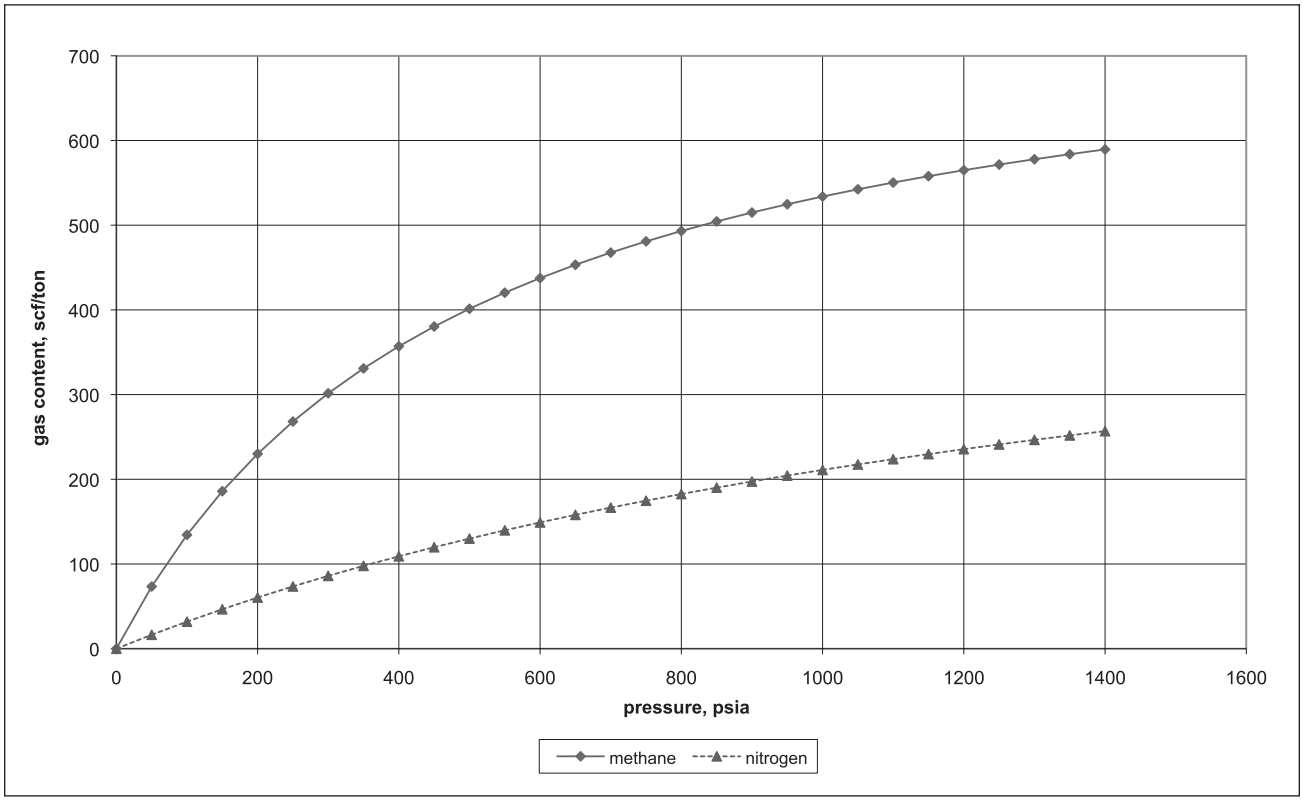



**Fig. 12–1.** Methane and nitrogen sorption isotherms[2]

Note that while the free gas is composed of equal parts of methane and nitrogen, the sorbed gas mixture is approximately five-sixths methane and one-sixth nitrogen. Based upon partial pressures of 500 psia, the single-component isotherms of figure 12–1 predict methane and nitrogen gas contents of 401.3 scf/ton and 130.0 scf ton, which sum to an erroneously high gas content of 531.3 scf/ton. This 20% error in total gas content is due to neglect of competition between the two gases for sorption sites and also results in inaccurate sorbed gas fractions.

## Early History of ECBM and $CO_2$ Sequestration in Coals

Enhanced coalbed methane recovery began in the early 1980s with laboratory studies and numerical simulations. Laboratory experiments using samples of Appalachian Basin coal by Fulton et al. demonstrated sorbed methane could be displaced by introduction of $CO_2$.[3] Methane gas sorbed onto the samples at pressures up to 200 psia was allowed to desorb naturally by venting to the atmosphere, or alternatively, $CO_2$ was sorbed onto the samples following the methane and then the gases were vented to the atmosphere. Average methane recovery factor increased from 43% under natural desorption to 79% with $CO_2$ present. Desorption of methane was accelerated in the presence of $CO_2$. Coal rank, proximate analyses, and sorption isotherms were not reported. This study concluded injection of $CO_2$ into coal seams would promote mine safety and enhance methane recovery from these unconventional reservoirs.

Enhanced coalbed methane recovery was first simulated by Collings.[4] It was assumed that a dry coal particle could be represented as a collection of capillary tubes holding methane by sorption and a constant flood gas concentration at the particle surface. Based on these assumptions, equations were developed describing gas composition as a function of distance from the particle surface and time. The derivation depended heavily on the kinetic theory of gases, and the assumption of a fixed number of sorption sites per unit mass of coal for all gases led to a single Langmuir volume constant for all gases. Coupling these equations with one for steady-state flow between injection and production wells allowed calculation of flood front shape and position as functions

of distance along the flow path over time. This study was limited to two-component gas mixtures (methane and $CO_2$ or nitrogen) and 1-D ECBM simulations. However, it accurately described flood gas composition over space and time and provided insights into expected flood behaviors based on the relative sorption strengths of the flood gas to methane. Gases such as nitrogen that sorb to coals less strongly than does methane exhibit soft, rounded flood fronts that travel rapidly through a coal deposit with minimal loss of flood gas to the coal. Gases such as $CO_2$ that sorb more strongly than methane have steep, slow-moving flood fronts and lose substantial mass to the coal. This original work catalyzed development of commercial ECBM simulators and pointed out the need for measurement of single-component sorption isotherms on the same coal sample.

A laboratory investigation of $CO_2$ injection into bituminous coal samples from the Pittsburgh coal seam by Reznik et al. employed 3.5 in. diameter core samples dried at 158°F (70°C) under vacuum for one to two months.[5] Although the samples were no longer at native conditions, this study demonstrated effective displacement of methane by $CO_2$ and mixtures of nitrogen and $CO_2$. Injection of 9 scf of $CO_2$ resulted in displacement of roughly 1 scf of methane. Further interpretation of this study is difficult, as isotherms or proximate analyses were not reported and the cycle times were significantly less than desorption times.

Laboratory experiments and numerical simulation of nitrogen flooding of a San Juan Basin coal were investigated by Puri and Yee.[6] These early studies demonstrated that coal gas production was indeed increased by reduction of methane partial pressure, while retarding or even stabilizing reservoir pressure decline. Flooding of a coal with an inert gas was shown to accelerate gas production and increase recovery beyond that of simple pressure depletion. The rapid ECBM evolution that followed these simple beginnings involved laboratory experiments, numerical simulations, and field tests to address both technical and economic issues.

Harpalani and Schraufnagel studied the effect of mechanical stress and desorption-induced matrix shrinkage on permeability of coals from the Piceance and Warrior basins.[7] Matrix shrinkage was found to be proportional to gas content, not pressure. Desorption of methane and $CO^2$ increased permeability by factors of 6 and 30, respectively, demonstrating in these specific experiments that permeability increase due to matrix shrinkage dominated permeability loss due to increased stress.

Amoco announced a field test of this process using nitrogen injection in the Tiffany area of La Plata County, Colorado, in the northern San Juan Basin.[8] Tiffany wells are completed in four seams of Cretaceous medium-volatile bituminous coal, and the field had been on continuous production since 1983. The pilot was comprised of 34 producers and 12 injectors on 160 ac spacing, with nitrogen sourced from a gas processing plant.

Simulation of coalbed methane recovery by nitrogen injection in a homogeneous reservoir by Arri et al. demonstrated a variety of simulators correctly described binary gas sorption physics.[9] Laboratory measurement of single-component methane and $CO_2$ as well as mixtures of these two gases by Greaves et al. demonstrated compositional variations during depletion and, by inference, the effect on ECBM response.[10]

Economics of nitrogen flooding of a single, heterogeneous coal seam were explored numerically by Stevenson et al.[11] Coal seam heterogeneity, described with a five-layer model, was found to have a minor influence on primary production and a major influence on ECBM. Presence of a high-permeability layer reduced the peak gas rate by approximately 25% but did not significantly affect timing of the peak gas rate. Time to nitrogen breakthrough was not addressed in this study. However, the nitrogen fraction in the produced gas stream increased more rapidly as permeability heterogeneity, that is, as permeability in one layer, increased. Methane recovery decreased with increasing permeability heterogeneity. Raising the permeability contrast from 1:1 to 100:1 reduced 30 year methane recovery from 95% to 38%. Economic impact of various permeability contrasts on nitrogen ECBM recovery was addressed by considering time to payout, internal rate of return (IRR), and discounted return on investment (DROI). While permeability heterogeneity minimally impacted the first parameter, it caused a strong deterioration of the second two.

A test to assess the viability of enhanced coalbed methane recovery in coal deposits (a micropilot test) was developed by Puri et al. and applied to a San Juan Basin coal.[12] As discussed in chapter 7, this test is comprised of three stages, each nominally three weeks in duration. It begins with injection of a flood gas into the target coal, followed by a shut-in period to allow injected gas to soak into the coal matrix, and then is completed with a production flow test. Frequent measurement of wellhead and downhole pressures and gas compositions throughout all three phases of a micropilot test permits use of pressure transient methods to determine reservoir properties and wellbore condition. It also allows calibration of numerical simulators for test interpretation.

Burlington Resources commenced field testing $CO_2$ ECBM in the Allison Unit, located in the San Juan Basin, in 1996.[13] After five years of continuous production from the field, the pilot was initiated with 16 producers, four injectors, and one pressure observation well on 160 ac spacing. $CO_2$, supplied from a pipeline running through the basin, was to be injected in bituminous Fruitland coals.

Chaback et al. measured sorption of binary methane-nitrogen mixtures and ternary oxygen-$CO_2$-nitrogen mixtures on medium-volatile Fruitland coal.[14] They demonstrated that their multicomponent sorption data, as well as that of Greaves et al., could be described using the extended Langmuir equation populated with single-component isotherm constants.[15] Sorption of nitrogen, methane, and $CO_2$ on bituminous coals was further investigated by Chaback et al.[16] This study concluded that sorption behavior of multicomponent gases could be described with the extended Langmuir equation using single-component sorption constants. The study also concluded that although the extended Langmuir formulation is not thermodynamically consistent, it is adequate for reservoir engineering purposes.

Coal seam response to gas injection for ECBM recovery is similar in many ways to conventional oil reservoir response to water injection for secondary recovery. Reservoir heterogeneity, which minimally impacts primary production in both reservoirs, strongly influences secondary recovery and degrades performance of any secondary flood. And similar to secondary recovery in conventional reservoirs, simulation of ECBM recovery and the associated economics require a more detailed reservoir description. Use of pressure falloff tests (PFOTs) to determine reservoir properties and to assess ECBM injection well condition was reported by Seidle and McAnear.[17] Pressure falloff tests of ECBM injectors similar to those of waterflood injectors were found to provide reliable estimates of permeability to gas, reservoir pressure, and wellbore condition. PFOT results were used to construct injectivity indices for estimation of nitrogen compression requirements. Seidle et al. combined spinner surveys, Hall plots, and pressure transient test analyses from two nitrogen injectors with reservoir simulation to investigate nitrogen injectivity, conformance of injected gas, and reservoir sweep efficiency.[18]

ECBM recovery from $CO_2$ injection in the Allison Unit of the San Juan Basin, screening criteria for $CO_2$ ECBM and sequestration project, and the implications for worldwide $CO_2$ sequestration were discussed by Stevens et al.[19] Analysis of the Allison $CO_2$ flood demonstrated increased methane production rates and recovery while sequestering substantial volumes of $CO_2$. Feasibility of $CO_2$ ECBM and sequestration in selected coals in Australia, Canada, China, India, and the United States were discussed on the basis of the following six reservoir screening criteria:

- **Homogeneous reservoir.** The target coal seam should be laterally continuous and vertically isolated from surrounding strata to insure $CO_2$ containment in the coal and efficient lateral sweep.
- **Simple structure.** Minimal faulting, folding, and structural complexity will minimize reservoir compartmentalization and $CO_2$ diversion.
- **Adequate permeability.** Absolute coal permeability on the order of 1 to 3 md was recommended for effective ECBM. *Note:* Sorption of $CO_2$ on coal swells the coal matrix and thus decreases permeability. In order to maintain injectivity during ECBM operations, the above permeabilities should be regarded as minimums.[20]
- **Optimal depth window.** As shallow coals have low pressure and consequently low gas contents, while deeper coals often lack permeability, each basin was speculated to have an optimal depth for $CO_2$ injection.
- **Coal geometry.** A coal deposit with a few thick seams over a short stratigraphic interval is preferable to one with multiple thin seams over a large interval.
- **Gas-saturated conditions.** From an economic viewpoint, ECBM of saturated coals is preferable to undersaturated coals due to earlier gas production and a larger in-place gas resource.

$CO_2$ ECBM and sequestration in Belgian and German coals was investigated by Wolf et al. via laboratory experiments and simulation.[21] These Westphalian-age coals were characterized with proximate, ultimate, and maceral analyses, methane and $CO_2$ sorption isotherms, and stress dependence of permeability and porosity. Laboratory experiments utilizing methane-saturated coal cores subjected to $CO_2$ injection were used to tune a

reservoir simulator. This simulator was then employed for field-scale predictions of $CO_2$ ECBM and sequestration in the Belgian coal. Important conclusions from this study included the observation of almost immediate $CO_2$ breakthrough in both core floods and a recommended well spacing of approximately 40 ac for Westphalian coals with a permeability of 1 md.

Project screening, design, and economics for $CO_2$ ECBM in San Juan Basin coals were studied by Stevens et al.[22] Simulation studies indicated use of this technology could slow the decline of basinwide coal gas production and increase coal gas recovery from the San Juan Basin by 20% over the course of 20 years. With a $CO_2$ supply cost estimated to be \$0.25/mcf to \$0.35/mcf, this study concluded many, if not most, of the CBM projects in the San Juan were candidates for $CO_2$ ECBM.

As part of a study of the influence of pore structure on coal transport properties, Clarkson and Bustin measured rates of methane and $CO_2$ sorption on Cretaceous coal samples from the Gates Formation in Canada.[23] Uptake of these gases on dry and wet coal was found to be best described with a model that accounted for nonlinear sorption, a bimodal pore distribution, and time-varying gas pressure boundary conditions. In general, $CO_2$ sorbed faster than methane, and both gases sorbed faster on dry coals than on wet. As the experimental data indicated sorption equilibrium required a maximum of 12 hr, situations where sorption kinetics are important for reservoir engineering purposes include well tests to evaluate fracture parameters, micropilot tests, and some field operations. In general, however, sorption kinetics can often be neglected in ECBM floods or $CO_2$ sequestration.

A study by Wong et al. pointed out that ECBM from $CO_2$ injection was generally not economic, but coal deposits could be employed to sequester $CO_2$ to mitigate greenhouse gas emissions.[24] Economic barriers to ECBM implementation would be reduced by sequestering $CO_2$ in the target coal. Producers of this gas that had previously been vented to the atmosphere would now presumably pay a disposal fee to be rid of it, eliminating one of the largest costs of an ECBM flood. The injected gas is either pure $CO_2$ or flue gas, which is 3% of a gas turbine exhaust stream or 13% of that from a coal-fired power plant. Noting that the $CO_2$ supply cost in the San Juan Basin was \$0.65/mcf, capture cost of $CO_2$ from industrial sources was estimated to cost between \$0.50/mcf and \$2.89/mcf. Economics of $CO_2$ removal from an electric power plant flue gas stream with an amine treatment plant were combined with simulated methane and $CO_2$ profiles for an Alberta coal gas field to estimate breakeven $CO_2$ sequestration costs. Assuming a $CO_2$ supply cost of \$2.89/mcf, breakeven economics would be obtained with a gas price of \$2.90/mcf. This study noted that $CO_2$ sorption is rank dependent and that the ratio of methane released to $CO_2$ sequestered is roughly 1:10 in subbituminous coals and 1:2 in bituminous coals.

Several additional studies sought to evaluate the $CO_2$ sequestration potential of various coals. These include the demonstration program for ECBM and $CO_2$ sequestration in Australian coals as detailed by Wong et al., the preliminary assessments of Warrior Basin coals by Pashin et al., and four Dutch coalfields by van Bergen et al.[25]

Analytical solutions of free and sorbed gas compositions during ECBM flooding or $CO_2$ sequestration were developed by Zhu et al.[26] This method assumed infinitely fast sorption kinetics, no moveable water, and one-dimensional flow between injector and producer. The solution paths in composition space were continuous waves or shocks. Plots of molar compositions as functions of dimensionless wave velocity were calculated for selected $CO_2$ and $N_2$ flood gas compositions. These plots indicated a continuous wave solution for nitrogen floods, while a shock solution occurred for $CO_2$ floods. With the only required inputs being distance between injector and producer, flood gas injection rate, and Langmuir isotherms, the strength and weakness of this method is minimal reservoir characteristics.

During this same time period, interpretation of the two field projects was in progress. As noted above, the BP Tiffany project in the northern San Juan Basin tested nitrogen ECBM response beginning in 1998. Pilot response was rapid, with gas production increasing by a factor of five during the first injection cycle, but nitrogen cut in the produced gas stream was not reported.[27] Due to surface equipment limitations, nitrogen was injected only during the cooler months, with the pilot being operated in blowdown mode over the hotter months. After four years of intermittent operation, nitrogen injection was suspended in early 2002 to evaluate pilot performance. Numerical simulation studies by Liang et al. and Reeves and Oudinot reported difficulties in matching nitrogen breakthrough times, produced gas compositions, and bottomhole pressures.[28]

The second ECBM field trial, also in the northern San Juan Basin, was conducted by Burlington Resources in the Allison Unit. Originally put on production in 1990, the unit had been on production for about five years

when $CO_2$ injection was initiated in 1996.[29] The pilot commenced with $CO_2$ injection into three Fruitland coal seams, while the producers were shut in for six months to permit longer residence or "soak" time for the $CO_2$. Interpretation of pilot response was compounded by this shut-in period, during which gas saturations changed due to water influx, and gas compositions changed due to $CO_2$ injection, many producing wells were recompleted or recavitated, and surface facilities debottlenecked. In August 2001, the pilot was shut in.

Reservoir behavior during enhanced coalbed methane recovery is more complicated than primary depletion of a coal deposit. Three additional elements include the following:

1. Absolute permeabilities vary due to the interplay of stresses and matrix shrinkage, especially when $CO_2$ is present.
2. Sorption kinetics influence short time events, such as early-time data from well tests.
3. Rapid breakthrough of injected gas and subsequent channeling over the course of the flood require a detailed geologic reservoir description.

All three of these factors were considered in a simulation study of the Burlington Allison $CO_2$ pilot by Reeves et al., which found them very difficult to properly model.[30]

A simulation study to understand general $CO_2$ ECBM behavior and subsequent economics was reported by Reeves and Oudinot.[31] Assuming $CO_2$ supply cost of $0.30/mcf and treating cost of $0.25/mcf, breakeven gas price was found to be $2.57/mcf. This study identified a $CO_2$ volume for a specific project, based upon reservoir properties and economic constraints, to maximize the net present value at a discount factor of 10% (PV10). $CO_2$ injection in excess of this volume resulted in additional sequestration but minimal additional methane recovery. Differences in simulated and actual bottomhole flowing pressures were ascribed to the primitive $CO_2$ swelling-permeability relation in the model. Actual $CO_2$ breakthrough was more rapid than predicted, and produced gas compositions were matched with varying degrees of success.

$CO_2$ ECBM and storage in the Medicine River (Mannville) coals of Alberta was evaluated by Mavor et al.[32] A series of three tests was developed to reduce economic risk associated with $CO_2$ ECBM and sequestration and to provide engineering details to design a $CO_2$ flood. Beginning with a single-well micropilot test followed by a five-well pilot and finally a nine-well pattern test, execution of all three tests was estimated to require seven to nine years. Tests of four models for ECBM simulation showed all models had difficulty in predicting produced gas compositions after $CO_2$ injection and all tended to overestimate displacement efficiency. With no simulation details provided, these limitations could be due to erroneous sorption physics or limited geological descriptions of the coal seams. Although the tested ECBM simulation models were incomplete, they were sufficient to demonstrate that the process was marginally economic. At the time of this writing, neither the Tiffany nitrogen flood nor the Allison $CO_2$ flood has been extended beyond the commercial demonstration stage. Operators in the basin are pursuing infill drilling rather than ECBM to achieve higher coal gas recovery from the Fruitland coal.

Pashin and MacIntyre clarified the $CO_2$ sequestration potential of Warrior Basin coals by comparing coal seam temperatures and pressures against the $CO_2$ critical point of 88°F (31°C) and 1,074 psia (7.41 MPaa).[33] Nearly all coals in this basin are above the critical temperature, but reservoir pressures in these compartmentalized reservoirs vary from normally pressured to deeply underpressured. Normally pressured coals are typically encountered in recharge areas along the basin margin, while deeply underpressured coals are found close to longwall mining operations and in compartments far from both mining activities and basin recharge areas. Assuming a pressure gradient of 0.433 psi/ft, the $CO_2$ critical pressure of 1,074 psia is reached at a depth of 2,446 ft. This study noted that supercritical $CO_2$ is employed as an organic solvent, and its reactivity and mobility in coal reservoirs above critical conditions should be investigated to better understand $CO_2$ sequestration potential in this and other coal basins.

The RECOPOL $CO_2$ sequestration demonstration project in the Carboniferous coals of the Upper Silesian Basin of Poland was described by van Bergen et al.[34] This project targeted six seams of high-volatile bituminous coals at depths of 900–1,250 m. Coal thicknesses ranged from 1.3 to 3.3 m. The project proposed drilling of an injection well midway between two existing coal wells. With injector-producer separations of 200 m, breakthrough of $CO_2$ was anticipated over the 1.5 years of proposed continuous $CO_2$ injection. Monitoring of $CO_2$ was to be accomplished by gas sampling at the surface and at the face of a nearby abandoned mine and

by time-lapse seismic. Gas samples would provide not only $CO_2$ concentrations but also isotope signatures in order to distinguish injected, industrially sourced $CO_2$ from naturally occurring $CO_2$. Seismic methods for $CO_2$ monitoring evaluated using synthetic data sets included high-resolution surface acquisition, vertical seismic profiling, and crosswell seismology. Crosswell seismology was found to provide the highest resolution and repeatability but lacked lateral resolution and was the most expensive.

Horizontal wells offer an operational strategy to mitigate the loss of coal permeability due to $CO_2$ injection. A simulation study by Bromhal et al. used generic coal properties and the Palmer-Mansoori model to determine sensitivity of cumulative methane production and total sequestered $CO_2$ to selected injector lengths and pressures.[35] The higher methane recoveries predicted for shorter injector lengths and lower injection pressures were explained by the longer breakthrough times and better sweep efficiencies seen in these scenarios. Maximum $CO_2$ sequestration occurred for injector lengths of 400 to 800 ft in a square drainage area 3,000 ft on a side (lateral lengths approximately 0.1 to 0.2 pattern length). Maximum sequestration was found to depend on coal swelling coefficients, mechanical properties, and sorption times.

Mavor et al. characterized the Medicine River (Mannville) coals of Alberta with micropilots, extended injections, and production testing in two wells using $CO_2$, nitrogen, and mixture of the two gases.[36] This work demonstrated the suitability of low-permeability coals (less than 1 md) for $CO_2$ sequestration and the highly variable nature of coal permeability. Absolute coal permeability was reduced by $CO_2$ swelling of the coal matrix but was increased during injection periods, when ballooning of the cleats dominated matrix swelling. Postinjection well tests yielded a skin factor more negative than preinjection tests, which was interpreted as extension of the induced fracture along planes of weakness or opening of preexisting fractures during injection. This study defined *hydrocarbon displacement efficiency* as the fraction of hydrocarbons removed from an area contacted by an injected fluid. The *hydrocarbon displacement ratio* was defined as the ratio of displaced hydrocarbon volume to injected fluid volume.

A $CO_2$ micropilot in anthracitic coals of the Qinshui Basin of China began with a 56 day production test, continued with a 13 day injection period, followed by a 42 day soak, and concluded with a 30 day production test.[37] Pressure buildups at the end of the two production tests and injectivity calculations indicated permeability of the coal decreased during $CO_2$ injection but rebounded during the final production test to 8 md, two-thirds the initial permeability of 12 md.

Inability to simulate gas composition and permeability changes seen in various micropilot tests was due in part to the assumption of infinitely fast sorption kinetics and the resultant matrix swelling or shrinkage. A simple conceptual model to overcome this limitation assumes sorption kinetics depend on pure gas species and coal properties, neglecting interference between components of the gas mixture and any irreversibility in sorption strains. This greatly simplifies experimental work, requiring only swelling or shrinkage measurements due to pure gases. Limited sorption kinetics data are currently available in the literature.

Rates of $CO_2$ and methane sorption on pulverized samples of Pennsylvanian coal from the Silesian Basin of Poland at 45°C and at pressures up to 4 MPaa were measured by Siemons et al.[38] Conceptualizing coal matrix as small crystalline aromatics embedded in large amorphous aliphatics, a two-step theoretical model was used to describe sorption kinetics. Beyond a particle size of about 2 mm, sorption times were independent of particle size. Maximum $CO_2$ sorption time on wet coal was roughly 8 hr, an order of magnitude faster than the 3.5 day sorption time of methane on the same coal.

Additional sorption kinetics experiments on pulverized samples of high-volatile bituminous coal from the Upper Silesian Basin of Poland were reported by Busch et al.[39] Sorption of both gases could be approximated with first order rate functions and more accurately described as the sum of two first order rate functions. Methane equilibration time on moist coal was roughly 45 hr, while that of $CO_2$ was about 8 hr, approximately six times faster than methane. For reservoir engineering purposes, sorption kinetics of both these gases can be described with first order rate equations and the appropriate sorption time constant. Extrapolation of these results to field-scale ECBM and sequestration proved problematic.

$H_2S$ sorption on samples of four coals from the WCSB and the associated matrix strains were measured by Chikatamarla et al.[40] Swelling/shrinkage coefficients due to pressure and sorption were reported for each gas and each coal. These coefficients were employed in porosity-pressure and permeability-pressure relations similar to

the Palmer-Mansoori model.[41] Use of these relations in simulations of acid gas sequestrations indicated injection of pure $H_2S$ would severely swell the matrix, reducing cleat permeability to values so low that sequestration of significant volumes would be impossible. Although the expressions did not include sorption kinetics, this study noted that experiment equilibration times at each pressure step ranged from 6 to 10 days. The implication is that sorption kinetics are important for understanding micropilot response and short-term well perturbations but not long-term fieldwide performance.

Siriwardane et al. modeled the effect of matrix deformation on permeability assuming volumetric strain of coal matrix is linearly related to coalbed gas content, calculating the subsequent reduction in porosity, and assuming permeability was related to the cube of porosity.[42] The proportionality constant between volumetric strain and gas content depends on the sorbing gas. Reservoir properties of the Allison Unit in the San Juan Basin reported by Reeves et al. and Reeves and Oudinot were combined with matrix swelling constants in simulations of selected Allison wells.[43] Assuming swelling constants of $3(10)^{-5}$ ton/scf and $1(10)^{-4}$ ton/scf for methane and $CO_2$, respectively, gas rates were specified in the simulation, and the resulting bottomhole pressures compared favorably with those from simulations by Reeves et al.[44]

## Linear Flooding of a Coal Deposit

Flooding of a coal deposit with nitrogen or $CO_2$ to increase coal gas recovery or injecting $CO_2$ into a coal seam to sequester it both involve two-phase gas and water flow in a naturally fractured reservoir. The permeability depends on the pressure and gas content of the coal. Composition of both the free and sorbed gas mixtures vary with space and time. The physics of ECBM floods and $CO_2$ sequestration are considerably more complicated than those of primary coal gas depletion. Accurate description of sorbed and free gas compositions and coal porosity and permeability changes during these processes is difficult and typically requires computer simulation. Injected gas will preferentially channel through the more permeable layers and natural fractures rather than flow smoothly, radially outward from an injection well. As a result, accurate simulation of flooding and sequestration in a coal requires detailed geological reservoir descriptions and a host of coal rock properties and sorption parameters. Nevertheless, insights into inert gas flooding and $CO_2$ sequestration can be obtained from a simple, semianalytical approach similar to that describing waterflooding of a conventional oil reservoir.[45] While not as accurate as computer models, such an approach yields "sense checks" on simulation results, rapid insight into flooding and sequestration behavior, and bounding rates and volumes for a given project.

Early response of a production well to injection of nitrogen or $CO_2$ in an adjacent well will be controlled by the most permeable path connecting the two wells. This path will likely be one or more natural fractures, either cleats formed during coalification or joints, faults, or tectonic fractures superimposed after coalification. Equations for free and sorbed gas compositions as a function of position in the channel and time can be developed by considering first convection in the channel and then mass balance between free and sorbed gases.

Assumptions for this problem include two wells completed in a single, homogenous coal seam of constant thickness and permeability. The cleats have no moveable water, and the matrix holds only pure methane. A pure gas, either nitrogen or $CO_2$, is injected into one well at a constant bottomhole pressure equal to initial reservoir pressure, while gas is produced from the second well, also operated at a constant bottomhole pressure. Both native and injected gases behave as ideal gases. Release of methane from the matrix and uptake of the injected gas onto the matrix both occur infinitely fast. The resulting gas mixture follows a linear path between the wells. Although free and sorbed gas compositions change with time, pressure and flow rate are assumed to be in steady state, with flow of the free gas described by the steady-state form of Darcy's law for compressible fluids. Combining this equation with the two-component Langmuir isotherm equation, equation (12.2), allows estimation of gas composition as a function of distance and time.

The linear, differential form of Darcy's law can be written as[46]

$$v = -\frac{k_g}{\mu_g}\frac{dp}{dx} \tag{12.5}$$

where

$v$ = gas velocity,
$k_g$ = gas permeability,
$\mu_g$ = gas viscosity,
$p$ = pressure, and
$x$ = distance.

Gas velocity can also be expressed as

$$v = \frac{q_g B_g}{A_c} \tag{12.6}$$

where

$q_g$ = gas flow rate,
$B_g$ = gas formation volume factor, and
$A_c$ = cross-sectional flow area.

Assuming an ideal gas, the formation volume factor is

$$B_g = \frac{p_{sc} T}{p T_{sc}} \tag{12.7}$$

where

$T_{sc}$ = standard temperature, °R,
$p_{sc}$ = standard pressure, psia, and
$T$ = reservoir temperature, °R.

Substituting (12.7) into (12.6), and then the resulting equation into (12.5), yields

$$\frac{q_g p_{sc} T}{A_c p T_{sc}} = -\frac{k_g}{\mu_g}\frac{dp}{dx}$$

Assuming a constant gas permeability and viscosity allows separation of variables and integration,

$$\frac{q_g p_{sc} T \mu_g}{A_c T_{sc} k_g}\int_0^x dx = -\int_{pinj}^{p} p dp$$

where

$p_{inj}$ = injection pressure.

Note that distance is measured from the injector.

$$\frac{q_g p_{sc} T \mu_g}{A_c T_{sc} k_g} x = -\frac{(p^2 - p_{inj}^2)}{2}$$

Solving for pressure as a function of distance,

$$p = \left[p_{inj}^2 - \frac{2 q_g p_{sc} T \mu_g}{A_c T_{sc} k_g} x\right]^{1/2}$$

Casting this result in field units, the pressure at any distance is given by

$$p = \left[ p_{inj}^2 - 8936.71 \frac{q_g T \mu_g}{A_c k_g} x \right]^{1/2} \tag{12.8}$$

where

$p$ = pressure, psia,
$p_{inj}$ = injection pressure, psia,
$q_g$ = gas flow rate, mcfd,
$T$ = reservoir temperature, °R,
$\mu_g$ = gas viscosity, cp,
$A_c$ = cross-sectional area, ft$^2$,
$k_g$ = gas permeability, md, and
$x$ = distance, ft.

Due to the assumption of steady-state flow, equation (12.8) gives the pressure at any distance for all time and all gas compositions. Assuming the producing well is located a distance $L$ from the injector and is operated at a constant bottomhole pressure, the gas flow rate is

$$q_g = 1.1190(10)^{-4} \frac{A_c k_g (p_{inj}^2 - p_{wf}^2)}{T \mu_g L} \tag{12.9}$$

where

$p_{wf}$ = producer bottomhole flowing pressure, psia, and
$L$ = distance between injector and producer, ft.

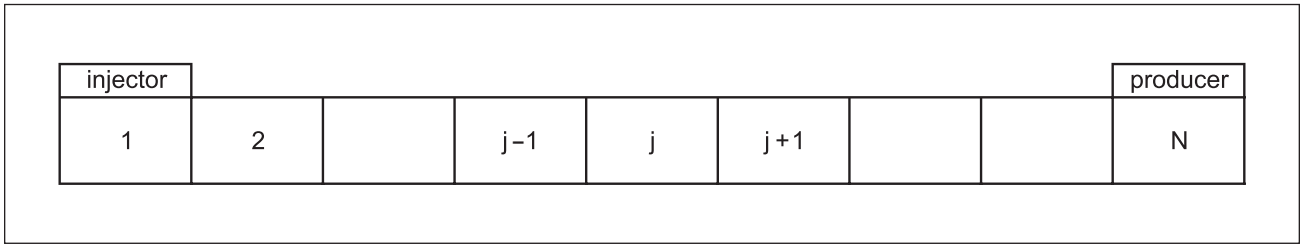



**Fig. 12–2.** Discretization of linear flow path between injector and producer

Discretizing the linear flow path between injector and producer into $N$ blocks as shown in figure 12–2, the moles of flood gas in block $j$ can be determined from the ideal gas law and the flood gas mole fraction

$$y_{2,j} p_j A_c \Delta L \phi = n_{2,j} RT$$

where

$y_{2,j}$ = flood gas mole fraction in free gas mixture in block $j$,
$p_j$ = pressure in block $j$,
$\Delta L$ = block width,
$\phi$ = porosity,
$n_{2,j}$ = moles of flood gas in free gas mixture in block $j$, and
$R$ = universal gas constant.

Solving for the number of moles of flood gas in the free gas mixture,

$$n_{2,j} = \frac{y_{2,j} p_j A_c \Delta L \phi}{RT} \tag{12.10}$$

The number of moles of flood gas convected into this block from the adjacent upstream block at a discrete time step can be determined from the ideal gas assumption

$$y_{2,j-1} p_{j-1} q_g B_g \Delta t = n_{2,in} RT$$

or

$$n_{2,in} = \frac{y_{2,j-1} p_{j-1} q_g B_{g,j-1} \Delta t}{RT} \tag{12.11}$$

where

$n_{2,in}$ = moles of flood gas convected into block $j$,
$y_{2,j-1}$ = flood gas mole fraction in free gas mixture in block $j$–1,
$B_{g,j-1}$ = flood gas formation volume factor in block $j$–1,
$p_{j-1}$ = pressure in block $j$–1,
$\Delta t$ = time step.

Similarly, the number of moles convected out of block $j$ during this time step can be determined from

$$y_{2,j} p_j q_g B_{g,k} \Delta t = n_{2,out} RT$$

Solving for the number of flood gas moles convected out

$$n_{2,out} = \frac{y_{2,j} p_j q_g B_{g,j} \Delta t}{RT} \tag{12.12}$$

Neglecting sorption of the flood gas for a moment, the moles of flood gas in the free gas mixture after the time step are given by an equation similar to (12.10)

$$n_{2,new} = \frac{y_{2,j,new} p_j A_c \Delta L \phi}{RT} \tag{12.13}$$

where

$n_{2,new}$ = moles of flood gas in block $j$ after a time step, and
$y_{2,new}$ = flood gas mole fraction in free gas mixture in block $j$ after a time step.

As sorption is temporarily neglected, the moles of flood gas in the free gas mixture of the block after a time step is the sum of the original moles plus the moles of flood gas convected in less those convected out

$$n_{2,new} = n_{2,j} + n_{2,in} - n_{2,out}$$

Substituting equations (12.10) through (12.13) into the above equation yields

$$\frac{y_{2,j,new} p_j A_c \Delta L \phi}{RT} = \frac{y_{2,j} p_j A_c \Delta L \phi}{RT} + \frac{y_{2,j-1} p_{j-1} q_g B_{g,j-1} \Delta t}{RT} - \frac{y_{2,j} p_j q_g B_{g,k} \Delta t}{RT}$$

Solving for the new flood gas mole fraction in the free gas mixture in this block,

$$y_{2,j,new} = y_{2,j} + y_{2,j-1}\frac{p_{j-1}}{p_j}\frac{q_g B_{g,j-1}\Delta t}{A_c \Delta L \phi} - y_{2,j}\frac{q_g B_{g,j}\Delta t}{A_c \Delta L \phi}$$

The normalized volume can be defined as the ratio of the volume of gas produced in the time step to the block pore volume,

$$V_{norm} = \frac{q_g \Delta t}{A_c \Delta L \phi}$$

where

$V_{norm}$ = normalized volume.

The mole fraction of flood gas in the free gas mixture can now be written

$$y_{2,j,new} = y_{2,j} + y_{2,j-1}\frac{p_{j-1}}{p_j}V_{norm}B_{g,j-1} - y_{2,j}V_{norm}B_{g,j} \tag{12.14}$$

Including sorption of flood gas in the block, mass conservation of the flood gas yields the net moles of flood gas convected into the block plus the moles of flood gas sorbed on the coal at the beginning of the time step equal the sum of the new free and sorbed flood gas moles. In field units, flood gas conservation in a block can be described on a molar basis as

$$\theta_j = \frac{379.4 A_c \Delta L \phi p_j y_{2,j,new}}{RT} + \frac{A_c \Delta L \rho_B V_{L2}}{32.037}\frac{\dfrac{y_{2,j,new}p_j}{p_{L2}}}{1 + \dfrac{(1-y_{2,j,new})p_j}{p_{L1}} + \dfrac{y_{2,j,new}p_j}{p_{L2}}} \tag{12.15}$$

where

$\theta_j$ = sum of convected and sorbed flood gas moles, and

$\rho_B$ = bulk coal density, g/cm$^3$.

Solving for the new flood gas mole fraction, $y_{2,j,new}$

$$0 = y_{2,j,new}^2 + B_j y_{2,j,new} - C_j \tag{12.16}$$

where the quadratic coefficients are defined as

$$B_j = \frac{1 + \dfrac{p_j}{p_{L1}} + \dfrac{RT\rho_B V_{L2}}{379.4(32.037)\phi p_{L2}} - \dfrac{RT\theta_j}{379.4\phi}\left[\dfrac{1}{p_{L2}} - \dfrac{1}{p_{L1}}\right]}{\left[\dfrac{p_j}{p_{L2}} - \dfrac{p_j}{p_{L1}}\right]} \tag{12.17}$$

and

$$C_j = \frac{RT\theta_j}{379.4 p_j \varphi}\frac{1 + \dfrac{p_j}{p_{L1}}}{\left[\dfrac{p_j}{p_{L2}} - \dfrac{p_j}{p_{L1}}\right]} \tag{12.18}$$

Mole fraction of the flood gas in the free gas mixture can be calculated as a function of space and time with the above equations. Assuming bottomhole pressures in the injector and producer are constant and a cross-sectional flow area of 1 $ft^2$, the gas flow rate and pseudosteady-state pressure distribution between the two wells can be calculated with equations (12.9) and (12.8), respectively. The boundary condition at the injector is a flood gas mole fraction of 1.0 in the free gas phase. Mole fractions of the flood gas due to convection after a time step are calculated with equation (12.14). Mole fractions of the flood gas due to convection and sorption after a time step are calculated sequentially along the flow path with equations (12.16), (12.17), and (12.18), with the physically unrealistic quadratic root being neglected. After discussion of flood gas load factor, methane recovery factor, and sweep efficiency, this method is illustrated in three examples below.

Sorbed volumes of methane and the flood gas in any gridblock can be calculated with the free gas composition and the multicomponent Langmuir isotherm, equation (12.2). The *flood gas load factor*, defined as the amount of flood gas sorbed along the flow path compared to the maximum flood gas sorption, can be written as

$$f = \frac{\sum_{k=1}^{N} V_{L2} \dfrac{\dfrac{y_{2,k} p_k}{p_{L2}}}{1 + \dfrac{(1-y_{2,k})p_k}{p_{L1}} + \dfrac{y_{2,k} p_k}{p_{L2}}}}{\sum_{k=1}^{N} V_{L2} \dfrac{p_k}{p_k + p_{L2}}} \tag{12.19}$$

where

$f$ = flood gas load factor.

Methane initially in place along this linear flow path is given by the single-component Langmuir isotherm equation.

$$V_{1,i} = \sum_{k=1}^{N} V_{L1} \frac{p_k}{p_k + p_{L1}}$$

At some later time during the flood, the methane remaining along the flow path is given by the multicomponent Langmuir isotherm.

$$V_{1,t} = \sum_{k=1}^{N} V_{L1} \frac{\dfrac{(1-y_{2,k})p_k}{p_{L1}}}{1 + \dfrac{(1-y_{2,k})p_k}{p_{L1}} + \dfrac{y_{2,k} p_k}{p_{L2}}}$$

A methane recovery factor at time $t$ can be defined as

$$rf_{1,t} = 1 - \frac{\sum_{k=1}^{N} V_{L1} \dfrac{\dfrac{(1-y_{2,k})p_k}{p_{L1}}}{1 + \dfrac{(1-y_{2,k})p_k}{p_{L1}} + \dfrac{y_{2,k} p_k}{p_{L2}}}}{\sum_{k=1}^{N} V_{L1} \dfrac{p_k}{p_k + p_{L1}}} \tag{12.20}$$

This simplified approach considers only the linear, high-permeability flow path between injector and producer. In actuality, an injected gas will contact a larger portion of the reservoir. Similar to waterflooding of a conventional oil reservoir, vertical and areal sweep efficiencies can be defined for ECBM. Sequestration efficiency can be written as

$$E_s = fE_vE_A \tag{12.21}$$

where

$E_s$ = sequestration efficiency,
$E_v$ = vertical sweep efficiency, and
$E_A$ = areal sweep efficiency.

Methane recovery efficiency at any time $t$ can be expressed as

$$E_1 = rf_{1,t}E_vE_A \tag{12.22}$$

where

$E_1$ = methane recovery efficiency.

Note that vertical and areal sweep efficiencies are also functions of time and are probably best determined from pilot testing in a particular coal seam and numerical simulation.

### Example 12.2. Nitrogen breakthrough in the Tiffany ECBM Pilot, San Juan Basin

As noted above, numerical simulations of the Tiffany ECBM Pilot by Liang et al. and Reeves and Oudinot reported difficulties in matching nitrogen breakthrough times and produced gas compositions.[47] Both studies employed 3-D models with multiple layers and large grid blocks. Such models have inherent limitations in describing rapid gas flow in small, linear, high-permeability channels thought to control flood gas breakthrough to producing wells. Thus the method outlined above was used to investigate free gas composition early in the nitrogen flood.

**Table 12–1.** Example 12.2 coal and well properties

| | | |
|---|---|---|
| Reservoir and injector pressure = | 1,600 | psia |
| Producer pressure = | 500 | psia |
| Temperature = | 120 | °F |
| Permeability = | 21 | md |
| Porosity = | 0.002 | fraction |
| Length = | 2,640 | ft |
| Coal density = | 1.80 | g/cm$^3$ |
| Gas viscosity = | 0.013 | cp |
| **San Juan in-situ methane isotherm** | | |
| $V_{L1}$ = | 421.0 | scf/ton |
| $p_{L1}$ = | 606.0 | psia |
| **San Juan in-situ nitrogen isotherm** | | |
| $V_{L2}$ = | 257.0 | scf/ton |
| $p_{L2}$ = | 1,429.0 | psia |

*Source:* Reeves, S., and Oudinot, A. 2005. The Tiffany Unit $N_2$-ECBM Pilot—a reservoir and economic analysis. Paper 0523 in *Proceedings of the 2005 International Coalbed Methane Symposium.* Tuscaloosa: University of Alabama.

Reservoir properties employed by Reeves and Oudinot in history matching pilot performance are presented in table 12–1. In-situ methane and nitrogen isotherms are shown in figure 12–3. Assuming nitrogen breaks through by following a linear, high-permeability path between injector and producer, the Tiffany well spacing of 160 ac implies a path length of 2,640 ft. This path was divided into 100 blocks, each with a length of 26.4 ft. Cross-sectional flow area was taken to be 1 $ft^2$, and a time step of 0.1 days was assumed. Geometric average permeability reported by Reeves and Oudinot was 13.4 md with an anisotropy ratio of 2.4, implying a maximum permeability of 21 md.

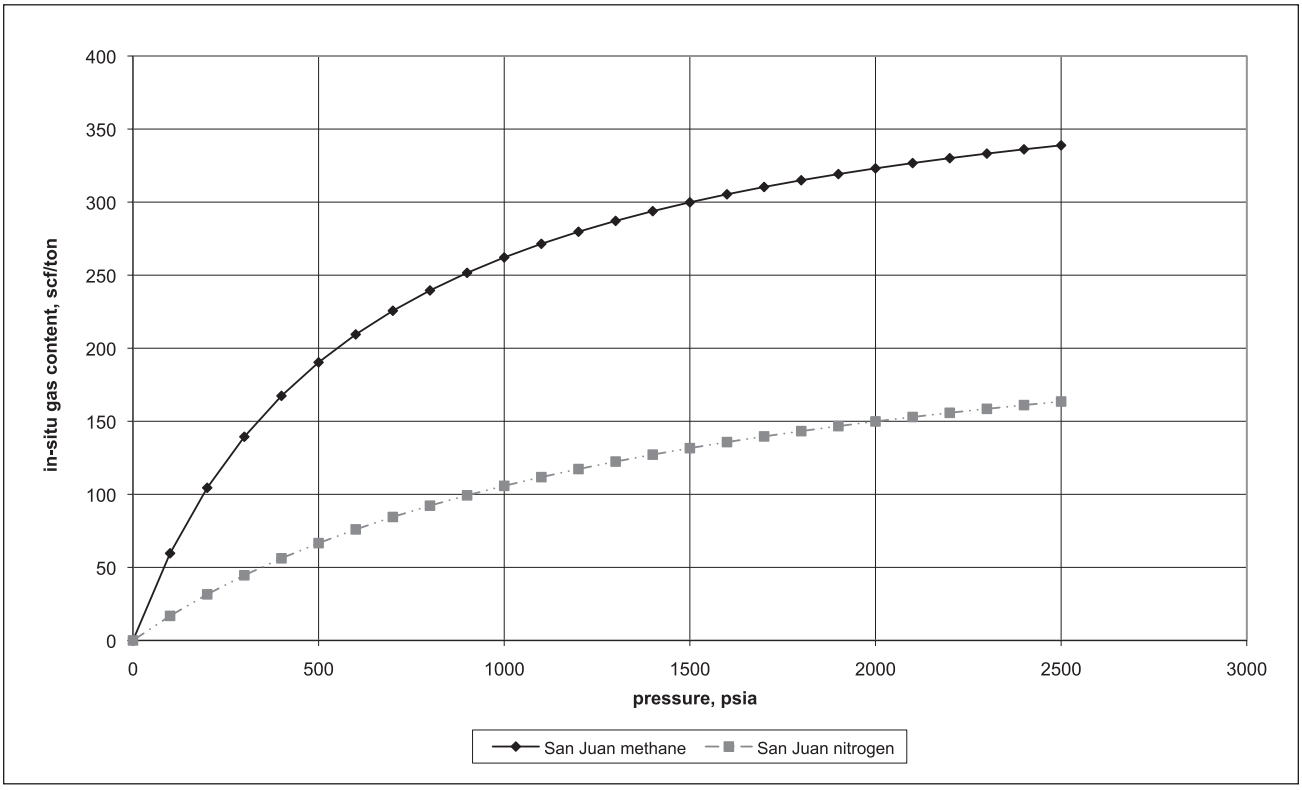



**Fig. 12–3.** Example 12.2 in-situ sorption isotherms[48]

The nitrogen mole fraction in the free gas is plotted as a function of distance in figure 12–4 for three times. After the first time step, 0.1 days, the nitrogen gas is present only in the first and second blocks. As methane sorbs on coal more strongly than does nitrogen, the nitrogen gas is readily convected along the linear flow path, giving a broad flood front. Breakthrough to the producing well, defined as a 1% nitrogen mole fraction in the produced gas stream, occurs after 33.5 days of injection. Time until the coal is one-half loaded with nitrogen, when the flood gas load factor defined by equation (12.19) equals 0.5, occurs at 30.9 days, three days before breakthrough of nitrogen at the producing well. Nitrogen fraction in the produced gas, plotted in figure 12–5, exhibits a moderate, nearly linear increase with time after breakthrough. Time to *floodout*, defined as time for the nitrogen fraction in the produced gas stream to rise to 99%, is 113.2 days. Consequently, time for the front to pass the producing well, that is the incremental time from breakthrough to floodout, is 79.7 days, three times longer than breakthrough time. Breakthrough times in nitrogen ECBM projects are typically only a fraction of frontal passage time. Consequently, produced gas from these projects will require separation throughout most of the flood life. Due to flooding response in slower beds of the coal seam and reservoir heterogeneity, actual produced gas composition is expected to show a slower rise than that predicted with this linear channel model. Times to a 50% nitrogen load factor and to floodout would be longer.

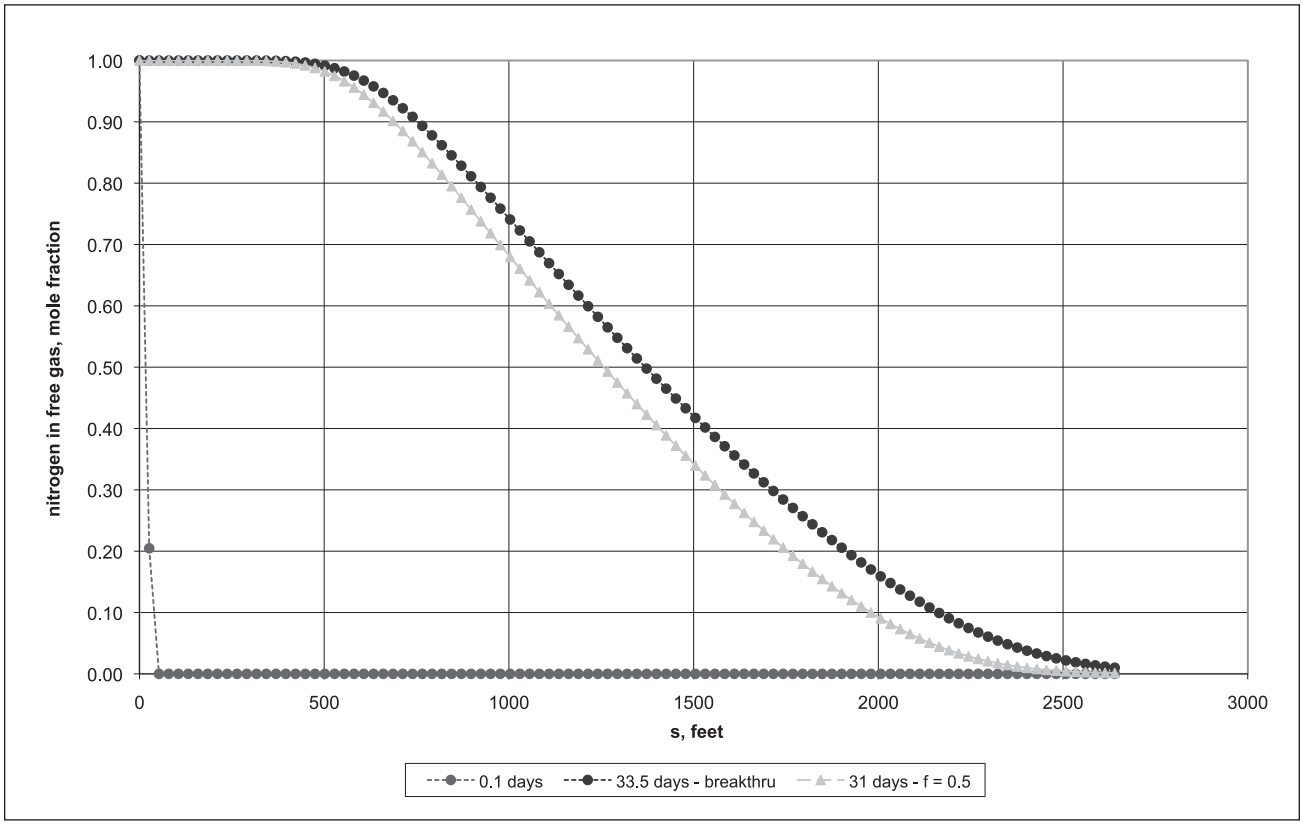



**Fig. 12–4.** Nitrogen mole fraction in free gas vs. distance

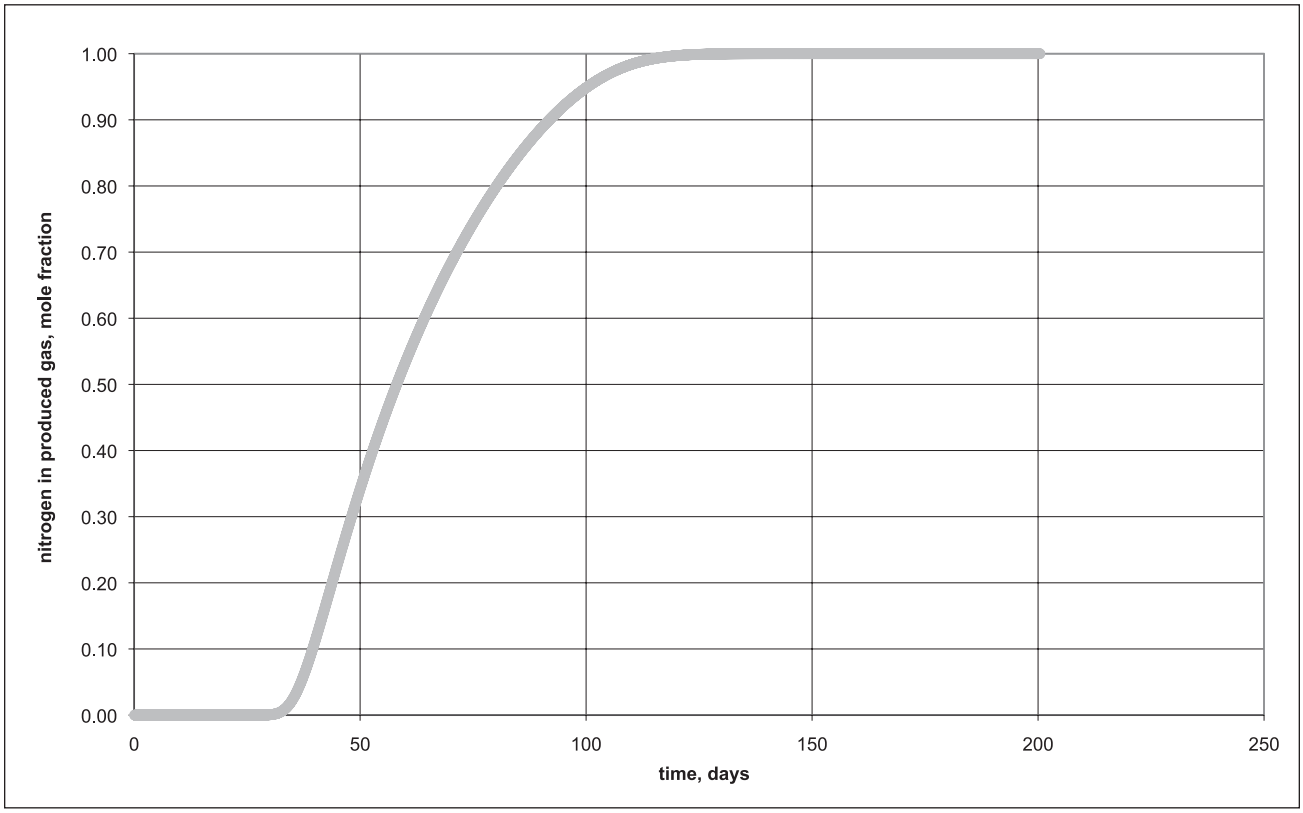



**Fig. 12–5.** Nitrogen mole fraction in produced gas vs. time

The load fraction of nitrogen in the coal and the methane recovery factor are plotted as a function of nitrogen in the produced gas stream in figure 12–6. To obtain a methane recovery of 90% would require treating a produced gas stream that is 67% nitrogen and entails considerable nitrogen lost in the coal seam, as the corresponding load factor is 91% of its maximum nitrogen capacity. Sorbed gas load factor and methane recovery factor, plotted as functions of time in figure 12–7, are nearly superimposed and indicate that 90% methane recovery would occur after 69 days of injection. Actual coal deposits have bedding planes, natural fractures, and other permeability heterogeneities that would flood at different speeds, smearing out the profiles predicted here with an idealized, single-channel approach.

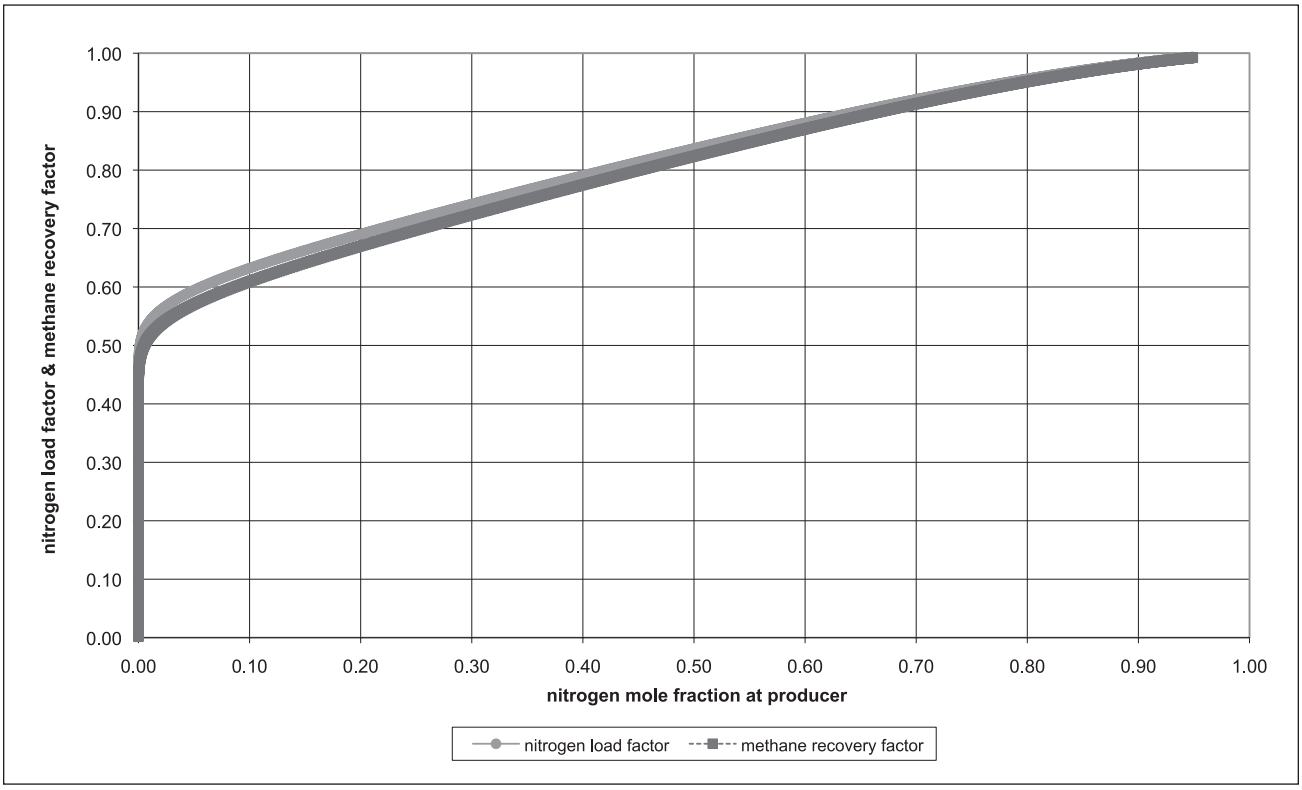



**Fig. 12–6.** Nitrogen load factor and methane recovery factor vs. nitrogen mole fraction at producer

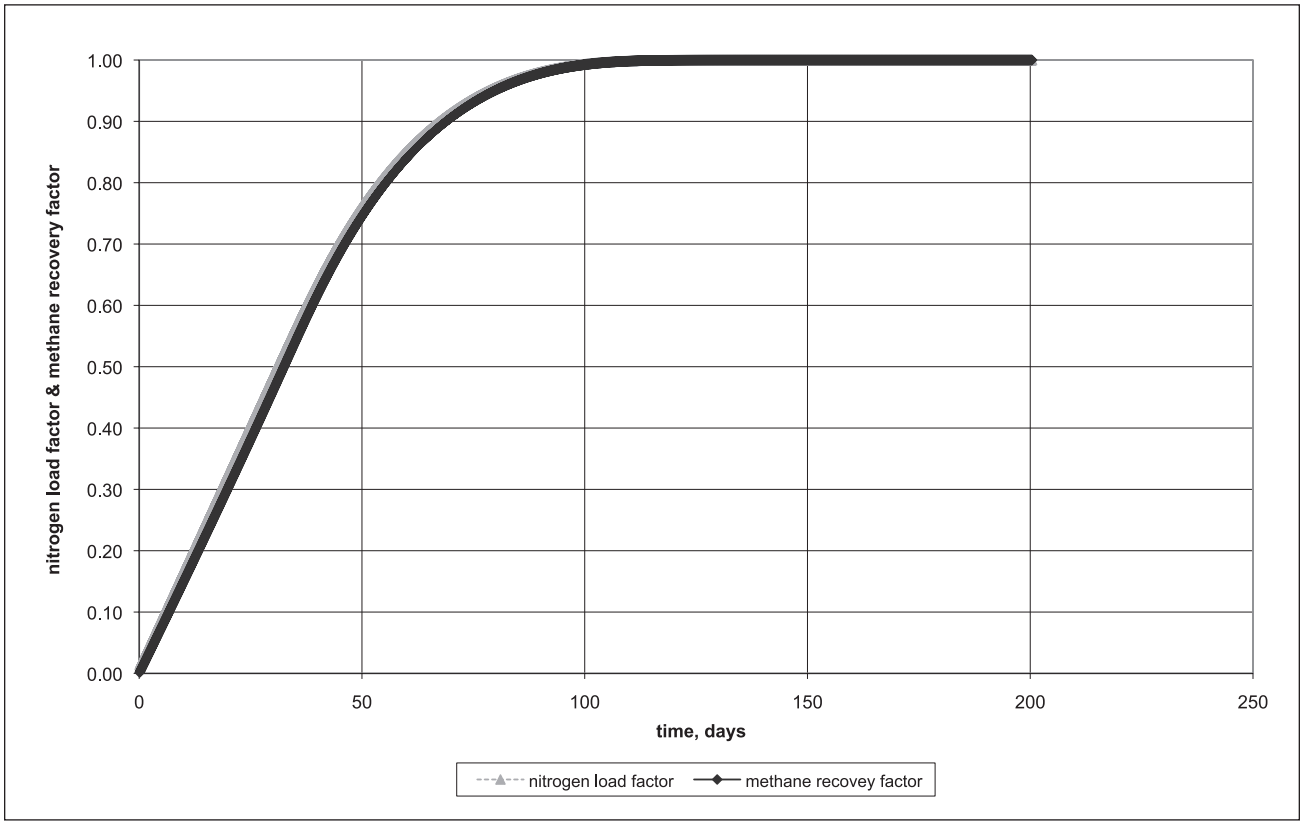



**Fig. 12–7.** Nitrogen load factor and methane recovery factor vs. time

### Example 12.3. Effect of Langmuir pressure on $CO_2$ breakthrough in ECBM

Coals can also be flooded with $CO_2$ to promote gas recovery. Use of two different $CO_2$ isotherms in the above method for linear flooding of a coal deposit demonstrates the effect of Langmuir pressure constants on ECBM. North San Juan Basin reservoir properties from example 12.2 are repeated in table 12–2, which also includes $CO_2$ Langmuir constants for sorption isotherms reported by Arri et al. and Pratt et al.[49] The isotherm reported by Arri et al., measured on a sample of low-volatile bituminous coal from the San Juan Basin, has a Langmuir volume constant nearly three times larger than that of methane. The $CO_2$ Langmuir pressure constant is about one-third the methane pressure constant. The isotherm reported by Pratt et al., measured on a sample of subbituminous coal from the Powder River Basin, also has a Langmuir volume constant nearly three times larger than the methane volume constant. The $CO_2$ Langmuir pressure is one-third more than that of methane. All three isotherms are plotted in figure 12–8.

As in example 12.2, the high-permeability channel between injector and producer was discretized as 100 blocks, each 26.4 ft in width, and having a cross-sectional flow area of 1 $ft^2$. The time step was 0.1 days.

Using the method developed above, $CO_2$ in the free gas phase predicted with the San Juan isotherms is plotted as a function of distance at three times in figure 12–9. At the first time step, $CO_2$ is present only in the first two grid blocks, similar to the nitrogen results of example 12.2 plotted in figure 12–4. In this flood, a sharp flood front forms, sweeping the channel like a piston, pushing methane ahead of it with little methane left behind the front. Time required to fill the coal with one-half the total $CO_2$ load (time to attain a load factor of 0.5) occurs at 249.5 days, well before the breakthrough time (1% $CO_2$ in the produced gas) of 490.0 days. This sharp front causes rapid frontal passage at the producing well, as seen in figure 12–10, where the $CO_2$ mole fraction rises from 1% to 99% in 27 days. The methane recovery factor at breakthrough is 97.6%. In contrast to a nitrogen flood, produced gas from a $CO_2$ flood has a higher methane fraction prior to frontal arrival, the front travels more slowly, and producing wells flood out more quickly. Time to $CO_2$ breakthrough in the producing well is typically much longer than frontal passage, resulting in different separation requirements than those of a nitrogen flood.

As seen in figure 12–11, the $CO_2$ load factor and methane recovery factor are nearly identical functions of $CO_2$ in the produced gas stream. Efficient displacement of methane and the resulting sharp flood front cause the sharp knees in these curves. Similarly, figure 12–12 shows $CO_2$ load fraction and methane recovery factor are nearly identical linear functions of time. Methane recovery of 90% occurs after 447 days of injection, 43 days prior to breakthrough. At this time, the $CO_2$ load factor is 0.887, roughly the same as the methane recovery factor.

**Table 12–2.** Example 12.3 coal and well properties

| | | |
|---|---|---|
| Injector pressure = | 1,600 | psia |
| Producer pressure = | 500 | psia |
| Temperature = | 120 | °F |
| Permeability = | 21 | md |
| Porosity = | 0.002 | fraction |
| Length = | 2,640 | ft |
| Coal density = | 1.80 | g/cm$^3$ |
| Gas viscosity = | 0.013 | cp |
| **San Juan in-situ methane isotherm** | | |
| $V_{L1}$ = | 421.0 | scf/ton |
| $p_{L1}$ = | 606.0 | psia |
| **San Juan in-situ $CO_2$ isotherm** | | |
| $V_{L2}$ = | 1,102.4 | scf/ton |
| $p_{L2}$ = | 204.5 | psia |
| **Powder River in-situ $CO_2$ isotherm** | | |
| $V_{L2}$ = | 1,182.6 | scf/ton |
| $p_{L2}$ = | 791.0 | psia |

*Sources:* Reeves, S., and Oudinot, A. 2005. Paper 0522; Arri, L. E., et al.; and Pratt, T. J., et al. 1999.

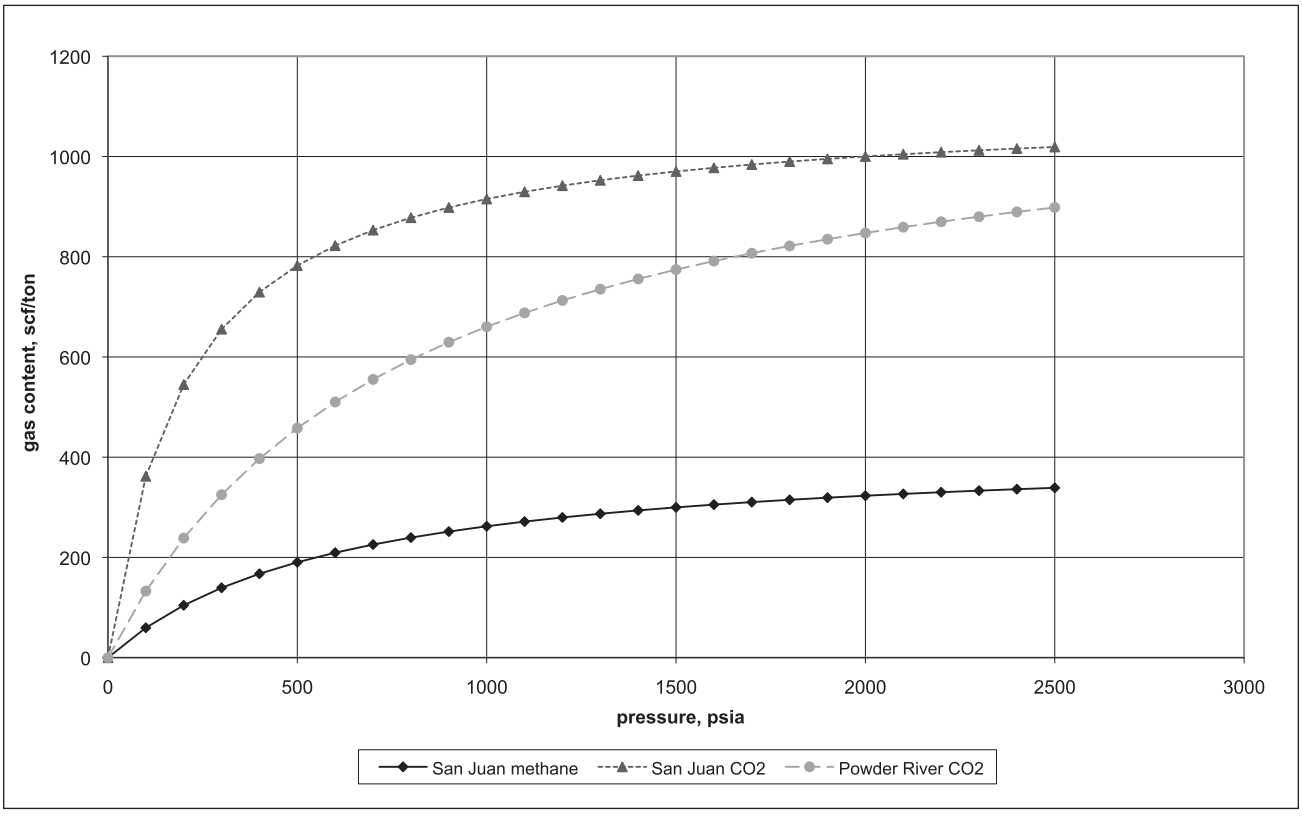



**Fig. 12–8**. Example 12.3 in-situ sorption isotherms[50]

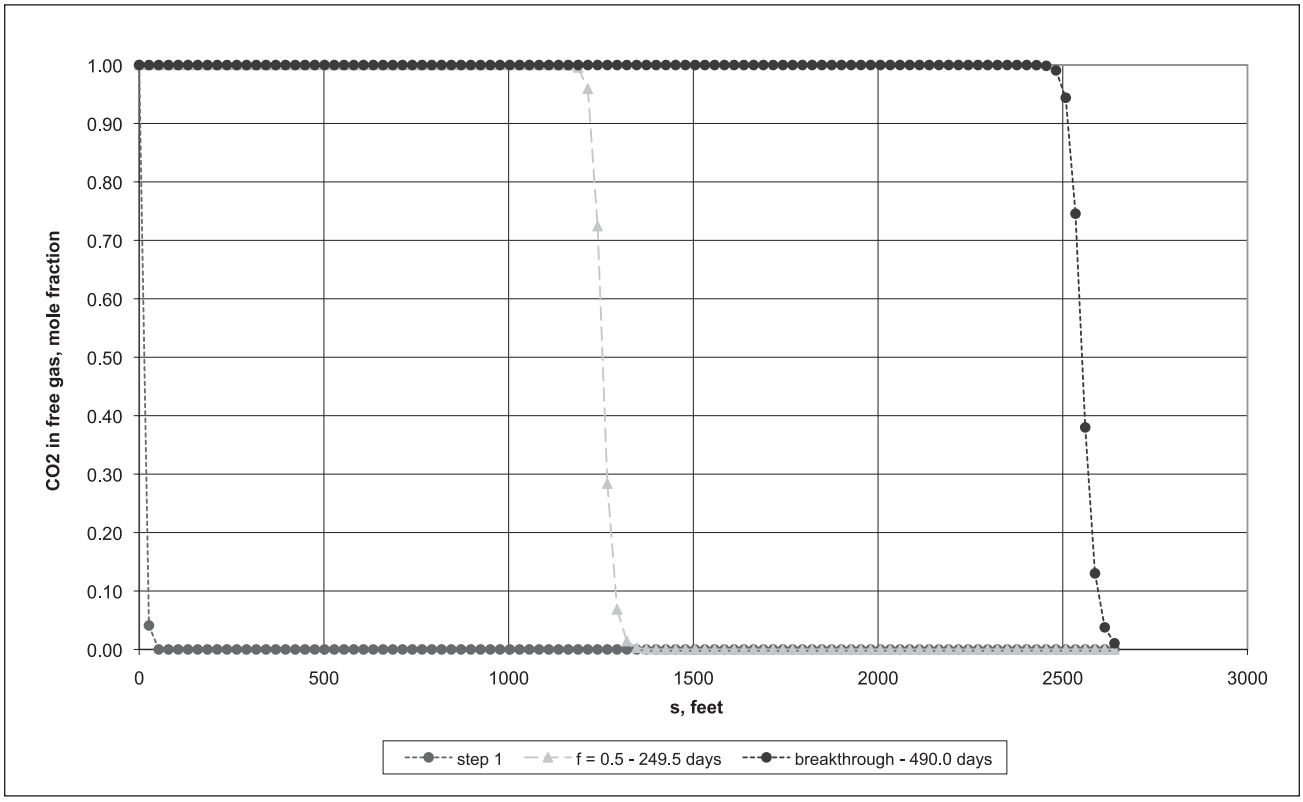



**Fig. 12–9.** Example 12.3 $CO_2$ mole fraction in free gas vs. distance—San Juan $CO_2$ isotherm

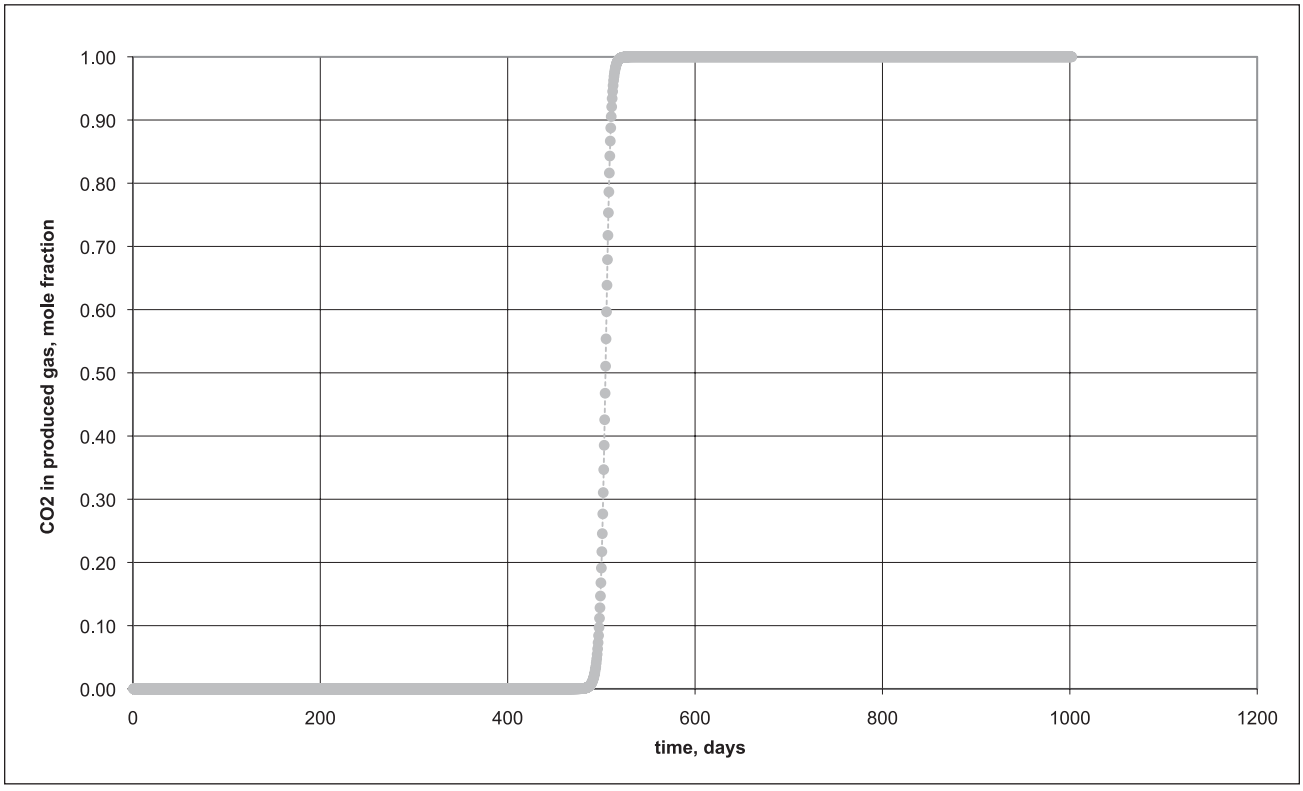



**Fig. 12–10.** Example 12.3 $CO_2$ mole fraction in produced gas vs. time—San Juan $CO_2$ isotherm

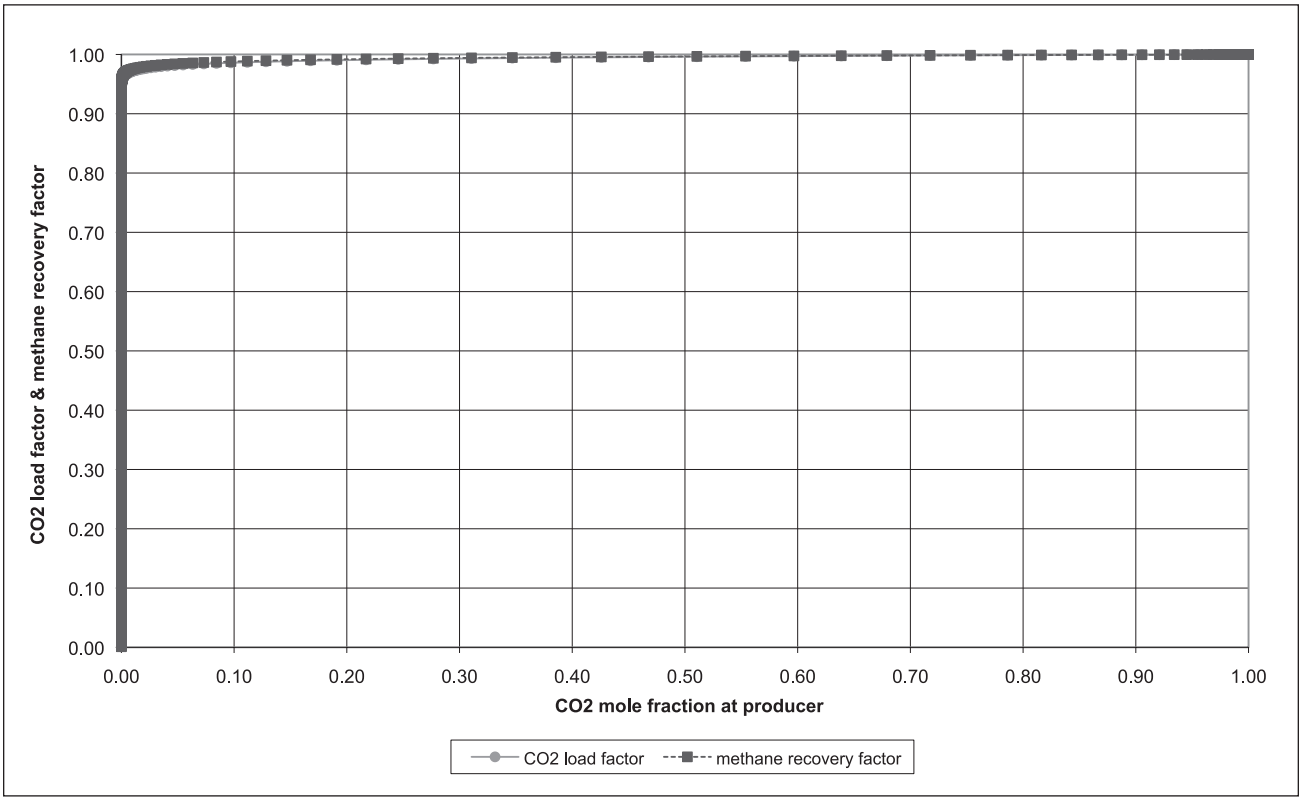



**Fig. 12–11.** Example 12.3 $CO_2$ load factor and methane recovery factor vs. $CO_2$ mole fraction at producer—San Juan $CO_2$ isotherm

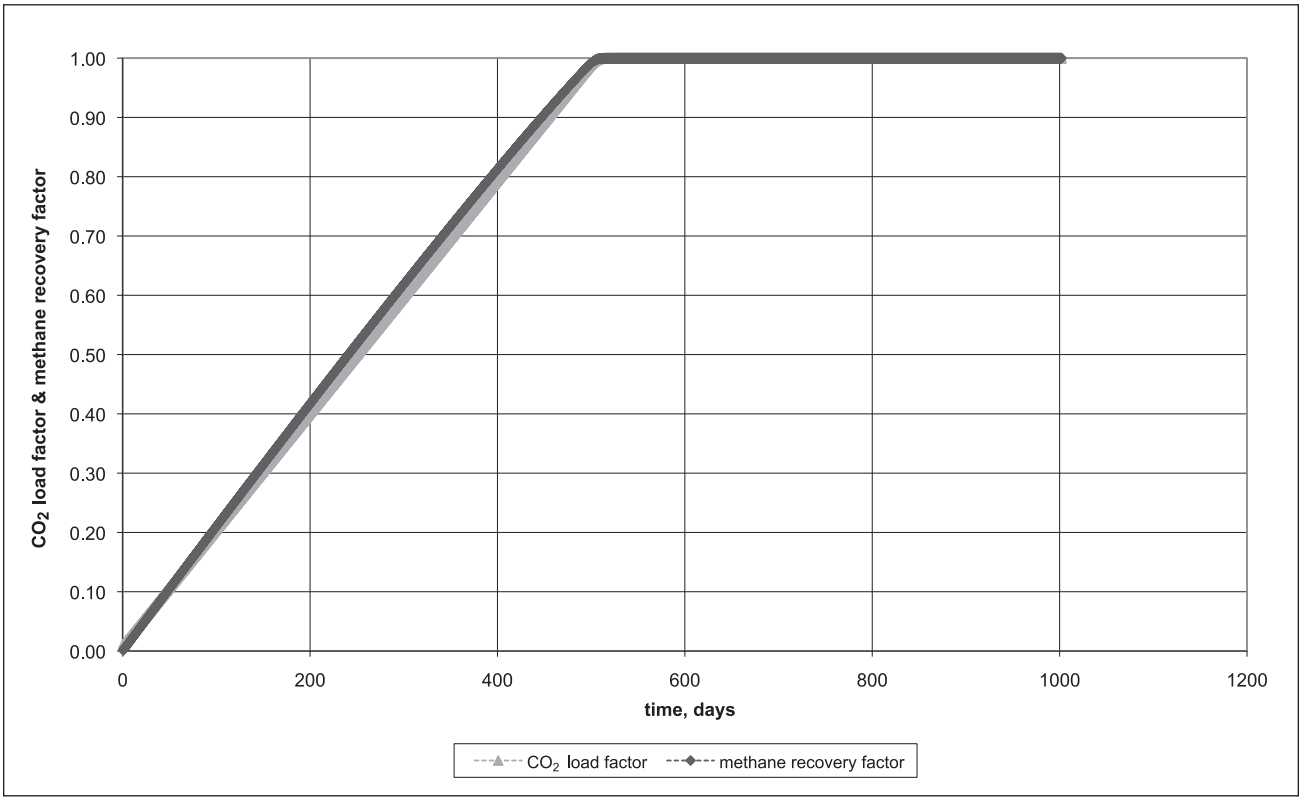



**Fig. 12–12.** Example 12.3 $CO_2$ load factor and methane recovery factor vs. time—San Juan $CO_2$ isotherm

Repeating the linear flood calculations with the Powder River Basin $CO_2$ isotherm yields a broader flood front that travels at a higher velocity, reaching the producing well sooner. $CO_2$ fraction in the free gas is plotted as a function of distance in figure 12–13 for the first time step, at a load factor of 0.5 (occurring at 185.0 days), and at breakthrough (occurring at 260.0 days). Frontal passage, depicted in figure 12–14, not only occurs sooner with this $CO_2$ isotherm but lasts longer, requiring 265.5 days for the $CO_2$ fraction to rise from 1% to 99%. $CO_2$ load factor and methane recovery factor as functions $CO_2$ fraction in the produced gas are depicted in figure 12–15 and as functions of time in figure 12–16. With this broader flood front, $CO_2$ at the produced well begins to rise at lower load factors and methane recovery, on the order of 65%, not 95%, but otherwise exhibits the same linearity as the previous cases. Time to floodout, defined as time required for produced gas composition to rise to 99% $CO_2$, occurs at roughly the same time, 520 days, with both $CO_2$ isotherms. Time required to recover 90% of the methane is 353.5 days, approximately three months after breakthrough. At this time, $CO_2$ in the produced gas stream has risen to 41% and the $CO_2$ load factor is 0.904. As noted in example 12.2, coal heterogeneities will broaden the flood front and prolong time to floodout. Various times for the nitrogen flood of example 12.2 and those of this example are compared in table 12–3.

**Table 12–3.** Calculated times for nitrogen and $CO_2$ ECBM response

| Time, days | $N_2$ SJB | $CO_2$ SJB | $CO_2$ PRB |
|---|---|---|---|
| 50% flood gas load | 30.9 | 249.5 | 185.0 |
| Breakthrough | 33.5 | 490.0 | 260.0 |
| Frontal passage | 79.7 | 26.5 | 265.5 |
| Floodout | 113.2 | 516.5 | 525.5 |
| 90% methane recovery | 68.9 | 447.0 | 353.5 |
| $CO_2$ in produced gas at 90% recovery | 66.7% | 0.0% | 41.3% |

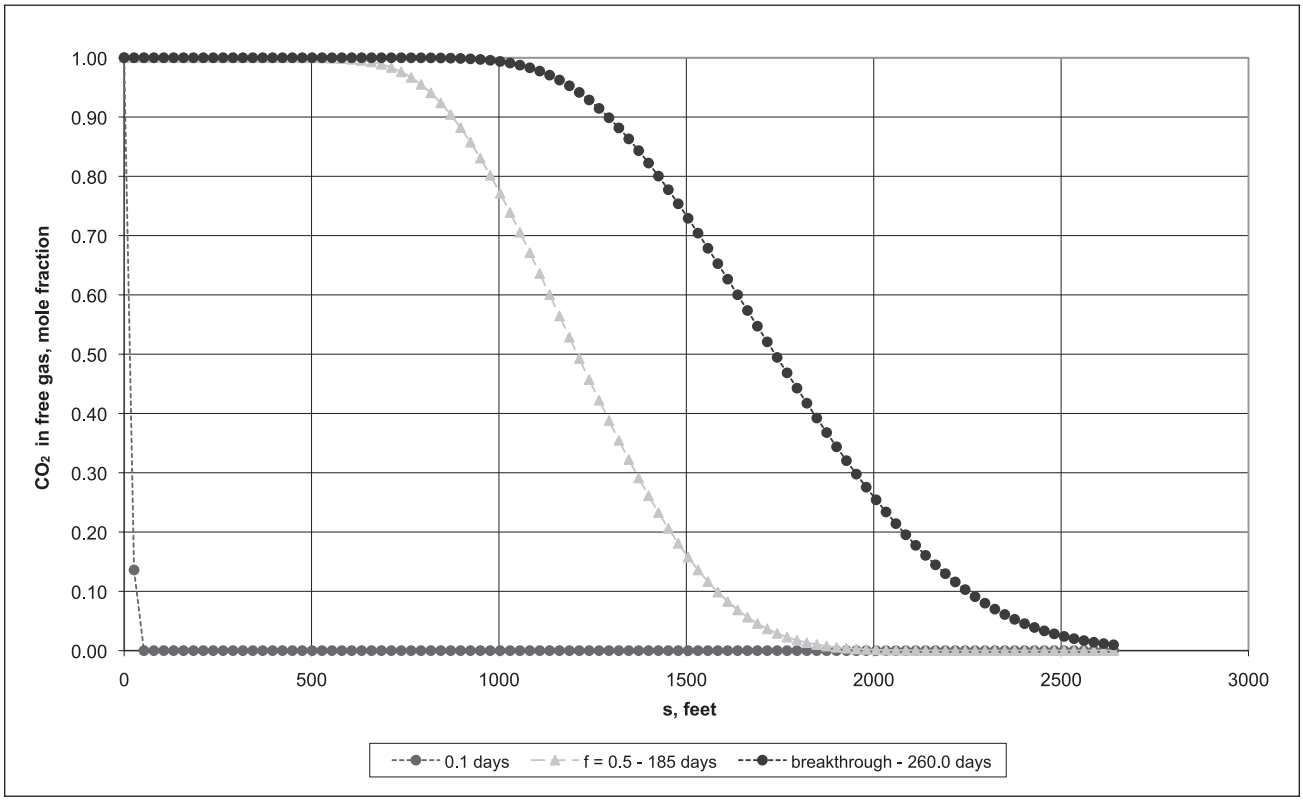



**Fig. 12–13.** Example 12.3 $CO_2$ mole fraction in free gas vs. distance—Powder River $CO_2$ isotherm

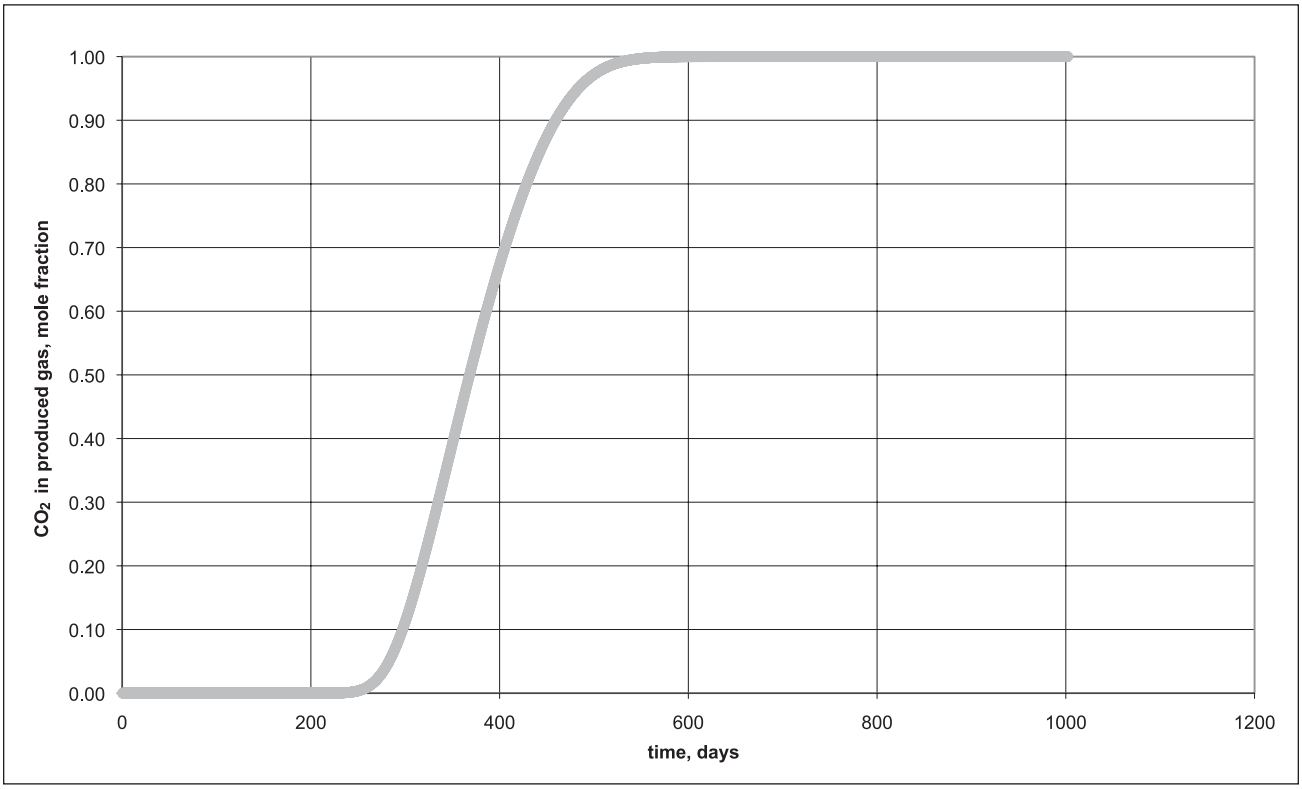



**Fig. 12–14.** Example 12.3 $CO_2$ mole fraction in produced gas vs. time—Powder River $CO_2$ isotherm

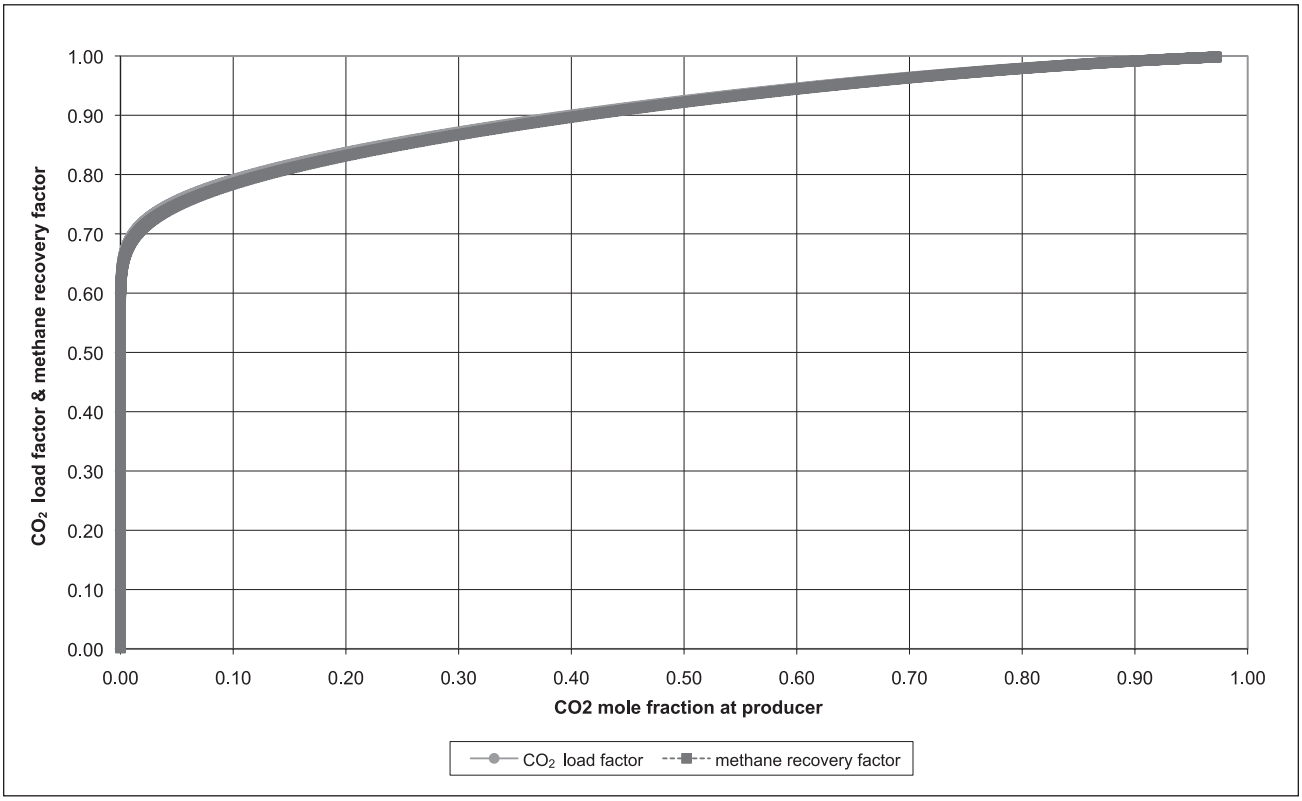



**Fig. 12–15.** Example 12.3 $CO_2$ load factor and methane recovery factor vs. $CO_2$ mole fraction at producer—Powder River $CO_2$ isotherm

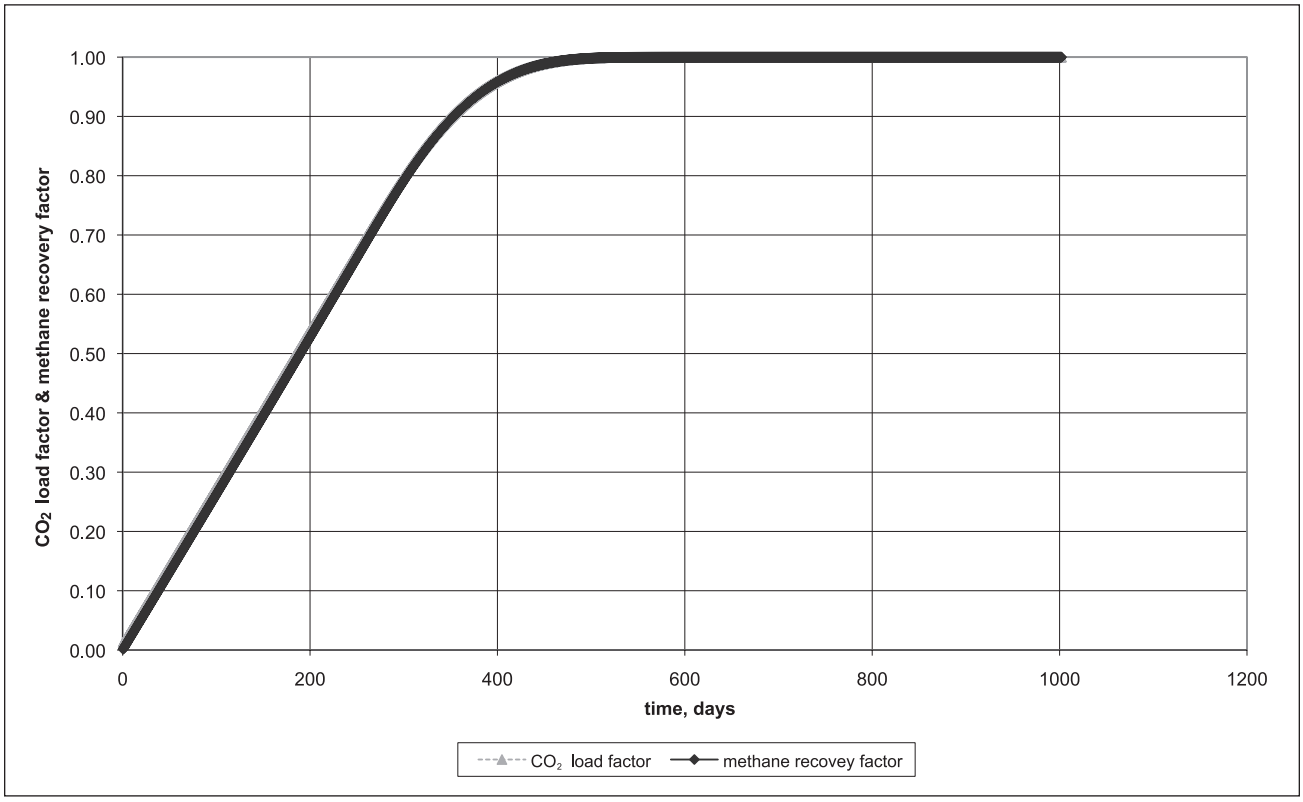



**Fig. 12–16.** Example 12.3 $CO_2$ load factor and methane recovery factor vs. time—Powder River $CO_2$ isotherm

## Coal Absolute Permeability Variation during ECBM or $CO_2$ Sequestration

Coal matrix swells or shrinks in response to changes in the sorbed gas composition and volume. Absolute permeability of a coal deposit changes due to this sorption-induced deformation, as well as stress effects. Replacing sorbed methane with a weaker sorbing gas such as nitrogen will result in overall shrinkage of the matrix, increasing cleat width and, hence, absolute coal permeability. On a field scale, sorption and stress effects of nitrogen flooding are additive, with injection opening up the cleats and nitrogen uptake shrinking the matrix. Nitrogen injectivity increases with time, all other parameters being equal. Increasing absolute permeability in areas contacted by nitrogen exacerbates channeling, reducing volumetric sweep efficiency. Gas mobility in the affected area is also increased due to relative permeability effects, as a larger cleat porosity combined with a slowly changing water volume yields a lower water saturation and, hence, higher gas relative permeability. At any given location in the reservoir, increasing permeability leads to more rapid nitrogen influx, aggravating fingering, accelerating breakthrough, and reducing overall flood performance.

Conversely, replacing sorbed methane with a stronger sorbing gas such as $CO_2$ will result in overall swelling of the matrix, decreasing cleat width and permeability. This permeability reduction acts contrary to the permeability increase due to cleat opening from gas injection. If the coal deposit reacts more strongly to changes in stress than in gas composition, permeability behavior similar to that of a weaker sorbing gas, as discussed above, is expected. If coal permeability is dominated by compositionally induced swelling, a net decrease in permeability results. On a field scale, injection of $CO_2$ in this case leads to decreased injectivity with time. Volumetric flood efficiency increases as high-permeability channels swell shut, forcing $CO_2$ into unswept areas. Gas mobility decreases due to reduced relative permeability to gas resulting from a smaller cleat porosity holding a slowly changing water volume. Decreasing permeability due to $CO_2$ contact at a given location blunts the flood front, retards breakthrough, and increases flood or sequestration performance.

As detailed in chapter 6, Mavor and Gunter extended the Palmer-Mansoori theory for coal permeability behavior to include multicomponent gases.[51] Coal matrix strain is assumed to be related to pressure through a Langmuirlike dependency, with total strain due to sorption of a multicomponent gas expressed similar to the multicomponent Langmuir isotherm equation. The Palmer-Mansoori theory normalizes porosity of the coal at a given pressure relative to porosity at atmospheric pressure and assumes a cubic dependency of the permeability ratio with that of porosity. Mavor and Gunter outline an iterative calibration procedure for this model utilizing coal rock properties and simulation of at least three well tests. With a two-component gas mixture, such as methane and nitrogen, these multicomponent Palmer-Mansoori equations contain six unknowns. These unknowns are the coal permeability and porosity at atmospheric pressure, the sorption strain at infinite pressure, $\varepsilon_\infty$, and pressure at a strain of 0.5 $\varepsilon_\infty$, for both of the two components of the gas mixture. Care must be exercised to obtain realistic values of the parameters, and nonunique solutions are expected. This theory assumes infinitely fast sorption kinetics.

Inclusion of matrix shrinkage and swelling into simulation of the Allison $CO_2$ pilot operation by Shi and Durucan improved matches of produced gas compositions, reservoir pressures, and injectivities.[52] Drawing on the explanation of this theory presented in chapter 6, change in coal stress due to changes in pressure and composition from injection of $CO_2$ into a methane-saturated coal can be written as

$$\sigma - \sigma_i = -\frac{\nu}{1-\nu}(p - p_i) + \frac{E\rho_{Bbbb}}{3(1-\nu)}\left[\sum_{k=1}^{N}\alpha_k V_k - \sum_{k=1}^{N}\alpha_k V_{ki}\right] \tag{12.23}$$

where

$\sigma$ = stress, psia or MPaa,
$\nu$ = Poisson's ratio,
$E$ = Young's modulus, psia or MPaa,
$\rho_B$ = bulk coal density, g/cm$^3$,
$\alpha_k$ = volumetric shrinkage/swelling coefficient for component $k$, ft$^3$/ft$^3$, and
$V_k$ = gas content of component $k$ calculated from equation (12.2), ft$^3$/ton or cm$^3$/g.

In addition to coal rock properties, the Shi-Durucan model requires volumetric shrinkage/swelling coefficients, $\alpha_j$s, for each component. Thus, description of permeability changes during a nitrogen flood of a methane-bearing coal deposit would require two such coefficients, determined empirically or through a simulation history match exercise. Using the latter approach, methane and $CO_2$ coefficients reported by Shi and Durucan for coals in the Allison Unit were $5.333(10)^{-4}$ ft$^3$/ft$^3$ and $6.805(10)^{-4}$ ft$^3$/ft$^3$, respectively.

Porosity and permeability changes were exponentially related to stress change,

$$\phi = \phi_i \exp[-c_f(\sigma - \sigma_i)] \tag{12.24}$$

where

$c_f$ = cleat volume compressibility, psia$^{-1}$ or MPa$^{-1}$.

$$\frac{k}{k_i} = \left(\frac{\phi}{\phi_i}\right)^3 \tag{12.25}$$

Sorption kinetics of both methane and $CO_2$ were described by Shi and Durucan with a sorption time of 10 days.

## Tank Model for $CO_2$ Sequestration

Sequestration of $CO_2$ in a depleted, dewatered coal can be described with a tank model. Although a tank model, representing the reservoir as a single node, cannot capture pressure, saturation, and composition gradients, it can describe overall reservoir behavior and $CO_2$ loading. Injection of a sorbing gas that swells the host coal deposit is arguably a very heterogeneous process with a constantly changing flow pattern. Higher permeability layers first accept gas then swell shut, forcing gas into the previously lower permeability, unswept channels. Simulation of such a process with a gridded model requires a good reservoir description in addition to the usual rock and fluid properties and well operating constraints. A tank model provides a bounding "sense check" on such simulation results.

Construction of a tank model for $CO_2$ sequestration begins with the assumption of pure $CO_2$ injection into a dry or dewatered single coal seam depleted of methane down to an abandonment pressure. With no gas production from the coal seam, the total amount of methane is constant and is described by

$$G_1 = 1.3597(10)^{-3} Ah\rho_B V_{L1} \frac{\dfrac{(1-y_2)\overline{p}}{p_{L1}}}{1+\dfrac{(1-y_2)\overline{p}}{p_{L1}}+\dfrac{y_2\overline{p}}{p_{L2}}} + 4.3560(10)^{-2} Ah\phi(1-S_{wi})\frac{1}{B_{g1}} \tag{12.26}$$

where

$G_1$ = methane gas volume in coal, mmcf,
$A$ = drainage area, ac,
$h$ = net coal thickness, ft,
$\overline{p}$ = average reservoir pressure, psia, and
$S_{wi}$ = irreducible water saturation, fraction.

Note the gas formation volume factor is calculated using the methane partial pressure, not average reservoir pressure.

Injection rate of $CO_2$ into the coal can be described with the p-squared form of Darcy's law

$$q_{inj} = \frac{k_g h}{1422 T \overline{Z}\overline{\mu}} \frac{p_{inj}^2 - \overline{p}^2}{\ln\left[\dfrac{r_e}{r_w}\right] - 0.75 + s} \tag{12.27}$$

where

$q_{inj}$ = gas injection rate, mcfd,
$k_g$ = effective permeability to gas, md,
$h$ = net coal thickness, ft,
$\overline{Z}$ = $CO_2$ gas deviation factor at average pressure,
$\overline{\mu}$ = $CO_2$ gas viscosity at average pressure, cp,
$p_{inj}$ = injection pressure, psia,
$\overline{p}$ = average reservoir pressure, psia,
$r_e$ = drainage radius, ft,
$r_w$ = wellbore radius, ft, and
$s$ = wellbore skin factor.

And the $CO_2$ mass balance is written

$$G_2 = 1.3597(10)^{-3} Ah\rho_B V_{L2} \frac{\dfrac{y_2 \overline{p}}{p_{L1}}}{1 + \dfrac{(1-y_2)\overline{p}}{p_{L1}} + \dfrac{y_2 \overline{p}}{p_{L2}}} + 4.3560(10)^{-2} Ah\phi(1 - S_{wi}) \frac{1}{B_{g2}} \tag{12.28}$$

where

$G_2$ = $CO_2$ gas volume in coal, mmcf.

Assuming a time step sufficiently small that the injection rate calculated from equation (12.27) can be considered constant, incremental $CO_2$ volume injected over a given time is

$$\Delta G_2 = 0.001 q_{inj} \Delta t$$

where

$\Delta G_2$ = incremental injected $CO_2$ volume, mmcf, and

$\Delta t$ = time step, days.

Cumulative $CO_2$ injected at the $k$th time is then simply

$$G_{2k} = \sum_k 0.001 q_{injk} \Delta t_k \tag{12.29}$$

The final component of a sequestration tank model is relationships between gas composition and pressure and coal porosity and permeability, such as the Shi-Durucan model above, equations (12.23), (12.24), and (12.25).

Sequestration of $CO_2$ in a coal seam is an iterative process that begins with calculation of porosity and permeability at initial conditions. Combining permeability with assumed injection well bottomhole pressure and wellbore skin factor, the current injection rate can be calculated from equation (12.27), followed by incremental and cumulative $CO_2$ volumes with equation (12.29). The methane and $CO_2$ mass balance relations, equations (12.26) and (12.28), are the two relations employed to solve for current reservoir pressure and $CO_2$ mole fraction in the free gas. Algebraic manipulation of the mass balance equations yields quadratics in the $CO_2$ free gas mole fraction, $y_2$, which can be solved iteratively to determine reservoir pressure and $y_2$.

Defining a rock and fluid parameter as

$$\gamma = \frac{32.037\phi(1 - S_{wi})pZ_{sc}T_{sc}}{\rho_B p_{sc} ZT}$$

the methane mass balance quadratic can be written

$$A_1 y_2^2 + B_1 y_2 + C_1 = 0$$

where

$$A_1 = \gamma p \left( \frac{1}{p_{L2}} - \frac{1}{p_{L1}} \right)$$

$$B_1 = \frac{735.47 G_1 p}{Ah\rho_B} \left( \frac{1}{p_{L2}} - \frac{1}{p_{L1}} \right) + V_{L1} \frac{p}{p_{L1}} - \gamma p \left( \frac{1}{p_{L2}} - \frac{1}{p} - \frac{2}{p_{L1}} \right)$$

$$C_1 = \frac{735.47G_1}{Ah\rho_B}\left(1+\frac{p}{p_{L1}}\right) - V_{L1}\frac{p}{p_{L1}} - \gamma\left(1+\frac{p}{p_{L1}}\right)$$

Similarly, the $CO_2$ mass balance quadratic can be written

$$A_2 y_2^2 + B_2 y_2 + C_2 = 0$$

where

$$A_2 = \gamma p\left(\frac{1}{p_{L1}} - \frac{1}{p_{L2}}\right)$$

$$B_2 = \frac{735.47G_2 p}{Ah\rho_B}\left(\frac{1}{p_{L2}} - \frac{1}{p_{L1}}\right) - V_{L2}\frac{p}{p_{L2}} - \gamma p\left(\frac{1}{p} + \frac{1}{p_{L1}}\right)$$

$$C_2 = \frac{735.47G_2 p}{Ah\rho_B}\left(\frac{1}{p} + \frac{1}{p_{L1}}\right)$$

Reservoir pressure and gas compositions obtained from solving the methane and $CO_2$ mass balance quadratics are used to compute new porosity and permeability values followed by a revised injection rate and incremental injected $CO_2$ volume. The example below illustrates this method for a San Juan coal seam.

### Example 12.4. $CO_2$ sequestration in San Juan coal

Injection of $CO_2$ into a single San Juan coal seam can be modeled using the tank model described above. Assuming a dewatered coal at an abandonment pressure of 100 psia, $CO_2$ is injected into a single well on 160 ac spacing at a bottomhole flowing pressure of 1,000 psia. Porosity and permeability are assumed to depend on pressure and gas composition according to the Shi-Durucan model. Reservoir and well properties are collected in table 12–4.

Initial methane in the 160 ac drainage area is 1,015.537 mmcf, and with a reservoir flow capacity of 1,462 md-ft, the initial $CO_2$ injection rate is 28 mmcfd. The injection rate, shown in figure 12–17, falls rapidly as the matrix swells upon sorption of the $CO_2$. After only three weeks of injection, the rate has fallen to one-half the initial value, 14 mmcfd, and after 50 years of injection, the rate is 39 mcfd. Permeability and porosity ratios, plotted in figure 12–18, drop to 0.14% and 11.2% of their initial values, respectively, over the 50 year injection period. The decrease in permeability due to $CO_2$ sequestration will serve to retard leakage of sequestered $CO_2$ out of the coal.

Total injected $CO_2$, plotted in figure 12–19, is equal to the initial methane volume after 73 days and rises to 4,629 mmcf after 50 years of injection. Total injected $CO_2$ reaches one-half the 50 year value after 636 days, 1.74 years, reflecting the steady decrease in permeability with increasing $CO_2$ sequestration noted above.

Free and sorbed gas mole fractions are plotted in figure 12–20. They show rapid initial changes but slowly vary after 10 years of injection, asymptotically approaching the 50 year free gas composition of 63% methane and 37% $CO_2$ and a sorbed gas composition of 18% methane and 82% $CO_2$. The increase in reservoir pressure is perhaps more modest than expected, reflecting the tremendous sorption capacity of coal for $CO_2$. As shown in figure 12–21, reservoir pressure rises from an initial value of 100 psia to 223 psia after 50 years, with most of that increase occurring early in the life of the injector. One-half the total pressure increment is reached after 1,135 days, 3.1 years.

Coal cleat compressibility strongly influences $CO_2$ sequestration behavior. A stiffer coal, with a smaller compressibility, will be less susceptible to matrix swelling and the consequent loss of permeability and porosity. To illustrate this behavior, the above $CO_2$ sequestration calculations were repeated with cleat compressibility reduced by an order of magnitude, from $1.0(10)^{-3}$ psia$^{-1}$ to $1.0(10)^{-4}$ psia$^{-1}$. The resulting $CO_2$ injection rate and cumulative injected $CO_2$ are compared with those from the above calculations in figures 12–22 and 12–23, respectively. Permeability of the stiffer coal does not decline as rapidly as in the more compliant coal, allowing more rapid $CO_2$ sequestration. After 2,370 days, or 6.5 years, average reservoir pressure and cumulative injected

$CO_2$ are within 1% of the 50 year values. The paradoxical rate behavior exhibited by the stiffer coal in figure 12–22 is due to a rapid reservoir pressure increase and associated $CO_2$ fill-up. These reduce injectivity more than does the stronger permeability loss of the more compliant coal.

The strong dependence of $CO_2$ sequestration behavior on cleat compressibility suggests not only that coal stiffness should be a primary screening criterion for sequestration candidates but also a field-based method for determination of cleat compressibility in an ongoing storage project.

**Table 12–4.** Example 12.4 tank model inputs

| | | |
|---|---|---|
| Area = | 160 | acres |
| Net coal thickness = | 43 | feet |
| Coal density = | 1.80 | $g/cm^3$ |
| Reservoir pressure = | 100 | psia |
| Injection pressure = | 1,000 | psia |
| Porosity = | 0.01 | fraction |
| Temperature = | 120 | °F |
| Gas permeability = | 34 | md |
| Irreducible water saturation = | 0.35 | fraction |
| Young's modulus = | 420,000 | psia |
| Poisson's ratio = | 0.35 | md |
| Cleat compressibility = | 0.001 | $psia^{-1}$ |
| Wellbore radius = | 0.204 | feet |
| Skin factor = | -2 | |
| time step = | 10 | days |
| | **In-situ methane isotherm** | |
| $V_{L1}$ = | 421.0 | scf/ton |
| $p_{L1}$ = | 606.0 | psia |
| | **In-situ $CO_2$ isotherm** | |
| $V_{L2}$ = | 1,102.4 | scf/ton |
| $p_{L2}$ = | 204.5 | psia |
| | **Shi-Durucan constants** | |
| $a_{meth}$ = | 0.0005333 | vol/vol |
| $a_{CO_2}$ = | 0.0006805 | vol/vol |

*Sources:* Arri, L. E., et al. 1992; Reeves, S., and Oudinot, A. 2005. Paper 0523; Reeves, S., and Oudinot, A. 2005. Paper 0522; Shi, J. Q., and Durucan, S. 2004; and Gash, B. W. 1991. *Measurement of "Rock Properties" in Coal for Coalbed Methane Production.* Paper SPE 22909. Presented at the Annual Technical Conference and Exhibition, Dallas, Texas, October 6–9.

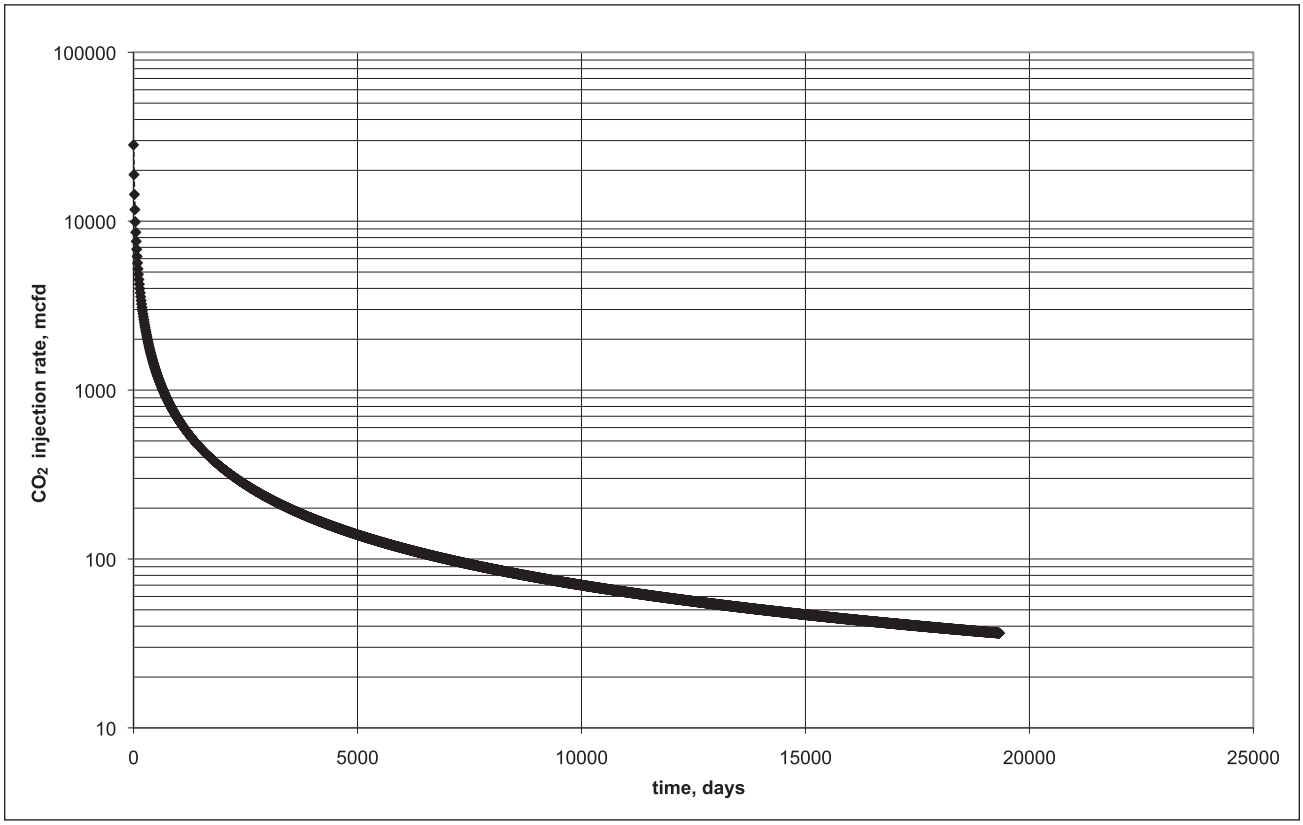



**Fig. 12–17.** Example 12.4 $CO_2$ injection rate vs. time

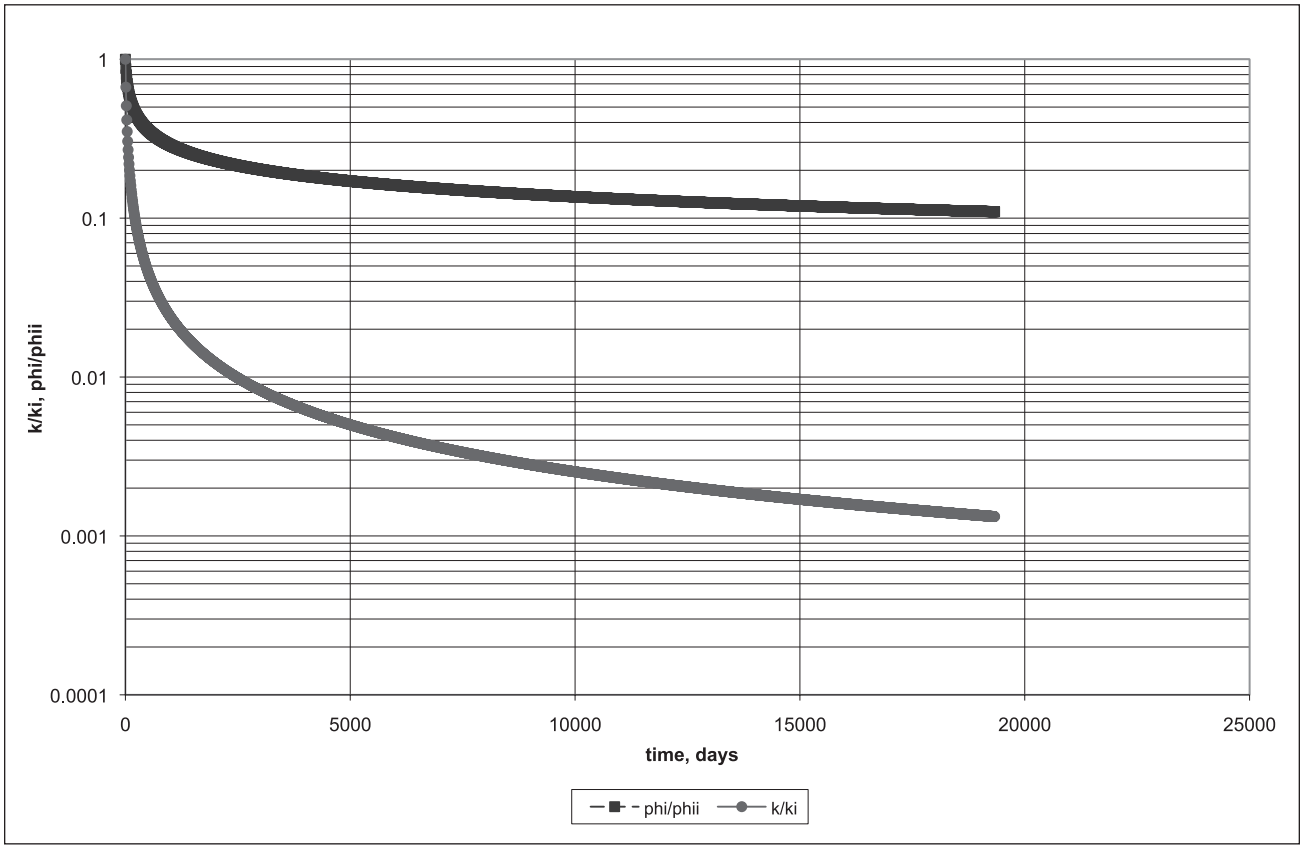



**Fig. 12–18.** Example 12.4 permeability and porosity ratios vs. time

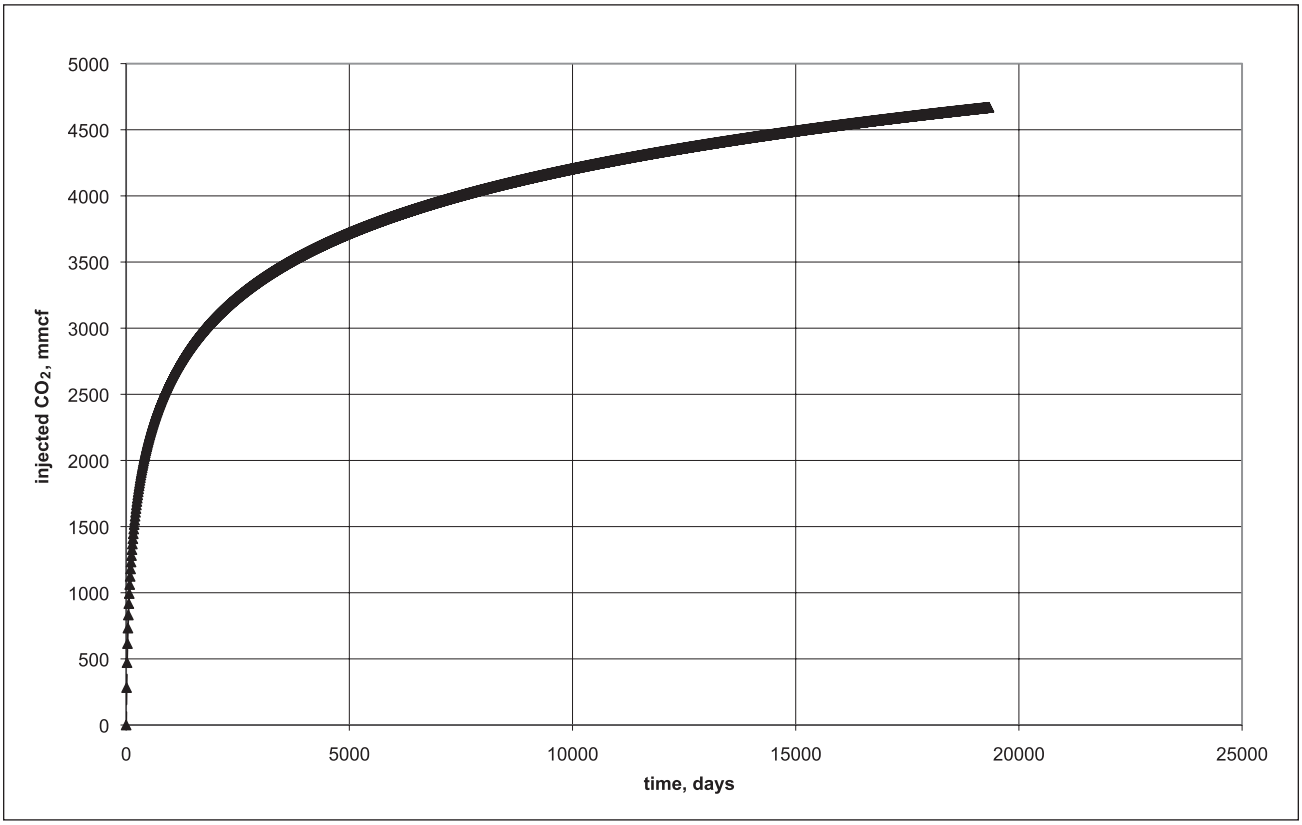



**Fig. 12–19.** Example 12.4 cumulative $CO_2$ injected vs. time

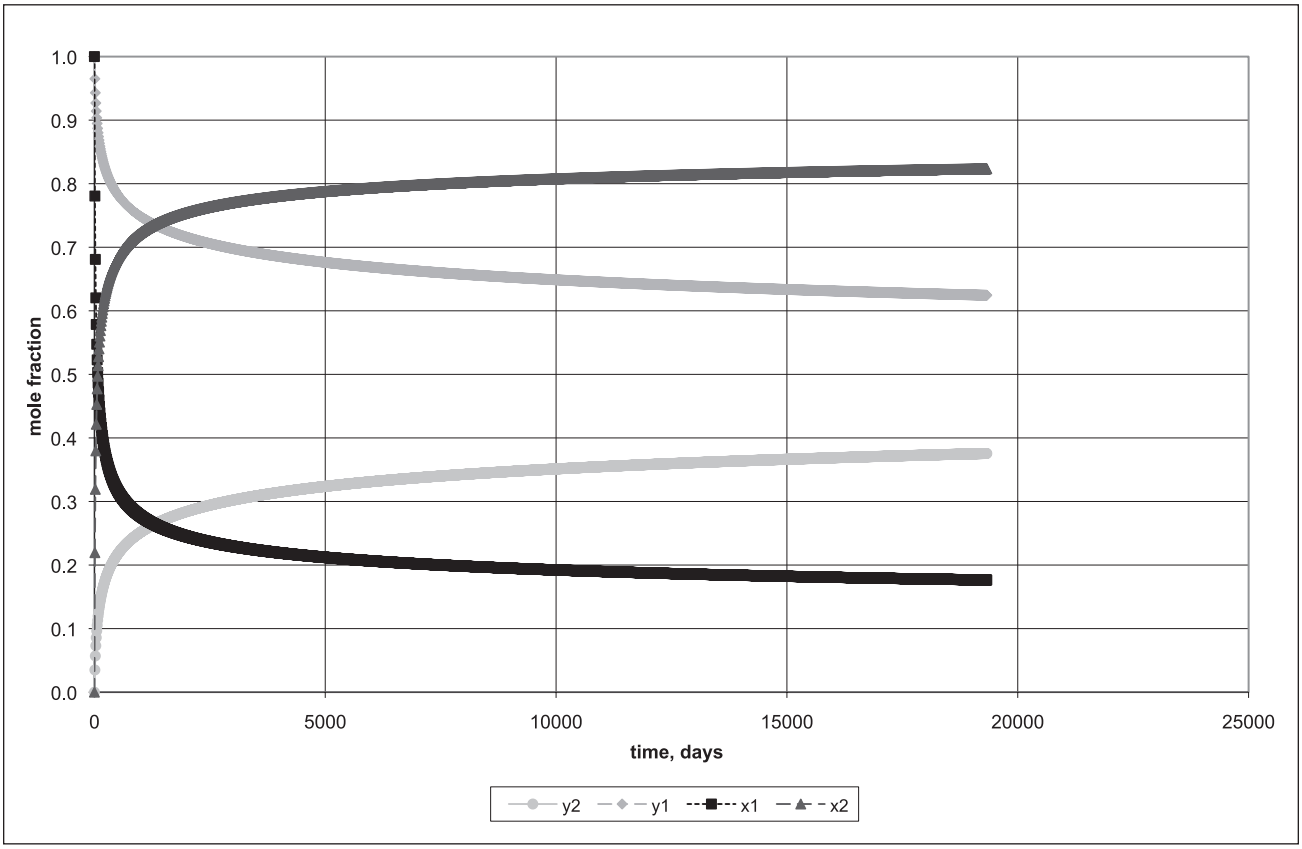



**Fig. 12–20.** Example 12.4 free and sorbed gas mole fractions vs. time

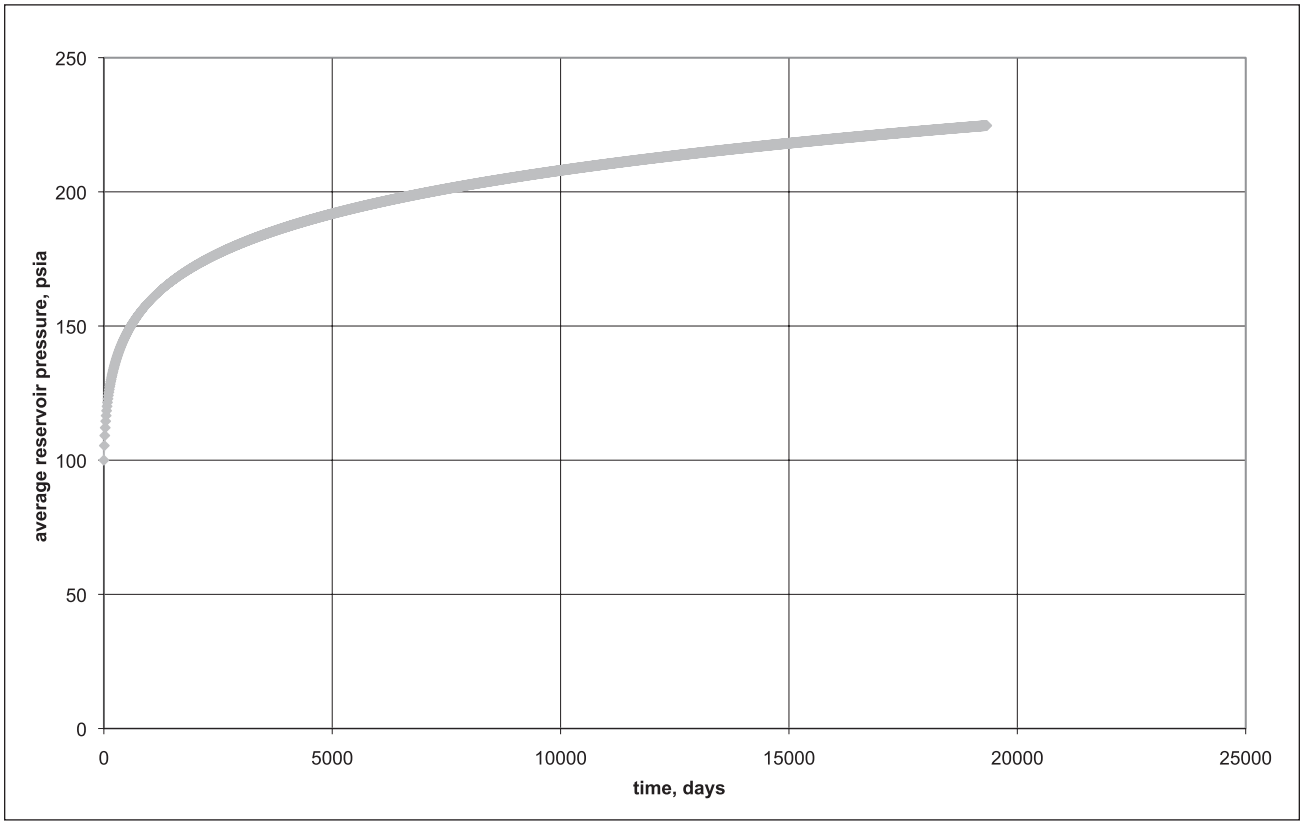



**Fig. 12–21.** Example 12.4 average reservoir pressure vs. time

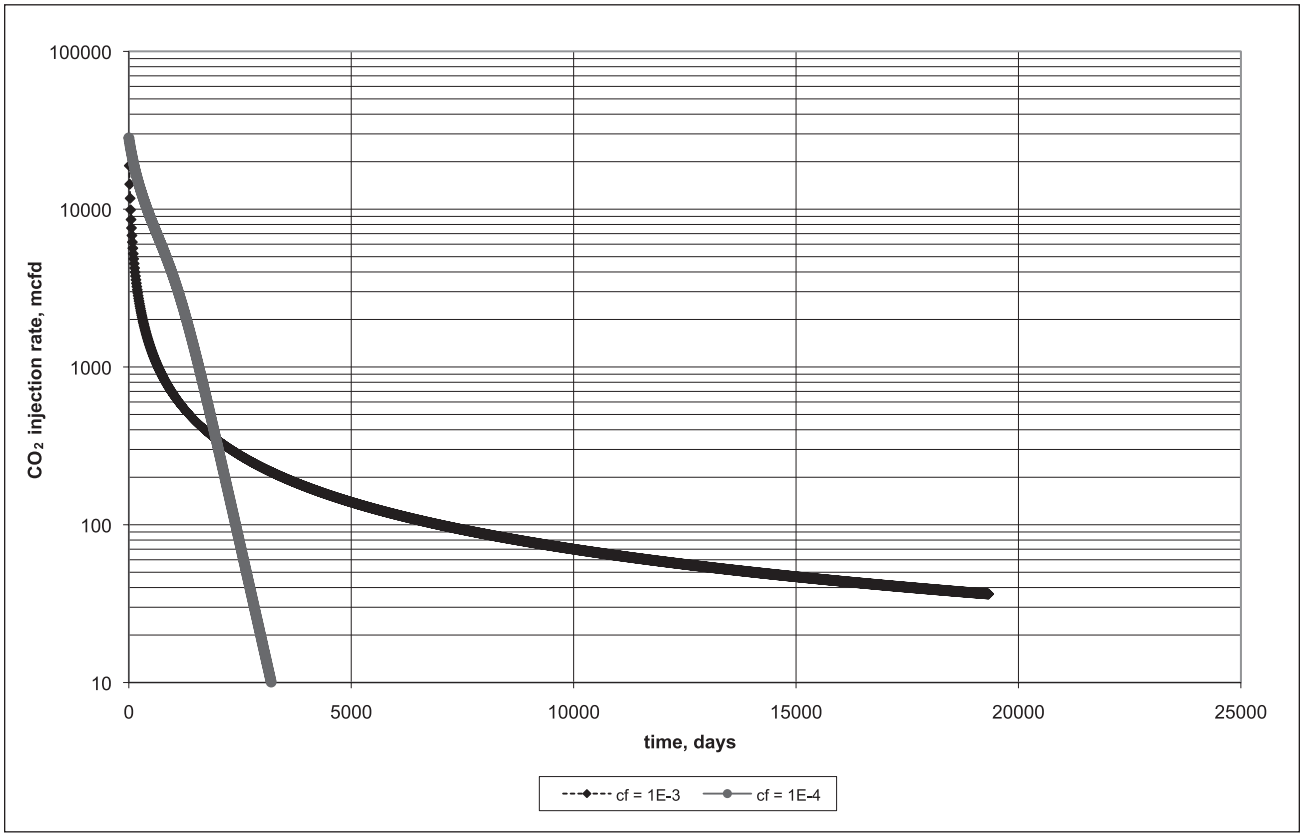



**Fig. 12–22.** Example 12.4 effect of cleat compressibility on $CO_2$ injection rate

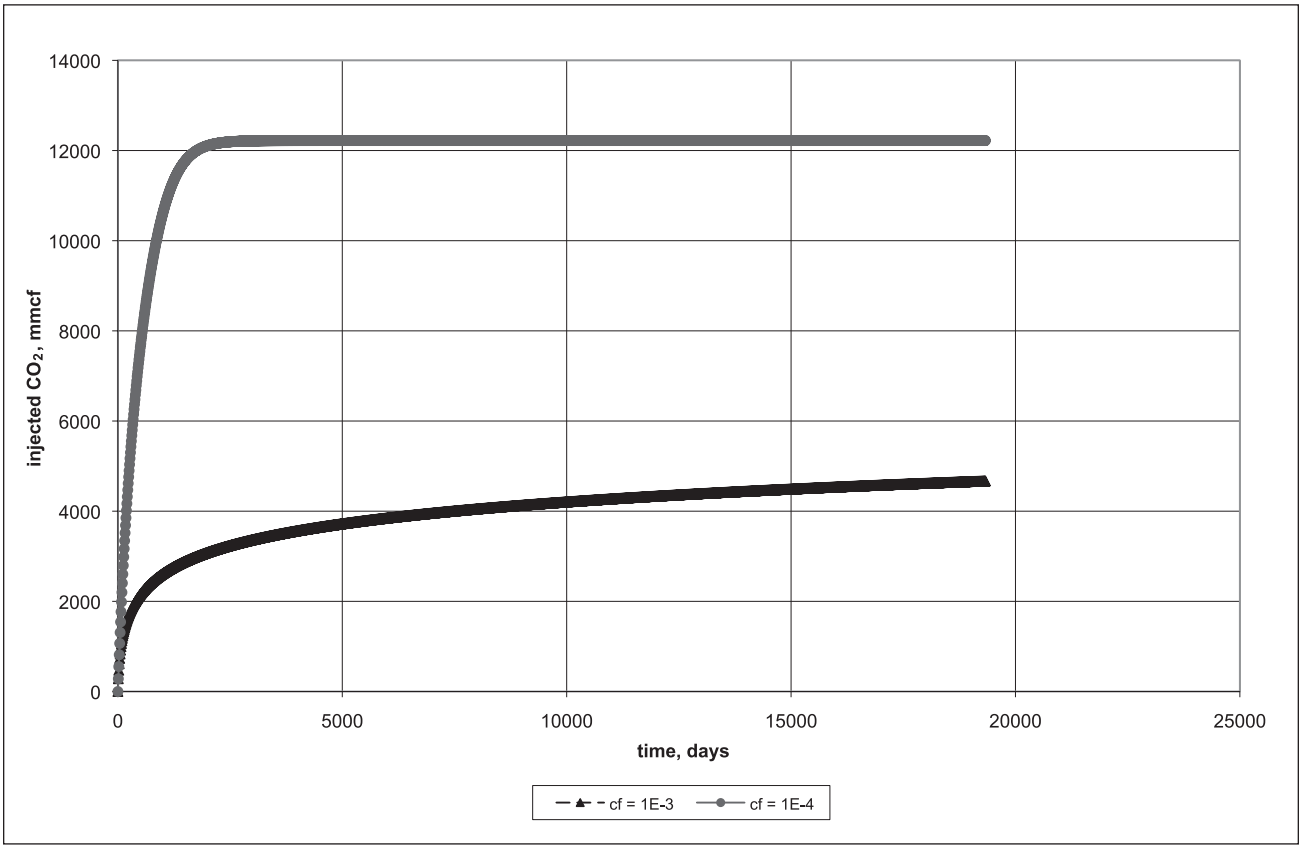



**Fig. 12–23.** Example 12.4 effect of cleat compressibility on injected $CO_2$ volume vs. time

# Nomenclature

| | |
|---|---|
| $A$ | Drainage area, ac |
| $A_c$ | Cross-sectional flow area, $ft^2$ |
| $B_g$ | Gas formation volume factor, res $ft^3$/scf |
| $B_j$ | Quadratic coefficient, equation (12.17) |
| $c_f$ | Cleat volume compressibility, $psia^{-1}$ or $Mpa^{-1}$ |
| $C_j$ | Quadratic coefficient, equation (12.18) |
| $E$ | Young's modulus, psia or MPaa |
| $E_1$ | Methane recovery efficiency |
| $E_A$ | Areal sweep efficiency |
| $E_s$ | Sequestration efficiency |
| $E_v$ | Vertical sweep efficiency |
| $f$ | Flood gas load factor, equation (12.19) |
| $G_1$ | Methane gas volume in coal, mmcf |
| $h$ | Net coal thickness, ft |
| $k$ | Absolute permeability, md |
| $K$ | Bulk modulus, psia |
| $k_g$ | Effective permeability to gas, md |
| $L$ | Distance between injection and production wells, ft |
| $\Delta L$ | Block width, ft |
| $M$ | Constrained axial modulus, psia |
| $N$ | Number of component gases or number of grid blocks |
| $n_{2,j}$ | Moles of flood gas in free gas mixture in block $j$ |
| $n_{2,new}$ | Moles of flood gas in block $j$ after a time step |
| $p$ | Total pressure, psia |
| $\overline{p}$ | Average reservoir pressure, psia |
| $p_{inj}$ | Injector bottomhole pressure, psia |
| $p_j$ | Partial pressure of component $j$ or pressure in block $j$ |
| $p_{Lk}$ | Component $k$ Langmuir pressure constant, scf/ton or $cm^3$/g |
| $p_{sc}$ | Standard pressure, psia |
| $p_{wf}$ | Producer bottomhole flowing pressure, psia |
| $p_\varepsilon$ | Pressure at a strain of 0.5 $\varepsilon_\infty$, psia or MPa |
| $q_g$ | Gas flow rate, mcfd |
| $q_{inj}$ | Gas injection rate, mcfd |
| $R$ | Universal gas constant |
| $r_e$ | Drainage radius, ft |
| $r_w$ | Wellbore radius, ft |
| $s$ | Wellbore skin factor |
| $S_{wi}$ | Irreducible water saturation, fraction |
| $T$ | Reservoir temperature, °R |
| $T_{sc}$ | Standard temperature, °R |
| $v$ | Gas velocity |
| $V_k$ | Sorbed quantity of component $k$, scf/ton or $cm^3$/g |
| $V_{Lk}$ | Component $k$ in-situ Langmuir volume constant, scf/ton or $cm^3$/g |
| $V_{norm}$ | Normalized volume |
| $V_T$ | Total gas content of the coal, scf/ton or $cm^3$/g |
| $x$ | Distance |
| $x_j$ | Sorbed gas mole fraction of component $j$ |
| $y_{2,j}$ | Flood gas mole fraction in free gas mixture in block $j$ |

$y_{2,\,conv}$ Flood gas mole fraction in free gas mixture in block *j* due to convection
$y_{2,\,new}$ New flood gas mole fraction in free gas mixture in block *j*
$y_j$ Free gas mole fraction of component *j*
$\overline{Z}$ Gas deviation factor at average pressure

## Greek

$\alpha_k$ Swelling coefficient for component *k*, $ft^3/ft^3$
$\varepsilon$ Sorption strain
$\varepsilon_\infty$ Sorption strain at infinite pressure
$\theta_j$ Sum of convected and sorbed flood gas moles in block *j*
$\overline{\mu}$ Gas viscosity at average pressure, cp
$\mu_g$ Gas viscosity, cp
$\nu$ Poisson's ratio
$\rho_B$ Bulk coal density, $g/cm^3$
$\sigma$ Stress, psia or MPaa
$\phi$ Porosity

## Subscripts

*i* Initial
*sc* Standard conditions

# References


1. Puri, R., and Yee, D. 1990. *Enhanced Coalbed Methane Recovery*. Paper SPE 20723. Presented at the Annual Technical Conference and Exhibition, New Orleans, Louisiana, September 23–26.
2. Ibid.
3. Fulton, P. F., Parente, C. A., Rogers, B. A., Shah, N. B., and Reznik, A.A. 1980. *A Laboratory Investigation of Enhanced Recovery of Methane from Coal Beds by Carbon Dioxide Injection*. Paper SPE 8930. Presented at the SPE/DOE Symposium on Unconventional Gas Recovery, Pittsburgh, Pennsylvania, May 18–21.
4. Collings, R. C. 1982. *The Feasibility of Enhanced Recovery of Methane from Coalbeds through Inert Gas Injection*. Master's thesis. University of Texas at Austin. December.
5. Reznik, A. A., Singh, P. K., and Foley, W. L. 1984. An analysis of the effect of $CO_2$ injection on the recovery of in situ methane from bituminous coal: An experimental simulation. *Society of Petroleum Engineers Journal*. V. 24 (no. 5). p. 521.
6. Puri, R., and Yee, D. 1990.
7. Harpalani, S., and Schraufnagel, R. A. 1990. *Influence of Matrix Shrinkage and Compressibility on Gas Production from Coalbed Methane Reservoirs*. Paper SPE 20729. Presented at the SPE Annual Technical Conference and Exhibition, New Orleans, Louisiana, September 23–26.
8. *Oil and Gas Journal*. 1991. Amoco plans test of nitrogen injection for coalbed methane. October 28. p. 30.
9. Arri, L. E., Yee, D., Morgan, W. D., and Jeansonne, M. W. 1992. *Modeling Coalbed Methane Production with Binary Gas Sorption*. Paper SPE 24363. Presented at the SPE Rocky Mountain Regional Meeting, Casper, Wyoming, May 18–21.
10. Greaves, K. H., Owen, L. B., McLennan, J. D., and Olszewski, A. 1993. Multi-component gas adsorption—desorption behavior of coal. Paper 9353 in *Proceedings of the 1993 International Coalbed Methane Symposium*. Tuscaloosa: University of Alabama.
11. Stevenson, M. D., Pinczewski, W. V., and Downey, R. A. 1993. *Economic Evaluation of Nitrogen Injection for Coalseam Gas Recovery*. Paper SPE 26199. Presented at the SPE Gas Technology Symposium, Calgary, Alberta, June 28–30.
12. Puri, R., Volz, R., and Duhrkopf, D. 1995. A micro-pilot approach to coalbed methane reservoir assessment. Paper 9556 in *Proceedings of the 1995 International Coalbed Methane Symposium*. Tuscaloosa: University of Alabama.
13. Stevens, S. H., Schoeling, L., and Pekot, L. 1999. $CO_2$ injection for enhanced coalbed methane recovery: Project screening and design. Paper 9934 in *Proceedings of the 1999 International Coalbed Methane Symposium*. Tuscaloosa: University of Alabama.
14. Chaback, J. J., Morgan, D., and Yee, D. 1996. *Sorption Irreversibilities and Mixture Compositional Behavior during Enhanced Coal Bed Methane Recovery Processes*. Paper SPE 35622. Presented at the Gas Technology Conference, Calgary, Alberta, April 28–May 1.
15. Chaback, J. J., et al. 1996; and Greaves, K. H., et al. 1993.
16. Chaback, J. J., Morgan, W. D., and Yee, D. 1996. Sorption of nitrogen, methane, carbon dioxide and their mixtures on bituminous coals at in-situ conditions. *Fluid Phase Equilibria*. V. 117 (no. 1–2). p. 289.
17. Seidle, J. P., and McAnear, J. F. 1995. *Pressure Falloff Testing of Enhanced Coalbed Methane Pilot Injection Wells*. Paper SPE 30731. Presented at the SPE Annual Technical Conference and Exhibition, Dallas, Texas, October 22–25.
18. Seidle, J. P., Sigdestad, C. A., Raterman, K. T., and Negahban, S. 1997. *Characterization of Enhanced Coalbed Methane Recovery Injection Wells*. Paper SPE 38861. Presented at the SPE Annual Technical Conference and Exhibition, San Antonio, Texas, October 5–8.
19. Stevens, S. H., Spector, D., and Reimer, P. 1998. *Enhanced Coalbed Methane Recovery Using $CO_2$ Injection: Worldwide Resource and $CO_2$ Sequestration Potential*. Paper SPE 48881. Presented at the SPE International Conference and Exhibition, Beijing, China, November 2–6.
20. Harpalani, S., and Schraufnagel, R. A. 1990; and Sereshki, F., Aziz, N. I., and Porter, I. 2004. Influence of gas type and pressure on permeability and volumetric characteristics of coal. Paper 0415 in *Proceedings of the 2004 International Coalbed Methane Symposium*. Tuscaloosa: University of Alabama.
21. Wolf, K-H. A. A., Hijman, R., Barzandji, O. H., and Bruining, J. 1999. Laboratory experiments and simulations on the environmentally friendly improvement of coalbed methane production by carbon dioxide injection. Paper 9905 in *Proceedings of the 1999 International Coalbed Methane Symposium*. Tuscaloosa: University of Alabama.
22. Stevens, S. H., et al. 1999.
23. Clarkson, C. R., and Bustin, R. M. 1999. The effect of pore structure and gas pressure upon the transport properties of coal: a laboratory and modeling study. 1. Isotherms and pore volume distributions. *Fuel*. V. 78. p. 1,333; and Clarkson, C. R., and Bustin, R. M. 1999. The effect of pore structure and gas pressure upon the transport properties of coal: A laboratory and modeling study. 2. Adsorption rate modeling. *Fuel*. V. 78. p. 1,345.
24. Wong, S., Gunter, W. D., and Mavor, M. J. 2000. *Economics of $CO_2$ Sequestration in Coalbed Methane Reservoirs*. Paper SPE 59785. Presented at the SPE/CERI Gas Technology Symposium, Calgary, Alberta, April 3–5.
25. Wong, S., MacLeod, K., Wold, M., Gunter, W. D., and Mavor, M. J., and Gale, J. 2001. $CO_2$-enhanced coalbed methane recovery demonstration pilot—a case for Australia. Paper 0148 in *Proceedings of the 2001 International Coalbed Methane Symposium*. Tuscaloosa: University of Alabama; Pashin, J. C., Groshong, R. H., Jr., and Carroll, R. E. 2001. Carbon sequestration potential of coalbed methane reservoirs in the Black Warrior Basin: A preliminary look. Paper 0143 in *Proceedings of the 2001 International Coalbed Methane Symposium*. Tuscaloosa: University of Alabama; and Van Bergen, F., Pagnier, H. J. M., Schreurs, H. C. E., Faaij, A. P. C., Hamelinck, C. N., Wolf, K-H. A. A., Barzandji, O. H., Jansen, D., and Ruijg, G. J. 2001. Inventory of the potential for enhanced coalbed methane production with carbon dioxide disposal in the Netherlands. Paper 0117 in *Proceedings of the 2001 International Coalbed Methane Symposium*. Tuscaloosa: University of Alabama.

26. Zhu, J., Jessen, K., Kovscek, A. R., and Orr, F. M., Jr. 2002. *Recovery of Coalbed Methane by Gas Injection*. Paper SPE 75255. Presented at the DPE/DOE Improved Oil Recovery Symposium, Tulsa, Oklahoma, April 13–17.
27. Reeves, S., and Oudinot, A. 2005. The Tiffany Unit $N_2$-ECBM Pilot—a reservoir and economic analysis. Paper 0523 in *Proceedings of the 2005 International Coalbed Methane Symposium*. Tuscaloosa: University of Alabama.
28. Liang, J., Raterman, K. T., and Robertson, E. P. 2003. A mechanistic model for $CO_2$ sequestration in Tiffany coal bed methane field. Paper 0339 in *Proceedings of the 2003 International Coalbed Methane Symposium*. Tuscaloosa: University of Alabama; and Reeves, S., and Oudinot, A. 2005. Paper 0523.
29. Stevens, S. H., et al. 1998; and Reeves, S., Taillefert, A., Pekot, L., and Clarkson, C. 2003. *The Allison Unit $CO_2$-ECBM Pilot: A Reservoir Modeling Study*. Topical Report. January 1, 2000–June 30, 2002. Award Number DE-FC26-0NT40924. U. S. Department of Energy.
30. Reeves, S., et al. 2003.
31. Reeves, S., and Oudinot, A. 2005. The Allison Unit $CO_2$-ECBM Pilot—a reservoir and economic analysis. Paper 0522 in *Proceedings of the 2005 International Coalbed Methane Symposium*. Tuscaloosa: University of Alabama.
32. Mavor, M. J., Gunter, W. D., Robinson, J. R., Law, D. H-S., and Gale, J. 2002. *Testing for $CO_2$ Sequestration and Enhanced Methane Production from Coal*. Paper SPE 75683. Presented at the SPE Gas Technology Symposium, Calgary, Alberta, April 30–May 2.
33. Pashin, J. C., and MacIntyre, M. R. 2003. Defining the supercritical phase window for $CO_2$ in coalbed methane reservoirs of the Black Warrior Basin: Implications for $CO_2$ sequestration and enhanced coalbed methane recovery. Paper 0316 in *Proceedings of the 2003 International Coalbed Methane Symposium*. Tuscaloosa: University of Alabama.
34. van Bergen, F., Pagnier, H. J. M., van der Meer, L. G. H., van den Belt, F. J. G., Winthaegan, P. L. A., and Krzystolik, P. 2003. Development of a field experiment of ECBM in the Upper Silesian Coal Basin of Poland (RECOPOL). Paper 0320 in *Proceedings of the 2003 International Coalbed Methane Symposium*. Tuscaloosa: University of Alabama.
35. Bromhal, G. S., Sams, W. N., Jikich, S., Ertekin, T., and Smith, D. H. 2004. Simulation of the effects of shrinkage and swelling on coal seam sequestration and coalbed methane production. Paper 0418 in *Proceedings of the 2004 International Coalbed Methane Symposium*. Tuscaloosa: University of Alabama.
36. Mavor, M. J., Gunter, W. D., and Robinson, J. R. 2004. *Alberta Multiwell Micro-Pilot Testing for CBM Properties, Enhanced Methane Recovery and $CO_2$ Storage Potential*. Paper SPE 90256. Presented at the SPE Annual Technical Meeting and Exhibition, Houston, Texas, September 26–29.
37. Robinson, J., Kadatz, B., Wong, S., Gunter, W., Sangli, F., and Zhiqiang, F. 2004. *ECBM Micro-Pilot Test in the Anthracitic Coals of the Qinshui Basin, China: Field Results & Preliminary Analysis*. Presented at Japan Coal Energy Center's Third International Workshop on Prospective Roles of $CO_2$ Sequestration in Coal Seams, Hokkaido University, Sapporo, Japan, October 5.
38. Siemons, N., Busch, A., Bruining, H., Krooss, B. M., and Gensterblum, Y. 2003. *Assessing the Kinetics and Capacity of Gas Adsorption in Coals by a Combined Adsorption/Diffusion Method*. Paper SPE 84340. Presented at the Annual Technical Conference and Exhibition, Denver, Colorado, October 5–8.
39. Busch, A., Krooss, B. M., and Gensterblum, Y. 2004. $CO_2$ and $CH_4$ sorption kinetics on coal: Experiments and potential application in CBM/ECBM modeling. Paper 0409 in *Proceedings of the 2004 International Coalbed Methane Symposium*. Tuscaloosa: University of Alabama.
40. Chikatamarla, L., Cui, X., and Bustin, R. M. 2004. Implications of volumetric swelling/shrinkage of coal in sequestration of acid gases. Paper 0435 in *Proceedings of the 2004 International Coalbed Methane Symposium*. Tuscaloosa: University of Alabama.
41. Palmer, I., and Mansoori, J. 1996. *How Permeability Depends on Stress and Pore Pressure in Coalbeds: A New Model*. Paper SPE 36737. Presented at the SPE Annual Technical Conference and Exhibition, Denver, Colorado, October 6–9.
42. Siriwardane, H. J., Smith, D. H., Gorucu, F., and Ertekin, T. 2006. *Influence of Shrinkage and Swelling of Coal on Production of Coalbed Methane and Sequestration of Carbon Dioxide*. Paper SPE 102767. Presented at the Annual Technical Conference and Exhibition, San Antonio, Texas, September 24–27.
43. Reeves, S., et al. 2003; and Reeves, S., and Oudinot, A. 2005. Paper 0522.
44. Reeves, S., et al. 2003.
45. Buckley, S. E., and Leverett, M. C. 1942. Mechanism of fluid displacement in sands. *Transactions*. AIME. V. 146. p. 107; and Welge, H. J. 1952. A simplified method for computing oil recoveries by gas or water drive. *Transactions*. AIME. V. 195. p. 91.
46. Craft, B. C., Hawkins, M. F., and Terry, R. E. 1991. *Applied Petroleum Reservoir Engineering*. 2nd ed. Englewood Cliffs, New Jersey: Prentice Hall; and Muskat, M. 1946. *The Flow of Homogeneous Fluids through Porous Media*. Ann Arbor, Michigan: J. W. Edwards.
47. Reeves, S., and Oudinot, A. 2005. Paper 0523; and Liang, J., et al. 2003.
48. Reeves, S., and Oudinot, A. 2005. Paper 0523.
49. Reeves, S., and Oudinot, A. 2005. Paper 0522; Arri, L. E., et al. 1992; and Pratt, T. J., Mavor, M. J., and DeBruyn, R. P. 1999. *Coal Gas Resource and Production Potential of Subbituminous Coal in the Powder River Basin*. Paper SPE 55599, presented at the SPE Rocky Mountain Regional Meeting, Gillette, Wyoming, May 15–18.
50. Arri, L. E., et all. 1992; Pratt, T. J., et al. 1999.
51. Mavor, M. J., and Gunter, W. D. 2004. *Secondary Porosity and Permeability of Coal vs. Gas Composition and Pressure*. Paper SPE 90255. Presented at the SPE Annual Technical Meeting and Exhibition, Houston, Texas, September 26–29; and Palmer, I., and Mansoori, J. 1996.
52. Shi, J. Q., and Durucan, S. 2004. A numerical simulation study of the Allison Unit $CO_2$-ECBM Pilot: The impact of matrix shrinkage and swelling on ECBM production and $CO_2$ injectivity. In *Proceedings of the 7th International Conference on Greenhouse Gas Control Technologies, Volume 1: Peer-Reviewed Papers and Plenary Presentations, IEA Greenhouse Gas Programme*. Cheltenham, UK.

# Index


## A

adsorption, 47, 125
air-dry basis, of gas content normalization, 110–111
Alberta, 15, 69
alluvial fans, 62
analogs
    construction of coal gas, 11–12, 19
    overview, 11
anthracites, 22
    coal rank of meta-, 69
    coal rank of semi-, 69
    coal reserves, 3, 4, 60–61
Appalachian Basin, isotherm variation between seams, 141
Arkoma Basin
    coal and well properties, 261
    coal well bottomhole flowing pressure, 260–262
    coal well decline curve analysis, 299–301
    horizontal well coal type curve, 10
Arkoma Basin Hartshorne coal
    cleat permeability and porosity, 159
    coal density, 27–28
    well and coal properties, 288
    wells cumulative gas production, 288, 289, 290
    wells depletion, 287–290
    wells gas production rates, 288, 289, 290
Arps, J. J., 297, 298
ash, 22. *See also* daf
    coal gas sorption and, 130–131
    density, moisture and coal organic fraction of coal, 36–39
    fraction, 23
ASTM, 19, 23, 24

## B

Barataria Basin, 64
basins
    coal permeability and, 165
    isotherm numbers and coal gas projects with, 143–145
    isotherm variation between formations in, 143, 144
bed moisture, 22
Bernard plot, for gas origin determination, 79
binary Langmuir sorption
    coalbed gas contents of two-component gas mixture and, 348–350
    in enhanced coalbed methane recovery, 348–350
    equations, 347–349
    overview, 347–348
biogenic coal gas
    coal geology and, 73, 77, 78, 79, 80
    generation, 77
    overview, 73, 77
biogenic gas
    in coal gas composition, 41, 73, 77, 78, 79, 80
    definition, 11, 73
bituminous coals, 22
    coal rank of high-volatile, 69
    coal rank of low-volatile, 69
    coal rank of medium-volatile, 69
    coal reserves, 3, 4, 60–61
bottomhole flowing pressure
    Arkoma Basin coal well, 260–262
    gas flow in coal equations, constant rate gas production, bounded drainage, and, 260–262
    gas flow in coal equations, constant rate gas production, infinite coal, and, 256–259
    gas flow in coal equations, gas production rate,, bounded drainage, and constant, 262–263
    of undersaturated Powder River Basin coal well, 264–266
    Warrior Basin coal well, 257–259
    water flow in coal and, 263–266
boundary-dominated flow, 253. *See also* pseudosteady-state flow
bounded drainage
    gas flow in coal equations, bottomhole flowing pressure, constant rate gas production, and, 260–262
    gas flow in coal equations, gas production rate,, constant bottomhole flowing pressure, and, 262–263
Bowen Basin, coal gas-water relative permeabilities, 172, 173
bulk and helium densities, 29
bulk density log, 81, 82–84
Bustin and Downey, 134, 136
butt cleats, 30, 31, 72, 156

## C

caliper logs, 81, 82, 84
carbon dioxide ($CO_2$)
  in coal gas composition, 40, 41, 43, 45, 73
  ECBM response in Powder River Basin, 370
  in enhanced coalbed methane recovery, 51, 325–326, 347, 350–354
  flooding in enhanced coalbed methane recovery, 353, 354
  mole fractions and Powder River Basin carbon dioxide isotherms, 370–371
  response in San Juan Basin Tiffany ECBM Pilot, 370
  sorption analysis, 33
  sorption isotherms for, 147–148
carbon dioxide injection
  in carbon dioxide sequestration, 352, 354, 355, 356, 372, 374, 375, 376–377, 378, 379, 380, 381
  in enhanced coalbed methane recovery, 347, 350, 351, 352, 353, 354, 356
  San Juan Basin coal, 378, 379, 380, 381
carbon dioxide isotherms
  Powder River Basin, 370–371
  San Juan Basin, 368–369
carbon dioxide sequestration, 211
  carbon dioxide injection in, 352, 354, 355, 356, 372, 374, 375, 376–377, 378, 379, 380, 381
  coal absolute permeability variation during, 372–373
  early history of, 350, 352–356
  enhanced coalbed methane recovery and, 51, 325–326, 347, 352–353, 354, 356–362, 372–373
  Greek symbols used in, 383
  linear flooding of coal deposit and, 356–362
  nomenclature, 382–383
  reservoir screening criteria for feasibility of, 352
  in San Juan coal, 376–381
  simulation, 325–326
  subscripts used in, 383
carbon dioxide sequestration, tank model
  equations, 374–376
  overview, 374–376
  San Juan Basin coal seam, 376–381
carbon/oxygen logs, 81, 82, 86
cased hole log, 81, 82, 84, 86
cell preservation index, 68
cement log, 81, 82, 86
characteristic (de)sorption time, 321
chemical contents of coal, 24
Cherokee Basin, coal type curve, 10
chi-square function ($X^2$), 25–26
  values, 27
chi-square goodness-of-fit test, 25–26
cleats, 1
  butt, 30, 31, 72, 156
  coal geology and, 72–73
  coal permeability and, 32–33, 70, 72, 155–163, 165–168, 174–175, 178
  coal rank and, 69, 72
  detection with wireline logs, 85–86
  development, 72, 86
  domains, 31
  face, 30, 31, 72, 156
  length, height and aperture, 31
  master, 31
  moderately developed, 86
  overview, 30–32, 72–73
  permeability, spacing and porosity, 32–33, 158, 159
  poorly developed cleat sections, 86
  porosity, 32–33, 36, 158, 159
  secondary, 31
  spacing, 70, 72, 156
  spacing and coal permeability, 70, 72, 158, 159
  stress and, 159
  strike, 31
  tertiary, 31
  well developed, 86
cleat compressibility, 52, 54, 159–160, 163, 165
  coal well simulation of undersaturated coal and, 335–338
  in Powder River Basin Big George coal simulation, 335–338
  San Juan Basin, 380, 381
  of selected coals, 53, 160
coal
  areas and depositional environments, 66
  fixed portions, 20
  gas saturation in, 247, 271
  grade, 19
  groups, 65
  lithotype, 72
  logs, 81
  mining, 1
  moisture content, 21, 22
  net pay, 3
  organic fraction of, 36–39
  overview, 1, 19, 60
  resources world estimates, 60–61
  sorption isotherm, 126
  thermal maturity ranks, 11
  water saturation in, 167, 247
  wireline log responses in, 82
coal absolute permeability, 155, 166, 167, 168, 172, 174
  theoretical, 156–159
  variation during carbon dioxide sequestration, 372–373
  variation during enhanced coalbed methane recovery, 372–373
coal body
  geometry, 68
  peat mires and, 67–68
  thickness and coal depositional environments, 66
  type, 68
coal cleats. *See* cleats
coal compressibility, 52–54
coal density
  Arkoma Basin Hartshorne, 27–28
  bulk, 36, 38
  coal rank and, 36, 82
  correlation *vs.* in-situ gas content, 40
  cutoffs, 3, 36
  macerals and, 37, 39
  matrix, 36
  of organic fraction, ash density and moisture density, 36–39
  overview, 36–40
  San Juan Basin Fruitland, 38–40
  wireline logs for, 81, 82, 83, 85

coal depletion of gas and water
Arkoma Basin coal wells, 287–290
coal permeability and, 272, 311–313
coal well decline curves and, 296–301
gas composition during, 301–311
gas production from dry coals and, 287–290
Greek symbols used in, 315
introduction, 271–272
negative decline and, 272, 273
nomenclature, 314–315
San Juan Basin well, 310–313
subscripts used in, 315
tank model, 272–287
undersaturated, 291–295
variable permeability, 311–313
Warrior Basin Marylee coal well, Rock Creek Project, 294–295
coal depletion tank model
equations, 272–273
overview, 272
Uinta Basin Drunkard's Wash Field Utah #25-7-6 example, 275–281
coal depletion tank model, hypothetical gas and water production profiles
coal and well parameters for isotherm sensitivities, 281
coal and well parameters for relative permeability sensitivities, 281
gas and water production rates, 283, 284, 285, 287
isotherm depletion traverse, 286
isotherm traverse, 282, 283, 284
overview, 281, 286
relative permeabilities traverse, 282, 285
Scenario A, 281, 282, 283
Scenario B, 281, 282, 283, 284
Scenario C, 281, 284, 285
Scenario D, 285, 286, 287
coal deposits
as gas reservoirs, 5, 16, 19, 59
as gas resource, 3
overview, 1, 3
worldwide, 3–5
coal deposition
rate, 61
setting, 61, 62
type, 61
coal depositional environments
alluvial fan, 62
basin variation of, 64
coal gas reservoir engineering and, 62
coal geologic ages and, 61, 69
coal geology and, 60–69
delta, 63–64
fluvial system, 63
lacustrine, 64
overview, 62
peat and, 61, 62, 63–64, 67–69
of selected coals, 65–67
shore-zone system, 64
variations and coal body thickness and areas, 66
coal distributions
coal geology and, 60–69
by geologic age, 60
by rank and location, 60
coal fundamentals, 19–53
Greek symbols used in, 55
nomenclature, 54–55
coal gas. *See also* gas and water mass balances in coals; gas flow in coal; methane; sorbed gas
analogs construction, 11–12, 19
in coal matrix, 1, 11, 13
contaminants, 43
emissions, 1
free, 3
generation *vs.* coal rank, 74
geoscience concepts, 1
industry standard coal pay cutoff, 3
overview, 1, 3
plays, 11
project characterization and required isotherm numbers, 139–145
coal gas composition
average, 45
biogenic gas in, 41, 73, 77, 78, 79, 80
carbon dioxide in, 40, 41, 43, 45, 73–74
coal gas origin and, 73–80
coal gas properties and, 40–47
coal geology and, 73–80
coal rank and, 41
contaminants, 43
ethane in, 40, 41, 45, 73, 75, 80
gas origin and, 41
$H_2S$ in, 43
heavier hydrocarbons (C2+), 40, 41, 45, 73, 75
lean gases in, 41
methane in, 40, 41, 45, 73–74, 75–77, 78, 79, 125
nitrogen in, 40, 43, 45, 73–74, 75
selected, 40
thermogenic gas in, 41, 73–77, 78, 79, 80
variation, 73
water vapor in, 43
wet gases in, 40, 45, 73
coal gas content, 11, 22. *See also* coalbed gas content
density correlation *vs.* in-situ, 40
gas composition during laboratory depletion, 306
coal gas exploitation, 59
current challenges to, 16–17
statistical nature of, 15–16
coal gas mass balance equations
coal gas reserves GRI well and, 224–227
full, 219–220
Jensen and Smith modified material balance method, 231–233
King Z* function for Powder River Basin Canyon coal, 221, 222
King Z* function for unidentified coal, 221
King Z* function simplification of full, 220–221
modified King method, 224–228
for multicomponent gases, 239–244
overview, 217–223
Powder River Basin Canyon coal gas reserves and, 227–228
reservoir properties of Powder River Basin Canyon coal and, 221–222
reservoir properties of unidentified coal and, 221
solution of, 224–228
for undersaturated coals, 238–239

coal gas origin
coal gas composition and, 73–80
coal geology and, 73–80
coal gas origin determination
Bernard plot for, 79
carbon and hydrogen isotopes in, 78–79
dryness ratio in, 79
isotopic variations in, 78–80
methane in, 78–79
coal gas pilots, 13
field operations, management focus and, 15
initial screening phases, 14
coal gas production, 5, 271. *See also* coal well gas production; gas production
coal well simulation and, 322, 327, 328–331
coalbed methane simulators development and, 322
from dry coals, 287–290
Powder River Basin Wyodak coal simulated and reported, 328–330
reduced pressure and, 347
coal gas properties
calculations, 41–45
coal gas composition and, 40–47
physical, 41, 42
pseudocritical, 43, 44
Z factor in, 41, 42, 43, 45–47
coal gas recovery. *See also* enhanced coalbed methane recovery
nitrogen and, 325
coal gas recovery factors
for multicomponent gases, 240–244
overview, 233–235
of Powder River Basin Canyon coal well, 236–237
San Juan Basin coal well abandonment pressure *vs.*, 311
of unidentified GRI well, 235–236
coal gas reservoirs, 1, 3, 16–17
as dry gas reservoirs, 41
coal gas reservoir engineering, 5
coal pay cutoff, 37
coal rank in, 3
common tests for, 29
development of, 3
emerging geoscience concepts and, 80–81
wireline logs for, 81, 82
coal gas reservoir simulators
coalbed methane simulators development and, 319
dual-porosity simulation models and, 319, 320
coal gas resources, 59
worldwide estimated, 3–5
coal gas saturation
in coal gas analog construction, 11
fully saturated, 5
undersaturation, 5, 11, 12, 16
coal gas simulators, 319
coalbed methane simulators development and, 320, 321
enhanced coalbed methane recovery and, 325
equations, 320–321
coal gas sorption. *See also* sorption
ash and moisture, daf and dmmf isotherms, and, 130–132
coal rank and, 133–134
gas content-pressure and, 125
Greek symbols used in, 151
introduction, 125
isotherm numbers and coal gas projects, 139–145
isotherms for carbon dioxide, nitrogen and other gases, 147–148
multicomponent Langmuir isotherms and, 148–149
nomenclature, 151
oversaturation and, 125, 149–150
pressure and, 125, 126
temperature and, 125, 126, 134–139
undersaturation and, 125, 146–147
coal gas sorption data
equations and, 126
Langmuir's equation and, 126–129
coal geologic ages, 11
coal depositional environments and, 61, 69
coal distributions by, 60
coal geology and, 60–69
five major, 60
coal geology
coal ages, distributions and depositional environments in, 60–69
coal cleats and, 72–73
coal gas origin and composition in, 73–80
coal rank and, 69–71
geoscience concepts for coal gas reservoir engineering and, 80–81
Greek symbols used in, 87
introduction, 59
nomenclature, 87
thermogenic and biogenic gas in, 73–80
wireline logs and, 81–87
coal inorganic components
ash, 22
moisture, 22
coal matrix. *See also* matrix
deformation due to sorption, 174–175
gas in, 1, 11, 13
overview, 174
permeability, 155, 156, 158, 167, 174, 180
strain coefficients, 174
and stress shrinkage influences on permeability, 175–180
coal organic components
fixed carbon, 22
volatile matter, 22
coal pay cutoff
coal gas reservoir engineering, 37
industry standard, 3
coal permeability, 4, 5, 15, 16
absolute permeability, 155, 156–159, 166, 167, 168, 172, 174, 372–373
basins and, 165
cleat spacing and, 70, 72, 158, 159
coal cleat, 32–33, 70, 72, 155–163, 165–168, 174–175, 178
coal matrix, 155, 156, 158, 167, 174, 180
coal porosity and, 32–33, 158, 159, 166–167, 174–180
coal seams and, 155, 156, 159, 160, 165, 166, 167, 170, 172, 173
coal well simulation and, 322–323, 325, 327
combined stress and matrix shrinkage influences on, 175–180
depletion and, 272, 311–313
depletion of variable, 311–313
depth data, 163–164

determination, 11, 17
effective, 166
fractures and, 156
gas-water relative permeabilities and, 155, 156, 166–173, 174
Greek symbols used in, 181
history matching and, 327–328
matrix deformation, sorption and, 174–175
nomenclature, 181
overview, 155–156
predicted decline with depletion, 165, 166
stress dependence on, 159–166
wireline logs and, 83, 86
coal permeability ratios, 176–180
San Juan Basin carbon dioxide sequestration, 378
coal pilots
data collection, 14
interpretation, 14
multiwell, 14, 17
coal porosity, 29
cleat, 32–33, 36, 158, 159
coal permeability and, 32–33, 158, 159, 166–167, 174–180
coal well simulation, 328
distributions *vs.* coal rank, 33, 34
dual behavior in coal well tests, 208–210
fixed carbon *vs.*, 33
fracture, 32
history matching and, 328
macerals and, 34–35
matrix, 32, 33, 36
overview, 32–36, 166–167
sorbed gas and, 35
vitrinite *vs.* total, 34–35
coal porosity ratios, 175–180
San Juan Basin carbon dioxide sequestration, 378
coal properties
deposition setting, 61, 62
deposition type, 61
nutrient supply, 61–62
peat temperature, 61, 62
plant communities, 61
redox potential, 61, 62
seven factors controlling, 61, 62
swamp acidity, 61, 62
coal rank, 3, 11
anisotropic, 69–70
anthracite, 69
chart, 20
cleats and, 69, 72
coal density and, 36, 82
coal distributions by, 60
coal gas composition and, 41
coal gas generation *vs.*, 74
coal gas sorption and, 133–134
coal geology and, 69–71
coal porosity distributions *vs.*, 33, 34
contours and structural contours, 71
cumulative gas generation *vs.*, 75
cumulative methane gas generation *vs.*, 76
gas generation and, 69, 75, 77
high, 20
high-volatile bituminous, 69
lignite, 69
low-volatile bituminous, 69
medium-volatile bituminous, 69
meta-anthracite, 69
methane daf sorption isotherms and, 134
nine, 69
overview, 19–22, 69–71
peat, 69, 71
semianthracite, 69
subbituminous, 69
thermal maturity and, 69
variation, 69–70
wireline logs and, 82, 83
coal reserves
anthracite, 3, 4, 60–61
bituminous, 3, 4, 60–61
lignite, 3, 4, 60–61
subbituminous, 3, 4, 60–61
worldwide, 3, 4, 60–61
coal reservoir, 1, 3
complexity during coalification, 64–65
geology, 59
naturally fractured, 30
physics and simulation insights, 322–323
coal reservoir properties
coal type curves, 5–10
of selected coals, 5–10
wireline logs for measuring specific, 81, 82, 83
coal rock properties
overview, 51–54
selected, 51, 52
coal sample
collection and preservation, 28–29
numbers and confidence limits, 25–28
coal seams, 1, 59, 80, 81
coal permeability and, 155, 156, 159, 160, 165, 166, 167, 170, 172, 173
gas flow in, 247–254
isotherm numbers and coal gas projects with single and multiple, 139–142
isotherm variation between, 141, 142
isotherm variation in single, 140
coal type
humic (banded), 19
overview, 19
sapropelic (unbanded), 19
coal waters, 1. *See also* water content of coal; water flow in coal
geochemistry of, 80
total dissolved solids in, 80
coal well decline curves
equations, 296–299, 301
overview, 296
coal well decline curve analysis
Arkoma Basin, 299–301
Uinta Basin Drunkard's Wash Field Utah #25-7-6, 298–299
coal well gas production
Arkoma Basin Hartshorne cumulative, 288, 289, 290
interpretation using Monte Carlo probabilistic methods and simulations, 15–16
profiles, 5
rates, 11
tests, 13–14
variability and risks, 15

coal well pressure transient tests
diagnostic fracture injection tests, 195–196
drawdown and buildup tests, 196–204
drillstem tests, 192–193
dual porosity behavior and, 208–210
Greek symbols used in, 213
injection/falloff tests, 185–192
interference tests, 210–211
introduction, 185
micropilot injectivity tests, 15, 211
nomenclature, 212–213
slug tests, 194
sorption compressibility and, 205–207
tank tests, 193–194
two-phase pseudopressures and, 207–208
coal well simulation. *See also* history matching
cleat compressibility effects in undersaturated coal, 335–338
coal gas production and, 322, 327, 328–331
coal permeability and, 322–323, 325, 327
coal porosity, 328
coalbed methane simulators development, 319–322
conventional reservoir simulation and, 319, 322, 324, 326, 327
deterministic, 323
enhanced coalbed methane recovery and carbon dioxide sequestration simulation, 325–326
gas and water production, 327, 328–330, 333, 334, 336, 337, 338, 339, 340
Greek symbols used in, 343
gridded model, 324, 331–335, 338–343
history matching and, 319, 326–331
nomenclature, 343
overview, 319
Powder River Basin, 323, 328–343
Powder River Basin Big George, 331–343
Powder River Basin Big George coal, 331–343
probabilistic, 323–325
pseudosteady-state flow and times, 341, 342
relative permeability and, 323, 328
required inputs, 326
San Juan Basin, 324
simulation insights into coal reservoir physics, 322–323
sorption time, 338–342
subscripts used in, 343
tank model, 324, 331–335, 338–343
of undersaturated coals with tank and gridded models, 331–335, 338
of undersaturation, 323, 331–335, 338
Warrior Basin, 324
coal well tests, 185. *See also* coal well pressure transient tests
dual porosity behavior in, 208–210
water production, 13–14
coal wells. *See also* horizontal wells
completion challenges, 17
Darcy flow and behavior of, 256, 341, 342
open hole logs for, 81
water in, 247
wireline logs and, 82
coalbed gas contents, 22, 23, 105
binary Langmuir sorption and, 348–350
of two-component gas mixture, 348–350
typical, 112–113
coalbed gas content determination, 25
direct methods, 93–102, 105–110
indirect methods, 93
introduction, 93
lost gas and, 102–104, 105
mass normalized gas contents and, 110–112
mud log method, 113
nomenclature, 122
number of samples in, 113–121
residual gas and, 104–105
sources of error in, 112
coalbed gas content determination, direct methods
curve fit methods, 93, 109–110
desorbed gas volumes measurement, 96–100
desorption and, 93–102
desorption data analysis, 93–94, 101–102
desorption sample collection, 94–96
desorption sampling techniques, 95–96
overview, 93–94
Smith and Williams method, 93, 106–108
U.S. Bureau of Mines (USBM) direct method, 93, 105–106
coalbed methane, 1, 73. *See also* enhanced coalbed methane recovery
horizontal wells and, 322
projects successful elements, 15
reservoirs, 3, 16
coalbed methane simulation
horizontal wells and, 322
models, 321–322
studies, 322
coalbed methane simulators development
coal gas production and, 322
coal gas reservoir simulators and, 319
coal gas simulators and, 320, 321
coalbed methane simulation models and, 321–322
dual-porosity simulation models and, 319, 321
Collings, R. C., 350
compaction, 64–65
compensated neutron log (CNI), 81, 82, 84, 85, 86
confidence limits, and sample numbers, 25–28
constant rate gas production
gas flow in coal equations, bottomhole flowing pressure, bounded drainage, and, 260–262
gas flow in coal equations, bottomhole flowing pressure, infinite coal, and, 256–259
continuous cores
desorption samples, 94, 95
overview, 94
conventional reservoir simulation
coal well simulation and, 319, 322, 324, 326, 327
history matching, 327
hydrocarbon production from, 319
coreholes, 15
correction factors (CF)
plot, 106, 107, 108
Smith and Williams, 106, 107, 108
critical point, 41
critical pressure, 41, 42
critical temperature, 41, 42
curve fit methods, 93
Amoco method, 109–110
Chase method, 109

desorption data and, 109–110
overview, 109

## D

daf (dry, ash-free)
basis of gas content normalization, 110, 111, 112
coal gas sorption and, 130–132
coal rank impact on methane daf sorption isotherms, 134
fractions and dmmf fractions comparison, 24
methane sorption isotherms, 140
Darcy flow
characteristic times for, 255–256
coal well behavior and, 256, 341, 342
Darcy's law, 73, 247
decline curve analysis, 1
deltas
coal depositions in, 63–64
fluvial-dominated, 63–64
tide-dominated, 63
wave-dominated, 63
depletion. *See also* coal depletion
coal permeability and predicted decline with, 165, 166
depressuring, 1, 5
dewatering interplay with, 272
desorbed gas, 94, 101
sample of cumulative, 101
desorbed gas fraction, 47–48
desorbed gas function, dimensionless, 48
desorbed gas volumes, 94
measurement, 96–100, 101
desorption, 125
characteristic time, 321
decline curve sample, 109
direct methods of coalbed gas content determination, and, 93–102
exponential gas release model of, 49–51
overview, 47–51
times, 50–51
unipore spherical coal particles model of, 49–51
desorption canisters
conventional, 98
overview, 95, 96, 97
sidewall core, 97, 98
whole core, 96, 97
desorption data
analysis, 93–94, 101–102
curve fit methods and, 109–110
set, 99–100
desorption pressure, 84–85, 291
log, 81, 82
desorption samples
collection, 94–96
continuous core, 94, 95
conventional whole core, 94, 95
drill cuttings, 94–95, 96
gas content uncertainty *vs.* numbers of, 115, 116, 117
numbers and types of needed, 113–121
pressure core, 95
sidewall core, 94, 96
techniques, 95–96
whole core, 93, 94, 95, 96, 114
wireline retrieved core, 94, 95
desorption tests, 3, 14, 29
apparatus development, 98
deterministic coal well simulation, 323
dewatering, 1, 5, 271. *See also* depletion
depressuring interplay with, 272
diagnostic fracture injection tests (DFITs), 195–196
diffusivity, 48, 102
dimensionless desorbed gas function, 48
dimensionless time, 47, 48, 50
direct methods
coalbed gas content determination, 93–102, 105–110
overview, 105
U.S. Bureau of Mines, 93, 105–106
distinct markers, 3
dmmf (dry, mineral-matter free)
basis of gas content normalization, 110, 111
coal gas sorption and, 130–132
fractions and daf fractions comparison, 24
Langmuir isotherms, 132
drainage. *See* bounded drainage
drawdown and buildup tests, 196–200
pressure buildup test example, 200–204
drill cuttings
desorption samples, 94–95, 96
in Smith and Williams method, 106, 107
drilling breaks, 3
drillstem tests (DSTs), 192–193
recommended flow and shut-in times, 192
dry, with-ash basis, of gas content normalization, 110
dry ash weight fraction, 37
reciprocal dry density *vs.*, 39
dry coals, 5
depletion of Arkoma Basin coal wells, 287–290
gas production from, 287–290
testing, 15
Z* function for, 287
dry gas reservoirs, 41
dryness ratio, 79
dual-porosity simulation models
coal gas reservoir simulators and, 319
coalbed methane simulators development and, 319, 321
Warren and Root, 319, 320
Dubinin equation, 136, 137, 139
Dubinin-Astakhov equation, 135
Dubinin-Radushkevich equation, 135, 137, 139

## E

effective porosity, 35
enhanced coalbed methane (ECBM) recovery, 211
binary Langmuir sorption and, 348–350
carbon dioxide breakthrough and Langmuir pressure, 366–372
carbon dioxide flooding in, 353, 354
carbon dioxide in, 51, 325–326, 347, 350–354
carbon dioxide injection in, 347, 350, 351, 352, 353, 354, 356
carbon dioxide sequestration and, 51, 325–326, 347, 352–353, 354, 356–362, 372–373
coal absolute permeability variation during, 372–373
coal gas simulators and, 325

early history of, 350–356
Greek symbols used in, 383
linear flooding of coal deposit and, 356–372
nitrogen flooding in, 351, 353, 354, 362, 366, 370, 372, 373
nitrogen fraction in, 351, 363–365
nitrogen in, 325, 347, 348, 349, 350, 351, 352, 353, 354, 355, 356, 362–366, 370, 372, 373
nitrogen injection in, 351, 352, 353, 356, 372, 373
nomenclature, 382–383
overview, 325, 347
Powder River Basin, 366–367, 370–372
reservoir screening feasibility criteria of, 352
San Juan Basin, 362–369
San Juan Basin Tiffany ECBM Pilot, 362–366
simulation, 325–326
subscripts used in, 383
two-component gas mixture and, 347, 348–350
equilibrium moisture, 22, 23, 25
estimated ultimate recovery (EUR), 288
ethane, in coal gas composition, 40, 41, 45, 73, 75, 80
exinites, 29

## F

face cleats, 30, 31, 72, 156
falloff tests, 185–186
coal well prefrac falloff test, 187–192
faults, 65
fixed carbon (FC), 22
coal porosity *vs.*, 33
flooding
enhanced coalbed methane recovery and carbon dioxide, 353, 354
enhanced coalbed methane recovery and nitrogen, 351, 353, 354, 362, 366, 370, 372, 373
linear flooding of coal deposit, 356–372
flow. *See also* gas flow; pseudosteady-state flow; water flow in coal
capacity, 59
Darcy, 255–256, 341, 342
fluvial systems, 63
formation
compressibility, 52
imaging logs, 81, 82, 86
Formation Micro Imager (FMI), 82, 86
Formation Microscanner (FMS), 82, 86
fractures. *See also* cleats
coal permeability and, 156
coal porosity of, 32
fold-related, 65
natural, 30–31
regional, 65
spacing, 31
systems, 30
fracturing, 64, 65
free gas, 73, 247
composition during depletion of San Juan Basin coal well, 310
composition during laboratory depletion, 309
mole fractions *vs.* time in San Juan Basin carbon dioxide sequestration, 379
Fruitland coal. *See* San Juan Basin Fruitland coal
fully saturated coal, 5, 291

## G

gamma ray log, 81, 82, 84, 85, 86
gas, 1
compressibility and sorption compressibility, 205, 206
diffusion, 47
dryness indices, 40
gravity, 41
wet, 40, 45, 73
gas composition during depletion
equations, 301–309
overview, 301
of San Juan Basin coal well, 310–311
gas composition during laboratory depletion
equations, 305–309
free gas composition, 309
gas contents and Langmuir isotherms, 306
overview, 305
gas content. *See also* coal gas content
calculated and measured, 137–139
coal density correlation *vs.* in-situ, 40
Great Divide Basin depth *vs.*, 118, 119, 120, 121
linearized plot of, 129
sidewall core measured, 116
uncertainty *vs.* numbers of desorption samples, 115, 116, 117
Warrior Basin Marylee coal, 292
wireline logs for, 83
gas content normalizations
air-dry basis, 110–111
dry, ash-free basis (daf), 110, 111, 112
dry, mineral-matter free (dmmf) basis, 110, 111
dry, with-ash basis, 110
in-situ basis, 110, 112
moist, ash-free basis, 110
"pure coal" basis, 110, 111
seven bases, 110–112
gas content-pressure
coal gas sorption and, 125
Langmuir's equation and, 125
sorption isotherm as, 126
gas desorption. *See* desorption
gas flow, 73
in coal seams, 247–254
gas flow in coal equations
bottomhole flowing pressure, constant rate gas production, bounded drainage, and, 260–262
bottomhole flowing pressure, constant rate gas production, infinite coal, and, 256–259
gas production rate, constant bottomhole flowing pressure, bounded drainage, and, 262–263
gas production rate, pseudosteady-state flow and, 262
Greek symbols used in, 267
nomenclature, 267–268
overview and development, 247–254
pseudosteady-state flow in, 253–254, 256, 262
real gas pseudopressure and, 247, 250, 256, 257, 258, 259, 260, 262

sorption, Darcy flow characteristic times, and, 255–256
subscripts used in, 267–268
gas generation
coal rank and, 69, 75, 77
coal rank *vs.* coal, 74
coal rank *vs.* cumulative, 75
methane, 74–77
gas mobility, 1, 271
gas per gram ($cm^3/g$), 93
gas production. *See also* coal gas production; gas and water production
negative decline and, 271
of undersaturated coals, 272
gas production rate, 1. *See also* constant rate gas production; gas and water production rates
Arkoma Basin Hartshorne coal wells, 288, 289, 290
gas flow in coal equations, constant bottomhole flowing pressure, bounded drainage, and, 262–263
gas flow in coal equations, pseudosteady-state flow, and, 262
variability in, 15
gas rates, 1. *See also* gas production rate
Gas Research Institute (GRI), 29, 95
Gas Research Institute coal well
coal gas recovery factor, 235–236
Jensen and Smith modified material balance method applied to, 231–232
King method applied to, 224–227
modified King method applied to, 229–230
gas reservoirs, 1. *See also* coal gas reservoirs
coal deposits as, 5, 16, 19, 59
dry, 41
engineering equations for conventional, 73
gas resources, 1
coal, 3–5, 59
conventional oil and gas, 4
gas saturation
in coal, 247, 271
definitions, 84
log, 84–85
gas and water mass balances in coals
coal gas mass balance equation and, 217–228
coal gas recovery factor and, 233–237
gas mass balance equation for multicomponent gases, and, 239–244
gas mass balance equation for undersaturated coals, and, 238–239
Greek symbols used in, 245
Jensen and Smith modified material balance method and, 231–233
modified King method and, 228–231
nomenclature, 245
subscripts used in, 245
gas and water production
coal well simulation of, 327, 328–330, 333, 334, 336, 337, 338, 339, 340
hypothetical profiles using coal depletion tank model, 281–287
Powder River Basin Wyodak coal well simulation of, 328–330, 333, 334, 336, 337, 338, 339, 340
Uinta Basin Drunkard's Wash Field Utah #25-7-6, 275, 277–281
Warrior Basin Marylee coal Rock Creek Project cumulative, 294, 295
gas and water production rates
Uinta Basin Drunkard's Wash Field Utah #25-7-6, 277, 278, 279, 280
using coal depletion tank model, 283, 284, 285, 287
Warrior Basin Marylee coal Rock Creek Project, 294, 295
gas-water relative permeabilities of coal, 155, 156, 174
measurement, 167–172
overview, 166–173
testing, 167
Uinta Basin Drunkard's Wash Field Utah #25-7-6, 276
gelification index (GI), 68
geology. *See also* coal geology
coal gas project characterization and complexity of, 143
geometry, matchstick, 156
geoscience concepts
coal gas, 1
coal gas reservoir engineering and emerging, 80–81
G-function tests, 195. *See also* diagnostic fracture injection tests
grain density, 36
Great Divide Basin
gas content *vs.* depth, 118, 119, 120, 121
measured gas contents, 118
Greek symbols usage
carbon dioxide sequestration, 383
coal depletion of gas and water, 315
coal fundamentals, 55
coal gas sorption, 151
coal geology, 87
coal well pressure transient tests, 213
coal well simulation, 343
enhanced coalbed methane recovery, 383
gas and water flow in coals, 267
gas and water mass balances in coals, 245
gridded model simulations, 324, 331–335, 338–343
groundwater index, 68


## H


$H_2S$, 43
half-saturation pressure, 126
heavier hydrocarbons (C2+), 40, 41, 45, 73, 75
helium density, 36
history matching
coal permeability and, 327–328
coal porosity and, 328
coal well simulation and, 319, 326–331
conventional reservoir simulation, 327
equations, 327–328
Powder River Basin Wyodak coal wells, 328–330
relative permeability and, 328
simulated and actual production comparisons, 327, 328–330
hole logs, 81, 82, 84, 85, 86
horizontal wells, 16
coalbed methane and, 322
coalbed methane simulation and, 322
Horseshoe Canyon, 15, 16
coal type curve, 9
probabilistic coal well simulation, 325
humic (banded) coal type, 19

humitites, 29
Al-Hussainy, R., 247, 250, 252
hydrocarbons
heavier, 40, 41, 45, 73, 75
plays, 11
production from conventional reservoir simulation, 319

## I

Illinois Basin, coal gas and sorption compressibilities, 205, 206
improved moisture, 23
indirect methods, of coalbed gas content determination, 93
inertinite macerals, 29
in-gauge hole log, 81, 82
inherent moisture, 22, 23, 25
injection. *See also* carbon dioxide injection
enhanced coalbed methane recovery and nitrogen, 351, 352, 353, 356, 372, 373
injection/falloff tests, 185–186. *See also* diagnostic fracture injection tests
coal well prefrac falloff test, 187–192
injectivity tests, micropilot, 15, 211
in-situ basis of gas content normalization, 110, 112
in-situ coal, 22
in-situ coalbed gas contents
coal density correlation *vs.*, 40
typical, 112–113
in-situ isotherms, 126, 144, 145
Powder River Basin, 367
San Juan Basin, 363, 367
Uinta Basin Drunkard's Wash Field Utah #25-7-6, 276
in-situ moisture, 22
interference tests, 210–211
International Organization for Standardization, 20
International Union of Pure and Applied Chemistry (IUPAC), 34
isotherm, 126. *See also* in-situ isotherms; sorption isotherms
coal and well parameters for sensitivities in, 281
data for San Juan Basin, Fruitland coal, 143, 145
high, low and average, 143, 144
methane, 139, 142, 143, 145, 150
traverses using coal depletion tank model, 281, 282, 283, 284, 286
variation between basin formations, 143, 144
variation between seams, 141, 142
variation in single seam, 140
isotherm equations, 126. *See also* Langmuir's equation
isotherm numbers required for characterization of coal gas projects
with basins, 143–145
geologic complexity and, 143
with multiple seams, 141–142
overview, 139
with single seam, 139–141

## J

Jensen and Smith modified material balance method
coal gas reserves GRI coal well and, 231–232
overview, 231
Powder River Basin Canyon coal well and, 232–233

## K

King method
coal gas reserves GRI well and, 224–227
modified, 224–225, 229–231
Powder River Basin Canyon coal gas reserves and, 227–228
King Z* function. *See also* Z* function
simplification of full coal gas mass balance equation, 220–221
King Z* function applications
to Powder River Basin Canyon coal, 221, 222
to unidentified coal, 221

## L

lacustrine environments, 64
Langmuir isotherms, 38, 128
dmmf, 132
gas composition during laboratory depletion, 306
methane sorption data and, 126, 127, 129
multicomponent (extended), 148–149
Langmuir pressure
constant as half-saturation pressure, 126
ECBM carbon dioxide breakthrough and, 366–372
Powder River Basin Canyon coal well, 232
Langmuir sorption, binary. *See* binary Langmuir sorption
Langmuir's equation, 73, 247
coal gas sorption data and, 126–129
gas-content pressure and, 125
overview, 126–129
Laterolog, 81, 82, 86
lean gases, 41
Lee, J., 196, 197
lignites, 22
coal rank, 69
coal reserves, 3, 4, 60–61
linear flooding of coal deposit
carbon dioxide sequestration and, 356–362
discretization of linear flow path between injector and producer, 358
enhanced coalbed methane recovery and, 356–372
equations, 356–362
Langmuir pressure, ECBM carbon dioxide breakthrough, and, 366–372
overview, 356
Powder River Basin, 366–367, 370–372
San Juan Basin, 362–369
San Juan Basin Tiffany ECBM Pilot, 362–366
liptinite macerals, 29
lost gas, 94
coalbed gas content determination and, 102–104, 105
plot sample, 103
lost time ratio (*LTR*), 106, 108

## M

macerals
coal density and, 37, 39
coal porosity and, 34–35
composition of selected coals, 30
inertinite, 29
liptinite, 29

overview, 29
vitrinite, 29, 34–35
mass balance equations
coal gas, 217–233, 238–244
overview, 217
master cleats, 31
matchstick geometry, 156
matrix. *See also* coal matrix
coal density, 36
porosity, 32, 33, 36
methane. *See also* coalbed methane
in coal gas composition, 40, 41, 45, 73–74, 75–77, 78, 79, 125
in coal gas origin determination, 78–79
daf sorption isotherms and coal rank, 134
isotherms, 139, 142, 143, 145, 150
sorption data and Langmuir isotherm, 126, 127, 129
sorption isotherms, 139, 140, 350
sorption isotherms on daf basis, 139, 140
methane gas generation
coal rank *vs.* cumulative, 76
volatile matter and, 75–77
microlog, 81, 82, 85–86
micropilot tests, 325
micropilot injectivity, 15, 211
mining industry, 3
mobile water porosity, 32, 36, 167, 326
modified King method
coal gas reserves GRI well and, 229–230
overview, 224–225
Powder River Basin Canyon coal well and, 230–231
moist, ash-free basis, of gas content normalization, 110
moisture. *See also* water
bed, 22
coal gas sorption and, 130–131
content of coal, 21, 22
density, ash and coal organic fraction density, 36–39
equilibrium, 22, 23, 25
holding capacity, 22
improved, 23
inherent, 22, 23, 25
in-situ, 22
Monte Carlo simulation methods
coal well gas production and, 15–16
probabilistic coal well simulation using, 15–16, 324–325
mud log, 81
method for coalbed gas content determination, 113
multicomponent gases
coal gas mass balance equation for, 239–244
recovery and San Juan Basin Fruitland coal wells, 242–244
recovery factor for, 240–244


## N


National Coal Board of the UK, 20
negative decline, 1
coal depletion and, 272, 273
gas production and, 271
rapid and slow, 2
Uinta Basin example of coal well, 271
nitrogen
in coal gas composition, 40, 43, 45, 73–74, 75
coal gas recovery and, 325
daf sorption isotherms, 147
ECBM response in Powder River Basin, 370
enhanced coalbed methane recovery and, 325, 347, 348, 349, 350, 351, 352, 353, 354, 355, 356, 362–366, 370, 372, 373
flooding in enhanced coalbed methane recovery, 351, 353, 354, 362, 366, 370, 372, 373
injection in enhanced coalbed methane recovery, 351, 352, 353, 356, 372, 373
load factor in San Juan Basin Tiffany ECBM Pilot, 365, 366
response in San Juan Basin Tiffany ECBM Pilot, 370
sorption isotherms, 147, 350
nitrogen fraction
in enhanced coalbed methane recovery, 351, 363–365
mole fraction of San Juan Basin Tiffany ECBM Pilot, 364
nomenclature
carbon dioxide sequestration, 382–383
coal depletion of gas and water, 314–315
coal fundamentals, 54–55
coal gas sorption, 151
coal geology, 87
coal well pressure transient tests, 212–213
coal well simulation, 343
coalbed gas content determination, 122
enhanced coalbed methane recovery, 382–383
gas and water flow in coals, 267–268
gas and water mass balances in coals, 245


## O


open hole log, 81, 82, 84, 86
organic fraction of coal, 36–39
oversaturation
apparent, 149–150
coal gas sorption and, 125, 149–150


## P–Q


Palmer-Mansoori porosity and permeability equations, 175–180, 373
Mavor and Gunter extension of, 373
partial pressure, 347
pay cutoff density, 83
peat
coal depositional environments and, 61, 62, 63–64, 67–69
coal rank, 69, 71
deposit rate and compressibility, 61
temperature, 61, 62
peat mires
coal bodies and, 67–68
planar, 67
raised or domed, 67
permeability. *See also* coal permeability; relative permeability
absolute, 155
definition, 59, 155
effective, 166
traverses, 281, 282, 285, 286
Piceance Basin, 5, 6, 31, 63
pilot testing, 14–15
Poisson's ratio, 51, 52
pore diameter, 32

pore volume compressibilities, 53
porosity. *See also* coal porosity; water porosity
effective, 35
wireline logs and, 86–87
Powder River Basin, 5, 6, 51, 59
bottomhole flowing pressure of undersaturated coal well in, 264–266
carbon dioxide isotherms, 370–371
carbon dioxide load factor and methane recovery factor *vs.* carbon dioxide mole fraction at producer, 371
carbon dioxide load factor and methane recovery factor *vs.* time, 371
carbon dioxide mole fraction in free gas *vs.* distance, 370
carbon dioxide mole fraction in produced gas *vs.* time, 371
coal and well properties, 367
coal depositional environment, 63, 65, 66
coal gas and sorption compressibilities, 205, 206
coal well simulations, 323, 328–343
daf methane sorption isotherms, 139, 140
Dietz 3 coal sample temperature and sorption isotherms, 134, 135, 136–139
ECBM carbon dioxide breakthrough and Langmuir pressure, 366–367, 370–372
enhanced coalbed methane recovery, 366–367, 370–372
high, low and average isotherms, 143, 144
in-situ sorption isotherms, 367
linear flooding of coal deposit, 366–367, 370–372
nitrogen and carbon dioxide ECBM response, 370
pseudosteady-state flow, 253, 254
sorption time, 255, 256
undersaturated coal and well properties, 264
Powder River Basin Big George coal
type curve, 9
well simulations, 331–343
Powder River Basin Big George coal well simulations
average reservoir pressure, 334, 337, 339, 340
average water saturation, 335, 338, 339, 341
cleat compressibility effects, 335–338
cumulative gas and water production, 334, 337, 339, 340
data, 338
gas and water production rates, 333, 336, 338, 339
sorption time, 338–343
time to pseudosteady-state flow, 341, 342
typical reservoir and well parameters, 331
using tank and gridded models, 331–335, 338–343
Powder River Basin Canyon coal
King method applied to gas reserves of, 227–228
King Z* function applied to, 221, 222
reservoir properties, 221–222
Powder River Basin Canyon coal well
coal gas recovery factor, 236–237
Jensen and Smith modified material balance method applied to, 232–233
Langmuir pressure for, 232
modified King method applied to, 227–228
Powder River Basin Wyodak coal
gas-water relative permeabilities, 172
simulated and reported gas profiles, 330
type curve, 8
wells comparison of simulated and actual production, 328–330
prefrac pressure falloff test
data, 187, 188
example, 187–192
log-log plot, 187, 189
plot of pressure data, 187, 189
semilog plot, equivalent time, 190, 191
semilog plot, Horner time, 190
pressure buildup test example
Cartesian plot, 201, 202
gas properties, 201
log-log plot of real gas pseudopressure difference, 201, 202
San Juan Basin Rincon Unit, 200–204
semilog plot, 203
summary of analyses, 204
test data, 200
pressure core desorption samples, 95
pressure falloff tests, 185. *See also* injection/falloff tests
pressure transient tests, 14. *See also* coal well pressure transient tests
pressure-gas content. *See* gas content-pressure
probabilistic coal well simulation
deterministic coal well simulation and, 323
Horseshoe Canyon, 325
Monte Carlo methods, 15–16, 324–325
production logs, 81, 86
proximate analysis, 29
overview, 22–25
wireline logs for, 81, 83
pseudocritical pressure, 42, 43
pseudocritical temperature, 42, 43
pseudosteady-state flow
coal well simulation of, 341, 342
gas flow in coal equations, gas production rate, and, 262
gas flow in coal equations and, 253–254, 256, 262
overview, 253
Powder River Basin Big George coal well simulation time to, 341, 342
time to reach, 253–254, 256, 341, 342
"pure coal" basis, of gas content normalization, 110, 111

## R

Raton Basin
isotherm variation between Vemejo and Raton formations in, 143, 144
Vemejo coal type curve, 8
Vemejo moisture and, 131
real gas law, 41
real gas pseudopressure
difference, 201
gas flow in coal equations and, 247, 250, 256, 257, 258, 259, 260, 262
Warrior Basin coal, 258
reciprocal dry density, 37
dry ash weight fraction *vs.*, 39
reciprocal time plot, 104–105
reduced Kitchoff equation, 136, 137, 139
reduced pressure, 41, 42
coal gas production and, 347
reduced temperature, 41, 42
relative permeability, 155, 166. *See also* gas-water relative permeabilities of coal
coal and well parameters for sensitivities in, 281

coal well simulation of, 323, 328
history matching and, 328
testing, 167
reservoirs. *See also* coal reservoir; gas reservoirs
screening feasibility criteria of carbon dioxide sequestration, 352
screening feasibility criteria of enhanced coalbed methane recovery, 352
reservoir engineering, 1. *See also* coal gas reservoir engineering
reservoir pressure
Powder River Basin Big George coal simulation average, 334, 337, 339, 340
San Juan Basin average, 380
reservoir simulation, 1. *See also* coal well simulation; conventional reservoir simulation
residual gas
coalbed gas content determination and, 104–105
definition and overview, 94, 104
resistivity log, 81, 82, 85
response time, 50
rock properties tests, 29

## S

San Juan Basin, 5, 6, 13, 31, 134
apparent oversaturation, 150
average reservoir pressure *vs.* time, 380
carbon dioxide injection rate *vs.* time, 378
carbon dioxide isotherms, 368–369
carbon dioxide sequestration, 376–381
Cedar Hill methane isotherms, 139, 142
cleat compressibility and carbon dioxide injection rate, 380
cleat compressibility and injected carbon dioxide volume *vs.* time, 381
coal and well properties, 367
coal depositional environment, 65, 66
coal type curve, 7
coal well simulation, 324
cumulative carbon dioxide injected *vs.* time, 379
dmmf Langmuir isotherms, 132
ECBM carbon dioxide breakthrough and Langmuir pressure, 366–369
enhanced coalbed methane recovery, 362–369
free and sorbed gas mole fractions *vs.* time, 379
ICM model stress-permeability coefficients, 178
in-situ sorption isotherms, 363, 367
isotherm variation between seams, 141, 142
linear flooding of coal deposit, 362–369
Palmer-Mansoori and ICM permeability and porosity ratios, 177, 178–180
permeability and porosity ratios *vs.* time, 378
pseudosteady-state flow, 253–254
reservoir and well properties, 377
sorption time, 255
undersaturated coal, 146
vitrinite reflectance *vs.* distance, 70–71
San Juan Basin coal well
coal properties, 310, 313
depletion, 310–313
free gas composition during depletion, 310
gas composition during depletion, 310–311
gas profiles, 312
recovery factors *vs.* abandonment pressure, 311
San Juan Basin Fruitland coal
coal density, 38–40
gas-water relative permeabilities of, 168–169
in-situ methane isotherms, 143, 145
isotherm data, 143, 145
methane sorption data and Langmuir isotherm, 126, 127, 129
multicomponent gas recovery, 242–244
Palmer-Mansoori coefficients, 176
single seam isotherm variation, 140
San Juan Basin Tiffany ECBM Pilot
coal and well properties, 362
enhanced coalbed methane recovery, 362–366
in-situ sorption isotherms example, 363
nitrogen and carbon dioxide response in, 370
nitrogen load factor and methane recovery *vs.* nitrogen mole fraction at producer, 365
nitrogen load factor and methane recovery *vs.* time, 366
nitrogen mole fraction in free gas *vs.* distance, 364
nitrogen mole fraction in produced gas *vs.* time, 364
sapropelic (unbanded) coal type, 19
saturated coal, 291
secondary cleats, 31
seismic reflectors, 3
seismic technologies, 80–81
shore-zone systems
backbarrier settings in, 64
coal depositions in, 64
tidal flat settings in, 64
sidewall core (SWC)
desorption canisters, 97, 98
desorption samples, 94, 96
measured gas contents, 116
Silesian Basin, 14
simulation of coal well performance. *See* coal well simulation
slug tests, 194
Smith and Williams method, 93
correction factors, 106, 107, 108
drill cuttings in, 106, 107
overview, 106–107
sonic log, 81, 82, 84
sorbed gas, 1, 3, 5, 73, 271, 272
coal porosity and, 35
mole fractions *vs.* time in San Juan Basin carbon dioxide sequestration, 379
sorption, 3, 47, 125. *See also* coal gas sorption
binary Langmuir, 347–350
capacity, 5
characteristic times for, 255–256
matrix deformation due to, 174–175
sorption compressibility, 53
coal well pressure transient tests and, 205–207
gas compressibility and, 205, 206
sorption data
coal gas, 126–129
methane, 126, 127, 129
sorption equations, 126. *See also* Langmuir's equation
sorption isotherms, 14, 29
for carbon dioxide, nitrogen and other gases, 147–148
coal, 126
daf methane, 139, 140

gas content-pressure as, 126
in-situ, 126, 144, 145
measurement, 126
methane, 139, 140, 350
nitrogen, 147, 350
nitrogen daf, 147
San Juan Basin in-situ, 363, 367
temperature impact on, 134, 135, 136–139
Warrior Basin Marylee coal, 292
sorption time, 50
coal well simulation of impact of, 338–342
Southern Ute, 114
spectral density (photoelectric) log, 81, 82, 84, 85
spontaneous potential log, 81, 82, 84
standard cubic feet of gas per ton (scf/ton), 93
*Standard Practice for Proximate Analysis of Coal and Coke*, 23
standard temperature and pressure (STP), 94, 101
stress
coal cleats and, 159
dependence on coal permeability, 159–166
and matrix shrinkage influences on coal permeability, 175–180
subbituminous coals, 22
coal rank, 69
coal reserves, 3, 4, 60–61
subscripts usage
carbon dioxide sequestration, 383
coal depletion of gas and water, 315
coal well simulation, 343
enhanced coalbed methane recovery, 383
gas and water flow in coals, 267–268
gas and water mass balances in coals, 245
sulfur content of coal, 23, 24
surface log, 81
surface time ratio (STR), 107
surface-to-in-seam (SIS) wells, 16
Sydney Basin, 62

## T

tank model. *See also* coal depletion tank model
carbon dioxide sequestration, 374–381
coal well simulation, 324, 331–335, 338–343
tank tests
overview, 193–194
schematic, 193
temperature
coal gas sorption and, 125, 126, 134–139
critical, 41, 42
peat, 61, 62
pseudocritical, 42, 43
reduced, 41, 42
sorption isotherms and, 134, 135, 136–139
standard temperature and pressure (STP), 94, 101
tertiary cleats, 31
thermal maturity, and coal rank, 69
thermogenic coal gas
coal geology and, 73–77, 78, 79, 80
overview, 73–77
thermogenic gas
in coal gas composition, 41, 73–77, 78, 79, 80
definition, 11, 73
tissue preservation index (TPI), 68
total dissolved solids (TDS), 80
two-component gas mixture
binary Langmuir sorption and, 348–350
coalbed gas contents of, 348–350
enhanced coalbed methane recovery and, 347, 348–350
two-phase pseudopressures, 207–208

## U

Uinta Basin, 70
Uinta Basin Drunkard's Wash Field Utah #25-7-6
coal depletion tank model, 275–281
coal well decline curve analysis, 298–299
coal well negative decline, 271
gas and water cumulative production, 277, 280
gas and water production, 275, 277–281
gas and water production rates, 277, 278, 279, 280
gas and water production step-by-step calculation, 278–279
gas-water relative permeabilities, 276
in-situ sorption isotherm, 276
reservoir and well properties, 275
ultimate analysis, 22, 25, 29
unconfined compressive strength (UCS), 52
undersaturated coals, 5, 11, 12, 16, 81, 84, 247
coal gas mass balance equation for, 238–239
coal well simulation with tank and gridded models, 331–335, 338
depletion of, 291–295
gas production of, 272
Warrior Basin Marylee Rock Creek Project, 291–292, 294–295
undersaturation, 81, 291
coal gas sorption and, 125, 146–147
coal well simulation of, 323, 331–335, 338
on isotherm knee, 11, 12
on isotherm plateau, 11, 12
overview, 125, 146–147
U.S. Bureau of Mines (USBM) direct method, 93, 105–106

## V

vitrinite macerals, 29
total coal porosity *vs.*, 34–35
vitrinite reflectance, 29
distance *vs.*, 70–71
procedure, 21
volatile matter relationship to, 21
void volume compressibility, 52, 53
volatile matter, 20, 22, 23
methane gas generation and, 75–77
vitrinite reflectance relationship to, 21

## W–X

Warren and Root dual-porosity simulation models, 319, 320
Warrior Basin, 5, 6, 59
coal depositional environment, 65, 66
coal gas properties and real gas pseudopressure, 258
coal type curve, 7
coal well bottomhole flowing pressure, 257–259

coal well simulation, 324
proximate analysis of, 24
pseudosteady-state flow, 253, 254, 256
sorption time, 255, 256
Warrior Basin Marylee coal
Blue Creek coal gas-water relative permeabilities, 170–172
sorption isotherm and gas content, 292
vitrinite reflectance *vs.* distance, 70
Warrior Basin Marylee coal Rock Creek Project
coal and well properties, 294
coal well depletion, 294–295
cumulative gas and water production, 294, 295
gas and water production rates, 294, 295
Langmuir constants and pressures, 291
undersaturated coal of, 291–292, 294–295
washed-out hole log, 85
water. *See also* moisture
in coal wells, 247
compressibility, 53
vapor, 43
water content of coal, 247. *See also* coal waters; gas and water mass balances in coals
estimation, 23, 25
overview and terminology, 22
water flow in coal
bottomhole flowing pressure and, 263–266
equations, 263–266
Greek symbols used in, 267
nomenclature, 267–268
Powder River Basin, 264–266
seams, 263–266
subscripts used in, 267–268
water porosity, 34
mobile, 32, 36, 167, 326
water production. *See* gas and water production
water saturation, 16
in coal, 167, 247
Powder River Basin Big George coal average, 335, 338, 339, 341
wireline logs for, 86, 87
Wattenberger, R. A., 196, 197
well performance analysis, 1
wet gases, in coal gas composition, 40, 45, 73
whole core
desorption canisters, 96, 97
desorption samples, 93, 94, 95, 96
wireline logs, 3, 14, 16, 59
bulk density log, 81, 82–84
caliper logs, 81, 82, 84
carbon/oxygen, 81, 82, 86
cased hole, 81, 82, 84, 86
cement, 81, 82, 86
cleat detection with, 85–86
coal density and, 81, 82, 83, 85
for coal gas reservoir engineering, 81, 82
coal geology and, 81–87
coal permeability and, 83, 86
coal rank and, 82, 83
coal wells and, 82
compensated neutron log, 81, 82, 84, 85, 86
desorption pressure, 81, 82
formation imaging logs, 81, 82, 86
Formation Micro Imager, 82, 86
Formation Microscanner, 82, 86
gamma ray, 81, 82, 84, 85, 86
gas content and, 83
gas saturation and, 84–85
hole, 81, 82, 84, 85, 86
in-gauge hole, 81, 82
Laterolog, 81, 82, 86
for measuring specific reservoir properties, 81, 82, 83
for mechanical properties, 83
microlog, 81, 82, 85–86
mud log, 81
open hole, 81, 82, 84, 86
openhole logs for coal wells, 81
overview, 81–87
porosity and, 86–87
production logs, 81, 86
proximate analysis and, 81, 83
resistivity, 81, 82, 85
responses in coals, 82
sonic, 81, 82, 84
spectral density (photoelectric), 81, 82, 84, 85
spontaneous potential, 81, 82, 84
surface log, 81
tools, 82–87
washed-out holes, 85
water saturation and, 86, 87
wireline retrieved core, desorption samples, 94, 95

## Y

Young's modulus, 51, 52

## Z

Z factors
average coal gas, 45–47
in coal gas properties, 41, 42, 43, 45–47
Z* function
for dry coals, 287
King, 220–222

## *The Essential Guide for Coal Gas Reservoir Engineering*

This straightforward introduction to coalbed methane gives insight and detail to industry professionals involved with this unique energy resource. Author John Seidle reviews global and U.S. coals and coalbed methane resources, takes the reader through the fundamentals of coal and its importance to coal gas production, and finishes with a discussion of the calculation of probabilistic coalbed methane reserves and pilot philosophy.

In this long-awaited book, Seidle also examines coal deposits as reservoirs, discusses the physics of gas storage in coal and its production, and covers basic equations of mass balance and production rates, negative decline, simulation of coal gas recovery, and enhanced coalbed methane recovery.

*Fundamentals of Coalbed Methane Reservoir Engineering* is an indispensable resource for students and practicing reservoir, production, and operations engineers, geoscientists, landmen, and managers.



John Seidle is a vice president with MHA Petroleum Consultants, Inc., in Denver, Colorado. He has 30 years of experience in coalbed methane and shale gas reservoir engineering. Privileged to work with others on more than 25 technical papers and six patents, he is also an instructor for industry courses. He is currently involved in unconventional gas reservoir engineering, reserve studies, and economic evaluations for domestic and international clients. He received his PhD from the University of Colorado, is a member of SPE, AAPG, and SPEE, and is a Registered Professional Engineer in Colorado, Oklahoma, and Wyoming.

## *Features and benefits*

- A better understanding of the unconventional gas resource called coalbed methane (CBM)
- Ability to analyze CBM exploration, development, and enhanced CBM opportunities
- Improved knowledge of important physics in coal gas production and improved ability to synthesize laboratory and field data into a cohesive picture
- Straightforward, practical answers for those involved in CBM on a daily basis

PennWell®

www.PennWellBooks.com

ISBN-13: 978-1-59370-001-0

90000

9 781593 700010